CAPACITY AND MECHANISMS OF UPTAKE OF SILVER BY JAROSITE FAMILY MINERALS

Peter Frank Cogram

A thesis for the degree of Doctor of Philosophy

Birkbeck

University of London

2016

The work presented in this thesis is the candidate's own.

Abstract

Jarosite is a family of iron-hydroxysulphate minerals that commonly occur in acidic, sulphate-rich environments and in ore processing wastes. Jarosite precipitation is used in hydrometallurgy to control Fe and other impurities. End-member jarosite *sensu stricto* contains potassium and has the chemical formula $KFe_3(SO_4)_2(OH)_6$, but extensive element substitution takes place in the crystal structure. Silver can be taken up by jarosite minerals and, in theory, Ag can form solid-solution series with K, Na and Pb in jarosite. This study carried out synthesis experiments, using a variety of sulphate starting solutions and temperatures, to form K-jarosite, Na-jarosite and Pb-jarosite minerals and determined their capacity for Ag by investigating them using powder X-ray diffraction (XRD), Rietveld refinement, electron microprobe analysis and inductively coupled plasma-atomic emission spectroscopy. Solid solution was found between Ag-jarosite and separately K-jarosite, Na-jarosite and Pb-jarosite, but with substantial hydronium (H_3O) content and vacancies in the Fe site. The average relative partitioning coefficients for Ag were 0.9 in K-jarosite, 1.3 in Na-jarosite and 1.17 in Pb-jarosite. Powder XRD analysis showed that, in the K-Ag-H_3O and Pb-Ag-H_3O-jarosite series, *d*-spacing values for the *hkl* 003 and 006 peaks indicated the unit-cell *c*-axis parameter decreased as Ag content increased. Rietveld refinement showed that, in K-Ag-H_3O-jarosite and Na-Ag-H_3O-jarosite, there were trends of increasing unit-cell *a*-axis parameters and decreasing *c*-axis parameters as Ag content increased. Rietveld refinement indicated decreasing K,Ag-O2 and K,Ag-O3 bond lengths as Ag content increased in K-Ag-H_3O-jarosite. Raman spectroscopic analysis showed the assigned v_1SO_4 and v_3SO_4 vibrational modes in some K-Ag-H_3O-jarosite series had higher wavenumbers (cm^{-1}), indicating higher bonding energies, as Ag content

increased. The XRD, Rietveld refinement and Raman data from this project will inform the evaluation of the Ag composition of jarosite minerals in complex natural mineral assemblages using these same techniques.

Table of Contents

List of Figures

List of Tables

Acknowledgements

I wish to thank my supervisor Professor Karen Hudson-Edwards of the Department of Earth and Planetary Sciences, Birkbeck, University of London, for her support, advice and other help; Dr Mark Welch of the Natural History Museum, London, for guidance and assistance with X-ray diffraction analysis and Rietveld refinement; Dr Andy Beard of the Department of Earth and Planetary Sciences, Birkbeck, for guidance and assistance with electron microprobe analysis; Steve Hirons of the Department of Earth and Planetary Sciences, Birkbeck, for advice and help with X-ray diffraction analysis; Jim Davy of the Earth Sciences Department, University College London, for advice and help with scanning electron microscope analysis; Dr Pam Murphy and Simon Crust of the Faculty of Science, Engineering and Computing, Kingston University, Surrey, for guidance and assistance with Raman spectroscopic analysis; Gary Tarbuck of the Wolfson Laboratory of Environmental Geochemistry, University College London, for advice and assistance with acid digestion of samples and inductively coupled plasma-atomic emission spectrometry analysis; Anthony Osborn of the Wolfson Laboratory of Environmental Geochemistry, University College London, for help with the synthesis of jarosite compounds; and Hank Sombroek of the Department of Earth and Planetary Sciences, Birkbeck, for preparation of polished resin blocks of the samples for electron microprobe analysis.

I received three-year funding through a Birkbeck postgraduate research studentship for this project.

1 INTRODUCTION

1.1 Importance of jarosite-family minerals and silver in the environment and hydrometallurgy

Jarosites form a family of iron hydroxysulphate minerals that commonly occur as secondary products in acidic (pH < 3.0) (Brown, 1971; Amoros et al., 1981), sulphate-rich environments formed by the oxidation of sulphide minerals, especially pyrite (FeS_2) (Baron and Palmer, 1996; Welch et al., 2008). The environments that jarosite minerals commonly form in include oxidised zones (gossans) of sulphide deposits (Brown, 1971; Craddock, 1995), areas of acid rock drainage and acid mine drainage (AMD), mine wastes, and acid sulphate soils from pyrite-bearing sediments (Brophy and Sheridan, 1965; Brown, 1971; Baron and Palmer, 1996; Dutrizac and Jambor, 2000; Becker and Gasharova, 2001; Welch et al., 2008; Murphy et al., 2009). Jarosite precipitation is also used for industrial uses and contaminated land remediation (Welch et al., 2007). In hydrometallurgy, especially the zinc industry, the precipitation of jarosite group phases is used in the processing of sulphide ore minerals to control Fe, sulphate, alkalis and other impurities (Dutrizac and Jambor, 1984; Groat et al., 2003; Murphy et al., 2009). These jarosites can contain Ag and other metals such as Cd, Cu, Ni, Pb and Zn (Sanchez et al., 1996; Ju et al., 2013; Kerolli-Mustafa et al., 2015). Significant losses of Ag can occur in the precipitation of jarosites in hydrometallurgical circuits (Dutrizac and Jambor, 1984), as well as in tailings as a by-product of the processing of economically important minerals (Cabri, 1987).

End-member jarosite *sensu stricto* contains potassium (K) and has the chemical formula $KFe_3(SO_4)_2(OH)_6$, while other end-member minerals in the jarosite

group also contain iron (Fe^{3+}) and sulphur (S^{6+}) (Scott, 1987; Jambor, 1999; Dutrizac and Jambor, 2000). In other end-member jarosite minerals, K^+ is replaced by, for example, sodium (Na^+) in natrojarosite, hydronium (H_3O^+) in hydronium jarosite, silver (Ag^+) in argentojarosite or lead (Pb^{2+}) in plumbojarosite (Jambor, 1999; Dutrizac and Jambor, 2000). Extensive element substitution may take place in the jarosite crystal structure (Scott, 1990; Jambor, 1999; Dutrizac and Jambor, 2000), which has the ability to incorporate 'much of the Periodic Table' as minor and trace elements (Burger et al., 2009). For example, element substitution in jarosite may also result in Fe^{3+} being replaced by aluminium (Al^{3+}), copper (Cu^{2+}), gallium (Ga^{3+}), chromium (Cr^{3+}) or vanadium (V^{3+}) (Dutrizac and Jambor, 2000; Basciano, 2008; Hudson-Edwards et al., 2008; Murphy et al., 2009) and in S^{6+} being replaced by phosphorus (P^{5+}) or arsenic (As^{5+}) (Jambor, 1999; Dutrizac and Jambor, 2000; Basciano, 2008).

Argentojarosite and Ag-bearing plumbojarosite can be valuable ores of Ag (Dutrizac and Jambor, 1984; Craddock, 1995). Silver is a precious metal for which the main uses include jewellery, as well as photography, plating, electrical applications and electronics (Blowes et al., 2003). The main mineral sources of Ag are native metal, electrum, chlorides, sulphides, sulfosalts, lead ores, iron and copper oxides and carbonates, occlusions in quartz, and jarosites in enrichment zones below orebodies (Hahn, 1929; Craddock, 1995). By contrast to Ag, the precious metal gold (Au) is not known to substitute for K^+ in jarosite (Fairchild, 1933; Jambor, 1999), but Au associated with jarosite in gossans has been reported (Darke et al., 1997).

Element substitution means that, in environments such as mine wastes, jarosite minerals are able to scavenge and act as sinks for potentially toxic elements such as As, Cr, Cu and Pb (Smith et al., 2006a; Hudson-Edwards et al., 2008;

Murphy et al., 2009; Kerolli-Mustafa et al., 2015) and precious metals such as Ag (Ju et al., 2013) that escaped extraction or were mobilised in the natural environment. The take-up of elements by jarosite may also take place at the mineral boundary through sorption or coprecipitation (Smith et al., 2006a). In addition, jarosite minerals are potential sources of acid generation (Desborough et al., 2010) and readily break down to release SO_4^{2-} and H^+, as well as metal cations such as K^+ and trace metals, when they are removed from their stability region and dissolve (Smith et al., 2006a; Welch et al., 2008).

1.2 Objectives

Silver can completely substitute in the *A* site of jarosite minerals, forming end-member argentojarosite [$AgFe_3(SO_4)_2(OH)_6$], and studies have suggested that Ag forms complete solid solution series with K and Na in synthetic jarosite in the presence of hydronium (H_3O^+) in the *A* site, and forms incomplete solid solution between Ag-rich and Pb-rich jarosites, with the series disrupted by a region of two phases (Dutrizac and Jambor, 1984 and 1987). These studies used X-ray diffraction (XRD) and chemical analysis to characterise the jarosite series, which were synthesised at 97ºC and 'elevated temperature'. Other studies have used Raman spectroscopy to characterise end-member synthesised Ag-H_3O-jarosite (Casas, et al., 2007) and natural argentojarosite (Frost et al., 2006). However, to date, K-Ag-H_3O-, Na-Ag-H_3O- and Pb-Ag-H_3O-jarosite solid solution series synthesised at low temperature (22ºC) have not been fully investigated and these jarosite series synthesised at higher temperatures have not been fully investigated by XRD and Rietveld refinement to determine changes in unit-cell parameters and atomic bond lengths, angles and positions or by Raman spectroscopy to determine changes in the wavenumbers of modes and so the bonding environment. Such knowledge of these

compounds is important for evaluating the Ag composition of naturally occurring jarosite minerals in complex mineral assemblages and of jarosite minerals in mine and metallurgical processing wastes. To this end, the aims of this study are to determine the capacity of synthetic K-, Na- and Pb-jarosite compounds for Ag, by analysing the *A*-site contents, and the characters of the Ag-bearing compounds. These aims are fulfilled by carrying out the following objectives:

- determine the structural characteristics of the K-Ag-H_3O jarosite, Na-Ag-H_3O jarosite and Pb-Ag-H_3O jarosite solid solution series compounds.
- compare the structures of Ag-bearing jarosite compounds synthesised, under various conditions, at hydrothermal temperatures (c. 97ºC and 140ºC) and at temperatures characteristic of the surface environment (c. 22ºC).

1.3 Outline of the thesis

The questions raised in the objectives set out in section 1.2 are answered by the experimental methods and results presented in this thesis. Chapter 2 reviews the mineral sources of Ag and the geochemistry of Ag in the surface environment. Chapter 3 presents the experimental methods and materials used in this project, including Munsell mineral colour analysis, scanning electron microscopy, X-ray powder diffraction and Rietveld refinement, electron microprobe analysis, Raman spectroscopy and chemical analysis. Chapter 4 presents the results of the experimental methods and explains how they help to characterise the natural and synthetic jarosite compounds. Chapter 5 discusses the uptake of silver by jarosite family minerals, including the effects of synthesis temperature and composition of starting solutions, as well as the relationship of unit-cell parameters to the ionic radii of *A*-site cations and Raman modes. The capacity of natural jarosite minerals for Ag

is also discussed. Chapter 6 presents conclusions and recommendations for future work. Appendix A lists the more than 40 minerals of the alunite supergroup. Appendix B contains theoretical background on the physical and chemical analytical techniques used in this project. Appendix C contains a table of product weights of K-Ag jarosites synthesised at 22ºC, 97ºC and 140ºC, and the concentrations of K and Ag in the starting solutions. Appendix D contains SEM secondary electron images of synthesised jarosite compounds. Appendix E contains XRD spectra. Appendix F contains Raman spectra. Appendix G contains a table of K, Na, Pb and Ag occupation of the *A* site and concentration in starting solutions, and partitioning coefficients for Ag in K-Ag, Na-Ag and Pb-Ag-jarosites between synthesis solutions and products. Appendix H contains figures of Ag partitioning in K-Ag-, Na-Ag- and Pb-Ag-jarosites in syntheses at different temperatures and using different concentrations of K, Na, Pb and Ag.

1.4 Summary

- Jarosite minerals form a family of iron-hydroxysulphate minerals that commonly occur as secondary products in acidic, sulphate-rich environments formed by the oxidation of sulphide ore deposits;
- end-member jarosite *sensu stricto* contains potassium and has the chemical formula $KFe_3(SO_4)_2(OH)_6$, but extensive element substitution may take place in the crystal structure, including Na, Pb, Ag and H_3O;
- argentojarosite and Ag-bearing plumbojarosite can be valuable ores of Ag;
- this study's aims are to determine the capacity of synthetic K-, Na- and Pb-jarosite compounds for Ag, by analysing the *A*-site contents, and the characters of the Ag-bearing compounds;

- these aims are fulfilled by carrying out the objectives of determining the structural characteristics of the jarosite solid solution series compounds; and comparing the structures of Ag-bearing jarosite compounds synthesised at hydrothermal temperatures (c. 97ºC and 140ºC) and at temperatures characteristic of the surface environment (c. 22ºC).

2 LITERATURE REVIEW

2.1 Silver in the environment

The main mineral sources of Ag are native silver, electrum (natural Ag-Au alloy) and in native copper, 'dry ores' such as silver chloride (cerargyrite AgCl), silver sulphide (argentite or acanthite Ag_2S) and sulfosalts, pyrite ores, argentiferous lead ores, iron oxide, Fe-Cu oxide, malachite [$Cu_2CO_3(OH)_2$] and siderite ($FeCO_3$), occlusions in quartz and jarosites associated with the supergene enrichment zones of orebodies between gossans and primary deposits (Hahn, 1929; Craddock, 1995). The main mineral deposits of Ag are low-sulphide quartz veins formed in fracture systems, sedimentary exhalative (sedex) Zn-Pb-Ag deposits, porphyry Cu deposits, epithermal quartz-alunite deposits, volcanogenic massive sulphide (VMS) deposits and supergene Ag-bearing jarosite deposits in sulphide oxidation zones (gossans) (Hahn, 1929; Craddock, 1995; Plumlee et al., 1995; Darke et al., 1997; Rice et al., 1998; Blowes et al., 2003). An example of supergene Ag-bearing jarosite minerals formed in the oxidation zone of VMS deposits is at Rio Tinto, Spain, and such jarosites may also form in the oxidation zones of felsic and mafic volcanic host rocks, as well as other sulphide deposits (Hahn, 1929; Amoros, et al., 1981; Craddock, 1995).

In the surface environment (298.15 K, 10^5 Pa) and in the Ag-O-H system, Ag occurs as Ag[+], Ag[2+], AgOH (aq), $Ag(OH)_2$[-], AgO[-], Ag_2O (s), Ag_2O_2 (s), Ag_2O_3 (s) and Ag (native silver) (Takeno, 2005). Silver exists in four oxidation states: 0, +1, +2 and +3; however, only 0 and +1 are important in soils (Lindsay, 1979) and the surface environment. Silver chemistry in soils and natural aqueous environments is largely limited to Ag(c) and Ag^+ with its minerals and complexes

(Lindsay, 1979). This is because, from the reaction $Ag^{2+} + e^{-} \leftrightarrow Ag^{+}$ log K^{o} 33.60, the ratio of Ag^{+}/Ag^{2+} is at unity at *pe* (electron activity/'concentration') 33.60. In moderately well-oxidised soil, *pe* is about 11, so the ratio of Ag^{+}/Ag^{2+} would be $10^{33.6–11.0} = 10^{22.6}$, and in the redox range of soils Ag^{+} is the predominant silver ion with very little Ag^{2+} and even less Ag^{3+} (Lindsay, 1979).

2.2 Jarosite-family minerals in the environment and in hydrometallurgy

2.2.1 Chemistry of the jarosite family of minerals

Jarosite-family minerals form part of the isostructural alunite supergroup, which has the general chemical formula $AB_3(TO_4)_2(OH)_6$ (Jambor, 1999; Dutrizac and Jambor, 2000; Smith et al., 2006a). There is extensive element substitution in the *A*, *B* and *T* sites in the alunite supergroup, which contains more than 40 end-member natural minerals (see Appendix A) (Jambor, 1999; Dutrizac and Jambor, 2000; Basciano, 2008). The *A* site of the various end-member alunite-supergroup minerals contains a total of 16 different ions: K, Na, H_3O, Ag, Pb, NH_4, Cu, Tl, Ca, Ba, Sr, Ce, La, Nd, Bi and Th (Jambor, 1999; Dutrizac and Jambor, 2000; Basciano, 2008). In the alunite supergroup, the *T* site contains S^{6+}, As^{5+} and/or P^{5+}, as well as Si^{4+} in two end-member minerals (Scott, 1987; Jambor, 1999; Dutrizac and Jambor, 2000). In the supergroup, the *B* site contains Al^{3+} or Fe^{3+}, as well as Ga^{3+} and V^{3+} in one mineral each (Dutrizac and Jambor, 2000; Basciano, 2008). Alunite minerals contain $Al^{3+} > Fe^{3+}$ occupying the *B* site, while in jarosite minerals *B*-site occupation is $Fe^{3+} > Al^{3+}$ (Jambor, 1999; Dutrizac and Jambor, 2000); in natural alunite and jarosite samples, extensive substitution between Al and Fe has been reported (Scott, 1987).

The jarosite family of end-member minerals contains the jarosite group (see Table 2.1) plus two members of the beudantite group ($Fe^{3+} > Al^{3+}$) and five members of the crandallite group ($Fe^{3+} > Al^{3+}$) (see Appendix A). End-member jarosite-group

minerals contain S^{6+} in the *T* site, whereas in the beudantite group there is As-S and P-S substitution and in the crandallite group P and As replace S (see Appendix A) (Jambor, 1999; Dutrizac and Jambor, 2000; Basciano, 2008). The jarosite group comprises eight minerals (see Table 2.1), including jarosite *sensu stricto*, natrojarosite, hydronium jarosite, argentojarosite and plumbojarosite (Dutrizac and Kaiman, 1976; Jambor, 1999; Dutrizac and Jambor, 2000; Drouet and Navrotsky, 2003). Analogues of all these minerals have been synthesised. Mercury jarosite [$Hg_{0.5}Fe_3(SO_4)_2(OH)_6$] and rubidium jarosite [$RbFe_3(SO_4)_2(OH)_6$] have also been synthesised but no natural examples are known (Dutrizac and Kaiman, 1976; Jambor, 1999). However, natural and synthetic jarosite minerals rarely have end-member compositions (Welch et al., 2008). Hydronium (H_3O) often substitutes for cations in the *A* site of jarosite (Majzlan et al., 2004; Basciano and Peterson, 2007), and the presence of H_3O as a substitute ion in the *A* site has been demonstrated by the use of nuclear magnetic resonance (NMR) spectroscopy (Ripmeester et al., 1986).

Table 2.1. End-member minerals of the jarosite group and synthetic analogues.

Mineral name	**Formula**	**Synthetic analogue**
Jarosite[1]	$KFe_3(SO_4)_2(OH)_6$	Potassium jarosite
Natrojarosite[1]	$NaFe_3(SO_4)_2(OH)_6$	Sodium jarosite
Hydronium jarosite[1]	$(H_3O)Fe_3(SO_4)_2(OH)_6$	Hydronium jarosite
Argentojarosite[1]	$AgFe_3(SO_4)_2(OH)_6$	Silver jarosite
Plumbojarosite[1]	$Pb_{0.5}Fe_3(SO_4)_2(OH)_6$	Lead jarosite
Ammoniojarosite[1]	$(NH_4)Fe_3(SO_4)_2(OH)_6$	Ammonium jarosite
Beaverite[1]	$Pb(Fe,Cu)_3(SO_4)_2(OH)_6$	Lead Fe-Cu-jarosite
Dorallcharite[1]	$Tl_{0.8}K_{0.2}Fe_3(SO_4)_2(OH)_6$	Thallium jarosite
No natural mineral	$Hg_{0.5}Fe_3(SO_4)_2(OH)_6$	Mercury jarosite[2]
No natural mineral	$RbFe_3(SO_4)_2(OH)_6$	Rubidium jarosite[2]

1 Jambor, 1999; Dutrizac and Jambor, 2000; Drouet and Navrotsky, 2003; Smith, 2004; Basciano, 2008; Hudson-Edwards et al., 2008. 2 Dutrizac and Kaiman, 1976; Jambor, 1999

Minerals of the alunite supergroup have the ability to incorporate many minor and trace elements into their crystal structure (Burger et al., 2009). A wide range of combinations of elements is possible in the *A*, *B* and TO_4 sites. Reported substitutions in the *A* site include Mn^{2+}, Mo^{2+} and ions of end-member alunite supergroup members Na^{+}, H_3O^{+}, Pb^{2+}, Ca^{2+}, Sr^{2+}, Ba^{2+}, Nd^{3+}, Ce^{3+} and La^{3+}, as well as other REEs Sm, Eu, Dy, Er and Yb; reported substitutions in the *B* site include Pb^{2+}, Mg^{2+}, Zn^{2+}, In^{3+}, Sb^{3+}, Cr^{3+} and Ti^{4+}, as well as ions of end-member alunite supergroup members Cu^{2+}, V^{3+} and Ga^{3+}; and reported substitutions in the *T* site include Cr^{6+}, Se^{6+} and Sb^{5+}, as well as P^{5+} and As^{5+} (Scott, 1987; Elgersma et al., 1993; Jambor, 1999; Sejkora, et al., 2001; Paktunc and Dutrizac, 2003; Welch et al., 2007, 2008; Burger et al., 2009). In addition, a reported substitution for TO_4^{2-} is CO_3^{2-} (Scott, 1987). Reported substitutions in the OH^{-} site are Cl^{-}, F^{-} and H_2O (Scott, 1987; Sejkora et al., 2001; Burger et al., 2009).

In synthetic jarosite, reported substitutions for S in the *T* site are As, Se and Cr, with a maximum As substitution of 17 mole % $AsO_4/(AsO_4 + SO_4)$, or $As/(As + S) = 0.17$ (Paktunc and Dutrizac, 2003). In synthesised jarosite- and alunite-group phases and analogues, substitution between Al^{3+}, Fe^{3+}, Cr^{3+} and V^{3+} in the *B* site has been reported (Murphy et al., 2009).

There is a strong relationship between occupancy of the crystallographic sites to maintain charge balance in alunite- and jarosite-group minerals (Scott, 1987; Burger, 2009). For example, studies have demonstrated coupled substitution of Pb^{2+} (Scott, 1987) and of Ba^{2+} and Sr^{2+} (Burger et al, 2009) for alkali cations in the monovalent *A* site combined with trivalent anions PO_4^{3-} and AsO_4^{3-} for SO_4^{2-} in the *T* site. In addition, a study of alunite supergroup minerals has reported the substitution

of AsO_3OH for AsO_4 and of PO_3OH for PO_4 to maintain charge balance where there are substitutions or vacancies in the *A* and *B* sites (Sejkora et al., 2001).

In non-stoichiometric jarosite group minerals in which there are deficiencies in occupancy of K^+, Na^+ or other substitute ions in the *A* site, studies often assume the site is occupied by hydronium (H_3O) (Basciano and Peterson, 2007; Desborough et al., 2010); however, occupancy by H_3O is not necessarily the case and often there may be vacancies in the *A* site (Majzlan et al., 2004).

Deficiencies in the *B* site are also reported to be charge balanced by the incorporation of water, in the form of hydronium, into the jarosite structure (Hudson-Edwards et al., 2008). Studies of natural alunite supergroup minerals have reported deficiencies in the *B* site (Scott, 1987; Rattray et al., 1996; Roca et al., 1999) and studies of synthesised jarosite-group minerals have shown deficiencies of Fe in the *B* site (Dutrizac and Kaiman, 1976; Basciano and Peterson, 2007, 2008; Hudson-Edwards et al., 2008). However, a vacancy in the *B* site may be compensated for by the addition of 4 H^+ (protonation) at the *B* site to form four *B*-OH_2 bonds per vacancy, so H_3O in the *A* site is not necessary for charge balance, hence vacancies in the *A* site are commonly seen (Kubisz, 1970; Basciano and Peterson, 2007, 2010). In addition, to maintain charge balance where substitutions or vacancies exist in crystallographic sites of alunite supergroup minerals, including jarosite, many studies have assumed the presence of H_2O in the OH^- site (Hendricks, 1937; Rattray et al., 1996; Sejkora et al., 2001; Drouet et al., 2004; Burger, 2009). These considerations have resulted in a modified general chemical formula being proposed for jarosite compounds:

$A_{1-x}(H_3O)_xFe_{3-y}[(OH)_{6-3y}(H_2O)_{3y}(SO_4)_2]$ (Kubisz, 1970).

Many solid solutions are complete among most or all synthetic jarosite species (Dutrizac and Jambor, 2000). Studies have reported solid solution involving K^+, Na^+ and H_3O^+ is extensive in synthetic alunite (Parker, 1962) and jarosite (Brophy et al., 1962; Brophy and Sheridan, 1965; Kubisz, 1970; Stoffregen and Cygan, 1990; Li et al., 1992; Jambor, 1999; Basciano and Peterson, 2007, 2008). Hydronium jarosite forms a complete solid-solution series with alkali jarosites. In addition, there is a complete solid solution among synthetic K, Na and NH_4 jarosites (Brophy and Sheridan, 1965), and another study has reported the incorporation of NH_4 in ammoniojarosite seems to be mainly at the expense of K^+ and H_3O^+ (Odum et al., 1982). Substitution involving K^+ and Pb^{2+} has also been shown to be extensive in jarosite (De Oliveira et al., 1996; Roca et al., 1999). Lead jarosite forms a solid-solution series with monovalent jarosites, but the series are not crystallographically perfect because order-disorder often results in superstructure effects in Pb-rich members, with *c* axis 34 Å (double axis length of monovalent jarosites) in Pb-jarosite (Dutrizac and Jambor, 1984, 1987a).

However, studies of natural minerals have reported only limited solid solution between K and Na in low-temperature jarosite and natrojarosite (Burger et al., 2009; Desborough et al., 2010), suggesting the presence of a solvus in the jarosite-natrojarosite system at temperatures below about 140ºC (Desborough et al., 2010). In one of these studies, hydronium-bearing jarosite was detected in only one relatively young supergene sample, suggesting H_3O-bearing jarosites are unstable over geological timescales. The extent of solid solution between Na, K, and H_3O affects the stability of natural jarosite and natrojarosite minerals (Desborough et al., 2010).

Synthetic Ag jarosite has been proposed to form an unbroken solid-solution series with K-jarosite in the presence of hydronium (Dutrizac and Jambor, 1984 and

2000), as well as with Na-H_3O jarosite (Dutrizac and Jambor, 1984). Solid solution between synthetic Ag-jarosite, NH_4-jarosite and H_3O-jarosite has also been reported (Roca et al., 2007). In addition, in synthetic systems, solid solution between Ag-H_3O and Pb-H_3O in jarosite has been reported; however, despite extensive solid solution between Ag-rich and Pb-rich jarosites, end-member compositions have not been achieved because of partial replacement of the non-ferrous metals by hydronium (Dutrizac and Jambor, 1984).

2.2.2 Crystal structure of the jarosite family of minerals

The crystal system of jarosite minerals is hexagonal and the crystal structure is in space group R-3m (Figueiredo and Pereira da Silva, 2011), and has trigonal symmetry (Figueiredo and Pereira da Silva, 2011). The structure has three formula units per unit cell (Z = 3), and in jarosite *sensu stricto* [$KFe_3(SO_4)_2(OH)_6$] the unit cell contains 3 K, 9 Fe, 6 S, 24 O and 18 (OH).

The structures of minerals in the alunite supergroup, which includes jarosite family minerals, are layered and based on octahedral-tetrahedral sheets (Jambor 1999; Hawthorne et al., 2000). These sheets are composed of variably distorted *B*-site cations in octahedral coordination (coordination number [CN] = 6) and *T*-site cation in tetrahedral coordination (CN = 4) (see Figure 1.1) (Dutrizac, 1980; Jambor, 1999; Figueiredo and Pereira da Silva, 2011). The $B^{3+}O_6$ octahedra are capped by the TO_4 tetrahedra and make up in-plane corner-sharing $B_3(OH)_6(TO_4)_2^-$ trimers, forming the layers. The interlayer space is filled by monovalent A^+ ions, which set the interlayer distance (Grohol and Nocera, 2007).

In jarosite, the B cation is Fe^{3+} in six-fold (octahedral) coordination with four OH^- and two O^{2-}, while the tetrahedra contain SO_4^{2-} (Brophy et al., 1962; Stoffregen et al., 2000). In alunite minerals, the B site is filled by Al^{3+}, which can form a solid

solution with Fe^{3+}. Fe^{3+} preference over Al^{3+} in the B site increases at higher acidity (pH < 3), lower temperature and/or increased Eh of formation (more oxidizing conditions) (Brophy et al., 1962; Burger et al., 2009). Other cations that are known to substitute in the B site include Zn^{2+}, Mg^{2+} and V^{4+} (Burger et al., 2009), Ga^{3+} and Cr^{3+} (Drouet and Navrotsky, 2003) and In^{3+} (Baron and Palmer, 2002).

The octahedra occur at the vertices of a 6^3 plane net, forming six-membered rings with the octahedra linked by corner-sharing four OH^- (see Figure 2.1) (Hawthorne et al., 2000). At the junction of three six-membered rings is a three-membered ring, and one set of apical vertices of those three octahedra link to a T-site tetrahedron (see Figure 2.1). The resultant sheets are held together by interstitial cations and hydrogen bonds.

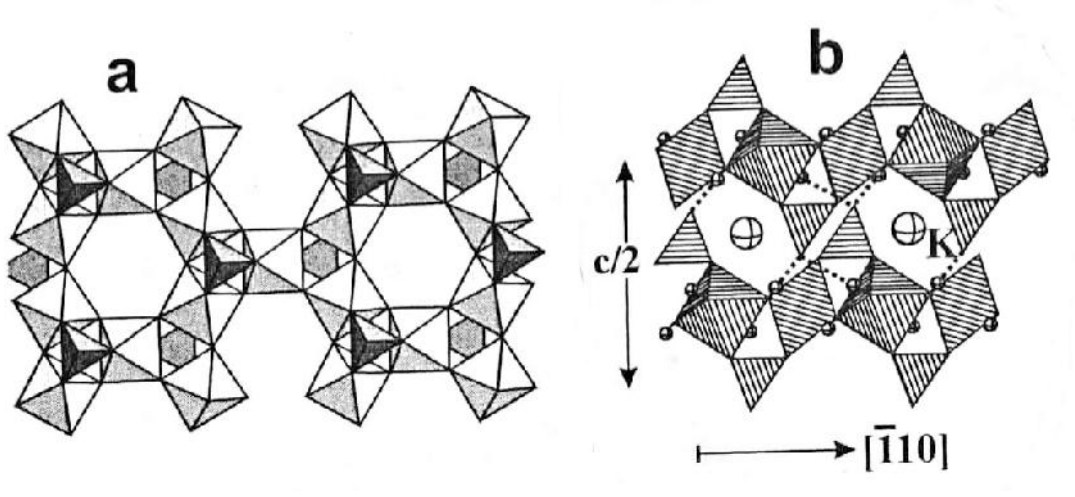

Figure 2.1. (a) Jarosite Fe-O and Fe-OH octahedra form six-membered rings with the octahedra linked by corner-sharing four OH^-. At the junction of three six-membered rings is a three-membered ring. (b) Fe octahedra corner share (four OH^-) to form sheets perpendicular to the *c* axis, and Fe octahedra also corner-share with SO_4 tetrahedra (two O^{2-}), aligned along (001) (From Hawthorne et al., 2000).

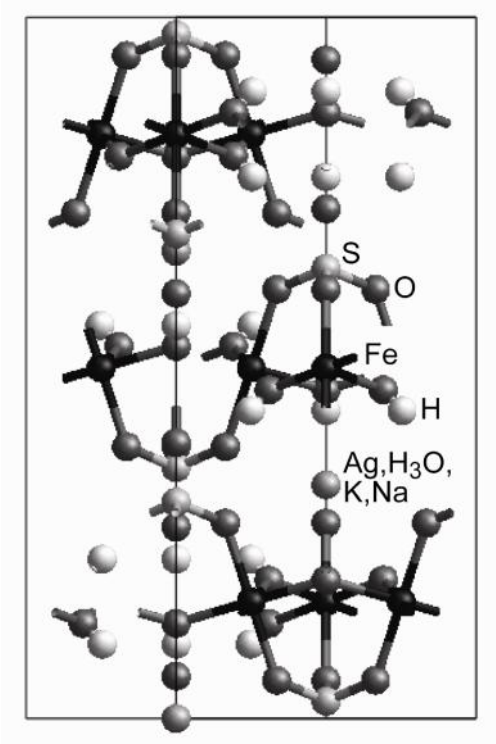

Figure 2.2. X–Z axis cut through a ball-and-spoke model of jarosite. The structure is composed of FeO_6 octahedra bonded to SO_4 tetrahedra, making a tetrahedral–octahedral–tetrahedral (T–O–T) sheetlike structure. *A*-site ions (Ag, H_3O, K, Na) are located between the T–O–T sheets.

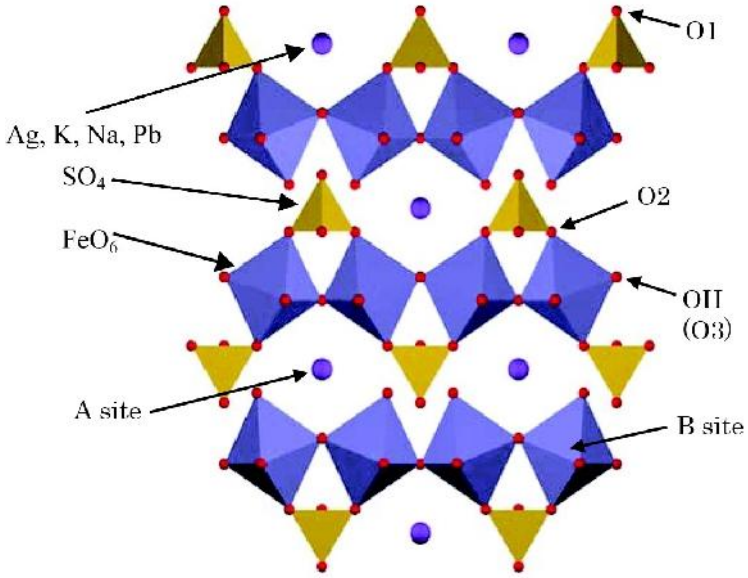

Figure 2.3. Jarosite structure of FeO_6 octahedra bonded to (corner-sharing with) SO_4 tetrahedra, forming sheets perpendicular to the *c* axis, with *A*-site ions (Ag, K, Na, Pb and H_3O) located between the tetrahedral–octahedral–tetrahedral sheets.

Fe octahedra corner share (four OH^-) to form sheets perpendicular to the *c* axis (Basciano and Peterson, 2007; Basciano, 2008), and Fe octahedra also corner-share with SO_4 tetrahedra (two O^{2-}), aligned along (001), i.e. perpendicular to the *c* axis (see Figures 2.1 and 2.2) (Jambor, 1999). This means substitutions in the B site mainly affect *a* axis dimension, with *a* decreasing as Al replaces Fe (Jambor, 1999). This is because Fe^{3+} (high spin) has a larger effective ionic radius (0.645 Å) in six-fold coordination than Al^{3+} (0.535 Å) (Shannon, 1976).

SO_4 tetrahedra (O1 bond), aligned along [001], occur as two crystallographically independent sites within a layer: one set of TO_4 points towards +*c* ('upward' along the *c* axis), alternating with other set pointing toward –*c* ('downward' along the *c* axis) (see Figure 2.1) (Stoffregen et al., 2000; Basciano and Peterson, 2007; Basciano, 2008). The oxygens and hydroxyls of the octahedra and tetrahedra form an icosahedron, amid which is the A cation. For compositions with the same TO_4, the length of the *c* parameter is mainly influenced by the size of the A-site cation (Jambor, 1999; Stoffregen et al., 2000).

The *A*-site cation is in 12-fold (icosahedral) coordination (CN = 12) (Figueiredo and Pereira da Silva, 2011) and the site is filled by monovalent K^+ in end-member jarosite, Na^+ in natrojarosite and Ag^+ in argentojarosite and divalent Pb^{2+} in plumbojarosite. Another monovalent cation that can also fill the A site is H_3O^+, which forms the end-member mineral hydronium jarosite.

The Fe^{3+} position in the jarosite structure can be described by a kagome lattice (of interlaced 2D triangles of atoms) (Wills et al., 2004; Basciano and Peterson, 2008). The jarosite group is a main model for studying spin frustration: kagome layers are formed from corner-sharing $Fe^{3+}{}_3$-(μ-$OH)_3$ triangles – the most highly frustrated two-dimensional lattice. Jarosite structures display novel physical

properties connected with geometrically frustrated magnetism, such as superconductivity (Grohol and Nocera, 2007).

2.2.3 Silver associated with members of the jarosite family of minerals

Silver is able to fill the *A* site of jarosite minerals and in natural environments forms argentojarosite, which is generally near the end-member composition (Jambor, 1999). The analogue of argentojarosite has been synthesised (Dutrizac and Kaiman, 1976; Jambor, 1999). Argentojarosite is of economic importance, being abundant enough at some localities to form ore minerals, while other subgroup members may be carriers of Ag. Silver-bearing jarosite was exploited at Rio Tinto, southern Spain, from pre-Roman times (Dutrizac and Jambor, 2000). End-member argentojarosite is almost as stable as K-jarosite (Dutrizac and Jambor, 2000), with the solubility products (at 298K) of jarosite and argentojarosite being reported as $10^{-12.50}$ and $10^{-11.55}$, respectively (Gaboreau and Veillard, 2004).

Silver is a common trace element in the oxidised zones of sulphide ore deposits and in mine waste and acid mine drainage (Scott, 1987; Darke et al., 1997; Leverett et al., 2005; Basciano and Peterson, 2010). Studies have reported Ag-bearing jarosites forming from the weathering of sulphides and sulfosalts at Mt Leyshon, northeast Queensland (Scott, 1987, 1990), with one Ag-containing natrojarosite sample having the formula: $Na_{0.47}K_{0.33}Ag_{0.01}(Fe_{2.58}Al_{0.59})(SO_4)_{1.91}(PO_4)_{0.08}(OH)_6$. Also, Ag associated with jarosite in oxidised zones has been reported to be enriched compared with sulphide ore deposits (Darke et al., 1997; Leverett et al., 2005).

Argentojarosite was first observed in 1925 as a secondary product from the weathering of sulphide-rich ore veins at Tintic Standard Mine, Dividend, Utah (Dutrizac and Jambor 2000). One of the principal sources of Ag is jarosite ores

associated with the enrichment zones of orebodies near the base of gossans (oxidised zones) above primary deposits, such as at Rio Tinto (Amoros et al., 1981; Craddock, 1995; Roca et al., 1999). Studies show Ag-bearing jarosite minerals in the gossan ores of Rio Tinto are argentojarosite and/or argentian plumbojarosite, and argentojarosite in dilute solid solution (Ag 230 ppm) in jarosite-beudantite [$PbFe_3(As,SO_4)_2(OH,H_2O)_6$] phases (Sanchez et al., 1996; Roca et al., 1999; Dutrizac and Jambor, 2000). The affinity of Pb for Ag has been known since antiquity, being used to recover the metal from primary ores and secondary products, including jarosite (Craddock, 1995). Argentiferous plumbojarosite is relatively common, and where abundant is typically from the weathering of Ag-bearing galena-rich veins. Argentiferous plumbojarosite was mined at Matagente, Peru, including by the Incas (Dutrizac and Jambor, 2000).

2.2.4 Occurrence and importance of jarosite minerals in the natural environment

Environments in which jarosite-family minerals commonly form as secondary products include gossans, areas of acid rock drainage and acid mine drainage (AMD), mine tailings, and acidic soils (Dutrizac and Jambor, 2000; Becker and Gasharova, 2001; Welch et al., 2008; Murphy et al., 2009). Jarosites form as secondary minerals in the oxidised zones (gossans) of sulphide deposits, particularly at the base of gossans (Craddock, 1995), by the reaction of dilute sulphuric acid (H_2SO_4), Fe^{3+} and other cations such as Ag^{+} and Pb^{2+} in ground water with gangue and wall-rock minerals (see Figure 1.3) (Brown, 1971; Craddock, 1995). Within saturated (phreatic) or vadose zones of mine tailings and acid sulphate soils, jarosites occur as yellow crusts and coatings (Basciano, 2008). In AMD fluvial environments, jarosite is one of the Fe hydroxides, oxyhydroxides or oxyhydroxysulphates

collectively termed ‘ochre’, ‘boulder coats’ or ‘yellowboy’ (Lottermoser, 2003). Other common Fe minerals in ochre include ferrihydrite ($Fe_5HO_8.4H_2O$), schewertmannite ($Fe_8O_8(SO_4)(OH)_6$) and FeOOH polymorphs goethite, ferroxyhyte, akaganeite and lepidocrocite. Ochre commonly occurs as bright reddish-yellow to yellowish-brown stains and coatings, and the precipitates are amorphous, poorly crystalline or crystalline (Lottermoser, 2003).

Figure 2.4 Pourbaix (Eh-pH) phase diagrams showing stability conditions of jarosite in the Fe-S-O-H system at 22˚C, 97˚C and 140˚C and of natrojarosite at 25˚C.

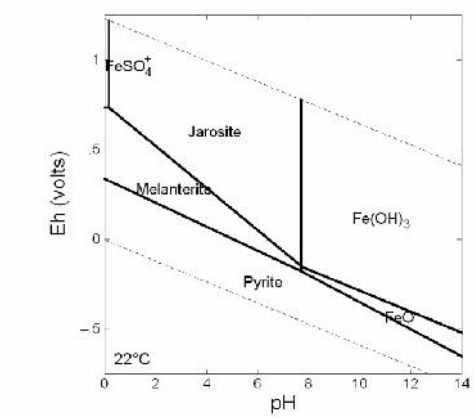

aFe = 10^{-1}, log SO_4^{2-} = $10^{-0.7}$, log K^+ = 10^{-2}

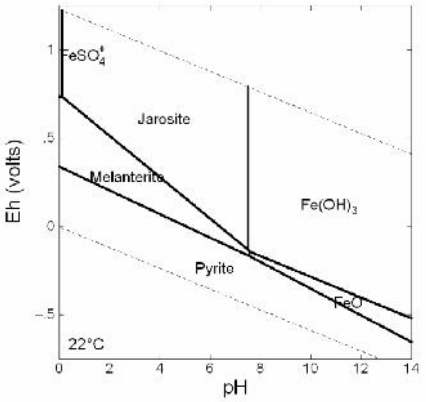

aFe = 10^{-1}, log SO_4^{2-} = 10^{-1}, log K^+ = 10^{-2}

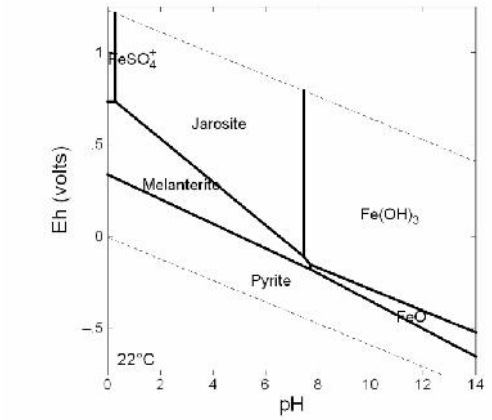

aFe = 10^{-1}, log SO_4^{2-} = $10^{-0.7}$, log K^+ = $10^{-2.7}$

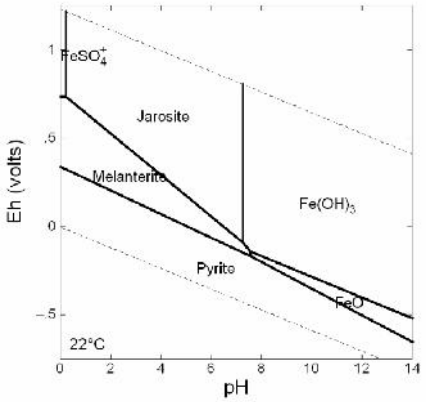

aFe = 10^{-1}, log SO_4^{2-} = 10^{-1}, log K^+ = $10^{-2.7}$

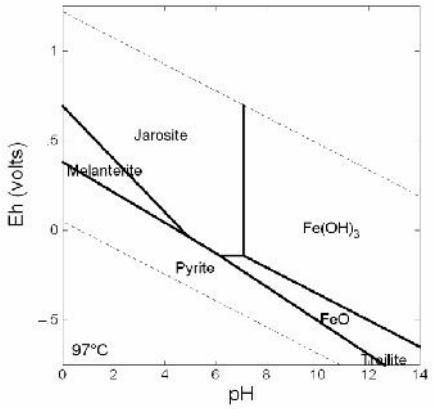

aFe = 10^{-1}, log SO_4^{2-} = $10^{-0.7}$, log K^+ = 10^{-2}

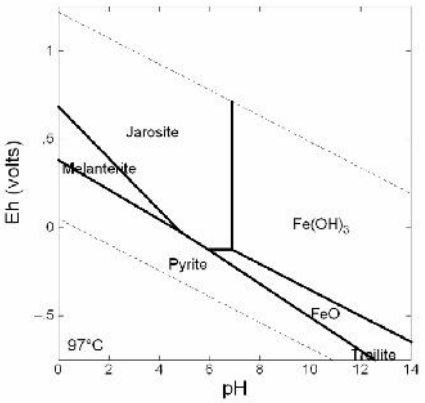

aFe = 10^{-1}, log SO_4^{2-} = 10^{-1}, log K^+ = 10^{-2}

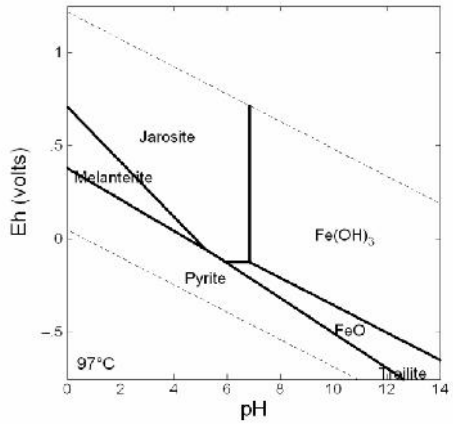

aFe = 10^{-1}, log SO_4^{2-} = $10^{-0.7}$, log K^+ = $10^{-2.7}$

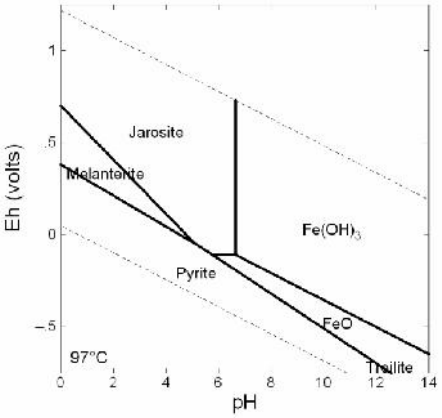

aFe = 10^{-1}, log SO_4^{2-} = 10^{-1}, log K^+ = $10^{-2.7}$

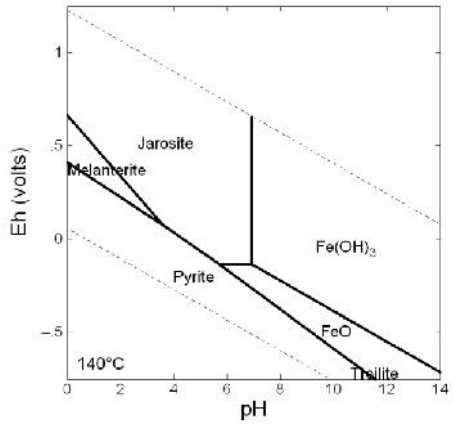

aFe = 10^{-1}, log SO_4^{2-} = $10^{-0.7}$, log K^+ = 10^{-2}

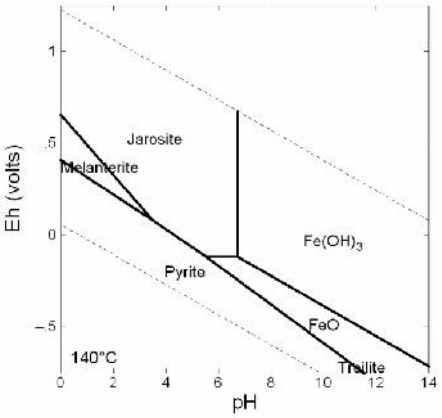

aFe = 10^{-1}, log SO_4^{2-} = 10^{-1}, log K^+ = 10^{-2}

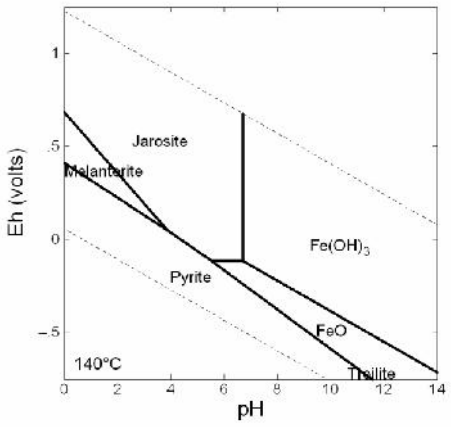

aFe = 10^{-1}, log SO_4^{2-} = $10^{-0.7}$, log K^+ = $10^{-2.7}$

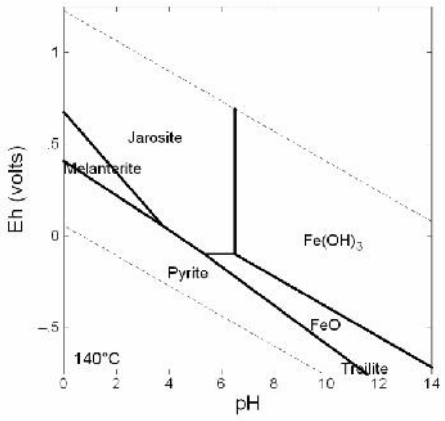

aFe = 10^{-1}, log SO_4^{2-} = 10^{-1}, log K^+ = $10^{-2.7}$

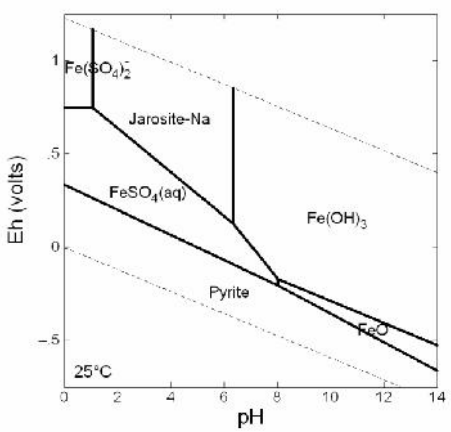

aFe = 10^{-1}, log SO_4^{2-} = $10^{-0.7}$, log Na^+ = 10^{-2}

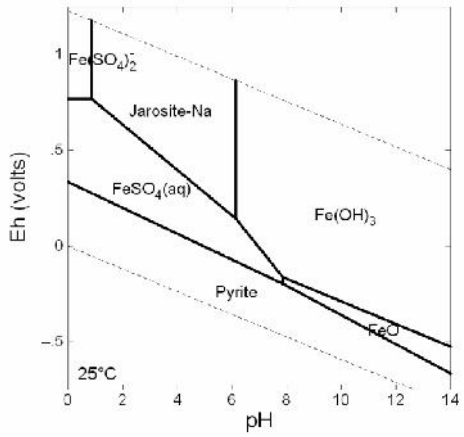

aFe = 10^{-1}, log SO_4^{2-} = 10^{-1}, log Na^+ = 10^{-2}

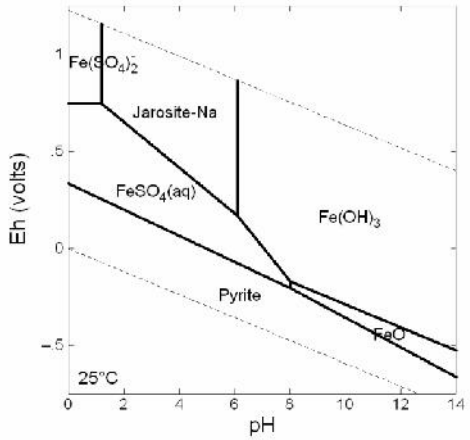

aFe = 10^{-1}, log SO_4^{2-} = $10^{-0.7}$, log Na^+ = $10^{-2.7}$

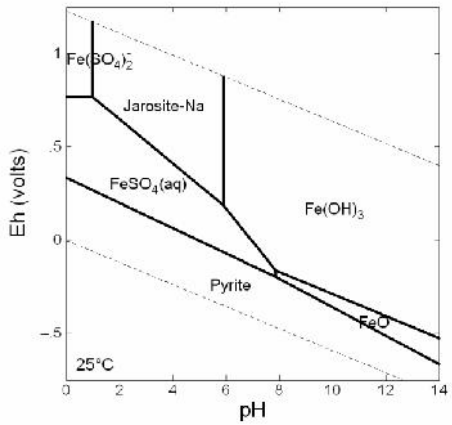

aFe = 10^{-1}, log SO_4^{2-} = 10^{-1}, log Na^+ = $10^{-2.7}$

Diagrams produced using the Geochemist's Workbench program and databases.

Jarosite minerals can also form in environments including acidic hypersaline lake sediments and evaporite basins, weathered coal refuse from pyritic coal seams,

nodules and disseminations in clays, and hot springs and hydrothermal vents, particularly through gases H_2S and SO_2 being dissolved and oxidised (Brophy and Sheridan, 1965; Baron and Palmer, 1996; Dutrizac and Jambor, 2000; Becker and Gasharova, 2001; Welch et al., 2008; Battler et al., 2013). Hypogene jarosite minerals have formed during albitisation, by hydrothermal alteration of alunitised volcanic rocks, as primary argentojarosite in polymetallic ore deposits, and in secondary quartzites (Dutrizac and Jambor, 2000).

Jarosite minerals have been reported in other geological environments that include glauconite sandstones, fillings in cavities in arkoses, bedded cherts, heavy-mineral assemblages in sandstone, and altered quartz porphyry oxidation products (Brophy and Sheridan, 1965). Jarosite, including chromium-jarosite, can form during the corrosion of Portland cement concrete (Becker and Gasharova, 2001; Tazaki et al., 1992). Jarosite-group minerals have accumulated as stalactites and fine-grained mud on massive pyrite in mines (Jamieson et al., 2005). In addition, the presence of jarosite on the surface of Mars has been reported (Papike et al., 2006).

Other jarosite group minerals commonly found in AMD settings are natrojarosite, hydronium jarosite and plumbojarosite, as well as As-bearing phases (Blowes et al., 2003). Other jarosites are rare compared with end-member K-jarosite, but this invariably contains hydronium, commonly with $K > H_3O > Na$ (Blowes et al., 2003). Hydronium jarosites exist where Fe-bearing sulphate solutions are deficient in alkalis due to the more rapid oxidation of pyrite than the country rocks, and the rapid neutralization of the solutions by, for example, carbonate rocks causing jarosite to precipitate before alkalis in the country rock can be dissolved. Hydronium jarosite has been found as crusts in mine dolomitic alteration zones, formed by oxidation after a gallery was opened (Brophy and Sheridan, 1965).

AMD forms from the oxidation of sulphide minerals such as pyrite (FeS_2) and produces acidic waters and secondary minerals such as metal-bearing sulphates, hydrosulphates, such as jarosite, and hydrous oxides, for example goethite (α-FeOOH). Jarosite group minerals form in strong acidity and moderate to highly oxidized sulphate-rich waters. Jarosites occur as yellow crusts and coatings within saturated (phreatic) or vadose zones of mine tailings and acid sulphate soils (Basciano, 2008). In the early stages of acid generation most K^+ is derived by the incongruent alteration of trioctahedral mica, such as biotite $[K_2(Fe,Mg)_6[Si_3AlO_{10}]_2(OH,F)_4]$ (Blowes et al., 2003). Jarosite minerals act as sinks for such interlayer monovalent cations from micas during weathering and bioleaching (Wang et al., 2007). Pb^{2+} in plumbojarosite is commonly derived from the weathering of the main ore of lead, galena (PbS) (Brophy and Sheridan, 1965; Blowes et al., 2003).

Weathering of hydrothermal minerals in acid-sulphate epithermal systems creates mineral products derived from sulphides, including jarosites, alunites and metals such as Ag, Bi, Cu and Pb (Scott, 1990). Alunite group minerals can form under acid oxidizing conditions in hypogene porphyry Cu and epithermal Au deposits. Jarosite group minerals can replace alunite group minerals during weathering, retaining the Na-K ratio of the parents and substantial Al. Jarosites that directly replace pyrite have low Al contents and Na-K ratios differing from alunite group minerals in the same sample (Scott, 1990).

Jarosite can form by precipitation of K^+ with Fe^{3+} and SO_4^{2-} generated by pyrite oxidation as follows (Blowes et al., 2003; Basciano, 2008):

$$K^+_{(aq)} + 3Fe^{3+}_{(aq)} + 2SO_4^{2-} + 6H_2O_{(l)} \leftrightarrow KFe_3(SO_4)_2(OH)_{6(s)} + 6H^+_{(aq)}$$

The equivalent equation applies for the formation of sodium-jarosite (natrojarosite) from Na^+ ions (Casas et al., 2007).

The Fe^{3+} and SO_4^{2-} required for jarosite formation can be supplied by processes other than sulphide mineral oxidation. Hypogene jarosites, for example, form as a result of the oxidation of H_2S gas to SO_4 and host-rock Fe^{2+} to Fe^{3+} upon ascent of hydrothermal fluids, and precipitation of the resultant oxidised species. In evaporative environments, the necessary ions for jarosite formation are provided by oxidation of sulphides, Fe(II)-bearing silicates and sulphate aerosols, and acidity from ferrolysis or sulphide oxidation (McArthur et al., 1991).

Bacteria can metabolise metals and sulphur, accelerating sulphide oxidisation, the release of metals into solution and the creation of AMD (Blowes et al., 2003). Bacterial oxidation of Fe^{2+} from pyrite and other sulphides aids the formation of jarosite (Sasaki and Konno, 2000; Becker and Gasharova, 2001). Acid tolerant (acidophile) bacterium *Thiobacillus ferrooxidans* is one of 18 bacteria species and four archaea species that are known oxidisers of pyrite. The process takes place either by direct interaction, with the microbe attaching to the mineral surface and solubilising it by enzymatic reactions, or by indirect interaction, with reactions taking place close to the mineral surface but not on it (Blowes et al., 2003).

Without such bacteria the rate of sulphide oxidation would stabilise below pH 3.5 (Blowes et al., 2003). Also, because abiotic oxidation of pyrite is slow, it has been suggested that *T. ferrooxidans* and other microbes are the driving force behind AMD pollution (Blowes et al., 2003). It has been stated that Fe^{2+} ion oxidation in high sulphate (~ 1 g l^{-1}) and highly acidic (< pH 3) waters can only occur with the assistance of microorganisms such as *T. ferrooxidans* (Schwertmann and Cornell, 2000). In reported experiments, jarosite has been synthesized within 1-6 months at

room temperature by aerating solutions of $Fe^{2+}SO_4$ and K_2SO_4 at pH 1-2, but if *T. ferrooxidans* is present, jarosite is able to form within days (Tazaki et al., 1992). *T. ferrooxidans* is able to accelerate the oxidation of Fe^{2+} to Fe^{3+} by five to six orders of magnitude than if it is absent (Tazaki et al., 1992).

Sasaki and Konno (2000) formed jarosite, argentojarosite and ammoniojarosite experimentally in the presence of *T. ferrooxidans*. Silver ions are extremely toxic to a wide range of bacteria, but *T. ferrooxidans* and *T. thiooxidans* accumulate Ag during the bioleaching of sulphide ores (Sasaki et al., 1995). In the hydrometallurgical bioleaching of metals from sulphides, jarosites are of great importance in controlling ferric iron solubility and remove Ag from solution to form argentojarosite (Wang et al., 2007). Argentojarosite can form in presence of *T. ferrooxidans* but neither bacteria nor extracellular substances make a direct contribution to its crystallization (Sasaki and Konno, 2000).

2.2.5 Jarosites in hydrometallurgy

The precipitation of jarosite group phases is used in hydrometallurgy, especially the zinc industry, to control Fe, sulphate, alkalis and other impurities (Groat et al., 2003; Murphy et al., 2009). Hydrometallurgical treatment of Zn sulphide ore involves separation of Zn from Fe, as most Zn processing concentrates contain 5-12% Fe. Processes involving the formation of jarosite remove Fe from acidic zinc sulphate solutions prior to Zn electrolysis (Dutrizac and Kaiman, 1976; Arslan and Arslan, 2003).

As well as Fe, these jarosites can contain Ag and other metals such as Cd, Cu, Ni, Pb, Zn (Sanchez et al., 1996; Ju, 2013; Kerolli-Mustafa, 2015). Argentojarosite and Ag-bearing plumbojarosite can be valuable ores of Ag and Pb, and precipitation of jarosites as controls of Fe and other impurities, including trace

metals, in hydrometallurgical circuits can lead to significant losses of Ag (Dutrizac and Jambor, 1984). In hydrometallurgy, much of the Ag present may enter the jarosite fraction and could be a cause of erratic recoveries of Ag 'values' (Dutrizac and Kaiman, 1976; Dutrizac and Jambor, 2000), as during conventional cyanidation processing of gossan, precipitation of Ag as argentojarosite can prevent its recovery (Dutrizac and Kaiman, 1976; May et al., 1973); cyanidation under conventional conditions recovers 40% of Ag from gossan ores of Rio Tinto, Spain (Roca et al., 1999). Studies have shown that, in zinc processing, Ag impurities are selectively incorporated in jarosite in preference to Na, NH_4 and Pb (Dutrizac and Jambor, 2000; Groat et al., 2003). Recovery of the Ag in jarosite formed hydrometallurgical processes requires the crystal structure to be destroyed. The jarosite residues can be decomposed by roasting and dissolution using NH_4ClH_2O (Ju et al., 2013) , cyanidation in alkaline media such as NaOH-CN^- or $Ca(OH)_2$-CN^- (Roca et al., 1999; Cruells et al., 2000; Dutrizac and Jambor 2000), or sulfidisation (Han et al., 2014); complexation is then used to remove Ag, as well as other metals, from the decomposition solids (Roca et al., 1999; Cruells et al., 2000).

In hydrometallurgy, jarosite is hazardous waste from zinc production and jarosite is converted to jarofix, a solidified, stabilised and inert material which can be disposed of in landfill (Cadena Zamudio, undated paper).

2.3 Synthesis methods for jarosite compounds

The factors affecting the extent of jarosite precipitation and the composition of jarosites are important for mineralogists in terms of understanding the partitioning of alkali ions during jarosite formation in supergene deposits and the extent of Ag, Pb and hydronium substitution for alkalis (Dutrizac, 1983).

Table 2.2: Examples of K, Na, Ag, Pb concentrations in reported jarosite syntheses

Compound	Temp	Reactants	A:Fe^{3+} ratio	Product formula
Dutrizac (1983)				
Na-jarosite[1]	97ºC	0.1 *M* $Fe_2(SO_4)_3$ + 0.3 *M* Na_2SO_4	Na^+:Fe^{3+} 3:1	$[Na_{0.8}(H_3O)_{0.2}]Fe_{2.8}(SO_4)_2(OH)_6$
Patino et al. (1998)				
Na-Ag-jarosite[2]		(Ag_2SO_4 + Na_2SO_4) + $Fe_2(SO_4)_3$		
	97ºC	0.6 *M* Na^+, 0.00048 *M* Ag^+, 0.4 *M* Fe^{3+}	Na^+:Ag^+:Fe^3 1.5:0.0012:1	$[Na_{0.675}Ag_{0.005}(H_3O)_{0.32}]Fe_3(SO_4)_2(OH)_6$
Basciano and Peterson (2008)				
Na-K-jarosite[3]		KCl + NaCl + $Fe_2(SO_4)_3.5H_2O$		
	140ºC	0.016 *M* K^+, 0.183 *M* Na^+, 0.3 *M* Fe^{3+}	(K^+:Na^+):Fe^{3+} 2:3	$[K_{0.11}Na_{0.85}(H_3O)_{0.04}]Fe_{2.96}(SO_4)_2(OH)_6$
	140ºC	0.144 *M* K^+, 0.02 *M* Na^+, 0.3 *M* Fe^{3+}	(K^+:Na^+):Fe^{3+} 1.64:3	$[K_{0.78}Na_{0.26}(H_3O)_{0.00}]Fe_{3.01}(SO_4)_2(OH)_6$
Dutrizac and Kaiman (1976)				
K-jarosite[4]	100ºC	0.1 *M* $Fe_2(SO_4)_3$ + 0.3 *M* KNO_3	K^+:Fe^{3+} 1:1.67	$[K_{0.86}(H_3O)_{0.14}]Fe_{2.49}(SO_4)_2(OH)_6$
Na-jarosite[4]	100ºC	0.1 *M* $Fe_2(SO_4)_3$ + 0.45 *M* Na_2SO_4	Na^+:Fe^{3+} 1:2.22	$[Na_{0.82}(H_3O)_{0.18}]Fe_{2.80}(SO_4)_2(OH)_6$
Ag-jarosite[4]	100ºC	0.1 *M* $Fe_2(SO_4)_3$ + 0.06 *M* Ag_2SO_4	Ag^+:Fe^{3+} 1:16.67	$[Ag_{0.91}(H_3O)_{0.09}]Fe_{2.78}(SO_4)_2(OH)_6$
Brown (1970)				
K-jarosite[5]	25ºC	K_2SO_4 + $FeSO_4.7H_2O$	K^+:Fe^{3+} 1:3	$[K_{0.97\text{-}1.00}(H_3O)_{0.03\text{-}0.00}]Fe_3(SO_4)_2(OH)_6$
		0.02 *M* K^+, 0.06 *M* Fe^{3+}, 0.095 *M* SO_4^{2-}		
		0.1 *M* K^+, 0.3 *M* Fe^{3+}, 0.491 *M* SO_4^{2-}		
		0.2 *M* K^+, 0.6 *M* Fe^{3+}, 0.95 *M* SO_4^{2-}		
Dutrizac and Jambor (1984)				
Ag-jarosite[6]		Ag_2SO_4 + $Fe_2(SO_4)_3$		
	60°C	0.1 *M* Ag^+, 0.3 *M* Fe^{3+}	Ag^+:Fe^{3+} 1:3	$[Ag_{0.84}(H_3O)_{0.16}]Fe_3(SO_4)_2(OH)_6$
	97ºC	0.1 *M* Ag^+, 0.3 *M* Fe^{3+}	Ag^+:Fe^{3+} 1:3	$[Ag_{0.86}(H_3O)_{0.14}]Fe_3(SO_4)_2(OH)_6$
	140ºC	0.1 *M* Ag^+, 0.3 *M* Fe^{3+}	Ag^+:Fe^{3+} 1:3	$[Ag_{0.91}(H_3O)_{0.09}]Fe_3(SO_4)_2(OH)_6$
	200°C	0.1 *M* Ag^+, 0.3 *M* Fe^{3+}	Ag^+:Fe^{3+} 1:3	$Ag_{1.00}Fe_3(SO_4)_2(OH)_6$
May et al. (1973)				
Ag-jarosite[7]	97ºC	0.063 *M* $Fe_2(SO_4)_3$ + 0.021 *M* Ag_2SO_4	Ag^+:Fe^{3+} 1:3	$[Ag_{0.903}(H_3O)_{0.097}]Fe_{2.97}(SO_4)_2(OH)_6$
Ag-jarosite[7]	97ºC	0.063 *M* $Fe_2(SO_4)_3$ + 0.021 *M* Ag_2SO_4	Ag^+:Fe^{3+} 1:3	$[Ag_{0.904}(H_3O)_{0.096}]Fe_3(SO_4)_2(OH)_6$
Dutrizac and Jambor (1983)				
Pb-jarosite[8]		$PbSO_4$ + $Fe_2(SO_4)_3$		
	97ºC	0.1 *M* Pb^{2+}, 0.3 *M* Fe^{3+}	Pb^{2+}:Fe^{3+} 1:3	$Pb_{0.242}(H_3O)_{0.516}Fe_{2.825}(SO_4)_2(OH)_{4.96}$
Dutrizac and Jambor (1984)				
Pb-Ag-jarosite[9]		(Ag_2SO_4 + $PbSO_4$) + $Fe_2(SO_4)_3$		
	97ºC	0.3 *M* Fe^{3+}, 0.1 *M* (0-0.1 Ag^+-Pb^{2+})	(Ag^++Pb^{2+}):Fe^{3+} 1:3	$[(H_3O)_xPb_{0.0}Ag_{0.775}]Fe_{2.6}(SO_4)_2(OH)_6$
	97ºC	0.3 *M* Fe^{3+}, 0.1 *M* (0-0.1 Pb^{2+}-Ag^+)	(Pb^{2+}+Ag^+):Fe^{3+} 1:3	$[(H_3O)_xPb_{0.26}Ag_{0.0}]Fe_{2.73}(SO_4)_2(OH)_6$
Dutrizac and Jambor (1987)				
Na-Ag-jarosite[10]		(Ag_2SO_4 + Na_2SO_4) + $Fe_2(SO_4)_3$		
	97ºC	0.06 *M* (Na^++Ag^+), 0.2 *M* Fe^{3+}	(Ag^++Na^+):Fe^{3+} 1:3.33	$[(Na,Ag)_{0.6\text{-}0.8}(H_3O)_{0.2\text{-}0.4}]Fe_{2.597\text{-}2.967}(SO_4)_2(OH)_6$
Forray et al. (2010)				
Pb-jarosite[11]		$Pb(NO_3)_2$ + $Fe_2(SO_4)_3.5H_2O$		
	95ºC	0.03 *M* Pb^{2+}, 0.108 *M* Fe^{3+}	Pb^{2+}:Fe^{3+} 1:3.6	$Pb_{0.13}(H_3O)_{0.74}Fe_{2.92}(SO_4)_2(OH)_{5.76}(H_2O)_{0.24}$
Grohol and Nocera (2007)				
K-jarosite[12]		K_2SO_4 + $Fe_2(SO_4)_3.5H_2O$		
	150ºC	0.13 *M* K^+, 0.652 *M* Fe^{3+}	K^+:Fe^{3+} 1:5	$[K_{0.73}(H_3O)_{0.27}]Fe_{2.93}(SO_4)_2(OH)_6$
Basciano and Peterson (2007a)				
K-jarosite[13]		K_2SO_4 + $Fe_2(SO_4)_3.5H_2O$		
	140ºC	0.023 *M* K^+, 0.163 *M* Fe^{3+}	K^+:Fe^{3+} 1:7.09	$[K_{0.857}(H_3O)_{0.143}]Fe_{2.96}(SO_4)_2(OH)_6$
Patino et al. (1994)				
Pb-Ag-jarosite[14]		$PbSO_4$ + Ag_2SO_4 + $Fe_2(SO_4)_3$		
	97ºC	0.6 *M* Fe^{3+}, 0.06 *M* Pb^{2+}, 0.00039 *M* Ag^+	Pb^{2+}:Ag^+:Fe^{3+} 0.1:0.00065:1	$[Pb_{0.32}Ag_{0.011}(H_3O)_{0.35}]Fe_3(SO_4)_2(OH)_6$
	97ºC	0.6 *M* Fe^{3+}, 0.06 *M* Pb^{2+}, 0.0002 *M* Ag^+	Pb^{2+}:Ag^+:Fe^{3+} 0.1:0.00033:1	$[Pb_{0.32}Ag_{0.0088}(H_3O)_{0.35}]Fe_3(SO_4)_2(OH)_6$
	97ºC	0.6 *M* Fe^{3+}, 0.06 *M* Pb^{2+}, 0.0001 *M* Ag^+	Pb^{2+}:Ag^+:Fe^{3+} 0.1:0.00017:1	$[Pb_{0.32}Ag_{0.0034}(H_3O)_{0.35}]Fe_3(SO_4)_2(OH)_6$
Basciano and Peterson (2008)				
Na-jarosite[15]		Na_2SO_4 + $Fe_2(SO_4)_3.5H_2O$		
	140ºC	0.014 *M* Na^+, 0.163 *M* Fe^{3+}	Na^+:Fe^{3+} 1:11.64	$[Na_{0.49}(H_3O)_{0.51}]Fe_{3.11}(SO_4)_2(OH)_6$

Key: 1 Dutrizac (1983), 2 Patino et al. (1998), 3 Basciano and Peterson (2008), 4 Dutrizac and Kaiman (1976), 5 Brown (1970), 6 Dutrizac and Jambor (1984), 7 May et al. (1973), 8 Dutrizac and Jambor (1983), 9 Dutrizac and Jambor (1984), 10 Dutrizac and Jambor (1987), 11 Forray et al. (2010), 12 Grohol and Nocera (2007), 13 Basciano and Peterson (2007a), 14 Patino et al. (1994), 15 Basciano and Peterson (2008).

Synthetic jarosites are often used as analogues for natural jarosites (Desborough et al., 2006). Therefore, one viewpoint holds that the methods used to create K-, Na-, Ag- and Pb-jarosites should simulate the geochemical conditions for the formation of natural jarosites by supergene or hydrothermal processes (Brown, 1970; Desborough et al., 2006; Swayze et al., 2008). Other experiments of jarosite synthesis have been carried out as research on jarosite processes used in the hydrometallurgical industry (Dutrizac and Jambor, 2000). Metallurgists are concerned with the effect of factors such as temperature, seeding and pH on the yield and composition of the jarosite product (Dutrizac, 1983).

Synthesis experiments to form jarosite minerals have been carried out at least since the 1930s (Fairchild, 1933). A variety of methods have been used in these jarosite syntheses, creating different amounts of product of various chemical compositions (see Table 2.2). Dutrizac and Jambor (2000) provide a summary of the literature on many of the synthesis parameters of jarosite formation, especially K- and Na-jarosite, and since that time there have been numerous other experiments. The following is a discussion of jarosite synthesis conditions.

2.3.1. Ferric iron media and concentrations

In synthesis experiments on jarosite, Brown (1970) used $FeSO_4.7H_2O$ in seven out of a total of eight syntheses and $Fe_2(SO_4)_3$ in the other, on the basis that Fe^{2+} or some ferrous complex is the dominant species of iron in natural aqueous solutions. Other studies have carried out biological syntheses of K-, Na- and Ag-jarosite by using bacteria such as *Thiobacillus ferrooxidans* to oxidize Fe(II) to Fe(III) (Sasaki et al., 1995; Sasaki and Konno, 2000). However, most studies have assumed the necessary presence of ferric iron for jarosite formation by using reactant $Fe_2(SO_4)_3$ or

$Fe_2(SO_4)_3.5H_2O$ to supply Fe(III) to synthesis experiments (Fairchild, 1933; Baron and Palmer, 1996). Examples of the molarities of $Fe_2(SO_4)_3$ or $Fe_2(SO_4)_3.nH_2O$ used are 0.351 *M* (Driscoll and Leinz, 2005), 0.2 *M* (Patino et al., 1998; Cruells et al., 2000), 0.1 *M* (Dutrizac and Kaiman, 1976; Dutrizac, 1983; Dutrizac and Jambor, 1987), 0.08 *M* (Frost et al., 2005), 0.078 *M* (Stoffregen, 1993), 0.063 *M* (May et al., 1973) and 0.0625 *M* (Stoffregen, 1993). An exception is $FeCl_3$ used, with $Fe_2(SO_4)_3.5H_2O$, by Basciano and Peterson (2007, 2008) to reduce the sulphate concentration in solution and thereby the amount of hydronium entering the jarosite structure.

The lower limit of Fe(III) concentration for jarosite precipitation is near 10^{-3} (0.001) *M* (Brown, 1971), while synthetic jarosites readily precipitate from sulphate-rich solutions containing 0.025-3.0 *M* Fe(III) (Brophy et al., 1962; Brophy and Sheridan, 1965; Brown, 1970). To synthesize K-, Na- and Ag-jarosite at 25ºC, Brown (1970) used the 1:3 molar ratio of $(K^+\text{-}Ag^+):Fe^{3+}$ or $(Na^+\text{-}Ag^+):Fe^{3+}$ in stoichiometric jarosite. This achieved K^+ occupancy of 97-100% in synthesised jarosite. In other studies 20% extra ferric sulphate was used (Fairchild, 1933; Brophy et al., 1962), raising the molar ratio to 1:3.6.

Experiments to synthesise K-, Na- and Ag-jarosites show ferric iron precipitation as jarosite increases with increasing alkali ions in solution until the $M^+:Fe^{3+}$ ratio is slightly above the stoichiometric ratio of 1:3 and thereafter is nearly independent of the amount of alkali (Dutrizac and Kaiman, 1976). Where excess alkali ions are used, the Fe composition of jarosite is independent of the Fe^{3+} concentration in the solution, even for relatively low Fe^{3+} concentrations, but the total amount of jarosite formed (yield) increases linearly with increasing Fe(III) (Dutrizac and Jambor, 2000).

As an illustration of this relationship, Dutrizac and Jambor (1984) reported that, in Ag-jarosite syntheses where there are excess 'alkali' (Ag^+) ions, initial Fe^{3+} concentration has a major influence on yield but little effect on composition. Ag-jarosite experiments using 250% excess Ag in solution resulted in products with fairly constant Ag and Fe contents (Fe ~ 28 wt % and Ag 18.4 wt %, compared with stoichiometric Fe 29.41 wt % and Ag 18.94 wt %) but with yields increasing linearly as the initial Fe concentration increases (as well as initial Ag proportionately).

However, most accurate analyses of synthetic jarosite show a slight deficiency of Fe relative to sulphate (Kubisz, 1970; Dutrizac and Kaiman, 1976). Because low Fe^{3+} concentration in the starting solution results in a deficiency of Fe^{3+} in the synthesised jarosite, and to achieve full Fe occupancy in the synthesis of H_3O-jarosite, Basciano and Peterson (2007a) used a high $Fe_2(SO_4)_3.nH_2O$ concentration of 0.82 *M*.

An equation for the precipitation of jarosites from homogeneous solutions containing alkali (A^+) ions is (Grohol and Nocera 2007):

$$3Fe^{3+} + 2A_2SO_4 + 6H_2O \rightarrow AFe_3(SO_4)_2(OH)_6 + 3A^+ + 6H^+$$

If alkali ions are insufficient or depleted then hydronium ions (H_3O^+) can substitute for alkali ions, resulting in a product with the general composition $A_x(H_3O)_{1-x}Fe_3(SO_4)_2(OH)_6$ ($0 < x < 1$). During this reaction, incomplete hydrolysis often results in substitution of H_2O for OH^-, leading to an excess positive charge. Every three such disorders can result in the displacement of one Fe^{3+} ion, leading to Fe deficiency and the general composition $K_x(H_3O)_{1-x}Fe_{3-y}(H_2O)_{3y}(OH)_{6-3y}(SO_4)_2$, where $y > 0$. The ratio of solubilised A^+/H_3O^+ ions in the reaction solutions will affect the amount of these ions in the jarosite product. Varying the H_3O^+ concentration is not practical, as jarosite precipitation is pH dependent: pH < 0.5 will

dissolve jarosite and pH > 2.5 will cause the precipitation of hematite (Fe_2O_3) impurity. So varying concentration of A^+ ions is better way of controlling A^+/H_3O^+ ratio, which can achieve reasonable spread of *x* values in $K_x(H_3O)_{1-x}Fe_{3-y}(H_2O)_{3y}(OH)_{6-3y}(SO_4)_2$.

2.3.2. Alkali or substitute cation media and concentrations

At least four different types of reactant have been used to supply K, Na, Ag and Pb in jarosite synthesis experiments:

- K_2SO_4, Na_2SO_4, Ag_2SO_4 and/or $PbSO_4$ (Brophy et al., 1962; Brown, 1970; May et al., 1973; Dutrizac and Kaiman, 1976; Dutrizac, 1983; Dutrizac and Jambor, 1984, 1987; Stoffregen, 1993; Patino et al., 1998; Cruells et al., 2000).
- KOH, NaOH and/or AgOH (Kubisz, 1970; Baron and Palmer, 1996; Driscoll and Leinz, 2005; Smith et al., 2006). Baron and Palmer (1996) used KOH rather than K_2SO_4 because they believed KOH would result in a higher K content in the jarosite precipitate. Kubisz (1970) recommended that alkali cations should be introduced as hydroxides to improve the sulphate-to-iron ratio in solution and so create purer alkali end-member jarosites with less hydronium content. This was because preparation of synthetic K-jarosite with K_2SO_4 and ferric sulphate creates a SO_3:Fe_2O_3 molar ratio of 3:1 as opposed to the stoichiometric ratio of 4:3.
- KNO_3, $NaNO_3$, $AgNO_3$ and/or $Pb(NO_3)_2$ (Dutrizac and Kaiman, 1976; Frost et al., 2005; Smith et al., 2006). In the synthesis of K-jarosite at 95ºC, Dutrizac and Kaiman (1976) used KNO_3 instead of K_2SO_4 on the basis that it results in a product richer in alkali, reducing the hydronium content. To synthesise Pb-jarosite at 95ºC, Smith et al. (2006) used $Pb(NO_3)_2$ in order to reduce the concentration of SO_4 in solution and hence hinder $PbSO_4$ precipitation.

● KCl and NaCl (Basciano and Peterson, 2007, 2008). KCl and NaCl were used by Basciano and Peterson (2007a, 2008) to reduce the sulphate concentration in solution in an effort to reduce the amount of hydronium entering the jarosite structure.

Jarosites can be precipitated from solutions with 0.05 *M* Na^+ (Dutrizac, 1999; Dutrizac and Jambor, 2000) or 0.02 *M* K^+ (Brown, 1970). However, very high alkali-sulphate concentrations (> 1.0 *M* Na_2SO_4) can result in the precipitation of alkali-Fe^{3+} sulphates instead of jarosites (Dutrizac and Jambor, 2000).

Slightly excess alkali concentrations (i.e. higher than stoichiometric) in the starting solution improve jarosite precipitate yield and alkali content (relative to hydronium content) (Dutrizac and Jambor, 2000). Use of a stoichiometric M^+:Fe^{3+} ratio does not give an optimum product: Fairchild (1933) claimed that an ideal M^+:Fe^{3+} stoichiometric ratio of 1:3 in the starting solution yields a product closest to end-member composition (Dutrizac and Jambor, 2000). A wide variety of alkali and substitute ion concentrations have been used in jarosite syntheses, some examples of which are given in Table 1.2.

2.3.3. Temperature of synthesis

Laboratory syntheses of jarosites have been carried out at temperatures ranging from 20ºC to 150ºC, to simulate natural and engineered (hydrometallurgical) environments, help to speed up the reaction and form purer compounds.

Brown (1970) states that it does not seem geologically reasonable for synthesis experiments simulating the surface occurrences of jarosites to use high temperatures and high initial concentrations of solutions, such as 105ºC and 0.505 *M* K^+, 1.948 *M* Fe^{3+} and 3.279 *M* SO_4^{2-} used by Brophy et al. (1962). Dutrizac and Jambor (2000) state that K-, Na- and NH_4-jarosites can all form at 25ºC but the formation rates are

very slow. Dutrizac and Jambor (1984) report that Ag-jarosite and K-jarosite precipitate slowly at 25°C. Brown (1970) synthesised K-jarosites at 25ºC (1 atm) over periods of four weeks to six months.

Studies show that the precipitation of synthetic jarosite becomes rapid at ~ 80ºC and is nearly complete in several hours at 100ºC (Brophy et al., 1962; Dutrizac and Kaiman, 1976). Higher temperatures significantly increase the amount of precipitate (yield) and slightly raise the alkali content (Dutrizac, 1983). Reaction rates increase rapidly above 100ºC, but there is an upper limit of jarosite formation at 180-200ºC, depending on solution composition. Commercially useful rates in hydrometallurgy generally require > 90ºC (Dutrizac and Jambor, 2000).

In synthesis experiments on Na-jarosite (Dutrizac, 1983; Dutrizac and Jambor, 2000), the amount of synthesised precipitate is strongly temperature-dependent but the composition of the jarosite is nearly temperature-independent (as shown by constant Na contents). At 97°C using glass reaction vessels, the synthesis of Na-jarosite (using 0.2 M Fe^{3+}, 0.15 M Na_2SO_4 and 5 g Na-jarosite seed) shows that reaction time sharply increases the percentage of iron precipitated as jarosite (and so the amount of product) up to a maximum at ~ 15 h and then it is constant. The percentage Fe precipitated is proportional to the amount of Na-jarosite formed (content ~ 33.5-34.2 wt % Fe in all jarosite precipitates; stoichiometric is 34.57 wt %), and the percentage Na content is nearly constant (3.5-3.8 wt %; stoichiometric is 4.74 wt %) (slight increase up to ~ 40 h) (Dutrizac, 1983; Dutrizac and Jambor, 2000). Over a reaction period of 24 h, the amount of Na-jarosite formed (shown by rising percentage of Fe precipitated while Na composition almost constant) increases sharply from 70°C to ~ 100°C, but then levels off at higher temperatures. At 140°C, a steady-state of Fe precipitated as Na-jarosite is reached within ~ 1 h (Dutrizac,

1983; Dutrizac and Jambor, 2000). The authors conclude that synthesis reactions are under thermodynamic control at > 100°C but are kinetically limited at lower temperatures.

At 100°C, H_3O-jarosite can precipitate (if no alkali is added) but the reaction is slow and incomplete except at higher temperatures (Dutrizac et al., 1980). H_3O-jarosite forms in autoclave at 130-160ºC (Dutrizac et al., 1980; Dutrizac and Jambor, 2000). However, the incorporation of H_3O in K-, Na- and Ag-jarosites is not favoured at high temperatures (≥ 110°C) (Dutrizac and Jambor, 1984).

Temperature has a significant effect on alkali jarosite and argentojarosite formation (Dutrizac and Jambor, 1984). In this study, Ag-jarosite was able to form at 60°C, but Na-jarosite did not. The yield of synthesised Ag-jarosite increased from 60°C to ≈ 110°C then levelled off to at least 230°C. At 90°C, the formation of argentojarosite (in syntheses series with alkali and plumbian jarosites) using Fe and Ag sulphates was virtually complete in 24 h. The Ag content increased steadily with increasing temperature, from ~ 16 wt. % at 60°C, ≈ 16.22 wt. % at 97°C, 17.2 wt. % at 140°C, until nearly ideal (stoichiometric 18.94 wt. %) at 200°C. At 230°C, Ag content was ~ 19 wt. %. These findings compare with the results of a study by May et al. (1973) in which two argentojarosites were synthesised at 97°C using Fe and Ag sulphates, but using HNO_3 or H_2SO_4 in the solutions, which yielded products with Ag content of 17.12 wt. % and 17.10 wt. % respectively.

2.3.4. Experimental techniques for heating of jarosite syntheses solutions

High-temperature syntheses of jarosites have been carried out using glass reaction vessels (commonly 2 litre) (Dutrizac, 1983), often with neck adaptors, one typically with a condenser attached to reduce solution loss through evaporation (Smith, 2004);

Ti autoclaves, which allow solutions to react at a variety of temperatures and pressures (Dutrizac, 1983; Smith, 2004), such as 130-160ºC (Dutrizac and Jambor, 2000); and stainless-steel pressure vessels ('bombs') with screw lids and Teflon linings, which also allow solutions to react at high temperatures and pressures, such as 140ºC and 3.58 atm (Basciano, 2008) and 150ºC (Grohol and Nocera, 2007).

Smith (2004) states that synthetic Pb-bearing jarosites can be made at varying temperatures by autoclave or by a slow-addition technique, to prevent the precipitation of $PbSO_4$. The slow-addition optimum temperature is similar to that of alkali jarosite formation in a reaction vessel, 97ºC (Dutrizac et al., 1980). For autoclave synthesis, optimum formation is at 130ºC (because small quantities of Fe_2O_3 form at 170ºC) (Dutrizac et al., 1980). Dutrizac and Jambor (1984) used 2 l glass reaction kettles to synthesise argentojarosite at 97°C and Ti autoclaves for higher temperatures (140°C and 150°C).

2.3.5. Acidity of synthesis solutions

The pH of the synthesis solution plays a major role in jarosite stability and the amount of precipitate, but has little effect on composition (Dutrizac, 1983; Dutrizac and Jambor, 2000). A key stage in jarosite formation is the hydrolysis of ferric iron sulphate, which releases protons (H^+) or sulphuric acid (H_2SO_4) into solution and increases acidity (Dutrizac, 1983; Dutrizac and Jambor, 2000). An equation for the hydrolysis of ferric iron to form jarosite, with each 1 mol Fe^{3+} precipitated producing 1 mol H_2SO_4, is (Dutrizac, 1983) (where M is a monovalent cation filling the A site):

$$0.5M_2SO_4 + 1.5Fe_2(SO_4)_3 + 6H_2O \rightarrow MFe_3(SO_4)_2(OH)_6 + 3H_2SO_4$$

An alternative reaction for jarosite formations is (Grohol and Nocera, 2007):

$$3Fe^{3+} + 2M_2SO_4 + 6H_2O \rightarrow MFe_3(SO_4)_2(OH)_6 + 3M^+ + 6H^+$$

Initial acid concentration, therefore, has a significant effect on Fe^{3+} precipitated and high acidity may retard synthetic jarosite precipitation (Brophy et al., 1962; Brown, 1970; Dutrizac, 1983; Dutrizac and Jambor, 2000). For this reason, initial pH of solution is critical to optimising jarosite formation and maximising yield (Smith, 2004). At 100ºC, the ideal starting pH value is 1.5-1.6 for jarosite formation, whereas other Fe compounds begin to form at pH values > 2 (Dutrizac and Jambor, 2000).

Dutrizac and Jambor (1984) state that pH values of 1.0-1.6 are near-optimum jarosite synthesis conditions. However, the amount of jarosite precipitated decreases sharply at pH < 1.5, because free acid in solution increasingly dominates acid released by hydrolysis, until free acid is too great for jarosite formation (including hydrolysis) (Dutrizac, 1983; Dutrizac and Jambor, 1984). At an initial pH of ≤ 0.5 no jarosite forms because equilibrium is displaced in favour of solution species (i.e., jarosite formation is not thermodynamically favourable), because free acid is too great. Jarosite formation is negligible at > 0.5 M H_2SO_4 (Dutrizac, 1983).

In synthesis experiments at 97°C, a constant amount of Na-jarosite precipitated using an initial solution pH of 1.5-2.0, whereas no Na-jarosite precipitated at pH < 0.5 (solution species in equilibrium) (Dutrizac, 1983; Dutrizac and Jambor, 2000). The amount of precipitate increased sharply between pH 0.5 and 1.5. The Na content of the jarosites was nearly constant at all pH values.

The acidity of initial solutions can be regulated using H_2SO_4 or $LiCO_3$ (Dutrizac, 1983; Dutrizac and Jambor, 1984). Dutrizac and Kaiman (1976) added 0.01 *M* H_2SO_4 to the initial solution to prevent ferric ion hydrolysis and precipitation of H_3O-jarosite in experiments using 0.1 *M* $Fe_2(SO_4)_3$. Lithium carbonate is used because Li does not form an end-member jarosite-type compound and because it

does not cause local precipitation of $Fe(OH)_3$ on addition (Dutrizac and Jambor, 1987; Dutrizac and Jambor, 2000), as the carbonate dissolves slowly enough to prevent local over-neutralisation with resulting Fe hydroxide precipitation (Dutrizac, 1983).

Higher temperatures are useful in combating high acidities (Dutrizac and Jambor, 2000). At 97°C, jarosite product yield falls steadily with increasing initial acid concentrations above 0.1 *M*. No jarosite is produced at 0.3 *M* H_2SO_4 (Dutrizac and Jambor, 1984). At 150°C, product yield is slightly greater at all acidities, but begins to decline after initial concentration of 0.4 *M* H_2SO_4. At 140°C, yield begins to decrease at ~ 0.3 *M* H_2SO_4. Increased temperature probably means increasing thermodynamic stability (i.e., over 24 h synthesis period, kinetic factors are not dominant at these temperatures).

2.3.6. Problems of Ag-jarosite synthesis

Problems can arise in the synthesis of Ag-jarosite because Ag_2SO_4 has low solubility and may precipitate when the sulphate concentration in solution is sufficiently high, contaminating the jarosite product. The solubility of Ag_2SO_4 is reported as ~ 0.03 *M* in water (0-240°C) (Dutrizac et al., 1975), or 0.02566 *M* (0.8 g/100 ml H_2O at 20ºC) (Dean, 1979). However, Dutrizac and Jambor (1984) state that Ag_2SO_4 has moderately high solubility in hot sulphate media.

2.3.7. Problems of Pb-jarosite synthesis

Anglesite ($PbSO_4$) has very low solubility of 0.00013 *M* (4.0 mg/100 ml H_2O at 20ºC) (Dean, 1979). During the synthesis of Pb-jarosite, this may cause a $PbSO_4$ impurity to precipitate. This problem is much less using a slow-addition technique

rather than an autoclave (Smith, 2004), and Pb-jarosite has been successfully synthesised at 95°C by a slow-addition method using 2 l glass reaction vessels with spiral condensers (Smith et al., 2006). However, autoclave synthesis commonly creates jarosite products with higher Pb content and greater crystallinity (Smith, 2004).

A method of removing $PbSO_4$ from Pb-jarosite is to leach the contaminant using 10% ammonium acetate (CH_3COONH_4) at room temperature. Dutrizac et al. (1980) used ammonium acetate to leach Pb sulphate from Pb-bearing jarosites and concluded that acetate did not decompose Pb-jarosite at 25ºC or 35ºC. At 50ºC, slight decomposition of Pb jarosite occurred, and at 70ºC to 90ºC this became significant. The authors conclude that ammonium acetate leaching must be done at low temperature to prevent Pb jarosite decomposition (Smith, 2004).

Dutrizac and Jambor (1983) successfully used this technique to selectively leach excess $PbSO_4$ from a Pb-jarosite precipitate by washing with four 1 l solutions of 10% ammonium acetate at 25°C. The Pb-jarosite was synthesised from a 1 l solution containing 0.3 *M* Fe^{3+} and 0.1 *M* $PbSO_4$. Dutrizac and Jambor (1984) were successful with the same leaching technique on Pb-jarosite and Ag-bearing Pb-jarosites synthesised from 1 l solutions each containing 0.3 *M* Fe^{3+} and 0.1 *M* $PbSO_4$ and/or Ag_2SO_4.

2.3.8. Solid solution

There is extensive solid solution involving K^+, Na^+ and H_3O^+ in jarosite family minerals (Brophy et al., 1962; Parker, 1962; Brophy and Sheridan, 1965; Kubisz, 1960, 1970; Stoffregen and Cygan, 1990; Li et al., 1992; Jambor, 1999). For example, hydronium jarosite forms a complete solid-solution series with alkali

jarosites, and there is a complete solid solution among K, Na and NH_4 jarosites (Brophy and Sheridan, 1965). Substitution involving K^+ and Pb^{2+} has been shown by de Oliveira et al. (1996) and Roca et al. (1999) to be extensive in jarosite. The incorporation of NH_4 in ammoniojarosite (Odum er al. 1982) seems to be mainly at the expense of K^+ and $(H_3O)^+$. Apparent deficiencies in K + Na + NH_4 *A*-site occupancy are generally attributed to $(H_3O)^+$.

Jambor (1999) states that natural argentojarosite is generally near the end-member composition, although in synthetic systems the solid solution between Ag-Pb (± H_3O) and Ag-K (± H_3O) has been shown to be complete (Ildefonse el al. 1986, Dutrizac and Jambor, 1984). Synthetic Ag-jarosite forms unbroken solid-solution series with K-jarosite in the presence of hydronium (Dutrizac and Jambor, 1984, 2000), and solid solutions are likely complete among most or all synthetic jarosite species (Dutrizac and Jambor, 2000).

Lead jarosite forms a solid-solution series with monovalent jarosites, but the series are not crystallographically perfect because order-disorder often results in superstructure effects in Pb-rich members, with a *c* axis of 34 Å (double axis length of monovalent jarosites) in Pb-jarosite (Dutrizac and Jambor, 1984, 1987a). Extensive solid solution between Ag-rich and Pb-rich jarosites has been shown by X-ray methods, but end-member compositions have not been achieved in syntheses because of partial replacement of non-ferrous metals by hydronium ion (Dutrizac and Jambor, 1984). The solid solution series Pb-Ag-H_3O is disrupted by a region in which two jarosite phases (near end-member Pb-rich and Ag-rich phases) are present (Dutrizac and Jambor, 1984).

2.3.9. Jarosite formation and order of stability

Jarosite stability is based on the extent of Fe formation (Dutrizac and Jambor, 2000). Iron precipitates as synthetic jarosite in the order K-jarosite > NH_4-jarosite > Na-jarosite (NH_4 only slightly > Na). Potassium precipitates in jarosite in preference to NH_4 and Na; for example, an Na-K or NH_4-K solution with 10 mol % K gives rise to jarosite solid-solution series with 80 mol % K. Ag jarosite is almost as stable as K jarosite in synthetic systems (Dutrizac 1983, 1991; Dutrizac and Jambor 1984). Ag-jarosite has notable thermal stability, greater than for K-, Na- and Pb-jarosites, which helps explain the significant and persistent Ag incorporation in hydrometallurgical jarosite processes (Dutrizac and Jambor 1984). Pb-jarosite has similar stability to Na-jarosite (Dutrizac and Jambor, 2000). Thallium-jarosite is only slightly less stable than K-jarosite and Rb-jarosite is somewhat less stable. Mercury-jarosite, which is difficult to synthesise, appears the least stable jarosite (Dutrizac and Jambor, 2000).

Standard free energies of formation data (see Table 2.3) show that jarosite is the preferred species:

$NaFe_3(SO_4)_2(OH)_6 + K^+ \rightarrow KFe_3(SO_4)_2(OH)_6 + Na^+$ $\Delta G°_{reaction}$ = -5.3 kcal/mole

The data also show the low stability of hydronium jarosite at low temperature [25°C/298K]:

$H_3OFe_3(SO_4)_2(OH)_6 + Na^+ \rightarrow NaFe_3(SO_4)_2(OH)_6 + H_3O^+$ $\Delta G°_{reaction}$ = -56.7 kcal/mole

However, the use of thermodynamics to predict behaviour in such systems is complicated by high and variable ionic strength and by extensive formation of solid solution compounds (Dutrizac and Jambor, 2000).

Table 2.3. Standard free energies of formation of selected jarosite minerals (after Dutrizac and Jambor, 2000) (Dutrizac, 1980, reported in Arslan and Arslan, 2003).

Jarosite subgroup mineral	Formula	$\Delta G°_{298}$ (kcal/mole)	M^+	$\Delta G°_{298}$ (kcal/mole)
Jarosite	$KFe_3(SO_4)_2(OH)_6$	-788.6	K^+	-67.5
Natrojarosite	$NaFe_3(SO_4)_2(OH)_6$	-778.4	Na^+	-62.6
Hydroniumjarosite	$H_3OFe_3(SO_4)_2(OH)_6$	-772.5	H_3O^+	0.0
Ammoniojarosite	$NH_4Fe_3(SO_4)_2(OH)_6$	-736.2	NH_4^+	-19.0
Argentojarosite	$AgFe_3(SO_4)_2(OH)_6$	-701.3	Ag^+	+18.4
Plumbojarosite	$Pb_{0.5}Fe_3(SO_4)_2(OH)_6$	-722.5	$0.5Pb^+$	-2.9

There is an induction period before appreciable jarosite forms when ferric sulphate-alkali sulphate solutions are heated rapidly to 90-100°C. Studies show this induction period is ~ 1 h (Dutrizac and Jambor, 2000). Once jarosite precipitation starts, the reaction is complete after 4-6 h at 95°C and after < 1 h at 140°C. The activation energy for jarosite precipitation is fairly high (as indicated by the induction period).

2.3.10. Drying temperature

Desborough et al. (2006, 2010) and Swayze et al. (2008) state that there are two types of naturally occurring low-temperature jarosites: 'young' (or 'modern') and 'mature'.

Young natural low-temperature K- and Na-jarosites contain (based on measurement of unit cell dimensions by XRD) H_3O in the alkali site and have alkali- or Fe-site vacancies. Young natural low-temperature K- and Na-jarosites are metastable and H_3O and alkali- and/or Fe-site vacancies disappear naturally over time through desiccation and recrystallization. Mature natural low-temperature K- and Na-jarosites lack alkali- or Fe-site vacancies, lack H_3O and consist of K- and Na-jarosite

end-members. Mature natural low-temperature jarosites resemble hydrothermal jarosites, rather than low-temperature (< 100°C) synthetic jarosites. The instability of H_3O-jarosite over geological timescales is indicated by the detection of hydronium only in young samples (Desborough et al., 2006 and 2010).

Heating of non-stoichiometric or hydronium-bearing jarosite products after synthesis is a common practice in experiments. Heating to > 110°C ("drying") after synthesis drives off structural water, creating a crystal structure similar to hydrothermal jarosite. The structural nature of the jarosite products is changed by driving off water molecules in vacant alkali and/or protonated hydroxyl sites, altering the cell dimensions, chemical composition and stability (or solubility) (Desborough et al., 2006 and 2010). Swayze et al. (2008) recommend that heating of jarosite to remove 'excess' water (not part of lattice structure) after synthesis should be carried out to ≤ 60ºC if the products are to be analogues for young natural low-temperature jarosites in mine waste. Driscoll and Leinz (2005) also dried the synthesized product at 60ºC. However, Desborough et al. (2006) state that drying should be at ≤ 95ºC, with the same aim.

2.3.11. Jarosite synthesis procedures used in this project

From the above discussion, in this project non-microbial syntheses of K-, Na-, Ag- and Pb-jarosites were carried out at three temperatures: surface temperature 22ºC (Brown, 1970); 'low' temperature 97ºC (Baron and Palmer, 1996, 2002; Drouet and Navrotsky, 2003; Dutrizac and Kaiman, 1976; Frost et al., 2005; Smith et al., 2006; Stoffregen, 1993); and high temperature 140ºC (Basciano and Peterson, 2007; Dutrizac and Kaiman, 1976). In order to investigate the effect of different drying

temperatures, for this project separate aliquots of synthesised K-Ag and Na-Ag jarosite products were dried at 60°C and 110°C.

2.4 Summary

- Jarosites associated with the supergene enrichment zones of orebodies are one of the main mineral sources of Ag;
- jarosite family minerals have the chemical formula $A Fe_3(SO_4)_2(OH)_6$ and there is extensive element substitution;
- jarosite precipitation is used in hydrometallurgy, especially the zinc industry, to control Fe, sulphate, alkalis and other impurities;
- significant losses of Ag can occur in the precipitation of jarosites in hydrometallurgical circuits;
- silver chemistry in soils and natural aqueous environments is largely limited to colloidal Ag and Ag^+ with its minerals and complexes;
- Ag-jarosite forms solid-solution series with both K-jarosite and Na-jarosite in the presence of hydronium in syntheses at hydrothermal temperatures, but it is not known if this is also the case with syntheses at temperatures consistent with the surface environment;
- extensive solid solution between Ag-rich and Pb-rich jarosites has been reported, but end-member compositions have not been achieved. The solid solution series Pb-Ag-H_3O is disrupted by a region comprising a near end-member Pb-rich phase and an Ag-rich phase.

3 EXPERIMENTAL METHODS AND MATERIALS

A variety of analytical techniques will be used in this project in an effort to provide data on Ag incorporated into the jarosite structure in competition with K, Na and Pb (see Appendix B). This will include X-ray diffraction and Rietveld refinement analysis, providing data on the crystal structure and information on how Ag incorporated in the *A* site of jarosite under different synthesis conditions changes the unit-cell *c* parameters. Rietveld refinement will also be able to provide information on the bond lengths and angles, and the atomic positions in the structure. In addition, Raman spectroscopy will enable comparison of the *c*-axis parameters of the different series of jarosite compounds with the wavenumbers of the assigned modes and so the bonding environment, indicating changing bond strength.

3.1 Collection of natural jarosite samples

Natural samples of jarosite, natrojarosite and argentojarosite were obtained from the Smithsonian Institution in Washington, D.C., United States, from mineral retailers via the Internet, and from the mineral collection of University College London/Birkbeck. A total of 48 samples were collected. The provenance of the ten jarosite mineral samples obtained from the Smithsonian Institution was Boolcoomatta, South Australia; Chuquicamata, Chile; Dividend, Utah, and Kingman, Arizona, U.S.; and Laurion, Attike, Greece. The known provenance of the other samples was Almeria, Spain; Arabia District, Esmeralda County, Iron Point District, Nyeco and Pershing County, Nevada, U.S.; Kapunda, South Australia; Laurion, Greece; Londonderry, Western Australia; Sierra Jarosa, Spain; Tintic District and Toole County, Utah, U.S.

3.2 Synthesis of K-, Na-, Pb-, Ag-, K-Ag-, Na-Ag- and Pb-Ag-jarosite compounds

The synthesis of jarosite compounds is discussed in Chapter 2.3, including various methods used in previous studies. For this project, synthetic samples were prepared in the Wolfson Laboratory at the Department of Earth and Planetary Sciences, Birkbeck College, University of London. Potassium-, Na-, Pb- and Ag-jarosites were synthesised in several series of experiments at 20ºC, 97ºC or 140ºC using different methods, detailed below. The chemicals used were AnalaR, Normapur or Alfa Aesar reagent grade or Premion.

3.2.1 Syntheses using K_2SO_4, Na_2SO_4 and Ag_2SO_4 at 22ºC [0.51 *M* $Fe_2(SO_4)_3.5H_2O$]

A total of nine syntheses were carried out at room temperature (22ºC) to make K-, Na- and Ag-jarosite and three intermediate products each of K-Ag and Na-Ag jarosites. For each synthesis, 0.51 *M* $Fe_2(SO_4)_3.5H_2O$ (25 g) was dissolved in a 100 ml solution of 18 MΩ cm^{-1} ultra-pure water, containing 0.01 *M* H_2SO_4 (0.1 ml), in a 250 ml polypropylene beaker. To each solution was added a total of 0.11 *M* Ag_2SO_4 and/or K_2SO_4 or Na_2SO_4 in varying amounts (see Table 3.1). (All chemicals were AnalaR Normapur.) The reagents were mixed into each solution by stirring for 15 min. The initial pH value of each solution was adjusted to 1.5-1.6 by the addition of H_2SO_4 or $LiCO_3$. Each solution was then poured into a 250 ml polypropylene bottle, which was covered but to which air was allowed to enter. The reaction time of each experiment was nine months. During this time the pH of each solution was monitored periodically and adjusted, where necessary, by the addition of H_2SO_4 or

$LiCO_3$ to ensure the value was between 1.0 and 1.6. Before adjustment, pH values reached a maximum of 1.9. Each synthesised product was filtered through Whatman #2 ashless filter paper, washed well with ultra-pure water to remove any residual acid, air-dried and stored in a desiccator.

Table 3.1 Syntheses using K_2SO_4, Na_2SO_4 and Ag_2SO_4 (0.51 *M* $Fe_2(SO_4)_3.5H_2O$)

Molar amount	Weight (g)	Molar amount	Weight (g)
0.11 *M* K_2SO_4	2.0	0.00 *M* Ag_2SO_4	0.0
0.0825 *M* K_2SO_4	1.5	0.0275 *M* Ag_2SO_4	0.9
0.055 *M* K_2SO_4	1.0	0.055 *M* Ag_2SO_4	1.8
0.0275 *M* K_2SO_4	0.5	0.0825 *M* Ag_2SO_4	2.7
0.00 *M* $(K,Na)_2SO_4$	0.0	0.11 *M* Ag_2SO_4	3.6
0.11 *M* Na_2SO_4	1.6	0.00 *M* Ag_2SO_4	0.0
0.0825 *M* Na_2SO_4	1.2	0.0275 *M* Ag_2SO_4	0.9
0.055 *M* Na_2SO_4	0.8	0.055 *M* Ag_2SO_4	1.8
0.0275 *M* Na_2SO_4	0.4	0.0825 *M* Ag_2SO_4	2.7

3.2.2 Syntheses using K_2SO_4, Na_2SO_4 and Ag_2SO_4 at 22ºC [0.075 *M* $Fe_2(SO_4)_3.5H_2O$]

A total of 13 syntheses were carried out at room temperature (22ºC) to make K-, Na- and Ag-jarosite and five intermediate products each of K-Ag and Na-Ag jarosites. For each synthesis, 0.075 *M* $Fe_2(SO_4)_3.5H_2O$ (7.35 g) (AnalaR Normapur) or $Fe_2(SO_4)_3.8H_2O$ (8.16 g) (Alfa Aesar, reagent grade) was dissolved in a 200 ml solution of 18 MΩ ultra-pure water with 0.01 *M* H_2SO_4 (0.2 ml) in a 250 ml

polypropylene beaker. To each solution was added a total of 0.03 *M* Ag_2SO_4 (Alfa Aesar, reagent grade) and/or K_2SO_4 or Na_2SO_4 (AnalaR Normapur) in varying amounts (see Table 3.2). The procedure was then the same as for the K-, Na- and Ag-jarosites synthesised at 22ºC using 0.51 *M* $Fe_2(SO_4)_3.5H_2O$ (see above) in 100 ml solutions, except the reaction time was 16 months.

Table 3.2 Syntheses using K_2SO_4, Na_2SO_4 and Ag_2SO_4 (0.075 *M* $Fe_2(SO_4)_3.5H_2O$)

Molar amount	Weight (g)	Molar amount	Weight (g)
0.03 *M* K_2SO_4	1.05	0.00 *M* Ag_2SO_4	0.00
0.025 *M* K_2SO_4	0.87	0.005 *M* Ag_2SO_4	0.31
0.02 *M* K_2SO_4	0.70	0.01 *M* Ag_2SO_4	0.62
0.015 *M* K_2SO_4	0.52	0.015 *M* Ag_2SO_4	0.94
0.01 *M* K_2SO_4	0.35	0.02 *M* Ag_2SO_4	1.25
0.005 *M* K_2SO_4	0.17	0.025 *M* Ag_2SO_4	1.56
0.00 *M* $(K,Na)_2SO_4$	0.00	0.03 *M* Ag_2SO_4	1.88
0.03 *M* Na_2SO_4	0.85	0.00 *M* Ag_2SO_4	0.00
0.025 *M* Na_2SO_4	0.71	0.005 *M* Ag_2SO_4	0.31
0.02 *M* Na_2SO_4	0.57	0.01 *M* Ag_2SO_4	0.62
0.015 *M* Na_2SO_4	0.43	0.015 *M* Ag_2SO_4	0.94
0.01 *M* Na_2SO_4	0.28	0.02 *M* Ag_2SO_4	1.25
0.005 *M* Na_2SO_4	0.14	0.025 *M* Ag_2SO_4	1.56

3.2.3 Syntheses using K_2SO_4, Na_2SO_4 and Ag_2SO_4 at 97ºC, dried at 60ºC

A total of nine syntheses were carried out at 97ºC to make K-, Na- and Ag-jarosite and three intermediate products each of K-Ag and Na-Ag jarosites. The solution preparation procedure and reagent quantities (see Table 3.1) used were the same as those used in the syntheses above at 22ºC [0.51 *M* $Fe_2(SO_4)_3.5H_2O$]. The initial pH values of the solutions were between 1.6 and 1.8. Each solution was then poured into 6 x 20 ml Teflon-lined stainless-steel vessels. The vessels were placed in an oven preheated to 97°C and heated for 4 h. The vessels were removed from the oven and cooled at room temperature for 30 min. The vessels were opened and the liquid poured through Whatman #2 ashless filter paper. The precipitate was rinsed on the filter paper with ultra-pure water to remove any residual acid. The solid was scraped from the bottom and sides of the Teflon linings and washed on to another Whatman #2 ashless filter paper and then rinsed thoroughly with ultra-pure water. The filter papers were placed on watch glasses and dried by heating at 60ºC for 1 h in an oven. The precipitates on the filter papers were scraped into separate glass containers and stored in a desiccator.

3.2.4 Syntheses using K_2SO_4, Na_2SO_4 and Ag_2SO_4 at 97ºC, dried at 110ºC

A total of nine syntheses were carried out at 97ºC to make K-, Na- and Ag-jarosite and three intermediate products each of K-Ag and Na-Ag jarosites. The same solution preparation procedure and reagent quantities (see Table 3.1) were used as those for the syntheses above at 97ºC, except that the precipitates on the filter papers were dried by heating at 110ºC for 1 h. The initial pH value of each solution was 1.6.

3.2.5 Syntheses using K_2SO_4, Na_2SO_4 and Ag_2SO_4 at 140ºC

A total of 13 syntheses were carried out at 140ºC to make K-, Na- and Ag-jarosite and five intermediate products each of K-Ag and Na-Ag jarosites. The experimental procedure was the same as that used in the synthesis above heated at 97ºC for 4 h with a drying temperature of 110ºC, except that the reagent quantities were different. For each synthesis, 0.15 *M* $Fe_2(SO_4)_3.5H_2O$ (7.35 g) was used, which was mixed with 0.06 *M* Ag_2SO_4 and/or K_2SO_4 or Na_2SO_4 in varying amounts (see Table 3.3). The initial pH values of the solutions were between 1.26 and 1.44.

Table 3.3 Syntheses using K_2SO_4, Na_2SO_4 and Ag_2SO_4 (0.15 *M* $Fe_2(SO_4)_3.5H_2O$)

Molar amount	Weight (g)	Molar amount	Weight (g)
0.06 *M* K_2SO_4	1.05	0.00 *M* Ag_2SO_4	0.00
0.05 *M* K_2SO_4	0.87	0.01 *M* Ag_2SO_4	0.31
0.04 *M* K_2SO_4	0.70	0.02 *M* Ag_2SO_4	0.62
0.03 *M* K_2SO_4	0.52	0.03 *M* Ag_2SO_4	0.94
0.02 *M* K_2SO_4	0.35	0.04 *M* Ag_2SO_4	1.25
0.01 *M* K_2SO_4	0.17	0.05 *M* Ag_2SO_4	1.56
0.00 *M* $(K, Na)_2SO_4$	0.00	0.06 *M* Ag_2SO_4	1.88
0.06 *M* Na_2SO_4	0.85	0.00 *M* Ag_2SO_4	0.00
0.05 *M* Na_2SO_4	0.71	0.01 *M* Ag_2SO_4	0.31
0.04 *M* Na_2SO_4	0.57	0.02 *M* Ag_2SO_4	0.62
0.03 *M* Na_2SO_4	0.43	0.03 *M* Ag_2SO_4	0.94
0.02 *M* Na_2SO_4	0.28	0.04 *M* Ag_2SO_4	1.25
0.01 *M* Na_2SO_4	0.14	0.05 *M* Ag_2SO_4	1.56

3.2.6 Syntheses using $PbSO_4$ and Ag_2SO_4 at 140ºC

A total of six syntheses were carried out at 140ºC to make Pb-jarosite and five Pb-Ag jarosites. The same solution preparation and heating procedures were used as in the syntheses above at 140ºC for 4 h with a drying temperature of 110ºC, using 0.15 *M* $Fe_2(SO_4)_3.5H_2O$ (7.35 g) mixed with 0.06 *M* $PbSO_4$ or $PbSO_4$ and Ag_2SO_4 (Alfa Aesar, Premion grade) in varying amounts (see Table 3.4). The initial pH values of the solutions were between 1.39 and 1.57. Each precipitate was scraped on to filter paper and rinsed with 400 ml of 10% ammonium acetate (40 g) (BDH, Prolabo grade) to leach excess $PbSO_4$. The precipitate was then rinsed on the filter paper with ultra-pure water before drying at 110ºC for 1 h.

Table 3.4 Syntheses using $PbSO_4$ and Ag_2SO_4 (0.15 *M* $Fe_2(SO_4)_3.5H_2O$)

Molar amount	Weight (g)	Molar amount	Weight (g)
0.06 *M* $PbSO_4$	1.82	0.00 *M* Ag_2SO_4	0.00
0.05 *M* $PbSO_4$	1.52	0.01 *M* Ag_2SO_4	0.31
0.04 *M* $PbSO_4$	1.21	0.02 *M* Ag_2SO_4	0.62
0.03 *M* $PbSO_4$	0.91	0.03 *M* Ag_2SO_4	0.94
0.02 *M* $PbSO_4$	0.61	0.04 *M* Ag_2SO_4	1.25
0.01 *M* $PbSO_4$	0.30	0.05 *M* Ag_2SO_4	1.56

3.2.7 Syntheses using $PbSO_4$ and Ag_2SO_4 at 22ºC

A total of six syntheses were carried out at room temperature (22ºC) to make Pb-jarosite and five Pb-Ag jarosites. For each synthesis, 0.075 *M* $Fe_2(SO_4)_3.5H_2O$ (7.35 g) (AnalaR, Normapur grade) or $Fe_2(SO_4)_3.8H_2O$ (8.16 g) (Alfa Aesar, reagent

grade) was dissolved in a 200 ml solution of 18 MΩ ultra-pure water with 0.02 *M* H_2SO_4 (0.2 ml) in a 250 ml polypropylene beaker. To each solution was added between 0.00013 *M* and 0.005 *M* $PbSO_4$ plus 0.025 *M* Ag_2SO_4 (Alfa Aesar, Premion grade); 0.001 *M* $PbSO_4$ (added in amounts of 0.0001 *M* every two to three weeks a total of ten times) plus 0.025 *M* Ag_2SO_4; and 0.001 *M* $PbSO_4$ (added in amounts of 0.0001 *M* every two to three weeks a total of ten times) (see Table 3.5). These concentrations were chosen on the basis of the solubilities of $PbSO_4$ and Ag_2SO_4 of 0.00013 *M* and 0.02566 *M* respectively in H_2O at 20ºC (Dean, 1979). The procedure was then the same as for the K-Ag and Na-Ag jarosites synthesised at 22ºC using 0.075 *M* $Fe_2(SO_4)_3.5H_2O$ (see above), except that the solid on the filter paper was rinsed with 400 ml 10% ammonium acetate (40 g) (BDH, Prolabo grade) to leach excess $PbSO_4$ and then rinsed again with ultra-pure water to remove any residual acid. The precipitate was then air-dried and stored in a desiccator.

Table 3.5 Syntheses using $PbSO_4$ and Ag_2SO_4 [0.075 *M* $Fe_2(SO_4)_3.5H_2O$]

Molar amount	Weight (g)	Molar amount	Weight (g)
0.00013 *M* $PbSO_4$	0.008	0.025 *M* Ag_2SO_4	1.56
0.00032 *M* $PbSO_4$	0.02	0.025 *M* Ag_2SO_4	1.56
0.001 *M* $PbSO_4$	0.06	0.025 *M* Ag_2SO_4	1.56
0.005 *M* $PbSO_4$	0.30	0.025 *M* Ag_2SO_4	1.56
0.0001 x 10^1 *M* $PbSO_4$	0.06	0.025 *M* Ag_2SO_4	1.56
0.0001 x 10^1*M* $PbSO_4$	0.06	0.0 *M* Ag_2SO_4	0.00

1 $PbSO_4$ was added in amounts of 0.006 g (0.0001 *M*) ten times (two or three weeks apart) over five months.

3.2.8 Annealing of synthesised K-, Na-, Ag-, K-Ag and Na-Ag-jarosites at 140ºC

Annealing was carried out on K-Ag and Na-Ag jarosite series samples synthesised at 97ºC (both dried at 60ºC and dried at 110ºC), which had been formed in solutions containing 0.51 M $Fe_2(SO_4)_3.5H_2O$. Each original synthesis solution had been retained and was poured into a 250 ml polypropylene beaker and the pH was adjusted, where necessary, with Li_2CO_3 powder to ensure the value was 1.0-1.6. Each solution was poured into 6 x 20 ml Teflon-lined stainless-steel vessels. An aliquot of the relevant jarosite sample was added as seed to each solution (see Tables 3.6 and 3.7). The vessels were placed in an oven preheated to 140ºC and heated for 3 h. The vessels were removed from the oven and cooled at room temperature for 30 min. The vessels were opened and the liquid poured through Whatman #2 ashless filter paper. The solid was scraped from the Teflon linings and washed on to the filter paper. The precipitate was rinsed on the filter paper with ≥ 500 ml ultra-pure

Table 3.6 Annealing of synthesised 1.02 M Fe^{3+} samples originally dried at 60ºC

Molar amounts in original solutions		Sample added (g)
0.11 *M* K_2SO_4	0.00 *M* Ag_2SO_4	2.0[1]
0.0825 *M* K_2SO_4	0.0275 *M* Ag_2SO_4	2.6[1]
0.055 *M* K_2SO_4	0.055 *M* Ag_2SO_4	4.3[1]
0.0275 *M* K_2SO_4	0.0825 *M* Ag_2SO_4	2.0[1]
0.00 *M* $(K, Na)_2SO_4$	0.11 *M* Ag_2SO_4	2.3[1]
0.11 *M* Na_2SO_4	0.00 *M* Ag_2SO_4	0.65
0.0825 *M* Na_2SO_4	0.0275 *M* Ag_2SO_4	2.9

0.055 *M* Na_2SO_4	0.055 *M* Ag_2SO_4	1.5[1]
0.0275 *M* Na_2SO_4	0.0825 *M* Ag_2SO_4	2.7

1 XRD analysis revealed unidentified, non-jarosite peak(s) in precipitate, so sample was rinsed in ultra-pure water and ammonium acetate, filtered and dried at 110°C.

Table 3.7 Annealing of synthesised 1.02 M Fe^{3+} samples originally dried at 110ºC

Molar amounts in original solutions		Sample added (g)
0.11 *M* K_2SO_4	0.00 *M* Ag_2SO_4	1.5
0.0825 *M* K_2SO_4	0.0275 *M* Ag_2SO_4	1.25
0.055 *M* K_2SO_4	0.055 *M* Ag_2SO_4	0.2
0.0275 *M* K_2SO_4	0.0825 *M* Ag_2SO_4	0.2
0.00 *M* $(K, Na)_2SO_4$	0.11 *M* Ag_2SO_4	0.25[1]
0.11 *M* Na_2SO_4	0.00 *M* Ag_2SO_4	0.25
0.0825 *M* Na_2SO_4	0.0275 *M* Ag_2SO_4	0.65
0.055 *M* Na_2SO_4	0.055 *M* Ag_2SO_4	0.1
0.0275 *M* Na_2SO_4	0.0825 *M* Ag_2SO_4	0.25

1 XRD analysis revealed unidentified, non-jarosite peak(s) in precipitate, so sample was rinsed in ultra-pure water and ammonium acetate, filtered and dried at 110°C.

water to remove any residual acid. The filter papers were placed on watch glasses and dried by heating at 110ºC for 1 h in an oven. The precipitates on the filter papers were scraped into separate glass containers and stored in a desiccator. For some samples (see Tables 3.6 and 3.7), XRD analysis revealed one or more non-jarosite peaks in the spectra. These samples were rinsed in ultra-pure water and ammonium acetate to remove any residue sulphates.

3.3 Characterisation of natural and synthetic jarosites

3.3.1 Determination of mineral colour

Colour analysis and Munsell colour charts (Munsell, 2000) have been used in studies as a method to characterise jarosite mineral samples (Smith, 2004; Frost et al., 2005; Jamieson et al., 2005; Smith et al., 2006a). For this project, a colour analysis of each synthesised jarosite sample was carried out using Munsell charts. The charts enable the colours of the samples to be characterised according to hue, value (lightness) and chroma (colourfulness). There are 10 hues in the Munsell charts: five main hues (red, purple, blue, green and yellow) and five intermediate hues (for example, YR is yellow-red), and each hue has 10 subdivisions. Value refers to lightness on a scale of 0–10, with 0 being dark and 10 being light. Chroma is degree of colourfulness, such as pastel, on a scale of 0–12, with 12 being maximum colourfulness.

3.3.2 Scanning electron microscopy

Scanning electron microscopy (SEM) has been used in previous studies of jarosite minerals to determine the crystal morphology and to provide semi-quantitative analyses of the chemical composition (Roca et al., 1993; Baron and Palmer, 1996; Sanchez et al., 1996; Sasaki and Konno, 2000; Smith et al., 2006a). For this project, SEM was used to determine the crystal morphology of synthetic jarosite samples with secondary electron imaging (SEI). Backscattered electron (BSE) and energy dispersive X-ray spectrometry (EDS) analyses were also undertaken. SEM analysis was carried out at the SEM Laboratory in the Rock and Ice Physics Laboratory, UCL, University of London, using a Jeol JSM-6480LV Variable Pressure Analytical Scanning Electron Microscope (SEM) with a high resolution of 3.0nm, equipped with Oxford Link EDS system and electron backscatter diffraction (EBSD) system.

Jarosite grain samples were mounted on Leit carbon double-sided adhesive tabs on 5 mm diameter aluminium stubs and then carbon or gold coated. A cobalt sample was used to calibrate the SEM. SEI of Au-coated samples was used for high-quality images of jarosite morphology. SEI of Au-coated samples used 7 kV accelerating voltage, 3.0 μm spot size and a working distance (WD) of 11 mm. SEI of carbon-coated samples used 1.5 kV and 10-12 mm WD, and BSE and EDS analyses of carbon-coated samples used 10 kV and 10-13 mm WD.

.

3.3.3 Powder X-ray diffraction and Rietveld refinement

X-ray diffraction (XRD) analysis is commonly used in studies to provide identification of jarosite family minerals (Brophy and Sheridan, 1965; May et al., 1973; Dutrizac and Kaiman, 1976; Desborough et al., 2006; Papike et al., 2006; Basciano and Peterson, 2007a, 2007b and 2008; Murphy et al., 2009). XRD analysis for mineral identification in this project was carried out using the Philips PW1876 powder diffractometer, PC-APD computer software and X'Menu graphics software in the Department of Earth and Planetary Sciences, Birkbeck, University of London. The anode material used was Cu, which has a $K\alpha_1$ wavelength of 1.54056 Å.

Mineral identification was carried out with X'Menu software, which uses the Joint Committee for Powder Diffraction Spectrometry (JCPDS) database and has a 'PC-identify' function that proposes a range of candidate minerals for each sample by comparing the automatically identified strongest spectrum of peaks (intensities, or counts per second), 2θ reference lines and calculated d-spacings within the sample to reference patterns. XRD peaks for synthetic and natural jarosites were indexed against JCPDS standard patterns: jarosite 10-0443 and 22-0827; hydronian jarosite 36-0427; natrojarosite 11-0302, 30-1203 and 36-0425; argentojarosite 25-1327 and

41-1398; hydronium jarosite 31-0650; and plumbojarosite 18-0698, 33-0759 and 39-1353.

Rietveld refinement of Co-radiation powder XRD data of the jarosite samples was also carried out for this project. This is a technique that has been used in other studies of jarosite group minerals (Basciano and Peterson, 2007 and 2008). The XRD analysis was carried out using a PANalytical X'Pert Pro diffractometer at the Natural History Museum, London. The instrument was fitted with an MPPC generator, PW3376/00 X-ray tube, PW3064 reflection-transmission spinner, PW3050/60 goniometer, X'Celerator detector, X'Pert Data Collector, Data Viewer and Database32, and X'Pert HighScore Plus software for crystallographic and Rietveld analyses. The instrument was operated at room temperature. Co radiation ($K\alpha_1$ λ = 1.78897 Å, $K\alpha_2$ λ = 1.79285 Å and α_2/α_1 intensity ratio = 0.5) was used for the analyses of the synthesised samples, which were run in reflection mode, and a monochromator was used. Continuous X-ray scans were used with a start angle of 10.00º 2θ and an end angle of 100.00º 2θ, a step size of 1.00º 2θ and a time per step of 40.0 s, except for additional scans of two samples using a time per step of 80 s. Before analysis, each sample was ground into a powder using a mortar and pestle.

Refinement of the unit-cell parameters, bond angles and lengths, and site occupancies of the mineral phases present in the jarosite compounds was carried out on the XRD data with the Rietveld method using the General Structure Analysis System (GSAS) program (Larson and Von Dreele, 2004) and the GSAS 'add-on' software EXPGUI ('Experiment Graphical User Interface'), a utility for viewing refinement fits and results (Toby, 2001).

3.3.4 Electron microprobe analysis

Electron microprobe analysis (EMPA) has been used in studies to provide chemical composition information on jarosite minerals, including natural samples (Ildefonse et al., 1984; Jamieson et al., 2005) and synthetic samples (Brophy and Sheridan, 1965; Lowers et al., 2005; Desborough et al., 2010). In this project, the chemical compositions of the natural and synthetic jarosite samples were analysed by electron microprobe spectroscopy in wavelength dispersive X-ray spectrometry (WDS) mode at the Electron Microprobe Suite, Department of Earth and Planetary Sciences, Birkbeck, University of London. Polished resin blocks of the synthetic and natural jarosite samples were prepared and these were analysed using a Jeol JXA-8100 electron microprobe, which operates under Windows XP Pro and Jeol analytical software. The accelerating voltage of the probe filament was 15 kV, the probe current was 2.5×10^{-8} amps and the spot beam diameter provides a spatial resolution of about 1 µm.

Prior to WDS analysis, the microprobe's backscattered electron imaging system was used to identify potential natural jarosite mineral grains. An Oxford Instruments energy dispersive X-ray spectrometry (EDS) system, equipped with INCA x-sight microanalytical software, was then used to analyse their qualitative chemical composition to confirm jarosite minerals for WDS analysis.

WDS analysis was carried out by the microprobe's three Joel XM-86030 Type H Spectrometers using LiF, PET, TAP crystals, as well as a layered dispersion elements (LDE) crystal to enable the quantitative analysis of the lighter element O. Elements analysed by TAP crystals were Na, Si, Al, As and Ga and by PET/LiF crystals were S, K, Pb, Fe, Ag, Au, P, V, Cr, Cu and Zn. Prior to WDS analysis, reference materials of known composition were used to calibrate the microprobe.

The standards used were pure metals, simple oxides or other natural minerals, including: albite (Na), pyrite (S), fayalite (Fe), quartz (Si) and apatite (P).

3.3.4.1 Benefits and limitations of EMPA of jarosites

The properties of jarosite that make EMPA analysis difficult and complicate the interpretation of the results, leading to potential errors of data interpretation, include sensitivity to the electron beam, small particle size and chemical heterogeneity (Lowers et al., 2005). Limitations of EMPA include the effects of interactions between the jarosite sample and the electron beam (Lowers et al., 2005).

Jarosite interactions with the beam may result in alkali cation migration and specimen damage at operating conditions varying from 10-20 kV, 5-30 nA (cup or PCD) and spot to 10 μm diameter beam. Migration of K and, to a greater degree, Na during microprobe analysis may result in loss of counts during analysis and an apparent cation deficiency (Lowers et al., 2005; Desborough et al., 2010). For example, at operating conditions of 15 kV, 20 nA and a spot beam, count losses of K of up to ~ 50% may result (Lowers et al., 2005). Reducing the accelerating voltage to 10 kV and beam diameter tend to minimise alkali loss. Using operating conditions of 10 kV, 20 nA and 5 μm diameter beam, Na and K count rates remain relatively constant for analysis times up to 30 s with no visible specimen damage.

If a sample contains high proportions of structural water and if the voltage of the electron beam is set too high, some water may be lost during analysis, leading to substantial error in elemental quantification (Smith, 2004). The structure of jarosite contains significant amounts of structural water, some of which is not strongly bound, while the samples are also likely to contain amounts of non-structural water remaining after drying during synthesis.

The operating conditions of the point analyses in this study included a spot (~ 1 μm) electron beam of 15 kV and 25 nA (2.5 x 10^{-8} A) for 10 s (S) and 20 s (K, Na, Ag, Pb and Fe). Monitoring of K and Na counts at these operating conditions using EDS showed little loss of intensities (c.f. Lowers et al., 2005).

Jarosites may be very fine-grained so that the grains are too small to resolve by EMPA (Desborough et al., 2010). Low-temperature jarosite minerals are generally very fine-grained, which prohibits their separation for chemical analysis (Desborough et al., 2010). Even a small electron beam may not resolve sub-micrometre intergrowths of different compositions of jarosite (Papike et al., 2006, 2007; Desborough et al., 2010). Analysis of jarosite volumes smaller than the excitation volume results in low totals of the elements of interest and incorrect cation ratios (Lowers et al., 2005). Operating conditions of 10 kV and 5 μm beam produce an excitation volume of ~ 4 μm^3 and operating conditions of 15 kV and 5 μm beam produce an excitation volume of ~ 8 μm^3. Data collected under circumstances where the jarosite volumes are smaller than the excitation volume must be used with caution when concluding that Fe deficiencies exist and/or H_3O^+ has substituted for K (Lowers et al., 2005). However, in this study, although the synthesised jarosites are very fine-grained, as indicated by the morphology studies, with some grains ≤ 1 μm, all the grains are in aggregates that form areas and volumes sufficiently large for EMPA. In addition, it has been shown that deficiencies in the K-monovalent site may not be due to the presence of H_3O^+ but rather to vacancies in the crystal structure (Majzlan et al., 2004).

Crystal chemistry of jarosite allows multiple substitutions in the lattice. Backscattered electron images can reveal chemical zonation within grains, information of which can be used to prevent analysis of overlapping chemical zones

(Lowers et al., 2005). However, orientation of chemical zones with depth is often not known; therefore, may be parallel to or intersect the chemical zones at depth within the excitation volume. Jarosite may display chemical zoning on a scale smaller than the excitation volume, resulting in more than one zone being analysed at one time. Interpretations of solid solution between end members (K, Na or H_3O) must consider the possibilities of heterogeneities in the excitation volume (Lowers et al., 2005).

A potential inaccuracy of the EMPA data obtained is if there is chemical heterogeneity or zonation in the samples. This is especially the case if the chemical zoning is of a scale smaller than the excitation volume of the beam, resulting in more than one zone being analysed at one time (Lowers et al., 2005). Backscattered electron images can reveal chemical zonation within grains and this information can be used to prevent analysis of overlapping zones (Lowers et al., 2005). However, backscattered electron images of the K-Ag, Na-Ag and Pb-Ag jarosite samples used in this study during identification of positions for point analyses by WDS indicated no chemical zonation within the synthesised crystals.

3.3.4.2 Interpretation of data and data quality

In EMPA of jarosite compounds, potential errors of data interpretation occur due to particle size being smaller (< 1 μm) than the electron beam (see section 3.3.4.1) and thus causing interactions. The EMPA readings of the content of the *A*-site cations in each synthesised jarosite compound often show substantial variation, indicating either significant heterogeneity or problems of obtaining good quality data from the samples. The standard deviations of the compositions of the *A*-site cations are generally relatively high. This is indicated by the analytical precision (in %) of the data measured by the coefficient of variation (C, ratio of standard deviation of population to the mean value) of the site occupancies of the *A*-site cations in each

sample (Table 3.8a-c). Of the compounds containing Na, only 1 out of 34 (3%) has a C value for Na of < 10%, while 8 (24%) have a C value of 20-29.99% and 16 (47%) have a C value of ≥ 50%. Of the K-containing compounds, only 2 out of 36 (6%) have a C value for K of < 10%, 13 (36%) have a C value of 10-19.99%, 11 (31%) have a C value of 20-29.99% and 6 (17%) have a C value of 30-39.99%, while 3 (8%) have a C value of ≥ 50%. Of the Pb-containing compounds, 1 out of 10 (10%) has a C value of < 10%, 1 (10%) has a C value of 30-30.99%, and 8 (80%) have a C value of more than ≥ 50%. In the Ag-containing compounds only 1 out of 72 (1%) has a C value for Ag of < 10%, while 14 (19%) have a C value of 10-19.99%, 23 (32%) have a C value of 20-29.99%, 17 (24%) have a C value of 30-39.99%, 10 (14%) have a C value of 40-49.99% and 8 (11%) have a C value of ≥ 50%.

Table 3.8a. EMPA mean *A*-site occupancy (occ) of K and Ag, standard deviation (s) and coefficient of variation (C) of synthesised K-Ag jarosites.

Sample	K occ	K s	K C	Ag occ	Ag s	Ag C
04	0.37	0.1411	38.11	0	0	0
06	0.60	0.0811	13.52	0.19	0.0409	21.53
06D	0.30	0.1024	34.13	0.06	0.0279	46.50
08	0.30	0.0913	30.43	0.29	0.0492	16.97
10	0.23	0.0364	15.83	0.14	0.0548	39.14
10D	0.22	0.0609	27.68	0.17	0.0702	41.29
12	0	0	0	0.31	0.0964	31.10
22	0.23	0.0486	21.13	0	0	0
24	0.25	0.0644	25.76	0.07	0.0281	40.14
24D	0.30	0.1521	50.70	0.09	0.0402	44.67
26	0.24	0.0450	18.75	0.07	0.0308	44.00
28	0.21	0.0272	12.95	0.10	0.0363	36.30
30	0	0	0	0.24	0.0627	26.13
40	0.26	0.0981	37.73	0.04	0.0100	25.00
55	0.43	0.0692	16.09	0	0	0
56	0.70	0.0451	6.44	0.16	0.0058	3.63
57	0.56	0.0643	11.48	0.26	0.0473	18.19
58	0.45	0.0819	18.20	0.27	0.0959	35.52
59	0.37	0.0579	15.65	0.35	0.1140	32.57
60	0.21	0.0432	20.57	0.60	0.1096	18.27
61	0	0	0	0.63	0.1848	29.33
62	0.55	0.0962	17.49	0	0	0
63	0.42	0.0881	20.98	0.24	0.0750	31.25
64	0.26	0.0471	18.12	0.30	0.0402	13.40
65	0.29	0.2155	74.31	0.34	0.0351	10.32
66	0	0	0	0.44	0.1517	34.48
71	0	0	0	0.66	0.0759	11.50
72	0	0	0	0.63	0.5282	83.84

73	0.32	0.0952	29.75	0	0	0
74	0.64	0.1881	29.39	0.06	0.0160	26.67
75	0.35	0.0588	16.80	0.10	0.0283	28.30
76	0.36	0.0262	7.28	0.15	0.0251	16.73
81	0.64	0.1119	17.48	0	0	0
82	0.40	0.1608	40.20	0.14	0.0484	34.57
83	0.30	0.0691	23.03	0.43	0.1129	26.26
84	0.10	0.0294	29.40	0.64	0.2127	33.23
89	0.55	0.0977	17.76	0	0	0
90	0.56	0.1279	22.84	0.05	0.0168	33.60
91	0.48	0.1640	34.17	0.04	0.0205	51.25
92	0.31	0.0641	20.68	0.09	0.0251	27.89
93	0.35	0.1235	35.29	0.12	0.0558	46.50
94	0.17	0.0994	58.47	0.28	0.1696	60.57
95	0	0	0	0.56	0.1768	31.57

Table 3.8b. EMPA mean *A*-site occupancy (occ) of Na and Ag, standard deviation (s) and coefficient of variation (C) of synthesised Na-Ag jarosites.

Sample	**Na occ**	**Na s**	**Na C**	**Ag occ**	**Ag s**	**Ag C**
12	0	0	0	0.31	0.0964	31.10
14	0.17	0.0404	23.76	0	0	0
16	0.10	0.0615	61.50	0.16	0.0574	35.88
18	0.05	0.0163	32.60	0.22	0.0390	17.73
20	0.04	0.0351	87.75	0.23	0.0460	20.00
30	0	0	0	0.24	0.0627	26.13
32	0.30	0.0894	29.80	0	0	0
34	0.10	0.0776	77.60	0.15	0.0336	22.40
36	0.04	0.0265	66.25	0.29	0.1328	45.79
38	0.01	0.0071	71.00	0.26	0.0510	19.62
38D	0.04	0.0283	70.75	0.23	0.1109	48.22
42	0.05	0.0087	17.40	0.20	0.0339	16.95
49	0.56	0.0289	5.16	0	0	0
50	0.25	0.1111	44.44	0.24	0.1031	42.96
51	0.16	0.0894	55.88	0.29	0.0808	27.86
52	0.05	0.0148	29.60	0.37	0.1394	37.68
53	0.03	0.0120	40.00	0.30	0.1127	37.57
54	0.01	0.0065	65.00	0.38	0.1402	36.89
61	0	0	0	0.63	0.1848	29.33
66	0	0	0	0.44	0.1517	34.48
67	0.65	0.1993	30.66	0	0	0
68	0.57	0.1699	29.81	0.09	0.1008	112.00
69	0.30	0.1759	58.63	0.12	0.1701	141.75
70	0.23	0.1778	77.30	0.33	0.2678	81.15
71	0	0	0	0.66	0.0759	11.50
72	0	0	0	0.63	0.5282	83.84
77	0.49	0.1878	38.33	0	0	0
78	0.05	0.0298	59.60	0.42	0.3550	84.52
79	0.06	0.0173	28.83	0.48	0.1452	30.25
80	0.03	0.0178	59.33	0.55	0.1466	26.65
85	0.55	0.1141	20.75	0	0	0
86	0.29	0.2672	92.14	0.35	0.2127	60.77
87	0.17	0.1014	59.65	0.50	0.1139	22.78
88	0.14	0.0711	50.79	0.49	0.0699	14.27
95	0	0	0	0.56	0.1768	31.57
96	0.56	0.1567	27.98	0	0	0
97	0.11	0.0374	34.00	0.46	0.2258	49.09
98	0.09	0.0312	34.67	0.55	0.1612	29.31
99	0.03	0.0088	29.33	0.57	0.1440	25.26

100	0.02	0.0093	46.50	0.63	0.1510	23.97
101	0.02	0.0112	56.00	0.50	0.1785	35.70

Table 3.8c. EMPA mean *A*-site occupancy (occ) of Pb and Ag, standard deviation (s) and coefficient of variation (C) of synthesised Pb-Ag jarosites.

Sample	**Pb occ**	**Pb s**	**Pb C**	**Ag occ**	**Ag s**	**Ag C**
43	n.d.	n.d.	n.d.	n.d.	n.d.	n.d.
44	0.03	0.0194	64.67	0.223	0.0599	26.86
45	0.006	0.0059	98.33	0.448	0.1279	28.55
46	n.d.	n.d.	n.d.	n.d.	n.d.	n.d.
47	0.006	0.0082	136.67	0.652	0.1546	23.71
48	0.009	0.0073	81.11	0.299	0.0433	14.48
61	0	0	0	0.63	0.1848	29.33
95	0	0	0	0.56	0.1768	31.57
102	0.004	0.0030	75.00	0.448	0.1322	29.51
103	0.003	0.0009	30.00	0.491	0.0752	15.32
104	0.025	0.0186	74.40	0.807	0.1974	24.46
105	0.047	0.0504	107.23	0.808	0.0881	10.90
106	0.018	0.0093	51.67	0.483	0.1374	28.45
107	0.03	0.0017	5.67	0	0	0

3.3.5 Raman spectroscopy

Raman spectroscopy has been used in studies to characterise jarosite minerals, including synthetic compounds (Serna et al., 1986; Sasaki et al., 1998; Casas et al., 2007; Murphy et al., 2009) and natural samples (Frost et al., 2006). Raman spectra can serve to identify the specific type of jarosite-group compound (Sasaki et al., 1998; Frost et al., 2006), including in poorly crystalline or low-concentration geochemical samples (Sasaki et al., 1998). Differences in the wavenumbers of $v_1(SO_4^{2-})$, $v_2(SO_4^{2-})$, $v_3(SO_4^{2-})$, $v_4(SO_4^{2-})$ and v_{OH} modes have been shown between K-, Na-, Ag-, H_3O- and Pb-jarosite (Frost et al., 2006). In addition, Raman spectroscopy has an advantage over infrared (IR) spectroscopy, another commonly used characterisation technique for jarosite minerals (Serna et al., 1986; Sasaki et al., 1998), as in aqueous solution, $v_1(SO_4^{2-})$, $v_2(SO_4^{2-})$, $v_3(SO_4^{2-})$ and $v_4(SO_4^{2-})$ modes are all Raman active in sulphate tetrahedra, compared with only $v_3(SO_4^{2-})$ and $v_4(SO_4^{2-})$ being IR active (Sasaki et al., 1998). Also, Raman spectra of the hydroxyl stretching region of jarosites have the advantage that bands due to adsorbed water are

eliminated and only jarosite OH stretching bands are observed, whereas the IR spectrum of K-jarosite shows a broad profile and a considerable number of overlapping bands of adsorbed water and hydroxyl (Frost et al., 2006).

Laser Raman microspectroscopic analyses were carried out at Kingston University using a Renishaw RM1000 Raman spectrometer and a Renishaw inVia Raman spectrometer, both of which were equipped with a thermoelectrically cooled charge coupled device (CCD) detector and a 514.5 nm Ar ion laser. The instruments were calibrated daily on a silicon standard at 520.5 cm^{-1}. The Renishaw RM1000 system was operated in confocal mode with the laser focused on the sample through the objective lens (magnification × 50) of an Olympus petrological microscope, and the Renishaw inVia system used a Leica DM2500 M microscope. Under these conditions the laser beam for analysis was restricted to an area of < 2 μm diameter.

Initial sample burn occurred at 100% laser beam power because of the hydrous content of the samples, so the laser beam power of the Renishaw RM1000 system was reduced from 100% to 25%. The laser power was reduced using neutral density filters and was typically between 1 mW and ~220 μW at the sample surface. The laser beam power of the Renishaw inVia system was reduced to 10% and was 6.76 mW at the sample surface. Following the reduction of beam power, the samples were inspected optically for any laser damage and none was observed.

Spectra were recorded over the frequency range 100 to 4000 cm^{-1}, using integration times of 60 s (except 120 s for one sample). The errors on the spectra were < 0.1 cm^{-1}. Peak fitting was performed using Galactic GRAMS/32 software with the Renishaw RM1000 spectrometer and WIRE 3.3 software with the Renishaw inVia spectrometer, both of which use a mixed Gaussian-Lorentzian curve. Depending on the quality of the spectra, between one and four spectra were obtained

over the full frequency range. The variation between the different spectra of individual samples was small and therefore the samples were assumed to be homogeneous.

.

3.3.6 Chemical analysis

Inductively coupled plasma-atomic emission spectrometry (ICP-AES) is a commonly used technique to analyse the chemical composition of jarosite minerals (Smith et al., 2006a; Basciano and Peterson, 2007a and 2008; Murphy et al., 2009). To prepare solutions of the samples for quantitative total elemental analysis by ICP-AES, acid digestion of the synthetic jarosite compounds was carried out. A commonly used acid to dissolve jarosite minerals is HCl (Sasaki et al., 1995; Smith et al., 2006a), sometimes in the form of aqua regia (3:1 HCl:HNO_3) (Basciano and Peterson 2007a and 2008). However, a problem encountered when using HCl to dissolve argentojarosite is the precipitation of AgCl (Sasaki et al., 1995). Consequently, for this project, trial dissolution using HCl of several of the synthetic Ag-containing jarosite compounds was carried out and this resulted in the formation of a precipitate. For this reason, an alternative method using HF was adopted to completely dissolve the jarosite compounds.

For the acid digestion of the jarosite compounds, approximately 90 mg of each dried synthetic compound were dissolved by adding 3 ml HF (38% wt) plus 1 ml HNO_3 (67% wt) in a Savillex vial with cap and heated at 150°C for 16 hrs. The resulting solutions were then evaporated at 110°C to incipient dryness. Then 1 ml HNO_3 was added to each and the resulting solutions were evaporated at 110°C to incipient dryness. Following this, 3 ml HNO_3 and 1 ml ultra-pure water were added. After digestion, the solutions were made up to 100 mL with ultra-pure water.

Following the acid digestion procedure, no visible solid remained. Following this, 10 ml of each solution were put in a 50 ml vial by pipette and 40 ml of ultra-pure water was added.

The resulting solutions were analyzed for Ag, Na, K, Pb, Fe and S by ICP-AES on a Varian 720-ES instrument, fitted with both a monochromator and a polychromator, at University College London. To calibrate the machine for the elements to be analysed, three standards were analysed: standard 1 contained 10 ppm S, 20 ppm Ag, K, Na and Pb, and 50 ppm Fe; standard 2 contained 20 ppm S, 40 ppm Ag, K, Na and Pb, and 80 ppm Fe; and standard 3 contained 30 ppm S, 60 ppm Ag, K, Na and Pb, and 100 ppm Fe. For drift calibration, standard 2 was analysed every seven samples and standards 1, 2 and 3 were analysed every 14 samples. Between every fourteen samples, a blank of ultrapure water was analysed. The wavelengths (nm) analysed for the elements were S 180.669 and S 181.972; Pb 217.000 and 220.353; Fe 234.350, 238.204 and 259.940; Ag 328.068 and 338.289; K 404.721, 766.491 and 769.897; and Na 568.821, 588.995 and 589.592.

The precision (in %) of ICP-AES analysis of K, Na, K-Ag, Na-Ag and Pb-Ag jarosites synthesised at 22ºC, 97ºC and 140ºC was calculated by analysing duplicates of samples 4, 14, 26, 47, 55, 60, 70, 76, 83, 87, 93, 101 and 105. Analytical precision (in %) of the results for these samples and duplicates is represented by the coefficient of variation (C) (standard deviation divided by the mean, times 100). The results (see Appendix I) show good analytical precision (C) figures of $\leq 6\%$ for the elements in all the above samples, except for K (18-32%) in sample 4; Na (23-97%), Ag (96%), Fe (94-95%) and S (94-95%) in sample 101; and Pb (20-22%) in sample 105.

3.4 Summary

- K-, Na-, Pb- and Ag-jarosites were synthesised in several series of experiments at 20ºC, 97ºC or 140ºC using different methods.
- Synthesis used K_2SO_4, Na_2SO_4, Ag_2SO_4 and $PbSO_4$ in different series of experiments at concentrations of 0-11 *M* or 0-0.06 *M*.
- Synthesis experiments used either 0.075 *M* $Fe_2(SO_4)_3.5H_2O$, 0.15 *M* $Fe_2(SO_4)_3.5H_2O$ or 0.51 *M* $Fe_2(SO_4)_3.5H_2O$.
- Colour analysis of each synthesised jarosite sample was carried out using Munsell charts.
- Scanning electron microscopy was used to determine the crystal morphology of synthetic jarosite samples with secondary electron imaging.
- Mineral identification by X-ray diffraction analysis was carried out using the Joint Committee for Powder Diffraction Spectrometry (JCPDS) database.
- The chemical compositions of the natural and synthetic samples were analysed by electron microprobe spectroscopy in wavelength dispersive X-ray spectrometry.
- Laser Raman microspectroscopic analyses were carried out using a Renishaw RM1000 Raman spectrometer or a Renishaw inVia Raman spectrometer.
- Acid digestion of the synthetic jarosite compounds was carried out prior to quantitative total elemental analysis by inductively coupled plasma-atomic emission spectrometry.

4 RESULTS

4.1 Characterisation of synthetic jarosite compounds

The products of the K-Ag, Na-Ag and Pb-Ag jarosite synthesis procedures were weighed and the result for each sample was recorded. These results are shown in the tables in Appendix C, which also show the 'ideal' or theoretical maximum weights of the jarosite products that could be produced from the amounts of reagents used in the synthesis experiments.

4.1.1 Munsell colour analysis

The synthesised jarosite compounds were ground to powders using a mortar and pestle and then the powders were compared with Munsell colour charts. The results of the Munsell colour analysis of each synthesised jarosite sample are shown in Table 4.1. The samples have been characterised with colours comprising 2.5Y 5/6, 7/6, 8/6, 5/8, 6/8, 7/8 and 8/8, and 10YR 5/6, 6/8 and 7/8. The colour names given by the Munsell charts for the notations are: 2.5Y 5/6 light olive yellow; 2.5Y 6/8 olive yellow; 2.5Y 7/6, 8/6, 5/8, 7/8 and 8/8 yellow; 10YR 5/6 yellowish brown; 10YR 6/8 brownish yellow; and 10YR 7/8 yellow. Most of this project's synthesised jarosite compounds have been characterised as yellow; however, there is a trend of compounds with high Ag content in the starting solutions being characterised as olive yellow.

These results compare with a reported Munsell colour for synthesised potassium jarosite of 10YR 8/7 (Smith, 2004; Smith et al., 2006a), while another study reports synthesised Ag-jarosite as being a yellow-brown precipitate (Frost et al., 2005), so the results for some of the compounds in this project are close to those

colours. A further study on natural jarosite-group minerals containing K, Na and H_3O, plus significant As, Pb and Zn, which are described as being dull orange-yellow, are given the Munsell colours 2.5Y 6-7 and 2.5Y 7-8 in samples from stalactites and Munsell colour 2.5Y 7/6 in a sample from mud on a mine wall (Jamieson et al., 2005). Therefore, the compounds in this project have colours similar to these.

Table 4.1: Munsell colours of synthesised K, Na, Pb, K-Ag, Na-Ag and Pb-Ag jarosites.

Sample	**Colour**	**Colour name**	**Starting solution**
Solutions containing 0.51 M $Fe_2(SO_4)_3.5H_2O$ heated at 97ºC and products dried at 60ºC			
4	2.5Y 7/8	Yellow	0.22 *M* K, 0.00 *M* Ag
6	2.5Y 7/8	Yellow	0.165 *M* K, 0.055 *M* Ag
8	2.5Y 8/8	Yellow	0.11 *M* K, 0.11 *M* Ag
10	2.5Y 7/8	Yellow	0.055 *M* K, 0.165 *M* Ag
12	2.5Y 6/8	Olive yellow	0.00 *M* K/Na, 0.22 *M* Ag
14	2.5Y 7/8	Yellow	0.22 *M* Na, 0.00 *M* Ag
16	2.5Y 6/8	Olive yellow	0.165 *M* Na, 0.055 *M* Ag
18	2.5Y 7/8	Yellow	0.11 *M* Na, 0.11 *M* Ag
20	2.5Y 7/8	Yellow	0.055 *M* Na, 0.165 *M* Ag
Solutions containing 0.51 M $Fe_2(SO_4)_3.5H_2O$ heated at 97ºC and products dried at 110ºC			
22	2.5Y 7/8	Yellow	0.22 *M* K, 0.00 *M* Ag
24	2.5Y 7/8	Yellow	0.165 *M* K, 0.055 *M* Ag
26	2.5Y 7/8	Yellow	0.11 *M* K, 0.11 *M* Ag
28	2.5Y 7/8	Yellow	0.055 *M* K, 0.165 *M* Ag
30	2.5Y 7/8	Yellow	0.00 *M* K/Na, 0.22 *M* Ag
32	10YR 6/8	Brownish yellow	0.22 *M* Na, 0.00 *M* Ag
34	2.5Y 7/8	Yellow	0.165 *M* Na, 0.055 *M* Ag
36	2.5Y 7/8	Yellow	0.11 *M* Na, 0.11 *M* Ag
38	2.5Y 7/8	Yellow	0.055 *M* Na, 0.165 *M* Ag
40	2.5Y 7/8	Yellow	0.5 *M* K, 0.1 *M* Ag
42	2.5Y 7/8	Yellow	0.5 *M* Na, 0.1 *M* Ag

Solutions containing 0.15 M $Fe_2(SO_4)_3.5H_2O$ heated at 140ºC and products dried at 110ºC			
43	2.5Y 7/8	Yellow	0.06 *M* Pb, 0.00 *M* Ag
44	2.5Y 7/8	Yellow	0.05 *M* Pb, 0.01 *M* Ag
45	2.5Y 7/8	Yellow	0.04 *M* Pb, 0.02 *M* Ag
46	10YR 7/8	Yellow	0.03 *M* Pb, 0.03 *M* Ag
47	2.5Y 7/8	Yellow	0.02 *M* Pb, 0.04 *M* Ag
48	2.5Y 7/8	Yellow	0.01 *M* Pb, 0.05 *M* Ag
49	2.5Y 7/8	Yellow	0.12 *M* Na, 0.00 *M* Ag
50	2.5Y 6/8	Olive yellow	0.10 *M* Na, 0.02 *M* Ag
51	2.5Y 6/8	Olive yellow	0.08 *M* Na, 0.04 *M* Ag
52	2.5Y 6/8	Olive yellow	0.06 *M* Na, 0.06 *M* Ag
53	2.5Y 6/8	Olive yellow	0.04 *M* Na, 0.08 *M* Ag
54	2.5Y 6/8	Olive yellow	0.02 *M* Na, 0.10 *M* Ag
55	2.5Y 7/8	Yellow	0.12 *M* K, 0.00 *M* Ag
56	2.5Y 7/8	Yellow	0.10 *M* K, 0.02 *M* Ag
57	2.5Y 7/8	Yellow	0.08 *M* K, 0.04 *M* Ag
58	2.5Y 7/8	Yellow	0.06 *M* K, 0.06 *M* Ag
59	2.5Y 7/8	Yellow	0.04 *M* K, 0.08 *M* Ag
60	2.5Y 7/8	Yellow	0.02 *M* K, 0.10 *M* Ag
61	2.5Y 6/8	Olive yellow	0.00 *M* M, 0.12 *M* Ag
Samples annealed at 140ºC and dried at 110ºC (from solutions originally containing 0.51 M $Fe_2(SO_4)_3.5H_2O$ heated at 97ºC and products dried at 60ºC)			
62	2.5Y 8/6	Yellow	0.22 *M* K, 0.00 *M* Ag
63	10YR 7/8	Yellow	0.165 *M* K, 0.055 *M* Ag
64	10YR 7/8	Yellow	0.11 *M* K, 0.11 *M* Ag
65	2.5Y 8/6	Yellow	0.055 *M* K, 0.165 *M* Ag
66	2.5Y 8/6	Yellow	0.00 *M* K/Na, 0.22 *M* Ag
67	2.5Y 8/8	Yellow	0.22 *M* Na, 0.00 *M* Ag
68	2.5Y 7/8	Yellow	0.165 *M* Na, 0.055 *M* Ag
69	2.5Y 7/6	Yellow	0.11 *M* Na, 0.11 *M* Ag
70	2.5Y 8/6	Yellow	0.055 *M* Na, 0.165 *M* Ag
Samples annealed at 140ºC and dried at 110ºC (from solutions originally containing 0.51 M $Fe_2(SO_4)_3.5H_2O$ heated at 97ºC and products dried at 110ºC)			
71	2.5Y 8/6	Yellow	0.00 *M* K/Na, 0.22 *M* Ag
81	2.5Y 8/6	Yellow	0.22 *M* K, 0.00 *M* Ag

82	2.5Y 7/8	Yellow	0.165 *M* K, 0.055 *M* Ag
83	2.5Y 6/8	Olive yellow	0.11 *M* K, 0.11 *M* Ag
84	2.5Y 6/8	Olive yellow	0.055 *M* K, 0.165 *M* Ag
85	2.5Y 8/8	Yellow	0.22 *M* Na, 0.00 *M* Ag
86	2.5Y 8/6	Yellow	0.165 *M* Na, 0.055 *M* Ag
87	2.5Y 7/8	Yellow	0.11 *M* Na, 0.11 *M* Ag
88	2.5Y 6/8	Olive yellow	0.055 *M* Na, 0.165 *M* Ag
Solutions containing 0.51 M $Fe_2(SO_4)_3.5H_2O$ were prepared at 22ºC and products air-dried at 22ºC			
72	2.5Y 8/6	Yellow	0.00 *M* K, 0.22 *M* Ag
73	2.5Y 8/6	Yellow	0.22 *M* K, 0.00 *M* Ag
74	2.5Y 8/6	Yellow	0.165 *M* K, 0.055 *M* Ag
75	2.5Y 8/6	Yellow	0.11 *M* K, 0.11 *M* Ag
76	2.5Y 8/6	Yellow	0.055 *M* K, 0.165 *M* Ag
77	2.5Y 8/6	Yellow	0.22 *M* Na, 0.00 *M* Ag
78	2.5Y 8/6	Yellow	0.165 *M* Na, 0.055 *M* Ag
79	2.5Y 8/6	Yellow	0.11 *M* Na, 0.11 *M* Ag
80	2.5Y 8/6	Yellow	0.055 *M* Na, 0.165 *M* Ag
Solutions containing 0.15 M $Fe_2(SO_4)_3.5H_2O$ were prepared at 22ºC and products air-dried at 22ºC			
89	2.5Y 5/6	Light olive yellow	0.12 *M* K, 0.00 *M* Ag
90	2.5Y 5/6	Light olive yellow	0.10 *M* K, 0.02 *M* Ag
91	2.5Y 5/6	Light olive yellow	0.08 *M* K, 0.04 *M* Ag
92	2.5Y 7/8	Yellow	0.06 *M* K, 0.06 *M* Ag
93	2.5Y 6/8	Olive yellow	0.04 *M* K, 0.08 *M* Ag
94	2.5Y 6/8	Olive yellow	0.02 *M* K, 0.10 *M* Ag
95	2.5Y 6/8	Olive yellow	0.00 *M* M, 0.12 *M* Ag
96	2.5Y 7/8	Yellow	0.12 *M* Na, 0.00 *M* Ag
97	2.5Y 7/8	Yellow	0.10 *M* Na, 0.02 *M* Ag
98	2.5Y 8/8	Yellow	0.08 *M* Na, 0.04 *M* Ag
99	2.5Y 5/8	Yellow	0.06 *M* Na, 0.06 *M* Ag
100	2.5Y 7/8	Yellow	0.04 *M* Na, 0.08 *M* Ag
101	2.5Y 6/8	Olive yellow	0.02 *M* Na, 0.10 *M* Ag
102	2.5Y 6/8	Olive yellow	0.00013 *M* Pb, 0.10 *M* Ag
103	2.5Y 6/8	Olive yellow	0.00032 *M* Pb, 0.10 *M* Ag
104	2.5Y 5/6	Light olive yellow	0.001 *M* Pb, 0.10 *M* Ag

105	2.5Y 5/6	Light olive yellow	0.005 *M* Pb, 0.10 *M* Ag
106	2.5Y 5/6	Light olive yellow	0.001 *M* Pb, 0.10 *M* Ag
107	2.5Y 5/8	Yellow	0.001 *M* Pb, 0.00 *M* Ag

4.1.2 Scanning electron microscopy

4.1.2.1 Morphology and grain size of synthetic jarosite compounds

SEM secondary-electron images of (Au-coated) synthetic samples 4-42 (even numbers) show end members of K-H_3O-jarosite, Ag-H_3O-jarosite and Na-H_3O-jarosite with distinctive morphologies, and K-Ag-H_3O and Na-Ag-H_3O-jarosite compounds display transitional forms between the end-member morphologies (see Table 4.2 and Appendix D). K-H_3O-jarosite crystals generally comprise rounded hexagonal plates on {0001} (Anthony et al., 2003) and discs, usually intergrown and in compact texture, with grain sizes of 1-20 µm, also as aggregates. Ag-H_3O-jarosite crystals comprise intergrown hexagonal plates on {0001} and dipyramidal (octahedral) rhombs with {01-12} and {0001} faces (Gasharova et al., 2005), both sometimes rounded, and in compact texture, with grain sizes of 4-25 µm. Na-H_3O-jarosite crystals are intergrown with pyramidal {01-12} and {0001} faces and rhombohedral {01-12} faces, in compact texture, with grain sizes of 1-20 µm.

Table 4.2. Morphology and grain size of synthetic K-Ag and Na-Ag jarosites

Sample	**Initial solution**	**Morphology**	**Grain size (µm)**
04	0.22 *M* K, 0.0 *M* Ag	Intergrown rounded plates and hexagonal plates, and rounded and angular aggregates	2-6
22	0.22 *M* K, 0.0 *M* Ag	Intergrown rounded plates, some with hexagonal faces, and aggregates	6-20
06	0.165 *M* K, 0.055 *M* Ag	Rounded hexagonal plates	2.5-4

24	0.165 *M* K, 0.055 *M* Ag	Intergrown plates and hexagonal plates, some rounded, and aggregates	5-10
06D	0.165 *M* K, 0.055 *M* Ag	Intergrown plates, some rounded	2-8
24D	0.165 *M* K, 0.055 *M* Ag	Intergrown rounded plates	15-40
08	0.11 *M* K, 0.11 *M* Ag	Rounded plates and hexagonal plates, and pyramidal rhombs	3.5-5
26	0.11 *M* K, 0.11 *M* Ag	Intergrown rounded plates	4-10
10	0.055 *M* K, 0.165 *M* Ag	Intergrown rounded plates and hexagonal plates, pyramidal rhombs, and aggregates	3-8
28	0.055 *M* K, 0.165 *M* Ag	Intergrown rounded plates, some with hexagonal faces, pyramidal rhombs, irregular, angular forms, and aggregates	2.5-6.5
40	0.5 *M* K, 0.1 *M* Ag	Intergrown rounded rhombs, rounded plates, some with hexagonal faces, and aggregates	2-8
12	0.22 *M* Ag, 0.0 *M* K	Intergrown hexagonal plates, some rounded, and pyramidal rhombs, some rounded	4-25
30	0.22 *M* Ag, 0.0 *M* K	Intergrown pyramidal rhombs, some rounded, and hexagonal plates, some rounded	10-20
14	0.22 *M* Na, 0.0 *M* Ag	Intergrown pyramidal rhombs	2-20
32	0.22 *M* Na, 0.0 *M* Ag	Intergrown pyramidal rhombs and pseudocubic rhombohedra	3-12
16	0.165 *M* Na, 0.055 *M* Ag	Intergrown pyramidal rhombs	1.5-25
34	0.165 *M* Na, 0.055 *M* Ag	Intergrown pyramidal rhombs and aggregates	1-8
18	0.11 *M* Na, 0.11 *M* Ag	Intergrown pyramidal rhombs	1-8
36	0.11 *M* Na, 0.11 *M* Ag	Intergrown pyramidal rhombs	1.5-10
20	0.055 *M* Na, 0.165 *M* Ag	Intergrown rounded plates, some with hexagonal faces, pyramidal rhombs, and irregular aggregates	3-20
38	0.055 *M* Na, 0.165 *M* Ag	Intergrown pyramidal rhombs	1-8
38D	0.055 *M* Na, 0.165 *M* Ag	Intergrown pyramidal rhombs and rounded plates, some with hexagonal faces	1-10
42	0.5 *M* Na, 0.1 *M* Ag	Intergrown pyramidal rhombs	1-6

4.1.2.2 Energy-dispersive X-ray spectroscopic analysis of K-Ag and Na-Ag jarosite products

The results of SEM energy-dispersive X-ray spectroscopic (EDS) analysis of the chemical compositions of the synthesised K-Ag-jarosite samples are shown in Tables 4.3 and 4.4, which also show the concentrations of cations in the synthesis starting solutions and the drying temperatures of the products. SEM analysis provides qualitative and partly quantitative chemical compositions (Gill, 1997), and the results of this project show generally declining content of K (Table 4.3) and Na (Table 4.4) in the jarosite compounds with decreasing alkali cation concentration in the starting solutions of the two series, which used different drying temperatures. The results also show increasing Ag content in the products with rising Ag cation concentration in the starting solutions.

Table 4.3: SEM EDS site occupancies of K-Ag jarosites synthesised at 97ºC

Series at 60°C drying temperature								
Sample	Na	K	Pb	Ag	H_3O	Fe	S	Starting solution
JS04[1]	0	0.76	0	0.00	0.24	2.89	2	0.22 *M* K, 0.00 *M* Ag
JS06[1]	0	0.62	0	0.14	0.24	2.50	2	0.165 *M* K, 0.055 *M* Ag
JS06D[1]	0	0.60	0	0.10	0.30	3.86	2	0.165 *M* K, 0.055 *M* Ag
JS08[1]	0	0.41	0	0.43	0.16	2.59	2	0.11 *M* K, 0.11 *M* Ag
JS10[1]	0	0.15	0	0.66	0.19	4.21	2	0.055 *M* K, 0.165 *M* Ag
JS10D[1]	0	0.23	0	0.53	0.24	3.65	2	0.055 *M* K, 0.165 *M* Ag
JS12[1]	0	0.00	0	0.80	0.20	3.92	2	0.00 *M* $M^{+,2+}$, 0.22 *M* Ag
Ave[3]	0	0.39	0	0.41	0.20	3.22	2	
Ave[4]	0	0.40	0	0.37	0.23	3.38	2	
Series at 110°C drying temperature								
Sample	Na	K	Pb	Ag	H_3O	Fe	S	Starting solution
JS22[2]	0	0.75	0	0.00	0.25	4.10	2	0.22 *M* K, 0.00 *M* Ag

JS24[2]	0	0.68	0	0.19	0.13	3.66	2	0.165 *M* K, 0.055 *M* Ag
JS24D[2]	0	0.63	0	0.13	0.24	3.99	2	0.165 *M* K, 0.055 *M* Ag
JS26[2]	0	0.49	0	0.37	0.14	3.65	2	0.11 *M* K, 0.11 *M* Ag
JS28[2]	0	0.13	0	0.81	0.06	2.03	2	0.055 *M* K, 0.165 *M* Ag
JS30[2]	0	0.00	0	0.86	0.14	3.40	2	0.00 *M* $M^{+,2+}$, 0.22 *M* Ag
JS40[2]	0	0.82	0	0.01	0.17	3.08	2	0.5 *M* K, 0.1 *M* Ag
Ave[5]	0	0.41	0	0.45	0.14	3.37	2	
Ave[6]	0	0.40	0	0.43	0.17	3.43	2	
Overall ave[7]	0	0.40	0	0.43	0.17	3.28	2	
Overall ave[8]	0	0.40	0	0.40	0.20	3.41	2	

Notes: 1 Solutions contained 0.51 *M* $Fe_2(SO_4)_3.5H_2O$ and were heated at 97ºC and products were dried at 60ºC.
2 Solutions contained 0.51 *M* $Fe_2(SO_4)_3.5H_2O$ and were heated at 97ºC and products were dried at 110ºC.
3 Average content of 60°C drying temperature series (excluding JS6D and 10D). 4 Average content of 60°C drying temperature series (excluding JS6 and 10). 5 Average content of 110°C drying temperature series (excluding JS24D and 40). 6 Average content of 110°C drying temperature series (excluding JS24 and 40).
7 Overall average of all products at 60°C and 110°C drying temperatures (excluding JS6D, 10D, 24D and 40).
8 Overall average of all products at 60°C and 110°C drying temperatures (excluding JS6, 10, 24 and 40).

Table 4.4: SEM EDS site occupancies of Na-Ag jarosites synthesised at 97ºC

Series at 60°C drying temperature

Sample	Na	K	Pb	Ag	H_3O	Fe	S	Starting solution
JS12[1]	0.00	0	0	0.80	0.20	3.92	2	0.00 M M^+, 0.22 M Ag
JS14[1]	0.73	0	0	0.00	0.27	3.51	2	0.22 M Na, 0.00 M Ag
JS16[1]	0.44	0	0	0.07	0.49	2.90	2	0.165 M Na, 0.055 M Ag
JS18[1]	0.10	0	0	0.63	0.27	3.03	2	0.11 M Na, 0.11 M Ag
JS20[1]	0.07	0	0	0.87	0.06	4.59	2	0.055 M Na, 0.165 M Ag
Ave[3]	0.27	0	0	0.47	0.26	3.59	2	

Series at 110°C drying temperature

Sample	Na	K	Pb	Ag	H_3O	Fe	S	Starting solution
JS30[2]	0.00	0	0	0.86	0.14	3.40	2	0.00 M M^+, 0.22 M Ag
JS32[2]	0.76	0	0	0.00	0.24	4.72	2	0.22 M Na, 0.00 M Ag
JS34[2]	0.41	0	0	0.47	0.12	3.90	2	0.165 M Na, 0.055 M Ag
JS36[2]	0.12	0	0	0.88	0.00	3.46	2	0.11 M Na, 0.11 M Ag
JS38[2]	0.01	0	0	0.84	0.15	2.20	2	0.055 M Na, 0.165 M Ag
JS38D[2]	0.02	0	0	0.77	0.21	3.18	2	0.055 M Na, 0.165 M Ag
JS42[2]	0.11	0	0	0.82	0.07	4.34	2	0.5 M Na, 0.1 M Ag
Ave[4]	0.26	0	0	0.61	0.13	3.54	2	

Ave[5]	0.26	0	0	0.60	0.14	3.73	2
Overall ave[6]	0.27	0	0	0.54	0.19	3.57	2
Overall ave[7]	0.27	0	0	0.54	0.19	3.66	2

Notes: 1 Solutions contained 0.51 *M* $Fe_2(SO_4)_3.5H_2O$ and were heated at 97ºC and products were dried at 60ºC. 2 Solutions contained 0.51 *M* $Fe_2(SO_4)_3.5H_2O$ and were heated at 97ºC and products were dried at 110ºC. 3 Average content of 60°C drying temperature series. 4 Average content of 110°C drying temperature series (excluding JS38D and 42). 5 Average content of 110°C drying temperature series (excluding JS38 and 42). 6 Overall average of all products at 60°C and 110°C drying temperatures (excluding JS38D and 42). 7 Overall average of all products at 60°C and 110°C drying temperatures (excluding JS38 and 42).

The composition (site occupancies) of the products 04 and 22 (Table 4.3) from the highest concentration of K (0.22 M) in the starting solutions are 0.76 and 0.75 respectively. The composition of the products 12 and 30 from the corresponding starting solutions for Ag (0.22 M) are 0.80 and 0.86 respectively, so the Ag content is slightly higher than the K content of the corresponding products. The composition of the products 08 and 26 from the starting solutions with equal concentrations of K and Ag (0.11 M) are K 0.41, Ag 0.43 and K 0.49, Ag 0.37 respectively. The average contents of K and Ag in the products of the two series of syntheses with initial solutions containing cations varying between 0 and 0.22 *M* (Table 4.3) are 0.40 and 0.43 respectively (excluding 6D, 10D and 24D) and 0.40 and 0.40 respectively (excluding 6, 10 and 24). On the basis of these average contents, the results for the two synthesis series in Tables 4.3 indicate that K and Ag are approximately equally incorporated into the structure of jarosite.

The *A*-site occupancies of the products 14 and 32 (Table 4.4) from the highest concentration of Na (0.22 M) in the starting solutions are 0.73 and 0.76 respectively, which compares with the occupancies of 0.80 and 0.86 respectively for the corresponding Ag products 12 and 30. Therefore, the Ag content is slightly higher than the Na content of the corresponding products. The site occupancies of products 18 and 36 from the starting solutions with equal concentrations of Na and Ag (0.11 M) are Na 0.10, Ag 0.63 and Na 0.12, Ag 0.88 respectively. The overall average

contents of Na and Ag in the products of the two series of syntheses with initial solutions containing cations varying between 0 and 0.22 *M* (Table 4.4) are 0.27 and 0.54 respectively. These average contents for the two synthesis series in Table 4.4 indicate that Ag is preferentially incorporated into the jarosite structure compared with Na approximately by a factor of two.

4.1.3 Powder XRD analysis and Rietveld refinement

4.1.3.1 Chemical compositions and d-values of main peaks of K-Ag-H_3O, Na-Ag-H_3O and Pb-Ag-H_3O jarosite compounds

XRD data provide information on unit-cell lengths and the degree of cation substitution in crystal structures (Schwertmann and Cornell, 2000), including jarosite subgroup minerals (Desborough et al., 2006). This is because variations in unit-cell dimensions are caused by differences between the ionic radii of elements contained in end-members of the jarosite subgroup (Brophy and Sheridan, 1965). Therefore, unit-cell variations can be used to estimate the elemental ratios in solid solution between end-members, that is, the extent of element substitutions (Desborough et al., 2006; Papike et al., 2006). Peak positions in XRD spectra can be used to determine unit-cell edge lengths (Schwertmann and Cornell, 2000). Structural incorporation of substituting cations in isomorphous minerals may be deduced from shifts in XRD peaks (Schwertmann and Cornell, 2000). Substitution of a smaller cation leads to a smaller unit cell, as indicated by shifts of all peaks towards higher 2θ angles. Theoretically, the unit-cell edge lengths of mixed phases (solid solution) should lie in a straight line between those of two end members, according to Vegard's rule (Schwertmann and Cornell, 2000).

XRD patterns produced from the samples were compared with reference patterns in the Joint Committee for Powder Diffraction Spectrometry (JCPDS) database. The JCPDS patterns were jarosite 10-0443 and (synthetic) 22-0827; hydromiumjarosite (synthetic) 36-0427; natrojarosite 11-0302, 30-1203 and (synthetic) 36-0425; argentojarosite (synthetic) 25-1327 and 41-1398; hydroniumjarosite (synthetic) 21-0932 and 31-0650; and plumbojarosite (natural) 18-0698, (synthetic) 33-0759 and (synthetic) 39-1353. The JCPDS patterns used to identify the presence of contaminant compound Ag_2SO_4 (silver sulphate) were 07-0203 and 27-1403. Cu radiation ($K\alpha_1$ λ = 1.54056 Å) was used to produce the profiles from the samples, which all contained Al peaks from the diffractometer's sample holder; these peaks were at ~ 38.40º 2θ ($K\alpha_1$ d-value ~ 2.34 Å) and ~ 44.60º 2θ ($K\alpha_1$ d-value ~ 2.03 Å) (Anthony et al., 2003).

Jarosite phases were identified in all the synthesised samples using the X'Menu software. These synthetic jarosite phases (see Table 4.5) were all consistent with the cations (K, Na, Pb and/or Ag) that were present in the starting solutions. The XRD spectra of the samples are shown in Appendix E. In some samples the XRD analysis identified peaks of Ag_2SO_4 or $PbSO_4$, indicating the presence of residual solutions that were not removed during washing. These samples were re-washed with 0.5 L 10% ammonium acetate and 1.0 L ultrapure water and then were re-analysed by XRD. Following this extra procedure, the XRD analysis showed that the synthesised samples still contaminated with Ag_2SO_4 were 10D, 20, 24, 38D, 40, 42 and 63, and the samples still contaminated with $PbSO_4$ were 43, 43D and 46D. In addition, an unidentified peak remained in each of JS06, 08 and 48.

Table 4.5: Phases identified by XRD in synthesised samples JS04-107. (Key: j = jarosite)

Sample	K-j	H_3O-K-j	Na-j	Pb-j	Ag-j	H_3O-j	Ag_2SO_4	$PbSO_4$
JS04	x					x		
JS06		x				x		
JS06D	x					x		
JS08		x			x			
JS10	x				x			
JS10D	x				x	x	x	
JS12					x			
JS14			x					
JS16			x		x			
JS18			x		x			
JS20			x		x		x	
JS22	x							
JS24	x				x		x	
JS24D		x			x			
JS26	x				x			
JS28	x				x			
JS30					x			
JS32			x					
JS34			x		x			
JS36			x		x			
JS38			x		x		x	
JS38D			x		x		x	
JS40			x		x		x	
JS42	x					x	x	
JS43				x		x		x
JS43D				x		x		x
JS44				x	x	x		
JS45				x	x	x		
JS46				x	x	x		

JS46D				x	x	x		x
JS47				x	x	x		
JS48				x	x	x		
JS49			x			x		
JS50			x		x	x		
JS51			x		x	x		
JS52			x		x	x		
JS53			x		x	x		
JS54			x		x	x		
JS55	x	x				x		
JS56	x	x				x		
JS57	x	x			x	x		
JS58	x	x			x	x		
JS59	x	x			x	x		
JS60	x	x			x	x		
JS61					x	x		
JS62	x					x		
JS63	x					x	x	
JS64	x					x		
JS65	x				x	x		
JS66					x	x		
JS67			x			x		
JS68			x		x	x		
JS69			x		x	x		
JS70			x		x	x		
JS71					x	x		
JS72					x	x		
JS73	x					x		
JS74	x					x		
JS75	x					x		
JS76	x				x	x		

JS77			x			x		
JS78			x		x	x		
JS79			x		x	x		
JS80			x		x	x		
JS81	x					x		
JS82	x					x		
JS83	x				x	x		
JS84	x				x	x		
JS85			x			x		
JS86			x		x	x		
JS87			x		x	x		
JS88			x		x	x		
JS89	x							
JS90	x					x		
JS91	x					x		
JS92	x					x		
JS93	x				x	x		
JS94	x				x			
JS95					x	x		
JS96			x			x		
JS97			x		x	x		
JS98			x		x	x		
JS99			x		x	x		
JS100			x		x	x		
JS101			x		x	x		
JS102				x	x	x		
JS103					x	x		
JS104				x	x	x		
JS105				x	x	x		
JS106				x	x	x		
JS107				x		x		

XRD peak broadening of synthesised Na-jarosite samples containing < 50% Na indicates inhomogeneity of samples (Basciano and Peterson, 2008). Peak broadening may be removed by grinding the samples and annealing at 140°C in the starting solutions, with two cycles achieving sharp XRD peaks and increasing the *A*-site occupancy of Na-jarosite (Basciano and Peterson, 2008). For this reason, samples JS04-38 (even numbers) were annealed at 140°C in an attempt to produce sharper peaks and increase site occupancy.

A problem that is caused by the use of Cu radiation for the XRD analysis of Fe-bearing minerals such as jarosite is that the X-rays are strongly absorbed, causing loss of X-ray intensity and high backgrounds as a result of fluorescence. This absorbance may be removed by a monochromator (Schwertmann and Cornell, 2000). For this reason, CoKα (λ = 1.78890 Å) or FeKα (λ = 1.93604 Å) X-ray radiation is preferable for Fe-rich phases (Schwertmann and Cornell, 2000). This problem makes identification of Fe-rich phases problematic using Cu radiation. Relatively high background intensities were especially noticeable, for example, in the XRD analyses results of JS24, 26, 28, 30, 43, 44, 49, 55, 60, 63, 72 and 78.

The issue of changes in peak positions with cation substitution relates to mineral identification using JCPDS patterns because these patterns are based on minerals that are not necessarily end-member jarosite subgroup phases. For example, the JCPDS pattern 25-1327 of argentojarosite represents data for synthesized products reported by May et al. (1973), for which the chemical formula is $Ag_{0.89-93}Fe_{2.93-3}(SO_4)_2(OH)_6$, and JCPDS pattern 30-1203 of natrojarosite represents data for synthesised products reported by Dutrizac and Kaiman (1976), for which the chemical formula is $Na_{0.82}Fe_{2.80}(SO_4)_2(OH)_6$. This makes problematical the matching

of standard patterns with peaks in synthesised jarosites of varying chemical compositions containing different proportions of cations. The differences in peak positions of the jarosite compounds in this project are shown in the XRD spectra in Appendix E.

The main peaks of the JCPDS patterns of jarosite (22-0827), natrojarosite (30-1203), argentojarosite (25-1327), hydronium jarosite (31-0650) and plumbojarosite (18-0698) are shown in Table 4.6. The strongest-intensity peaks of these JCPDS patterns are closely comparable with the main peaks of the K-Ag-H_3O, Na-Ag-H_3O and Pb-Ag-H_3O jarosite compounds synthesised in this project, which are also listed in Table 4.6. The maximum-intensity peaks (100) are consistent with those of the JCPDS patterns, except for a few of the Na-Ag-H_3O and Pb-Ag-H_3O jarosite compounds in which these peaks are consistent with the pattern for hydronium jarosite and indicate the high H_3O content in the samples. Some of the sample series show changing highest-intensity d-value peaks in accordance with the JCPDS patterns as the proportion of the different cations occupying the *A* site changes. For example, the K-Ag-H_3O-jarosite series of samples 04, 06, 08, 10 and 12, which has declining K content and increasing Ag content through the series, has the highest-intensity d-value peaks of 3.081, 3.076, 3.073, 3.072 and 3.064 Å, respectively. These decreasing d-values are consistent with the changing *A*-site occupation as K^+ content decreases and Ag^+ content increases, according to the equivalent peaks in the JCPDS patterns of 3.08 Å in jarosite and 3.062 Å in argentojarosite.

The Na-Ag-H_3O-jarosite series show no consistent trends of main peaks (Table 4.6). Two of the seven sample series show main peaks declining from 3.067 and 3.083 Å for Na-H_3O-jarosite products 49 and 67, respectively, to 3.064 and

3.076 Å for Ag-H_3O-jarosite products 61 and 66, respectively; the relatively high d-values of 3.083 and 3.076 Å for samples 67 and 66, respectively, indicate the effect of the highest-intensity peak of 3.08 Å of hydronium jarosite, as the compounds in these series are relatively high in hydronium. Additionally, another of the Na-H_3O-jarosite series shows the highest-intensity peaks increasing from 3.067 Å for Na-H_3O jarosite product 85 to 3.085 Å for Ag-H_3O jarosite product 71, again suggesting the effect of H_3O-jarosite. Table 4.6 also includes Na-H_3O-jarosite samples 14, 32 and 77, the strongest peaks of which are 5.082, 5.066 and 5.075 Å, respectively. These are consistent with the strongest peak (5.10 Å) of hydronium jarosite (31-0650), rather than the strongest peak (3.06 Å) of natrojarosite (30-1203), and indicate the high proportion of H_3O in the samples shown by EMPA and ICP-AES. A similar effect is seen in Pb-H_3O-jarosite samples 43 and 43D, whose strongest peaks are 5.11 and 5.101 Å, respectively, rather than 3.066 Å as in plumbojarosite JCPDS pattern 18-0698.

Table 4.6: XRD powder patterns: main peaks[1] (*d*-values in Å) of samples JS04-107 and chemical compositions (site occupancies).

No.	**K/Na/Pb**	**Ag**	**H_3O**	**Fe**	**Main peaks**						
22-0827	K				3.08 (100)	3.11 (75)	5.09 (70)	5.93 (45)	1.977 (45)	1.825 (45)	3.65 (40)
31-0650			H_3O		5.10 (100)	3.13 (90)	3.09 (65)	1.839 (30)	1.990 (20)	5.67 (18)	5.97 (16)
25-1327		Ag			3.062 (100)	5.98 (50)	3.681 (30)	2.524 (30)	2.218 (30)	1.979 (25)	3.127 (20)
30-1203	Na				3.06 (100)	3.12 (90)	5.06 (90)	2.24 (50)	1.98 (50)	1.83 (50)	5.57 (40)
18-0698	Pb				3.066 (100)	5.933 (95)	1.829 (70)	3.114 (45)	1.976 (45)	6.232 (35)	3.657 (30)
K-Ag-H_3O jarosite compounds											
JS04	0.65	0	0.35	2.55	3.081 (100)	5.095 (63)	3.122 (57)	1.983 (22)	2.276 (20)	5.951 (18)	5.688 (18)
JS06	0.5	0.18	0.32	2.88	3.076 (100)	5.085 (47)	3.13 (43)	5.969 (30)	1.984 (23)	1.834 (19)	3.669 (16)
JS06D	0.52	0.15	0.33	2.56	3.086 (100)	3.132 (52)	5.106 (45)	5.981 (29)	2.268 (23)	1.987 (20)	3.682 (20)
JS08	0.41	0.3	0.29	2.72	3.073 (100)	5.074 (47)	3.123 (44)	5.941 (37)	1.984 (24)	1.836 (22)	3.668 (22)
JS10	0.25	0.41	0.34	2.72	3.072 (100)	5.955 (36)	3.128 (35)	1.984 (28)	5.075 (25)	1.839 (17)	2.239 (16)
JS10D	0.27	0.44	0.29	2.71	3.088 (100)	3.15 (38)	6.044 (32)	6.003 (30)	5.13 (23)	3.705 (23)	2.247 (22)

JS22	0.64	0	0.36	2.59	3.09 (100)	5.113 (76)	3.13 (60)	2.283 (24)	1.986 (22)	1.836 (21)	5.973 (20)
JS24	0.53	0.15	0.32	2.62	3.069 (100)	3.078 (67)	5.087 (38)	3.12 (37)	2.254 (35)	2.824 (18)	1.83 (17)
JS24D	0.52	0.14	0.34	2.59	3.076 (100)	3.123 (54)	5.079 (46)	1.983 (30)	5.947 (25)	2.264 (25)	1.836 (19)
JS26	0.44	0.25	0.31	2.74	3.07 (100)	3.119 (40)	5.062 (35)	2.249 (35)	2.256 (32)	5.919 (24)	1.981 (24)
JS28	0.27	0.56	0.17	2.57	3.045 (100)	5.876 (52)	5.004 (34)	1.435 (31)	2.774 (26)	1.974 (24)	2.227 (23)
JS40	0.26	0.04	0.7	2.87	3.183 (100)	3.085 (96)	2.882 (75)	2.652 (66)	5.104 (56)	3.128 (54)	1.985 (29)
JS55	0.43	0	0.57	2.75	3.081 (100)	5.106 (70)	3.121 (54)	5.738 (28)	2.289 (26)	1.829 (24)	1.983 (23)
JS56	0.7	0.16	0.14	2.33	3.088 (100)	5.117 (56)	3.128 (43)	5.979 (29)	1.986 (23)	2.277 (22)	2.551 (19)
JS57	0.47	0.23	0.3	2.8	3.08 (100)	5.097 (38)	3.126 (38)	5.979 (32)	2.268 (25)	1.984 (24)	2.544 (17)
JS58	0.38	0.34	0.28	2.82	3.102 (100)	3.149 (32)	6.058 (31)	2.27 (28)	5.142 (27)	1.84 (23)	3.707 (21)
JS59	0.29	0.45	0.26	2.83	3.083 (100)	5.993 (49)	3.135 (36)	1.986 (26)	5.106 (23)	2.542 (21)	2.253 (21)
JS60	0.16	0.68	0.16	2.96	3.07 (100)	5.959 (65)	3.128 (34)	2.781 (33)	2.227 (28)	1.983 (25)	3.68 (24)
JS62	0.61	0	0.39	2.87	3.093 (100)	5.129 (68)	3.13 (62)	1.987 (24)	2.291 (23)	5.758 (22)	5.996 (21)
JS63	0.49	0.21	0.3	2.46	3.09 (100)	5.119 (47)	3.13 (42)	5.987 (36)	1.987 (25)	3.68 (16)	5.738 (14)
JS64	0.37	0.36	0.27	2.76	3.071 (100)	5.087 (36)	5.943 (33)	5.67 (24)	3.123 (24)	1.982 (23)	2.819 (21)
JS65	0.15	0.37	0.48	2.98	3.082 (100)	3.14 (57)	5.991 (36)	5.106 (34)	1.987 (26)	1.841 (21)	3.691 (20)
JS73	0.78	0	0.22	2.4	3.092 (100)	3.137 (48)	5.126 (47)	2.273 (25)	1.988 (25)	1.837 (24)	6.007 (24)
JS74	0.68	0.06	0.26	2.52	3.078 (100)	5.092 (49)	3.121 (46)	1.982 (33)	2.267 (31)	5.955 (20)	1.832 (19)
JS75	0.64	0.14	0.22	2.49	3.082 (100)	5.101 (41)	3.127 (39)	2.265 (28)	5.973 (23)	1.983 (21)	1.834 (19)
JS76	0.37	0.26	0.37	2.33	3.078 (100)	5.10 (89)	3.14 (77)	5.613 (30)	1.84 (28)	2.236 (28)	1.986 (27)
JS81	0.6	0	0.4	2.81	3.086 (100)	3.131 (48)	5.111 (39)	5.981 (37)	1.986 (23)	1.837 (20)	2.268 (19)
JS82	0.44	0.24	0.32	2.87	3.078 (100)	5.973 (54)	3.133 (41)	3.682 (29)	1.984 (26)	5.10 (23)	1.839 (21)
JS83	0.29	0.46	0.25	2.91	3.081 (100)	6.005 (63)	3.142 (34)	3.697 (25)	1.987 (23)	2.24 (20)	1.843 (19)
JS84	0.09	0.68	0.23	2.94	3.092 (100)	6.042 (42)	3.157 (31)	1.994 (29)	2.248 (26)	2.55 (22)	1.85 (22)
JS89	0.73	0	0.27	2.49	3.081 (100)	3.121 (61)	5.091 (49)	1.832 (33)	2.272 (31)	1.983 (27)	5.955 (20)
JS90	0.69	0.05	0.26	2.55	3.088 (100)	3.133 (57)	5.119 (46)	1.836 (27)	1.987 (27)	5.989 (25)	3.684 (20)
JS91	0.65	0.1	0.25	2.68	3.084 (100)	3.127 (63)	5.11 (58)	1.984 (28)	1.834 (26)	2.271 (24)	5.971 (23)
JS92	0.6	0.15	0.25	2.61	3.082 (100)	3.13 (45)	5.104 (45)	1.985 (31)	1.836 (28)	2.264 (26)	5.973 (26)
JS93	0.43	0.35	0.22	2.72	3.078 (100)	3.13 (44)	5.975 (37)	5.092 (26)	1.984 (26)	3.678 (19)	1.837 (19)
JS94	0.28	0.52	0.2	2.71	3.075 (100)	5.977 (41)	3.133 (30)	1.984 (25)	3.682 (24)	5.085 (20)	1.838 (19)
Na-Ag-H3O jarosite compounds											
JS14	0.57	0	0.43	2.91	5.082 (100)	3.075 (96)	3.134 (88)	5.601 (34)	1.839 (32)	1.985 (25)	2.238 (24)

JS16	0.33	0.37	0.3	2.92	3.064 (100)	3.125 (51)	5.055 (42)	5.939 (32)	1.981 (22)	3.678 (19)	1.838 (18)
JS18	0.1	0.63	0.27	2.72	3.065 (100)	5.949 (47)	3.128 (33)	1.983 (27)	2.222 (26)	1.84 (24)	3.678 (22)
JS20	0.06	0.71	0.23	2.71	3.064 (100)	5.951 (47)	3.13 (29)	2.223 (25)	3.679 (22)	1.982 (21)	2.527 (19)
JS32	0.55	0	0.45	2.87	5.066 (100)	3.127 (97)	3.069 (91)	1.837 (32)	5.58 (31)	2.24 (22)	1.984 (21)
JS34	0.12	0.21	0.67	2.97	3.067 (100)	5.957 (38)	3.131 (34)	5.062 (26)	3.681 (22)	1.983 (22)	2.225 (18)
JS36	0.05	0.31	0.64	2.83	3.071 (100)	5.975 (54)	3.138 (28)	2.227 (27)	3.692 (24)	1.986 (21)	1.843 (21)
JS38	0.04	0.61	0.35	2.59	3.066 (100)	5.957 (48)	2.223 (25)	3.133 (25)	3.684 (24)	1.983 (21)	1.841 (19)
JS38D	0.07	0.65	0.28	2.68	3.067 (100)	5.963 (43)	1.984 (26)	3.684 (25)	3.134 (25)	2.223 (22)	1.841 (21)
JS42	0.09	0.7	0.21	2.63	3.068 (100)	5.967 (49)	2.224 (28)	3.135 (26)	3.687 (24)	1.984 (23)	2.529 (18)
JS49	0.47	0	0.53	2.64	3.067 (100)	3.122 (95)	5.059 (91)	5.597 (32)	1.835 (27)	1.982 (20)	5.943 (18)
JS50	0.33	0.25	0.42	3.04	3.071 (100)	5.078 (79)	3.13 (64)	5.613 (34)	5.965 (30)	1.983 (22)	2.53 (20)
JS51	0.2	0.47	0.33	2.9	3.074 (100)	3.132 (43)	5.084 (39)	5.989 (38)	1.985 (30)	2.24 (14)	2.778 (14)
JS52	0.09	0.67	0.24	2.93	3.069 (100)	5.967 (48)	3.135 (25)	1.984 (20)	2.773 (19)	2.53 (19)	2.23 (19)
JS53	0.04	0.77	0.19	2.98	3.066 (100)	5.963 (52)	2.227 (34)	3.133 (26)	1.983 (26)	2.777 (21)	3.683 (20)
JS54	0.01	0.83	0.16	2.98	3.064 (100)	5.943 (48)	2.222 (33)	3.126 (24)	2.768 (23)	3.678 (22)	2.526 (21)
JS67	0.65	0	0.35	2.91	3.083 (100)	5.108 (80)	3.142 (79)	1.988 (25)	5.64 (25)	6.017 (23)	1.842 (23)
JS68	0.57	0.09	0.34	2.74	3.076 (100)	3.137 (53)	5.993 (43)	5.097 (42)	1.986 (24)	1.838 (18)	2.537 (16)
JS69	0.4	0.19	0.41	3.16	3.078 (100)	5.10 (88)	3.135 (85)	5.989 (36)	5.64 (29)	1.986 (26)	1.839 (26)
JS70	0.25	0.33	0.42	2.68	3.083 (100)	6.023 (51)	3.147 (25)	1.989 (23)	2.234 (22)	3.708 (20)	1.844 (19)
JS77	0.67	0	0.33	2.86	5.075 (100)	3.131 (95)	3.069 (88)	5.589 (40)	1.983 (29)	1.839 (19)	2.236 (17)
JS78	0.11	0.42	0.47	2.88	3.094 (100)	5.13 (65)	3.128 (51)	5.76 (33)	2.291 (28)	5.987 (21)	1.986 (21)
JS79	0.06	0.48	0.46	2.78	3.067 (100)	5.971 (45)	2.221 (33)	1.983 (28)	3.686 (25)	1.84 (21)	2.766 (18)
JS80	0.03	0.82	0.15	3.02	3.073 (100)	5.993 (42)	2.225 (36)	3.694 (26)	3.14 (24)	1.986 (22)	1.841 (21)
JS85	0.57	0	0.43	2.98	3.067 (100)	3.128 (87)	5.082 (87)	1.834 (26)	5.973 (23)	1.983 (23)	5.613 (21)
JS86	0.29	0.35	0.36	2.73	3.08 (100)	6.015 (46)	3.143 (34)	2.235 (28)	5.104 (24)	1.987 (22)	2.538 (20)
JS87	0.17	0.5	0.33	2.53	3.075 (100)	5.985 (38)	5.091 (32)	3.135 (28)	2.535 (20)	3.691 (17)	1.985 (18)
JS88	0.11	0.56	0.33	2.97	3.081 (100)	6.005 (51)	3.143 (38)	5.10 (27)	1.987 (26)	2.238 (22)	2.537 (19)
JS96	0.68	0	0.32	3.01	3.071 (100)	3.128 (93)	5.077 (80)	5.592 (33)	1.836 (31)	1.981 (27)	2.238 (27)
JS97	0.37	0.41	0.22	2.96	3.068 (100)	3.128 (50)	5.069 (43)	5.965 (33)	3.682 (24)	1.983 (23)	1.839 (17)
JS98	0.14	0.68	0.18	2.86	3.068 (100)	5.969 (48)	3.133 (32)	1.983 (29)	2.224 (24)	3.684 (23)	1.84 (23)
JS99	0.04	0.8	0.16	2.86	3.066 (100)	5.969 (47)	3.685 (27)	1.983 (26)	2.223 (22)	3.133 (22)	1.84 (21)
JS100	0.02	0.81	0.17	2.84	3.066 (100)	5.971 (54)	3.683 (26)	3.133 (25)	1.983 (24)	2.222 (24)	1.84 (20)
JS101	0.01	0.83	0.16	2.84	3.07 (100)	5.977 (54)	2.223 (26)	3.691 (26)	3.137 (25)	1.984 (24)	1.841 (23)

Pb-Ag-H3O jarosite compounds

JS43	0.179	0	0.821	3	5.11 (100)	3.09 (86)	3.134 (70)	5.969 (23)	1.99 (23)	1.834 (23)	2.273 (21)
JS43D	0.168	0	0.832	3.15	5.101 (100)	3.086 (65)	3.131 (45)	3.068 (38)	5.957 (23)	5.679 (20)	1.839 (19)
JS44	0.081	0.281	0.638	3.01	3.076 (100)	5.122 (65)	3.139 (61)	3.09 (61)	5.983 (51)	3.131 (50)	1.986 (27)
JS45	0.082	0.502	0.416	2.97	3.071 (100)	5.969 (59)	3.134 (35)	5.092 (21)	3.687 (21)	1.985 (21)	1.84 (20)
JS46	0.046	0.701	0.253	3	3.066 (100)	5.951 (52)	2.772 (25)	3.678 (23)	3.13 (22)	2.529 (21)	2.246 (18)
JS47	0.021	0.766	0.213	2.98	3.074 (100)	5.983 (58)	2.23 (28)	2.776 (25)	3.694 (21)	2.533 (20)	1.843 (19)
JS48	0.021	0.765	0.214	3	3.066 (100)	5.957 (60)	2.223 (25)	3.681 (23)	3.13 (22)	2.771 (20)	2.53 (19)
JS102	0.006	0.826	0.168	2.8	3.067 (100)	5.979 (50)	3.059 (48)	2.222 (24)	1.841 (24)	3.689 (23)	1.984 (23)
JS103	0.028	0.822	0.15	2.89	3.068 (100)	5.971 (49)	2.223 (38)	3.686 (23)	2.768 (22)	3.134 (19)	1.84 (19)
JS104	0.02	0.853	0.127	2.92	3.069 (100)	5.977 (55)	3.687 (28)	1.984 (24)	3.135 (23)	1.84 (21)	2.53 (21)
JS105	0.063	0.824	0.113	2.85	3.072 (100)	5.991 (57)	3.694 (27)	1.986 (24)	2.225 (23)	3.137 (22)	1.841 (20)
JS106	0.036	0.799	0.165	2.78	3.068 (100)	5.973 (52)	2.223 (26)	3.687 (24)	1.984 (23)	3.135 (22)	1.84 (21)
JS107	0.258	0	0.742	2.91	3.087 (100)	5.991 (43)	3.132 (43)	1.987 (30)	5.111 (30)	1.837 (26)	2.549 (25)
Ag-H3O jarosite compounds											
JS12	0	0.78	0.22	2.71	3.064 (100)	5.943 (50)	3.129 (26)	2.223 (24)	1.983 (22)	1.84 (21)	2.527 (19)
JS30	0	0.63	0.37	2.62	3.061 (100)	5.941 (47)	2.224 (41)	2.768 (31)	3.678 (26)	3.13 (21)	1.982 (20)
JS61	0	0.85	0.15	2.93	3.064 (100)	5.949 (60)	3.677 (24)	1.981 (24)	1.838 (22)	3.13 (22)	2.225 (21)
JS66	0	0.44	0.56	3.03	3.076 (100)	3.142 (69)	5.133 (57)	5.997 (51)	3.097 (49)	5.716 (37)	1.988 (31)
JS71	0	0.76	0.24	2.98	3.085 (100)	6.033 (54)	3.149 (28)	2.237 (23)	3.708 (21)	1.99 (20)	2.541 (18)
JS72	0	0.63	0.37	2.84	3.097 (100)	5.141 (58)	3.14 (57)	1.989 (28)	2.282 (24)	1.837 (24)	6.017 (20)
JS95	0	0.85	0.15	2.86	3.073 (100)	5.991 (65)	2.224 (28)	3.694 (28)	1.842 (25)	3.141 (24)	1.986 (23)

Note: 1 Peaks at 2.34 and 2.03 removed because these are Al peaks of the diffractometer holder.

Differences between the XRD peak positions of the 006 (*hkl*) reflections (2θ degree angles) of jarosite, natrojarosite and mixtures of both end-members shown on X-ray diffractograms have been compared as these result from the respective *c*-axis dimensions of the unit cells (Desborough et al., 2010), as do the 003 reflections. The different positions (*d* values) of the 003 and 006 reflections, using Cu radiation, of synthesised K-Ag-H_3O- and Na-Ag-H_3O-jarosite compounds are listed in Table 4.7 and those of the Pb-Ag-H_3O-jarosite samples are listed in Table 4.8. These *d* values provide indicators of the variations in *c*-axis parameters of these synthesised jarosite

products. In theory, these *c*-axis parameters should vary according to the proportions of cations with different ionic radii occupying the *A* site. In 12-fold coordination, the ionic radius of Na^+ is 1.39 Å and K^+ is 1.64 Å (Shannon, 1976), Ag^+ is 1.48 Å (Dutrizac and Jambor, 2000) and H_3O^+ is 1.52 Å (Basciano and Peterson, 2008). However, a crystal structure study of the argentojarosite end-member suggests that the coordination of Ag^+ is between six-fold and 12-fold (Groat *et al.*, 2003). In 12-fold coordination in end-member argentojarosite, Ag^+ has a predicted ionic radius of 1.48-1.56 Å; however, the crystal structure study suggests Ag^+ in the *A* site of argentojarosite has an ionic radius of 1.35-1.36 Å (Groat et al., 2003). This experimental radius for Ag^+ indicates the cation is in nine-fold coordination, according to the study; by comparison, Ag^+ in eight-fold coordination has an effective ionic radius of 1.28 Å (Shannon, 1976).

Tables 4.7 and 4.8 also list the positions of the *hkl* 003 and 006 reflections in the JCPDS patterns of jarosite (22-0827), natrojarosite (30-1203), argentojarosite (25-1327), hydronium jarosite (31-0650) and plumbojarosite (18-0698). The *d* values of the 003 and 006 reflections in the JCPDS pattern for argentojarosite (25-1327) are smaller than the values for natrojarosite (30-1203), indicating the Ag^+ cation is smaller than the Na^+ cation. The *d* values of the patterns are closely comparable with the *d* values of the K-, Na-, Pb- and Ag-jarosite analogues synthesised in this study. In Table 4.7, the positions of the 003 and 006 reflections in samples 04, 06, 08, 10 and 12 (a series of K-Ag jarosite analogues synthesised at 97°C), for example, show generally declining *d*-spacing values from 5.688 Å and 2.847 Å, respectively, for the jarosite product (04) containing K-H_3O only to 5.538 Å and 2.763 Å, respectively, for the jarosite product (12) containing Ag-H_3O only. These results are consistent with the smaller radius of the Ag^+ cation compared with K^+. The other series of K-

Ag-H_3O-jarosite analogues – samples 22-30 (synthesised at 97°C); 55-61, 62-66, and 71 and 81-84 (synthesised at 140°C); and 72-76 and 89-95 (synthesised at 22°C) – show similar generally declining trends of 003 and 006 reflection *d*-spacing values. However, the sample showing a significant deviation from this trend is 72, a jarosite product containing Ag-H_3O only, which has anomalously large *d*-spacing values for 003 and 006 reflections of 5.74 Å and 2.855 Å, respectively.

Table 4.7. XRD peaks (*d*-values in Å) of K-Ag and Na-Ag synthetic samples. Peak shifts of c parameters should be most pronounced, indicated by *hkl* indices of 003 and 006.

Number	**Type**	***hkl* 003**	***hkl* 006**	**Number**	**Type**	***hkl* 003**	***hkl* 006**
22-0827	K	5.72	2.861				
31-0650	H3O	5.67	2.835	31-0650	H3O	5.67	2.835
			2.783	30-1203	Na	5.57	2.783
25-1327	Ag	5.55	2.763	25-1327	Ag	5.55	2.763
JS04	K-H3O	5.688	2.847	JS14	Na-H3O	5.601	2.793
JS06	K-Ag-H3O	5.661	2.828	JS16	Na-Ag-H3O	5.559	2.784
JS06D	K-Ag-H3O	5.674	2.83	JS18	Na-Ag-H3O	5.545	2.766
JS08	K-Ag-H3O	5.649	2.82	JS20	Na-Ag-H3O	5.55	2.766
JS10	K-Ag-H3O	5.61	2.788	JS12	Ag-H3O	5.538	2.763
JS10D	K-Ag-H3O	5.663	2.815				
JS12	Ag-H3O	5.538	2.763				
JS22	K-H3O	5.721	2.853	JS32	Na-H3O	5.58	2.791
JS24	K-Ag-H3O	5.629	2.824	JS34	Na-Ag-H3O	5.576	2.773
JS24D	K-Ag-H3O	5.652	2.825	JS36	Na-Ag-H3O	5.568	2.778
JS26	K-Ag-H3O	5.606	2.809	JS38	Na-Ag-H3O	5.538	2.772
JS28	K-Ag-H3O	5.519	2.774	JS38D	Na-Ag-H3O	5.557	2.773
JS30	Ag-H3O	5.523	2.768	JS30	Ag-H3O	5.523	2.768
JS40	K-Ag-H3O	5.685	2.838	JS42	Na-Ag-H3O	5.555	2.774
JS55	K-H3O	5.738	2.86	JS49	Na-H3O	5.597	2.801

JS56	K-Ag-H3O	5.723	2.854	JS50	Na-Ag-H3O	5.613	2.8
JS57	K-Ag-H3O	5.679	2.835	JS51	Na-Ag-H3O	5.603	2.778
JS58	K-Ag-H3O	5.716	2.834	JS52	Na-Ag-H3O	5.564	2.773
JS59	K-Ag-H3O	5.636	2.81	JS53	Na-Ag-H3O	5.559	2.777
JS60	K-Ag-H3O	5.589	2.781	JS54	Na-Ag-H3O	5.531	2.768
JS61	Ag-H3O	5.543	2.767	JS61	Ag-H3O	5.543	2.767
JS62D	K-H3O	5.758	2.874	JS67	Na-H3O	5.64	2.798
JS63D	K-Ag-H3O	5.738	2.856	JS68	Na-Ag-H3O	5.634	2.807
JS64D	K-Ag-H3O	5.67	2.819	JS69D	Na-Ag-H3O	5.64	2.807
JS65D	K-Ag-H3O	5.71	2.841	JS70	Na-Ag-H3O	5.608	2.788
JS66D	Ag-H3O	5.596	2.777	JS66D	Ag-H3O	5.596	2.777
JS73	K-H3O	5.712	2.842	JS77	Na-H3O	5.589	2.785
JS74	K-Ag-H3O	5.676	2.831	JS78	Na-Ag-H3O	5.76	2.868
JS75	K-Ag-H3O	5.678	2.83	JS79	Na-Ag-H3O	5.549	2.766
JS76	K-Ag-H3O	5.613	2.789	JS80	Na-Ag-H3O	5.566	2.773
JS72	Ag-H3O	5.74	2.855	JS72	Ag-H_3O	5.74	2.855
JS81	K-H3O	5.716	2.835	JS85	Na-H3O	5.613	2.787
JS82	K-Ag-H3O	5.622	2.813	JS86	Na-Ag-H3O	5.62	2.789
JS83	K-Ag-H3O	5.61	2.79	JS87	Na-Ag-H3O	5.613	2.782
JS84D	K-Ag-H3O	5.665	2.807	JS88D	Na-Ag-H3O	5.617	2.79
JS71D	Ag-H3O	5.627	2.792	JS71D	Ag-H3O	5.627	2.792
JS89	K-H3O	5.6848	2.8404	JS96	Na-H3O	5.592	2.7899
JS90	K-Ag-H3O	5.7176	2.8408	JS97	Na-Ag-H3O	5.5797	2.7722
JS91	K-Ag-H3O	5.6993	2.8417	JS98	Na-Ag-H3O	5.5519	2.7714
JS92	K-Ag-H3O	5.6721	2.8281	JS99	Na-Ag-H3O	5.5537	2.7664
JS93	K-Ag-H3O	5.6416	2.8108	JS100	Na-Ag-H3O	5.5502	2.7659
JS94	K-Ag-H3O	5.6061	2.7818	JS101	Na-Ag-H3O	5.571	2.7689
JS95	Ag-H3O	5.5623	2.7697	JS95	Ag-H3O	5.5623	2.7697

The Na-Ag-H_3O-jarosite analogue series 12-20 (synthesised at 97°C) shows *d*-values of 003 and 006 reflections (see Table 4.7) decreasing from 5.601 Å and 2.793 Å, respectively, in the jarosite compound with Na-H_3O only in the *A* site to

5.538 Å and 2.763 Å, respectively, in the Ag-H_3O product. These results are consistent with the radius of the Ag^+ cation being smaller than that of Na^+ and, therefore, Ag+ being in 9-fold coordination. However, the *d*-values of the 003 and 006 reflections in the JCPDS patterns of natrojarosite and argentojarosite are of similar respective magnitudes (Table 4.7); therefore, the decrease in *d*-values may be the result of the higher H_3O content of the Na-H_3O compound than the Ag-H_3O compound. Additionally, one intermediate product (sample 20) has slightly high *d*-values relative to the previous intermediate product (sample 18); these may be explained by the EMPA compositional results, which show vacancies (Fe = 2.92) in the *B* site of sample 18, which for charge balance may cause protonation of four Fe-OH bonds for each vacancy and result in deprotonation of H_3O and a vacancy in the *A* site (Basciano and Peterson, 2010). (The assumption throughout this project is that Fe^{3+} only occupies the *B* site of the products and the cations K^+, Na^+, Pb^+, Ag^+ and/or H_3O^+ only occupy the *A* site of the products.) The Na-Ag-H_3O jarosite product series 30-38/38D (synthesised at 97°C) also shows a generally declining trend of *d*-values for 003 and 006 reflections from 5.58 Å and 2.791 Å, respectively, in the Na-H_3O product to 5.523 Å and 2.768 Å, respectively, in the Ag-H_3O product; however, one intermediate product (sample 34) has a relatively low 006 d-value of 2.773 Å. The results of both these series are generally consistent with the Ag^+ cation having a smaller radius than Na^+ and, therefore, being likely to be in 9-fold coordination.

The Na-Ag-H_3O jarosite analogue series 49-54 and 61 (synthesised at 140°C) shows a generally decreasing trend of *d*-values from the Na-H_3O product to the Ag-H_3O product. However, the Na-H_3O product's (sample 49) 003 d-value of 5.597 Å increases to 5.613 Å in the first intermediate product in the series, which may be

explained by the low Fe occupancy (2.33) and consequent reduced H_3O content of sample 49. There is also an increase from the d-value of 5.531 Å of the final Na-Ag-H_3O intermediate product in the series (sample 54) to 5.543 Å in the Ag-H_3O product, which also may be explained by the low Fe occupancy (2.86) and consequent reduced H_3O content of sample 54. The Na-Ag jarosite analogues in sample series 66-70 (synthesised at 140°C) have *d*-values for 003 and 006 reflections that decrease from 5.64 Å and 2.798 Å, respectively, in the product with Na-H_3O only in the *A* site to 5.596 Å and 2.777 Å, respectively, in the product with Ag-H_3O only in the *A* site. These results also indicate the Ag^+ cation has a smaller radius than Na^+; however, one intermediate Na-Ag-H_3O jarosite product (sample 69) in the series has a relatively high 003 *d*-value of 5.64 Å and two intermediate products (samples 68 and 69) have high 006 *d*-values of 2.807 Å, so provide contradictory evidence on the cation sizes. However, EMPA compositional data show sample 69 has a relatively low Na content (0.28) and high H_3O content (0.51), which may explain the high 003 and 006 *d*-values because of the relatively large size of the hydronium cation; the compositional data do not provide an explanation for the high 006 *d*-value of sample 68, even taking into account the assumed H_3O content and the Fe vacancies in the *B* site.

The Na-Ag-H_3O-jarosite analogues in sample series 71 and 85-88 (synthesised at 140°C) show a generally increasing trend of *d*-values for 003 and 006 reflections from 5.613 Å and 2.787 Å, respectively, in the product with Na-H_3O only in the *A* site to 5.627 Å and 2.792 Å, respectively, in the product with Ag-H_3O only in the *A* site, so indicate the Ag^+ cation is larger than the Na^+ cation and is in 12-fold coordination. However, the 003 *d*-value of one intermediate product (sample 86) is relatively high (5.62 Å) and the 006 *d*-value of another intermediate product (sample

87) is relatively low (2.782 Å). In the Na-Ag-H_3O jarosite analogue series 72 and 77-80 (synthesised at 22°C), the 003 and 006 *d*-values increase from 5.589 Å and 2.785 Å, respectively, in the Na-H_3O product to 5.74 Å and 2.855 Å, respectively, in the Ag-H_3O product; however, the intermediate Na-Ag-H_3O products in the series do not show a clear trend of *d*-values. This provides contradictory evidence from the *d*-values for 003 and 006 peaks on the respective sizes of the ionic radii of the Na and Ag cations and, therefore, whether Ag is in 9-fold or 12-fold coordination. In the Na-Ag-H_3O-jarosite series JS95-101 (synthesised at 22°C), the 003 and 006 *d*-values decrease from 5.592 Å and 2.7899 Å, respectively, in the Na-H_3O product to 5.5623 Å and 2.7697 Å, respectively, in the Ag-H_3O product, which is consistent with the reported *d*-values of the 003 and 006 reflections in the JCPDS patterns for natrojarosite and argentojarosite. However, there is some variation within this overall trend. In the intermediate compounds of the series, the 003 reflection's *d*-value increases from 5.5519 Å for JS98 to 5.5537 Å for JS99, but then declines again to 5.5502 Å for JS100; however, the *d*-value then increases to 5.571 Å for JS101. In

Table 4.8. XRD *hkl* 003 and 006 peaks (*d*-values in Å) of Pb-Ag JS samples. Peak shifts of *c* parameters should be most pronounced, indicated by *hkl* indices of 003 and 006 peaks

Number	**Type**	***hkl* 003**	***hkl* 006**	**Number**	**Type**	***hkl* 003**	***hkl* 006**
31-0650	H_3O	5.67	2.835	31-0650	H_3O	5.67	2.835
25-1327	Ag	5.55	2.763	25-1327	Ag	5.55	2.763
18-0698	Pb	11.3	2.812	18-0698	Pb	11.3	2.812
	Pb	5.64	2.823		Pb	5.64	2.823
JS43	$Pb_{0.18}H_3O_{0.82}$	5.69	2.84	JS102	$Pb_{0.01}Ag_{0.83}H_3O_{0.16}$	5.5641	2.7693
JS43D	$Pb_{0.17}H_3O_{0.83}$	5.679	2.838	JS103	$Pb_{0.03}Ag_{0.82}H_3O_{0.15}$	5.5763	2.7684
JS44	$Pb_{0.08}Ag_{0.28}H_3O_{0.64}$	5.707	2.836	JS104	$Pb_{0.02}Ag_{0.85}H_3O_{0.13}$	n.d.	2.7697
JS45	$Pb_{0.08}Ag_{0.50}H_3O_{0.42}$	5.64	2.807	JS105	$Pb_{0.06}Ag_{0.82}H_3O_{0.12}$	5.578	2.7705

JS46	$Pb_{0.05}Ag_{0.70}H_3O_{0.25}$	5.545	2.772	JS106	$Pb_{0.04}Ag_{0.80}H_3O_{0.16}$	n.d.	2.7689
JS46D	$Pb_{0.04}Ag_{0.58}H_3O_{0.38}$	5.608	2.768	JS107	$Pb_{0.26}H_3O_{0.74}$	5.7011	2.8408
JS47	$Pb_{0.02}Ag_{0.77}H_3O_{0.21}$	5.578	2.776	JS95	$Ag_{0.86}H_3O0.14$	5.5623	2.7697
JS48	$Pb_{0.02}Ag_{0.77}H_3O_{0.21}$	5.554	2.771				
JS61	$Ag_{0.86}H_3O_{0.14}$	5.543	2.767				

addition, the d-value for the 006 reflection increases from 2.7659 Å for JS100 to 2.7689 Å for JS101 and 2.7697 Å for JS95. The reasons for these variations are not clear because they cannot be explained by the chemical compositional data.

The *d*-values for the 003 and 006 reflections of the Pb-Ag-H_3O-jarosite compounds in series JS43-48 & 61 and JS95 & 102-107 do not indicate the reported doubled *c*-axis dimension of plumbojarosite (Hawthorne et al., 2000; Basciano and Peterson, 2010), the doubled size represented by the 003 *d*-value of 11.3 Å in JCPDS pattern 18-0698 (see Table 4.8); however, the *d*-values for the 003 and 006 reflections of the synthesised Pb-Ag-H_3O compounds are consistent with their low Pb contents and high H_3O contents. For samples 43 and 44, the *d*-value results are consistent with H_3O^+ being the dominant *A*-site cation in the chemical compositions and the JCPDS patterns in Table 4.8, with H_3O-jarosite having a larger *d*-value for the 003 reflection than Ag-jarosite and Pb-jarosite; the results are also consistent with the larger ionic radius of H_3O^+ of 1.52 Å in 12-fold coordination compared with 1.49 Å for Pb^{2+} (Shannon, 1976) and 1.48 Å for Ag^+. For sample 45, the 003 *d*-value is consistent with the chemical composition of Pb^{2+} plus H_3O^+ being equal to Ag^+; and for samples 46-48 and 61 the results are consistent with Ag^+ being the dominant cation. In samples 95 and 102-106, Ag^+ is the dominant cation in the chemical compositions and the 003 and 006 d-values are similar; however, in Pb-H_3O-jarosite sample 107, these d-values increase, which is consistent with the JCPDS patterns.

Powder X-ray diffraction analysis of the synthesized samples was also carried out using a PANalytical X'Pert Pro diffractometer and Co radiation ($K\alpha_1$ λ = 1.78897 Å), which, as noted above, is more suitable for Fe-bearing minerals than Cu radiation. X'Pert HighScore Plus software was used for the crystallographic analyses. All the samples contained jarosite phases and a contaminant phase of Ag_2SO_4 was found to be present in samples JS12, 30 and 38, which was not discovered using Cu radiation.

4.1.3.2 Rietveld refinement of XRD data

Refinement of the crystal structures, unit-cell parameters, site occupancies, and bond lengths and angles of the mineral phases present in the jarosite compounds was carried out on the Co-radiation XRD data with the Rietveld method using the General Structure Analysis System (GSAS) (Larson and Von Dreele, 2004) and EXPGUI (Toby, 2001) programs. The space group used was R-3m (Rbar3m) and the lattice was centric R-centred (Rhombohedral symmetry) trigonal (Laue classification) with interaxial angles of $\alpha = 90^o$ and $\gamma = 120^o$. Refinement was carried out of atomic co-ordinates, with initial atomic co-ordinates based on those reported by Basciano and Peterson (2007, 2008), and U_{iso} (thermal) isotropic displacement factors. Refinement was also carried out of the background using a ('type 2') pseudo-voigt function (six terms) and the histogram scale factor. Refinement of the profile (peak shape) parameters included the Gaussian peak width terms U, V and W and asymmetry, shift and transparency.

The results of the Rietveld refinements of the jarosite phases in the samples are shown in Table 4.9. In the table, the chi-squared (X^2) statistical test value provides an assessment of how well the observed data fit the theoretical (model) data

(goodness of fit), as also do the R-factor (Rp) and weighted R-factor (Rwp) values (Young, 1993) and the Durbin-Watson d-statistic (DWd) values (Basciano and Peterson, 2008). The Rp, Rwp and DWd values for goodness of fit are, for most samples, reasonably comparable with the values reported by Basciano and Peterson (2007, 2008) for Rietveld refinements on synthesised K-H_3O and Na-H_3O jarosite series. These reported values for K-H_3O jarosites were Rp 0.0329-0.0359, Rwp 0.0429-0.0499 and DWd 0.523-0.745 (Basciano and Peterson, 2007) and for Na-H_3O jarosites were Rp 0.0313-0.0355, Rwp 0.0436-0.0465 and DWd 0.547-0.740 (Basciano and Peterson, 2008).

During the Rietveld refinement of the synthesised samples' XRD profiles, the fit was in some cases improved by the inclusion of more than one phase (see Table 4.9), suggesting those samples are inhomogeneous. This raises the possibility that there may be a lack of solid solution and immiscibility in K-Ag and Na-Ag jarosites under the synthesis conditions used, a condition that has been reported in low-temperature synthesised K-Na jarosites (Desborough et al., 2006, 2010), as well as in natural jarosites (Swayze et al., 2008). However, against this conclusion is that more than one phase was included in the refinements of only a minority of samples.

Table 4.9 shows the Rietveld-refined *a* parameters of synthesised K-H_3O-jarosite products 04 and 22 (7.3266 Å and 7.3282 Å, respectively) are shorter than those of Na-H_3O-jarosite products 14 and 32 (7.3421 Å and 7.3426 Å, respectively), and the *c* parameters for K-H_3O-jarosites 04 and 22 (17.0797 Å and 17.0823 Å) are longer than those for Na-H_3O-jarosites 14 and 32 (16.7008 Å and 16.7158 Å). These values are consistent with reported *a* and *c* parameter values for K-jarosite and Na-jarosite. For example, for K-jarosite, *a* values of 7.288 Å (Brophy and Sheridan, 1965), 7.29 Å (Sasaki and Konno, 2000; Anthony et al., 2003), 7.303 Å (K 0.95 site

occupancy) (Basciano and Peterson, 2007a) and 7.315 Å (K 0.92) (Dutrizac and Kaiman, 1976) have been reported; for Na-jarosite, *a* values of 7.33 Å (Dutrizac and Kaiman, 1976; Serna et al., 1986), 7.3346 Å (Hawthorne et al., 2000) and 7.3388 Å (Na 0.49), 7.342 Å (Na 0.35) and 7.3474 Å (Na 0.24) (Basciano and Peterson, 2008) have been reported. For K-jarosite, *c* values of 17.06 Å (Sasaki and Konno, 2000), 17.119 Å (K 0.92) (Dutrizac and Kaiman, 1976), 17.16 (Anthony et al., 2003), 17.192 Å (Brophy and Sheridan, 1965) and 17.204 Å (K 0.95) (Basciano and Peterson, 2007a) have been reported; for Na-jarosite, *c* values of 16.70 Å (Dutrizac and Kaiman, 1976) and 16.8105 Å (Na 0.49), 16.8574 Å (Na 0.35) and 16.9253 Å (Na 0.24) (Basciano and Peterson, 2008) have been reported. In Table 4.9, Ag-H_3O-jarosite products 12 and 30 have *a* parameter values of 7.3582 Å and 7.3584 Å, respectively, and *c* parameter values of 16.6095 Å and 16.6099 Å, respectively, whereas reported parameters for Ag-jarosite are *a* 7.336 Å and *c* 16.564 Å (Dutrizac and Jambor, 1987), *a* 7.3398 Å and *c* 16.538 Å (Groat et al., 2003), *a* 7.346 Å and *c* 16.668 Å (Ag 0.86) (Ildefonse et al., 1986), *a* 7.347 Å and *c* 16.58 Å (May et al., 1973), *a* 7.348 Å and *c* 16.551 Å (Ag 0.96) (Kato and Miura, 1977) and *a* 7.35 Å and *c* 16.55 Å (Dutrizac and Kaiman, 1976), and reported values for H_3O-jarosite are *a* 7.355 Å and *c* 16.98 Å (Brophy and Sheridan, 1965), *a* 7.347 Å and *c* 16.994 Å (Dutrizac and Kaiman, 1976), *a* 7.35 Å and *c* 16.99 Å (Serna et al., 1986), and *a* 7.3552 Å and *c* 16.9945 Å (Basciano and Peterson, 2007a, 2008).

In all refinements of the K-Ag-H_3O and Na-Ag-H_3O-jarosite compounds, improved fits were achieved with vacancies in the Fe site, shown by results of < 1 in the refinements (see Table 4.9). Vacancies in the Fe site represent Fe:SO_4 ratios lower than the ideal 3:2, which have been commonly reported in synthetic studies (Kubisz, 1970; Dutrizac and Jambor, 2000; Desborough et al., 2006; Basciano and

Table 4.9. Rietveld refinement of synthetic Na-, K- and H_3O-jarosite site occupancies and unit-cell parameters (*a* and *c* in Å).

Sample	Starting solution	Rwp	Rp	Dwd	χ^2	Na	K	Ag	H_3O	Fe	a	c
K-Ag-H_3O-jarosite compounds												
Solutions containing 0.51 M $Fe_2(SO_4)_3.5H_2O$ heated at 97ºC and products dried at 60ºC												
JS04	0.22 *M* K, 0.00 *M* Ag	0.0740	0.0572	0.650	1.704	0.00	0.65	0.00	0.35	0.8042	7.3266	17.0797
JS06D	0.165 *M* K, 0.055 *M* Ag	0.0743	0.0584	0.649	1.632	0.00	0.71	0.09	0.20	0.8676	7.3388	16.9475
JS08c1	0.11 *M* K, 0.11 *M* Ag	0.0662	0.0474	0.361	2.964	0.00	0.53	0.28	0.19	0.9576	7.3426	16.9212
JS10	0.055 *M* K, 0.165 *M* Ag	0.0944	0.0692	0.426	2.481	0.00	0.32	0.38	0.30	0.7790	7.3479	16.7611
Solutions containing 0.51 M $Fe_2(SO_4)_3.5H_2O$ heated at 97ºC and products dried at 110ºC												
JS22	0.22 *M* K, 0.00 *M* Ag	0.0582	0.0426	0.487	2.398	0.00	0.61	0.00	0.39	0.7980	7.3282	17.0823
JS24	0.165 *M* K, 0.055 *M* Ag	0.0465	0.0350	0.468	2.377	0.00	0.63	0.10	0.27	0.7593	7.3377	16.9522
JS26i2	0.11 *M* K, 0.11 *M* Ag	0.0408	0.0278	0.319	4.379	0.00	0.45	0.20	0.35	0.7800	7.3397	16.8842
JS28c1	0.055 *M* K, 0.165 *M* Ag	0.0401	0.0294	0.288	3.995	0.00	0.30	0.43	0.27	0.9248	7.3470	16.7442
Solutions containing 0.15 M $Fe_2(SO_4)_3.5H_2O$ heated at 140ºC and products dried at 110ºC												
JS55	0.12 *M* K, 0.00 *M* Ag	0.0759	0.0581	0.608	1.828	0.00	0.32	0.00	0.68	0.7588	7.3137	17.1687
JS56	0.10 *M* K, 0.02 *M* Ag	0.0809	0.0613	0.543	1.991	0.00	0.71	0.09	0.20	0.8040	7.3242	17.0630
JS57	0.08 *M* K, 0.04 *M* Ag	0.0754	0.0588	0.651	1.677	0.00	0.56	0.21	0.23	0.8066	7.3302	16.9781
JS58	0.06 *M* K, 0.06 *M* Ag	0.0747	0.0579	0.650	1.603	0.00	0.38	0.35	0.27	0.8480	7.3358	16.8922
JS59	0.04 *M* K, 0.08 *M* Ag	0.0801	0.0603	0.585	1.788	0.00	0.46	0.39	0.15	0.8168	7.3391	16.8087
JS60	0.02 *M* K, 0.10 *M* Ag	0.0890	0.0656	0.501	2.107	0.00	0.34	0.55	0.11	0.8340	7.3475	16.6935
Solutions containing 0.51 M $Fe_2(SO_4)_3.5H_2O$ prepared at 22ºC and products air-dried at 22ºC												
JS73	0.22 *M* K, 0.00 *M* Ag	0.0717	0.0527	0.364	3.033	0.00	0.67	0.00	0.33	0.7310	7.3172	17.0031
JS74	0.165 *M* K, 0.055 *M* Ag	0.0784	0.0604	0.603	1.787	0.00	0.61	0.08	0.31	0.7801	7.3168	16.9719
JS75	0.11 *M* K, 0.11 *M* Ag	0.0836	0.0636	0.533	2.011	0.00	0.37	0.19	0.44	0.7673	7.3224	16.9411
JS76b1	0.055 *M* K, 0.165 *M* Ag	0.1056	0.0816	0.451	2.432	0.00	0.37	0.26	0.37	0.7756	7.3336	16.8748
Na-Ag-H_3O-jarosite compounds												
Solutions containing 0.51 M $Fe_2(SO_4)_3.5H_2O$ heated at 97ºC and products dried at 60ºC												
JS14b	0.22 *M* Na, 0.00 *M* Ag	0.0749	0.0576	0.550	2.050	0.66	0.00	0.00	0.34	0.8701	7.3421	16.7008

JS16	0.165 *M* Na, 0.055 *M* Ag	0.0907	0.0665	0.451	2.464	0.35	0.00	0.27	0.38	0.8136	7.3492	16.6505
JS18	0.11 *M* Na, 0.11 *M* Ag	0.0910	0.0695	0.515	2.260	0.30	0.00	0.53	0.17	0.8047	7.3556	16.6134
JS20	0.055 *M* Na, 0.165 *M* Ag	0.0940	0.0725	0.477	2.346	0.20	0.00	0.56	0.24	0.7989	7.3539	16.6091
Solutions containing 0.51 M $Fe_2(SO_4)_3.5H_2O$ heated at 97ºC and products dried at 110ºC												
JS32	0.22 *M* Na, 0.00 *M* Ag	0.0607	0.0447	0.448	2.598	0.51	0.00	0.00	0.49	0.7724	7.3426	16.7158
JS34	0.165 *M* Na, 0.055 *M* Ag	0.0806	0.0594	0.629	1.801	0.47	0.00	0.43	0.10	0.7615	7.3528	16.6375
JS36	0.11 *M* Na, 0.11 *M* Ag	0.0969	0.0725	0.481	2.422	0.03	0.00	0.61	0.36	0.7477	7.3583	16.6155
JS38b1	0.055 *M* K, 0.165 *M* Ag	0.0958	0.0726	0.523	2.216	0.04	0.00	0.61	0.35	0.7274	7.3593	16.6103
Solutions containing 0.15 M $Fe_2(SO_4)_3.5H_2O$ heated at 140ºC and products dried at 110ºC												
JS49b1	0.12 *M* Na, 0.00 *M* Ag	0.0879	0.0690	0.362	2.883	0.47	0.00	0.00	0.53	0.8808	7.3380	16.7932
JS50	0.10 *M* Na, 0.02 *M* Ag	0.0991	0.0684	0.339	3.208	0.16	0.00	0.23	0.61	0.9418	7.3472	16.7537
JS51	0.08 *M* Na, 0.04 *M* Ag	0.0878	0.0645	0.496	2.254	0.22	0.00	0.38	0.40	0.8272	7.3474	16.6663
JS52	0.06 *M* Na, 0.06 *M* Ag	0.0847	0.0667	0.560	1.927	0.17	0.00	0.45	0.38	0.6558	7.3483	16.6193
JS53	0.04 *M* Na, 0.08 *M* Ag	0.0863	0.0681	0.542	1.961	0.06	0.00	0.57	0.37	0.7072	7.3482	16.6019
JS54	0.02 *M* Na, 0.10 *M* Ag	0.0887	0.0694	0.535	2.037	0.04	0.00	0.66	0.30	0.7775	7.3501	16.5989
Solutions containing 0.51 M $Fe_2(SO_4)_3.5H_2O$ prepared at 22ºC and products air-dried at 22ºC												
JS78	0.165 *M* Na, 0.055 *M* Ag	0.0859	0.0663	0.551	1.909	0.09	0.00	0.61	0.30	0.7773	7.3477	16.5654
JS80b1	0.055 *M* Na, 0.165 *M* Ag	0.1037	0.0814	0.495	2.068	0.03	0.00	0.68	0.29	0.8295	7.3474	16.5535
Ag-H_3O-jarosite compounds												
Solutions containing 0.51 M $Fe_2(SO_4)_3.5H_2O$ heated at 97ºC and products dried at 60ºC												
JS12	0.00 *M* M^+, 0.22 *M* Ag	0.1030	0.0772	0.440	2.509	0.00	0.00	0.65	0.35	0.7693	7.3582	16.6095
Solutions containing 0.51 M $Fe_2(SO_4)_3.5H_2O$ heated at 97ºC and products dried at 110ºC												
JS30	0.00 *M* M^+, 0.22 *M* Ag	0.0677	0.0464	0.200	9.215	0.00	0.00	0.63	0.37	0.7905	7.3562	16.6005
Solutions containing 0.15 M $Fe_2(SO_4)_3.5H_2O$ heated at 140ºC and products dried at 110ºC												
JS61	0.00 *M* M^+, 0.12 *M* Ag	0.0789	0.0617	0.687	1.592	0.00	0.00	0.76	0.24	0.8356	7.3485	16.5013
Solutions containing 0.51 M $Fe_2(SO_4)_3.5H_2O$ prepared at 22ºC and products air-dried at 22ºC												
JS72	0.00 *M* M^+, 0.22 *M* Ag	0.0904	0.0707	0.364	3.032	0.00	0.00	0.74	0.26	0.8027	7.3495	16.5551

Key: χ^2 = chi-squared test value, Rp = Rietveld pattern value, wRp = weighted Rietveld pattern value, and DWd = Durbin-Watson d-statistic value. The notation b, c and h on the samples refers to the second, third or eighth attempt at refinement; b1, b2, b3, c1, c2, c3, d2 and d3 refer to the jarosite phase number in the refinement; and l refers to longer scans of 80 s per step.

Peterson, 2007), such as 73% Fe^{3+} occupancy (Fe:SO_4 value of 2.2:2) (Baron and Palmer, 1996). Fe^{3+} deficiencies result in excess anion charge in the crystal structure, leading to charge neutrality (balance) in the structure of these non-stoichiometric jarosites to be maintained by protonation of hydroxyl groups, substituting H_2O for OH^- in $FeO_2(OH,H_2O)_4$ octahedra (Kubisz, 1970; Drouet et al., 2004; Desborough et al., 2006; Basciano and Peterson, 2007; Burger et al., 2009). H_2O groupings possibly also occupy Fe vacant sites (Kubisz, 1970). Full Fe occupancy results in larger jarosite unit-cell parameters than where there are vacancies (Basciano and Peterson, 2008). Fe deficiency decreases unit-cell volume (large change in *c*, minor change in *a*) by shortening the Fe-OH (Fe-O3) bond length (Basciano and Peterson, 2007).

Rietveld refinement of the crystal structures produced the interatomic distances and bond angles shown in Table 4.10 for Na-H_3O-jarosite sample 49, Na-Ag-H_3O-jarosite samples 50-54 (all synthesised at 140ºC), and 78 and 80 (both synthesised at 22ºC), K-H_3O-jarosite sample 55, K-Ag-H_3O-jarosite samples 56-60 (all synthesised at 140ºC) and 73-76 (synthesised at 22ºC), and Ag-H_3O-jarosite samples 61 (synthesised at 140ºC) and 72 (synthesised at 22ºC). These sample series have been selected as being representative of series synthesised at 22ºC (low temperature) and 140ºC (high temperature) (see Appendix F for data for samples 04-80). Rietveld refinement of K-Ag-H_3O-jarosite compounds reveals generally decreasing K,Ag-O2 and K,Ag-O3 bond lengths as Ag content increases (although there are some inconsistencies within the series). The same trends are not evident in the Na-Ag-H_3O-jarosite compounds, possibly because the ionic radii of Na^+ and Ag^+ are of relatively similar sizes and the H_3O contents are relatively high in many of the samples.

Rietveld refinement also produced the atom positions and occupancies of samples 04-80 shown in Tables 4.11a and 4.11b. It should be noted that there are some substantial differences between the refined occupancies and the occupancies from EMPA. For example, the Na occupancy of sample 49 is refined at 0.47, whereas it is 0.56 from EMPA; the Ag occupancy of sample 61 is refined at 0.76, whereas it is 0.54 from EMPA. Where there are site vacancies, charge balance of the structure may be maintained by substitution of H_3O^+ in the *A* site or protonation of OH^- to H_2O (Kubisz, 1970). The refined structure of K-H_3O-jarosite sample 55 (K occupancy 0.32) has atom positions (see Table 4.11a) similar to reported positions for two synthesised K-H_3O-jarosite compounds (K occupancies 0.60 and 0.70), although both had full Fe occupancy (Basciano and Peterson, 2007). The refined structure of Na-H_3O-jarosite sample 49 (Na occupancy 0.47) has atom positions (see Table 4.11b) similar to reported positions for a synthesised Na-H_3O-jarosite compound (Na occupancy 0.49), although this had full Fe occupancy (Basciano and Peterson, 2008). The refinements show changing atomic positions of O2 and O3 (OH), to which the *A*-site atom is bonded, with changing compositions of Ag. A general trend in the atomic positions of O2 and O3 on the *z* axis is evident in the K-Ag-H_3O-jarosite sample series 55-61 (synthesised at 140ºC); however, no clear trend is apparent in the corresponding Na-Ag-H_3O-jarosite sample series 49-54 & 61. In the K-Ag-H_3O-jarosite sample series 72-76 (synthesised at 22ºC) a trend in the atomic positions of O3 on the *z* axis is apparent; in the corresponding Na-Ag-H_3O jarosite sample series 72, 78 and 80, a trend in the atomic positions of O2 on the *x* and *y* axes is apparent and of O3 on the *z* axis.

Table 4.10 Rietveld refinement interatomic distances (Å) and angles of K-Ag- and Na-Ag-jarosites synthesised at 22ºC, 97ºC and 140ºC.

					Synthesis temperature 97ºC					
Bonds	**JS04**	**JS06D**	**JS08**	**JS10**	**JS12**	**JS22**	**JS24**	**JS26**	**JS28**	**JS30**
	$K_{0.65}$ $H_3O_{0.35}$	$K_{0.71}$ $Ag_{0.09}$ $H_3O_{0.20}$	$K_{0.53}$ $Ag_{0.28}$ $H_3O_{0.19}$	$K_{0.32}$ $Ag_{0.38}$ $H_3O_{0.30}$	$Ag_{0.65}$ $H_3O_{0.35}$	$K_{0.61}$ $H_3O_{0.39}$	$K_{0.63}$ $Ag_{0.10}$ $H_3O_{0.27}$	$K_{0.27}$ $Ag_{0.18}$ $H_3O_{0.55}$	$K_{0.30}$ $Ag_{0.43}$ $H_3O_{0.27}$	$Ag_{0.63}$ $H_3O_{0.37}$
K,Ag – O2 × 6	2.994 (4)	3.01468 (4)	3.050 (11)	3.034 (6)	2.98574 (22)	2.9931 (31)	2.9758 (24)	2.95389 (1)	2.98760 (3)	2.97451 (2)
K,Ag – O3 × 6	2.822 (4)	2.83248 (5)	2.725 (11)	2.694 (6)	2.70820 (17)	2.8371 (27)	2.8019 (24)	2.80780 (2)	2.80256 (4)	2.74384 (2)
Fe – O2 × 2	2.046 (5)	2.114 (6)	2.112 (11)	1.997 (7)	2.10845 (16)	2.062 (4)	2.0472 (34)	2.08572 (2)	2.16386 (4)	2.11923 (2)
Fe – O3 × 4	2.0167 (17)	2.0104 (18)	1.9224 (30)	2.0346 (22)	2.00690 (15)	2.0015 (11)	2.0068 (10)	1.99907 (1)	2.01902 (2)	2.02132 (1)
S – O1 × 1	1.479 (7)	1.529 (8)	1.515 (21)	1.267 (10)	1.37218 (11)	1.543 (6)	1.511 (5)	1.53553 (2)	1.58893 (4)	1.56600 (0)
S – O2 × 3	1.483 (5)	1.421 (5)	1.370 (12)	1.487 (5)	1.43269 (11)	1.469 (4)	1.4889 (28)	1.48463 (1)	1.40089 (1)	1.42922 (1)
O2 - K,Ag – O2 × 6	69.29 (10)	67.73 (9)	67.75 (18)	69.29 (13)	66.877 (1)	69.01 (7)	68.87 (6)	68.024 (0)	66.347 (0)	66.669 (0)
O2 - K,Ag – O2 × 6	110.71 (10)	112.27 (9)	112.25 (18)	110.71 (13)	113.123 (1)	110.99 (7)	111.13 (6)	111.976 (0)	113.653 (0)	113.331 (0)
O2 - K,Ag – O3 × 6	71.80 (14)	70.20 (14)	76.05 (30)	70.72 (18)	69.097 (5)	72.24 (10)	71.70 (8)	71.143 (1)	67.797 (1)	67.947 (1)
O2 - K,Ag – O3 × 6	108.20 (14)	109.80 (14)	103.95 (30)	109.28 (18)	110.903 (5)	107.76 (10)	108.30 (8)	108.857 (1)	112.203 (1)	112.053 (1)
O2 - K,Ag – O3 × 12	57.77 (8)	59.15 (9)	60.78 (18)	69.29 (13)	59.919 (1)	58.19 (6)	59.043 (0)	59.342 (0)	60.287 (0)	59.882 (0)
O2 - K,Ag – O3 × 12	122.23 (8)	120.85 (9)	119.22 (18)	110.71 (13)	120.081 (1)	121.81 (6)	120.957 (0)	120.658 (0)	119.713 (0)	120.118 (0)
O3 - K,Ag – O3 × 6	61.85 (13)	61.69 (14)	52.10 (34)	63.60 (17)	61.874 (5)	60.65 (9)	61.29 (8)	60.695 (1)	62.943 (1)	63.336 (1)
O3 - K,Ag – O3 × 6	118.15 (13)	118.31 (14	127.90 (34)	116.40 (17)	118.126 (5)	119.35 (9)	118.71 (8)	119.305 (1)	117.057 (1)	116.664 (1)
O2 - Fe – O3 × 4	87.68 (12)	88.94 (13)	86.8 (4)	86.89 (20)	87.767 (3)	88.60 (9)	87.93 (7)	88.146 (0)	88.124 (1)	87.385 (0)
O2 - Fe – O3 × 4	92.32 (12)	91.06 (13)	93.2 (4)	93.11 (20)	92.233 (3)	91.40 (9)	92.07 (7)	91.854 (0)	91.876 (1)	92.615 (0)
O3 - Fe – O3 × 2	88.02 (20)	87.49 (23)	77.0 (6)	88.49 (27)	87.857 (1)	88.60 (14)	89.25 (12)	89.587 (0)	87.115 (0)	89.094 (0)
O3 - Fe – O3 × 2	91.98 (20)	92.51 (23)	103.0 (6)	91.51 (27)	92.143 (1)	91.40 (14)	90.75 (12)	90.413 (0)	92.885 (0)	90.906 (0)
O1 - S – O2 × 3	110.84 (27)	108.59 (29)	106.3 (6)	113.9 (4)	106.886 (2)	109.71 (20)	109.63 (17)	107.679 (0)	104.829 (0)	105.455 (0)
O2 - S – O2 × 3	108.07 (28)	110.33 (28)	112.4 (5)	104.8 (5)	111.928 (2)	109.23 (20)	109.32 (17)	111.202 (0)	113.688 (0)	113.171 (0)

	Synthesis temperature 140ºC								*Synthesis temperature 22ºC*		
Bonds	**JS55**	**JS56**	**JS57**	**JS58**	**JS59**	**JS60**	**JS61**	**JS73**	**JS74**	**JS75**	**JS76**	**JS72**
	$K_{0.32}$ $H_3O_{0.68}$	$K_{0.71}$ $Ag_{0.09}$ $H_3O_{0.20}$	$K_{0.56}$ $Ag_{0.21}$ $H_3O_{0.23}$	$K_{0.38}$ $Ag_{0.35}$ $H_3O_{0.27}$	$K_{0.46}$ $Ag_{0.39}$ $H_3O_{0.15}$	$K_{0.34}$ $Ag_{0.55}$ $H_3O_{0.11}$	$Ag_{0.76}$ $H_3O_{0.24}$	$K_{0.67}$ $H_3O_{0.33}$	$K_{0.61}$ $Ag_{0.08}$ $H_3O_{0.31}$	$K_{0.37}$ $Ag_{0.19}$ $H_3O_{0.44}$	$K_{0.37}$ $Ag_{0.26}$ $H_3O_{0.37}$	$Ag_{0.74}$ $H_3O_{0.26}$
K,Ag – O2 × 6	2.97785(23)	2.98724(26)	2.97751(25)	2.98459(10)	2.96464(11)	2.94844(32)	2.95930(21)	3.00593(11)	3.02113(13)	2.99377(4)	3.0614(4)	2.9951(5)
K,Ag – O3 × 6	2.84616(18)	2.85561(21)	2.85479(20)	2.85253(8)	2.82147(9)	2.75587(25)	2.73381(16)	2.77891(8)	2.78448(10)	2.84001(3)	2.77527(31)	2.6808(6)
Fe – O2 × 2	2.01216(15)	2.09847(18)	2.09583(17)	2.11432(7)	2.11037(8)	2.13769(23)	2.10658(15)	2.03634(7)	2.06263(9)	2.07309(3)	2.08957(28)	2.0717(6)
Fe – O3 × 4	1.98702(16)	1.98324(18)	1.99911(17)	2.00134(7)	2.00257(8)	2.01157(22)	2.01611(14)	2.00467(8)	2.00357(9)	2.0015=75(2)	2.01922(28)	2.00319(34)
S – O1 × 1	1.52036(13)	1.61279(16)	1.65744(15)	1.62225(6)	1.56306(7)	1.41866(17)	1.50063(12)	1.44251(6)	1.40025(7)	1.53493(2)	1.39850(22)	1.4340(5)
S – O2 × 3	1.50993(12)	1.43700(13)	1.44741(12)	1.43066(5)	1.45289(6)	1.45205(16)	1.45061(10)	1.46940(5)	1.43526(6)	1.45262(2)	1.40998(19)	1.43527(24)
O2 - K,Ag – O2 × 6	70.188(2)	68.300(2)	68.094(2)	67.549(1)	67.364(1)	66.585(2)	66.843(1)	69.273(1)	68.735(1)	68.423(0)	68.042(3)	67.427(5)
O2 – K,Ag – O2 × 6	109.812(2)	111.700(2)	111.906(2)	112.451(1)	112.636(1)	113.415(2)	113.157(1)	110.727(1)	111.265(1)	111.577(0)	111.958(3)	112.573(5)
O2 - K,Ag – O3 × 6	74.242(5)	72.288(6)	71.120(6)	70.265(2)	69.883(3)	68.456(7)	68.356(5)	72.233(3)	71.618(3)	71.222(1)	70.021(9)	69.769(16)
O2 - K,Ag – O3 × 6	105.758(5)	107.712(6)	108.880(6)	109.735(2)	110.117(3)	111.544(7)	111.644(5)	107.767(3)	108.382(3)	108.778(1)	109.979(9)	110.231(16)
O2 - K,Ag – O3 × 12	57.385(1)	59.012(1)	58.954(1)	59.389(0)	59.515(0)	60.123(1)	59.767(1)	57.892(0)	58.341(0)	58.598(0)	58.741(1)	59.409(2)
O2 - K,Ag – O3 × 12	122.615(1)	120.988(1)	121.046(1)	120.611(0)	120.485(0)	119.877(1)	120.233(1)	122.108(0)	121.659(0)	121.402(0)	121.259(1)	120.591(2)
O3 - K,Ag – O3 × 6	59.383(5)	59.323(6)	60.858(6)	61.249(2)	61.527(3)	62.347(8)	63.013(5)	61.120(3)	61.189(3)	61.283(1)	62.551(10)	61.829(17)
O3 - K,Ag – O3 × 6	120.617(5)	120.677(6)	119.142(6)	118.751(2)	118.473(3)	117.653(8)	116.987(5)	118.880(3)	118.811(3)	118.717(1)	117.449(10)	118.171(17)
O2 - Fe – O3 × 4	88.817(3)	89.708(4)	89.036(3)	89.315(1)	88.636(2)	87.178(5)	87.180(3)	87.983(2)	88.483(2)	89.057(1)	88.734(6)	87.791(12)
O2 - Fe – O3 × 4	91.181(3)	90.292(4)	90.964(3)	90.685(1)	91.364(2)	92.822(5)	92.820(3)	92.017(2)	91.517(2)	90.941(1)	91.266(6)	92.209(12)
O3 - Fe – O3 × 2	89.610(1)	89.114(1)	87.352(1)	86.882(0)	87.783(0)	89.667(2)	89.750(1)	89.628(1)	89.964(1)	87.377(0)	88.950(2)	86.870(4)
O3 - Fe – O3 × 2	90.390(1)	90.886(1)	92.648(1)	93.118(0)	92.217(0)	90.333(2)	90.250(1)	90.372(1)	90.036(1)	92.621(0)	91.050(2)	93.130(4)
O1 - S – O2 × 3	111.054(2)	107.030(2)	107.109(2)	106.659(1)	107.100(1)	105.935(3)	106.535(2)	111.326(1)	110.446(1)	109.551(0)	112.342(4)	108.556(7)
O2 - S – O2 × 3	107.843(2)	111.798(2)	111.727(2)	112.131(1)	111.734(1)	112.764(2)	112.241(2)	107.554(1)	108.479(1)	109.391(0)	106.454(5)	110.371(6)

					Synthesis temperature 22ºC					
Bonds	**JS14**	**JS16**	**JS18**	**JS20**	**JS12**	**JS32**	**JS34**	**JS36**	**JS38**	**JS30**
	$Na_{0.66}$ $H_3O_{0.34}$	$Na_{0.35}$ $Ag_{0.27}$ $H_3O_{0.38}$	$Na_{0.30}$ $Ag_{0.53}$ $H_3O_{0.17}$	$Na_{0.20}$ $Ag_{0.56}$ $H_3O_{0.24}$	$Ag_{0.65}$ $H_3O_{0.35}$	$Na_{0.51}$ $H_3O_{0.49}$	$Na_{0.47}$ $Ag_{0.43}$ $H_3O_{0.10}$	$Na_{0.03}$ $Ag_{0.61}$ $H_3O_{0.36}$	$Na_{0.04}$ $Ag_{0.61}$ $H_3O_{0.35}$	$Ag_{0.63}$ $H_3O_{0.37}$
Na,Ag – O2 × 6	3.003 (4)	3.004 (5)	2.989 (5)	2.94763 (26)	2.98574 (22)	2.959 (4)	2.960 (4)	2.935 (5)	2.882 (5)	2.97451 (2)
Na,Ag – O3 × 6	2.7917 (32)	2.703 (5)	2.726 (6)	2.74808 (20)	2.70820 (17)	2.7753 (27)	2.710 (5)	2.725 (7)	2.701 (7)	2.74384 (2)
Fe – O2 × 2	2.055 (5)	2.013 (6)	2.122 (6)	2.17821 (19)	2.10845 (16)	1.971 (4)	2.053 (6)	2.083 (7)	2.072 (5)	2.11923 (2)
Fe – O3 × 4	2.0053 (13)	2.0095 (18)	2.0009 (19)	1.99476 (18)	2.00690 (15)	1.9933 (10)	2.0047 (18)	2.0007 (22)	2.0080 (22)	2.02132 (1)
S – O1 × 1	1.530 (7)	1.359 (9)	1.473 (10)	1.47741 (15)	1.37218 (11)	1.505 (6)	1.412 (9)	1.468 (11)	1.459 (11)	1.56600 (0)
S – O2 × 3	1.454 (5)	1.478 (5)	1.415 (5)	1.41801 (13)	1.43269 (11)	1.543 (4)	1.478 (4)	1.482 (5)	1.530 (6)	1.42922 (1)
O2 - Na,Ag – O2 × 6	68.06 (8)	68.65 (10)	67.71 (9)	65.734 (1)	66.877 (1)	69.58 (8)	67.85 (10)	67.26 (12)	67.38 (13)	66.669 (0)
O2 - Na,Ag – O2 × 6	111.94 (8)	111.35 (10)	112.27 (9)	114.266 (1)	113.123 (1)	110.42 (8)	112.15 (10)	112.74 (12)	112.62 (13)	113.331 (0)
O2 - Na,Ag – O3 × 6	70.37 (12)	71.02 (14)	70.20 (14)	68.165 (6)	69.097 (5)	72.75 (9)	70.36 (14)	69.84 (18)	69.65 (19)	67.947 (1)
O2 - Na,Ag – O3 × 6	109.63 (12)	108.98 (14)	109.80 (14)	111.835 (6)	110.903 (5)	107.25 (9)	109.64 (14)	110.16 (18)	110.35 (19)	112.053 (1)
O2 - Na,Ag – O3 × 12	58.80 (7)	58.29 (9)	59.15 (9)	61.194 (0)	59.919 (1)	57.69 (6)	59.05 (9)	59.64 (12)	59.44 (13)	59.882 (0)
O2 - Na,Ag – O3 × 12	121.20 (7)	121.71 (9)	120.85 (9)	118.806 (0)	120.081 (1)	122.31 (6)	120.95 (9)	120.36 (12)	120.56 (13)	120.118 (0)
O3 - Na,Ag – O3 × 6	62.01 (11)	62.01 (14)	61.47 (16)	61.093 (6)	61.874 (5)	60.79 (9)	61.65 (14)	61.39 (18)	61.93 (17)	63.336 (1)
O3 - Na,Ag – O3 × 6	117.99 (11)	117.99 (14)	118.53 (16)	118.907 (6)	118.126 (5)	119.21 (9)	118.35 (14)	118.61 (18)	118.07 (17)	116.664 (1)
O2 - Fe – O3 × 4	89.18 (11)	87.90 (16)	88.33 (19)	65.734 (1)	87.767 (3)	88.68 (9)	87.36 (16)	87.36 (21)	85.60 (19)	87.385 (0)
O2 - Fe – O3 × 4	90.82 (11)	92.10 (16)	91.67 (19)	114.266 (1)	92.233 (3)	91.32 (9)	92.64 (16)	92.64 (21)	94.40 (19)	92.615 (0)
O3 - Fe – O3 × 2	88.36 (16)	87.22 (23)	88.27 (26)	68.165 (6)	87.857 (1)	89.57 (14)	87.69 (25)	88.11 (31)	87.58 (31)	89.094 (0)
O3 - Fe – O3 × 2	91.64 (16)	92.28 (23)	91.73 (26)	111.835 (6)	92.143 (1)	90.43 (14)	92.31 (25)	91.89 (31)	92.42 (31)	90.906 (0)
O1 - S – O2 × 3	110.11 (24)	111.12 (33)	105.5 (4)	61.194 (0)	106.886 (2)	111.58 (19)	107.61 (31)	105.8 (4)	104.9 (4)	105.455 (0)
O2 - S – O2 × 3	108.82 (25)	107.78 (35)	113.12 (33)	118.806 (0)	111.928 (2)	107.28 (21)	111.26 (29)	112.92 (33)	113.60 (32)	113.171 (0)
				Synthesis temperature 140ºC					*Synthesis temperature 22ºC*	
Bonds	**JS49**	**JS50**	**JS51**	**JS52**	**JS53**	**JS54**	**JS61**	**JS72**	**JS78**	**JS80**
	$Na_{0.47}$ $H_3O_{0.53}$	$Na_{0.16}$ $Ag_{0.23}$ $H_3O_{0.61}$	$Na_{0.22}$ $Ag_{0.38}$ $H_3O_{0.40}$	$Na_{0.17}$ $Ag_{0.45}$ $H_3O_{0.38}$	$Na_{0.06}$ $Ag_{0.57}$ $H_3O_{0.37}$	$Na_{0.04}$ $Ag_{0.66}$ $H_3O_{0.30}$	$Ag_{0.76}$ $H_3O_{0.24}$	$Ag_{0.74}$ $H_3O_{0.26}$	$Na_{0.09}$ $Ag_{0.61}$ $H_3O_{0.30}$	$Na_{0.03}$ $Ag_{0.68}$ $H_3O_{0.29}$
Na,Ag – O2 × 6	3.04325(3)	3.0756(4)	2.98579(29)	2.84718(25)	2.89087(25)	2.93743(25)	2.95930(21)	2.9951(5)	2.92830(3)	2.92698(15)
Na,Ag – O3 × 6	2.80482(4)	2.80433(27)	2.70981(22)	2.71940(20)	2.71332(19)	2.74239(19)	2.73381(16)	2.6808(6)	2.74412(2)	2.73857(11)
Fe – O2 × 2	1.97703(3)	2.02518(22)	1.96822(19)	2.07450(19)	2.11065(18)	2.15295(19)	2.10658(15)	2.0717(6)	2.14599(2)	2.16617(10)
Fe – O3 × 4	1.98091(2)	1.98903(24)	2.01129(20)	1.99962(18)	2.00291(17)	1.99667(17)	2.01611(14)	2.00319(34)	1.99987(2)	1.00908(10)
S – O1 × 1	1.40326(3)	1.37004(18)	1.37276(15)	1.55166(16)	1.53964(15)	1.50083(14)	1.50063(12)	1.4340(5)	1.55299(2)	1.54274(9)
S – O2 × 3	1.47401(1)	1.41631(16)	1.51651(14)	1.55564(14)	1.49988(13)	1.44048(13)	1.45061(10)	1.43527(24)	1.44887(1)	1.43950(7)
O2 - Na,Ag – O2 × 6	69.767(0)	68.828(3)	69.487(3)	67.359(2)	66.727(2)	66.090(1)	66.843(1)	67.427(5)	66.107(0)	65.764(1)
O2 – Na,Ag – O2 × 6	110.233(0)	111.172(3)	110.513(3)	112.641(2)	113.273(2)	113.910(1)	113.157(1)	112.573(5)	113.893(0)	114.236(1)
O2 - Na,Ag – O3 × 6	73.628(1)	72.207(8)	71.805(7)	69.948(6)	69.003(6)	68.467(5)	68.356(5)	69.769(16)	68.205(1)	67.264(3)
O2 - Na,Ag – O3 × 6	106.372(1)	107.793(8)	108.195(7)	110.052(6)	110.997(6)	111.533(5)	111.644(5)	110.231(16)	111.795(1)	112.736(3)
O2 - Na,Ag – O3 × 12	57.690(0)	58.380(1)	57.562(1)	59.539(1)	60.086(1)	60.785(0)	59.767(1)	59.409(2)	60.688(0)	60.899(0)
O2 - Na,Ag – O3 × 12	122.310(0)	121.620(1)	122.438(1)	120.461(1)	119.914(1)	119.215(0)	120.233(1)	120.591(2)	119.312(0)	119.101(0)
O3 - Na,Ag – O3 × 6	59.683(1)	60.392(8)	62.180(7)	61.411(6)	61.736(6)	61.336(6)	63.013(5)	61.829(17)	61.800(1)	62.621(3)
O3 - Na,Ag – O3 × 6	120.317(1)	119.608(8)	117.820(7)	118.589(6)	118.264(6)	118.664(6)	116.987(5)	118.171(17)	118.200(0)	117.379(3)
O2 - Fe – O3 × 4	88.747(1)	88.417(5)	87.535(5)	85.502(4)	86.131(4)	87.760(4)	87.180(3)	87.791(12)	87.548(0)	86.979(2)
O2 - Fe – O3 × 4	91.253(1)	91.583(5)	92.465(5)	94.498(4)	93.869(4)	92.240(4)	82.820(3)	92.209(12)	92.452(0)	93.021(2)
O3 - Fe – O3 × 2	89.591(0)	89.671(1)	88.173(2)	87.965(1)	88.063(1)	88.948(1)	89.750(1)	86.870(4)	89.605(0)	89.797(1)
O3 - Fe – O3 × 2	90.409(0)	90.329(1)	91.827(2)	92.035(1)	91.937(1)	91.052(1)	90.250(1)	93.130(4)	90.395(0)	90.203(1)
O1 - S – O2 × 3	113.285(0)	112.121(4)	111.706(3)	104.405(2)	104.123(2)	103.546(2)	106.535(2)	108.556(7)	103.624(0)	102.802(1)
O2 - S – O2 × 3	105.403(1)	106.696(4)	107.146(3)	114.027(2)	114.249(1)	114.690(1)	112.241(2)	110.371(6)	114.631(0)	115.236(1)

Table 4.11a. Rietveld-refined atom positions (*x*, *y*, *z*), isotropic displacement parameters (U_{iso}) and occupancies of K-Ag-H_3O-jarosite compounds synthesised at 22ºC, 97ºC and 140ºC.

Sample	**Site**	**Multiple**	**x**	**y**	**z**	U_{iso}	**Occupancy**
Synthesis temperature 97ºC							
4	K	3	0	0	0	0.025	0.65
$K_{0.65}$	Fe	9	0.16667	-0.16667	-0.16667	0.075	0.8042
$H_3O_{0.35}$	S	6	0	0	0.309467	0.047	1
	O1	6	0	0	0.396036	0.049	1
	O2	18	0.224154	-0.224154	-0.05475	0.045	1
	O3	18	0.131971	-0.131971	0.132993	0.048	1
6D	K	3	0	0	0	0.025	0.71
$K_{0.71}$	Ag	3	0	0	0	0.025	0.09
$Ag_{0.09}$	Fe	9	0.16667	-0.16667	-0.16667	0.083	0.8676
$H_3O_{0.20}$	S	6	0	0	0.309523	0.034	1
	O1	6	0	0	0.399748	0.045	1
	O2	18	0.227395	-0.227395	-0.05054	0.028	1
	O3	18	0.131934	-0.131934	0.13469	0.04	1
8	K	3	0	0	0	0.025	0.53
$K_{0.53}$	Ag	3	0	0	0	0.025	0.28
$Ag_{0.28}$	Fe	9	0.16667	-0.16667	-0.16667	0.029	0.9577
$H_3O_{0.19}$	S	6	0	0	0.304788	-0.005	1
	O1	6	0	0	0.394304	0.089	1
	O2	18	0.22996	-0.22996	-0.051263	-0.01	1
	O3	18	0.10864	-0.10864	0.138794	0.002	1
10	K	3	0	0	0	0.025	0.32
$K_{0.32}$	Ag	3	0	0	0	0.025	0.38
$Ag_{0.38}$	Fe	9	0.16667	-0.16667	-0.16667	0.025	0.779
$H_3O_{0.30}$	S	6	0	0	0.312665	0.025	1
	O1	6	0	0	0.388285	0.025	1
	O2	18	0.226473	-0.226473	-0.056543	0.025	1
	O3	18	0.128797	-0.128797	0.127533	0.025	1
12	Ag	3	0	0	0	0.025	0.65
$Ag_{0.65}$	Fe	9	0.16667	-0.16667	-0.16667	0.025	0.8111
$H_3O_{0.35}$	S	6	0	0	0.310024	0.025	1
	O1	6	0	0	0.392644	0.025	1
	O2	18	0.225844	-0.225844	-0.047661	0.025	1
	O3	18	0.125903	-0.125903	0.130745	0.025	1
Synthesis temperature 97ºC							
22	K	3	0	0	0	0.058	0.61
$K_{0.61}$	Fe	9	0.16667	-0.16667	-0.16667	0.066	0.798
$H_3O_{0.39}$	S	6	0	0	0.30847	0.04	1
	O1	6	0	0	0.39878	0.054	1
	O2	18	0.224389	-0.224389	-0.053867	0.047	1
	O3	18	0.130315	-0.130315	0.134934	0.032	1
24	K	3	0	0	0	0.065	0.63
$K_{0.63}$	Ag	3	0	0	0	0.025	0.1
$Ag_{0.10}$	Fe	9	0.16667	-0.16667	-0.16667	0.055	0.7593
$H_3O_{0.27}$	S	6	0	0	0.309305	0.044	1
	O1	6	0	0	0.398441	0.052	1
	O2	18	0.222988	-0.222988	-0.053529	0.05	1
	O3	18	0.129762	-0.129762	0.133618	0.033	1
26	K	3	0	0	0	0.025	0.45
$K_{0.45}$	Ag	3	0	0	0	0.078	0.2
$Ag_{0.20}$	Fe	9	0.16667	-0.16667	-0.16667	0.025	0.78
$H_3O_{0.35}$	S	6	0	0	0.308	0.017	1
	O1	6	0	0	0.4025	0.259	1
	O2	18	0.224	-0.224	-0.0505	0.007	1
	O3	18	0.131	-0.131	0.136	0.024	1
28	K	3	0	0	0	0.031	0.3
$K_{0.30}$	Ag	3	0	0	0	0.068	0.43
$Ag_{0.43}$	Fe	9	0.16667	-0.16667	-0.16667	0.093	0.9248
$H_3O_{0.27}$	S	6	0	0	0.30895	0.058	1
	O1	6	0	0	0.40386	0.235	1

	O2	18	0.226913	-0.226913	-0.045799	0.041	1
	O3	18	0.132767	-0.132767	0.133564	0.009	1
30	Ag	3	0	0	0	0.057	0.63
$Ag_{0.63}$	Fe	9	0.16667	-0.16667	-0.16667	0.057	0.7905
$H_3O_{0.37}$	S	6	0	0	0.30993	0.048	1
	O1	6	0	0	0.401021	0.087	1
	O2	18	0.224133	-0.224133	-0.047482	0.045	1
	O3	18	0.128853	-0.128853	0.13019	0.037	1
Synthesis temperature 140ºC							
55	K	3	0	0	0	0.025	0.32
$K_{0.32}$	Fe	9	0.16667	-0.16667	-0.16667	0.025	0.7588
$H_3O_{0.68}$	S	6	0	0	0.308091	0.041	1
	O1	6	0	0	0.396645	0.056	1
	O2	18	0.22221	-0.222095	-0.056837	0.076	1
	O3	18	0.12851	-0.128506	0.135984	0.051	1
56	K	3	0	0	0	0.025	0.71
$K_{0.71}$	Ag	3	0	0	0	0.025	0.09
$Ag_{0.09}$	Fe	9	0.16667	-0.16667	-0.16667	0.025	0.804
$H_3O_{0.20}$	S	6	0	0	0.307	0.032	1
	O1	6	0	0	0.402	0.074	1
	O2	18	0.225	-0.225	-0.052	0.037	1
	O3	18	0.129	-0.129	0.138	0.032	1
57	K	3	0	0	0	0.02	0.56
$K_{0.56}$	Ag	3	0	0	0	0.13	0.21
$Ag_{0.21}$	Fe	9	0.16667	-0.16667	-0.16667	0.05	0.8066
$H_3O_{0.23}$	S	6	0	0	0.3074	0.055	1
	O1	6	0	0	0.405022	0.101	1
	O2	18	0.22438	-0.224376	-0.051013	0.032	1
	O3	18	0.1315	-0.131498	0.136393	0.048	1
58	K	3	0	0	0	0.035	0.38
$K_{0.38}$	Ag	3	0	0	0	0.071	0.35
$Ag_{0.35}$	Fe	9	0.16667	-0.16667	-0.16667	0.06	0.848
$H_3O_{0.27}$	S	6	0	0	0.308036	0.037	1
	O1	6	0	0	0.404071	0.115	1
	O2	18	0.225461	-0.225461	-0.049577	0.027	1
	O3	18	0.132057	-0.132057	0.136563	0.03	1
59	K	3	0	0	0	0.19	0.46
$K_{0.46}$	Ag	3	0	0	0	0.035	0.39
$Ag_{0.39}$	Fe	9	0.16667	-0.16667	-0.16667	0.056	0.8168
$H_3O_{0.15}$	S	6	0	0	0.309886	0.038	1
	O1	6	0	0	0.402877	0.08	1
	O2	18	0.22409	-0.224091	-0.048864	0.034	1
	O3	18	0.13109	-0.131093	0.135453	0.044	1
60	K	3	0	0	0	0.175	0.34
$K_{0.34}$	Ag	3	0	0	0	0.033	0.55
$Ag_{0.55}$	Fe	9	0.16667	-0.16667	-0.16667	0.05	0.834
$H_3O_{0.11}$	S	6	0	0	0.311018	0.034	1
	O1	6	0	0	0.396001	0.048	1
	O2	18	0.223618	-0.223618	-0.046196	0.037	1
	O3	18	0.129435	-0.129435	0.132352	0.033	1
61	Ag	3	0	0	0	0.06	0.76
$Ag_{0.76}$	Fe	9	0.16667	-0.16667	-0.16667	0.049	0.8356
$H_3O_{0.24}$	S	6	0	0	0.310634	0.036	1
	O1	6	0	0	0.401081	0.06	1
	O2	18	0.22408	-0.224077	-0.047583	0.022	1
	O3	18	0.12961	-0.129611	0.131392	0.02	1
Synthesis temperature 22ºC							
73	K	3	0	0	0	0.042	0.67
$K_{0.67}$	Fe	9	0.16667	-0.16667	-0.16667	0.054	0.731
$H_3O_{0.33}$	S	6	0	0	0.30959	0.047	1
	O1	6	0	0	0.394428	0.044	1
	O2	18	0.225332	-0.225332	-0.055172	0.04	1
	O3	18	0.12873	-0.12873	0.132304	0.063	1
74	K	3	0	0	0	0.082	0.61
$K_{0.61}$	Ag	3	0	0	0	0.03	0.08
$Ag_{0.08}$	Fe	9	0.16667	-0.16667	-0.16667	0.058	0.7801
$H_3O_{0.31}$	S	6	0	0	0.309017	0.036	1

	O1	6	0	0	0.391521	0.027	1
	O2	18	0.22722	-0.227216	-0.053858	0.033	1
	O3	18	0.12913	-0.129125	0.132742	0.068	1
75	K	3	0	0	0	0.141	0.37
$K_{0.37}$	Ag	3	0	0	0	0.034	0.19
$Ag_{0.19}$	Fe	9	0.16667	-0.16667	-0.16667	0.057	0.7673
$H_3O_{0.44}$	S	6	0	0	0.309556	0.046	1
	O1	6	0	0	0.40016	0.048	1
	O2	18	0.225403	-0.225403	-0.052472	0.055	1
	O3	18	0.131782	-0.131782	0.135536	0.043	1
76	K	3	0	0	0	0.095	0.37
$K_{0.37}$	Ag	3	0	0	0	0.025	0.26
$Ag_{0.26}$	Fe	9	0.16667	-0.16667	-0.16667	0.025	0.7756
$H_3O_{0.37}$	S	6	0	0	0.3125	0.025	1
	O1	6	0	0	0.395375	0.03	1
	O2	18	0.23066	-0.230664	-0.052596	0.025	1
	O3	18	0.13098	-0.130976	0.131635	0.03	1
72	Ag	3	0	0	0	0.025	0.74
$Ag_{0.74}$	Fe	9	0.16667	-0.16667	-0.16667	0.025	0.8027
$H_3O_{0.26}$	S	6	0	0	-0.3106	0.025	1
	O1	6	0	0	0.390231	0.025	1
	O2	18	0.22363	-0.22363	-0.054048	0.025	1
	O3	18	0.1251	-0.1251	0.13025	0.025	1

Table 4.11b. Rietveld-refined atom positions (*x*, *y*, *z*), isotropic displacement parameters (U_{iso}) and occupancies of Na-Ag-H_3O-jarosite compounds synthesised at 22ºC, 97ºC and 140ºC.

Sample	**Site**	**Multiple**	**x**	**y**	**z**	U_{iso}	**Occupancy**
Synthesis temperature 97ºC							
14	Na	3	0	0	0	0.209	0.66
$Na_{0.66}$	Fe	9	0.16667	-0.16667	-0.16667	0.067	0.8701
$H_3O_{0.34}$	S	6	0	0	0.31108	0.038	1
	O1	6	0	0	0.402681	0.041	1
	O2	18	0.225952	-0.225952	-0.052193	0.046	1
	O3	18	0.130582	-0.130582	0.134369	0.023	1
16	Na	3	0	0	0	0.025	0.35
$Na_{0.35}$	Ag	3	0	0	0	0.025	0.27
$Ag_{0.27}$	Fe	9	0.16667	-0.16667	-0.16667	0.025	0.8136
$H_3O_{0.38}$	S	6	0	0	0.311004	0.025	1
	O1	6	0	0	0.392622	0.025	1
	O2	18	0.225019	-0.225019	-0.054311	0.025	1
	O3	18	0.126297	-0.126297	0.130481	0.025	1
18	Na	3	0	0	0	0.025	0.3
$Na_{0.30}$	Ag	3	0	0	0	0.025	0.53
$Ag_{0.53}$	Fe	9	0.16667	-0.16667	-0.16667	0.025	0.8047
$H_3O_{0.17}$	S	6	0	0	0.308746	0.025	1
	O1	6	0	0	0.397393	0.025	1
	O2	18	0.226295	-0.226295	-0.047375	0.025	1
	O3	18	0.126283	-0.126283	0.132478	0.025	1
20	Na	3	0	0	0	0.025	0.2
$Na_{0.20}$	Ag	3	0	0	0	0.025	0.56
$Ag_{0.56}$	Fe	9	0.16667	-0.16667	-0.16667	0.025	0.7989
$H_3O_{0.24}$	S	6	0	0	0.307866	0.025	1
	O1	6	0	0	0.396818	0.025	1
	O2	18	0.224444	-0.224444	-0.043235	0.025	1
	O3	18	0.126616	-0.126616	0.133968	0.025	1
12	Ag	3	0	0	0	0.025	0.65
$Ag_{0.65}$	Fe	9	0.16667	-0.16667	-0.16667	0.025	0.8111
$H_3O_{0.35}$	S	6	0	0	0.310024	0.025	1
	O1	6	0	0	0.392644	0.025	1
	O2	18	0.225844	-0.225844	-0.047661	0.025	1
	O3	18	0.125903	-0.125903	0.130745	0.025	1

Synthesis temperature 97ºC							
32	Na	3	0	0	0	0.025	0.51
$Na_{0.51}$	Fe	9	0.16667	-0.16667	-0.16667	0.045	0.7724
$H_3O_{0.49}$	S	6	0	0	0.31112	0.056	1
	O1	6	0	0	0.401139	0.075	1
	O2	18	0.220564	-0.220564	-0.056148	0.059	1
	O3	18	0.127442	-0.127442	0.134688	0.052	1
34	Na	3	0	0	0	0.025	0.47
$Na_{0.47}$	Ag	3	0	0	0	0.025	0.43
$Ag_{0.43}$	Fe	9	0.16667	-0.16667	-0.16667	0.025	0.7615
$H_3O_{0.10}$	S	6	0	0	0.309282	0.033	1
	O1	6	0	0	0.394162	0.044	1
	O2	18	0.222699	-0.222699	-0.050938	0.032	1
	O3	18	0.125906	-0.125906	0.13132	0.045	1
36	Na	3	0	0	0	0.025	0.03
$Na_{0.03}$	Ag	3	0	0	0	0.025	0.61
$Ag_{0.61}$	Fe	9	0.16667	-0.16667	-0.16667	0.025	0.7477
$H_3O_{0.36}$	S	6	0	0	0.308968	0.039	1
	O1	6	0	0	0.397312	0.05	1
	O2	18	0.221445	-0.221445	-0.048581	0.047	1
	O3	18	0.126046	-0.126046	0.132497	0.05	1
38	Na	3	0	0	0	0.025	0.04
$Na_{0.04}$	Ag	3	0	0	0	0.025	0.61
$Ag_{0.61}$	Fe	9	0.16667	-0.16667	-0.16667	0.025	0.7266
$H_3O_{0.35}$	S	6	0	0	0.307921	0.042	1
	O1	6	0	0	0.392383	0.062	1
	O2	18	0.2202	-0.2202	-0.047106	0.053	1
	O3	18	0.125485	-0.125485	0.130927	0.05	1
30	Ag	3	0	0	0	0.057	0.63
$Ag_{0.63}$	Fe	9	0.16667	-0.16667	-0.16667	0.057	0.7905
$H_3O_{0.37}$	S	6	0	0	0.30993	0.048	1
	O1	6	0	0	0.401021	0.087	1
	O2	18	0.224133	-0.224133	-0.047482	0.045	1
	O3	18	0.128853	-0.128853	0.13019	0.037	1
Synthesis temperature 140ºC							
49	Na	3	0	0	0	0.025	0.45
$Na_{0.47}$	Fe	9	0.166667	-0.16667	-0.16667	0.025	0.8773
$H_3O_{0.53}$	S	6	0	0	0.309936	0.027	1
	O1	6	0	0	0.393497	0.038	1
	O2	18	0.22681	-0.226805	-0.058095	0.038	1
	O3	18	0.1268	-0.1268	0.136698	0.029	1
50	Na	3	0	0	0	0.025	0.16
$Na_{0.16}$	Ag	3	0	0	0	0.025	0.23
$Ag_{0.23}$	Fe	9	0.16667	-0.16667	-0.16667	0.025	0.9418
$H_3O_{0.61}$	S	6	0	0	0.309317	0.021	1
	O1	6	0	0	0.391092	0.037	1
	O2	18	0.23023	-0.23023	-0.05585	0.036	1
	O3	18	0.127982	-0.127982	0.136264	0.022	1
51	Na	3	0	0	0	0.02	0.22
$Na_{0.22}$	Ag	3	0	0	0	0.032	0.38
$Ag_{0.38}$	Fe	9	0.16667	-0.16667	-0.16667	0.054	0.8272
$H_3O_{0.40}$	S	6	0	0	0.310415	0.042	1
	O1	6	0	0	0.392782	0.117	1
	O2	18	0.22262	-0.222617	-0.056572	0.05	1
	O3	18	0.12697	-0.126967	0.130526	0.035	1
52	Na	3	0	0	0	0.025	0.17
$Na_{0.17}$	Ag	3	0	0	0	0.025	0.45
$Ag_{0.45}$	Fe	9	0.16667	-0.16667	-0.16667	0.025	0.6558
$H_3O_{0.38}$	S	6	0	0	0.309175	0.076	1
	O1	6	0	0	0.40254	0.164	1
	O2	18	0.214951	-0.214951	-0.047445	0.084	1
	O3	18	0.125978	-0.125978	0.13216	0.056	1
53	Na	3	0	0	0	0.025	0.06
$Na_{0.06}$	Ag	3	0	0	0	0.025	0.57
$Ag_{0.57}$	Fe	9	0.16667	-0.16667	-0.16667	0.025	0.7072
$H_3O_{0.37}$	S	6	0	0	0.309332	0.06	1
	O1	6	0	0	0.402071	0.135	1

	O2	18	0.21905	-0.21905	-0.046045	0.065	1
	O3	18	0.1263	-0.126928	0.131666	0.044	1
54	Na	3	0	0	0	0.025	0.04
$Na_{0.04}$	Ag	3	0	0	0	0.025	0.66
$Ag_{0.66}$	Fe	9	0.16667	-0.16667	-0.16667	0.042	0.7775
$H_3O_{0.30}$	S	6	0	0	0.309197	0.038	1
	O1	6	0	0	0.399614	0.114	1
	O2	18	0.223332	-0.223332	-0.044463	0.037	1
	O3	18	0.126873	-0.126873	0.133519	0.033	1
61	Ag	3	0	0	0	0.06	0.76
$Ag_{0.76}$	Fe	9	0.16667	-0.16667	-0.16667	0.049	0.8356
$H_3O_{0.24}$	S	6	0	0	0.310634	0.036	1
	O1	6	0	0	0.401081	0.06	1
	O2	18	0.22408	-0.224077	-0.047583	0.022	1
	O3	18	0.12961	-0.129611	0.131392	0.02	1
Synthesis temperature 22ºC							
77	n.d.						
78	Na	3	0	0	0	0.025	0.09
$Na_{0.09}$	Ag	3	0	0	0	0.061	0.61
$Ag_{0.61}$	Fe	9	0.16667	-0.16667	-0.16667	0.053	0.7773
$H_3O_{0.30}$	S	6	0	0	0.309454	0.038	1
	O1	6	0	0	0.403203	0.03	1
	O2	18	0.22269	-0.22269	-0.044481	0.046	1
	O3	18	0.12786	-0.12786	0.133387	0.29	1
79	n.d.						
80	Na	3	0	0	0	0.025	0.03
$Na_{0.03}$	Ag	3	0	0	0	0.068	0.68
$Ag_{0.68}$	Fe	9	0.16667	-0.16667	-0.16667	0.066	0.8295
$H_3O_{0.29}$	S	6	0	0	0.309409	0.04	1
	O1	6	0	0	0.402606	0.049	1
	O2	18	0.22303	-0.223031	-0.043193	0.045	1
	O3	18	0.12913	-0.129132	0.132341	0.02	1
72	Ag	3	0	0	0	0.025	0.74
$Ag_{0.74}$	Fe	9	0.16667	-0.16667	-0.16667	0.025	0.8027
$H_3O_{0.26}$	S	6	0	0	-0.3106	0.025	1
	O1	6	0	0	0.390231	0.025	1
	O2	18	0.22363	-0.22363	-0.054048	0.025	1
	O3	18	0.1251	-0.1251	0.13025	0.025	1

4.1.4 Raman spectroscopy

4.1.4.1 Chemical composition and wavenumbers (cm^{-1}) of modes v_1(S-O) and v_3(S-O), v_2(S-O) and v_4(S-O), vOH, δOH, γOH, Fe-OH and Fe-O

Jarosite exhibits spectral features as a result of the vibrational frequencies of the molecular bonds of sulphate groups, hydroxyl groups and metal-oxygen bonds, as well as lattice vibrations and iron excitations (Bishop and Murad, 2005). Sulphate tetrahedra in aqueous solution possess *Td* symmetry and vibrational frequencies occur as a result of $v_1(SO_4^{2-})$ symmetric stretching, $v_2(SO_4^{2-})$ symmetric bending, $v_3(SO_4^{2-})$ asymmetric stretching and $v_4(SO_4^{2-})$ asymmetric bending, which are all

Raman active (Sasaki et al., 1998; Myneni, 2000). The symmetric vibrational modes produce more intense bands compared with the other sulphate vibrations because of changes in polarisability (Myneni, 2000). Sulphates of jarosite have C3v symmetry (monodentate, corner-sharing) and one v_1, one v_2, two v_3 and two v_4 frequencies are exhibited (Bishop and Murad, 2005; Myneni, 2000). Fundamental frequencies and combinations and overtones are all observed (Bishop and Murad, 2005). In jarosites, other vibrational frequencies occur as a result of hydroxyl ν(OH) stretching, δ(OH) in-plane bending and γ(OH) out-of-plane bending, as well as cation bonding in Fe-O and Fe-OH (Serna et al., 1986; Sasaki et al., 1998; Frost et al., 2006; Casas et al., 2007; Ling et al., 2016).

The results of Raman spectroscopic analyses of some of the jarosites synthesised in this project enabled the detected vibrational frequencies (wavenumbers, cm^{-1}) of the spectral peaks to be assigned to particular modes, which are shown in Table 4.12. These assignments were made on the basis of comparisons with reported frequencies and assigned modes (Serna et al., 1986; Sasaki et al., 1998; Frost et al., 2006; Casas et al., 2007; Murphy et al., 2009; Ling et al., 2016) and comparison with detected peaks in samples of the RRUFF Project database of Raman spectra at the University of Arizona (see Table 4.13). For the synthesised K-Ag jarosites of this project, the modes assigned to detected ranges of vibrational frequencies (wavenumbers) are: Fe-O 221.1-228.4 cm^{-1}, 274.1-307.0 cm^{-1}, 353.3-371.9 cm^{-1}, 432.4-438.1 cm^{-1}; $v_2(SO_4)$ 451.3-458.8 cm^{-1}; Fe-OH 556.9-576.1 cm^{-1}; $v_4(SO_4)$ 620.9-627.3 cm^{-1}; $v_1(SO_4)$ 965.8-1013.6 cm^{-1}; $v_3(SO_4)$ 1082.6-1110.1 cm^{-1}, 1120.2-1125.2 cm^{-1}, 1140.4-1166.8 cm^{-1}; and ν(OH) 3378.5-3419.9 cm^{-1}. For the synthesised Na-Ag jarosites, the vibrational frequencies and assigned modes are: Fe-O 224.6-228.4 cm^{-1}, 296.0-309.8 cm^{-1}, 358.9-371.9 cm^{-1}, 435.9-441.4 cm^{-1}; $v_2(SO_4)$

450.7-458.8 cm^{-1}; Fe-OH 555.4-570.6 cm^{-1}; $v_4(SO_4)$ 621.8-625.8 cm^{-1}; $v_1(SO_4)$ 966.6-1016.2 cm^{-1}; $v_3(SO_4)$ 1088.0-1114.3 cm^{-1}, 1122.2-1125.2 cm^{-1}, 1140.4-1165.3 cm^{-1}; and v(OH) 3378.5-3417.2 cm^{-1}. For the synthesised Pb-Ag jarosites, the vibrational frequencies and assigned modes are: Fe-O 217.6-226.4 cm^{-1}, 277.0 cm^{-1}, 336.1-362.0 cm^{-1}, 422.2-437.6 cm^{-1}; Fe-OH 558.2-573.4 cm^{-1}; $v_4(SO_4)$ 618.8-622.1 cm^{-1}; $v_1(SO_4)$ 976.7-1012.0 cm^{-1}; $v_3(SO_4)$ 1101.2-1104.4 cm^{-1}, 1121.8 cm^{-1}, 1156.5-1172.2 cm^{-1}; and v(OH) 3385.0-3449.6 cm^{-1}. In the Pb-Ag jarosites, no peaks were present that could be assigned to $v_2(SO_4)$.

The Raman spectra of the synthesised K-Ag, Na-Ag and Pb-Ag jarosites also contained bands (see Table 4.12) that have not been reported in previous Raman studies. These include peaks at 3581.8-3595.3 cm^{-1} in K-Ag samples, 3578.3-3593.5 cm^{-1} in Na-Ag samples and 3584-3589.8 cm^{-1} in Pb-Ag samples. Of these, the only strong bands were in Ag-sample JS72 at 3592.4 cm^{-1}; in all the other samples the band strengths were weak. These peaks have been assigned to a hydroxyl stretching mode, v(OH), or water stretching mode, $v(H_2O)$, on the basis of evidence from other studies. Raman peaks at 3515 cm^{-1} were assigned to v(OH) in Sasaki et al. (1998), whereas IR peaks at 3501 cm^{-1} were assigned to $v(H_2O)$ in Powers et al. (1975). IR peaks at ~ 3550 cm^{-1} (medium band strength) in synthetic Na-jarosite and K-jarosite and ~ 3550 cm^{-1} (weak band strength) in natural jarosite were assigned to $v(H_2O)$ in Bishop and Murad (2005). Peaks at 3459.7, 3410.5 and 3385.5 cm^{-1} were assigned to v(OH) in synthesised K-jarosite [chemical formula $K_{1.06}Na_{0.01}Fe_{3.30}(SO_4)_2(OH)_6$] and peaks at 3428.4, 3385.7 and 3357.1 cm^{-1} were assigned to v(OH) in Na-jarosite [chemical formula $Na_{1.05}Fe_{3.30}(SO_4)_2(OH)_6$] in Ling et al. (2016). A study of the IR spectrum of K-jarosite reports a broad profile centred on 3356 cm^{-1} with overlapping bands of v(OH) (hydroxyl stretching) modes and adsorbed water extending from

3590 to 2600 cm^{-1}, although Raman analysis does not detect bands of adsorbed water (Frost et al., 2006). IR spectral bands at ~ 3600 cm^{-1} have been assigned to *v*(OH) bands in the sulphates gypsum and ettringite (Myneni, 2000).

Spectral bands were detected at 3075.1-3080.1 cm^{-1} in K-Ag samples, 3075.1-3082 cm^{-1} in Na-Ag samples and 3077.3-3081 cm^{-1} in Pb-Ag samples. These bands were strong in Ag-jarosite samples JS72 and JS61, and in K-Ag samples JS24, JS26, JS55, JS57, JS58, JS59, JS60, JS74 and JS76, and Na-Ag samples JS16, JS42, JS54 and JS77; these bands were medium strength in Na-Ag samples JS34, JS49, JS51, JS52, JS53, JS78, JS79 and JS80; and all other of these peaks were weak. These peaks have been assigned to *v*(OH), on the basis of the IR study of K-jarosite by Frost et al. (2006), mentioned above, reporting a broad profile centred on 3356 cm^{-1} with overlapping bands of *v*(OH) modes from 3590 to 2600 cm^{-1}. For the same reason, two further band ranges have been assigned to *v*(OH). First, peaks at 2760.2-2762.5 cm^{-1} in K-Ag samples and 2752.5-2760.2 cm^{-1} in Na-Ag samples. Ag-jarosite sample JS72 has a medium-strength band at 2760.2 cm^{-1}; all other bands in the range are weak. Second, peaks at 2573.6-2580.5 cm^{-1} in K-Ag samples, 2574.9-2583.1 cm^{-1} in Na-Ag samples and 2574.9-2581.5 cm^{-1} in Pb-Ag samples. Again, only Ag-jarosite sample JS72 has a medium-strength band; all other bands in the range are weak.

Spectral bands were present at 1668.0-1690.5 cm^{-1} in K-Ag samples, 1598.4-1687.5 cm^{-1} in Na-Ag samples and 1668.0-1682.7 cm^{-1} in Pb-Ag samples. These have been assigned to $2v_3(SO_4^{2-})/2\delta OH$, on the basis of reported IR bands at 1634s cm^{-1} in synthetic K-jarosite and at 1639s cm^{-1} in synthetic Na-jarosite and at 1630m cm^{-1} in natural K-jarosite, which were assigned to $\delta(H_2O)$ (in-plane bending) (Bishop and Murad, 2005). In addition, RRUFF Project jarosite samples R060113

(K-jarosite), R070493 (K-jarosite), R050289 (Na-jarosite), R050471 (Na-jarosite) and 060097 (Ag-jarosite) show weak, broad peaks at 1672.5-1692.2 cm^{-1}. The spectra from the Raman analysis of the synthesised jarosite compounds of this project are contained in Appendix G.

In Raman spectra, frequency differences in vibrational modes with different *A*-site substitutions in the jarosite structure may be caused by the heaviness (atomic number) of the elements present (Murphy et al., 2009). These frequency differences may be due to differences in the bonding to the metal cations, so revealing small but important structural differences with cation substitution, which may be due to different electronic configurations (Murphy et al., 2009); in this study, these differences may be the result of the substitution of Ag (a transition metal) for K or Na (alkali metals). In some of the synthesised products in this study, the assigned vibrational modes of the synthesised K-H_3O-jarosite compounds have higher wavenumbers (cm^{-1}) than their Ag-H_3O equivalents, which is consistent with some reported modes but not with others (Serna et al., 1996; Sasaki et al., 1998; Frost et al., 2006; Murphy et al., 2009): samples 22 (K-H_3O) and 30 (Ag-H_3O) (both 97°C), respectively, ν(OH) (3411.7 and 3393.7), $\nu_3(SO_4)$ (lower reading, 1104.5 and 1088), $\nu_1(SO_4)$ (lower reading, 1009.3 and 972.12), and $\nu_4(SO_4)$ (627.16 and 624.4). Therefore, these results are not consistent with predicted stronger bonds for heavier elements (Murphy et al., 2009). In some other cases, the K-H_3O-jarosite compounds have lower wavenumbers than their Ag-H_3O equivalents, thereby providing evidence of stronger bonds for Ag: products 22 and 30, respectively, $\nu_3(SO_4)$ (upper reading, 1158.4 and 1163.9) and $\nu_2(SO_4)$ (432.6 and 438.12); products 55 (K-H_3O) and 61

Table 4.12a. Raman frequencies (wavenumbers, cm^{-1}) and mode assignments in synthetic K-Ag jarosite compounds.

Mode	**JS22**	**JS73**	**JS55**	**JS24**	**JS74**	**JS26**	**JS08**	**JS75**	**JS28**	**JS76**	**JS56**	**JS57**	**JS58**	**JS59**	**JS60**	**JS30**	**JS72**	**JS61**
Rietveld fitting content	$K_{0.61}H_3O_{0.39}$	$K_{0.67}H_3O_{0.33}$	$K_{0.32}H_3O_{0.68}$	$K_{0.63}Ag_{0.10}H_3O_{0.27}$	$K_{0.61}Ag_{0.08}H_3O_{0.31}$	$K_{0.27}Ag_{0.18}H_3O_{0.55}$	$K_{0.53}Ag_{0.28}H_3O_{0.19}$	$K_{0.37}Ag_{0.19}H_3O_{0.44}$	$K_{0.30}Ag_{0.43}H_3O_{0.27}$	$K_{0.37}Ag_{0.26}H_3O_{0.37}$	$K_{0.71}Ag_{0.09}H_3O_{0.20}$	$K_{0.56}Ag_{0.21}H_3O_{0.23}$	$K_{0.38}Ag_{0.35}H_3O_{0.27}$	$K_{0.46}Ag_{0.39}H_3O_{0.15}$	$K_{0.34}Ag_{0.55}H_3O_{0.11}$	$Ag_{0.63}H_3O_{0.37}$	$Ag_{0.74}H_3O_{0.26}$	$Ag_{0.76}H_3O_{0.24}$
Temp. of formation	97ºC	22ºC	140ºC	97ºC	22ºC	97ºC	97ºC	22ºC	97ºC	22ºC	140ºC	140ºC	140ºC	140ºC	140ºC	97ºC	22ºC	140ºC
Temp. of drying	110ºC	22ºC	110ºC	110ºC	22ºC	110ºC	60ºC	22ºC	110ºC	22ºC	110ºC	110ºC	110ºC	110ºC	110ºC	110ºC	22ºC	110ºC
Un-assigned			3586.4w	3595.3w	3586.4w	3586.37 w				3592.4w	3584.1w	3585.2w	3586.4w	3581.8w	3585.2		2592.4s	3584.1w
*v*OH									3417.3									
*v*OH	3411.7	3414.7	3412.08		3413.26		3413.1	3410.01	3410.4	3411.18	3416.78	3408.5s						
*v*OH				3407.6		3406.19	3407.6		3407.6				3403.84					
*v*OH									3399.3									

*v*OH									3395.2					3397.95				
*v*OH															3384.97	3393.7	3373.43	3384.97
Un-assigned									3123.4							3378.5		
Un-assigned	3077.7w	3080.1w	3077.3s	3075.1s	3078.5s	3077.3s	3079.2w	3078.8w		3077.6s	3079.8w	3078.5s	3078.5s	3078.5s	3078.5s		3080.1s	3078.5s
Un-assigned												2762.5w					2760.2	
Un-assigned			2578.8w		2576.2w	2573.6w				2577.8w		2577.5w	2477.5w		2576.2w		2580.5	2574.9w
Un-assigned		2409.88	2409.55		2410.9	2409.55				2413.92		2412.2s	2408.21	2409.55	2410.9		2413.92	2408.21
Un-assigned			2292.76		2294.13	2296.87				2295.83		2292.76					2299.93	
Un-assigned			2206.08		2204.69	2206.08				2205.02	2207.46	2206.08	2204.69	2207.46	2203.31		2207.79	2204.69
Un-assigned			2167.24		2165.85	2167.24		2165.85		2167.57	2167.24	2165.85	2165.85	2165.85	2165.85		2167.57	2165.85
Un-assigned		2167.57	2103.01		2104.42	2104.42		2103.01		2104.75	2103.01	2103.01	2103.01	2103.01	2103.01		2104.75	2104.42
Un-assigned		2103.35	2008.52								2007.1	2012.77	2014.19	2015.61	2012.77			2011.36

Un-assigned																		
$2\nu_3(SO_4^{2-})$ / 2δOH#		1681.61	1682.74		1690.12			1690.48			1682.74	1679.78	1673.87	1672.39	1676.83			1667.95
$2\nu_3(SO_4^{2-})$ / 2δOH			1404.72 s															
HOH																	1232.12	
$\nu_3(SO_4^{2-})$							1166.8											
$\nu_3(SO_4^{2-})$				1162.6			1161.3									1163.9		
$\nu_3(SO_4^{2-})$	1158.4	1158.46	1154.93		1154.93	1159.66		1156.88	1153	1158.46	1156.51	1156.51	1156.51	1156.51	1156.51			1156.51
$\nu_3(SO_4^{2-})$																1140.4		
$\nu_3(SO_4^{2-})$	1125.2		1123.38	1122.6	1123.38	1121.8		1121.8		1122.18		1121.8	1121.8		1120.22		1122.18	
$\nu_3(SO_4^{2-})$	1110.1						1108.8		1108.8							1110.1		
$\nu_3(SO_4^{2-})$	1104.5	1103.18	1101.22	1106.1	1102.1	1104.39		1104.77		1104.77	1101.22	1102.81	1101.22	1101.22	1104.39		1104.77	1104.39
$\nu_3(SO_4^{2-})$				1100.5						1082.56						1088		

$\nu_1(SO_4^{2-})$	1013.5			1013.6			1013.6		1012.2							1013.5		
$\nu_1(SO_4^{2-})$	1009.3	1007.58	1007.2	1006.7	1007.2	1008.8	1009.5	1009.18	1009.5	1009.18	1007.2	1008.8	1008.8	1008.8	1010.4		1012.39	1012
$\nu_1(SO_4^{2-})$†									972.26	965.82						972.12	969.04	
$\nu_4(SO_4^{2-})$	627.16			627.3			627.3											
$\nu_4(SO_4^{2-})$		624.21	623.81		623.81	623.81	621.8	624.21	623.16	620.85	623.81	623.81	622.13	622.13	622.13	624.4	622.53	622.13
Unassigned							595.6			592.32						592.67		
Fe-OH	573.35	572.12	570.04	572.11	573.41		569.4	572.12		570.44								
Fe-OH						564.98	565.2		561.07		566.66	564.98	563.29	561.6	563.29	562.31	562.01	559.92
Fe-OH							556.9											
$\nu_2(SO_4^{2-})$	456.06	453.27	452.96		454.67	451.26	452.1		452.06	456.79	451.26	451.26				458.82		
$\nu_2(SO_4^{2-})$	432.6	432.85	432.44	438.26	432.44	432.44	436.9	432.85	435.5	434.56	430.73	432.44	434.16	434.16	437.58	438.12	437.99	437.58
Fe-O																371.89		

Fe-O	363.61	357.21	353.34		356.8	356.8	361.0		358.23	360.66	353.34	355.07	353.34	356.8	358.52	360.85	362.39	360.25
Fe-O	302.9	300.05		303.04	301.37	301.37	301.7	301.79	304.42	301.79		301.37	301.37	303.11	304.85	307.04	305.26	304.85
Fe-O			299.64									299.64						
Fe-O										274.06								
Fe-O*	228.38	223.27	222.85	223.01	224.6	224.6	225.8	225.02	225.77	226.77	222.85	222.85	221.1	222.85	224.6	227	226.77	224.6
Un-assigned		138.75	138.33		140.1	138.33		140.52		138.75	138.33	138.33	138.33	138.33	138.33		138.75	138.33

Key: B-O* = B-O (or OH-O, Frost et al,. 2006b); † = similar peak and assignment reported at http://www.sci.qut.edu.au/sci_schps.html; # Assigned to δ(H2O) in mid-IR study of synthetic K-jarosite in Bishop and Murad (2005); s = strong; w = weak; sh = shoulder; b = broad; sp = sharp

Table 4.12b: Raman frequencies (wavenumbers, cm^{-1}) and mode assignments in synthetic Na-Ag jarosite compounds.

Mode	**JS32**	**JS49b1**	**JS16**	**JS34**	**JS78**	**JS36**	**JS38b1**	**JS80**	**JS50**	**JS51**	**JS52**	**JS53**	**JS54**	**JS30**	**JS72**	**JS61**
Rietveld fitting content	$Na_{0.02}$ $H_3O_{0.98}$	$Na_{0.47}$ $H_3O_{0.53}$	$Na_{0.35}$ $Ag_{0.27}$ $H_3O_{0.38}$	$Na_{0.47}$ $Ag_{0.43}$ $H_3O_{0.10}$	$Na_{0.09}$ $Ag_{0.61}$ $H_3O_{0.30}$	$Na_{0.03}$ $Ag_{0.61}$ $H_3O_{0.36}$	$Na_{0.04}$ $Ag_{0.61}$ $H_3O_{0.35}$	$Na_{0.31}$ $Ag_{0.68}$ $H_3O_{0.29}$	$Na_{0.16}$ $Ag_{0.23}$ $H_3O_{0.61}$	$Na_{0.22}$ $Ag_{0.38}$ $H_3O_{0.40}$	$Na_{0.17}$ $Ag_{0.45}$ $H_3O_{0.38}$	$Na_{0.06}$ $Ag_{0.57}$ $H_3O_{0.37}$	$Na_{0.04}$ $Ag_{0.66}$ $H_3O_{0.30}$	$Ag_{0.63}$ $H_3O_{0.37}$	$Ag_{0.74}$ $H_3O_{0.26}$	$Ag_{0.76}$ $H_3O_{0.24}$
Formation temp.	97ºC	140ºC	97ºC	97ºC	22ºC	97ºC	97ºC	22ºC	140ºC	140ºC	140ºC	140ºC	140ºC	97ºC	22ºC	140ºC
Drying temp.	110ºC	110ºC	60ºC	110ºC	22ºC	110ºC	110ºC	22ºC	110ºC	110ºC	110ºC	110ºC	110ºC	110ºC	22ºC	110ºC

Unassigned		3578.6w		3578.3w	3585.5w					3586.6w	3585.5w	3585.5w	3584.4w		3592.4s	3584.1w
*v*OH	3417.2															
*v*OH	3408.9	3405.3							3401.76							
*v*OH	3399.2		3399.3	3396.77						3398.23						
*v*OH			3392.4	3392.05	3389.69	3393.8	3388.2	3388.79			3384.07	3382.89	3393.51	3393.7	3373.43	3384.97
*v*OH														3378.5w		
Unassigned		3078.8	3079.2w	3076.1	3078.8	3082w	3081.9w	3078.8	3078.8w	3078.8	3080.1	3077.6	3078.8s		3080.1s	3078.5s
Unassigned													2752.5w		2760.2	
Unassigned		2576.5w								2581.8w	2579.2w	2583.1w	2475.2w		2580.5	2574.9w
Unassigned		2409.88		2410.9						2411.22	2412.57	2408.53	2412.57		2413.92	2408.21
Unassigned										2295.83			2291.72		2299.93	
Unassigned		2206.41								2205.02	2207.79	2205.02	2206.41		2207.79	2204.69
Unassigned		2166.18		2167.24						2167.57	2166.18	2167.57	2167.57		2167.57	2165.85
Unassigned		2104.75		2103.01	2167.57			2167.57		2104.75	2103.35	2103.35	2103.35		2104.75	2104.42
Unassigned		2020.2			2103.35			2103.35	2015.95	2018.78	2014.53	2017.37	2013.11			2011.36

$2\nu_3(SO_4^{2-})$ / 2δOH#		1687.52		1673.87	1680.14			1681.61	1687.52	1678.66	1684.57	1680.14	1666.82			1667.95
HOH															1232.12	
$\nu_3(SO_4^{2-})$	1165.3						1163.9						1160.03	1163.9		
$\nu_3(SO_4^{2-})$	1159.7	1158.46	1158.5	1158.08	1158.46	1159.9	1154.2	1156.88	1158.46	1158.46	1158.46	1158.46				1156.51
$\nu_3(SO_4^{2-})$														1140.4		
$\nu_3(SO_4^{2-})$				1123.38									1122.18		1122.18	
$\nu_3(SO_4^{2-})$	1108.7		1114.3			1107.4	1110.1							1110.1		
$\nu_3(SO_4^{2-})$		1106.35		1105.97	1106.35			1106.35	1106.35	1106.35	1106.35	1106.35	1104.77		1104.77	1104.39
$\nu_3(SO_4^{2-})$														1088		
$\nu_3(SO_4^{2-})$	1013.5	1012.39	1012.2	1012	1012.39	1012.2	1013.5	1012.39	1012.39	1012.39	1012.39	1012.39	1012.39	1013.5	1012.39	1012
$\nu_1(SO_4^{2-})$†							966.61							972.12	969.04	
$\nu_4(SO_4^{2-})$	652															
$\nu_4(SO_4^{2-})$	625.78	622.53	623.2	622.13	622.53	621.78	624.4	622.53	622.53	622.53	622.53	622.53	622.53	624.4	622.53	622.13
Unassigned														592.67		
B-OH	570.59															

B-OH	563.69	563.69	563.8		563.69	561.07	567.83	562.01	562.01	562.01	560.32	560.32		562.31	562.01	559.92
B-OH				558.23			558.17						558.63			
$v_2(SO_4^{2-})$			450.7											458.82		
$v_2(SO_4^{2-})$	439.5	437.99	438.3	435.87	439.7	436.88	438.12	437.99	437.99	436.28	437.99	437.99	437.99	438.12	437.99	437.58
B-O						366.51	366.37							371.89		
B-O	364.99	360.66		360.25	362.39		359.47	365.84	360.66	360.66	362.39	358.94	362.39	360.85	362.39	360.25
B-O	309.79	300.05	303	303.11	307	304.42	308.42	307	303.53	305.26	305.26	305.26	305.26	307.04	305.26	304.85
B-O	296															
B-O*	228.38	225.02	227.2	224.6	226.77	227.15	228.38	226.77	226.77	225.02	225.02	225.02	225.02	227	226.77	224.6
Unassigned		136.98		138.33	138.75			140.52	136.98	138.75	138.75	138.75	138.75		138.75	138.33

Key: B-O* = B-O (or OH-O, Frost et al,. 2006b); † = similar peak and assignment reported at http://www.sci.qut.edu.au/sci_schps.html; # Assigned to δ(H2O) in mid-IR study of synthetic K-jarosite in Bishop and Murad (2005); s = strong; w = weak; sh = shoulder; b = broad; sp = sha

Table 4.12c. Raman frequencies (wavenumbers, cm^{-1}) and mode assignments in synthetic Pb-Ag jarosite compounds.

Sample	**JS43**	**JS43d**	**JS44**	**JS45**	**JS46D**	**JS47**	**JS48**	**JS61**
A-site	$Pb_{0.179}$	$Pb_{0.168}$	$Pb_{0.081}Ag_{0.281}$	$Pb_{0.082}Ag_{0.502}$	$Pb_{0.041}Ag_{0.58}$	$Pb_{0.021}Ag_{0.766}$	$Pb_{0.021}Ag_{0.765}$	$Ag_{0.76}$
content	$H_3O_{0.821}$	$H_3O_{0.832}$	$H_3O_{0.638}$	$H_3O_{0.416}$	$H_3O_{0.379}$	$H_3O_{0.213}$	$H_3O_{0.214}$	$H_3O_{0.24}$
Unass					3589.8w	3587.5w	3587.5w	3584.1
vOH	3441.43	3449.63						
vOH	3430.88							
vOH			3417.96					
vOH				3402.66				
vOH					3384.97	3389.69	3390.87	3384.97
Unass	3080.99	3077.29	3078.52	3078.52	3078.52	3077.29	3078.52	3078.52
Unass					2581.5w			2574.9w
Unass		2406.86			2410.9	2410.9	2408.21	2408.21
Unass							2296.87	
Unass					2204.69	2206.08	2206.08	2204.69
Unass	2165.85	2165.85	2167.24	2167.24	2167.24	2167.24	2167.24	2165.85
Unass	2104.42	2103.01	2103.01	2103.01	2104.42	2103.01	2103.01	2104.42
Unass			2017.03	2012.77	2015.61	2022.7	2018.45	2011.36
Unass			1965.84					
$2v_3(SO_4^{2-})$ / 2δOH #			1678.31	1676.83	1678.31	1679.78	1682.74	1667.95
$v_3(SO_4^{2-})$		1172.24						
$v_3(SO_4^{2-})$	1169.09		1162.8					
$v_3(SO_4^{2-})$				1159.66	1156.51	1158.08	1158.08	1156.51
$v_3(SO_4^{2-})$ / δOH		1121.8						
$v_3(SO_4^{2-})$	1101.22	1102.81	1102.81	1104.39	1102.81	1104.39	1104.39	1104.39
$v_1(SO_4^{2-})$	1012	1012	1012	1012	1012	1012	1010.4	1012
$v_1(SO_4^{2-})$†		976.7						
$v_4(SO_4^{2-})$	618.78	620.46	620.46	620.46	620.46	620.46	620.46	622.13
Fe-OH	573.41	573.41	568.35	563.29				559.92
Fe-OH					558.23	559.92	559.92	
$v_2(SO_4^{2-})$								
Fe-O	435.87	435.87		434.16	437.58	437.58	437.58	437.58
Fe-O	422.17		429.02					
Fe-O	336.05	336.05	358.52	361.98	360.25	358.52	358.52	360.25
Fe-O			306.58	306.58	304.85	304.85	304.85	304.85
Fe-O	277.02							
Fe-O*	224.6	217.59	224.6	226.35	222.85	224.6	224.6	224.6
Unass	134.79	134.79	134.79	136.56	138.33	138.33	138.33	138.33

Key: Unass = unassigned Fe-O* = Fe-O (or OH-O, Frost et al. 2006b) ; † = similar peak and assignment reported at http://www.sci.qut.edu.au/sci_schps.html; # Assigned to $\delta(H_2O)$ in mid-IR study of synthetic K-jarosite in Bishop and Murad (2005). s = strong; w = weak; sh = shoulder; b = broad; sp = sharp
A-site contents of 43-48 are Rietveld refinement data and the content of 61 is combined data.

Table 4.13. Reported Raman frequencies (wavenumbers, cm^{-1}) and mode assignments in synthetic jarosite compound end-members, and in other jarosite-family compounds.

Mode	JS22	K[1]	K[2]	K[5]	K[6]	JS32	Na[1]	Na[2]	Na[3]	Na[7]	Na[8]	JS30	Ag[2]	Ag[4]	Ag[9]	Ag[10]	H_3O[1]	H_3O[4]
*v*OH														3440.3				3452.0
*v*OH						3417.2												
*v*OH	3411.7			3410.67s	3412.36s	3408.9					3401.95s							3410.9
*v*OH						3399.2	3399		3394	3388.85s		3393.7		3394.2	3380.52s	3384.38s		3383.2
*v*OH							3368					3378.5w		3371.6				3372.0
Unassigned	3077.7w																	
Unassigned															2215.73w			
Unassigned				2006.74w	2012.29w						2005.74w				2017.10w			
Unassigned				1688.55w	1692.17w					1672.52w	1679.83w				1679.62w			
$v_3(SO_4^{2-})$	1158.4	1161	1153.33	1154.36	1159.91s	1165.3	1160	1154.24w	1152w	1153.76	1155.29	1163.9	1160.58w	1153.6	1157	1157	1163	1154.3
$v_3(SO_4^{2-})$						1159.7						1140.4						
$v_3(SO_4^{2-})$	1125.2																	
$v_3(SO_4^{2-})$	1110.1	1112	1102.63s	1102.29s	1109.77s	1108.7	1114	1112.59	1105	1109.41s	1105.15s	1110.1	1107.16	1104.5	1110.72s	1108.79	1099	1102.9
$v_3(SO_4^{2-})$	1104.5																	
$v_3(SO_4^{2-})$												1088						

$\nu_1(SO_4^{2-})$	1013.5	1015	1006.67	1009.73s	1013.35	1013.5	1014	1012.10	1007	1012.98s	1010.65	1013.5	1012.10	1011	1016.22s	1016.22	1011	1007.3
$\nu_1(SO_4^{2-})$	1009.3																	
$\nu_1(SO_4^{2-})$†										974.41sh		972.12			975.73w			
Unassigned											840.95b							
$\nu_4(SO_4^{2-})$						652								648.9				642.6
$\nu_4(SO_4^{2-})$	627.16	625	624.61s	625.96	631.51	625.78	627	624.61sp	617sp	625.36s	623.03	624.4	622.80sp	627.6	626.67s	624.75	619	624.3
$\nu_4(SO_4^{2-})$														621.0				
$\nu_4(SO_4^{2-})$														614.2				
γOH		560	576.63w	573.89	591.01w	570.59	571	570.29w	559w	567.51w	563.25	592.67	573.91w		576.53w	578.46w	563	576.4
O-Fe						563.69								562.7				
Fe-OH												562.31		558.5				554.7
O-Fe	573.35																530	
$\nu_2(SO_4^{2-})$														476.9				465.7
$\nu_2(SO_4^{2-})$	456.06		453.50					450.78sh				458.82		451.4				453.4
$\nu_2(SO_4^{2-})$		442			444.54s		445		445sh	444.09s	441.76s		448.97sh	440.6	445.40s	445.40s		433.6

O-Fe	432.6	434.49s	436.97s		439.5		444.44s	437s			438.12	441.73s					
O-Fe						406					371.89						
O-Fe	363.61	357.53w	354.05		364.99	365	367.49w	357w	365.02w	356.90w	360.85	362.96w		368.26w		382	
O-Fe	302.9	301.40	300.05	303.67w	309.79	303					307.04	305.93sp		308.48s	310.41		
O-Fe					296	295	298.68	288	295.59	299.05							
O-Fe	228.38	223.54s	222.91s	230.39s	228.38	228	227.16	220	224.24s	219.98s	227	228.07	224.8	229.41s	227.48		224.1
Unassigned														188.91w			
Unassigned				147.47w		142			139.39w	140.91				142.63w	142.63sw	110	

Key: 1 = Serna et al. (1986); 2 = Sasaki et al (1998); 3 = Casas et al. (2007) [$Na_{0.53}(H_3O)_{0.47}Fe_{1.79}(OH)_6(SO_4)_2$]; 4 = Frost et al. (2006) (natural jarosite); 5 = RRUFF project R060113; 6 = RRUFF project R070493; 7 = RRUFF project R050289; 8 = RRUFF project R050471; 9 = RRUFF project 060097; 10 = RRUFF project 060098. s = strong; w = weak; sh = shoulder; b = broad; sp = sharp † = www.sci.qut.edu.au/sci_schps.html; RRUFF Project (integrated database of Raman spectra, XRD and chemistry data at the University of Arizona): http://rruff.info/jarosite/display=default/ 5 = RRUFF Project R060113, Jarosite, Iron Blossom Mine, East Tintic District, Eureka, Utah, USA; 6 = RRUFF Project R070493, Jarosite, Maria Josefa Mine, Rhodalquilar, Almeria Province, Spain; 7 = RRUFF Project R050289, Natrojarosite, Bristol Mine, Pioche, Lincoln County, Nevada, USA; 8 = RRUFF Project R050471, Natrojarosite, Bristol Mine, Pioche, Lincoln County, Nevada, USA; 9 = RRUFF Project 060097, Argentojarosite, Locality unknown; 10 = RRUFF Project 060098, Argentojarosite, Tintic Standard Mine, Dividend, Utah, USA.

(Ag-H_3O) (both 140°C), respectively, $v_3(SO_4)$ (1101.22 and 1104.39; 1154.93 and 1156.51), $v_1(SO_4)$ (1007.2 and 1012) and $v_2(SO_4)$ (432.44 and 437.58); and products 73 (K-H_3O) and 72 (Ag-H_3O) (both 22°C), respectively, $v_3(SO_4)$ (lower reading, 1103.18 and 1104.77), $v_1(SO_4)$ (1007.58 and 1012.39) and $v_2(SO_4)$ (432.85 and 437.99).

In all cases, the assigned modes of Ag-H_3O-jarosite compounds do not have higher wavenumbers than their Na-H_3O equivalents, but some have the same wavenumbers, which is consistent with some reported modes but not with others (see Tables 4.12 and 4.13) (Sasaki et al., 1998; Frost et al., 2006; RRUFF projects 060097 and 060098). The Na-H_3O modes with higher wavenumbers than their Ag-H_3O equivalents are: products 32 (Na-H_3O) and 30 (Ag-H_3O) (both 97°C), respectively, v(OH) (3399.2 and 3393.7), $v_3(SO_4)$ (1108.7 and 1088; 1165.3 and 1163.9), $v_4(SO_4)$ (625.78 and 624.4) and $v_2(SO_4)$ (439.5 and 438.12); products 49 (Na-H_3O) and 61 (Ag-H_3O) (both 140°C), respectively, v(OH) (3405.3 and 3384.97) and $v_3(SO_4)$ (1106.35 and 1104.39; and 1158.46 and 1156.51); and products 77 (Na-H_3O) and 72 (Ag-H_3O) (both 22°C), respectively, v(OH) (3401.76 and 3373.43), $v_3(SO_4)$ (1107.94 and 1104.77; 1156.88 and 1122.18), $v_4(SO_4)$ (624.21 and 622.53) and $v_2(SO_4)$ (441.41 and 437.99). Therefore, these results are also not consistent with predicted stronger bonds for heavier elements (Murphy et al., 2009).

The Pb-H_3O-jarosite compounds (samples 43/43d) have lower wavenumbers than their Ag-H_3O equivalent (sample 61) for the assigned modes of $v_3(SO_4)$ (1101.22/1102.81 and 1104.39 respectively) and $v_4(SO_4)$ (618.78/620.46 and 622.13), thereby providing evidence of stronger bonds for Ag. The Pb-H_3O-jarosite compounds have higher wavenumbers than their Ag-H_3O equivalent for the assigned modes of v(OH) (3441.43/3449.63 and 3384.97 respectively) and $v_3(SO_4)$ (1172.24

and 1156.51), indicating weaker bonds for Ag. The Pb-H_3O and Ag-H_3O jarosite products have the same wavenumber for $\nu_1(SO_4)$ (1012). Pb is a heavier element than Ag but the chemical analyses indicate low Pb content in the Pb-H_3O and Pb-Ag-H_3O jarosite compounds. A study (Smith, 2004) has reported that, in plumbojarosite, broadening of the peaks corresponding to $\nu_1(SO_4^{2-})$ and $\nu_3(SO_4^{2-})$ owing to two overlapping peaks assigned to two types of sulphate groups, SO_4^{2-} ions adjacent and not adjacent to Pb^{2+} ions in ordered plumbojarosite structure with half the *A* sites filled with Pb and half the *A* sites vacant; however, the Raman spectra of this project did not display such broad peaks for Pb-H_3O-jarosite, although this may be because of the low Pb content and high H_3O content of the compounds.

In the series of synthesised K-Ag-H_3O- and Na-Ag-H_3O-jarosite compounds, no consistent trend is discernible in the wavenumbers of the assigned modes with increasing Ag content of the products. However, the K-Ag-H_3O jarosite series in which trends may be observed are: samples 22 (K-H_3O)-30 (Ag-H_3O) (97°C), $\nu_4(SO_4)$ (decreasing cm^{-1}); 55 (K-H_3O)-61 (Ag-H_3O) (140°C), ν(OH) (decreasing cm^{-1}), $\nu_3(SO_4)$ (increasing cm^{-1}) and ν_1SO_4 (increasing cm^{-1}); and 72 (Ag-H_3O), 73 (K-H_3O)-76 (K-Ag-H_3O) (22°C), ν(OH) (decreasing cm^{-1}), $\nu_1(SO_4)$ (increasing cm^{-1}) and $\nu_2(SO_4)$ (increasing cm^{-1}). The Na-Ag-H_3O jarosite series in which trends may be observed are: 30 (Ag-H_3O), 32 (Na-H_3O)-38 (Na-Ag-H_3O) (97°C), $\nu_3(SO_4)$ (increasing cm^{-1}, except the Na-H_3O and Ag-H_3O products) and $\nu_2(SO_4)$ (increasing cm^{-1}, except the Na-H_3O product); 49 (Na-H_3O)-54 (Na-Ag-H_3O) and 61 (Ag-H_3O) (140°C), ν(OH) (decreasing cm^{-1}) and $\nu_3(SO_4)$ (decreasing cm^{-1}); and 72 (Ag-H_3O) and 77 (Na-H_3O)-80 (Na-Ag-H_3O) (22°C), $\nu_2(SO_4)$ (decreasing cm^{-1}). The Pb-Ag-H_3O-jarosite series 43/43d (Pb-H_3O)-48 (Pb-Ag-H_3O) and 61 (Ag-H_3O) (140°C) shows a trend of generally decreasing wavenumbers for modes ν(OH) and $\nu_3(SO_4)$

(upper range) and a trend of generally increasing wavenumbers for modes $v_3(SO_4)$ (lower range) and $v_4(SO_4)$. An increasing trend indicates growing bond strength with increasing Ag content of the synthesised jarosite compounds; a decreasing trend indicates declining bond strength with increasing Ag content.

In the Fe-O modes, the synthesised K-Ag-H_3O-jarosite compounds have lower ranges of wavenumbers than the Na-Ag-H_3O jarosite products, which is not consistent with some reported modes (Casas et al., 2007; Murphy et al., 2009; RRUFF project R050471), but is with other reported modes (Sasaki et al., 1998; Murphy et al., 2009; RRUFF project R060113). The Pb-Ag-H_3O-jarosite compounds have lower ranges of wavenumbers than the equivalent Na-Ag-H_3O-jarosites for the Fe-O modes. Relative to the equivalent K-Ag-H_3O-jarosites, the Pb-Ag-H_3O-jarosites have a lower range of wavenumbers for one Fe-O mode and higher ranges of wavenumbers for two other Fe-O modes. Therefore, these results provide contradictory evidence on any relationship between Fe-O bonding and *A*-site substitution.

4.1.5 Electron microprobe analysis (EMPA) of synthesised jarosites

4.1.5.1 Compositions of synthesised K-Ag, Na-Ag and Pb-Ag jarosites

The results of EMPA of the synthetic K-Ag-H_3O, Na-Ag-H_3O and Pb-Ag-H_3O jarosite compounds are shown in the chemical compositions (weight percent) and site occupancies listed in Appendix J. The site occupancies, as well as the concentrations of cations in the starting solutions, of the synthetic K-Ag-H_3O and Na-Ag-H_3O jarosites are also shown in Tables 4.14 and 4.15, respectively. The results show a generally declining content of K (Table 4.14) and Na (Table 4.15) in the jarosite compounds with declining alkali cation concentration in the starting solutions of each series with different initial Fe sulphate concentrations. Similar

results for synthetic Pb-Ag-H_3O jarosites are shown in Table 4.16. Accompanying these trends of declining K, Na and Pb contents is a complementary trend of generally increasing Ag content as the concentration of this cation increases in the starting solutions. However, the results have some anomalous contents, so some series show only poor or fairly poor linear relationships between the content of the cations in the products. Good linear relationships are shown by K-Ag-H_3O jarosite series 22-30, synthesised at 97ºC, with an R^2 value of 0.8356; series 62-66 and 71 & 81-84, both synthesised at 140ºC, with R^2 values of 0.8407 and 0.9390, respectively; and series 89-95, synthesised at 22ºC, with an R^2 value of 0.8779. The Na-Ag-H_3O jarosite compounds with good linear relationships are series 12-30, 30-38 and 30-38D, synthesised at 97ºC, with R^2 values of 0.9835, 0.9105 and 0.9041, respectively; series 49-54 & 61, 66-70 and 71 & 85-88, synthesised at 140ºC, with R^2 values of 0.7472, 0.8755 and 0.9915, respectively; and series 72 & 77-80 and 95-101, synthesised at 22ºC, with R^2 values of 0.9486 and 0.9534, respectively. The other K-Ag-H_3O and Na-Ag-H_3O series have R^2 values of ≤ 0.6859.

Table 4.14. EMPA site occupancies of K-Ag jarosites synthesised at 22ºC, 97ºC and 140ºC, and the concentrations of K and Ag in the starting solutions.

Sample	Na	K	Pb	Ag	H_3O	Fe	S	Starting solution
Solutions containing 0.51 M $Fe_2(SO_4)_3.5H_2O$ heated at 97ºC and products dried at 60ºC								
JS04	0	0.37	0	0.00	0.63	3.04	2	0.22 *M* K, 0.00 *M* Ag
JS06	0	0.60	0	0.19	0.21	3.06	2	0.165 *M* K, 0.055 *M* Ag
JS06D	0	0.30	0	0.06	0.64	2.99	2	0.165 *M* K, 0.055 *M* Ag
JS08	0	0.30	0	0.29	0.41	2.85	2	0.11 *M* K, 0.11 *M* Ag
JS10	0	0.23	0	0.14	0.63	3.03	2	0.055 *M* K, 0.165 *M* Ag
JS10D	0	0.22	0	0.17	0.61	3.03	2	0.055 *M* K, 0.165 *M* Ag
JS12	0	0.00	0	0.31	0.69	3.09	2	0.00 *M* K, 0.22 *M* Ag
Solutions containing 0.51 M $Fe_2(SO_4)_3.5H_2O$ heated at 97ºC and products dried at 110ºC								
JS22	0	0.23	0	0.00	0.77	2.95	2	0.22 *M* K, 0.00 *M* Ag

JS24	0	0.25	0	0.07	0.68	2.41	2	0.165 *M* K, 0.055 *M* Ag
JS24D	0	0.30	0	0.09	0.61	3.04	2	0.165 *M* K, 0.055 *M* Ag
JS26	0	0.24	0	0.07	0.69	2.93	2	0.11 *M* K, 0.11 *M* Ag
JS28	0	0.21	0	0.10	0.69	3.03	2	0.055 *M* K, 0.165 *M* Ag
JS30	0	0.00	0	0.24	0.76	3.12	2	0.00 *M* K, 0.22 *M* Ag
JS40	0	0.26	0	0.04	0.70	2.87	2	0.5 *M* K, 0.1 *M* Ag
Solutions containing 0.15 M $Fe_2(SO_4)_3.5H_2O$ heated at 140ºC and products dried at 110ºC								
JS55	0	0.43	0	0.00	0.57	2.56	2	0.12 *M* K, 0.00 *M* Ag
JS56	0	0.70	0	0.16	0.14	2.33	2	0.10 *M* K, 0.02 *M* Ag
JS57	0	0.56	0	0.26	0.18	2.86	2	0.08 *M* K, 0.04 *M* Ag
JS58	0	0.45	0	0.27	0.28	2.83	2	0.06 *M* K, 0.06 *M* Ag
JS59	0	0.37	0	0.35	0.28	2.79	2	0.04 *M* K, 0.08 *M* Ag
JS60	0	0.21	0	0.60	0.19	2.87	2	0.02 *M* K, 0.10 *M* Ag
JS61	0	0.00	0	0.63	0.37	3.02	2	0.00 *M* K, 0.12 *M* Ag
Samples annealed at 140ºC and dried at 110ºC (from solutions originally containing 0.51 M $Fe_2(SO_4)_3.5H_2O$ heated at 97ºC and products dried at 60ºC)								
JS62	0	0.55	0	0.00	0.45	2.88	2	0.22 *M* K, 0.00 *M* Ag
JS63	0	0.42	0	0.24	0.34	2.46	2	0.165 *M* K, 0.055 *M* Ag
JS64	0	0.26	0	0.30	0.44	2.76	2	0.11 *M* K, 0.11 *M* Ag
JS65	0	0.29	0	0.34	0.37	2.88	2	0.055 *M* K, 0.165 *M* Ag
JS66	0	0.00	0	0.44	0.56	2.91	2	0.00 *M* K, 0.22 *M* Ag
Samples annealed at 140ºC and dried at 110ºC (from solutions originally containing 0.51 M $Fe_2(SO_4)_3.5H_2O$ heated at 97ºC and products dried at 110ºC)								
JS71	0	0.00	0	0.66	0.34	2.35	2	0.00 *M* K, 0.22 *M* Ag
JS81	0	0.64	0	0.00	0.36	2.86	2	0.22 *M* K, 0.00 *M* Ag
JS82	0	0.40	0	0.14	0.46	2.70	2	0.165 *M* K, 0.055 *M* Ag
JS83	0	0.30	0	0.43	0.27	2.38	2	0.11 *M* K, 0.11 *M* Ag
JS84	0	0.10	0	0.64	0.26	2.19	2	0.055 *M* K, 0.165 *M* Ag
Solutions containing 0.51 M $Fe_2(SO_4)_3.5H_2O$ were prepared at 22ºC and products air-dried at 22ºC								
JS72	0	0.00	0	0.63	0.37	2.84	2	0.00 *M* K, 0.22 *M* Ag
JS73	0	0.32	0	0.00	0.68	2.80	2	0.22 *M* K, 0.00 *M* Ag
JS74	0	0.64	0	0.06	0.30	2.88	2	0.165 *M* K, 0.055 *M* Ag
JS75	0	0.35	0	0.10	0.55	2.93	2	0.11 *M* K, 0.11 *M* Ag
JS76	0	0.36	0	0.15	0.49	2.92	2	0.055 *M* K, 0.165 *M* Ag
Solutions containing 0.15 M $Fe_2(SO_4)_3.5H_2O$ were prepared at 22ºC and products air-dried at 22ºC								
JS89	0	0.55	0	0.00	0.45	2.06	2	0.12 *M* K, 0.00 *M* Ag

JS90	0	0.56	0	0.05	0.39	2.58	2	0.10 *M* K, 0.02 *M* Ag
JS91	0	0.48	0	0.04	0.48	2.91	2	0.08 *M* K, 0.04 *M* Ag
JS92	0	0.31	0	0.09	0.60	3.03	2	0.06 *M* K, 0.06 *M* Ag
JS93	0	0.35	0	0.12	0.53	2.91	2	0.04 *M* K, 0.08 *M* Ag
JS94	0	0.17	0	0.28	0.55	2.12	2	0.02 *M* K, 0.10 *M* Ag
JS95	0	0.00	0	0.56	0.44	2.98	2	0.00 *M* K, 0.12 *M* Ag

Table 4.15. EMPA site occupancies of Na-Ag jarosites synthesised at 22ºC, 97ºC and 140ºC, and the concentrations of Na and Ag in the starting solutions.

Sample	Na	K	Pb	Ag	H_3O	Fe	S	Starting solution
Solutions containing 0.51 M $Fe_2(SO_4)_3.5H_2O$ heated at 97ºC and products dried at 60ºC								
JS12	0.00	0	0	0.31	0.69	3.09	2	0.00 *M* Na, 0.22 *M* Ag
JS14	0.17	0	0	0.00	0.83	3.01	2	0.22 *M* Na, 0.00 *M* Ag
JS16	0.10	0	0	0.16	0.74	2.99	2	0.165 *M* Na, 0.055 *M* Ag
JS18	0.05	0	0	0.22	0.73	2.92	2	0.11 *M* Na, 0.11 *M* Ag
JS20	0.04	0	0	0.23	0.73	3.06	2	0.055 *M* Na, 0.165 *M* Ag
Solutions containing 0.51 M $Fe_2(SO_4)_3.5H_2O$ heated at 97ºC and products dried at 110ºC								
JS30	0.00	0	0	0.24	0.76	3.09	2	0.00 *M* Na, 0.22 *M* Ag
JS32	0.30	0	0	0.00	0.70	2.72	2	0.22 *M* Na, 0.00 *M* Ag
JS34	0.10	0	0	0.15	0.75	3.03	2	0.165 *M* Na, 0.055 *M* Ag
JS36	0.04	0	0	0.29	0.64	3.04	2	0.11 *M* Na, 0.11 *M* Ag
JS38	0.01	0	0	0.26	0.73	3.06	2	0.055 *M* Na, 0.165 *M* Ag
JS38D	0.04	0	0	0.23	0.73	3.05	2	0.055 *M* Na, 0.165 *M* Ag
JS42	0.05	0	0	0.20	0.75	3.07	2	0.5 *M* Na, 0.1 *M* Ag
Solutions containing 0.15 M $Fe_2(SO_4)_3.5H_2O$ heated at 140ºC and products dried at 110ºC								
JS49	0.56	0	0	0.00	0.44	2.29	2	0.12 *M* Na, 0.00 *M* Ag
JS50	0.25	0	0	0.24	0.51	2.85	2	0.10 *M* Na, 0.02 *M* Ag
JS51	0.16	0	0	0.29	0.55	2.86	2	0.08 *M* Na, 0.04 *M* Ag
JS52	0.05	0	0	0.37	0.58	2.90	2	0.06 *M* Na, 0.06 *M* Ag
JS53	0.03	0	0	0.30	0.67	2.89	2	0.04 *M* Na, 0.08 *M* Ag
JS54	0.01	0	0	0.38	0.61	2.86	2	0.02 *M* Na, 0.10 *M* Ag
JS61	0.00	0	0	0.63	0.37	3.02	2	0.00 *M* Na, 0.12 *M* Ag
Samples annealed at 140ºC and dried at 110ºC (from solutions originally containing 0.51 M $Fe_2(SO_4)_3.5H_2O$ heated at 97ºC and products dried at 60ºC)								
JS66	0.00	0	0	0.44	0.56	2.91	2	0.00 M Na, 0.22 M Ag

JS67	0.65	0	0	0.00	0.35	2.91	2	0.22 M Na, 0.00 M Ag
JS68	0.57	0	0	0.09	0.34	2.74	2	0.165 M Na, 0.055 M Ag
JS69	0.30	0	0	0.12	0.58	3.16	2	0.11 M Na, 0.11 M Ag
JS70	0.23	0	0	0.33	0.44	2.72	2	0.055 M Na, 0.165 M Ag
Samples annealed at 140ºC and dried at 110ºC (from solutions originally containing 0.51 M $Fe_2(SO_4)_3.5H_2O$ heated at 97ºC and products dried at 110ºC)								
JS71	0.00	0	0	0.66	0.34	2.35	2	0.00 *M* Na, 0.22 *M* Ag
JS85	0.55	0	0	0.00	0.45	2.76	2	0.22 *M* Na, 0.00 *M* Ag
JS86	0.29	0	0	0.35	0.36	2.73	2	0.165 *M* Na, 0.055 *M* Ag
JS87	0.17	0	0	0.50	0.33	2.53	2	0.11 *M* Na, 0.11 *M* Ag
JS88	0.14	0	0	0.49	0.37	2.63	2	0.055 *M* Na, 0.165 *M* Ag
Solutions containing 0.51 M $Fe_2(SO_4)_3.5H_2O$ were prepared at 22ºC and products air-dried at 22ºC								
JS72	0.00	0	0	0.63	0.37	2.84	2	0.00 *M* Na, 0.22 *M* Ag
JS77	0.49	0	0	0.00	0.51	2.86	2	0.22 *M* Na, 0.00 *M* Ag
JS78	0.05	0	0	0.42	0.53	2.88	2	0.165 *M* Na, 0.055 *M* Ag
JS79	0.06	0	0	0.48	0.46	2.78	2	0.11 *M* Na, 0.11 *M* Ag
JS80	0.03	0	0	0.55	0.42	2.70	2	0.055 *M* Na, 0.165 *M* Ag
Solutions containing 0.15 M $Fe_2(SO_4)_3.5H_2O$ were prepared at 22ºC and products air-dried at 22ºC								
JS95	0.00	0	0	0.56	0.44	2.98	2	0.00 *M* Na, 0.12 *M* Ag
JS96	0.56	0	0	0.00	0.44	3.04	2	0.12 *M* Na, 0.00 *M* Ag
JS97	0.11	0	0	0.46	0.43	3.02	2	0.10 *M* Na, 0.02 *M* Ag
JS98	0.09	0	0	0.55	0.36	2.96	2	0.08 *M* Na, 0.04 *M* Ag
JS99	0.03	0	0	0.57	0.40	2.74	2	0.06 *M* Na, 0.06 *M* Ag
JS100	0.02	0	0	0.63	0.35	3.08	2	0.04 *M* Na, 0.08 *M* Ag
JS101	0.02	0	0	0.50	0.48	3.07	2	0.02 *M* Na, 0.10 *M* Ag

Table 4.16. EMPA site occupancies of Pb-Ag jarosites synthesised at 22ºC and 140ºC, plus the concentrations of Pb and Ag in the starting solutions.

Sample	Na	K	Pb	Ag	H_3O	Fe	S	Starting solution
Solutions containing 0.15 M $Fe_2(SO_4)_3.5H_2O$ heated at 140ºC and products dried at 110ºC								
JS43	n.d.	n.d	n.d.	n.d.	n.d.	n.d.	-	0.06 *M* Pb, 0.00 *M* Ag
JS43D	n.d.	n.d	n.d.	n.d.	n.d.	n.d.	-	0.06 *M* Pb, 0.00 *M* Ag
JS44	0	0	0.030	0.223	0.717	2.80	2	0.05 *M* Pb, 0.02 *M* Ag
JS45	0	0	0.006	0.448	0.546	2.61	2	0.04 *M* Pb, 0.04 *M* Ag
JS46	n.d.	n.d	n.d.	n.d.	n.d.	n.d.	-	0.03 *M* Pb, 0.06 *M* Ag

JS47	0	0	0.006	0.652	0.342	2.46	2	0.02 *M* Pb, 0.08 *M* Ag
JS48	0	0	0.009	0.299	0.692	3.11	2	0.01 *M* Pb, 0.10 *M* Ag
JS61	0	0	0	0.630	0.370	3.02	2	0.00 *M* Pb, 0.12 *M* Ag
Solutions containing 0.15 M $Fe_2(SO_4)_3.5H_2O$ were prepared at 22ºC and products air-dried at 22ºC								
JS102	0	0	0.004	0.448	0.548	2.99	2	0.00013 *M* Pb, 0.05 *M* Ag
JS103	0	0	0.003	0.491	0.506	3.02	2	0.00032 *M* Pb, 0.05 *M* Ag
JS104	0	0	0.025	0.807	0.168	3.15	2	0.001 *M* Pb, 0.05 *M* Ag
JS105	0	0	0.047	0.808	0.145	2.73	2	0.005 *M* Pb, 0.05 *M* Ag
JS106	0	0	0.018	0.483	0.499	3.21	2	0.001 *M* Pb, 0.05 *M* Ag
JS107	0	0	0.030	0.000	0.970	2.91	2	0.001 *M* Pb, 0.00 *M* Ag

The K *A*-site contents of samples synthesised at 97ºC vary from 0.37 in JS04 (ideal site occupancy 1.0), from an initial solution concentration of 0.22 *M* K (0.00 *M* Ag) (and an Fe:K ratio in the starting solution of 4.64:1, so with excess Fe compared with the stoichiometric ratio of 3:1), to 0.21 in JS28, from a starting-solution K concentration of 0.055 *M* (and 0.165 *M* Ag) (Fe:K ratio 18.55:1). Sample JS06 has the highest K content at 0.60, which is substantially higher than the other products synthesised at 97ºC, from an initial concentration of 0.165 *M* K (and 0.055 *M* Ag) in the starting solution (Fe:K ratio 6.18:1); the duplicate JS06D has a K content of 0.30. Sample JS22 has a K content of 0.23, from the same synthesis starting solution concentrations as sample 04.

The Na contents of the jarosite products synthesised at 97ºC vary from 0.30 in JS32, from an initial solution concentration of 0.22 *M* Na (0.00 *M* Ag) (Fe:Na ratio in 4.64:1), to 0.01 in JS38, from a starting-solution Na concentration of 0.055 *M* (and 0.165 *M* Ag) (Fe:Na ratio 18.55:1). Sample JS34 has an Na content of 0.10, from an initial solution concentration of 0.165 *M* Na (and 0.055 *M* Ag) (Fe:Na ratio 6.18:1).

In the syntheses at 97ºC, JS12 and JS30 have Ag contents of 0.31 and 0.24, respectively, both from starting-solution concentrations of 0.22 *M* Ag (with no alkali

cations). However, sample JS08 has a relatively high Ag product content of 0.29 from a starting solution concentration of 0.11 *M* Ag (and 0.11 *M* K), as does sample JS06 with an Ag product content of 0.19 from a solution concentration of 0.055 *M* Ag (and 0.165 *M* K); the duplicate JS06D has an Ag content of 0.06.

In the syntheses carried out at 97ºC, there are no significant differences in the alkali and Ag cation contents, or corresponding H_3O contents, between the products dried at 60ºC and those dried at 110ºC (Lowers et al., 2005). There is also no significant difference in Fe contents between the products dried at 60ºC and those dried at 110ºC, which would potentially affect the structural water content by protonation of hydroxyl to balance the overall charge where there is Fe deficiency.

The results from the samples synthesised at 140ºC indicate a higher alkali and Ag content, and correspondingly lower H_3O content, than the samples synthesised at lower temperature. Sample JS55 has a K content of 0.43, from an initial solution concentration of 0.12 *M* K (with no Ag) (Fe:K ratio 2.5:1), which compares with the K content of 0.37 in JS04, synthesised at 97ºC and with 0.22 *M* K (Fe:K ratio 4.64:1) in the starting solution. JS49 has an Na content of 0.56 and JS50 has an Na content of 0.25, from starting-solution concentrations of 0.12 *M* (with no Ag) (Fe:Na ratio 2.5:1) and 0.10 *M* Na (and 0.02 *M* Ag) (Fe:Na ratio 3:1), respectively, which compare with 0.30 in JS32, synthesised at 97ºC using 0.22 *M* Na (with no Ag) (Fe:Na ratio 4.64:1). JS61 has an Ag content of 0.63, from an initial solution concentration of 0.12 *M* Ag (and no K or Na) (Fe:Ag ratio 2.5:1), which compares with Ag contents of 0.31 in JS12 and 0.24 in JS30 in syntheses both at 97ºC using 0.22 *M* Ag (and no alkali cation) (Fe:Ag ratio 4.64:1). In the Pb-Ag series synthesised at 140ºC, JS44 has the highest Pb content of 0.03, from a starting-solution concentration of 0.05 *M* Pb (and 0.02 *M* Ag).

In the products synthesised at 22ºC, the K contents are comparable with the equivalents synthesised at 97ºC, although there is variability; for example, JS73 has a K content of 0.32 compared with 0.23 in JS22 and 0.37 in JS04, and JS76 has a content of 0.36 compared with 0.23 in JS10, 0.22 in JS10D and 0.21 in JS28, while JS74 has a content of 0.64 compared with 0.60 in JS06, 0.30 in JS06D and 0.30 in JS24D. A trend of lower Na content is shown in the products synthesised at 22ºC compared with the equivalents synthesised at 97ºC; for example, JS78 has an Na content of 0.05 compared to 0.10 in JS16 and 0.10 in JS34, and JS80 has a content of 0.03 compared to 0.04 in JS20. In the products synthesised at 22ºC, a higher Ag content (0.63) is shown in the Ag end member (JS72), compared with the equivalent syntheses at 97ºC (0.31 and 0.24, respectively), although the content is the same as equivalent made at 140ºC (0.63); however, this result may be anomalous. In the K-Ag-H_3O series synthesised at 22ºC, the Ag contents are comparable with those in their equivalents synthesised at 97ºC. In the Na-Ag-H_3O series synthesised at 22ºC, the Ag contents are higher than in their equivalents synthesised at 97ºC.

The K-Ag and Na-Ag products synthesised at 97ºC with 0.51 *M* $Fe_2(SO_4)_3.5H_2O$ in the starting solutions have average Fe contents of 2.97 (± 0.56). This compares with an average Fe content of 2.85 (± 0.15) for the compounds synthesised at 22ºC using 0.51 *M* $Fe_2(SO_4)_3.5H_2O$. The K-Ag-H_3O and Na-Ag-H_3O products synthesised at 140ºC with 0.15 *M* $Fe_2(SO_4)_3.5H_2O$ in the starting solutions have average Fe contents of 2.76 (± 0.47). The results show the syntheses that used the highest concentrations of Fe^{3+} in the starting solutions (0.51 *M* $Fe_2(SO_4)_3.5H_2O$) resulted in the highest occupancy of the Fe site in the products. The degree of occupation of the Fe site varied with synthesis temperature: most products made at 97ºC had close to full occupancy, while those made at 22ºC contained significant Fe

site vacancies. Products synthesised at 140ºC contained slightly higher Fe site occupancies than those made at 22ºC, in spite of the lower concentration of Fe in the starting solutions (0.15 *M* $Fe_2(SO_4)_3.5H_2O$).

The results for the K-Ag-H_3O-jarosite series indicate the issue of data quality of EMPA of powder jarosite samples (see section 3.3.4). In five out of seven of the series, the EMPA results show the end-member K-H_3O-jarosite compound (synthesised from the starting solution with the highest K concentration in the series) has a K content that is lower than the K content of the first intermediate K-Ag-H_3O-jarosite compound (synthesised from the starting solution with the second highest K concentration). This could suggest there is an effect caused by the presence of the two cations that increases total incorporation of the cations into the jarosite structure. The samples involved are: 4 (K occupancy 0.37) and 6 (K 0.60, Ag 0.19); 22 (K 0.23) and 24 (K 0.25, Ag 0.07); 55 (K 0.43) and 56 (K 0.70, Ag 0.16); 73 (K 0.32) and 74 (K 0.64, Ag 0.06); and 89 (K 0.55) and 90 (K 0.56, Ag 0.05). The result is also seen in the Rietveld refinement analysis of K-Ag-H_3O-jarosite series samples 4 (K 0.65) and 6D (K 0.71, Ag 0.09); 22 (K 0.61) and 24 (K 0.63, Ag 0.10); and 55 (K 0.32) and 56 (K 0.71, Ag 0.09). The same type of result does not arise with the other analyses used, except for ICP-AES analysis of sample 66 (Ag 0.44) and 70 (Ag 0.45, Na 0.20).

4.1.5.2 Effects of temperature and starting solution composition on EMPA compositional data

The EMPA results show that, in the K-Ag-H_3O jarosite products synthesised at 22ºC, the K and Ag contents are comparable with the equivalents synthesised at 97ºC, although there is some variability (see Table 4.14) in products synthesised at 140ºC.

In the Na-Ag-H_3O jarosite compounds synthesised from starting solutions in which Na and Ag each varies between 0 *M* and 22 *M*, there is little difference between the Na contents of intermediate products synthesised at 22ºC compared with the equivalents synthesised at 97ºC (see Table 4.15); however, the Na end member synthesised at 22ºC has a substantially higher Na occupancy (0.49) than the two equivalents synthesised at 97ºC (0.17 and 0.30). In these samples, the Ag contents are substantially higher in the compounds synthesised at 22ºC than their equivalents synthesised at 97ºC; this may be related to the different lengths of time of synthesis, which was 12 months at 22ºC and 4 hours at 97ºC. The equivalent compounds synthesised at 140ºC have higher Na contents than the equivalents synthesised at 22ºC and 97ºC. The Ag contents of the compounds synthesised at 22ºC are higher than the equivalents synthesised at both 97ºC and 140ºC, which again may be related to the period of synthesis. The results of ICP-AES analysis showed generally higher A-site occupancies in these same compounds than EMPA. ICP-AES analysis also indicated the relatively high Ag contents in the compounds synthesised at 22ºC; it also indicated relatively low contents in the compounds synthesised at 140ºC compared with the original compounds synthesised at 97ºC, which suggests the annealing experiment was not successful in these samples.

In the K-Ag-H_3O and Na-Ag-H_3O jarosite products synthesised at 97ºC, the EMPA results show no significant differences in the alkali and Ag cation contents, or corresponding H_3O contents, between the products dried at 60ºC and those dried at 110ºC.

The concentrations of Pb and Ag in the starting solutions were substantially different between the series of Pb-Ag-H_3O samples synthesised at 22ºC and the series synthesised at 140ºC. Nevertheless, the Pb contents were very low in both

series, indicating problems of incorporating Pb in the jarosite structure. However, the Ag contents were generally relatively high in the compounds synthesised at 22ºC compared with those synthesised at 140ºC; again this may relate to the relatively long period of synthesis in the experiments at 22ºC.

4.1.6 Inductively coupled plasma-atomic emission spectroscopy

The bulk-composition data (in parts per million, ppm) from ICP-AES analysis of the synthetic K-Ag-H_3O, Na-Ag-H_3O and Pb-Ag-H_3O jarosite compounds (see Appendix K) were used to calculate the *A*-site occupancies of K^+, Na^+ or Pb^{2+} and Ag^+ and the *B*-site occupancy of Fe^{3+}. Difference of these *A*-site occupancies from 1.0 was used to calculate their hydronium occupancy, and it was assumed there was no H_2O substitution in the *A* or *B* site or protonation of OH^- (Kubisz, 1970; Murphy et al, 2009; Basciano and Peterson, 2010). The site occupancies were calculated based on the normalisation of the bulk-composition data for S to a site occupancy of 2.0 (Basciano and Peterson, 2010). The site occupancies calculated from the results of ICP-AES analysis of the synthetic K-Ag-H_3O, Na-Ag-H_3O and Pb-Ag-H_3O jarosite compounds show generally declining contents of K (Table 4.17), Na (Table 4.18), and Pb (Table 4.19) respectively with declining K^+, Na^+ or Pb^{2+} cation concentration in the starting solutions of each series. Accompanying these trends of declining K, Na and Pb contents are complementary trends of generally increasing Ag content as the concentration of Ag increases in the starting solutions. These trends are present irrespective of differences in the initial Fe sulphate concentration in the starting solutions of the different series. The results show anomalous, excessive *A*-site occupancies in some of the products: in K-Ag-H_3O jarosite products 40 and 76; in Na-Ag-H_3O jarosite products 80 and 101; and in Ag-H_3O jarosite

product 72. In Pb-H_3O jarosite product 107, there is excessive Fe content. In addition, there are no data for samples 49 (Na-H_3O jarosite product) and 56 (K-Ag-H_3O jarosite product), as these were not analysed.

Table 4.17. ICP-AES site occupancies of K-Ag jarosites synthesised at 22ºC, 97ºC and 140ºC, and the concentrations of K and Ag in the starting solutions.

Sample	Na	K	Pb	Ag	H_3O	Fe	S	Starting solution
Solutions containing 0.51 M $Fe_2(SO_4)_3.5H_2O$ heated at 97ºC and products dried at 60ºC								
JS04	0	0.66	0	0.00	0.34	2.60	2	0.22 *M* K, 0.00 *M* Ag
JS06	0	0.50	0	0.18	0.32	2.88	2	0.165 *M* K, 0.055 *M* Ag
JS06D	0	0.52	0	0.15	0.33	2.56	2	0.165 *M* K, 0.055 *M* Ag
JS08	0	0.41	0	0.30	0.29	2.72	2	0.11 *M* K, 0.11 *M* Ag
JS10	0	0.25	0	0.41	0.34	2.72	2	0.055 *M* K, 0.165 *M* Ag
JS10D	0	0.27	0	0.44	0.29	2.71	2	0.055 *M* K, 0.165 *M* Ag
JS12	0	0.00	0	0.78	0.22	2.71	2	0.00 *M* K, 0.22 *M* Ag
Solutions containing 0.51 M $Fe_2(SO_4)_3.5H_2O$ heated at 97ºC and products dried at 110ºC								
JS22	0	0.64	0	0.00	0.36	2.59	2	0.22 *M* K, 0.00 *M* Ag
JS24	0	0.53	0	0.15	0.32	2.62	2	0.165 *M* K, 0.055 *M* Ag
JS24D	0	0.52	0	0.14	0.34	2.59	2	0.165 *M* K, 0.055 *M* Ag
JS26	0	0.44	0	0.25	0.31	2.74	2	0.11 *M* K, 0.11 *M* Ag
JS28	0	0.27	0	0.56	0.17	2.57	2	0.055 *M* K, 0.165 *M* Ag
JS30	0	0.00	0	1.00	0.00	2.62	2	0.00 *M* K, 0.22 *M* Ag
JS40	0	0.41	0	1.66	0.00	1.51	2	0.5 *M* K, 0.1 *M* Ag
Solutions containing 0.15 M $Fe_2(SO_4)_3.5H_2O$ heated at 140ºC and products dried at 110ºC								
JS55	0	0.37	0	0.36	0.27	2.56	2	0.12 *M* K, 0.00 *M* Ag
JS56	0	n.d.	0	n.d.	n.d.	n.d.	n.d.	0.10 *M* K, 0.02 *M* Ag
JS57	0	0.47	0	0.23	0.30	2.80	2	0.08 *M* K, 0.04 *M* Ag
JS58	0	0.38	0	0.34	0.28	2.82	2	0.06 *M* K, 0.06 *M* Ag
JS59	0	0.29	0	0.45	0.26	2.83	2	0.04 *M* K, 0.08 *M* Ag
JS60	0	0.16	0	0.68	0.16	2.96	2	0.02 *M* K, 0.10 *M* Ag
JS61	0	0.00	0	0.85	0.46	2.93	2	0.00 *M* K, 0.12 *M* Ag
Samples annealed at 140ºC and dried at 110ºC (from solutions originally containing 0.51 M $Fe_2(SO_4)_3.5H_2O$ heated at 97ºC and products dried at 60ºC)								
JS62	0	0.61	0	0.00	0.39	2.87	2	0.22 *M* K, 0.00 *M* Ag

JS63	0	0.49	0	0.21	0.30	3.36	2	0.165 *M* K, 0.055 *M* Ag
JS64	0	0.37	0	0.36	0.27	3.44	2	0.11 *M* K, 0.11 *M* Ag
JS65	0	0.15	0	0.37	0.48	2.98	2	0.055 *M* K, 0.165 *M* Ag
JS66	0	0.00	0	0.44	0.56	3.03	2	0.00 *M* K, 0.22 *M* Ag
Samples annealed at 140ºC and dried at 110ºC (from solutions originally containing 0.51 M $Fe_2(SO_4)_3.5H_2O$ heated at 97ºC and products dried at 110ºC)								
JS71	0	0.00	0	0.76	0.24	2.98	2	0.00 *M* K, 0.22 *M* Ag
JS81	0	0.60	0	0.00	0.40	2.81	2	0.22 *M* K, 0.00 *M* Ag
JS82	0	0.44	0	0.24	0.32	2.87	2	0.165 *M* K, 0.055 *M* Ag
JS83	0	0.29	0	0.46	0.25	2.91	2	0.11 *M* K, 0.11 *M* Ag
JS84	0	0.09	0	0.68	0.23	2.94	2	0.055 *M* K, 0.165 *M* Ag
Solutions containing 0.51 M $Fe_2(SO_4)_3.5H_2O$ were prepared at 22ºC and products air-dried at 22ºC								
JS72	0	0.00	0	2.10	0.00	1.88	2	0.00 *M* K, 0.22 *M* Ag
JS73	0	0.78	0	0.00	0.22	2.40	2	0.22 *M* K, 0.00 *M* Ag
JS74	0	0.68	0	0.06	0.26	2.52	2	0.165 *M* K, 0.055 *M* Ag
JS75	0	0.64	0	0.14	0.22	2.49	2	0.11 *M* K, 0.11 *M* Ag
JS76	0	0.42	0	1.07	0.00	1.99	2	0.055 *M* K, 0.165 *M* Ag
Solutions containing 0.15 M $Fe_2(SO_4)_3.5H_2O$ were prepared at 22ºC and products air-dried at 22ºC								
JS89	0	0.73	0	0.00	0.27	2.49	2	0.12 *M* K, 0.00 *M* Ag
JS90	0	0.69	0	0.05	0.26	2.55	2	0.10 *M* K, 0.02 *M* Ag
JS91	0	0.65	0	0.10	0.25	2.68	2	0.08 *M* K, 0.04 *M* Ag
JS92	0	0.60	0	0.15	0.25	2.61	2	0.06 *M* K, 0.06 *M* Ag
JS93	0	0.43	0	0.35	0.22	2.72	2	0.04 *M* K, 0.08 *M* Ag
JS94	0	0.28	0	0.52	0.20	2.71	2	0.02 *M* K, 0.10 *M* Ag
JS95	0	0.00	0	0.85	0.15	2.86	2	0.00 *M* K, 0.12 *M* Ag

Table 4.18. ICP-AES site occupancies of Na-Ag jarosites synthesised at 22ºC, 97ºC and 140ºC, and the concentrations of Na and Ag in the starting solutions.

Sample	Na	K	Pb	Ag	H_3O	Fe	S	Starting solution
Solutions containing 0.51 M $Fe_2(SO_4)_3.5H_2O$ heated at 97ºC and products dried at 60ºC								
JS12	0.00	0	0	0.78	0.22	2.71	2	0.00 *M* Na, 0.22 *M* Ag
JS14	0.57	0	0	0.00	0.43	2.91	2	0.22 *M* Na, 0.00 *M* Ag
JS16	0.33	0	0	0.37	0.30	2.92	2	0.165 *M* Na, 0.055 *M* Ag
JS18	0.10	0	0	0.63	0.27	2.72	2	0.11 *M* Na, 0.11 *M* Ag
JS20	0.06	0	0	0.71	0.23	2.71	2	0.055 *M* Na, 0.165 *M* Ag

Solutions containing 0.51 M $Fe_2(SO_4)_3.5H_2O$ heated at 97ºC and products dried at 110ºC								
JS30	0.00	0	0	1.00	0.00	2.62	2	0.00 *M* Na, 0.22 *M* Ag
JS32	0.55	0	0	0.00	0.45	2.87	2	0.22 *M* Na, 0.00 *M* Ag
JS34	0.16	0	0	0.55	0.29	2.97	2	0.165 *M* Na, 0.055 *M* Ag
JS36	0.03	0	0	0.72	0.25	2.83	2	0.11 *M* Na, 0.11 *M* Ag
JS38	0.01	0	0	0.97	0.02	2.59	2	0.055 *M* Na, 0.165 *M* Ag
JS38D	0.05	0	0	0.77	0.18	2.68	2	0.055 *M* Na, 0.165 *M* Ag
JS42	0.09	0	0	0.70	0.21	2.63	2	0.5 *M* Na, 0.1 *M* Ag
Solutions containing 0.15 M $Fe_2(SO_4)_3.5H_2O$ heated at 140ºC and products dried at 110ºC								
JS49	n.d.	0	0	n.d.	n.d.	n.d.	n.d.	0.12 *M* Na, 0.00 *M* Ag
JS50	0.33	0	0	0.25	0.42	3.04	2	0.10 *M* Na, 0.02 *M* Ag
JS51	0.20	0	0	0.47	0.33	2.90	2	0.08 *M* Na, 0.04 *M* Ag
JS52	0.09	0	0	0.67	0.24	2.93	2	0.06 *M* Na, 0.06 *M* Ag
JS53	0.04	0	0	0.77	0.19	2.98	2	0.04 *M* Na, 0.08 *M* Ag
JS54	0.01	0	0	0.83	0.16	2.98	2	0.02 *M* Na, 0.10 *M* Ag
JS61	0.00	0	0	0.85	0.15	2.93	2	0.00 *M* Na, 0.12 *M* Ag
Samples annealed at 140ºC and dried at 110ºC (from solutions originally containing 0.51 M $Fe_2(SO_4)_3.5H_2O$ heated at 97ºC and products dried at 60ºC)								
JS66	0.00	0	0	0.44	0.56	3.03	2	0.00 *M* Na, 0.22 *M* Ag
JS67	0.59	0	0	0.00	0.41	3.12	2	0.22 *M* Na, 0.00 *M* Ag
JS68	0.51	0	0	0.13	0.36	3.00	2	0.165 *M* Na, 0.055 *M* Ag
JS69	0.40	0	0	0.19	0.51	3.16	2	0.11 *M* Na, 0.11 *M* Ag
JS70	0.20	0	0	0.45	0.35	2.97	2	0.055 *M* Na, 0.165 *M* Ag
Samples annealed at 140ºC and dried at 110ºC (from solutions originally containing 0.51 M $Fe_2(SO_4)_3.5H_2O$ heated at 97ºC and products dried at 110ºC)								
JS71	0.00	0	0	0.76	0.24	2.98	2	0.00 *M* Na, 0.22 *M* Ag
JS85	0.57	0	0	0.00	0.43	2.98	2	0.22 *M* Na, 0.00 *M* Ag
JS86	0.55	0	0	0.08	0.37	3.02	2	0.165 *M* Na, 0.055 *M* Ag
JS87	0.13	0	0	0.60	0.27	2.99	2	0.11 *M* Na, 0.11 *M* Ag
JS88	0.11	0	0	0.56	0.33	2.97	2	0.055 *M* Na, 0.165 *M* Ag
Solutions containing 0.51 M $Fe_2(SO_4)_3.5H_2O$ were prepared at 22ºC and products air-dried at 22ºC								
JS72	0.00	0	0	2.10	0.00	1.88	2	0.00 *M* Na, 0.22 *M* Ag
JS77	0.67	0	0	0.00	0.33	2.86	2	0.22 *M* Na, 0.00 *M* Ag
JS78	0.11	0	0	0.71	0.18	2.68	2	0.165 *M* Na, 0.055 *M* Ag
JS79	0.03	0	0	0.80	0.17	2.76	2	0.11 *M* Na, 0.11 *M* Ag
JS80	0.03	0	0	1.93	0.42	1.92	2	0.055 *M* Na, 0.165 *M* Ag

Solutions containing 0.51 M $Fe_2(SO_4)_3.5H_2O$ were prepared at 22ºC and products air-dried at 22ºC								
JS95	0.00	0	0	0.85	0.15	2.86	2	0.00 *M* Na, 0.12 *M* Ag
JS96	0.68	0	0	0.00	0.32	3.01	2	0.12 *M* Na, 0.00 *M* Ag
JS97	0.37	0	0	0.41	0.22	2.96	2	0.10 *M* Na, 0.02 *M* Ag
JS98	0.14	0	0	0.68	0.18	2.86	2	0.08 *M* Na, 0.04 *M* Ag
JS99	0.04	0	0	0.80	0.16	2.86	2	0.06 *M* Na, 0.06 *M* Ag
JS100	0.02	0	0	0.81	0.17	2.84	2	0.04 *M* Na, 0.08 *M* Ag
JS101	0.03	0	0	1.93	0.42	1.92	2	0.02 *M* Na, 0.10 *M* Ag

Table 4.19. ICP-AES site occupancies of Pb-Ag jarosites synthesised at 22ºC and 140ºC, and the concentrations of Pb and Ag in the starting solutions.

Sample	Na	K	Pb	Ag	H_3O	Fe	S	Starting solution
Solutions containing 0.15 M $Fe_2(SO_4)_3.5H_2O$ heated at 140ºC and products dried at 110ºC								
JS43	0	0	0.179	0.00	0.821	3.00	2	0.06 *M* Pb, 0.00 *M* Ag
JS43D	0	0	0.168	0.00	0.832	3.15	2	0.06 *M* Pb, 0.00 *M* Ag
JS44	0	0	0.081	0.281	0.638	3.01	2	0.05 *M* Pb, 0.02 *M* Ag
JS45	0	0	0.082	0.502	0.416	2.97	2	0.04 *M* Pb, 0.04 *M* Ag
JS46	0	0	0.046	0.701	0.253	3.00	2	0.03 *M* Pb, 0.06 *M* Ag
JS46D	0	0	0.041	0.58	0.379	2.91	2	0.03 *M* Pb, 0.06 *M* Ag
JS47	0	0	0.021	0.766	0.213	2.98	2	0.02 *M* Pb, 0.08 *M* Ag
JS48	0	0	0.021	0.765	0.214	3.00	2	0.01 *M* Pb, 0.10 *M* Ag
JS61	0	0	0.000	0.857	0.143	2.93	2	0.00 *M* Pb, 0.12 *M* Ag
Solutions containing 0.15 M $Fe_2(SO_4)_3.5H_2O$ were prepared at 22ºC and products air-dried at 22ºC								
JS95	0	0	0.00	0.856	0.144	2.86	2	0.00 *M* Pb, 0.12 *M* Ag
JS102	0	0	0.006	0.826	0.168	2.80	2	0.00013 *M* Pb, 0.10 *M* Ag
JS103	0	0	0.028	0.822	0.150	2.89	2	0.00032 *M* Pb, 0.10 *M* Ag
JS104	0	0	0.020	0.853	0.127	2.92	2	0.001 *M* Pb, 0.10 *M* Ag
JS105	0	0	0.063	0.824	0.113	2.85	2	0.005 *M* Pb, 0.10 *M* Ag
JS106	0	0	0.036	0.799	0.165	2.78	2	0.001 *M* Pb, 0.10 *M* Ag
JS107	0	0	0.258	0.00	0.742	9.8	2	0.001 *M* Pb, 0.00 *M* Ag

4.1.7 Combined data from EMPA, ICP-AES and Rietveld refinement

The occupancies of the *A* sites of the synthesised K-Ag-, Na-Ag- and Pb-Ag-jarosite products based on a combination of the results of EMPA, ICP-AES and Rietveld

refinement are shown in Tables 4.20, 4.21 and 4.22, respectively. The occupancies shown in this table are mainly taken from the ICP-AES analysis, but where there is a lack of data or the data are considered inaccurate, EMPA or Rietveld refinement data are used. The jarosite products for which changes have been made to the ICP-AES occupancy data are K-Ag-jarosite series 04-12, 22-30, 55-61, and 72-76; Na-Ag-jarosite series 30-38, 49-54 & 61, 66-70, 72 & 77-80, and 71 & 85-88; and Pb-Ag-jarosite sample 107.

Table 4.20: Combined data of site occupancies of K-Ag jarosites synthesised at 22ºC, 97ºC and 140ºC, and the concentrations of K and Ag in the starting solutions.

Sample	Na	K	Pb	Ag	H_3O	Fe	S	Starting solution
Solutions containing 0.51 M $Fe_2(SO_4)_3.5H_2O$ heated at 97ºC and products dried at 60ºC								
JS04	0	0.65	0	0.00	0.35	2.55	2	0.22 *M* K, 0.00 *M* Ag
JS06	0	0.50	0	0.18	0.32	2.88	2	0.165 *M* K, 0.055 *M* Ag
JS06D	0	0.52	0	0.15	0.33	2.56	2	0.165 *M* K, 0.055 *M* Ag
JS08	0	0.41	0	0.30	0.29	2.72	2	0.11 *M* K, 0.11 *M* Ag
JS10	0	0.25	0	0.41	0.34	2.72	2	0.055 *M* K, 0.165 *M* Ag
JS10D	0	0.27	0	0.44	0.29	2.71	2	0.055 *M* K, 0.165 *M* Ag
JS12	0	0.00	0	0.78	0.22	2.71	2	0.00 *M* K, 0.22 *M* Ag
Solutions containing 0.51 M $Fe_2(SO_4)_3.5H_2O$ heated at 97ºC and products dried at 110ºC								
JS22	0	0.64	0	0.00	0.36	2.59	2	0.22 *M* K, 0.00 *M* Ag
JS24	0	0.53	0	0.15	0.32	2.62	2	0.165 *M* K, 0.055 *M* Ag
JS24D	0	0.52	0	0.14	0.34	2.59	2	0.165 *M* K, 0.055 *M* Ag
JS26	0	0.44	0	0.25	0.31	2.74	2	0.11 *M* K, 0.11 *M* Ag
JS28	0	0.27	0	0.56	0.17	2.57	2	0.055 *M* K, 0.165 *M* Ag
JS30	0	0.00	0	0.63	0.00	2.62	2	0.00 *M* K, 0.22 *M* Ag
JS40	0	0.26	0	0.04	0.70	2.87	2	0.5 *M* K, 0.1 *M* Ag
Solutions containing 0.15 M $Fe_2(SO_4)_3.5H_2O$ heated at 140ºC and products dried at 110ºC								
JS55	0	0.43	0	0.00	0.57	2.75	2	0.12 *M* K, 0.00 *M* Ag
JS56	0	0.70	0	0.16	0.14	2.33	2	0.10 *M* K, 0.02 *M* Ag
JS57	0	0.47	0	0.23	0.30	2.80	2	0.08 *M* K, 0.04 *M* Ag
JS58	0	0.38	0	0.34	0.28	2.82	2	0.06 *M* K, 0.06 *M* Ag
JS59	0	0.29	0	0.45	0.26	2.83	2	0.04 *M* K, 0.08 *M* Ag

JS60	0	0.16	0	0.68	0.16	2.96	2	0.02 *M* K, 0.10 *M* Ag
JS61	0	0.00	0	0.85	0.46	2.93	2	0.00 *M* K, 0.12 *M* Ag
Samples annealed at 140ºC and dried at 110ºC (from solutions originally containing 0.51 M $Fe_2(SO_4)_3.5H_2O$ heated at 97ºC and products dried at 60ºC)								
JS62	0	0.61	0	0.00	0.39	2.87	2	0.22 *M* K, 0.00 *M* Ag
JS63	0	0.49	0	0.21	0.30	2.46	2	0.165 *M* K, 0.055 *M* Ag
JS64	0	0.37	0	0.36	0.27	2.76	2	0.11 *M* K, 0.11 *M* Ag
JS65	0	0.15	0	0.37	0.48	2.98	2	0.055 *M* K, 0.165 *M* Ag
JS66	0	0.00	0	0.44	0.56	3.03	2	0.00 *M* K, 0.22 *M* Ag
Samples annealed at 140ºC and dried at 110ºC (from solutions originally containing 0.51 M $Fe_2(SO_4)_3.5H_2O$ heated at 97ºC and products dried at 110ºC)								
JS71	0	0.00	0	0.76	0.24	2.98	2	0.00 *M* K, 0.22 *M* Ag
JS81	0	0.60	0	0.00	0.40	2.81	2	0.22 *M* K, 0.00 *M* Ag
JS82	0	0.44	0	0.24	0.32	2.87	2	0.165 *M* K, 0.055 *M* Ag
JS83	0	0.29	0	0.46	0.25	2.91	2	0.11 *M* K, 0.11 *M* Ag
JS84	0	0.09	0	0.68	0.23	2.94	2	0.055 *M* K, 0.165 *M* Ag
Solutions containing 0.51 M $Fe_2(SO_4)_3.5H_2O$ were prepared at 22ºC and products air-dried at 22ºC								
JS72	0	0.00	0	0.63	0.37	2.84	2	0.00 *M* K, 0.22 *M* Ag
JS73	0	0.78	0	0.00	0.22	2.40	2	0.22 *M* K, 0.00 *M* Ag
JS74	0	0.68	0	0.06	0.26	2.52	2	0.165 *M* K, 0.055 *M* Ag
JS75	0	0.64	0	0.14	0.22	2.49	2	0.11 *M* K, 0.11 *M* Ag
JS76	0	0.37	0	0.26	0.37	2.33	2	0.055 *M* K, 0.165 *M* Ag
Solutions containing 0.15 M $Fe_2(SO_4)_3.5H_2O$ were prepared at 22ºC and products air-dried at 22ºC								
JS89	0	0.73	0	0.00	0.27	2.49	2	0.12 *M* K, 0.00 *M* Ag
JS90	0	0.69	0	0.05	0.26	2.55	2	0.10 *M* K, 0.02 *M* Ag
JS91	0	0.65	0	0.10	0.25	2.68	2	0.08 *M* K, 0.04 *M* Ag
JS92	0	0.60	0	0.15	0.25	2.61	2	0.06 *M* K, 0.06 *M* Ag
JS93	0	0.43	0	0.35	0.22	2.72	2	0.04 *M* K, 0.08 *M* Ag
JS94	0	0.28	0	0.52	0.20	2.71	2	0.02 *M* K, 0.10 *M* Ag
JS95	0	0.00	0	0.85	0.15	2.86	2	0.00 *M* K, 0.12 *M* Ag

Table 4.21: Combined data of site occupancies of Na-Ag jarosites synthesised at 22ºC, 97ºC and 140ºC, and the concentrations of Na and Ag in the starting solutions.

Sample	Na	K	Pb	Ag	H_3O	Fe	S	Starting solution
Solutions containing 0.51 M $Fe_2(SO_4)_3.5H_2O$ heated at 97ºC and products dried at 60ºC								
JS12	0.00	0	0	0.78	0.22	2.71	2	0.00 *M* Na, 0.22 *M* Ag

JS14	0.57	0	0	0.00	0.43	2.91	2	0.22 *M* Na, 0.00 *M* Ag
JS16	0.33	0	0	0.37	0.30	2.92	2	0.165 *M* Na, 0.055 *M* Ag
JS18	0.10	0	0	0.63	0.27	2.72	2	0.11 *M* Na, 0.11 *M* Ag
JS20	0.06	0	0	0.71	0.23	2.71	2	0.055 *M* Na, 0.165 *M* Ag
Solutions containing 0.51 M $Fe_2(SO_4)_3.5H_2O$ heated at 97ºC and products dried at 110ºC								
JS30	0.00	0	0	0.63	0.00	2.62	2	0.00 *M* Na, 0.22 *M* Ag
JS32	0.55	0	0	0.00	0.45	2.87	2	0.22 *M* Na, 0.00 *M* Ag
JS34	0.12	0	0	0.21	0.67	2.97	2	0.165 *M* Na, 0.055 *M* Ag
JS36	0.05	0	0	0.31	0.64	2.83	2	0.11 *M* Na, 0.11 *M* Ag
JS38	0.04	0	0	0.61	0.35	2.59	2	0.055 *M* Na, 0.165 *M* Ag
JS38D	0.07	0	0	0.65	0.28	2.68	2	0.055 *M* Na, 0.165 *M* Ag
JS42	0.09	0	0	0.70	0.21	2.63	2	0.5 *M* Na, 0.1 *M* Ag
Solutions containing 0.15 M $Fe_2(SO_4)_3.5H_2O$ heated at 140ºC and products dried at 110ºC								
JS49	0.47	0	0	0.00	0.53	2.64	2	0.12 *M* Na, 0.00 *M* Ag
JS50	0.33	0	0	0.25	0.42	3.04	2	0.10 *M* Na, 0.02 *M* Ag
JS51	0.20	0	0	0.47	0.33	2.90	2	0.08 *M* Na, 0.04 *M* Ag
JS52	0.09	0	0	0.67	0.24	2.93	2	0.06 *M* Na, 0.06 *M* Ag
JS53	0.04	0	0	0.77	0.19	2.98	2	0.04 *M* Na, 0.08 *M* Ag
JS54	0.01	0	0	0.83	0.16	2.98	2	0.02 *M* Na, 0.10 *M* Ag
JS61	0.00	0	0	0.85	0.15	2.93	2	0.00 *M* Na, 0.12 *M* Ag
Samples annealed at 140ºC and dried at 110ºC (from solutions originally containing 0.51 M $Fe_2(SO_4)_3.5H_2O$ heated at 97ºC and products dried at 60ºC)								
JS66	0.00	0	0	0.44	0.56	3.03	2	0.00 *M* Na, 0.22 *M* Ag
JS67	0.65	0	0	0.00	0.35	2.91	2	0.22 *M* Na, 0.00 *M* Ag
JS68	0.57	0	0	0.09	0.34	2.74	2	0.165 *M* Na, 0.055 *M* Ag
JS69	0.40	0	0	0.19	0.41	3.16	2	0.11 *M* Na, 0.11 *M* Ag
JS70	0.23	0	0	0.33	0.44	2.72	2	0.055 *M* Na, 0.165 *M* Ag
Samples annealed at 140ºC and dried at 110ºC (from solutions originally containing 0.51 M $Fe_2(SO_4)_3.5H_2O$ heated at 97ºC and products dried at 110ºC)								
JS71	0.00	0	0	0.76	0.24	2.98	2	0.00 *M* Na, 0.22 *M* Ag
JS85	0.57	0	0	0.00	0.43	2.98	2	0.22 *M* Na, 0.00 *M* Ag
JS86	0.29	0	0	0.35	0.36	2.73	2	0.165 *M* Na, 0.055 *M* Ag
JS87	0.17	0	0	0.50	0.33	2.53	2	0.11 *M* Na, 0.11 *M* Ag
JS88	0.11	0	0	0.56	0.33	2.97	2	0.055 *M* Na, 0.165 *M* Ag
Solutions containing 0.51 M $Fe_2(SO_4)_3.5H_2O$ were prepared at 22ºC and products air-dried at 22ºC								
JS72	0.00	0	0	0.63	0.37	2.84	2	0.00 *M* Na, 0.22 *M* Ag

JS77	0.67	0	0	0.00	0.33	2.86	2	0.22 *M* Na, 0.00 *M* Ag
JS78	0.11	0	0	0.42	0.47	2.88	2	0.165 *M* Na, 0.055 *M* Ag
JS79	0.06	0	0	0.48	0.46	2.78	2	0.11 *M* Na, 0.11 *M* Ag
JS80	0.03	0	0	0.82	0.15	3.02	2	0.055 *M* Na, 0.165 *M* Ag
Solutions containing 0.51 M $Fe_2(SO_4)_3.5H_2O$ were prepared at 22ºC and products air-dried at 22ºC								
JS95	0.00	0	0	0.85	0.15	2.86	2	0.00 *M* Na, 0.12 *M* Ag
JS96	0.68	0	0	0.00	0.32	3.01	2	0.12 *M* Na, 0.00 *M* Ag
JS97	0.37	0	0	0.41	0.22	2.96	2	0.10 *M* Na, 0.02 *M* Ag
JS98	0.14	0	0	0.68	0.18	2.86	2	0.08 *M* Na, 0.04 *M* Ag
JS99	0.04	0	0	0.80	0.16	2.86	2	0.06 *M* Na, 0.06 *M* Ag
JS100	0.02	0	0	0.81	0.17	2.84	2	0.04 *M* Na, 0.08 *M* Ag
JS101	0.01	0	0	0.83	0.16	2.84	2	0.02 *M* Na, 0.10 *M* Ag

Table 4.22. Combined data of site occupancies of Pb-Ag jarosites synthesised at 22ºC and 140ºC, and the concentrations of Pb and Ag in the starting solutions.

Sample	Na	K	Pb	Ag	H_3O	Fe	S	Starting solution
Solutions containing 0.15 M $Fe_2(SO_4)_3.5H_2O$ heated at 140ºC and products dried at 110ºC								
JS43	0	0	0.179	0.00	0.821	3.00	2	0.06 *M* Pb, 0.00 *M* Ag
JS43D	0	0	0.168	0.00	0.832	3.15	2	0.06 *M* Pb, 0.00 *M* Ag
JS44	0	0	0.081	0.281	0.638	3.01	2	0.05 *M* Pb, 0.02 *M* Ag
JS45	0	0	0.082	0.502	0.416	2.97	2	0.04 *M* Pb, 0.04 *M* Ag
JS46	0	0	0.046	0.701	0.253	3.00	2	0.03 *M* Pb, 0.06 *M* Ag
JS46D	0	0	0.041	0.58	0.379	2.91	2	0.03 *M* Pb, 0.06 *M* Ag
JS47	0	0	0.021	0.766	0.213	2.98	2	0.02 *M* Pb, 0.08 *M* Ag
JS48	0	0	0.021	0.765	0.214	3.00	2	0.01 *M* Pb, 0.10 *M* Ag
JS61	0	0	0.000	0.857	0.143	2.93	2	0.00 *M* Pb, 0.12 *M* Ag
Solutions containing 0.15 M $Fe_2(SO_4)_3.5H_2O$ were prepared at 22ºC and products air-dried at 22ºC								
JS95	0	0	0.00	0.856	0.144	2.86	2	0.00 *M* Pb, 0.12 *M* Ag
JS102	0	0	0.006	0.826	0.168	2.80	2	0.00013 *M* Pb, 0.10 *M* Ag
JS103	0	0	0.028	0.822	0.150	2.89	2	0.00032 *M* Pb, 0.10 *M* Ag
JS104	0	0	0.020	0.853	0.127	2.92	2	0.001 *M* Pb, 0.10 *M* Ag
JS105	0	0	0.063	0.824	0.113	2.85	2	0.005 *M* Pb, 0.10 *M* Ag
JS106	0	0	0.036	0.799	0.165	2.78	2	0.001 *M* Pb, 0.10 *M* Ag
JS107	0	0	0.258	0.00	0.742	2.91	2	0.001 *M* Pb, 0.00 *M* Ag

4.2 Silver content of natural jarosite samples

The EMPA analysis of the natural jarosite, natrojarosite and argentojarosite samples obtained for this project indicates that the samples have only trace levels of Ag, except for sample 34, which is argentojarosite (see Table 4.23). Sample 34 has *A*-site occupancies of Ag 0.64, Pb 0.011 and Au 0.005, plus, by difference from 1.0, H_3O 0.333. Therefore, the analysis provided no useful data for this project.

Table 4.23. EMPA site occupancies for natural jarosite samples.

Sample	Na	K	Ag	Pb	Au	H3O	Fe	Al	S	As	P
JN_01											
JN_02	0.114	0.071	0	0	0.006	0.809	3.236	0.014	1.996	0	0.004
JN_03	0.114	0.002	0	0	0.002	0.882	3.196	0.002	2	0	0
JN_04	0.084	0.115	0	0	0.004	0.797	3.196	0.028	1.998	0	0.002
JN_05	0.056	0.029	0	0	0.002	0.913	2.596	0.001	1.968	0.032	0
JN_05_Na	0.127	0.003	0	0	0.002	0.868	2.506	0.002	1.989	0.011	0
JN_05_K	0.003	0.048	0	0	0.002	0.947	2.663	0.001	1.953	0.047	0
JN_06	0.002	0.712	0	0.019	0.002	0.265	3.202	0.004	1.988	0.008	0.004
JN_15	0.2	0.759	0.003	0.071	0.004	0	2.446	0.453	1.97	0.007	0.023
JN_16	0.162	0.532	0	0	0.003	0.303	2.218	0.384	1.995	0	0.005
JN_17	0.466	0.567	0	0.001	0.004	0	2.2	0.864	1.978	0	0.022
JN_18	0.077	0.692	0	0	0.004	0.227	2.511	0.446	1.965	0.003	0.032
JN_19	0.192	0.379	0	0	0.003	0.426	2.447	0.11	1.997	0	0.003
JN_20	0.115	0.551	0	0	0.005	0.329	1.992	1.004	1.978	0.002	0.02
JN_21	0.054	0.739	0	0.001	0.004	0.201	2.464	0.219	1.998	0.001	0.001
JN_22	0.354	0.422	0	0.001	0.003	0.219	2.554	0.099	1.997	0.001	0.002
JN_23	0.01	0.555	0	0	0.004	0.431	2.821	0.098	1.826	0	0.174
JN_24	0.167	0.324	0	0	0.003	0.506	2.989	0.011	1.972	0.006	0.022
JN_25	0.008	0.859	0	0.048	0.003	0.034	2.76	0.083	1.966	0.024	0.01
JN_26	0.287	0.211	0	0.001	0.006	0.494	2.563	0.206	1.994	0	0.006
JN_26_Na	0.329	0.134	0	0.001	0.007	0.528	2.461	0.225	1.995	0	0.005
JN_26_K	0.188	0.39	0	0.003	0.003	0.413	2.801	0.159	1.993	0	0.007
JN_27	0.32	0.066	0	0.124	0.004	0.362	2.855	0.13	1.985	0.012	0.003
JN_28	0.063	0.412	0	0.045	0.003	0.432	2.704	0.134	1.962	0.013	0.025
JN_31	0.045	0.457	0	0	0.002	0.496	2.698	0.17	1.993	0.003	0.004
JN_33	0.407	0.059	0	0.001	0.004	0.528	2.525	0.212	1.992	0	0.008
JN_34	0	0	0.64	0.011	0.005	0.333	2.755	0.012	1.996	0.003	0.001
JN_45	0.191	0.688	0.001	0.001	0.004	0.114	2.75	0.274	2	0	0
JN_46	0.189	0.392	0	0.001	0.005	0.412	2.983	0.085	1.999	0.001	0

4.3 Summary

- The synthesised jarosite compounds have been given Munsell colour numbers 2.5Y 5/6, 7/6, 8/6, 5/8, 6/8, 7/8 and 8/8, and 10YR 5/6, 6/8 and 7/8. Most of the compounds have a Munsell colour of yellow, but some compounds with high Ag content in the starting solutions are olive yellow;
- SEM secondary-electron images indicate differences in morphology between K-H_3O, Na-H_3O and Ag-H_3O-jarosite compounds;
- powder XRD analysis indicates K-Ag-H_3O jarosite series with declining K content and increasing Ag content show a trend of generally declining d-values for the strongest peaks as the relative proportions of the two cations in the *A* site change;
- the XRD results for the Na-Ag-H_3O-jarosite series show no consistent trends of changing *d*-values of main peaks as the quantity of Na and Ag occupying the *A* site changes. This is likely to be related to the high proportion of H_3O in the compounds, which is also the case with the Pb-Ag-H_3O-jarosites;
- XRD peak positions of *hkl* 003 and 006 reflections give information on changing *c*-axis parameter of the unit cell, as the parameter varies according to the ionic radii of cations occupying the *A* site;
- the K-Ag-H_3O-jarosite series show generally declining *d*-spacing values for 003 and 006 reflections as K content decreases and Ag content increases, consistent with the smaller ionic radius of Ag^+ compared with K^+;
- the Na-Ag-H_3O-jarosite series show *d*-spacing values for the 003 and 006 reflections decrease from the Na-H_3O-jarosite compound to the Ag-H_3O-

jarosite compound, which is consistent with the ionic radius of Ag^+ being smaller than that of Na^+. However, within each series, although there is a general decline, there are inconsistent *d* values for some intermediate compounds;

- in the Pb-Ag-H_3O-jarosite compounds, the *d*-values for the 003 and 006 reflections do not indicate the reported doubled *c*-axis dimension (11.3 Å) of plumbojarosite, but the *d*-values of the samples are consistent with their low Pb contents and high H_3O contents;
- Rietveld refinement of the XRD data indicates the *a*-axis parameters of K-H_3O-jarosite compounds are shorter (7.3172-7.3282 Å) and the *c*-axis parameters are longer (17.0031-17.1687 Å) than those of Na-H_3O-jarosite (7.338-7.3426 Å and 16.7008-16.7932 Å) and Ag-H_3O-jarosite (7.3485-7.3582 Å and 16.5013-16.6095 Å), which are consistent with published data. These results indicate the ionic radius of the Ag^+ cation is smaller than the radius of the Na^+ cation;
- Rietveld refinement of the intermediate Na-Ag-H_3O-jarosite compounds in the different series gives contradictory evidence on the effect of Ag content on the length of the *a*- and *c*-axis parameters and so on whether the ionic radius of Ag^+ is larger or smaller than that of Na^+, and therefore on whether Ag^+ in the *A* site is likely to be in 12-fold or 9-fold coordination;
- Rietveld refinement of K-Ag-H_3O-jarosite compounds reveals generally decreasing K,Ag-O2 and K,Ag-O3 bond lengths as Ag content increases (although there are some inconsistencies within the series). The same trends are not evident in the Na-Ag-H_3O-jarosite compounds, possibly because the ionic radii of Na^+ and Ag^+ are of relatively similar sizes

compared with K^+, whichever the coordination of Ag^+, and the H_3O contents are relatively high in many of the samples;

- Rietveld refinement of K-Ag-H_3O and Na-Ag-H_3O-jarosite compounds reveals changing atomic positions of O2 and O3 (OH), to which the *A*-site atom is bonded, with changing composition of Ag;
- the assigned Raman vibrational modes of some of the synthesised K-H_3O-jarosite products have higher wavenumbers (cm^{-1}) than their Ag-H_3O equivalents, but others do not. The same is the case with the Pb-H_3O-jarosite compounds and Ag-H_3O-jarosite compounds. The assigned modes of Ag-H_3O-jarosite compounds do not have higher wavenumbers than their Na-H_3O equivalents, but some have the same wavenumbers. Consequently, the results do not provide consistent evidence on predicted stronger bonds for heavier elements;
- EMPA and ICP-AES analysis of the chemical composition of the synthetic K-Ag-H_3O-, Na-Ag-H_3O- and Pb-Ag-H_3O-jarosite compounds show generally declining contents of K, Na and Pb, respectively, with declining K^+, Na^+ or Pb^{2+} cation concentration in the starting solutions, and complementary trends of generally increasing Ag^+ contents as Ag increases in the starting solutions.

5 DISCUSSION

5.1 Capacity and mechanisms of uptake of silver by synthesised jarosite-family minerals

5.1.1 Influence of synthesis temperature on the K-Ag-H_3O, Na-Ag-H_3O and Pb-Ag-H_3O compound characteristics

5.1.1.1 Influence of synthesis temperature on *A*-site occupancies

Compositional information on the K, Na, Pb and Ag occupancies of the *A* site of the jarosite compounds synthesised in this project is provided by EMPA, ICP-AES and Rietveld refinement of powder XRD data. Several studies have suggested increased cation occupancies of jarosite structural sites with increased temperature of synthesis (e.g., Murphy et al., 2009); however, the compositional data from the different analytical techniques used in this project indicate inconsistent trends in the *A*-site occupancies of the different jarosite series. The results of the different analyses show that the K-Ag-H_3O and Na-Ag-H_3O-jarosite product series have generally declining mean and median *A*-site occupancies of both K + Ag and Na + Ag, respectively, and Ag-only cations as synthesis temperature increases from 22ºC to 97ºC. However, the occupancies generally increase as synthesis temperature increases from 97ºC to 140ºC. There are variations in the differences in occupancies between products synthesised at 22ºC and those made at 140ºC according to analysis technique. The EMPA results show the mean and median K and Ag *A*-site occupancies of the K-Ag-H_3O-jarosite product series are generally higher in those synthesised at 140ºC compared with those synthesised at 22ºC; the ICP-AES results show the opposite trend in occupancies in the majority of cases. In the Na-Ag-H_3O-jarosite products, the EMPA results show the Na and Ag occupancies are generally lower in the series synthesised at 140ºC than in those synthesised at 22ºC; this is also the case with the

ICP-AES analysis results. The Rietveld refinement results show that, in the K-Ag-H_3O-jarosite product series, the K and Ag occupancies rise with increased synthesis temperature from 22ºC to 97ºC and 140ºC; in the Na-Ag-jarosite product series, the opposite trend is seen in Na and Ag occupancies. A combination of data from the different analysis techniques shows that the K + Ag mean and median *A*-site occupancies of the K-Ag-H_3O-jarosite product series decrease as synthesis temperature increases from 22ºC to 97ºC and from 22ºC to 140ºC, whereas the Ag-only occupancies generally increase. As temperature increases from 97ºC to 140ºC, there is a decrease in mean occupancy and an increase in median occupancy of K + Ag, and there are increases in mean and median occupancy of Ag-only. In the Na-Ag-H_3O-jarosite product series, the combined data show that, in most cases, the Na + Ag and Ag-only mean and median *A*-site occupancies decrease as synthesis temperature increases from 22ºC to 97ºC and from 22ºC to 140ºC. As temperature increases from 97ºC to 140ºC, the mean and median occupancies of Na + Ag increase, whereas for Ag-only they decrease. For the Pb-Ag-H_3O-jarosite products, the EMPA and ICP-AES results both show declining Pb and Ag *A*-site occupancies with increasing synthesis temperature. The details of these general findings are discussed in the following sections.

5.1.1.1.1 EMPA data of *A*-site occupancies

The EMPA results for the K-Ag-H_3O-jarosite samples synthesised at 22ºC, 97ºC and 140ºC using 0.51 *M* $Fe_2(SO_4)_3.5H_2O$ and at 22ºC and 140ºC using 0.15 *M* $Fe_2(SO_4)_3.5H_2O$ show cation occupancy (total of K and Ag) of the *A*-site decreases as the synthesis temperature is increased from 22ºC (mean 0.52, median 0.52, range 0.34-0.70) to 97ºC (mean 0.35, median 0.34, range 0.23-0.59); however, there is an

increase in occupancy as the temperature is increased to 140ºC (mean 0.65, median 0.66, range between 0.43 and 0.86) (see Table 5.1 and Figure 5.1). The same trends are generally seen for the Ag-only occupancies: there is a decline in the mean but increase in the median occupancy from 22ºC (mean 0.21, median 0.11, range 0.04-0.63) to 97ºC (mean 0.17, median 0.15, range 0.06-0.31) and an increase in the mean and median to 140ºC (mean 0.39, median 0.35, range 0.14-0.66) (see Figure 5.1a). A possible reason for these trends is that the difference in synthesis period between ~ 1 year at 22ºC and 4 hours at 97ºC is sufficient to result in greater occupancies at the lower temperature, whereas the increase in temperature to 140ºC is sufficiently high to outweigh this effect.

Table 5.1: EMPA *A*-site occupancies of K + Ag, Na + Ag, and Ag and synthesis temperature of K-Ag-H_3O and Na-Ag-H_3O-jarosite compounds

Cation	Mean	Med.	Range	Temp	Mean	Med.	Range	Temp	Mean	Med.	Range	Temp
Synthesis solution 0.51 M $Fe_2(SO_4)_3.5H_2O$ and 0.15 M $Fe_2(SO_4)_3.5H_2O$												
K+Ag	0.52	0.52	0.34-70	22	0.35	0.34	0.23-59	97	0.65	0.66	0.43-86	140
Ag	0.21	0.11	0.04-63	22	0.17	0.15	0.06-31	97	0.39	0.35	0.14-66	140
Na+Ag	0.57	0.57	0.47-64	22	0.27	0.27	0.17-33	97	0.50	0.49	0.33-66	140
Ag	0.54	0.55	0.42-63	22	0.23	0.23	0.15-31	97	0.32	0.32	0.09-63	140

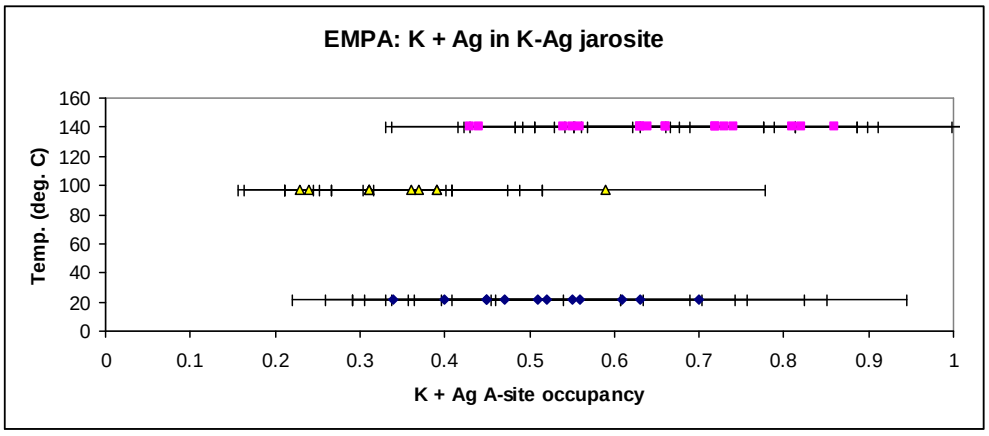

Figure 5.1: EMPA total *A*-site occupancy of K + Ag in K-Ag-H_3O-jarosite samples synthesised using 0.51 *M* $Fe_2(SO_4)_3.5H_2O$ and 0.15 *M* $Fe_2(SO_4)_3.5H_2O$ at 22˚C, 97˚C and 140˚C. (Error bars show series mean precision or C in %, see Appendix I.)

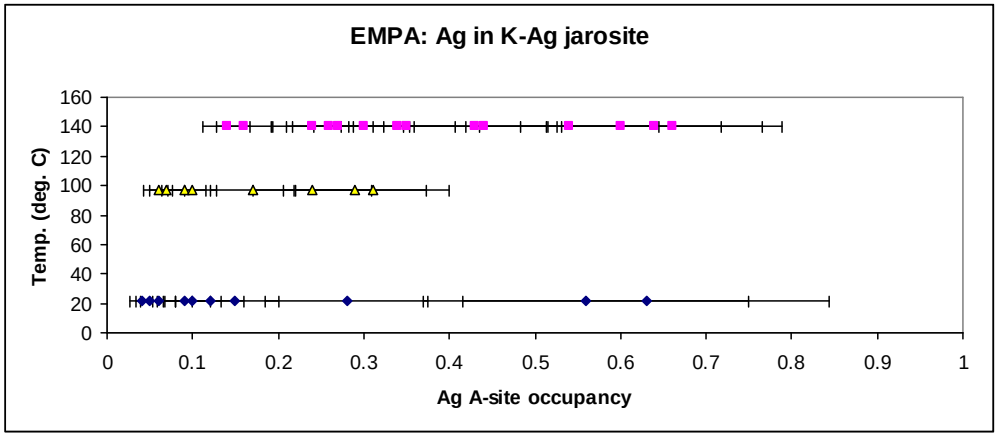

Figure 5.1a: EMPA total *A*-site occupancy of Ag in K-Ag-H_3O-jarosite samples synthesised using 0.51 *M* $Fe_2(SO_4)_3.5H_2O$ and 0.15 *M* $Fe_2(SO_4)_3.5H_2O$ at 22˚C, 97˚C and 140˚C. (Error bars show series mean precision or C in %, see Appendix I.)

The EMPA results for the Na-Ag-H_3O-jarosite samples synthesised at 22ºC, 97ºC and 140ºC using 0.51 *M* $Fe_2(SO_4)_3.5H_2O$ and at 22ºC and 140ºC using 0.15 *M* $Fe_2(SO_4)_3.5H_2O$ show the *A*-site cation occupancies (total of Na and Ag) decrease as the synthesis temperature is increased from 22ºC (mean 0.57, median 0.57, range 0.47-0.64) to 97ºC (mean 0.27, median 0.27, range 0.17-0.33) and 140ºC (mean 0.50, median 0.49, range 0.33-0.66) (see Table 5.1 and Figure 5.1b). However, there is an increase in occupancies as the temperature is increased from 97ºC to 140ºC, although the occupancies at 140ºC are below those at 22ºC. Similar trends are seen for the Ag-only occupancies: there is a decline from 22ºC (mean 0.54, median 0.55, range 0.42-0.63) to 97ºC (mean 0.23, median 0.23, range 0.15-0.31) and then a lesser increase to 140ºC (mean 0.32, median 0.32, range 0.09-0.63) (see Figure 5.1c). A possible reason for these trends is that the difference in synthesis period between ~ 1 year at 22ºC and 4 hours at 97ºC and 140ºC is sufficient to result in greater occupancies at the lower temperature, while the increase in temperature from 97ºC to 140ºC increases *A*-site occupancies.

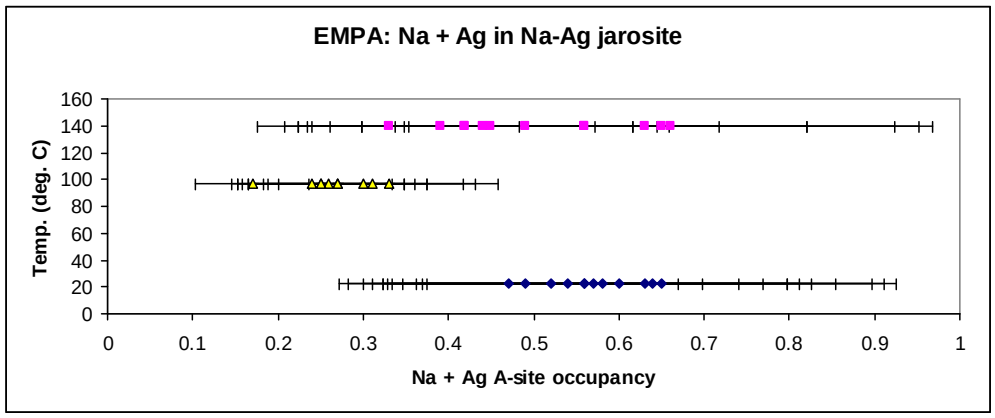

Figure 5.1b: EMPA total *A*-site occupancy of Na + Ag in Na-Ag-H_3O-jarosite samples synthesised using 0.51 *M* $Fe_2(SO_4)_3.5H_2O$ and 0.15 *M* $Fe_2(SO_4)_3.5H_2O$ at 22˚C, 97˚C and 140˚C. (Error bars show series mean precision or C in %, see Appendix I.)

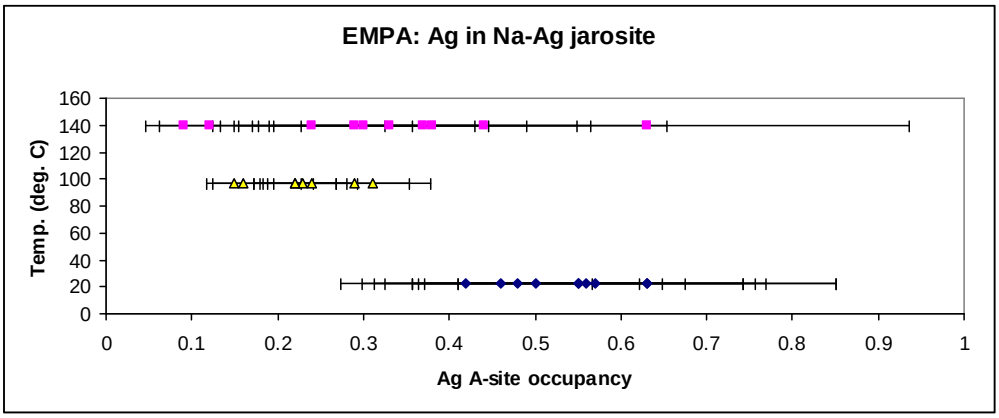

Figure 5.1c: EMPA total *A*-site occupancy of Ag in Na-Ag-H_3O-jarosite samples synthesised using 0.51 *M* $Fe_2(SO_4)_3.5H_2O$ and 0.15 *M* $Fe_2(SO_4)_3.5H_2O$ at 22˚C, 97˚C and 140˚C. (Error bars show series mean precision or C in %, see Appendix I.)

The EMPA results for the K-Ag-H_3O-jarosite samples indicate that, of the products synthesised using 0.51 *M* $Fe_2(SO_4)_3.5H_2O$, the lowest *A*-site cation occupancies (total of K and Ag) are found for those synthesised at 97ºC (content mean 0.35, median 0.33, range between 0.23 and 0.59), compared with those synthesised at 22ºC (mean 0.53, median 0.48, range 0.34-0.70). There is an increase in occupancies, however, in those synthesised at 140ºC (mean 0.62, median 0.64, range 0.44-0.74) (see Table 5.2 and Figure 5.2). This is also the case for the mean Ag-only contents of these K-Ag-jarosite samples (see Figure 5.2a): 0.17 at 97ºC; 0.24 at 22ºC; and 0.40 at 140ºC. However, apart from the Ag-jarosite end-member,

the median (0.13) and range (0.06-0.15) of Ag contents is lower in the products made at 22ºC than in the products made at 97ºC (median 0.14 and range 0.06-0.31); therefore, the increase in synthesis temperature increases the median and range of Ag *A*-site contents. In the products synthesised at 140ºC, the Ag contents are: mean 0.40, median 0.39, range 0.14-0.66; therefore, they have higher *A*-site Ag contents than those synthesised at 97ºC or 22ºC, a finding supported by the results for the K-Ag-H_3O-jarosite samples synthesised using 0.15 *M* $Fe_2(SO_4)_3.5H_2O$ (see Table 5.2 and Figure 5.2b). These results indicate that the increase in synthesis temperature to 140ºC increases *A*-site content (mean 0.71, median 0.72, range 0.43-0.86) compared with the products made at 22ºC (mean 0.51, median 0.50, range 0.40-0.61). The Ag-only contents of these samples also show this trend: mean 0.19, median 0.11, range 0.04-0.56 at 22ºC; and mean 0.36, median 0.31, range 0.16-0.60 at 140ºC (see Figure 5.2c). The lower contents of the samples synthesised at 97ºC compared with the samples synthesised at 22ºC in the series using 0.51 *M* $Fe_2(SO_4)_3.5H_2O$ may be explained by the difference between their periods of synthesis, which were 4 hours and ~ 1 year, respectively.

Table 5.2: EMPA *A*-site occupancy of K + Ag, Na + Ag, Pb + Ag and Ag and synthesis temperature of K-Ag-H_3O, Na-Ag-H_3O and Pb-Ag-H_3O-jarosite compounds according to Fe concentration in the synthesis solution

Cation	Mean	Med.	Range	Temp	Mean	Med.	Range	Temp	Mean	Med.	Range	Temp
Synthesis solution 0.51 M $Fe_2(SO_4)_3.5H_2O$												
K+Ag	0.53	0.48	0.34-70	22	0.35	0.33	0.23-59	97	0.62	0.64	0.44-74	140
Ag	0.24	0.13	0.06-63	22	0.17	0.14	0.06-31	97	0.40	0.39	0.14-66	140
Na+Ag	0.54	0.54	0.47-63	22	0.27	0.27	0.17-33	97	0.55	0.58	0.44-66	140
Ag	0.52	0.52	0.42-63	22	0.23	0.23	0.15-31	97	0.27	0.27	0.09-44	140
Synthesis solution 0.15 M $Fe_2(SO_4)_3.5H_2O$												
K+Ag	0.51	0.50	0.40-61	22					0.71	0.72	0.43-86	140
Ag	0.19	0.11	0.04-56	22					0.36	0.31	0.16-60	140
Na+Ag	0.59	0.57	0.52-65	22					0.47	0.44	0.33-63	140
Ag	0.55	0.57	0.46-63	22					0.36	0.34	0.24-54	140

Pb+Ag	0.53	0.53	0.03-86	22			0.46	0.45	0.25-66	140
Ag	0.60	0.53	0.45-81	22			0.45	0.45	0.22-65	140

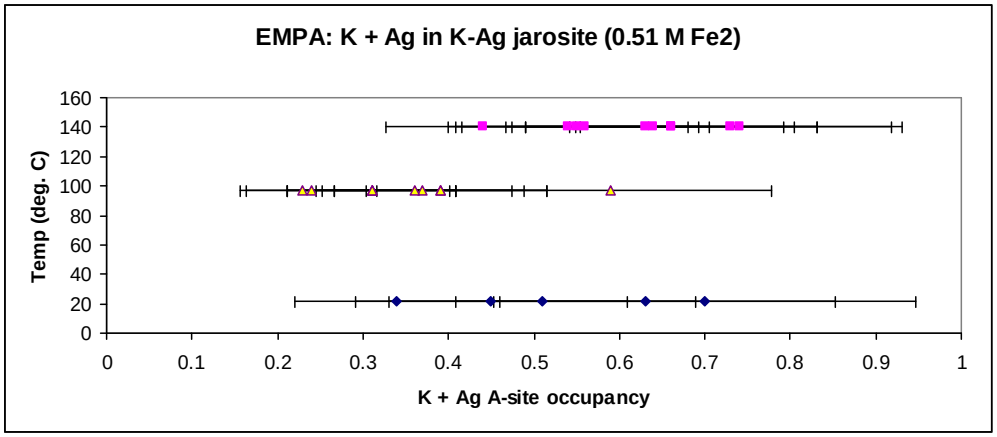

Figure 5.2: EMPA total *A*-site occupancy of K + Ag in K-Ag-H_3O-jarosite samples synthesised using 0.51 *M* $Fe_2(SO_4)_3.5H_2O$ at 22˚C, 97˚C and 140˚C. (Error bars show series mean precision or C in %, see Appendix I.)

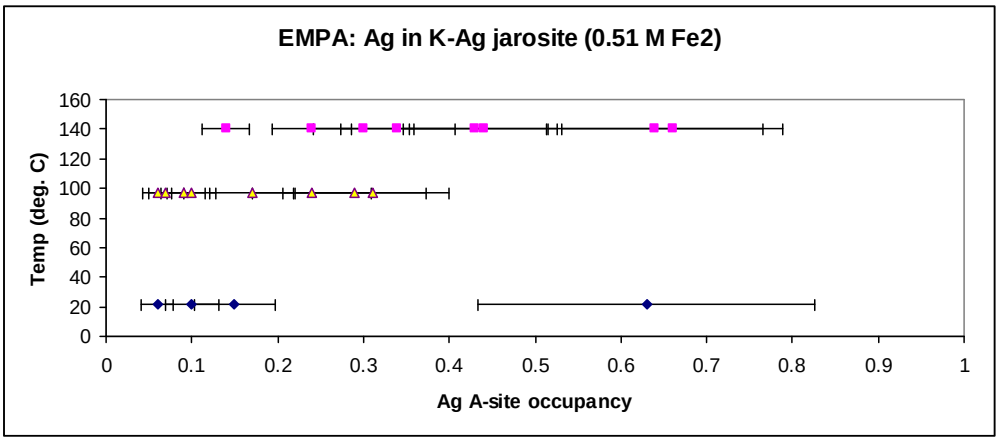

Figure 5.2a: EMPA total *A*-site occupancy of Ag in K-Ag-H_3O-jarosite samples synthesised using 0.51 *M* $Fe_2(SO_4)_3.5H_2O$ at 22˚C, 97˚C and 140˚C. (Error bars show series mean precision or C in %, see Appendix I.)

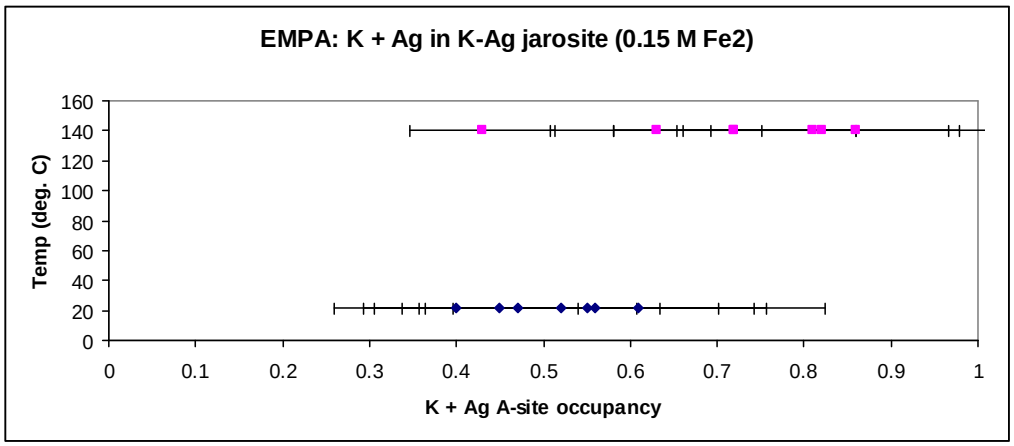

Figure 5.2b: EMPA total *A*-site occupancy of K + Ag in K-Ag-H_3Ojarosite samples synthesised using 0.15 *M* $Fe_2(SO_4)_3.5H_2O$ at 22˚C, 97˚C and 140˚C. (Error bars show series mean precision or C in %, see Appendix I.)

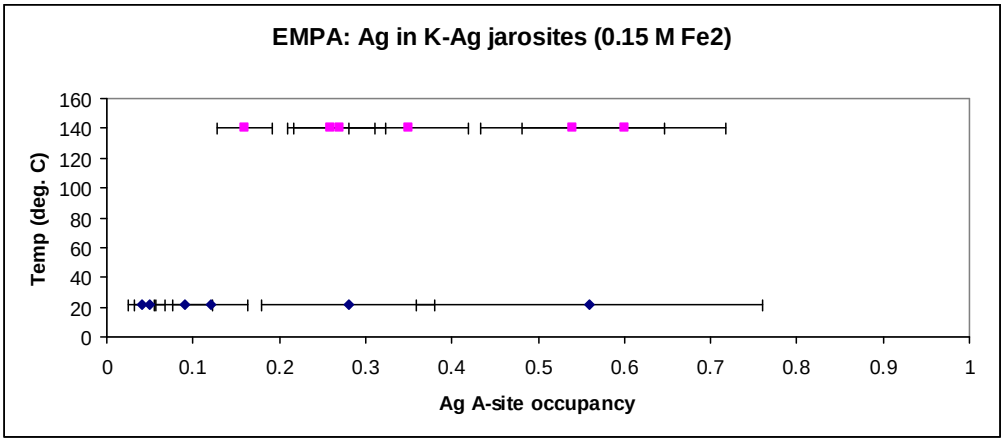

Figure 5.2c: EMPA total *A*-site occupancy of Ag in K-Ag-H_3O-jarosite samples synthesised using 0.15 *M* $Fe_2(SO_4)_3.5H_2O$ at 22˚C, 97˚C and 140˚C. (Error bars show series mean precision or C in %, see Appendix I.)

The EMPA results for the Na-Ag-H_3O-jarosite samples synthesised using 0.51 *M* $Fe_2(SO_4)_3.5H_2O$ indicate that, as in the K-Ag-H_3O-jarosite samples, the lowest *A*-site contents (total of Na and Ag), on average, are found in the products synthesised at 97ºC (mean 0.27, median 0.27, range 0.17-0.33), compared with those synthesised at 22ºC (mean 0.54, median 0.54, range 0.47-0.63) or 140ºC (mean 0.55, median 0.58, range 0.44-0.66) (see Figure 5.2d). This is also the case for the Ag-only contents of these Na-Ag-jarosite samples (see Figure 5.2e): mean 0.23, median 0.23, range 0.15-0.31 at 97ºC; mean 0.52, median 0.52, range 0.42-0.63 at 22ºC; and mean 0.27, median 0.27, range 0.09-0.44 at 140ºC. However, the products synthesised at 140ºC have slightly higher Na plus Ag *A*-site contents but lower Ag-only contents than those synthesised at 22ºC. The lower contents of the samples synthesised at 97ºC and 140ºC compared with those made at 22ºC may be explained by the difference in synthesis periods, which were 4 hours and ~ 1 year, respectively.

In the Na-Ag-H_3O-jarosite samples synthesised using 0.15 *M* $Fe_2(SO_4)_3.5H_2O$ (see Figure 5.2f), the products synthesised at 22ºC (mean 0.59, median 0.57, range 0.52-0.65) have higher *A*-site contents, on average, than those synthesised at 140ºC (mean 0.47, median 0.44, range 0.33-0.63). The Ag-only

contents of these samples also show this trend: mean 0.55, median 0.57, range 0.46-0.63 at 22ºC; and mean 0.36, median 0.34, range 0.24-0.54 at 140ºC (see Figure 5.2g). Therefore, these results contradict the results (above) for the syntheses using 0.51 *M* $Fe_2(SO_4)_3.5H_2O$, in which the products synthesised at 140ºC have higher average contents than those made at 22ºC. As a consequence, it is not sufficient for the lower contents of the samples synthesised at 140ºC compared with the samples synthesised at 22ºC in the 0.15 *M* $Fe_2(SO_4)_3.5H_2O$ data set to be explained by the difference between their periods of synthesis (4 hours and ~ 1 year, respectively). It

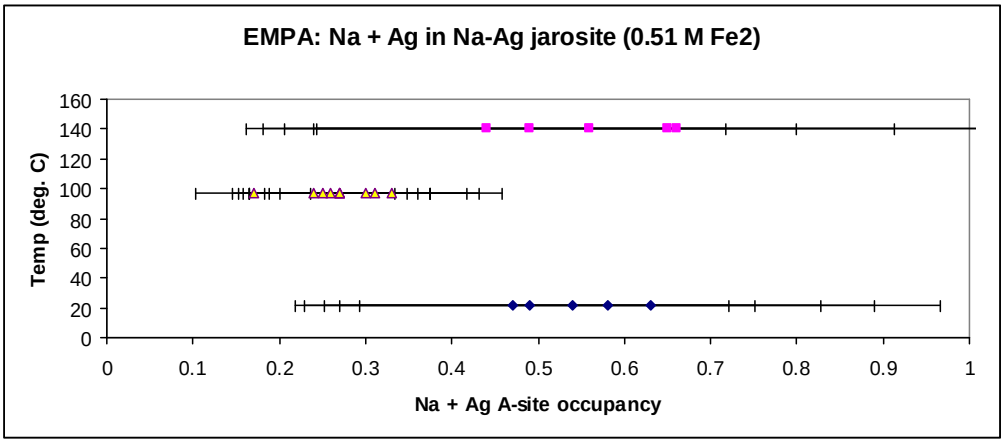

Figure 5.2d: EMPA total *A*-site occupancy of Na + Ag in Na-Ag-H_3O-jarosite samples synthesised using 0.51 *M* $Fe_2(SO_4)_3.5H_2O$ at 22˚C, 97˚C and 140˚C. (Error bars show series mean precision or C in %, see Appendix I.)

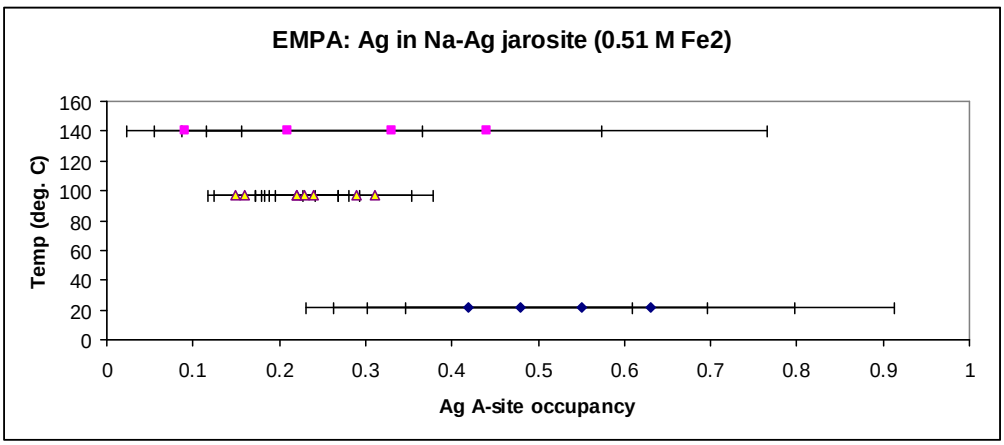

Figure 5.2e: EMPA total *A*-site occupancy of Ag in Na-Ag-H_3O-jarosite samples synthesised using 0.51 *M* $Fe_2(SO_4)_3.5H_2O$ at 22˚C, 97˚C and 140˚C. (Error bars show series mean precision or C in %, see Appendix I.)

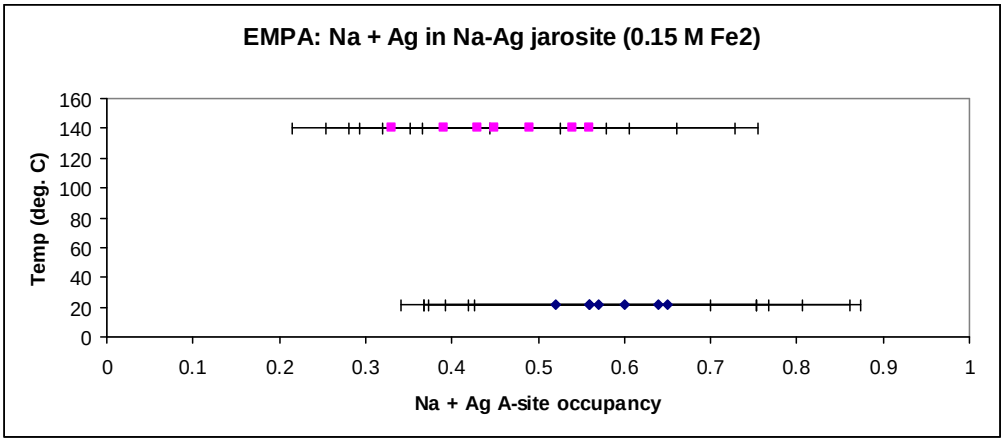

Figure 5.2f: EMPA total *A*-site occupancy of Na + Ag in Na-Ag-H_3O-jarosite samples synthesised using 0.15 *M* $Fe_2(SO_4)_3.5H_2O$ at 22˚C, 97˚C and 140˚C. (Error bars show series mean precision or C in %, see Appendix I.)

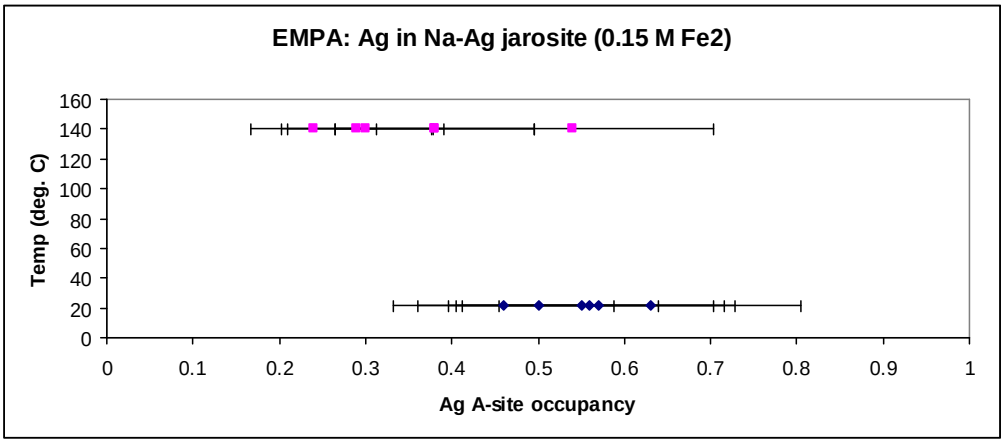

Figure 5.2g: EMPA total *A*-site occupancy of Ag in Na-Ag-H_3O-jarosite samples synthesised using 0.15 *M* $Fe_2(SO_4)_3.5H_2O$ at 22˚C, 97˚C and 140˚C. (Error bars show series mean precision or C in %, see Appendix I.)

is more likely that inaccurate results have been caused by the problems of EMPA of jarosite compounds, including sample sensitivity to the electron beam causing interactions and small particle size (< 1 μm) (see section 4.1.5).

The EMPA results for the Pb-Ag-H_3O-jarosite samples synthesised using 0.15 *M* $Fe_2(SO_4)_3.5H_2O$ (see Figure 5.2h) indicate the products synthesised at 22ºC (mean 0.53, median 0.53, range 0.03-0.86) have higher *A*-site contents, on average, than those synthesised at 140ºC (mean 0.46, median 0.45, range 0.25-0.66). The Ag-only contents of these samples also show this trend (see Figure 5.2i): mean 0.60, median 0.53, range 0.45-0.81 at 22ºC; and mean 0.45, median 0.45, range 0.22-0.65

at 140ºC. As with the Na-Ag-jarosite samples (above), the lower contents of the samples synthesised at 140ºC compared with those made at 22ºC may be explained by the difference between their synthesis periods (4 hours and ~ 1 year, respectively) or by inaccurate results created by the problems of EMPA of jarosite compounds.

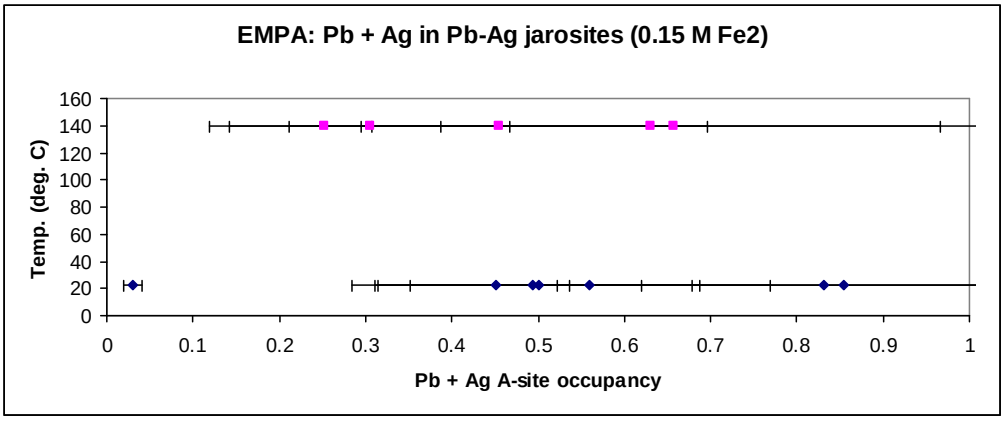

Figure 5.2h: EMPA total *A*-site occupancy of Pb + Ag in Pb-Ag-H_3O-jarosite samples synthesised using 0.15 *M* $Fe_2(SO_4)_3.5H_2O$ at 22˚C, 97˚C and 140˚C. (Error bars show series mean precision or C in %, see Appendix I.)

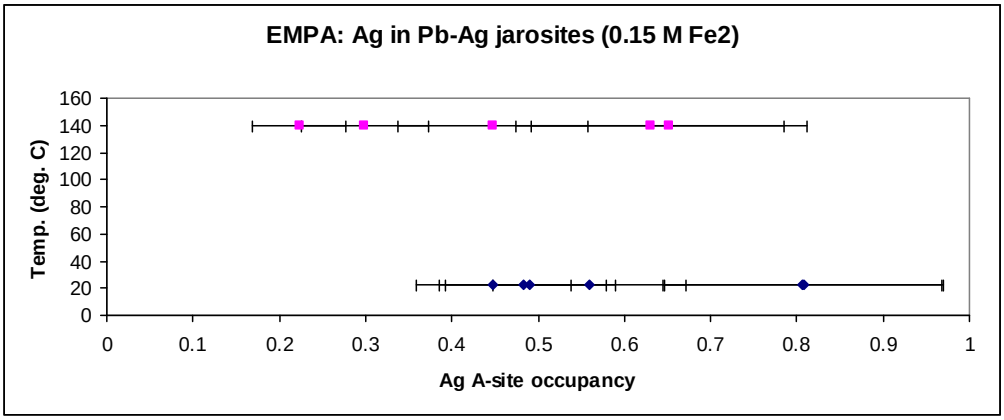

Figure 5.2i: EMPA total *A*-site occupancy of Ag in Pb-Ag-H_3O-jarosite samples synthesised using 0.15 *M* $Fe_2(SO_4)_3.5H_2O$ at 22˚C, 97˚C and 140˚C. (Error bars show series mean precision or C in %, see Appendix I.)

5.1.1.1.2 ICP-AES data on *A*-site occupancies

The ICP-AES results for the K-Ag-H_3O-jarosite samples synthesised at 22ºC, 97ºC and 140ºC using 0.51 *M* $Fe_2(SO_4)_3.5H_2O$ and at 22ºC and 140ºC using 0.15 *M* $Fe_2(SO_4)_3.5H_2O$ show cation occupancy (total of K and Ag) of the *A*-site decreases as the synthesis temperature is increased from 22ºC (mean 0.77, median 0.77, range

0.73-0.85) to 97ºC (mean 0.72, median 0.68, range 0.64-1.00) and 140ºC (mean 0.67, median 0.71, range 0.37-0.85) (see Table 5.3 and Figure 5.3). The opposite trend is seen for the Ag-only occupancies: there is an increase in occupancy as

Table 5.3: ICP-AES *A*-site occupancies of K + Ag, Na + Ag and Ag and synthesis temperature of K-Ag-H_3O and Na-Ag-H_3O-jarosite compounds

Cation	Mean	Med.	Range	Temp	Mean	Med.	Range	Temp	Mean	Med.	Range	Temp
Synthesis solution 0.51 M $Fe_2(SO_4)_3.5H_2O$ and 0.15 M $Fe_2(SO_4)_3.5H_2O$												
K+Ag	0.77	0.77	0.74-85	22	0.72	0.68	0.64-1	97	0.67	0.71	0.37-85	140
Ag	0.28	0.15	0.05-85	22	0.40	0.30	0.14-1	97	0.47	0.44	0.21-85	140
Na+Ag	0.80	0.83	0.67-85	22	0.74	0.74	0.55-1	97	0.67	0.65	0.44-85	140
Ag	0.74	0.80	0.41-85	22	0.69	0.72	0.37-1	97	0.51	0.46	0.13-85	140

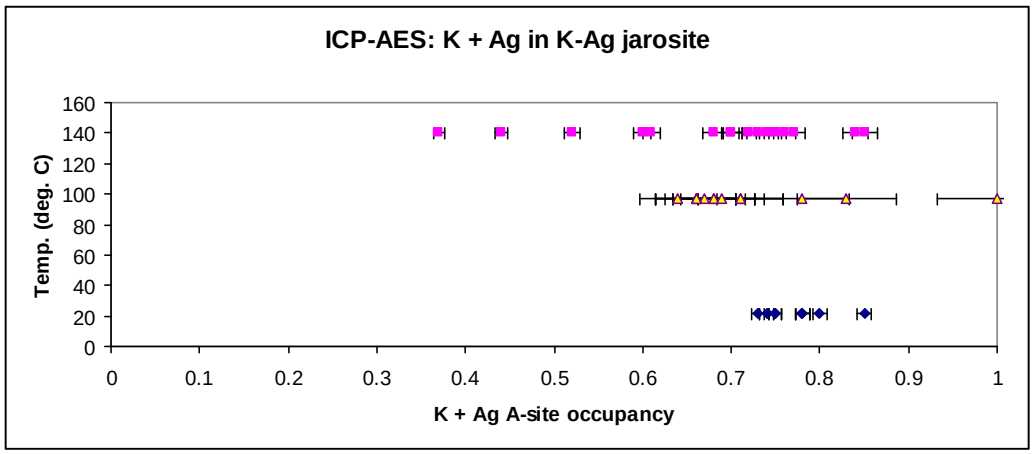

Figure 5.3: ICP-AES total *A*-site occupancy of K + Ag in K-Ag-H_3O-jarosite samples synthesised using 0.51 *M* $Fe_2(SO_4)_3.5H_2O$ and 0.15 *M* $Fe_2(SO_4)_3.5H_2O$ at 22˚C, 97˚C and 140˚C. (Error bars show series mean precision or C in %, see Appendix H.)

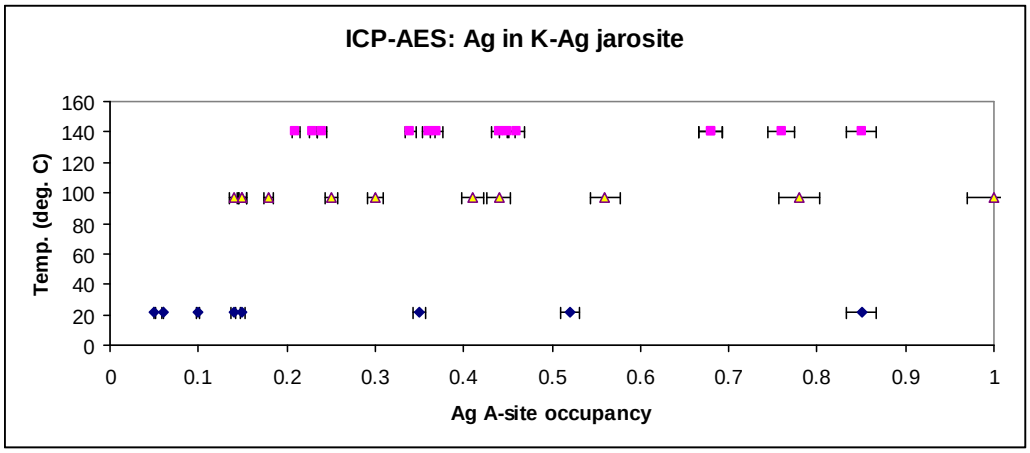

Figure 5.3a: ICP-AES total *A*-site occupancy of Ag in K-Ag-H_3O-jarosite samples synthesised using 0.51 *M* $Fe_2(SO_4)_3.5H_2O$ and 0.15 *M* $Fe_2(SO_4)_3.5H_2O$ at 22˚C, 97˚C and 140˚C. (Error bars show series mean precision or C in %, see Appendix H.)

synthesis temperature increases from 22ºC (mean 0.28, median 0.15, range 0.05-0.85) to 97ºC (mean 0.40, median 0.30, range 0.14-1.00) and 140ºC (mean 0.47, median 0.44, range 0.21-0.85) (see Figure 5.3a).

The ICP-AES results for the Na-Ag-H_3O-jarosite samples synthesised at 22ºC, 97ºC and 140ºC using 0.51 *M* $Fe_2(SO_4)_3.5H_2O$ and at 22ºC and 140ºC using 0.15 *M* $Fe_2(SO_4)_3.5H_2O$ show the *A*-site cation occupancies (total of Na and Ag) decrease as the synthesis temperature is increased from 22ºC (mean 0.80, median 0.83, range 0.67-0.85) to 97ºC (mean 0.74, median 0.74, range 0.55-1.00) and 140ºC (mean 0.67, median 0.65, range 0.44-0.85) (see Table 5.3 and Figure 5.3b). Similar trends are seen for the Ag-only occupancies: there is a decline from 22ºC (mean 0.74, median 0.80, range 0.41-0.85) to 97ºC (mean 0.69, median 0.72, range 0.37-1.00) and 140ºC (mean 0.51, median 0.46, range 0.13-0.85) (see Figure 5.3c). A possible reason for these trends is that the difference in synthesis period between ~ 1 year at 22ºC and 4 hours at 97ºC and 140ºC is sufficient to result in greater occupancies at the lower temperature, although the lower *A*-site occupancies with increase in temperature from 97ºC to 140ºC is not readily explainable.

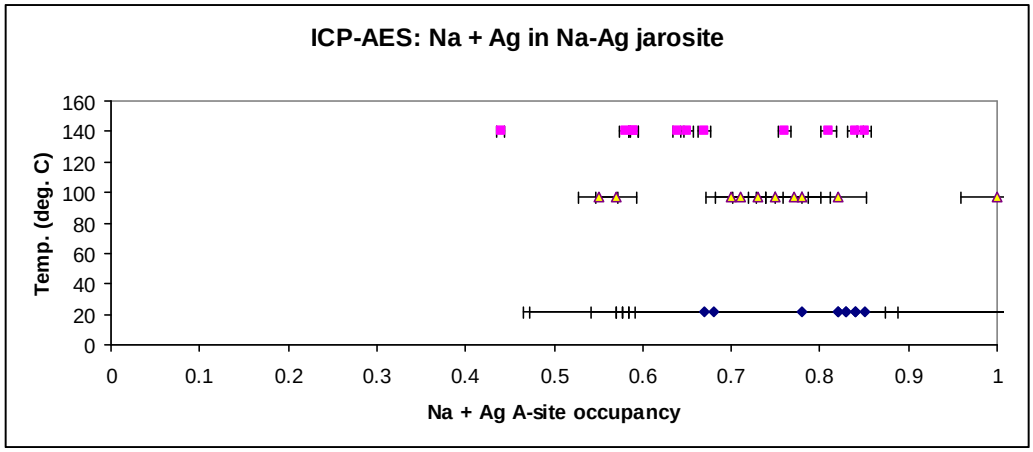

Figure 5.3b: ICP-AES total *A*-site occupancy of Na + Ag in Na-Ag-H_3O-jarosite samples synthesised using 0.51 *M* $Fe_2(SO_4)_3.5H_2O$ and 0.15 *M* $Fe_2(SO_4)_3.5H_2O$ at 22˚C, 97˚C and 140˚C. (Error bars show series mean precision or C in %, see Appendix H.)

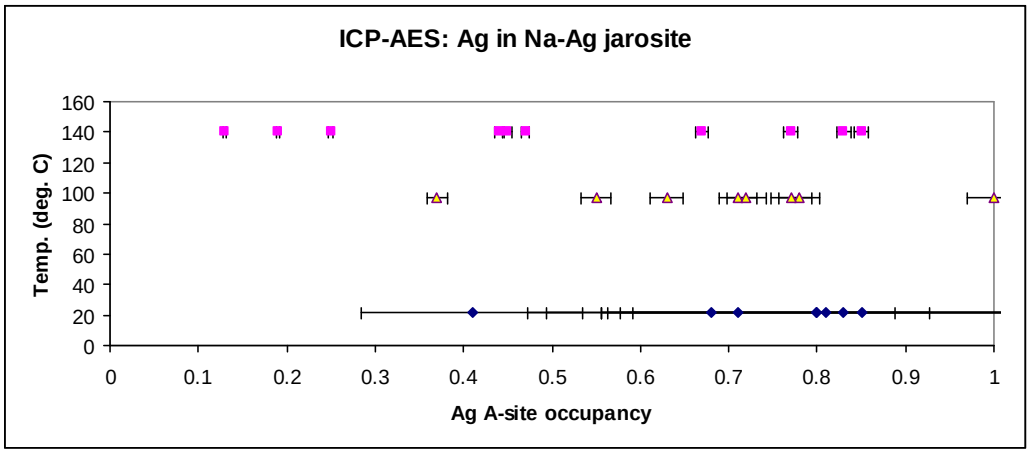

Figure 5.3c: ICP-AES total *A*-site occupancy of Ag in Na-Ag-H_3O-jarosite samples synthesised using 0.51 *M* $Fe_2(SO_4)_3.5H_2O$ and 0.15 *M* $Fe_2(SO_4)_3.5H_2O$ at 22˚C, 97˚C and 140˚C. (Error bars show series mean precision or C in %, see Appendix H.)

The breakdown of the ICP-AES results for the K-Ag-H_3O-jarosite samples shows those synthesised using 0.51 *M* $Fe_2(SO_4)_3.5H_2O$ indicate higher *A*-site contents (total of K and Ag), on average, in the products synthesised at 22ºC (mean 0.77, median 0.78, range 0.74-0.78) than in those synthesised at 97ºC (mean 0.72, median 0.68, range 0.64-1.00) and 140ºC (mean 0.66, median 0.69, range 0.44-0.77) (see Table 5.4 and Figure 5.3d). Although there were data for only three out of five samples synthesised at 22ºC, the two missing samples were products synthesised using starting solutions with the highest concentrations of Ag, so the absence of these data is highly unlikely to have altered the observed occupancy trend. The results of the Ag-only contents of these K-Ag-H_3O-jarosite samples show an increase with the increase in temperature (see Figure 5.3e) from 97ºC (mean 0.40, median 0.28 and range 0.14-1.00) to 140ºC (mean 0.44, median 0.41 and range 0.21-0.76). The Ag-only results show an increase in occupancy from synthesis at 22ºC (mean 0.10, median 0.10 and range 0.06-0.14) to synthesis at 97ºC; however, data were obtained for only two out of five samples in the series synthesised at 22ºC, and

these were samples with the highest Ag concentrations in the starting solutions, so the data obtained were inadequate for identifying trends in the data.

The ICP-AES results for the K-Ag-H_3O-jarosite samples synthesised using 0.15 *M* $Fe_2(SO_4)_3.5H_2O$ (see Table 5.4 and Figure 5.3f) do not indicate that the increase in synthesis temperature to 140ºC increases total K and Ag *A*-site content (mean 0.70, median 0.73, range 0.37-0.85) compared with the products made at 22ºC (mean 0.77, median 0.75, range 0.73-0.85), which may be explained by the difference between their periods of synthesis (4 hours and ~ 1 year, respectively). However, the Ag-only contents of these samples contradict this finding because they do show increasing content with increased temperature of synthesis from 22ºC to 140ºC: mean 0.34, median 0.25, range 0.05-0.85 at 22ºC; and mean 0.51, median 0.45, range 0.23-0.85 at 140ºC (see Figure 5.3g).

Table 5.4: ICP-AES *A*-site occupancy of K + Ag, Na + Ag, Pb + Ag and Ag and synthesis temperature of K-Ag-H_3O, Na-Ag- H_3O and Pb-Ag- H_3O-jarosite compounds according to Fe concentration in the synthesis solution

Cation	Mean	Med.	Range	Temp	Mean	Med.	Range	Temp	Mean	Med.	Range	Temp
Synthesis solution 0.51 M $Fe_2(SO_4)_3.5H_2O$												
K+Ag	0.77	0.78	0.74-78	22	0.72	0.68	0.64-1	97	0.66	0.69	0.44-77	140
Ag	0.10	0.10	0.06-14	22	0.40	0.28	0.14-1	97	0.44	0.41	0.21-76	140
Na+Ag	0.77	0.82	0.67-83	22	0.74	0.74	0.55-1	97	0.58	0.59	0.44-65	140
Ag	0.76	0.76	0.71-80	22	0.62	0.67	0.37-78	97	0.30	0.32	0.13-45	140
Synthesis solution 0.15 M $Fe_2(SO_4)_3.5H_2O$												
K+Ag	0.77	0.75	0.73-85	22					0.70	0.73	0.37-85	140
Ag	0.34	0.25	0.05-85	22					0.51	0.45	0.23-85	140
Na+Ag	0.81	0.84	0.68-85	22					0.75	0.79	0.58-85	140
Ag	0.73	0.81	0.41-85	22					0.64	0.72	0.25-85	140
Pb+Ag	0.77	0.84	0.26-90	22					0.57	0.67	0.18-79	140
Ag	0.83	0.83	0.80-85	22					0.60	0.70	0.28-77	140

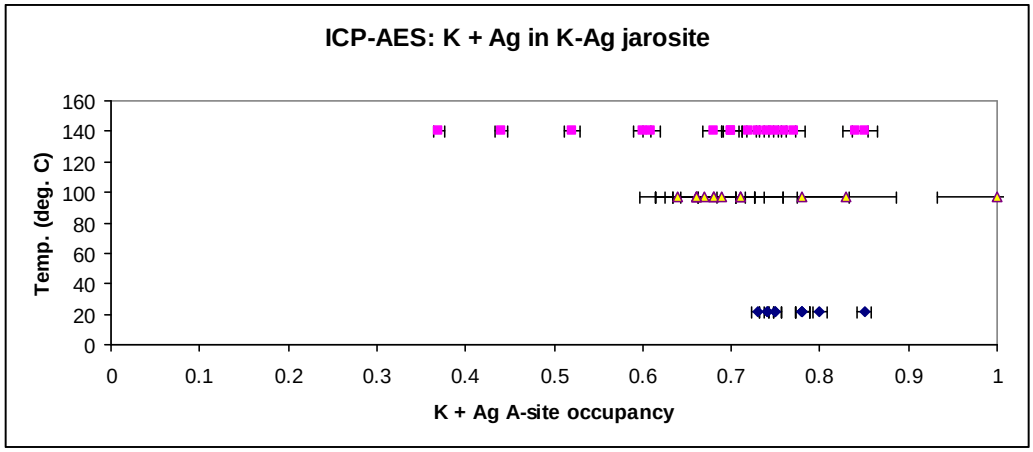

Figure 5.3d: ICP-AES total *A*-site content of K + Ag in K-Ag-H_3O-jarosite samples synthesised using 0.51 *M* $Fe_2(SO_4)_3.5H_2O$. (Error bars show series mean precision or C in %, see Appendix H.)

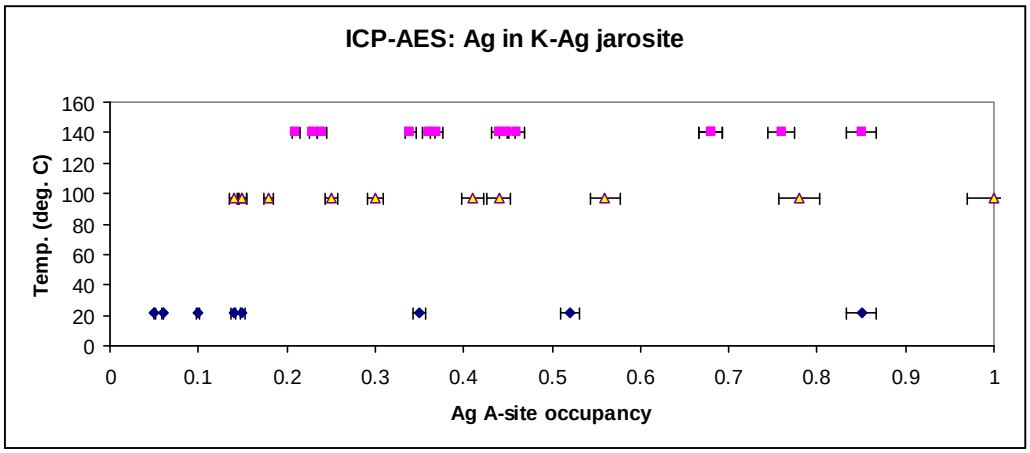

Figure 5.3e: ICP-AES total *A*-site content of Ag in K-Ag-H_3O-jarosite samples synthesised using 0.51 *M* $Fe_2(SO_4)_3.5H_2O$. (Error bars show series mean precision or C in %, see Appendix H.)

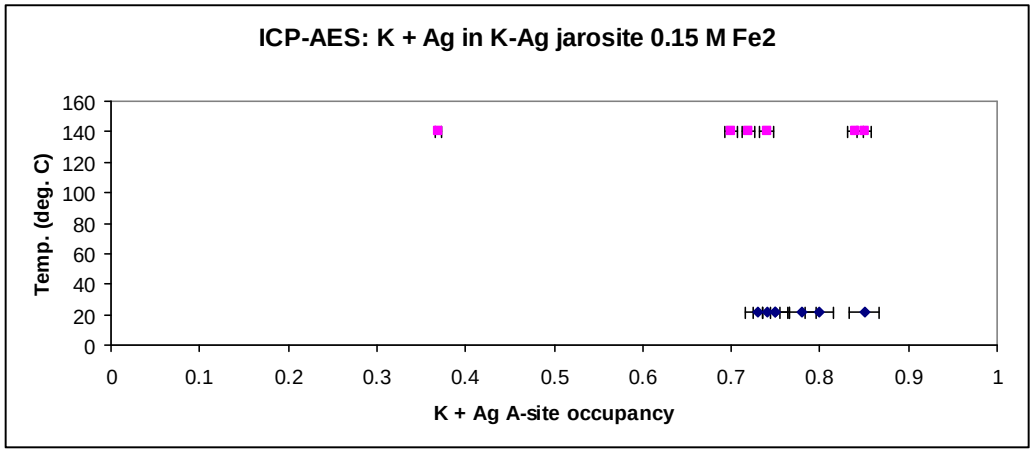

Figure 5.3f: ICP-AES total *A*-site content of K + Ag in K-Ag-H_3O-jarosite samples synthesised using 0.15 *M* $Fe_2(SO_4)_3.5H_2O$. (Error bars show series mean precision or C in %, see Appendix H.)

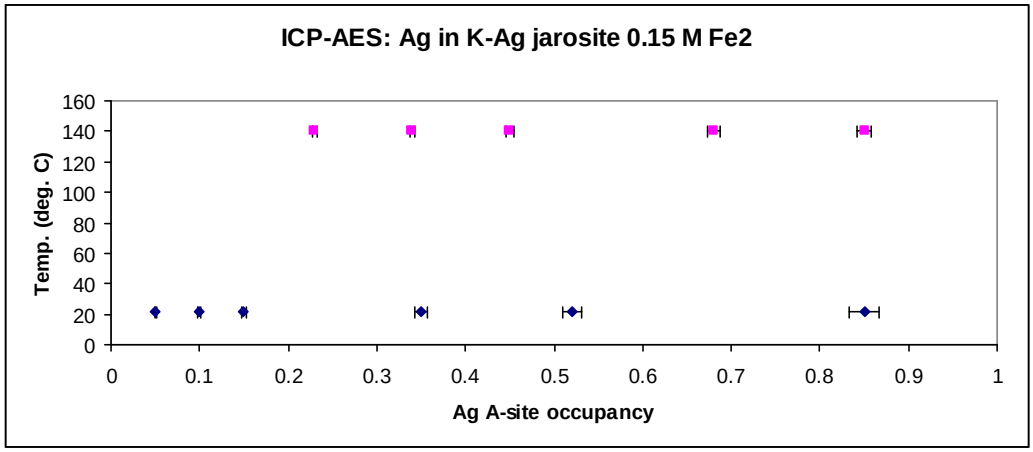

Figure 5.3g: ICP-AES total *A*-site content of Ag in K-Ag-H_3O-jarosite samples synthesised using 0.15 *M* $Fe_2(SO_4)_3.5H_2O$. (Error bars show series mean precision or C in %, see Appendix H.)

The ICP-AES results for the Na-Ag-H_3O-jarosite samples synthesised using 0.51 *M* $Fe_2(SO_4)_3.5H_2O$ show the *A*-site contents (total of Na and Ag), on average, decrease as the synthesis temperature is increased from 22ºC (mean 0.77, median 0.82, range 0.67-0.83) to 97ºC (mean 0.74, median 0.74, range 0.55-1.00) and 140ºC (mean 0.58, median 0.59, range 0.44-0.65) (see Table 5.4 and Figure 5.3h). There is also a decrease in the Ag-only contents of these Na-Ag-H_3O-jarosite samples as synthesis temperature is increased (see Figure 5.3i): mean 0.76, median 0.76, range 0.71-0.80 at 22ºC; mean 0.62, median 0.67, range 0.37-0.78 at 97ºC; and mean 0.30, median 0.32, range 0.13-0.45 at 140ºC.

This trend in Na + Ag content change in the Na-Ag-H_3O-jarosite samples synthesised using 0.51 *M* $Fe_2(SO_4)_3.5H_2O$ is repeated in the samples synthesised using 0.15 *M* $Fe_2(SO_4)_3.5H_2O$ (see Figure 5.3j): the products synthesised at 22ºC have higher Na + Ag *A*-site occupancies (mean 0.81, median 0.84, range 0.68-0.85), on average, than those synthesised at 140ºC (mean 0.75, median 0.79, range 0.58-0.85). The Ag-only contents of these samples also show this trend: mean 0.73, median 0.81, range 0.41-0.85 at 22ºC; and mean 0.64, median 0.72, range 0.25-0.85 at 140ºC (see Figure 5.3k).

The lower total Na + Ag and Ag-only contents of the samples synthesised at 140ºC than the samples synthesised at 22ºC in the series using 0.51 *M* $Fe_2(SO_4)_3.5H_2O$ and the series using 0.15 *M* $Fe_2(SO_4)_3.5H_2O$ may be explained by the difference between their periods of synthesis, which were 4 hours and ~ 1 year, respectively. This may also be the reason for the samples synthesised at 97ºC having lower contents than those synthesised at 22ºC; however, the reason for the samples synthesised at 97ºC having higher contents than those synthesised at 140ºC is unclear.

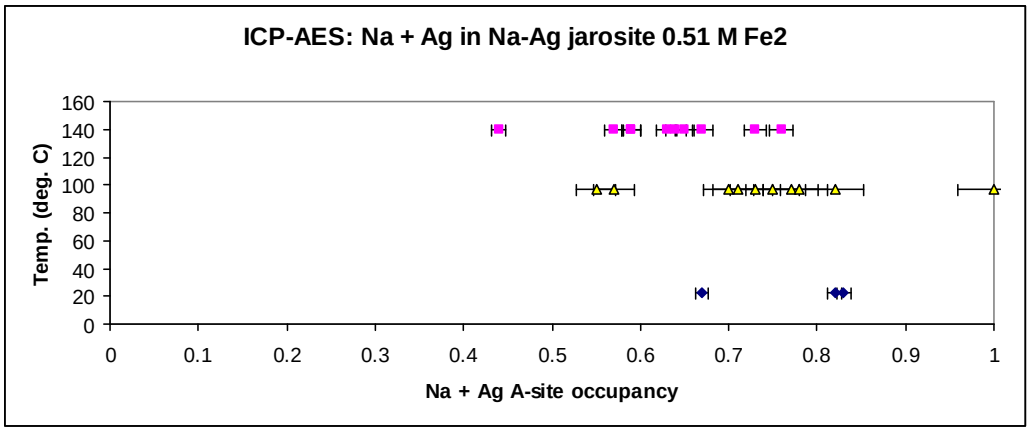

Figure 5.3h: ICP-AES total *A*-site content of Na + Ag in Na-Ag-H_3O-jarosite samples synthesised using 0.51 *M* $Fe_2(SO_4)_3.5H_2O$. (Error bars show series mean precision or C in %, see Appendix H.)

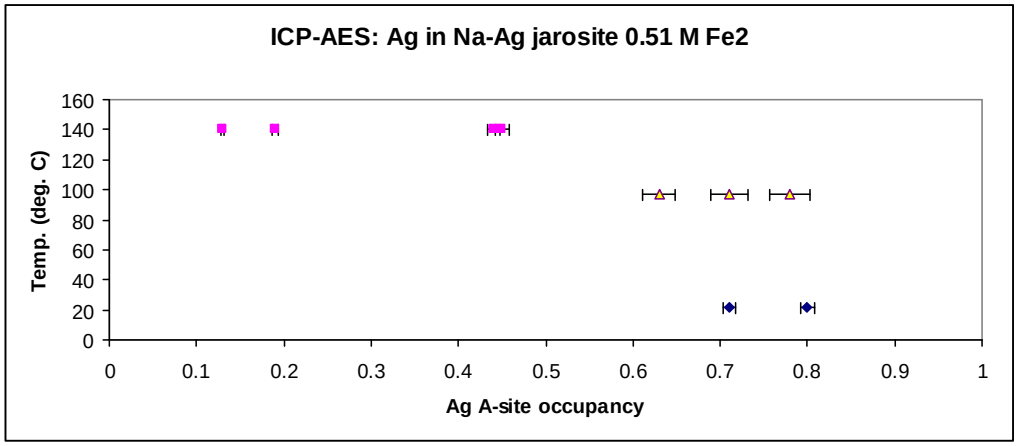

Figure 5.3i: ICP-AES total *A*-site content of Ag in Na-Ag-H_3O-jarosite samples synthesised using 0.51 *M* $Fe_2(SO_4)_3.5H_2O$. (Error bars show series mean precision or C in %, see Appendix H.)

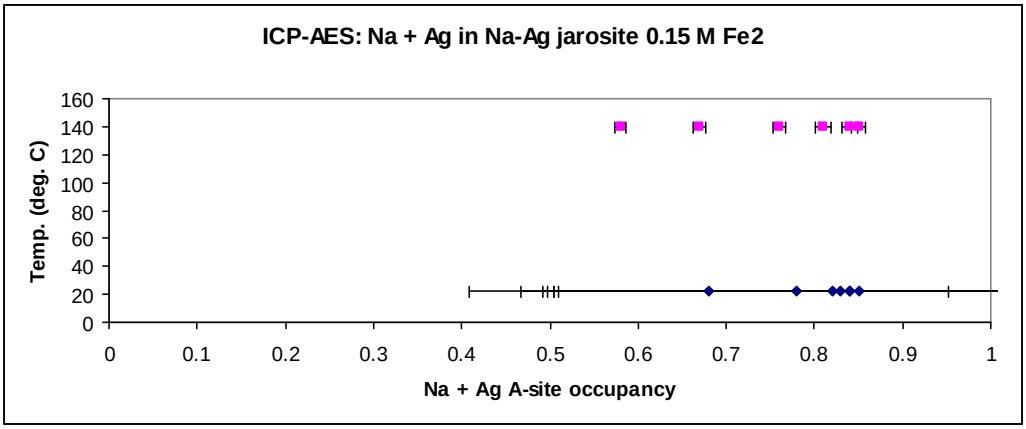

Figure 5.3j: ICP-AES total *A*-site content of Na + Ag in Na-Ag-H_3O-jarosite samples synthesised using 0.15 *M* $Fe_2(SO_4)_3.5H_2O$. (Error bars show series mean precision or C in %, see Appendix H.)

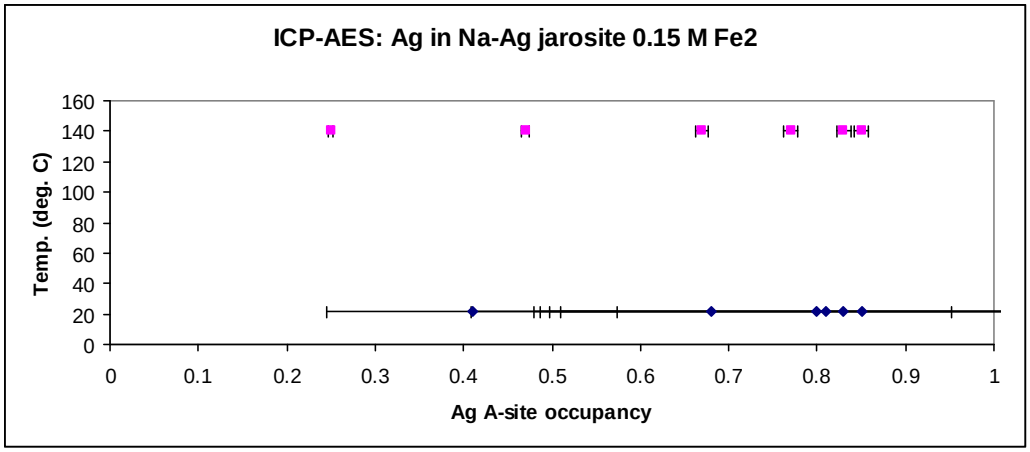

Figure 5.3k: ICP-AES total *A*-site content of Ag in Na-Ag-H_3O-jarosite samples synthesised using 0.15 *M* $Fe_2(SO_4)_3.5H_2O$. (Error bars show series mean precision or C in %, see Appendix H.)

The ICP-AES results for the Pb-Ag-H_3O-jarosite samples synthesised using 0.15 *M* $Fe_2(SO_4)_3.5H_2O$ (see Table 5.4 and Figure 5.3l) indicate the products synthesised at 22ºC have higher Pb + Ag *A*-site occupancies (mean 0.77, median 0.84, range 0.26-0.90), on average, than those synthesised at 140ºC (mean 0.57, median 0.67, range 0.18-0.79). The Ag-only contents of these samples also show this trend: mean 0.83, median 0.83, range 0.80-0.85 at 22ºC; and mean 0.60, median 0.70, range 0.28-0.77 at 140ºC (see Figure 5.3m). As with some of the K-Ag and Na-Ag samples, the lower *A*-site contents of the Pb-Ag samples synthesised at 140ºC

compared with the samples synthesised at 22ºC may be explained by the difference between their periods of synthesis, which were 4 hours and ~ 1 year, respectively.

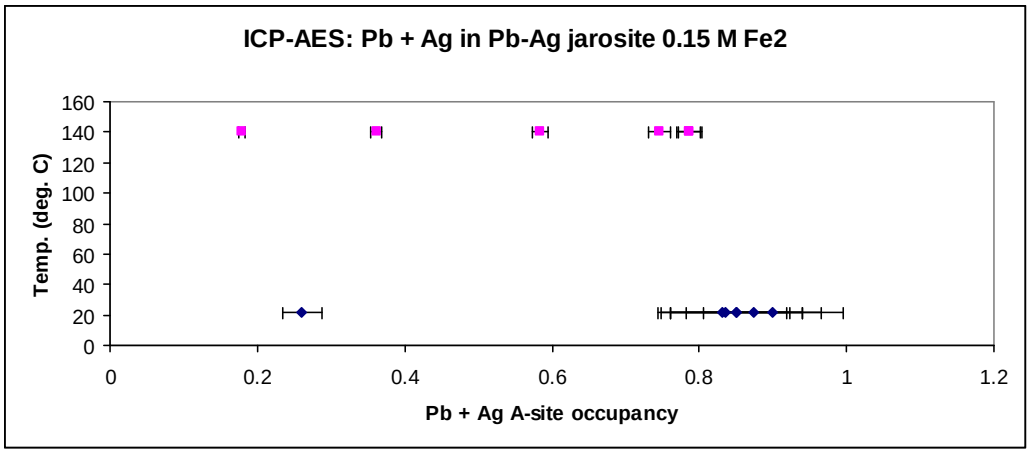

Figure 5.3l: ICP-AES total *A*-site content of Pb + Ag in Pb-Ag-H_3O-jarosite samples synthesised using 0.15 *M* $Fe_2(SO_4)_3.5H_2O$. (Error bars show series mean precision or C in %, see Appendix H.)

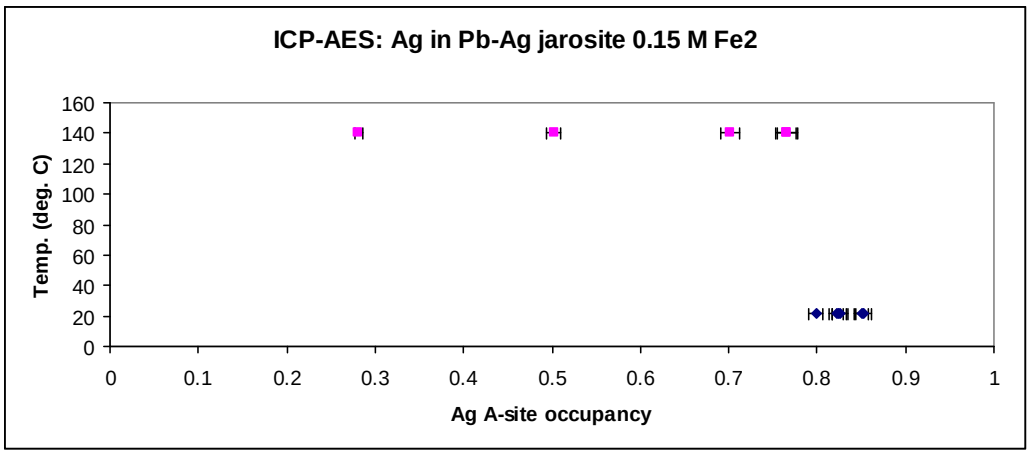

Figure 5.3m: ICP-AES total *A*-site content of Ag in Pb-Ag-H_3O-jarosite samples synthesised using 0.15 *M* $Fe_2(SO_4)_3.5H_2O$. (Error bars show series mean precision or C in %, see Appendix H.)

5.1.1.1.3 Rietveld refinement data of *A*-site occupancies

Rietveld refinement of the powder XRD results for the K-Ag-H_3O-jarosite compounds synthesised at 22ºC and 97ºC using 0.51 *M* $Fe_2(SO_4)_3.5H_2O$ and at 140ºC using 0.15 *M* $Fe_2(SO_4)_3.5H_2O$ shows the *A*-site occupancies (total of K and Ag) increase as the synthesis temperature is increased from 22ºC (mean 0.66, median 0.67, range 0.58-0.74) to 97ºC (mean 0.68, median 0.69, range 0.45-0.81) and 140ºC

(mean 0.73, median 0.77, range 0.32-0.89) (see Table 5.5 and Figure 5.4). There is also an increase in the Ag-only contents of these K-Ag-H_3O-jarosite compounds as synthesis temperature is increased (see Figure 5.4a): mean 0.32, median 0.23, range

Table 5.5: Rietveld refined *A*-site occupancy of K + Ag, Na + Ag and Ag and synthesis temperature of K-Ag-H_3O and Na-Ag-H_3O-jarosite compounds

Cation	Mean	Med.	Range	Temp	Mean	Med.	Range	Temp	Mean	Med.	Range	Temp
Synthesis solution 0.51 M $Fe_2(SO_4)_3.5H_2O$												
K+Ag	0.66	0.67	0.58-74	22	0.68	0.69	0.45-0.81	97	-	-	-	-
Ag	0.32	0.23	0.08-74	22	0.34	0.33	0.09-0.65	97	-	-	-	-
Na+Ag	0.72	0.71	0.70-74	22	0.69	0.65	0.51-0.90	97	-	-	-	-
Ag	0.68	0.68	0.61-74	22	0.54	0.59	0.27-65	97	-	-	-	-
Synthesis solution 0.15 M $Fe_2(SO_4)_3.5H_2O$												
K+Ag	-	-	-	-	-	-	-	-	0.73	0.77	0.32-89	140
Ag	-	-	-	-	-	-	-	-	0.39	0.37	0.09-76	140
Na+Ag	-	-	-	-	-	-	-	-	0.60	0.61	0.39-76	140
Ag	-	-	-	-	-	-	-	-	0.51	0.51	0.23-76	140

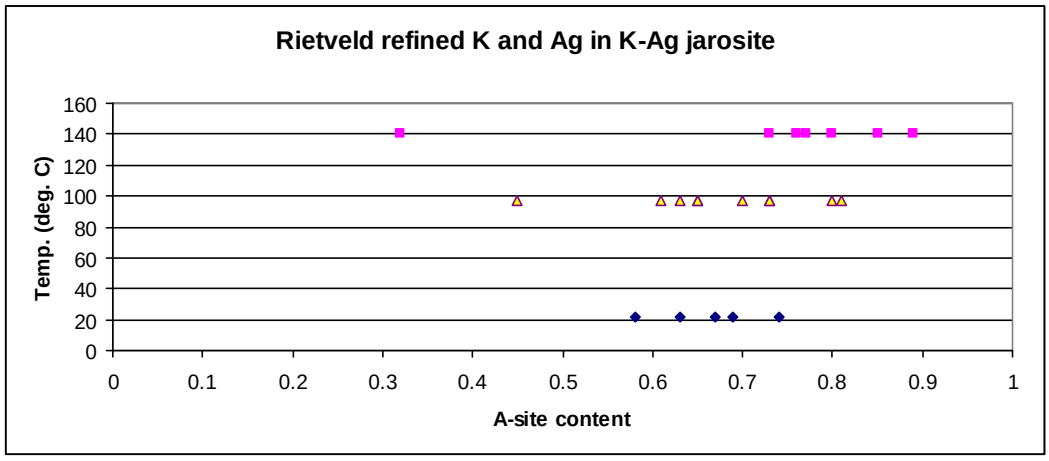

Figure 5.4: Rietveld refined total *A*-site occupancies of K + Ag in K-Ag-H_3O-jarosite compounds synthesised at 22˚C, 97˚C and 140˚C.

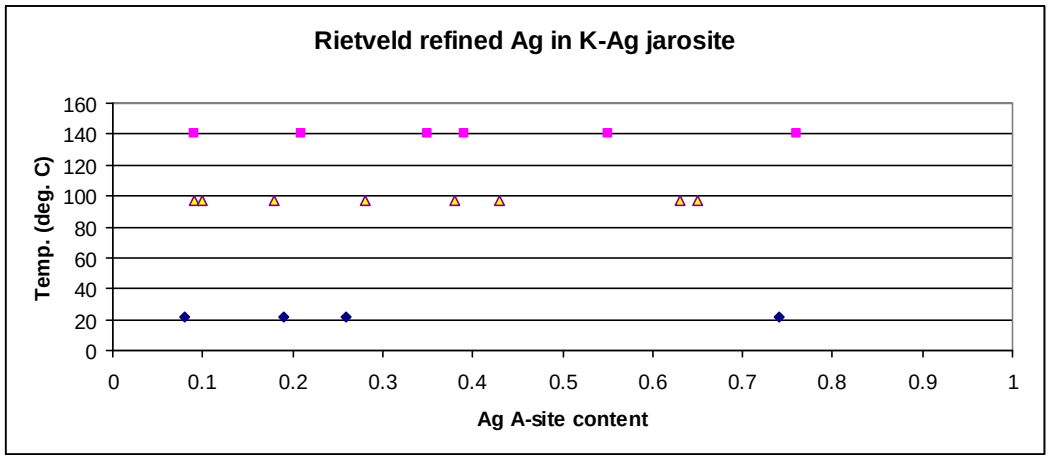

Figure 5.4a: Rietveld refined *A*-site occupancies of Ag in K-Ag-H_3O-jarosite compounds synthesised at 22˚C, 97˚C and 140˚C.

0.19-0.74 at 22ºC; mean 0.34, median 0.33, range 0.09-0.65 at 97ºC; and mean 0.39, median 0.37, range 0.09-0.76 at 140ºC.

Unlike the K-Ag-H_3O-jarosite products, Rietveld refinement of the Na-Ag-H_3O-jarosite compounds synthesised at 22ºC and 97ºC using 0.51 *M* $Fe_2(SO_4)_3.5H_2O$ and at 140ºC using 0.15 *M* $Fe_2(SO_4)_3.5H_2O$ shows the *A*-site occupancies (total of Na and Ag) decrease as the synthesis temperature increases from 22ºC (mean 0.72, median 0.71, range 0.71-0.74) to 97ºC (mean 0.69, median 0.65, range 0.51-0.83) and 140ºC (mean 0.60, median 0.61, range 0.39-0.76) (see Table 5.5 and Figure 5.4b). There is also a decrease in the Ag-only contents of the Na-Ag-H_3O-jarosite samples as synthesis temperature is increased (see Figure 5.4c): mean 0.68, median 0.68, range 0.61-0.74 at 22ºC; mean 0.54, median 0.59, range 0.27-0.65 at 97ºC; and mean 0.51, median 0.51, range 0.23-0.76 at 140ºC. The 22ºC data consist of only three samples out of a series of five because no data are available for two, but the missing data are for the two samples with the highest Ag concentrations in the starting solutions, so are unlikely to have affected the trend.

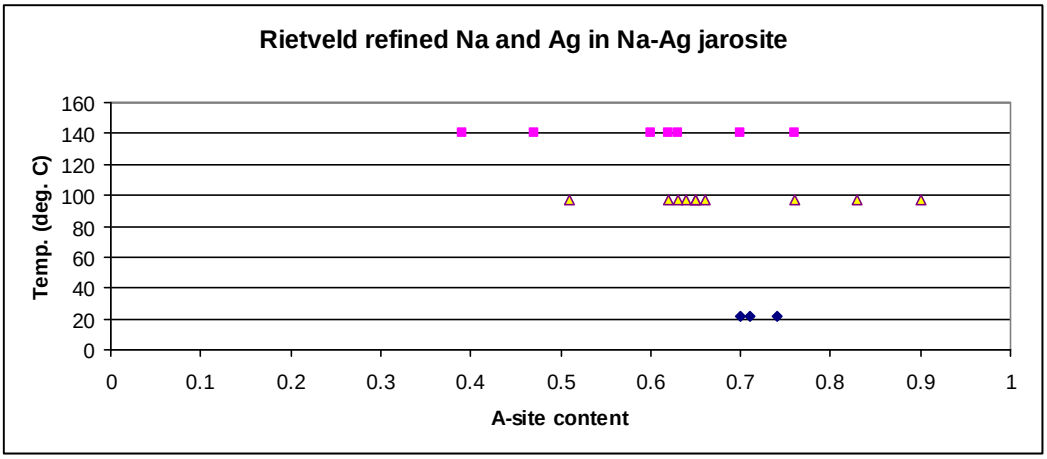

Figure 5.4b: Rietveld refined total *A*-site occupancies of Na + Ag in Na-Ag-H_3O-jarosite compounds synthesised at 22˚C, 97˚C and 140˚C.

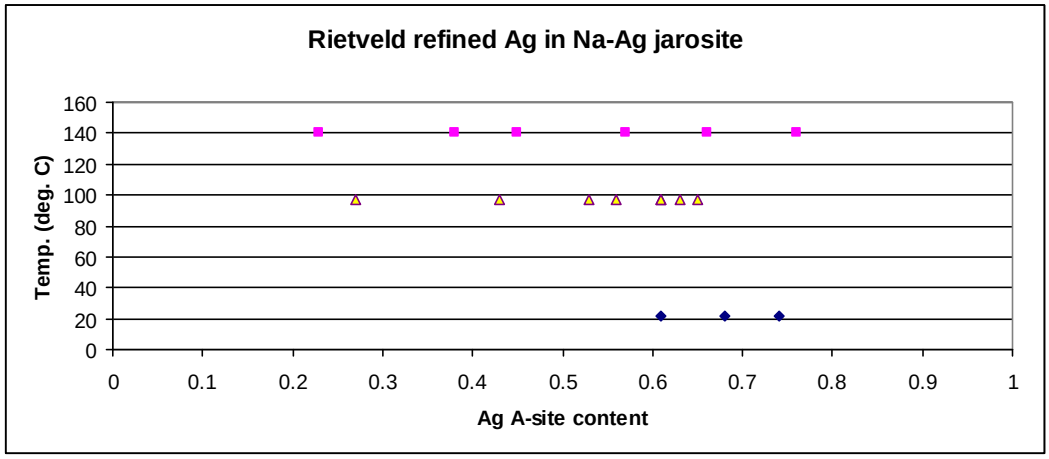

Figure 5.4c: Rietveld refined *A*-site occupancies of Ag in Na-Ag-H_3O-jarosite compounds synthesised at 22˚C, 97˚C and 140˚C.

The results of the EMPA, ICP-AES and Rietveld refinement of the K-Ag-H_3O, Na-Ag-H_3O and Pb-Ag-H_3O-jarosite product series indicate inconsistent trends in the *A*-site occupancies as synthesis temperature changes. Increases in occupancy as synthesis temperature is raised from 22ºC to 97ºC are seen in the median content of Ag in K-Ag jarosite from the EMPA results, as well as in the Ag-only contents from ICP-AES analysis; such an increase is also seen in the K + Ag and Ag-only occupancies of these products from Rietveld refinement. Otherwise, the general trend is for *A*-site occupancies to decrease as synthesis temperature is raised from 22ºC to 97ºC; this may be explained by the difference between how long the products were synthesised at these temperatures, which was 4 hours and ~ 1 year, respectively. There is an approximately equal split between trends in occupancies in the product series that show these rising as temperature is increased to 140ºC and those that show occupancies declining. In addition, data are missing for several samples in the EMPA, ICP-AES and Rietveld refinement results for the K-Ag-H_3O, Na-Ag-H_3O and Pb-Ag-H_3O-jarosite product series. There are also results for some samples that seem anomalous, such as the Ag occupancy of 1.00 in JS30, although the removal of this result from its series does not alter the trend observed. For these

reasons, a combined table of *A*-site occupancies for the three techniques has been created to analyse trends in the products' contents as synthesis temperature varies (see next sub-section). The combined data are based on the ICP-AES results but replaced by EMPA or Rietveld refinement results where ICP-AES data are lacking or anomalous.

5.1.1.1.4 Combined data from analysis results of *A*-site occupancies

The combined data from the results of EMPA, ICP-AES and Rietveld refinement (see Tables 4.20, 4.21 and 4.22) of the K-Ag-H_3O-jarosite samples synthesised at 22ºC, 97ºC and 140ºC using 0.51 *M* $Fe_2(SO_4)_3.5H_2O$ and at 22ºC and 140ºC using 0.15 *M* $Fe_2(SO_4)_3.5H_2O$ show cation occupancy (total of K and Ag) of the *A*-site decreases as the synthesis temperature is increased from 22ºC (mean 0.75, median 0.75, range 0.63-0.85) to 97ºC (mean 0.70, median 0.69, range 0.63-0.83) and 140ºC (mean 0.69, median 0.72, range 0.43-0.86) (see Table 5.6 and Figure 5.5). However, there is an opposite, increasing trend for the Ag-only occupancies as temperature is increased from 22ºC (mean 0.31, median 0.20, range 0.05-0.85) to 97ºC (mean 0.41, median 0.37, range 0.14-0.78) and 140ºC (mean 0.45, median 0.41, range 0.16-0.85) (see Figure 5.5a).

Table 5.6: Combined data results of *A*-site occupancies of K + Ag, Na + Ag and Ag and synthesis temperature of K-Ag-H_3O and Na-Ag-H_3O-jarosite compounds.

Cation	Mean	Med.	Range	Temp	Mean	Med.	Range	Temp	Mean	Med.	Range	Temp
Synthesis solution 0.51 M $Fe_2(SO_4)_3.5H_2O$ and 0.15 M $Fe_2(SO_4)_3.5H_2O$												
K+Ag	0.75	0.75	0.63-85	22	0.70	0.69	0.63-83	97	0.69	0.72	0.43-86	140
Ag	0.31	0.20	0.05-85	22	0.41	0.37	0.14-78	97	0.45	0.41	0.16-85	140
Na+Ag	0.74	0.80	0.54-85	22	0.61	0.64	0.33-78	97	0.66	0.66	0.44-85	140
Ag	0.67	0.74	0.41-85	22	0.53	0.62	0.21-78	97	0.50	0.49	0.09-85	140

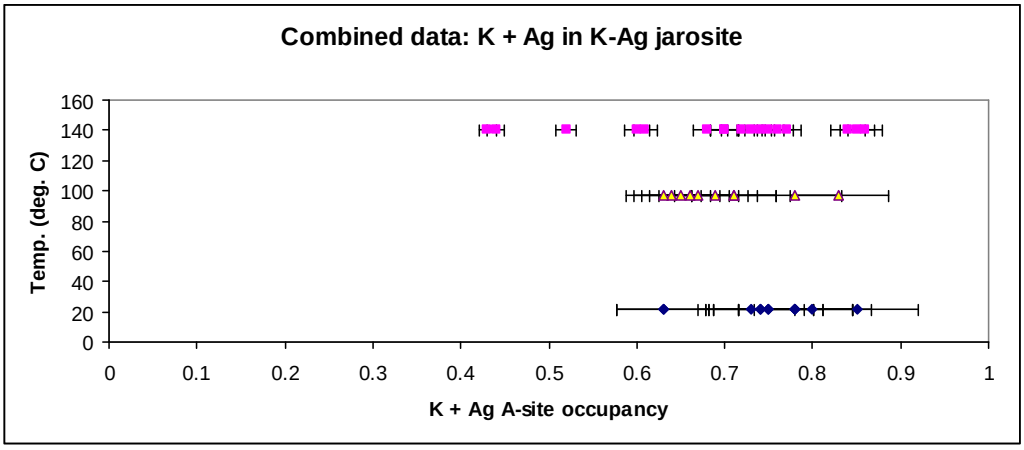

Figure 5.5: Combined data on total *A*-site occupancy of K + Ag in K-Ag-H_3O-jarosite samples synthesised using 0.51 *M* $Fe_2(SO_4)_3.5H_2O$ and 0.15 *M* $Fe_2(SO_4)_3.5H_2O$ at 22˚C, 97˚C and 140˚C. (Error bars show series mean precision or C in %, see Appendices H and I.)

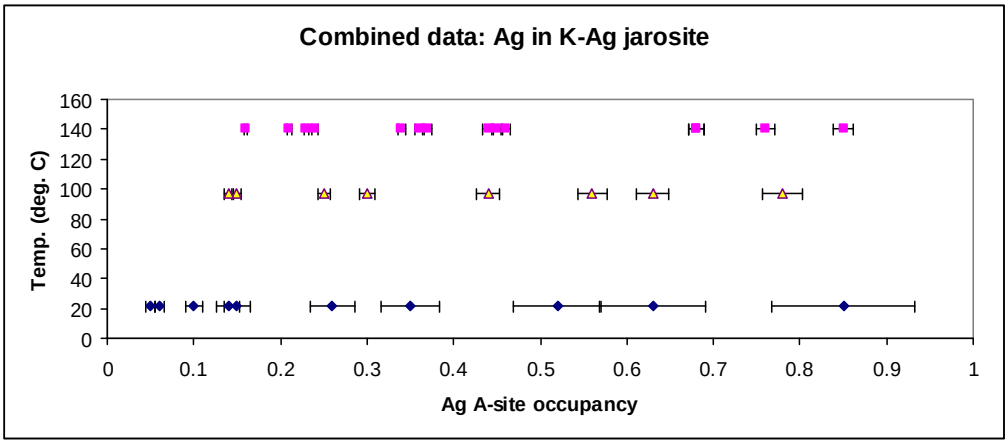

Figure 5.5a: Combined data on total *A*-site occupancy of Ag in K-Ag-H_3O-jarosite samples synthesised using 0.51 *M* $Fe_2(SO_4)_3.5H_2O$ and 0.15 *M* $Fe_2(SO_4)_3.5H_2O$ at 22˚C, 97˚C and 140˚C. (Error bars show series mean precision or C in %, see Appendices H and I.)

The combined data results for the Na-Ag-H_3O-jarosite samples synthesised at 22ºC, 97ºC and 140ºC using 0.51 *M* $Fe_2(SO_4)_3.5H_2O$ and at 22ºC and 140ºC using 0.15 *M* $Fe_2(SO_4)_3.5H_2O$ show the *A*-site cation occupancies (total of Na and Ag) decrease as the synthesis temperature is increased from 22ºC (mean 0.74, median 0.80, range 0.53-0.85) to 97ºC (mean 0.61, median 0.64, range 0.33-0.78), and then increase as temperature increases from 97ºC to 140ºC (mean 0.66, median 0.66, range 0.44-0.85) (see Table 5.6 and Figure 5.5b). The Ag-only occupancies show a declining trend as temperature is increased from 22ºC (mean 0.67, median 0.74,

range 0.41-0.85) to 97ºC (mean 0.53, median 0.62, range 0.21-0.78) and 140ºC (mean 0.50, median 0.49, range 0.09-0.85) (see Figure 5.5c).

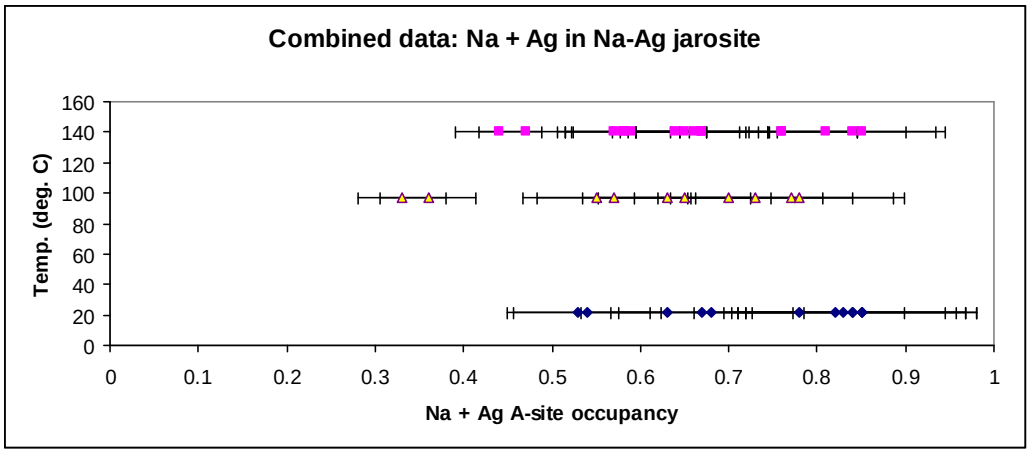

Figure 5.5b: Combined data on total *A*-site occupancy of Na + Ag in Na-Ag-H_3O-jarosite samples synthesised using 0.51 *M* $Fe_2(SO_4)_3.5H_2O$ and 0.15 *M* $Fe_2(SO_4)_3.5H_2O$ at 22˚C, 97˚C and 140˚C. (Error bars show series mean precision or C in %, see Appendices H and I.)

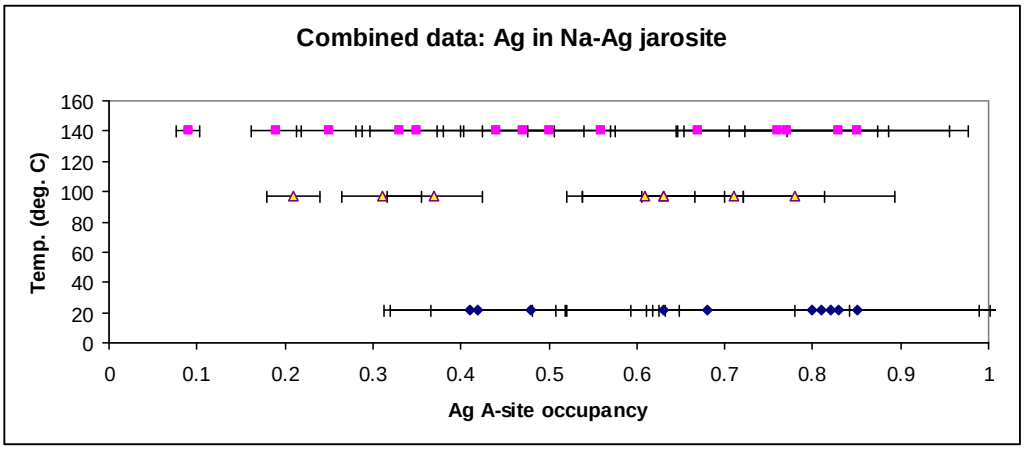

Figure 5.5c: Combined data on total *A*-site occupancy of Ag in Na-Ag-H_3O-jarosite samples synthesised using 0.51 *M* $Fe_2(SO_4)_3.5H_2O$ and 0.15 *M* $Fe_2(SO_4)_3.5H_2O$ at 22˚C, 97˚C and 140˚C. (Error bars show series mean precision or C in %, see Appendices H and I.)

The breakdown of the combined data for the K-Ag-H_3O-jarosite samples shows those synthesised using 0.51 *M* $Fe_2(SO_4)_3.5H_2O$ indicate higher *A*-site occupancies (total of K and Ag) of the products synthesised at 22ºC (mean 0.71, median 0.74, range 0.63-0.78) than in those synthesised at 97ºC (mean 0.70, median 0.69, range 0.64-0.83) and 140ºC (mean 0.66, median 0.69, range 0.44-0.77) (see

Table 5.7 and Figure 5.5d). The results of the Ag-only contents of these K-Ag-H_3O-jarosite samples show an increase in occupancy with increase in temperature (see Figure 5.5e) from 22ºC (mean 0.27, median 0.20 and range 0.06-0.63) to 97ºC (mean 0.41, median 0.37 and range 0.14-0.78) and 140ºC (mean 0.44, median 0.41 and range 0.21-0.76).

Table 5.7: Combined data results of K + Ag, Na + Ag, Pb + Ag and Ag *A*-site occupancy and synthesis temperature of K-Ag-H_3O, Na-Ag-H_3O and Pb-Ag-H_3O-jarosite compounds.

Cation	Mean	Med.	Range	Temp	Mean	Med.	Range	Temp	Mean	Med.	Range	Temp
Synthesis solution 0.51 M $Fe_2(SO_4)_3.5H_2O$												
K+Ag	0.71	0.74	0.63-78	22	0.70	0.69	0.64-83	97	0.66	0.69	0.44-77	140
Ag	0.27	0.20	0.06-63	22	0.41	0.37	0.14-63	97	0.44	0.41	0.21-76	140
Na+Ag	0.64	0.63	0.53-85	22	0.61	0.64	0.33-78	97	0.62	0.65	0.44-76	140
Ag	0.59	0.56	0.42-82	22	0.53	0.62	0.21-78	97	0.40	0.40	0.09-76	140
Synthesis solution 0.15 M $Fe_2(SO_4)_3.5H_2O$												
K+Ag	0.77	0.75	0.73-85	22	-	-	-	-	0.73	0.74	0.43-86	140
Ag	0.34	0.25	0.05-85	22	-	-	-	-	0.45	0.40	0.16-85	140
Na+Ag	0.81	0.83	0.68-85	22	-	-	-	-	0.71	0.76	0.47-85	140
Ag	0.73	0.81	0.41-85	22	-	-	-	-	0.64	0.72	0.25-85	140
Pb+Ag	0.77	0.84	0.26-90	22	-	-	-	-	0.61	0.75	0.18-85	140
Ag	0.83	0.83	0.80-85	22	-	-	-	-	0.64	0.73	0.28-85	140

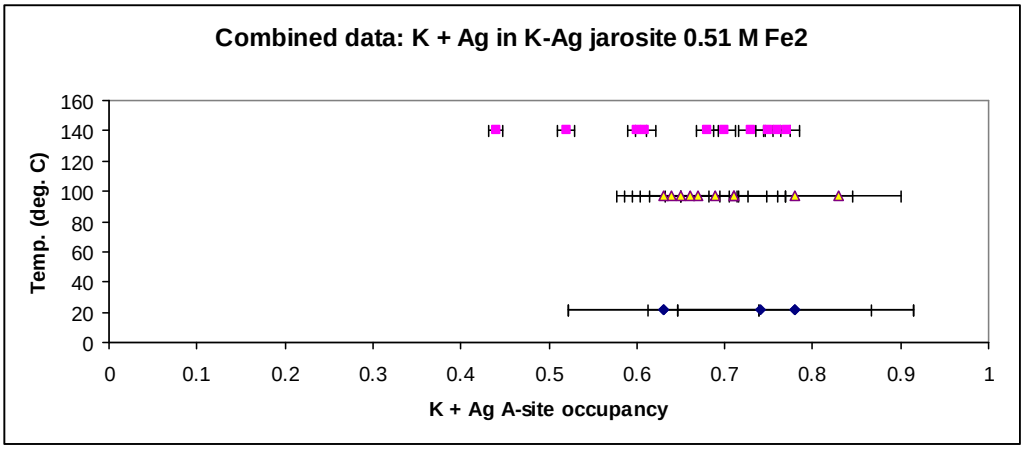

Figure 5.5d: Combined data on total *A*-site occupancy of K + Ag in K-Ag-H_3O-jarosite samples synthesised using 0.51 *M* $Fe_2(SO_4)_3.5H_2O$. (Error bars show series mean precision or C in %, see Appendices H and I.)

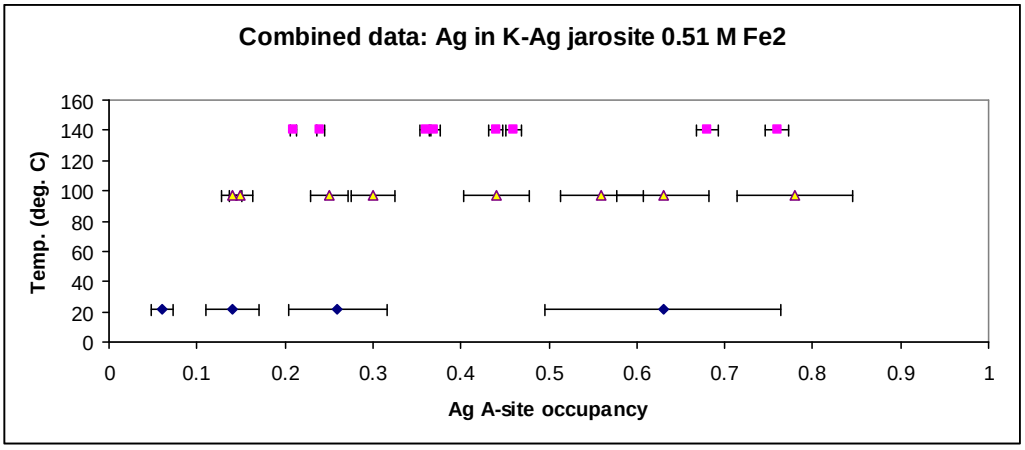

Figure 5.5e: Combined data on total *A*-site occupancy of Ag in K-Ag-H_3O-jarosite samples synthesised using 0.51 *M* $Fe_2(SO_4)_3.5H_2O$. (Error bars show series mean precision or C in %, see Appendices H and I.)

The combined data for the K-Ag-H_3O-jarosite samples synthesised using 0.15 *M* $Fe_2(SO_4)_3.5H_2O$ (see Table 5.7 and Figure 5.5f) indicate occupancy decreases with increase of synthesis temperature from 22ºC (mean 0.77, median 0.75, range 0.73-0.85) to 140ºC (mean 0.73, median 0.74, range 0.43-0.86). However, the Ag-only contents do show increased content with higher temperature of synthesis: mean 0.34, median 0.25, range 0.05-0.85 at 22ºC; and mean 0.45, median 0.40, range 0.16-0.85 at 140ºC (see Figure 5.5g).

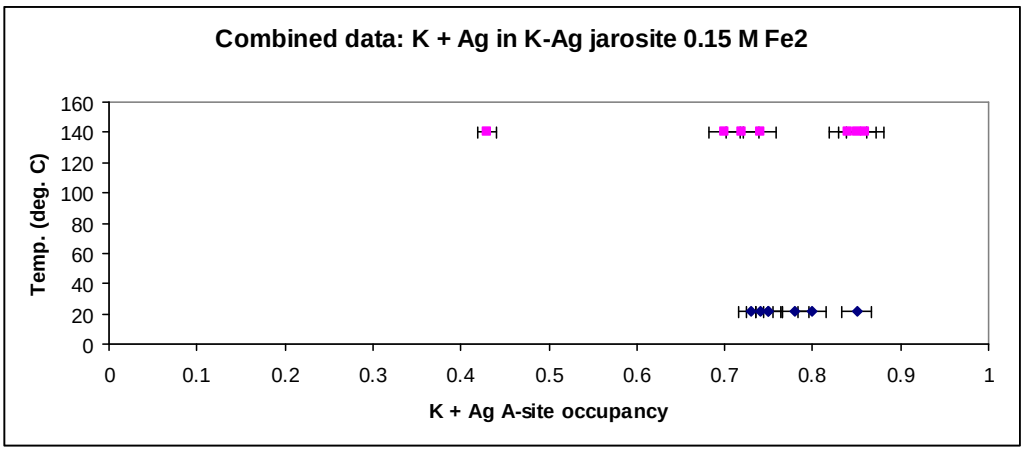

Figure 5.5f: Combined data on total *A*-site occupancy of K + Ag in K-Ag-H_3O-jarosite samples synthesised using 0.15 *M* $Fe_2(SO_4)_3.5H_2O$. (Error bars show series mean precision or C in %, see Appendices H and I.)

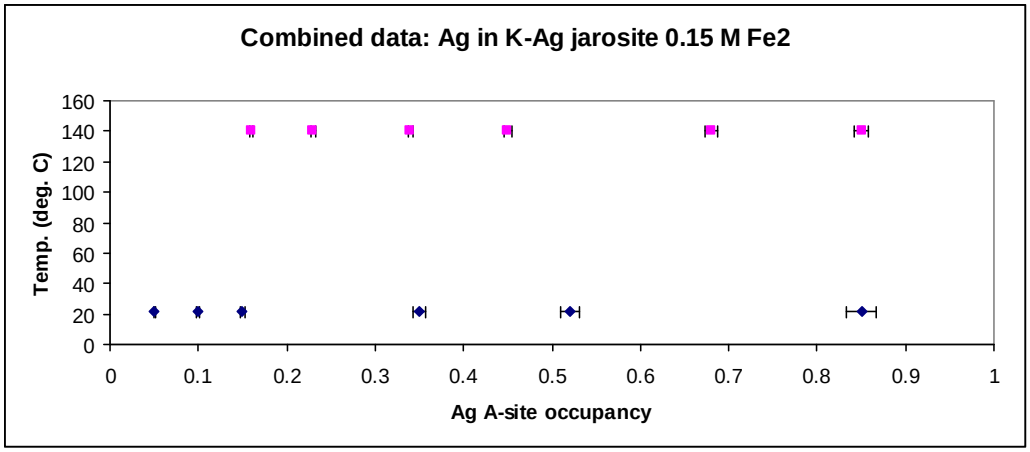

Figure 5.5g: Combined data on total *A*-site occupancy of Ag in K-Ag-H_3O-jarosite samples synthesised using 0.15 *M* $Fe_2(SO_4)_3.5H_2O$. (Error bars show series mean precision or C in %, see Appendices H and I.)

The combined data for the Na-Ag-H_3O-jarosite samples synthesised using 0.51 *M* $Fe_2(SO_4)_3.5H_2O$ show the mean *A*-site content (total of Na and Ag) decreases slightly (although the median content increases slightly) as the synthesis temperature is increased from 22ºC (mean 0.64, median 0.63, range 0.53-0.85) to 97ºC (mean 0.61, median 0.64, range 0.33-0.78), but then increases slightly to 140ºC (mean 0.62, median 0.65, range 0.44-0.76) (see Table 5.7 and Figure 5.5h). There is a decrease in the mean Ag-only content (but increase in the median content) of these Na-Ag-H_3O-jarosite samples as synthesis temperature is increased (see Figure 5.5i) from 22ºC (mean 0.59, median 0.56, range 0.42-0.82) to 97ºC (mean 0.53, median 0.62, range 0.21-0.78); the contents then decrease as synthesis temperature is increased to 140ºC (mean 0.40, median 0.40, range 0.09-0.76).

The trend in the Na-Ag-H_3O-jarosite samples synthesised using 0.15 *M* $Fe_2(SO_4)_3.5H_2O$ is also decreasing *A*-site contents as synthesis temperature increases from 22ºC (mean 0.81, median 0.83, range 0.68-0.85) to 140ºC (mean 0.71, median 0.76, range 0.47-0.85) (see Figure 5.5j). The Ag-only contents of these samples also show this trend: mean 0.73, median 0.81, range 0.41-0.85 at 22ºC; and mean 0.64, median 0.72, range 0.25-0.85 at 140ºC (see Figure 5.5k).

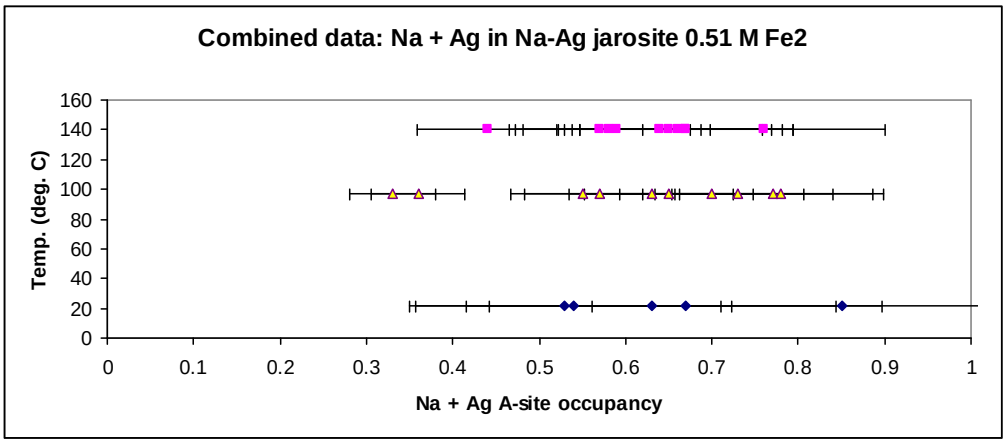

Figure 5.5h: Combined data on total *A*-site occupancy of Na + Ag in Na-Ag-H_3O-jarosite samples synthesised using 0.51 *M* $Fe_2(SO_4)_3.5H_2O$. (Error bars show series mean precision or C in %, see Appendices H and I.)

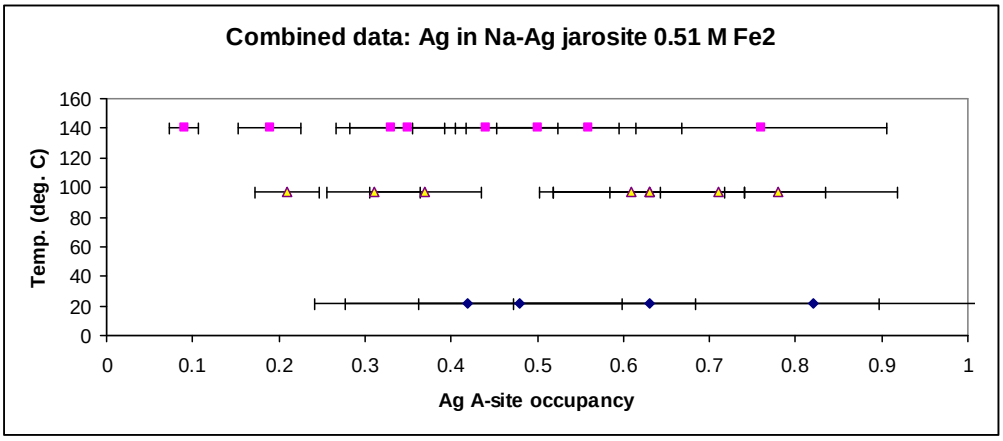

Figure 5.5i: Combined data on total *A*-site occupancy of Ag in Na-Ag-H_3O-jarosite samples synthesised using 0.51 *M* $Fe_2(SO_4)_3.5H_2O$. (Error bars show series mean precision or C in %, see Appendices H and I.)

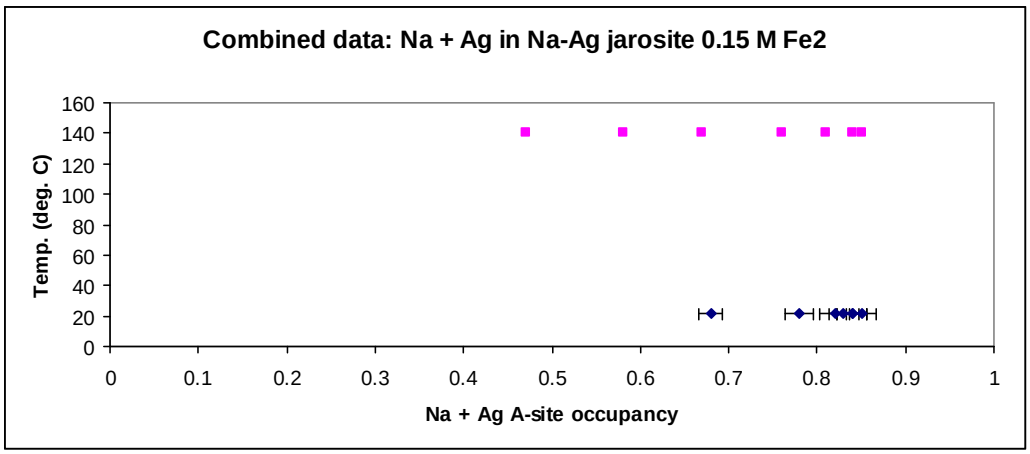

Figure 5.5j: Combined data on total *A*-site occupancy of Na + Ag in Na-Ag-H_3O-jarosite samples synthesised using 0.15 *M* $Fe_2(SO_4)_3.5H_2O$. (Error bars show series mean precision or C in %, see Appendices H and I.)

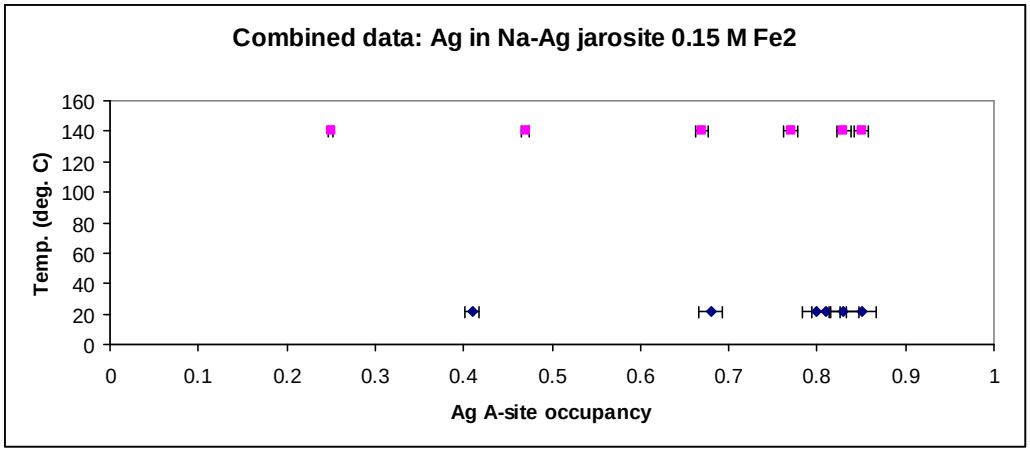

Figure 5.5k: Combined data on total *A*-site occupancy of Ag in Na-Ag-H_3O-jarosite samples synthesised using 0.15 *M* $Fe_2(SO_4)_3.5H_2O$. (Error bars show series mean precision or C in %, see Appendices H and I.)

The combined data results for the Pb-Ag-H_3O-jarosite compounds synthesised using 0.15 *M* $Fe_2(SO_4)_3.5H_2O$ (see Table 5.7) indicate the products made at 22ºC have higher Pb + Ag *A*-site occupancies (mean 0.77, median 0.84, range 0.26-0.90), on average, than those synthesised at 140ºC (mean 0.61, median 0.75, range 0.18-0.85) (see Figure 5.5l). The Ag-only contents of these products also show this trend: mean 0.83, median 0.83, range 0.80-0.85 at 22ºC; and mean 0.64, median 0.73, range 0.28-0.85 at 140ºC (see Figure 5.5m). The lower *A*-site contents of the

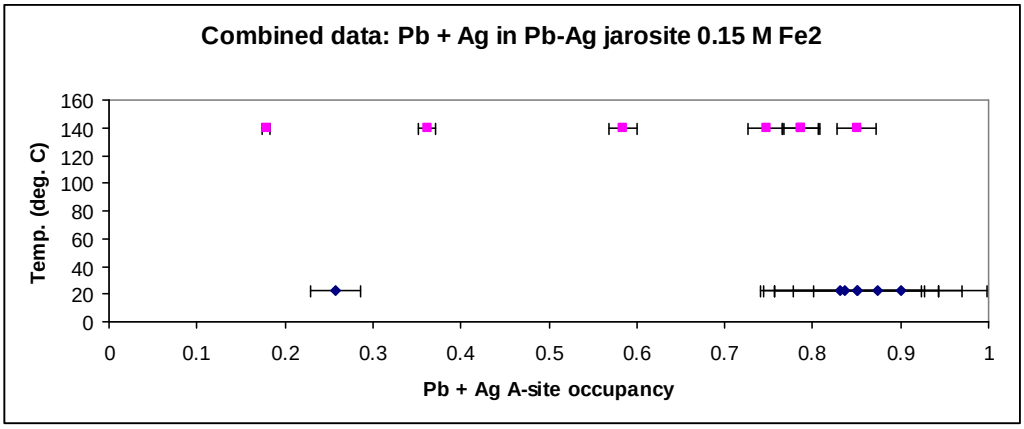

Figure 5.5l: Combined data on total *A*-site occupancy of Pb + Ag in Pb-Ag-H_3O-jarosite samples synthesised using 0.15 *M* $Fe_2(SO_4)_3.5H_2O$. (Error bars show series mean precision or C in %, see Appendices H and I.)

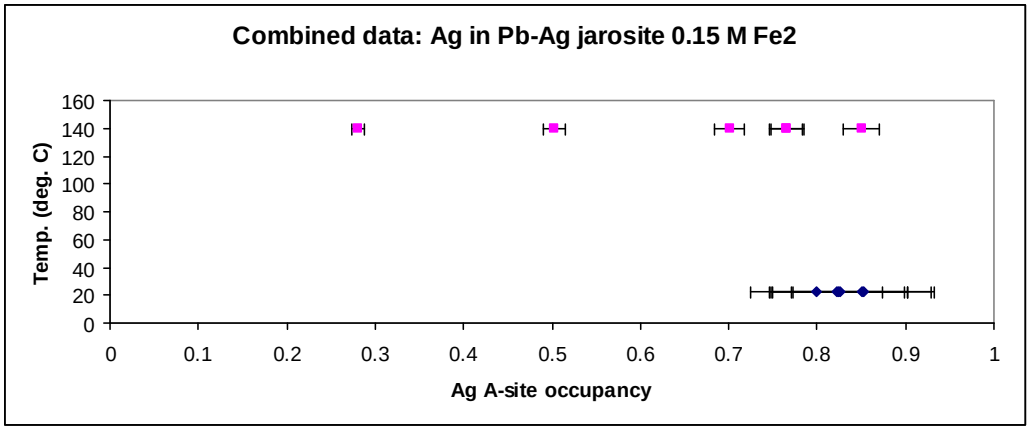

Figure 5.5m: Combined data on total *A*-site occupancy of Ag in Pb-Ag-H_3O-jarosite samples synthesised using 0.15 *M* $Fe_2(SO_4)_3.5H_2O$. (Error bars show series mean precision or C in %, see Appendices H and I.)

Pb-Ag products synthesised at 140ºC compared with those made at 22ºC may be explained by the difference between their periods of synthesis, which were 4 hours and ~ 1 year, respectively.

5.1.1.2 Influence of temperature on *B*-site occupancies

Lower temperatures of synthesis may result in jarosite compounds with greater amounts of Fe vacancies in the *B* sites of their crystal structures (Swayze et al., 2008), although synthetic K- and Na-jarosites prepared at 95°C have shown variation of products between high Fe-deficiency and low Fe-deficiency (Swayze et al., 2008). Vacancies of Fe in the *B* sites may affect the amount of cations (K, Na, Pb or Ag) required in the *A* site, or the amount of hydronium substitution, to maintain charge balance (Kubiscz, 1970).

5.1.1.2.1 EMPA results of *B*-site occupancies

EMPA indicates a decrease in the proportion of *B*-site vacancies with increase in synthesis temperature from 22°C to 97°C in the combined K-Ag-H_3O and Na-Ag-H_3O-jarosite compounds (see Table 5.8 and Figure 5.6), and in the K-Ag- and Na-

Ag-jarosite compounds synthesised with 0.51 *M* $Fe_2(SO_4)_3.5H_2O$ in the starting solutions (see Figure 5.6a) (Murphy et al., 2009). The proportion of vacancies then increases with the increase in temperature from 97°C to 140°C, and by a greater amount than the previous decrease, so the vacancies are higher in the compounds made at 140°C than in those made at 22°C. In the K-Ag-H_3O and Pb-Ag-H_3O jarosite compounds synthesised with 0.15 *M* $Fe_2(SO_4)_3.5H_2O$ in the starting solutions (see Table 5.8 and Figures 5.6b and 5.6c) the vacancies decrease with the synthesis temperature increase from 22°C to 140°C; in the Na-Ag jarosite compounds the opposite trend is seen (Figure 5.6d).

Table 5.8: EMPA data of *B*-site occupancies and synthesis temperature of K-Ag-, Na-Ag- and Pb-Ag-jarosite compounds.

Samples	Mean	+/-	Temp	Mean	+/-	Temp	Mean	+/-	Temp
Synthesis solutions 0.51 M $Fe_2(SO_4)_3.5H_2O$ and 0.15 M $Fe_2(SO_4)_3.5H_2O$									
All	2.86	0.80	22	2.97	0.56	97	2.73	0.54	140
Synthesis solutions 0.51 M $Fe_2(SO_4)_3.5H_2O$									
All	2.84	0.14	22	2.97	0.56	97	2.70	0.24	140
K-Ag	2.87	0.06	22	2.97	0.56	97	2.64	0.45	140
Na-Ag	2.81	0.11	22	3.01	0.29	97	2.74	0.42	140
Synthesis solution 0.15 M $Fe_2(SO_4)_3.5H_2O$									
All	2.87	0.81	22	-	-	-	2.76	0.47	140
K-Ag	2.66	0.60	22	-	-	-	2.75	0.42	140
Na-Ag	2.98	0.24	22	-	-	-	2.81	0.52	140
Pb-Ag	2.80	0.34	22	-	-	-	3.00	0.27	140

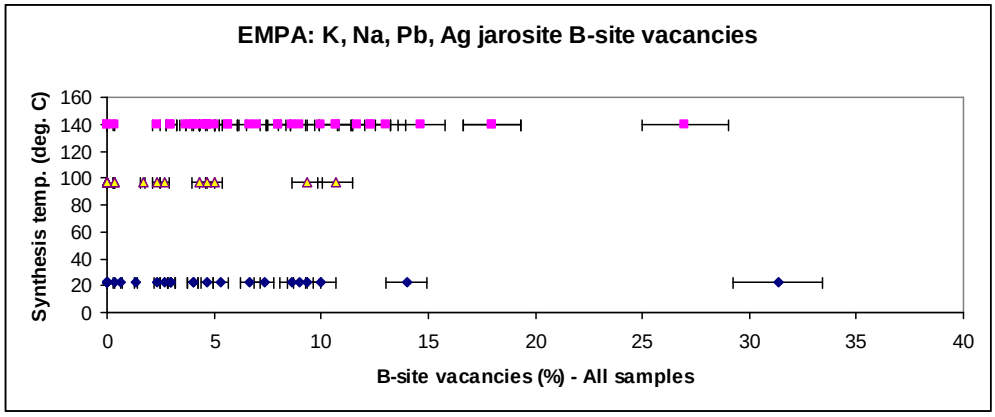

Figure 5.6: Synthesis temperature (22°C, 97°C and 140°C) vs *B*-site vacancies in EMPA of K-Ag-H_3O, Na-Ag-H_3O and Pb-Ag-H_3O-jarosite compounds [0.51 *M* $Fe_2(SO_4)_3.5H_2O$ and 0.15 *M* $Fe_2(SO_4)_3.5H_2O$ solutions]. (Error bars show mean precision or C in %, see Appendix I.)

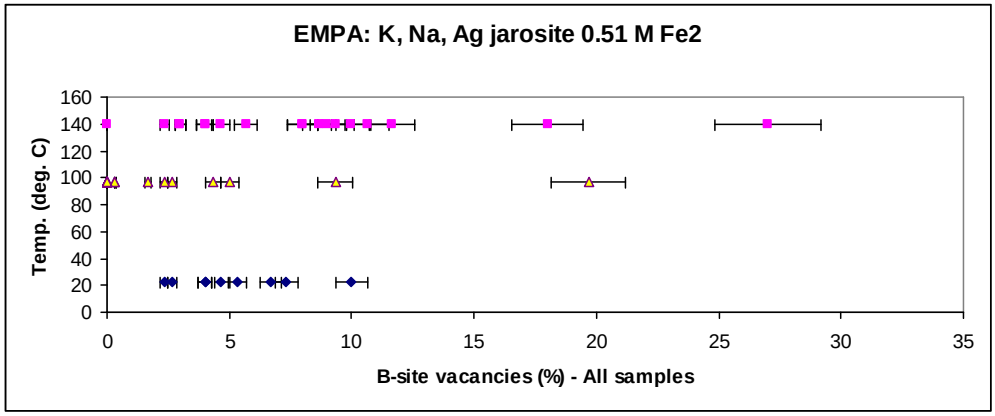

Figure 5.6a: Synthesis temperature (22°C, 97°C and 140°C) vs *B*-site vacancies in EMPA of K-Ag-H_3O and Na-Ag-H_3O-jarosite compounds [0.51 *M* $Fe_2(SO_4)_3.5H_2O$ solutions]. (Error bars show mean precision or C in %, see Appendix I.)

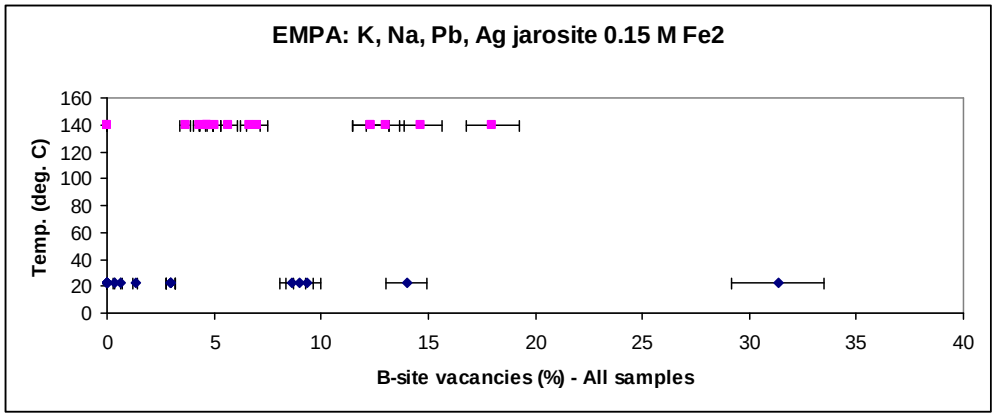

Figure 5.6b: Synthesis temperature (22°C and 140°C) vs *B*-site vacancies in EMPA of K-Ag-H_3O, Na-Ag-H_3O and Pb-Ag-H_3O-jarosite compounds [0.15 *M* $Fe_2(SO_4)_3.5H_2O$ solutions]. (Error bars show mean precision or C in %, see Appendix I.)

The EMPA results show the K-Ag and Na-Ag products synthesised at 97ºC with 0.51 *M* $Fe_2(SO_4)_3.5H_2O$ in the starting solutions have combined average Fe contents of 2.97 (± 0.56) (see Table 5.8). However, if outliers with anomalously low Fe contents (JS24 and 32) are removed from the data set (Rollinson, 1993), the average Fe content is 3.01 (± 0.16). In the samples synthesised at 140ºC using 0.51 *M* $Fe_2(SO_4)_3.5H_2O$, the average Fe content is 2.70 (± 0.24). If the outliers (JS63, 71, 83 and 84) with anomalously low Fe contents are removed from the 140ºC data set, the average Fe content is 2.80 (± 0.36), so remains lower than that of the 97ºC data set in spite of the higher temperature of synthesis. This compares with an average Fe

content of 2.84 (± 0.14) for the compounds synthesised at 22ºC using 0.51 *M* $Fe_2(SO_4)_3.5H_2O$; that is, the average content is higher than that of the 140ºC data set in spite of the lower temperature of synthesis.

The K-Ag, Na-Ag and Pb-Ag products synthesised at 140ºC with 0.15 *M* $Fe_2(SO_4)_3.5H_2O$ in the starting solutions have mean Fe contents of 2.76 (± 0.47). If the outliers with anomalously high Fe content (JS48) and low Fe contents (JS47, 49 and 56) are removed from the data set, the average Fe content is 2.82 (± 0.26). This compares with an average Fe content of 2.87 (± 0.81) for the compounds synthesised at 22ºC using 0.15 *M* $Fe_2(SO_4)_3.5H_2O$. If the outliers with anomalously high Fe contents (JS104 and 106) and low Fe contents (JS89 and 94) are removed from the data set, the average Fe content is 2.93 (± 0.35); that is, the average content is higher than that of the 140ºC data set in spite of the lower temperature of synthesis.

The EMPA results show the syntheses at 97ºC and using the highest concentration of Fe^{3+} in the starting solutions [0.51 *M* $Fe_2(SO_4)_3.5H_2O$] resulted in the highest (full) occupancy of the *B* site in the combined K-Ag and Na-Ag jarosite products' crystal structure. The products made at 22ºC and 140ºC contained substantial Fe site vacancies. In the syntheses using starting solutions containing 0.15 *M* $Fe_2(SO_4)_3.5H_2O$ and in those using starting solutions containing 0.51 *M* $Fe_2(SO_4)_3.5H_2O$, the products made at 22ºC contained higher average Fe site occupancies than those made at 140ºC. This result may be explained by the longer period of synthesis (1 year) of the products made at 22ºC compared with the synthesis period (4 hours) of the products made at 140ºC.

In both the K-Ag- and the Na-Ag-jarosite products synthesised with 0.51 *M* $Fe_2(SO_4)_3.5H_2O$ in the starting solutions, the lowest *B*-site vacancies are in those made at 97ºC (mean Fe contents 2.97 ± 0.56 and 3.01 ± 0.29, respectively), while the

vacancies are lower in those made at 22ºC (mean Fe contents 2.87 ± 0.06 and 2.81 ± 0.11, respectively) than in those made at 140ºC (mean Fe contents 2.64 ± 0.45 and 2.74 ± 0.42, respectively) (see Figures 5.6c and 5.6d). In the K-Ag-jarosite products synthesised with 0.15 *M* $Fe_2(SO_4)_3.5H_2O$ in the starting solutions, lower Fe vacancies are in the products made at 140ºC (mean Fe content 2.75 ± 0.42) than in those made at 22ºC (mean Fe content 2.66 ± 0.60) (see Figure 5.6e); in the Na-Ag jarosites, the products made at 22ºC (mean Fe content 2.98 ± 0.24) have lower Fe vacancies than in those made at 140ºC (mean Fe content 2.81 ± 0.52) (see Figure 5.6f).

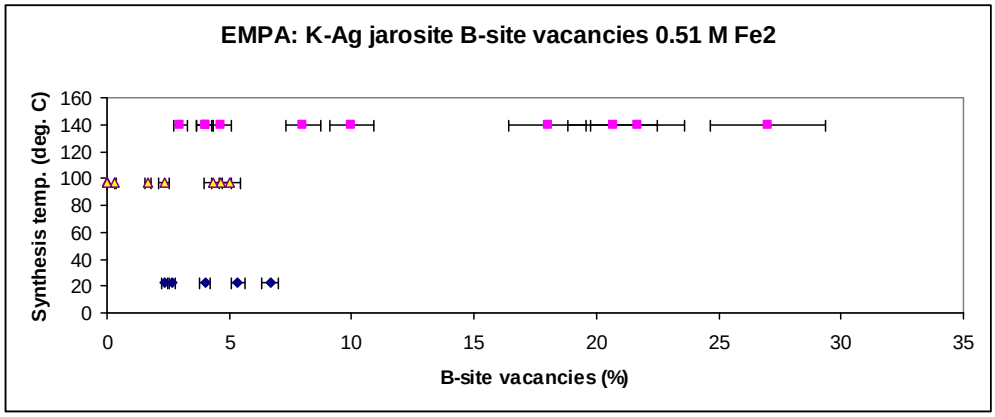

Figure 5.6c: Synthesis temperature (22°C, 97°C and 140°C) vs *B*-site vacancies in EMPA of K-Ag-H_3O-jarosite compounds [0.51 *M* $Fe_2(SO_4)_3.5H_2O$ solutions]. (Error bars show mean precision or C in %, see Appendix I.)

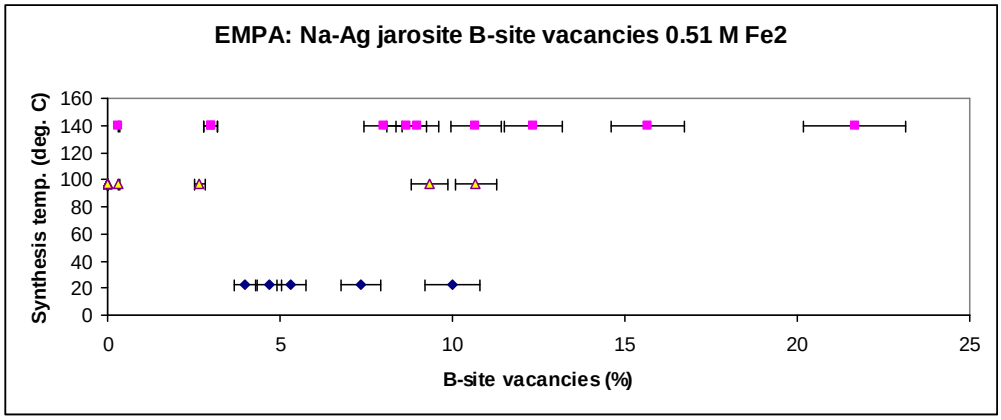

Figure 5.6d: Synthesis temperature (22°C, 97°C and 140°C) vs *B*-site vacancies in EMPA of Na-Ag-H_3O-jarosite compounds [0.51 *M* $Fe_2(SO_4)_3.5H_2O$ solutions]. (Error bars show mean precision or C in %, see Appendix I.)

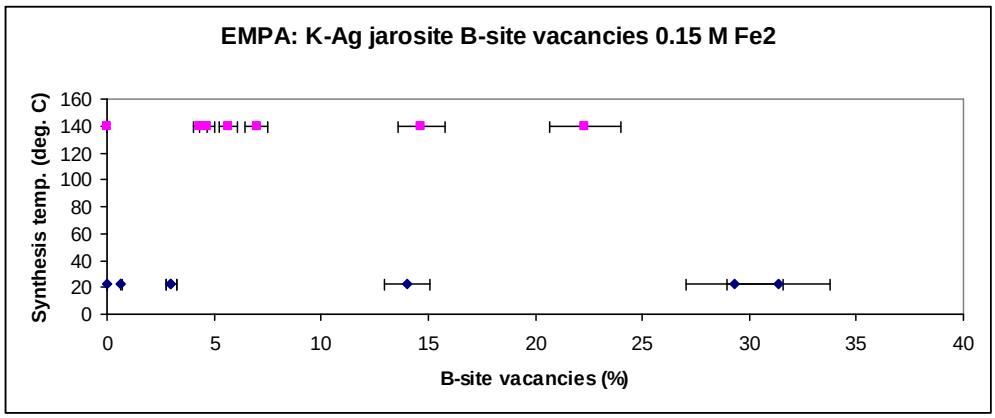

Figure 5.6e: Synthesis temperature (22°C and 140°C) vs *B*-site vacancies in EMPA of K-Ag-H_3O-jarosite compounds [0.15 *M* $Fe_2(SO_4)_3.5H_2O$ solutions]. (Error bars show mean precision or C in %, see Appendix I.)

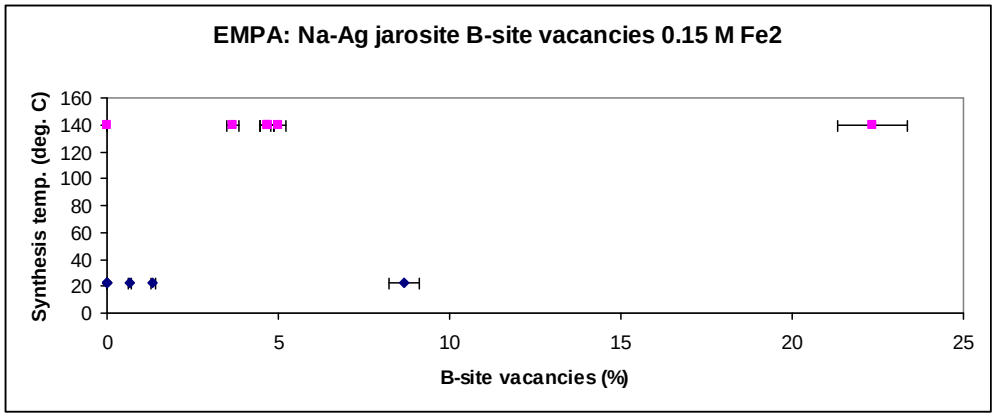

Figure 5.6f: Synthesis temperature (22°C and 140°C) vs *B*-site vacancies in EMPA of Na-Ag-H_3O-jarosite compounds [0.15 *M* $Fe_2(SO_4)_3.5H_2O$ solutions]. (Error bars show mean precision or C in %, see Appendix I.)

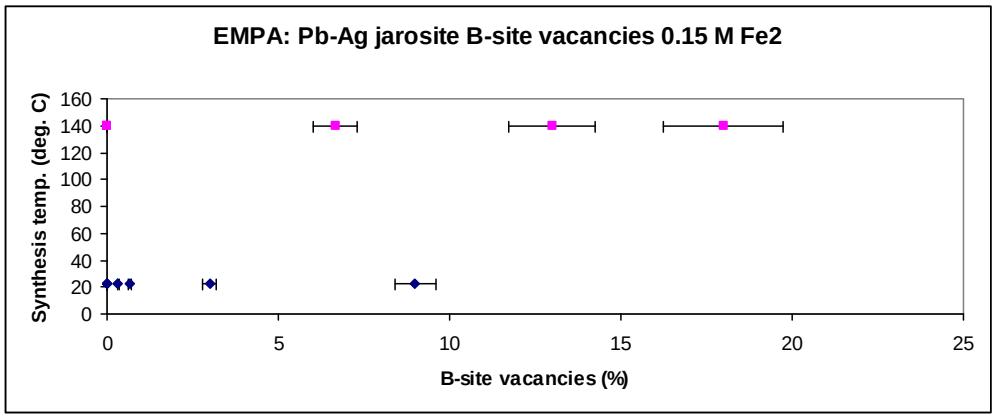

Figure 5.6g: Synthesis temperature (22°C and 140°C) vs *B*-site vacancies in EMPA of Pb-Ag-H_3O-jarosite compounds [0.15 *M* $Fe_2(SO_4)_3.5H_2O$ solutions]. (Error bars show mean precision or C in %, see Appendix I.)

In the Pb-Ag-jarosite product series, synthesised with 0.15 *M*

$Fe_2(SO_4)_3.5H_2O$ in the starting solutions, the EMPA results show mean Fe contents

are 3.00 (± 0.27) in the products synthesised at 22ºC and 2.80 (± 0.34) in the products synthesised at 140ºC. Consequently, *B*-site vacancies increase in the products synthesised at a higher temperature (see Figure 5.6g).

5.1.1.2.2 ICP-AES results of *B*-site occupancies

The ICP-AES results indicate decreasing *B*-site vacancies (increasing Fe occupancies) in the K-Ag, Na-Ag and Pb-Ag-jarosite compounds with increasing temperature of synthesis (see Table 5.9). In the results for the K-Ag and Na-Ag jarosite compounds synthesised with 0.51 *M* $Fe_2(SO_4)_3.5H_2O$ in the starting solutions, the *B*-site vacancies decrease as synthesis temperature increases from 22°C to 97°C and 140°C (see Figure 5.7). The mean Fe contents are 2.39 (± 0.51) in the products made at 22°C, 2.67 (± 1.16) in those made at 97°C and 3.02 (± 0.42) in those made at 140°C. The K-Ag, Na-Ag and Pb-Ag jarosite compounds synthesised with 0.15 *M* $Fe_2(SO_4)_3.5H_2O$ in the starting solutions also have lower *B*-site vacancies in the products made at higher temperature (see Figure 5.7a): mean Fe content is 2.79 (± 0.30) in the products made at 22°C and 2.95 (± 0.20) in those made at 140°C.

Table 5.9: ICP-AES data of *B*-site occupancies and synthesis temperature of K-Ag-, Na-Ag- and Pb-Ag-jarosite compounds

Samples	Mean	+/-	Temp	Mean	+/-	Temp	Mean	+/-	Temp
Synthesis solutions 0.51 M $Fe_2(SO_4)_3.5H_2O$ and 0.15 M $Fe_2(SO_4)_3.5H_2O$									
All	2.66	0.78	22	2.67	1.16	97	2.98	0.46	140
Synthesis solutions 0.51 *M* $Fe_2(SO_4)_3.5H_2O$									
All	2.39	0.51	22	2.67	1.16	97	3.02	0.42	140
K-Ag	2.26	0.38	22	2.58	1.07	97	3.02	0.42	140
Na-Ag	2.42	0.54	22	2.76	0.21	97	3.02	0.14	140
Synthesis solution 0.15 M $Fe_2(SO_4)_3.5H_2O$									
All	2.79	0.30	22	-	-	-	2.95	0.20	140
K-Ag	2.66	0.20	22	-	-	-	2.86	0.10	140
Na-Ag	2.89	0.12	22	-	-	-	2.96	0.08	140
Pb-Ag	2.85	0.07	22	-	-	-	2.99	0.16	140

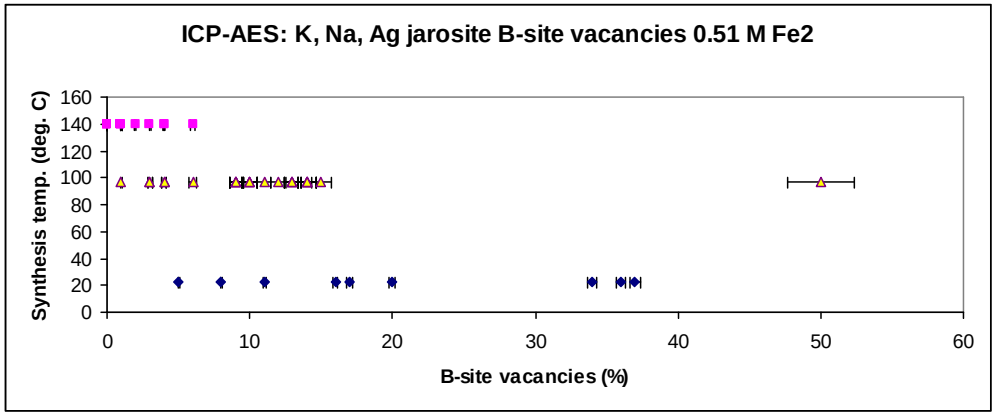

Figure 5.7: Synthesis temperature (22°C, 97°C and 140°C) vs *B*-site vacancies in ICP-AES of K-Ag-H_3O and Na-Ag-H_3O-jarosite compounds [0.51 *M* $Fe_2(SO_4)_3.5H_2O$ solutions]. (Error bars show series mean precision or C in %, see Appendix H.)

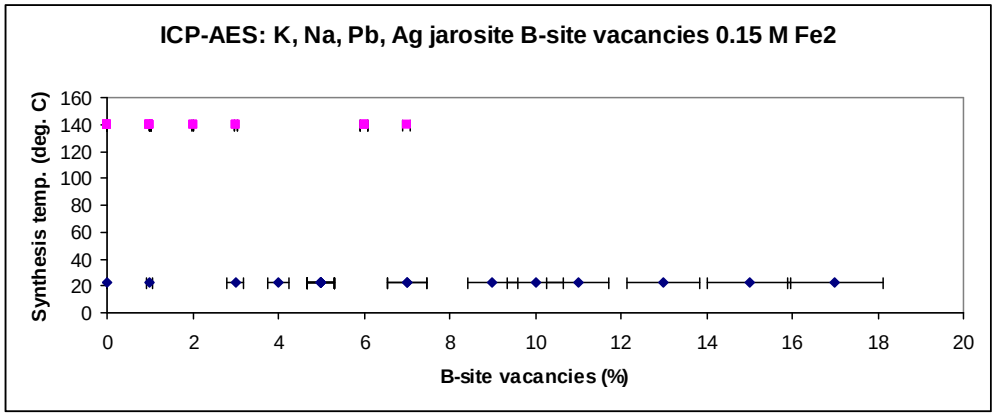

Figure 5.7a: Synthesis temperature (22°C and 140°C) vs *B*-site vacancies in ICP-AES of K-Ag-H_3O, Na-Ag-H_3O and Pb-Ag-H_3O-jarosite compounds [0.15 *M* $Fe_2(SO_4)_3.5H_2O$ solutions]. (Error bars show series mean precision or C in %, see Appendix H.)

The ICP-AES results show that in both the K-Ag-jarosite and the Na-Ag-jarosite products synthesised with 0.51 *M* $Fe_2(SO_4)_3.5H_2O$ in the starting solutions, the percentage of *B*-site vacancies is higher the lower the temperature of synthesis (see Figures 5.7b and 5.7c). The mean Fe occupancy is highest at 3.02 ± 0.42 in the K-Ag-jarosite products and 3.02 ± 0.14 in the Na-Ag-jarosite products made at the highest temperature of 140ºC, and is 2.58 ± 1.07 and 2.76 ± 0.21, respectively, in the products made at 97ºC and 2.26 ± 0.38 and 2.42 ± 0.54, respectively, in those made at 22ºC. In the K-Ag-jarosite and Na-Ag-jarosite products synthesised with 0.15 *M* $Fe_2(SO_4)_3.5H_2O$ in the starting solutions, lower Fe vacancies are found in the

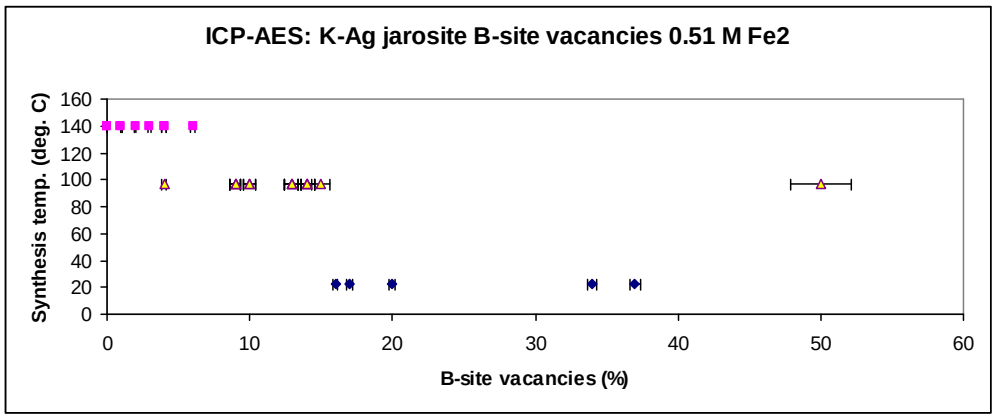

Figure 5.7b: Synthesis temperature (22°C, 97°C and 140°C) vs *B*-site vacancies in ICP-AES of K-Ag-H_3O-jarosite compounds [0.51 *M* $Fe_2(SO_4)_3.5H_2O$ solutions]. (Error bars show series mean precision or C in %, see Appendix H.)

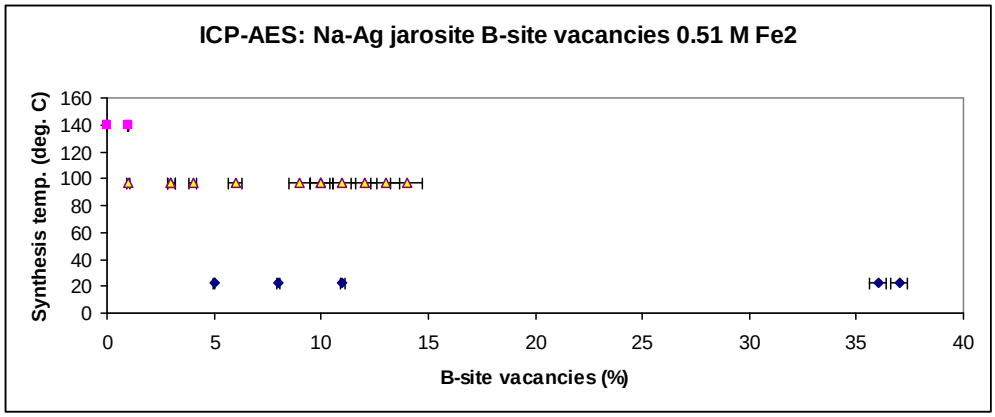

Figure 5.7c: Synthesis temperature (22°C, 97°C and 140°C) vs *B*-site vacancies in ICP-AES of Na-Ag-H_3O-jarosite compounds [0.51 *M* $Fe_2(SO_4)_3.5H_2O$ solutions]. (Error bars show series mean precision or C in %, see Appendix H.)

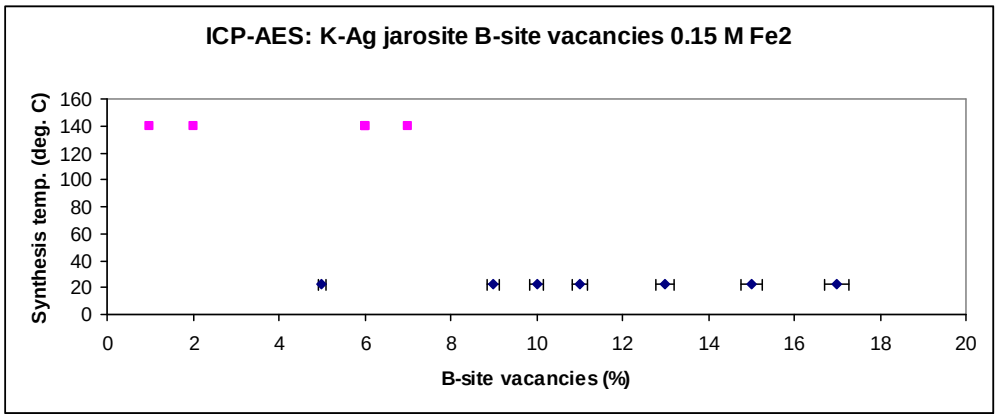

Figure 5.7d: Synthesis temperature (22°C and 140°C) vs *B*-site vacancies in ICP-AES of K-Ag-H_3O-jarosite compounds [0.15 *M* $Fe_2(SO_4)_3.5H_2O$ solutions]. (Error bars show series mean precision or C in %, see Appendix H.)

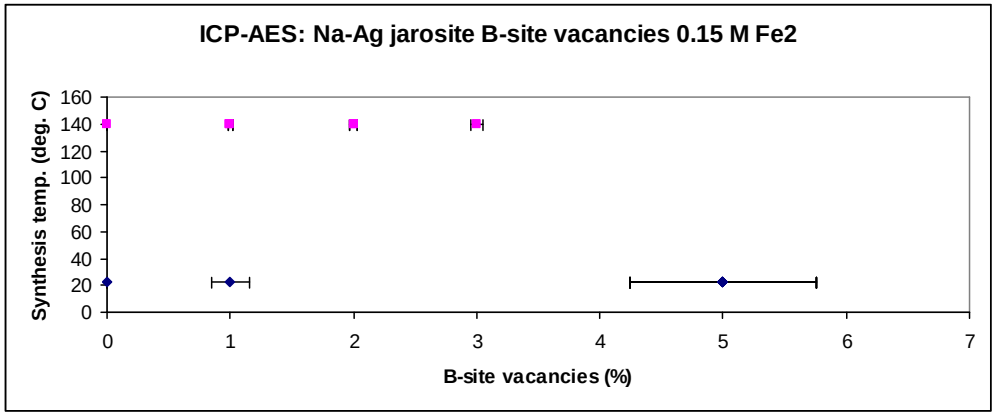

Figure 5.7e: Synthesis temperature (22°C and 140°C) vs *B*-site vacancies in ICP-AES of Na-Ag-H_3O-jarosite compounds [0.15 *M* $Fe_2(SO_4)_3.5H_2O$ solutions]. (Error bars show series mean precision or C in %, see Appendix H.)

products made at 140ºC (mean Fe content 2.86 ± 0.10 and 2.96 ± 0.08, respectively) than in those made at 22ºC (2.66 ± 0.20 and 2.89 ± 0.12, respectively) (see Figures 5.7d and 5.7e).

In the Pb-Ag-jarosite product series, synthesised with 0.15 *M* $Fe_2(SO_4)_3.5H_2O$ in the starting solutions, the ICP-AES results show mean Fe contents are 2.85 (± 0.07) in the products synthesised at 22ºC and 2.99 (± 0.16) in the products synthesised at 140ºC. Consequently, *B*-site vacancies decrease in the products synthesised at a higher temperature (see Figure 5.7f).

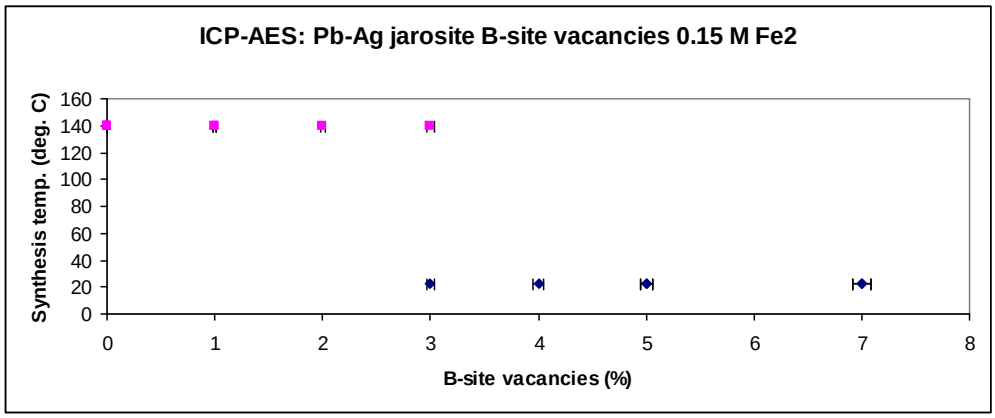

Figure 5.7f: Synthesis temperature (22°C and 140°C) vs *B*-site vacancies in ICP-AES of Pb-Ag-H_3O-jarosite compounds [0.15 *M* $Fe_2(SO_4)_3.5H_2O$ solutions]. (Error bars show mean precision or C in %, see Appendix H.)

5.1.1.2.3 Rietveld refinement results of *B*-site occupancies

The Rietveld refinement of powder XRD data for the K-Ag- and Na-Ag-jarosite products indicates Fe vacancies in the B site decrease as synthesis temperature increases (see Table 5.10 and Figure 5.8). The same trend is observable in the K-Ag-jarosite product series: in the samples synthesised with 0.51 *M* $Fe_2(SO_4)_3.5H_2O$ in the starting solutions, the mean Fe occupancies are 2.52 (± 0.32) at 22ºC and 2.64 (± 0.10) at 97ºC; and in the samples synthesised with 0.15 *M* $Fe_2(SO_4)_3.5H_2O$, 2.77 (± 0.44) at 140ºC (see Figure 5.8a). In the Na-Ag-jarosite series, in the products synthesised with 0.51 *M* $Fe_2(SO_4)_3.5H_2O$ in the starting solutions, the overall mean Fe occupancies are 2.79 (± 0.20) at 97ºC, compared with 2.91 (± 0.11) at 22ºC; and

Table 5.10: Rietveld refinement data of *B*-site occupancies and synthesis temperature of K-Ag-H_3O and Na-Ag-H_3O-jarosite compounds

Samples	Mean	+/-	Temp	Mean	+/-	Temp	Mean	+/-	Temp
Synthesis solutions 0.51 M $Fe_2(SO_4)_3.5H_2O$ and 0.15 M $Fe_2(SO_4)_3.5H_2O$									
All	2.64	0.38	22	2.72	0.25	97	2.84	0.51	140
Synthesis solutions 0.51 M $Fe_2(SO_4)_3.5H_2O$									
K-Ag	2.52	0.32	22	2.64	0.10	97	-	-	-
Na-Ag	2.91	0.11	22	2.79	0.20	97	-	-	-
Synthesis solution 0.15 M $Fe_2(SO_4)_3.5H_2O$									
K-Ag	-	-	-	-	-	-	2.77	0.44	140
Na-Ag	-	-	-	-	-	-	2.91	0.27	140

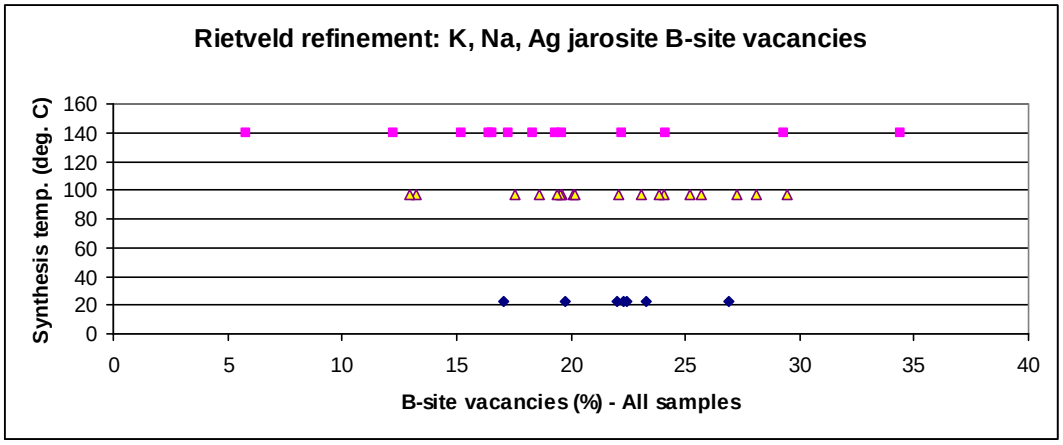

Figure 5.8: Synthesis temperature (22°C, 97°C and 140°C) vs *B*-site vacancies from Rietveld refinement of K-Ag-H_3O and Na-Ag-H_3O-jarosite compounds [0.51 *M* $Fe_2(SO_4)_3.5H_2O$ and 0.15 *M* $Fe_2(SO_4)_3.5H_2O$ solutions].

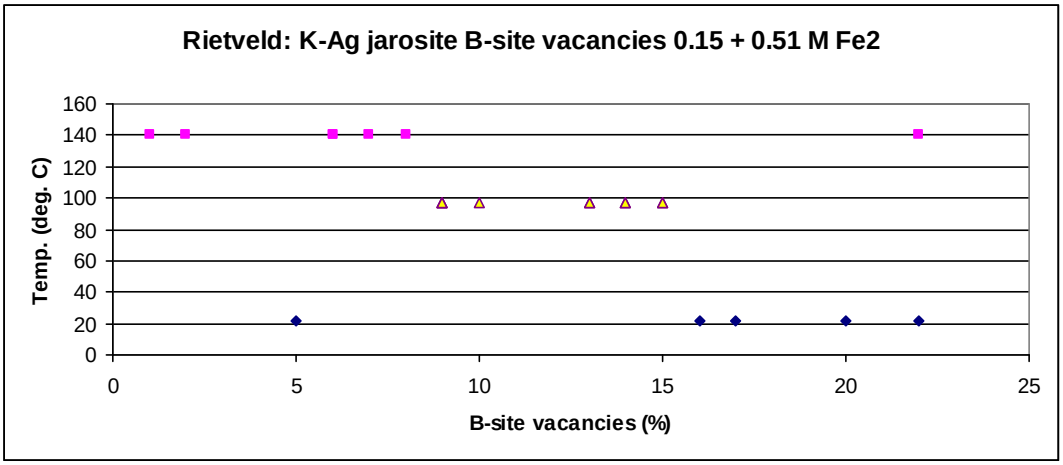

Figure 5.8a: Synthesis temperature (22°C, 97°C and 140°C) vs *B*-site vacancies from Rietveld refinement of K-Ag-H_3O-jarosite compounds [0.51 *M* $Fe_2(SO_4)_3.5H_2O$ and 0.15 *M* $Fe_2(SO_4)_3.5H_2O$ solutions].

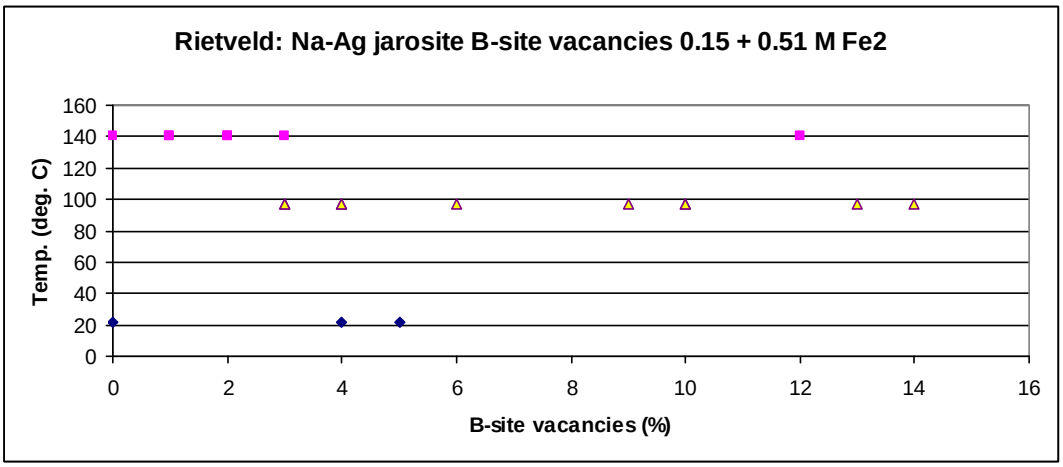

Figure 5.8b: Synthesis temperature (22°C, 97°C and 140°C) vs *B*-site vacancies from Rietveld refinement of Na-Ag-H_3O-jarosite compounds [0.15 *M* $Fe_2(SO_4)_3.5H_2O$ and 0.15 *M* $Fe_2(SO_4)_3.5H_2O$ solutions].

(in the products synthesised with 0.15 *M* $Fe_2(SO_4)_3.5H_2O$) the mean occupancy is 2.91 (± 0.27) at 140ºC (see Figure 5.9b).

5.1.1.2.4 Combined data results of *B*-site occupancies

On the basis of a combination of data from the different analytical techniques used to study the chemical composition of the jarosite products (see Tables 4.20-22), an increase in the synthesis temperature from 22°C to 97°C and 140°C results, in general, in a decrease in the proportion of *B*-site vacancies in the crystal structure

(Murphy et al., 2009). The results for all the K-Ag-, Na-Ag- and Pb-Ag-jarosite compounds show the products synthesised at the highest temperature (140°C) have the lowest percentage of Fe vacancies (mean Fe occupancy 2.89 ± 0.56) (see Table 5.11 and Figure 5.9), whereas the products synthesised at 22°C and 97°C have similar Fe contents to each other of 2.76 ± 0.43 and 2.72 ± 0.25, respectively. Of the products synthesised with 0.51 *M* $Fe_2(SO_4)_3.5H_2O$ in the starting solutions, the samples made at 140°C have the lowest percentage of *B*-site vacancies (mean Fe occupancy 2.87 ± 0.41), while the mean Fe occupancies are 2.72 ± 0.25 for those made at 97°C and 2.68 ± 0.35 for those made at 22°C (see Figure 5.9a). The same

Table 5.11: Combined data of *B*-site occupancies and synthesis temperature of K-Ag-H_3O, Na-Ag-H_3O and Pb-Ag-H_3O-jarosite compounds

Samples	Mean	+/-	Temp	Mean	+/-	Temp	Mean	+/-	Temp
Synthesis solutions 0.51 M $Fe_2(SO_4)_3.5H_2O$ and 0.15 M $Fe_2(SO_4)_3.5H_2O$									
All	2.76	0.43	22	2.72	0.25	97	2.89	0.56	140
Synthesis solutions 0.51 *M* $Fe_2(SO_4)_3.5H_2O$									
All	2.68	0.35	22	2.72	0.25	97	2.87	0.41	140
K-Ag	2.52	0.32	22	2.68	0.20	97	2.86	0.40	140
Na-Ag	2.88	0.14	22	2.76	0.21	97	2.92	0.24	140
Synthesis solution 0.15 M $Fe_2(SO_4)_3.5H_2O$									
All	2.80	0.31	22	-	-	-	2.90	0.26	140
K-Ag	2.66	0.20	22	-	-	-	2.78	0.45	140
Na-Ag	2.89	0.12	22	-	-	-	2.91	0.27	140
Pb-Ag	2.86	0.08	22	-	-	-	2.99	0.16	140

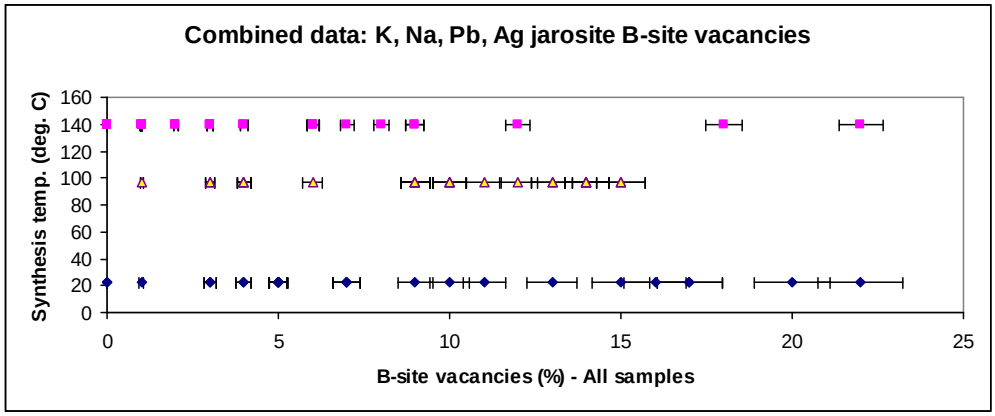

Figure 5.9: Synthesis temperature (22°C, 97°C and 140°C) vs *B*-site vacancies from combined data of all K-Ag-H_3O, Na-Ag-H_3O and Pb-Ag-H_3O-jarosite compounds [0.51 *M* $Fe_2(SO_4)_3.5H_2O$ and 0.15 *M* $Fe_2(SO_4)_3.5H_2O$ solutions]. (Error bars show series mean precision or C in %, see Appendices H and I.)

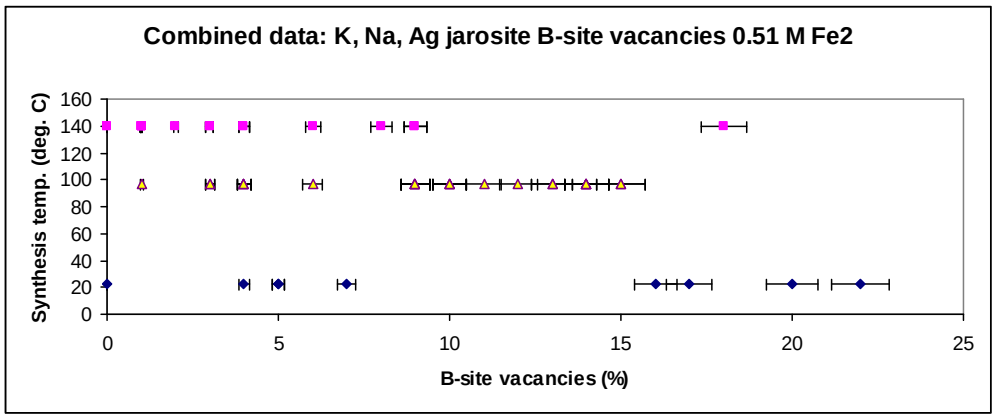

Figure 5.9a: Synthesis temperature (22°C, 97°C and 140°C) vs *B*-site vacancies from combined data of all K-Ag-H_3O and Na-Ag-H_3O-jarosite compounds [0.51 *M* $Fe_2(SO_4)_3.5H_2O$ solutions]. (Error bars show series mean precision or C in %, see Appendices H and I.)

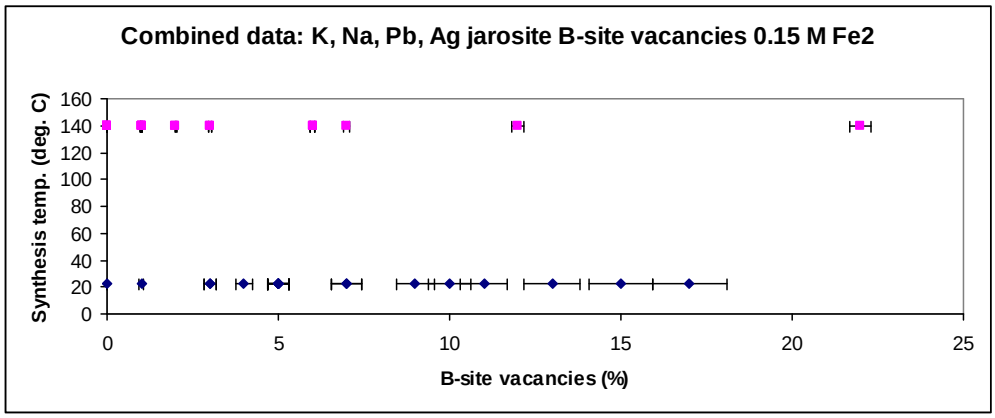

Figure 5.9b: Synthesis temperature (22°C and 140°C) vs *B*-site vacancies from combined data of all K-Ag-H_3O, Na-Ag-H_3O and Pb-Ag-H_3O-jarosite compounds [0.15 *M* $Fe_2(SO_4)_3.5H_2O$ solutions]. (Error bars show series mean precision or C in %, see Appendices H and I.)

trend is seen in the products synthesised with 0.15 *M* $Fe_2(SO_4)_3.5H_2O$ in the starting solutions (see Figure 5.9b): mean Fe occupancies are 2.90 ± 0.26 at 140°C and 2.80 ± 0.31 at 22°C.

The combined data for the separate K-Ag, Na-Ag and Pb-Ag-jarosite series (with 0.51 *M* $Fe_2(SO_4)_3.5H_2O$ and with 0.15 *M* $Fe_2(SO_4)_3.5H_2O$ in the starting solutions) show that the percentage of Fe vacancies decreases (Fe occupancy increases) as the temperature of synthesis increases (see Table 5.11 and Figures 5.9c, 5.9d, 5.9e, 5.9f and 5.9g). The exception is the Na-Ag-jarosite series (with 0.51 *M*

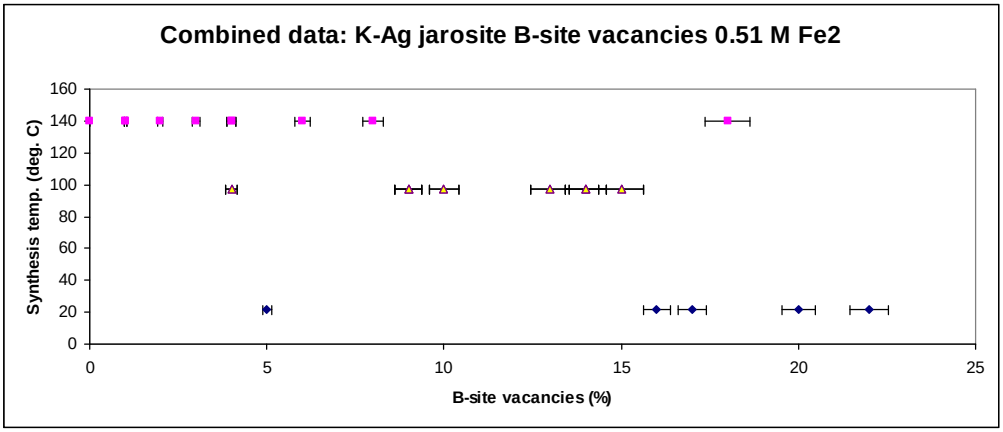

Figure 5.9c: Synthesis temperature (22°C, 97°C and 140°C) vs *B*-site vacancies from combined data of K-Ag-H_3O-jarosite compounds [0.51 *M* $Fe_2(SO_4)_3.5H_2O$ solutions]. (Error bars show series mean precision or C in %, see Appendices H, I.)

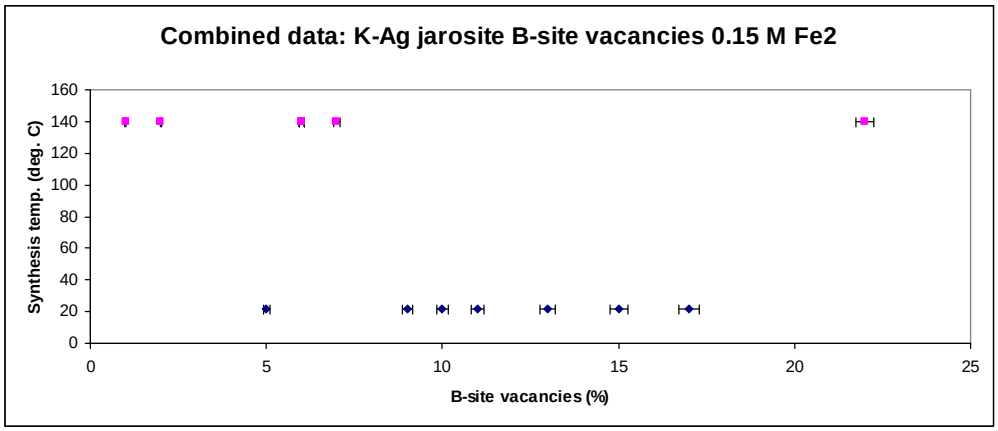

Figure 5.9d: Synthesis temperature (22°C and 140°C) vs *B*-site vacancies from combined data of K-Ag-H_3O-jarosite compounds [0.15 *M* $Fe_2(SO_4)_3.5H_2O$ solutions]. (Error bars show series mean precision or C in %, see Appendices H, I.)

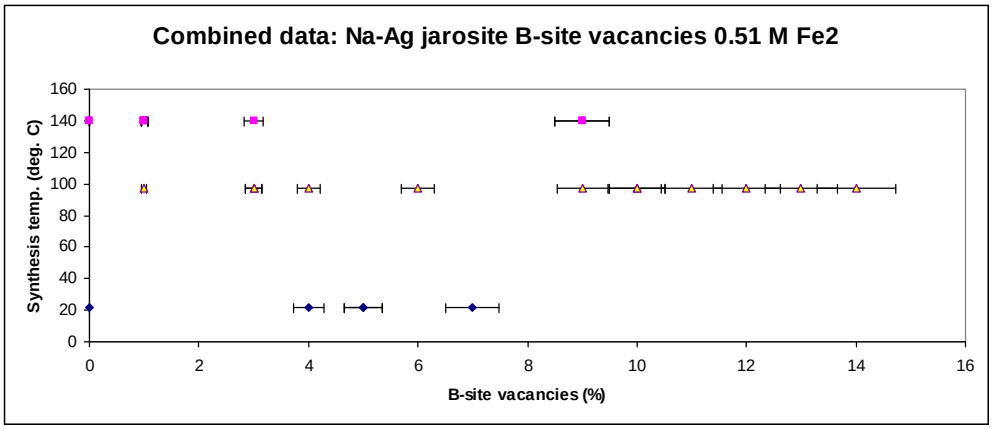

Figure 5.9e: Synthesis temperature (22°C, 97°C and 140°C) vs *B*-site vacancies from combined data of Na-Ag-H_3O-jarosite compounds [0.51 *M* $Fe_2(SO_4)_3.5H_2O$ solutions]. (Error bars show series mean precision or C in %, see Appendices H, I.)

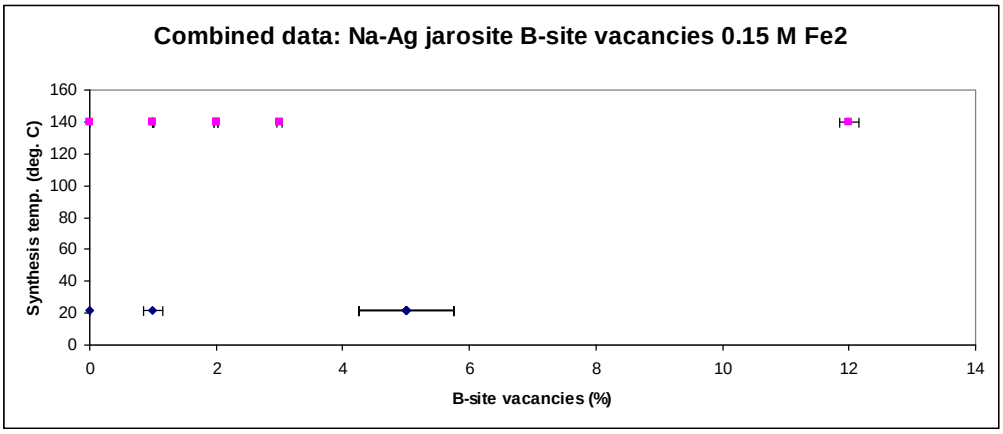

Figure 5.9f: Synthesis temperature (22°C and 140°C) vs *B*-site vacancies from combined data of Na-Ag-H_3O-jarosite compounds [0.15 *M* $Fe_2(SO_4)_3.5H_2O$ solutions]. (Error bars show series mean precision or C in %, see Appendices H, I.)

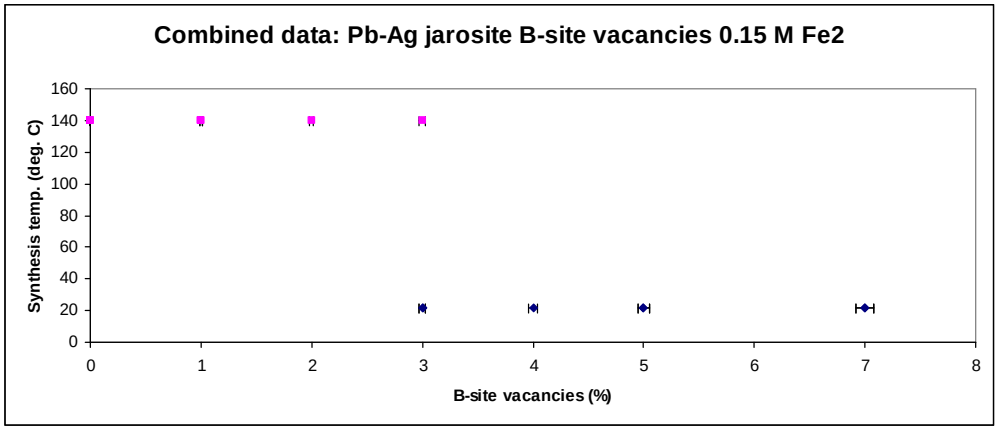

Figure 5.9g: Synthesis temperature (22°C and 140°C) vs *B*-site vacancies from combined data of Pb-Ag-H_3O-jarosite compounds [0.15 *M* $Fe_2(SO_4)_3.5H_2O$ solutions]. (Error bars show series mean precision or C in %, see Appendices H, I.)

$Fe_2(SO_4)_3.5H_2O$ in the starting solutions), as the products made at 22°C (mean Fe occupancy 2.88 ± 0.14) have fewer Fe vacancies than those made at 97°C (mean Fe occupancy 2.76 ± 0.21).

5.1.2 Influence of starting composition on the final chemistry of the synthesised K-Ag-H_3O, Na-Ag-H_3O and Pb-Ag-H_3O compounds

A range of starting solutions in the synthesis of jarosite compounds has been used in this project. The concentrations of K^+ and Na^+ were in separate series with Ag^+

involving 0, 0.055, 0.11, 0.165 and 0.22 *M* and 0, 0.02, 0.04, 0.06, 0.08, 0.10 and 0.12 *M* of each cation in 100 ml solutions and 0. 0.01, 0.02, 0.03, 0.04, 0.05 and 0.06 *M* of each in 200 ml solutions. In addition, two concentrations of Fe^{3+} were used: 0.15 *M* $Fe_2(SO_4)_3.5H_2O$ and 0.51 *M* $Fe_2(SO_4)_3.5H_2O$. In two Pb^{2+}-Ag^{+} series, concentrations of 0, 0.01, 0.02, 0.03, 0.04, 0.05 and 0.06 *M* of each cation and 0, 0.0001, 0.00013, 0.00032, 0.001 and 0.005 *M* Pb and 0.25 *M* Ag were used. In the former series Fe was 0.15 *M* $Fe_2(SO_4)_3.5H_2O$ and in the latter series Fe was 0.075 *M* $Fe_2(SO_4)_3.5H_2O$.

The different analytical techniques used (EMPA, ICP-AES, and Rietveld refinement of XRD data) all show increasing K, Na, Pb and Ag contents in the synthesised jarosite compounds as the concentration of the respective cations increases in the starting solutions of the series of synthesis experiments.

The EMPA compositional results for the K-Ag-H_3O- and Na-Ag-H_3O-jarosite synthesis products show generally declining K and Na contents with decreasing alkali cation concentration in the starting solutions of each series. The results are similar for Pb-Ag-H_3O-jarosite samples (synthesised at 140ºC). There are also complementary trends of generally increasing Ag content as the concentration of this cation increases in the starting solutions. However, the results have some anomalous contents, so the different series of compounds generally show only poor or fairly poor linear relationships between the content of K, Na and Pb cations and Ag cations in the products, with only three series showing good linear relationships between the content of alkali and Ag cations with R^2 values of ≥ 0.8356.

In the K-Ag-H_3O-jarosite compounds, the K content is consistently higher than the Ag content even when the Ag concentration in the starting solutions is three times the K concentration, such as in JS10 and JS28. The residual H_3O content is

higher than the K content even in samples with the highest concentration (0.22 *M*) of K in the starting solutions, such as JS04, 22, 73, although JS62 and 81 contain more K than H_3O. However, the high (residual) H_3O contents in the samples synthesised at 97ºC are also likely to have been the result of the excess Fe in the starting solutions, with the Fe:K ratio 4.64:1 compared with the stoichiometric jarosite ratio of 3:1. By contrast, sample 56 has a K *A*-site occupation of 0.70 and sample 57 has a K content of 0.56 from starting solutions with K^+ concentrations of 0.10 *M* and 0.08 *M*, respectively, and Fe:K ratios of 3:1 and 3.75:1, respectively. In the same series, samples 60 and 61 have Ag contents of 0.60 and 0.63, respectively, from starting solutions with Ag concentrations 0.10 *M* and 0.12 *M*, respectively. Of the other K-Ag-H_3O-jarosite compound series, the only samples with Ag contents above 0.5 are end-member samples 72 (0.63) and 71 (0.66), as well as sample 84 (0.64) from a starting-solution Ag^+ concentration of 0.165 *M* and Fe ratio of 4.64:1.

In the Na-Ag-H_3O-jarosite compounds synthesised at 97ºC, the Ag *A*-site occupation is consistently higher than the Na content, even when the concentration of Na^+ in the starting solution was three times that of Ag^+ (samples 16 and 34) or five times that of Ag^+ (JS42). In the series JS49-54 and 61 (synthesised at 140ºC), only sample 50 has a higher Na content (0.25) than Ag (0.24) and this is from a starting solution in which the Na concentration was five times that of the Ag concentration. Series JS72 and 77-80 (synthesised at 22ºC) and 71 and 85-88 (synthesised at 140ºC) have higher Ag contents than Na contents in all intermediate products. Series JS66-70 (synthesised at 140ºC) has higher Na content than Ag content in two of the intermediate products: sample 68 (Na 0.57 and Ag 0.09), for which the Na^+ concentration in the starting solution was three times that of Ag^+; and sample 69 (Na 0.30 and Ag 0.12) from a starting solution with equal concentrations

of Na^+ and Ag^+, so this is a contradictory result to the other series. The residual H_3O content is higher than the Na content and the Na+Ag content in all the products synthesised at 97ºC, although this may be explained by the excess of Fe^{3+} in the starting solutions, with an Fe:(Na+Ag) ratio of 4.64:1. In the series JS49-54 and 61 (synthesised at 140ºC), the H_3O content is higher than the Na+Ag content in all the intermediate products, with an Fe:(Na+Ag) ratio of 2.5:1 in the starting solutions. The end-member jarosite products of this series have Na and Ag contents of 0.56 and 0.63 respectively. In the other Na-Ag-H_3O jarosite compound series, only the end-member products have Na or Ag contents higher than 0.5.

In the Pb-Ag-H_3O jarosite compounds, the Ag content is consistently higher than the Pb content even when the concentration of Pb in the starting solutions is 2.5 times the concentration of Ag (sample 44). However, in the low-temperature compounds (synthesised at 22ºC) the Ag concentration in the starting solutions is a minimum of 10 times the Pb concentration. The residual H_3O content is higher than the Pb content in all samples.

5.1.2.1 Partitioning coefficients for Ag in synthesised jarosite compounds

The relative incorporation of K, Na, Pb and Ag in the synthesised jarosite products may also be indicated by comparing their molar concentrations (*M*) in the synthesis starting solutions with their molar concentrations in the *A* site of the jarosite precipitates (Dutrizac and Jambor, 1987). Tables 5.12 and 5.13 show relative partitioning coefficients for the various jarosite compounds and product series between K and Ag, Na and Ag, and Pb and Ag (see also Appendix G). The partitioning coefficients are based on the *A*-site occupancies from the combined data of the analysis techniques used in this project (see Section 4.1.7 and Appendix G).

The partitioning coefficient of each compound is calculated from the *A*-site occupancy of Ag divided by the total *A*-site occupancy of Ag and K (Ag/Ag+K), Na (Ag/Ag+Na) or Pb (Ag/Ag+Pb) in the K-Ag-, Na-Ag- or Pb-Ag-jarosite products, respectively; and from the Ag concentration (*M*) divided by the total concentration of Ag and K (Ag/Ag+K), Na (Ag/Ag+Na) or Pb (Ag/Ag+Pb) in the synthesis solutions. The partitioning coefficient is the ratio of the former to the latter: $Ag/(Ag+X)_{product}$ / $Ag/(Ag+X)_{solution}$ (where X is K, Na or Pb). The graphs below (Figures 5.10a-p) illustrate this relative partitioning, in which a straight line between 0 and 1 would indicate ideal solid solution between the two phases (Ag-jarosite and K-jarosite or Na-jarosite), with the ratio of the cations' molar concentrations in the starting solutions being equal to the ratio of the cations' site occupancies in the products (Dutrizac and Jambor, 1987).

Table 5.12: Partitioning coefficients for Ag in K-Ag- and Na-Ag-jarosites as ratio of Ag/Ag+(K or Na) in products to Ag/Ag+(K or Na) in synthesis solutions.

Sample	**[Ag/Ag+K]j**	**[Ag/Ag+K]sol**	**P. coeff.**	**Sample**	**[Ag/Ag+Na]j**	**[Ag/Ag+Na]sol**	**P. coeff.**
Solutions containing 0.51 M $Fe_2(SO_4)_3.5H_2O$ heated at 97ºC and products dried at 60ºC							
JS04	0	0	0	JS12	1	1	1
JS06	0.265	0.25	1.06	JS14	0	0	0
JS06D	0.224	0.25	0.896	JS16	0.529	0.25	2.116
JS08	0.423	0.5	0.846	JS18	0.863	0.5	1.726
JS10	0.621	0.75	0.828	JS20	0.922	0.75	1.229
JS10D	0.62	0.75	0.827	**JS12-20**	**3.314**	**2.5**	**1.326**
JS12	1	1	1				
JS04-12	**3.153**	**3.5**	**0.901**				
Solutions containing 0.51 M $Fe_2(SO_4)_3.5H_2O$ heated at 97ºC and products dried at 110ºC							
JS22	0	0	0	JS30	1	1	1
JS24	0.221	0.25	0.884	JS32	0	0	0
JS24D	0.212	0.25	0.848	JS34	0.636	0.25	2.544
JS26	0.362	0.5	0.724	JS36	0.861	0.5	1.722
JS28	0.675	0.75	0.9	JS38	0.938	0.75	1.251
JS30	1	1	1	JS38D	0.903	0.75	1.204
JS22-30	**2.47**	**2.75**	**0.898**	**JS30-38**	**4.338**	**3.25**	**1.335**
Samples annealed at 140ºC and dried at 110ºC [from 0.51 M $Fe_2(SO_4)_3.5H_2O$ solutions heated at 97ºC, products dried at 60ºC]							
JS62	0	0	0	JS66	1	1	1
JS63	0.3	0.25	1.2	JS67	0	0	0
JS64	0.493	0.5	0.986	JS68	0.136	0.25	0.544
JS65	0.712	0.75	0.949	JS69	0.322	0.5	0.644
JS66	1	1	1	JS70	0.589	0.75	0.785
JS62-66	**2.505**	**2.5**	**1.002**	**JS66-70**	**2.047**	**2.5**	**0.819**
Samples annealed at 140ºC and dried at 110ºC [from 0.51 M $Fe_2(SO_4)_3.5H_2O$ solutions heated at 97ºC, products dried at 110ºC]							
JS71	1	1	1	JS71	1	1	1
JS81	0	0	0	JS85	0	0	0
JS82	0.353	0.25	1.412	JS86	0.547	0.25	2.188
JS83	0.613	0.5	1.226	JS87	0.746	0.5	1.492
JS84	0.883	0.75	1.177	JS88	0.836	0.75	1.115
JS71, 81-84	**2.849**	**2.5**	**1.140**	**JS71, 85-88**	**3.129**	**2.5**	**1.252**

Solutions containing 0.51 M $Fe_2(SO_4)_3.5H_2O$ prepared at 22ºC and products air-dried at 22ºC							
JS72	1	1	1	JS72	1	1	1
JS73	0	0	0	JS77	0	0	0
JS74	0.081	0.25	0.324	JS78	0.792	0.25	3.168
JS75	0.179	0.5	0.358	JS79	0.889	0.5	1.778
JS76	0.413	0.75	0.551	JS80	0.965	0.75	1.287
JS72-76	**1.673**	**2.5**	**0.669**	**JS72, 77-80**	**3.646**	**2.5**	**1.458**
Solutions containing 0.15 M $Fe_2(SO_4)_3.5H_2O$ heated at 140ºC and products dried at 110ºC							
JS55	0	0	0	JS49	0	0	0
JS56	0.186	0.167	1.114	JS50	0.431	0.167	2.581
JS57	0.329	0.333	0.988	JS51	0.701	0.333	2.105
JS58	0.472	0.5	0.944	JS52	0.882	0.5	1.764
JS59	0.608	0.667	0.912	JS53	0.951	0.667	1.426
JS60	0.81	0.833	0.972	JS54	0.988	0.833	1.186
JS61	1	1	1	JS61	1	1	1
JS55-61	**3.405**	**3.5**	**0.973**	**JS49-54, 61**	**4.953**	**3.5**	**1.415**
Solutions containing 0.075 M $Fe_2(SO_4)_3.5H_2O$ were prepared at 22ºC and products air-dried at 22ºC							
JS89	0	0	0	JS95	1	1	1
JS90	0.068	0.167	0.407	JS96	0	0	0
JS91	0.133	0.333	0.399	JS97	0.526	0.167	3.15
JS92	0.2	0.5	0.4	JS98	0.829	0.333	2.489
JS93	0.449	0.667	0.673	JS99	0.952	0.5	1.904
JS94	0.65	0.833	0.78	JS100	0.976	0.667	1.463
JS95	1	1	1	JS101	0.988	0.833	1.186
JS89-95	**2.5**	**3.5**	**0.714**	**JS95-101**	**5.271**	**3.5**	**1.506**

Key: j = jarosite product; sol. = synthesis solution; P. coeff. = partitioning coefficient. [Ag/Ag+K]j = Ag *A*-site occupancy divided by total *A*-site occupancy of Ag and K in K-Ag-jarosite product. [Ag/Ag+Na]j = Ag *A*-site occupancy divided by total *A*-site occupancy of Ag and Na in Na-Ag-jarosite product. [Ag/Ag+K]sol = Ag concentration (*M*) divided by total concentration of Ag and K in synthesis solution. [Ag/Ag+Na]sol = Ag concentration (*M*) divided by total concentration of Ag and Na in synthesis solution.

In Table 5.12, the partitioning coefficients for Ag in the K-Ag-jarosite compounds are, in general, less than 1 (the mean value for the seven series of K-Ag-jarosite compounds is 0.900), which indicates that K is preferentially incorporated in the products relative to Ag. The coefficients for Ag in the different K-Ag-jarosite series synthesised in solutions containing 0.22 *M* K+Ag and 0.51 *M* $Fe_2(SO_4)_3.5H_2O$ are 0.901 (JS04-12), 0.898 (JS22-30), 1.002 (JS62-66), 1.140 (JS71, 81-84) and 0.669 (JS72-76) (Table 5.14). These compare with partitioning coefficients for Ag in the K-Ag-jarosite series synthesised in solutions containing 0.12 *M* K+Ag (100 ml solution) or 0.06 *M* K+Ag (200 ml solution) and 0.15 *M* $Fe_2(SO_4)_3.5H_2O$ and 0.075 *M* $Fe_2(SO_4)_3.5H_2O$, respectively, of 0.973 (JS55-61) and 0.714 (JS89-95). Therefore, the data indicate differences in chemical composition of the synthesis starting solutions have, in general, no substantial effect on the relative partitioning between Ag and K in K-Ag-jarosite compounds. However, the lowest relative partitioning coefficients of Ag are for the two K-Ag-jarosite series synthesised at low

temperature (22ºC): 0.669 for series JS72-76 and 0.714 for JS89-95; that is, K has a greater preference for occupation of the jarosite structure, compared with Ag, at lower temperature of synthesis. This conclusion is also supported by the partitioning coefficients for the K-Ag-jarosite series synthesised at 97ºC and 140ºC. The two product series synthesised at 97ºC have Ag partitioning coefficients of 0.901 (JS04-22) and 0.898 (JS22-30), while for the series synthesised at 140ºC the coefficients are higher at 1.002 (JS62-66), 1.140 (JS71, 81-84) and 0.973 (JS55-61). The mean of the relative partitioning coefficients for Ag in the three K-Ag-jarosite series synthesised at 140ºC is 1.038 and indicates that, at the highest temperature of synthesis of 140ºC, Ag is at least equally incorporated into the jarosite structure compared with K or is even slightly preferentially incorporated into the structure.

In Table 5.12, the K-Ag-jarosite series JS04-12 and JS22-30 synthesised at 97ºC and with synthesis solutions containing 0.22 *M* K+Ag and 0.51 *M* $Fe_2(SO_4)_3.5H_2O$ show relatively high Ag partitioning coefficients (1.06, 0.896, 0.884 and 0.848) for the products (06, 06D, 24 and 24D, respectively) synthesised from solutions containing the lowest Ag concentration of 0.055 *M* (indicating relatively high initial uptake of Ag in K-Ag-jarosite compounds). The values of the partitioning coefficients then decrease slightly in the other intermediate products with increasing Ag concentration in the synthesis solutions, except for JS28, which is the intermediate product in the JS22-30 series with the highest concentration of Ag in the synthesis solution, until the coefficients rise to 1 in the Ag-only products. The trends in the partitioning coefficients' values of the two series are illustrated by the shape of curves formed by the points in Figures 5.10a and 5.10b, which initially have slightly decreasing gradients after the point for the first intermediate product (indicating slightly declining uptake of Ag into the jarosite structure relative to K as

Ag concentration in the synthesis solutions is increased) and then increasing gradients towards the point (with a value of 1) for the Ag-only product.

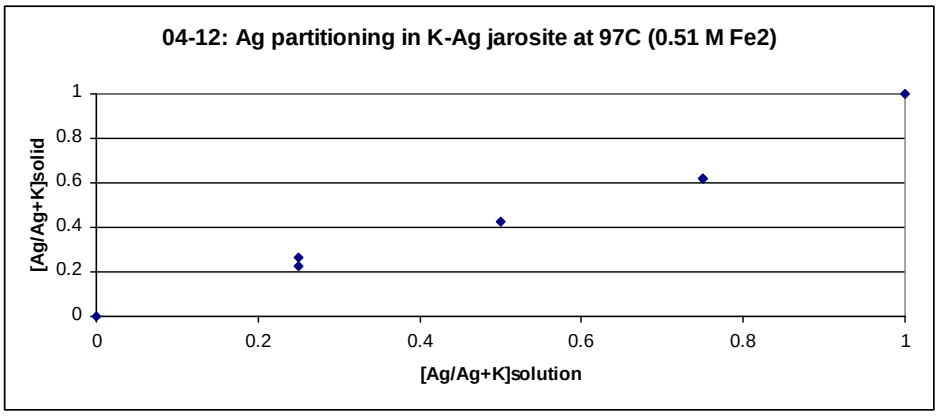

Figure 5.10a: JS04-12: 0.22 M (K+Ag) and 0.51 M $Fe_2(SO_4)_3.5H_2O$ at 97ºC.

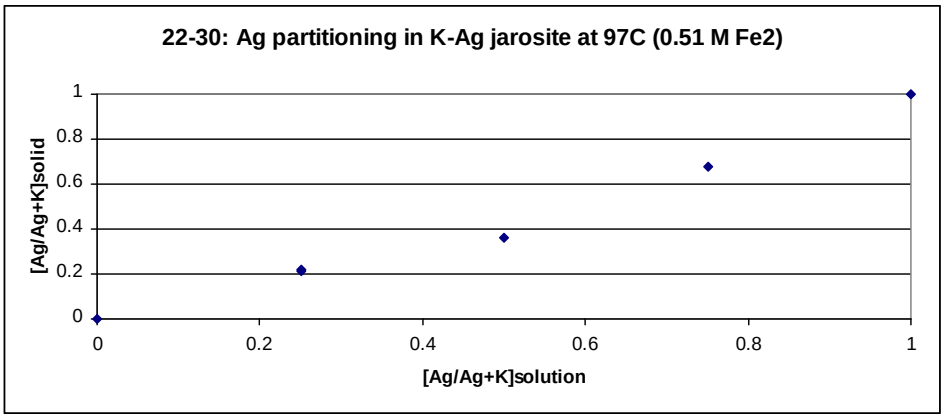

Figure 5.10b: JS22-30: 0.22 M (K+Ag) and 0.51 M $Fe_2(SO_4)_3.5H_2O$ at 97ºC.

The three K-Ag-jarosite series synthesised at 140ºC (JS55-61, 62-66 and 71 & 81-84) show the same trends as the two series synthesised at 97ºC of relatively high initial Ag partitioning coefficient values (see Table 5.12) and then slightly declining values (except JS60 in series 55-61), until increasing to 1 in the Ag-only compound; however, in series 71, 81-84, the values of the intermediate products are all above 1, so the value (1.177) for the last intermediate product (JS84) decreases to 1 for the Ag-only product (JS71). The trends in the partitioning coefficients' values of the three series are illustrated by the shape of curves formed by the points in Figures 5.10c, 5.10d and 5.10e. In Figures 5.10c and 5.10d, these curves initially have

slightly decreasing gradients after the point for the first intermediate product and then increasing gradients; in Figure 5.10e, the curve continues to have a slightly decreasing gradient after the point for the first intermediate product (again indicating slightly declining relative uptake of Ag compared to K, and so Ag concentration is possibly moving closer to saturation in the synthesis solutions relative to incorporation of Ag in the jarosite structure).

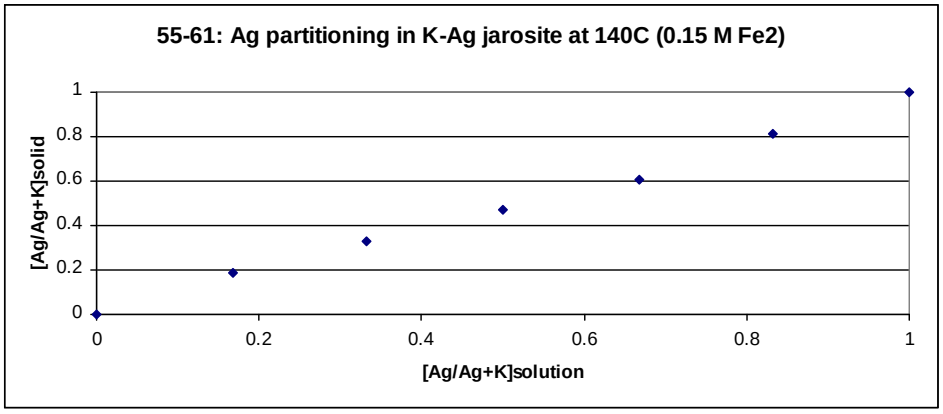

Figure 5.10c: JS55-61: 0.12 M (K+Ag), 0.15 M $Fe_2(SO_4)_3.5H_2O$ at 140ºC.

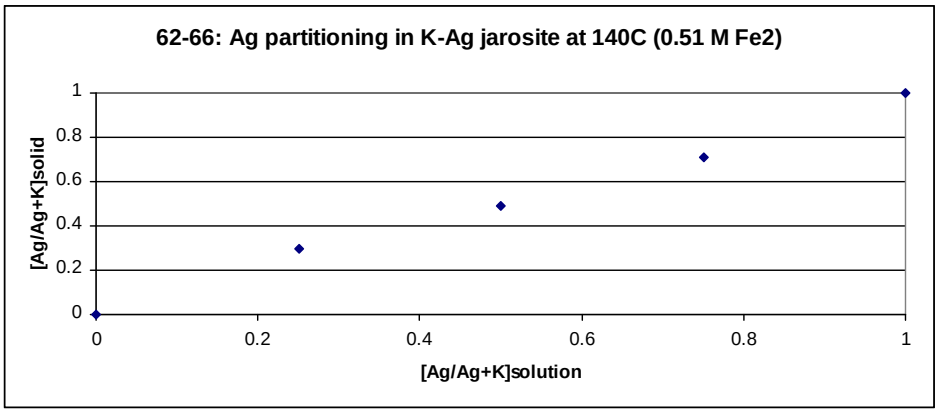

Figure 5.10d: JS62-66: 0.22 M (K+Ag), 0.51 M $Fe_2(SO_4)_3.5H_2O$ at 140ºC.

In contrast, the two K-Ag-jarosite series synthesised at 22ºC have relatively low Ag partitioning coefficients for the first intermediate products, indicating relatively low initial Ag uptake. In series JS72-76, the Ag partitioning coefficients then gradually increase through the series to 1; in series JS89-95, the Ag partitioning coefficients remain around 0.4 for three intermediate products and then gradually

increase to 1. The trends in the partitioning coefficients' values of the two series are illustrated by the shape of curves formed by the points in Figures 5.10f and 5.10g. Figures 5.10f shows the curve gradient increasing after the point for the first intermediate product, indicating Ag has a growing preference for incorporation in the jarosite structure as the concentration of Ag in the synthesis solution increases. In Figure 5.10g, the curve gradients described by the points are initially approximately equal, representing the partitioning coefficients of around 0.4 for the first three intermediate products, indicating K concentration is at saturation level in the synthesis solutions for these products, and then the gradients increase through the series as solution K concentration declines and Ag concentration increases.

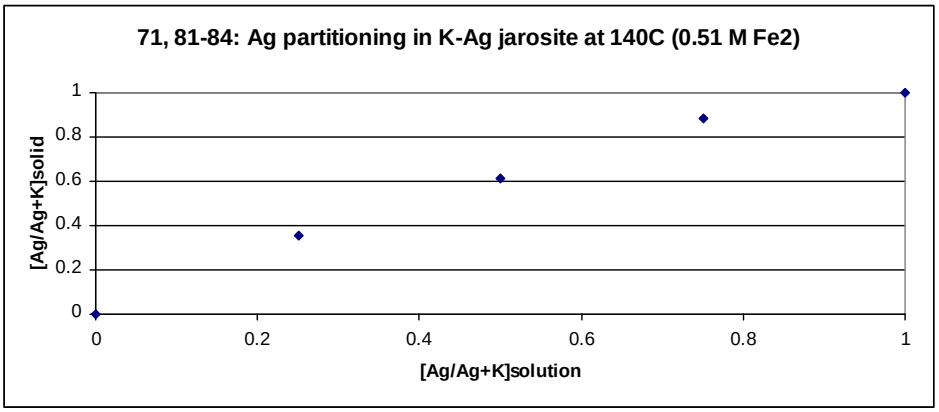

Figure 5.10e: JS71, 81-84: 0.22 M (K+Ag), 0.51 M $Fe_2(SO_4)_3.5H_2O$ at 140ºC.

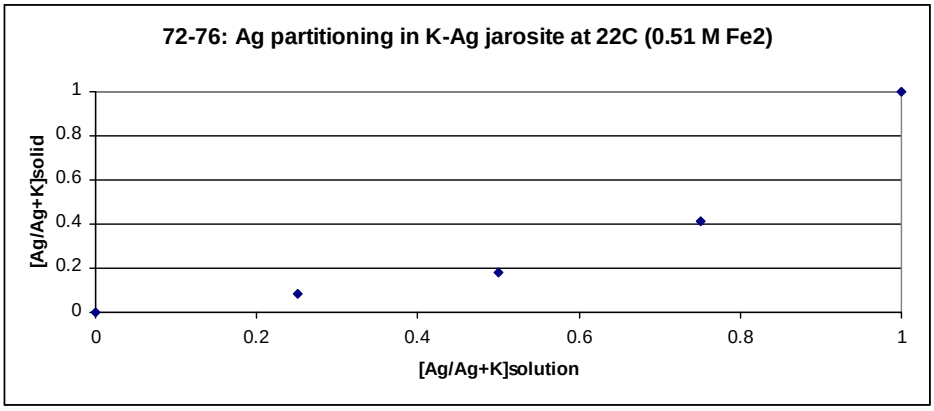

Figure 5.10f: JS72-76: 0.22 M (K+Ag) and 0.51 M $Fe_2(SO_4)_3.5H_2O$ at 22ºC.

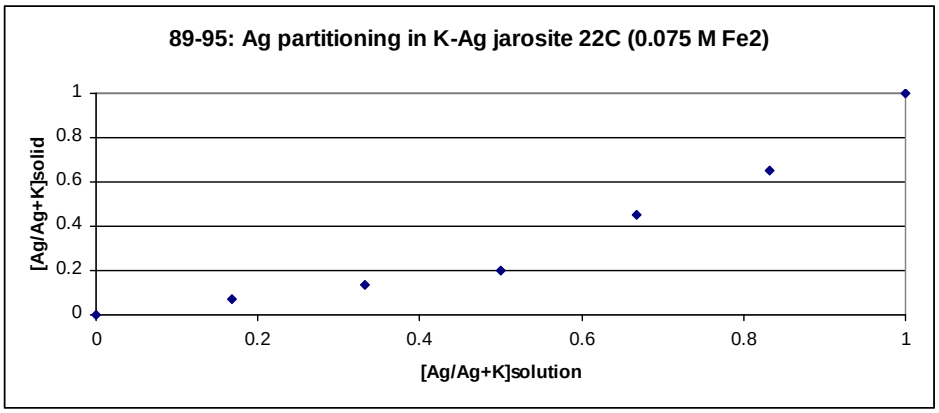

Figure 5.10g: JS89-95: 0.06 M (K+Ag), 0.075 M $Fe_2(SO_4)_3.5H_2O$ at 22ºC.

In comparison to the K-Ag-jarosites, the partitioning coefficients for Ag in the Na-Ag-jarosite series are, in general, greater than 1 (the mean value for the seven series of Na-Ag-jarosite compounds is 1.302), indicating that Ag is preferentially incorporated in these products compared to Na. The partitioning coefficients for Ag in the different Na-Ag-jarosite series synthesised in solutions containing 0.22 *M* Na+Ag and 0.51 *M* $Fe_2(SO_4)_3.5H_2O$ are 1.326 (JS12-20), 1.335 (JS30-38), 0.819 (JS66-70), 1.252 (JS71, 85-88) and 1.458 (JS72, 77-80) (Table 5.12). The coefficient of 0.819 for the series JS66-70 appears to be an anomalous result. These values compare with partitioning coefficients for Ag in the Na-Ag-jarosite series synthesised in solutions containing 0.12 *M* Na+Ag (100 ml solution) or 0.06 *M* Na+Ag (200 ml solution) and 0.15 *M* $Fe_2(SO_4)_3.5H_2O$ or 0.075 *M* $Fe_2(SO_4)_3.5H_2O$, respectively, of 1.415 (JS49-54 & 61) and 1.506 (JS95-101). The series (JS49-54 & 61 and JS95-101) synthesised from solutions with the lowest concentrations of Na+Ag (Fe:[Na+Ag] ratio 2.5:1) in the starting solutions are two of the three series with the highest partitioning coefficients for Ag. However, there are no substantial differences between the partitioning coefficients for Ag in the different Na-Ag-jarosite series (in the other series, the Fe:[Na+Ag] ratio is 4.64:1), apart from the anomalous result for series JS66-70. The partitioning coefficients for Ag in Na-Ag-

jarosite in this project are lower than, but approximately consistent with, the reported limiting partitioning coefficient of ~ 2.0 for Ag in Na-jarosite synthesised at 97ºC from dilute silver solutions of 0.03 *M* [Ag_2SO_4 + Na_2SO_4] in sulphate media containing 0.2 *M* $Fe_2(SO_4)_3$ (Dutrizac and Jambor, 1987).

The two Na-Ag-jarosite series synthesised at low temperature (22ºC) have the highest relative partitioning coefficients for Ag: 1.458 for series JS72 & 77-80 and 1.506 for JS95-101. This is consistent with the results for the two K-Ag-jarosite series synthesised at 22ºC, which had the lowest Ag partitioning coefficients of the K-Ag-jarosite series and, concomitantly, relative partitioning was highest for the preferentially incorporated cation, K. In the two Na-Ag-jarosite series synthesised at 22ºC (JS72 & 77-80 and JS95-101), the relative partitioning coefficients for Ag are highest (3.168 and 3.15) in the compounds (JS78 and 97, respectively) synthesised from solutions with the lowest Ag concentrations in the respective series (see Table 5.12); therefore there is a relatively high initial uptake of Ag into the Na-Ag-jarosite compounds. In both series, the partitioning coefficients then progressively decrease as the concentration of Ag is increased in the synthesis solutions, until the partitioning coefficient is 1 in the Ag-only compounds. This trend of decreasing partitioning coefficients for these two series is illustrated in Figures 5.10h and 5.10i. In these figures, the curve described by the points shows a progressive change towards a lower gradient away from the source, which indicates that the Ag concentration in solution is increasingly approaching saturation point relative to incorporation of Ag into the jarosite structure. This is the case even though there is substantial difference between the Ag concentrations in the synthesis solutions of the two series: in series JS72 & 77-80, Ag concentration varies between 0.055 and 0.22 *M*; and in series JS95-101, Ag concentration is 0.01-0.06 *M*.

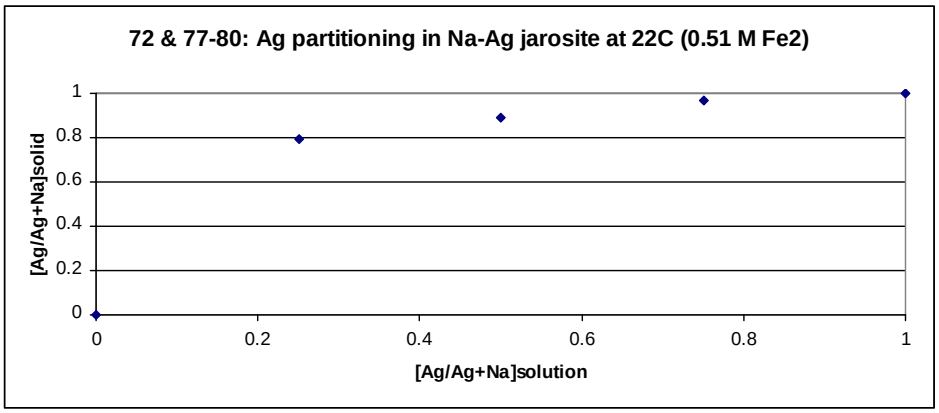

Figure 5.10h: JS72,77-80: 0.22 M (Na+Ag), 0.51 M $Fe_2(SO_4)_3.5H_2O$ at 22ºC.

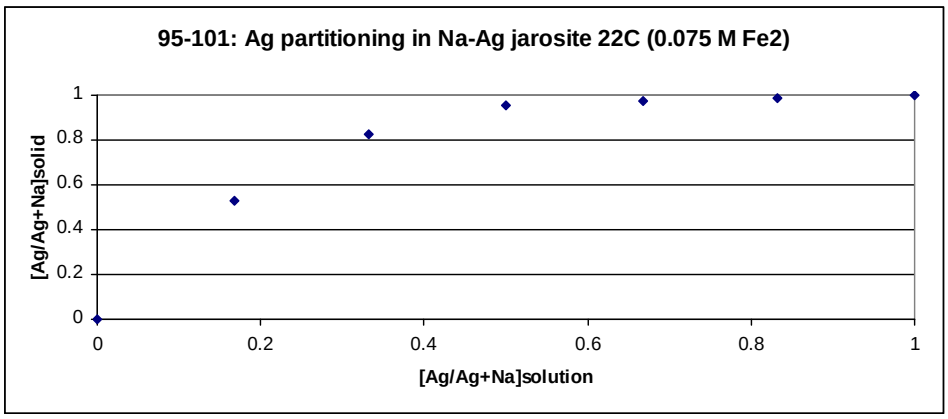

Figure 5.10i: JS95-101: 0.06 M (Na+Ag), 0.075 M $Fe_2(SO_4)_3.5H_2O$ at 22ºC.

The Na-Ag-jarosite series JS12-20 and JS30-38 synthesised at 97ºC and from solutions containing 0.22 *M* Na+Ag and 0.51 *M* $Fe_2(SO_4)_3.5H_2O$ also show relatively high Ag partitioning coefficients (2.116 and 2.544) for the products (JS16 and 34, respectively) synthesised from solutions containing the series' lowest Ag concentration of 0.055 *M* (see Table 5.12). As with the products synthesised at 22ºC, this indicates relatively high initial uptake of Ag in the Na-Ag-jarosite compounds. The partitioning coefficients then progressively decrease in both series as the concentration of Ag increases in the synthesis solutions, which is illustrated in Figures 5.10j and 5.10k by the curve formed by the points having a progressively lower gradient. This indicates that, as with the products synthesised at 22ºC, the Ag

concentration in solution is increasingly approaching saturation point relative to incorporation of Ag into the jarosite structure.

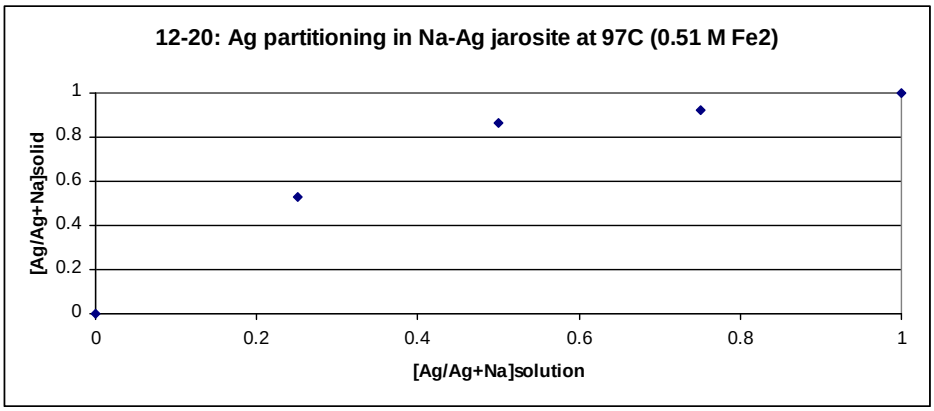

Figure 5.10j: JS12-20: 0.22 M (Na+Ag), 0.51 M $Fe_2(SO_4)_3.5H_2O$ at 97ºC.

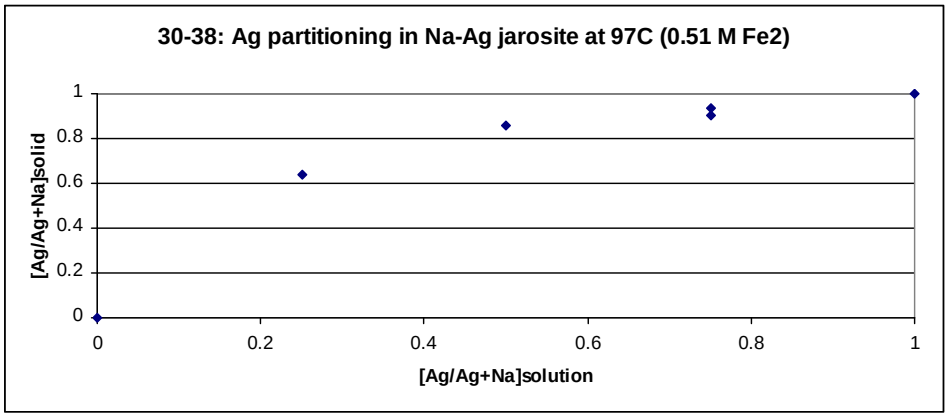

Figure 5.10k: JS30-38: 0.22 M (Na+Ag), 0.51 M $Fe_2(SO_4)_3.5H_2O$ at 97ºC.

Two of the three Na-Ag-jarosite series synthesised at 140ºC (JS49-54 & 61 and JS71 & 85-88) show the same trends as the series synthesised at 22ºC and 97ºC of relatively high initial Ag partitioning coefficient values (2.581 and 2.188) in the first intermediate products (JS50 and 86, respectively) and then progressively declining values (see Table 5.12). The trends in the partitioning coefficients' values of these two series are illustrated by the shape of curves formed by the points in Figures 5.10l and 5.10n, which have decreasing gradients after the point for the first intermediate product, indicating slightly declining relative uptake of Ag compared to Na, and possible Ag concentration reaching saturation in the synthesis solutions

relative to Ag incorporated in the jarosite structure. However, the other Na-Ag-jarosite series synthesised at 140ºC (JS66-70) displays a different trend of a relatively low partitioning coefficient (0.544) for the first intermediate product (JS68) and then increasing partitioning coefficients to the value of 1 for the Ag-only product, indicating Ag has a growing preference for incorporation in the jarosite structure as the concentration of Ag in the synthesis solution increases. This trend is illustrated by the shape of curve formed by the points in Figure 5.10m, which shows progressively increasing gradients. Series JS66-70 was synthesised under the same conditions as series JS71 & 85-88 and, therefore, the partitioning coefficients for series JS66-70 are anomalous.

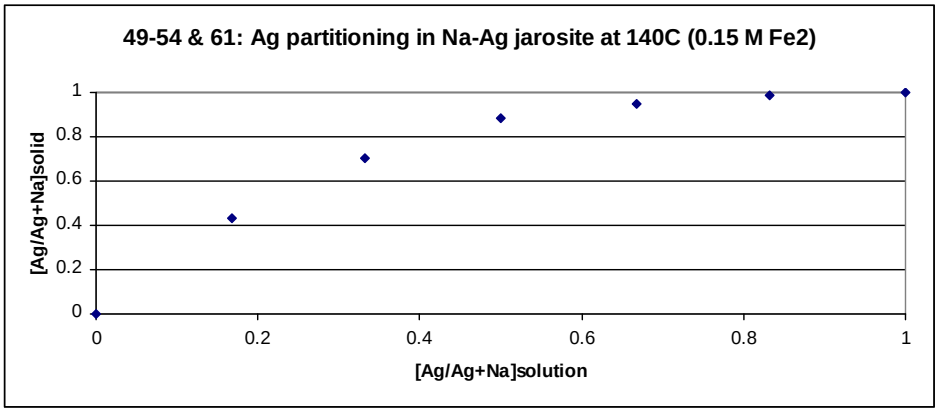

Figure 5.10l: JS49-54,61: 0.12 M (Na+Ag), 0.15 M $Fe_2(SO_4)_3.5H_2O$ at 140ºC.

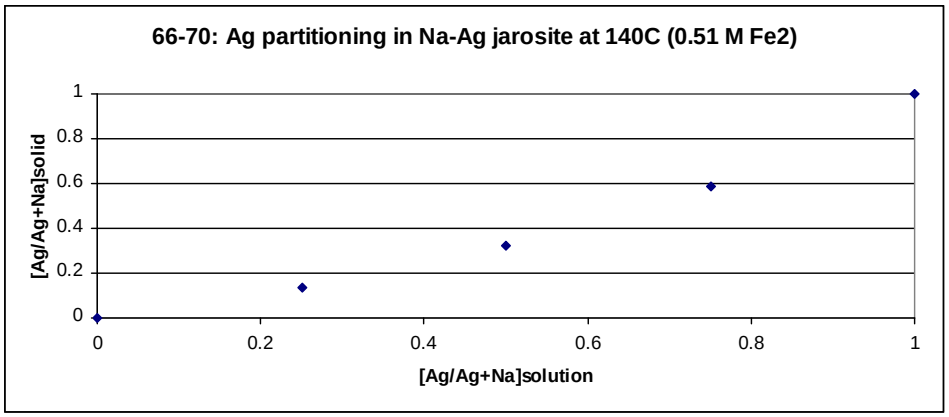

Figure 5.10m: JS66-70: 0.22 M (Na+Ag), 0.51 M $Fe_2(SO_4)_3.5H_2O$ at 140ºC.

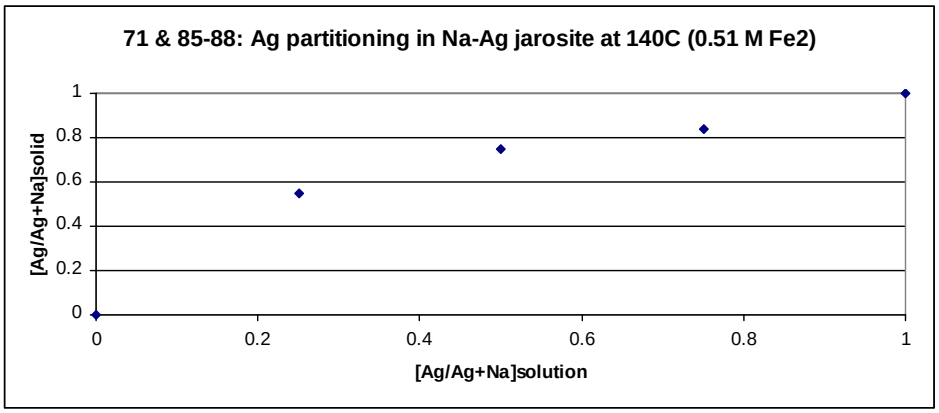

Figure 5.10n: JS71, 85-88: 0.22 M (Na+Ag), 0.51 M $Fe_2(SO_4)_3.5H_2O$ at 140ºC.

Table 5.13: Partitioning coefficients for Ag in Pb-Ag-jarosites as ratio of Ag/Ag+Pb in products to Ag/Ag+Pb in synthesis solutions.

Sample	[Ag/Ag+Pb]j	[Ag/Ag+Pb]sol	P. coeff.
Solutions containing 0.15 M $Fe_2(SO_4)_3.5H_2O$ heated at 140ºC and products dried at 110ºC			
JS43	0	0	0
JS43D	0	0	0
JS44	0.776	0.286	2.713
JS45	0.86	0.5	1.72
JS46	0.938	0.667	1.406
JS46D	0.934	0.667	1.4
JS47	0.973	0.8	1.216
JS48	0.973	0.909	1.07
JS61	1	1	1
JS43-48, 61	**6.454**	**4.829**	**1.337**
Solutions containing 0.075 M $Fe_2(SO_4)_3.5H_2O$ were prepared at 22ºC and products air-dried at 22ºC			
JS95	1	1	1
JS102	0.993	0.998	0.995
JS103	0.967	0.994	0.973
JS104	0.977	0.98	0.997
JS105	0.929	0.909	1.022
JS106	0.957	0.98	0.977
JS107	0	0	0
JS95, 102-107	**5.823**	**5.861**	**0.994**

Key: j = jarosite product; sol. = synthesis solution; P. coeff. = partitioning coefficient. [Ag/Ag+Pb]j = Ag *A*-site occupancy divided by total *A*-site occupancy of Ag and Pb in Pb-Ag-jarosite product. [Ag/Ag+Pb]sol = Ag concentration (*M*) divided by total concentration of Ag and Pb in synthesis solution.

The partitioning coefficients for Ag in the two Pb-Ag-jarosite series are close to or higher than 1 (the series mean is 1.166), which indicates that Ag is preferentially incorporated in the products relative to Pb (see Table 5.13). The partitioning coefficient for Ag in Pb-Ag-jarosite series JS43-48 & 61 synthesised in solutions containing 0.06-12 *M* Pb+Ag and 0.15 *M* $Fe_2(SO_4)_3.5H_2O$) (Fe:[Pb+Ag] ratio 2.5:1 to 5:1) is 1.337. The partitioning coefficient for Ag in Pb-Ag-jarosite series JS95 & 102-107 synthesised in solutions containing 0.05013-0.06 *M* Pb+Ag and 0.075 *M* $Fe_2(SO_4)_3.5H_2O$ (Fe:[Pb+Ag] ratio 2.5:1 to ~3:1) is 0.994, so is close to

unity. However, the concentrations of Pb in the synthesis solutions of this series are low (ranging between 0.00013 *M* and 0.005 *M*), which were chosen because of the low solubility of $PbSO_4$; therefore, the overwhelming predominance of Ag means the series result provides a limited indicator of relative partitioning between Ag and Pb.

In Pb-Ag-jarosite series JS43-48 & 61, the product (JS44) synthesised from a solution containing the lowest Ag concentration of 0.02 *M* has the highest Ag partitioning coefficient of 2.713 (see Table 5.13), indicating relatively high initial uptake of Ag in the Pb-Ag-jarosite structure. The partitioning coefficients then progressively decrease in the series as the concentration of Ag increases in the synthesis solutions, which is illustrated in Figure 5.10o by the curve formed by the points having a progressively lower gradient. This indicates that the Ag concentration in solution is increasingly approaching saturation point relative to incorporation of Ag into the jarosite structure. In series 95 & 102-107, no such trend is discernible (see Figure 5.10p) as the Ag concentration is constant at 0.05 *M* in the synthesis solutions, except for 0.06 *M* in the Ag-only synthesis experiment (JS95).

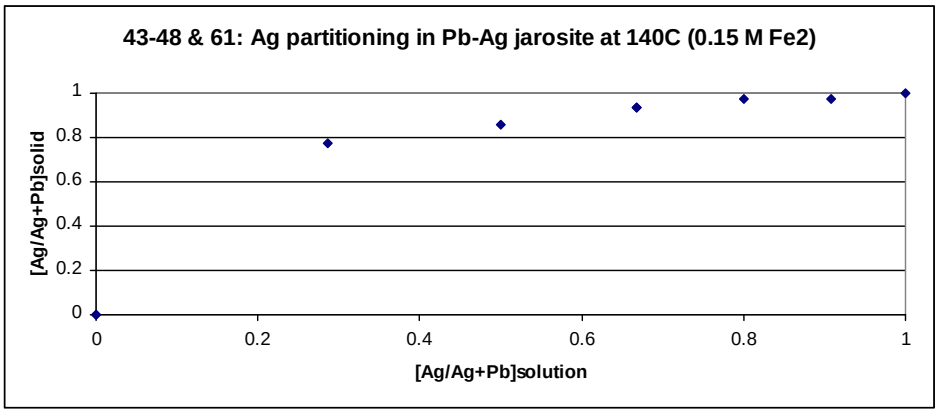

Figure 5.10o: JS43-48 & 61: 0.12 M (Pb+Ag), 0.15 M $Fe_2(SO_4)_3.5H_2O$ at 140ºC.

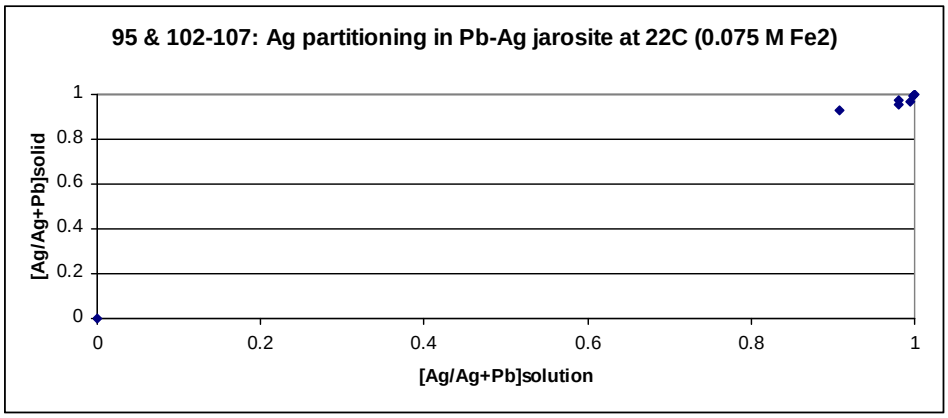

Figure 5.10p: JS95&102-107: 0.06&0.025 M Ag, 0.075 M $Fe_2(SO_4)_3.5H_2O$ at 22ºC.

5.1.3 Relationship of unit-cell parameters to other characteristics

5.1.3.1 Ionic radii of *A*-site cations

5.1.3.1.1 XRD analysis

In the data from powder XRD analysis using Cu radiation, the different positions (*d* values) of the *hkl* 003 and 006 reflections of synthesised K-Ag-H_3O-jarosite and Na-Ag-H_3O-jarosite samples indicate variations in *c*-axis parameters of the unit cells of the compounds, which are caused by differences between the ionic radii of cations substituting in the *A* site of the crystal structure (see Tables 4.7 and 4.8). This study's XRD results provide contradictory evidence on whether Ag^+ in the *A* site is likely to be in 12-fold coordination or in nine-fold coordination, the latter being reported by a jarosite crystal structure study (Groat *et al.*, 2003). The K-Ag-H_3O-jarosite compounds show generally declining *d*-spacing values in each series as K content declines and Ag content increases, which is consistent with the smaller Ag^+ cation (ionic radius of 1.48 Å in 12-fold coordination) compared with the K^+ cation (1.64 Å) and the H_3O^+ cation (1.52 Å). In Na-Ag-H_3O-jarosite series 12-20 and 30-38/38D (both synthesised at 97°C) and series 49-54 & 61 (synthesised at 140°C), the 003 and 006 reflections show a generally declining trend of *d*-values as Ag increases, which may indicate the Ag^+ cation has a smaller radius than the Na^+ cation (1.39 Å). If it

does, this may indicate Ag^+ is in nine-fold coordination, for which an experimental radius of 1.35-1.36 Å has been reported (Groat et al., 2003). An alternative explanation is that the declining trend of *d*-values in these series may be the result of the relatively high H_3O content in the Na-Ag-H_3O-jarosite compounds synthesised from starting solutions containing high Na. However, Na-Ag-H_3O jarosite series 71 & 85-88 (synthesised at 140°C) shows a generally increasing trend of *d*-values from 5.613 Å and 2.787 Å in Na-H_3O-jarosite to 5.627 Å and 2.792 Å in Ag-H_3O-jarosite, which is consistent with the Ag^+ cation having a larger radius than Na^+ and, therefore, being in 12-fold coordination. The other three series of Na-Ag-H_3O-jarosite products do not provide clear increasing or decreasing trends in the *d*-values. Theoretically, possible explanations for the lack of trends in the *d*-values of these series may be low Na content and high H_3O content or, in other cases, low Fe occupancy and consequent relatively low H_3O content and vacancies in the *A* site. However, the chemical compositional data are not consistent with these explanations for the changes in *d*-values of series 66-70 and 95-101, although the *d*-values are smaller for the Ag-H_3O-jarosite compounds than the Na-H_3O-jarosite compounds. The chemical compositional data for series 72 & 77-80 are potentially consistent with these explanations, except for Ag-H_3O-jarosite sample 72, which has anomalously large *d*-values more consistent with the JCPDS pattern for hydronium jarosite, even though the H_3O occupancy is 0.37, and larger than those for Na-H_3O-jarosite sample 77.

5.1.3.1.2 Rietveld refinement

Rietveld refinement of XRD data indicates the K-Ag-H_3O-jarosite and Na-Ag-H_3O-jarosite compounds show a trend of increasing *a* parameter and decreasing *c*

parameter as K^+ or Na^+ occupancy of the *A* site declines and Ag^+ occupancy increases, which is consistent with reported end-member values for jarosite, natrojarosite and argentojarosite (see Table 4.9). In the Na-H_3O-jarosite product with very high H_3O occupancy of the *A* site (sample 49), the refined *c* parameters are higher than those of the next Na-Ag-H_3O-jarosite products in the series (samples 34 and 50 respectively), which is consistent with reported end-member values for natrojarosite, hydronium jarosite and argentojarosite.

The refined unit-cell parameters for K-Ag-H_3O- and Na-Ag-H_3O-jarosite in Table 4.9 are consistent with reported *a*-axis and *c*-axis values for K-, Na-, Ag- and H_3O-jarosites. In the K-Ag-H_3O-jarosite series (04-12, 22-30, 55-61 and 72-76), there is a trend of increasing *a* parameter as K site occupancy declines and Ag occupancy increases, while the *c* parameter decreases, which is consistent with reported end-member values (May *et al.*, 1973; Dutrizac and Kaiman, 1976; Kato and Miura, 1977; Basciano and Peterson, 2007). In the Na-Ag-H_3O-jarosite series (12-20; 30-38; 49-54 and 61; 72, 78 and 80), the trend is for the *a* parameter to increase as Na site occupancy declines and Ag occupancy increases, while the *c* parameter declines, which is consistent with the ionic radius of Ag^+ in jarosite being smaller than Na^+ (May *et al.*, 1973; Dutrizac and Kaiman, 1976; Kato and Miura, 1977; Basciano and Peterson, 2008).

Tables 4.11a and 4.11b show isotropic displacement (U_{iso}) values for the Rietveld refined structures of the selected K-, Na- and Ag-bearing synthesised jarosite compounds. These U_{iso} values may provide information on whether Ag^+ in argentojarosite has an ionic radius of 1.35-1.36 Å and is in nine-fold coordination or is in 12-fold coordination (ionic radius 1.48 Å) (Groat *et al.*, 2003). It is suggested by Groat *et al.* (2003) that in argentojarosite the internal energy (*U*) values

(displacement values) of Ag^+ are anomalously high and this could indicate the Ag atom is located slightly off the *A* site, with correspondingly reduced occupancy, because the void is too large for the Ag^+ ion, which tries to locally achieve lower coordination numbers. In this project, the U_{iso} values generated by Rietveld refinement of K-Ag-H_3O-jarosite compounds indicate no consistent relationship is identifiable between the values of K and Ag. In Table 4.11a, in four samples, the U_{iso} value for Ag^+ is higher than the value for K^+: JS26 and 28 (synthesised at 97ºC) and JS57 and 58 (synthesised at 140ºC). In addition, in the series JS55-61, the U_{iso} value for Ag^+ (0.06) in Ag-H_3O-jarosite sample 61 is higher than the value for K^+ (0.025) in K-H_3O-jarosite sample 55. However, in six samples, the U_{iso} value for K^+ is higher than the value for Ag^+: JS24 (synthesised at 97ºC) , JS59 and 60 (synthesised at 140ºC), and JS74, 75 and 76 (synthesised at 22ºC). In addition, in the series JS22-30 and JS72-76, the U_{iso} values for K^+ (0.058 and 0.042, respectively) in the K-H_3O-jarosite compounds are higher than the values for Ag^+ (0.057 and 0.025, respectively) in the Ag-H_3O-jarosite compounds. In four samples, the U_{iso} value for Ag^+ is the same as the value for K^+: JS04, 08 and 10 (synthesised at 97ºC) and JS56 (synthesised at 140ºC). In addition, in the series JS04-12 (synthesised at 97ºC), the U_{iso} value (0.025) for Ag^+ in the Ag-H_3O-jarosite compound is the same as the value for K^+ in the K-H_3O-jarosite compound.

In Table 11b, in Na-Ag jarosite samples 51 (synthesised at 140ºC), 78 and 80 (both synthesised at 22ºC), the U_{iso} values for Ag^+ (0.032, 0.061 and 0.068, respectively) are higher than the values for Na^+ (0.02, 0.025 and 0.025, respectively). In series JS30-38 (synthesised at 97ºC) and JS49-54 & 61 (synthesised at 140ºC), the U_{iso} values for Ag^+ (0.057 and 0.06, respectively) in the Ag-H_3O-jarosite compounds are higher than the values for Na^+ (0.025 in both series) in Na-H_3O-jarosite. The U_{iso}

value for Na^+ (0.209) is higher than the value for Ag^+ (0.025) only in the respective Na-H_3O- and Ag-H_3O-jarosite compounds of series JS12-20 (synthesised at 97ºC). In samples 16, 18, 20, 34, 36 and 38 (synthesised at 97ºC) and samples 50, 52, 53 and 54 (synthesised at 140ºC), the U_{iso} value for Ag^+ (0.025) is the same as the value for Na^+.

5.1.3.1.3 Raman spectroscopy

Studies have compared the unit-cell parameters of jarosite group compounds with the wavenumbers of their modes (Sasaki et al., 1998; Frost et al., 2004, 2006; Murphy et al., 2009). Unit-cell parameters vary with the size of the ionic radius of the cation in the *A* site of the jarosite structure (Brophy and Sheridan, 1965; Desborough et al., 2010). A relationship between SO_4 band position and ionic radius in jarosite has been reported, specifically the symmetric stretching band (v_1SO_4) (Frost *et al*., 2004); ionic radius affects the polarisability of SO_4^{2-} vibrations. In theory, unit-cell parameter differences indicate different bond lengths due to size of ionic radii, which potentially are related to bonding strength and may result in changes in the wavenumbers of vibrational modes (Murphy et al., 2009). Reportedly, Raman spectra of jarosite-group compounds are characterised by a tendency for wavenumbers assigned to vibrational modes $v_1(SO_4^{2-})$ and $v_3(SO_4^{2-})$, and three vibrational modes of Fe-O bonds, to decrease with an increase in the *c* unit-cell parameter, whereas wavenumbers assigned to $v_2(SO_4^{2-})$ and $v_4(SO_4^{2-})$ are independent of the value of *c* (Sasaki et al., 1998); however, Frost et al. (2006) report the relationship is tenuous, and is questionable for bands assigned to Fe-O vibrations. In addition, it has been reported that previous studies have found no

correlation between the *c* parameter and any of the νSO_4 Raman wavenumbers (Murphy et al., 2009).

In this project, differences in Raman spectra are evident between compounds with different compositions of Ag and/or K or Na cations, especially in the νSO_4 and νOH bands. The spectra differences indicate differences in bonding and symmetry of the compounds as a result of *A*-site cation composition of the products. For the νOH bands, a decrease in wavenumbers is evident between the end-members of the K-Ag-H_3O-, Na-Ag-H_3O and Pb-Ag-H_3O-jarosite series, indicating decreasing bond strength. For the ν_1SO_4 band, there are increasing wavenumber trends as Ag content increases in the different K-Ag-H_3O-jarosite series synthesised at 22ºC, 97ºC and 140ºC. By contrast, there is no change in wavenumbers across two of the Na-Ag-H_3O-jarosite series (synthesised at 22ºC and 140ºC), whereas for series 30-38 (synthesised at 97ºC) there is no change in wavenumbers between the end-members but a general wavenumber increase in the intermediate members as Ag content increases. There is no change in wavenumbers in the Pb-Ag-H_3O-jarosite series. For the ν_3SO_4 band, there are increasing wavenumber trends as Ag content increases in the K-Ag-H_3O-jarosite series synthesised at 22ºC and 140ºC; in the series synthesised at 97ºC there is no change in wavenumber between the end-members and no clear trend in the wavenumbers of the intermediate members. In the Na-Ag-H_3O-jarosites, there is an increasing wavenumber trend as Ag content increases in the series synthesised at 97ºC and decreasing trends in the series synthesised at 22ºC and 140ºC. In the Pb-Ag-H_3O-jarosite series, there is an increasing wavenumber trend as Ag content increases. In other modes of the K-H_3O-jarosite compounds there is no consistent evidence of whether the various Raman modes of Ag-H_3O-jarosite compounds have higher wavenumbers than K-H_3O-jarosite compounds and

so have higher bonding energies. None of the other modes for Ag-H_3O-jarosite compounds have higher wavenumbers than the Na-H_3O equivalents, but some have the same wavenumbers. Consequently, no consistent trend is discernible in the wavenumbers of the assigned modes, so there is no clear evidence of whether bond strength grows with increasing Ag content of the jarosite compounds.

Table 5.14 compares the Raman wavenumbers with the Rietveld refined *c*-axis parameters of selected synthesised K-Ag-H_3O- and Na-Ag-H_3O-jarosite compounds

Table 5.14 Rietveld-refined *c* parameters and Raman wavenumbers of selected[1] jarosite compounds synthesised at 97°C, 140°C and 22°C.

Number	Compound	Temp (°C)	*c* parameter	*v*OH	$v_3(SO_4)$	$v_1(SO_4)$	$v_4(SO_4)$	$v_2(SO_4)$
JS22	K-H_3O	97	17.0823	3411.7	1110.1	1009.3	627.16	432.6
JS24	K-Ag-H_3O	97	16.9522	3407.6	1106.1	1006.7	627.3	438.26
JS26	K-Ag-H_3O	97	16.8897	3406.19	1104.39	1008.8	623.81	432.44
JS28	K-Ag-H_3O	97	16.8358	3410.4	1108.8	1009.5	623.16	435.5
JS30	Ag-H_3O	97	16.5995	3393.7	1110.1	1013.5	624.4	438.12
JS55	K-H_3O	140	17.1687	3412.08	1101.22	1007.2	623.81	432.44
JS56	K-Ag-H_3O	140	17.063	3416.78	1101.22	1007.2	623.81	430.73
JS57	K-Ag-H_3O	140	16.9781	3408.55	1102.81	1008.8	623.81	432.44
JS58	K-Ag-H_3O	140	16.8922	3403.84	1101.22	1008.8	622.13	434.16
JS59	K-Ag-H_3O	140	16.8087	3397.95	1101.22	1008.8	622.13	434.16
JS60	K-Ag-H_3O	140	16.6935	3384.97	1104.39	1010.4	622.13	437.58
JS61	Ag-H_3O	140	16.5913	3384.97	1104.39	1012	622.13	437.58
JS73	K-H_3O	22	17.0031	3414.71	1103.18	1007.58	624.21	432.85
JS74	K-Ag-H_3O	22	16.9719	3413.26	1102.81	1007.2	623.81	432.44
JS75	K-Ag-H_3O	22	16.9411	3410.01	1104.77	1009.18	624.21	432.85
JS76	K-Ag-H_3O	22	16.8748	3411.18	1104.77	1009.18	620.85	434.56
JS72	Ag-H_3O	22	16.5551	3373.43	1104.77	1012.39	622.53	437.99
JS32	Na-H_3O	97	16.7231	3399.2	1108.7	1013.5	625.78	439.5
JS34	Na-Ag-H_3O	97	16.6375	3396.77	1105.97	1012	622.13	435.87
JS36	Na-Ag-H_3O	97	16.6155	3393.8	1107.4	1012.2	621.78	436.88
JS38	Na-Ag-H_3O	97	16.6103	3388.2	1110.1	1013.5	624.4	438.12
JS30	Ag-H_3O	97	16.5995	3378.5	1110.1	1013.5	624.4	438.12
JS49	Na-H_3O	140	16.8017	3405.3	1106.35	1012.39	622.53	437.99
JS50	Na-Ag-H_3O	140	16.7537	3401.76	1106.35	1012.39	622.53	437.99
JS51	Na-Ag-H_3O	140	16.6663	3398.23	1106.35	1012.39	622.53	436.28
JS52	Na-Ag-H_3O	140	16.6193	3384.07	1106.35	1012.39	622.53	437.99
JS53	Na-Ag-H_3O	140	16.6019	3382.89	1106.35	1012.39	622.53	437.99
JS54	Na-Ag-H_3O	140	16.5989	3393.51	1104.77	1012.39	622.53	437.99
JS61	Ag-H_3O	140	16.5913	3384.97	1104.39	1012	622.13	437.58
JS77	Na-H_3O	22	n.d.	3401.76	1107.94	1012.39	624.21	441.41
JS78	Na-Ag-H_3O	22	16.5654	3389.69	1106.35	1012.39	622.53	439.7
JS79	Na-Ag-H_3O	22	n.d.	3384.97	1105.97	1012	622.13	439.29
JS80	Na-Ag-H_3O	22	16.5535	3388.79	1106.35	1012.39	622.53	437.99
JS72	Ag-H_3O	22	16.5551	3373.43	1104.77	1012.39	622.53	437.99

Key: 1 Selected jarosite sample series are representative of the different synthesis starting solutions and temperatures used.

in this study. (Selected jarosite sample series are representative of the different synthesis starting solutions and temperatures used.) Most of the assigned Raman modes of the synthesised jarosite series (20 out of 30) have poor or fairly poor linear relationships (R^2 values of ≤ 0.6082) between the Raman wavenumbers and the *c*-axis parameters; however, in one-third (10 out of 30) of the modes of the different series (eight for K-Ag-H_3O-jarosite compounds; two for Na-Ag-H_3O-jarosite compounds) there is a good linear relationship between the wavenumbers and the *c*-axis parameters (see Figure 5.11). Good or fairly good linear relationships (R^2 values) were identified in sample numbers 22-30 (K-Ag-H_3O) for *v*OH (0.7859); numbers 55-61 (K-Ag-H_3O) for *v*OH (0.9005), v_1SO_4 (0.8992), v_4SO_4 (0.7187) and v_2SO_4 (0.8304); numbers 72-76 (K-Ag-H_3O) for *v*OH (0.9605), v_1SO_4 (0.9168) and v_2SO_4 (0.9661); numbers 49-54 and 61 (Na-Ag-H_3O) for *v*OH (0.7783); and numbers 72, 78 and 80 (Na-Ag-H_3O) for v_2SO_4 (0.9847) (see Figure 4.1.3). There are no Rietveld refinement data for the Pb-H_3O- and Pb-Ag-H_3O-jarosite products.

Figure 5.11 R^2 values of Raman wavenumbers (cm^{-1}) of modes *v*OH, v_1SO_4, v_2SO_4, v_3SO_4 and v_4SO_4 compared with refined *c* parameters for selected series of K-Ag-H_3O-jarosite compounds synthesised at 22ºC, 97ºC and 140ºC.

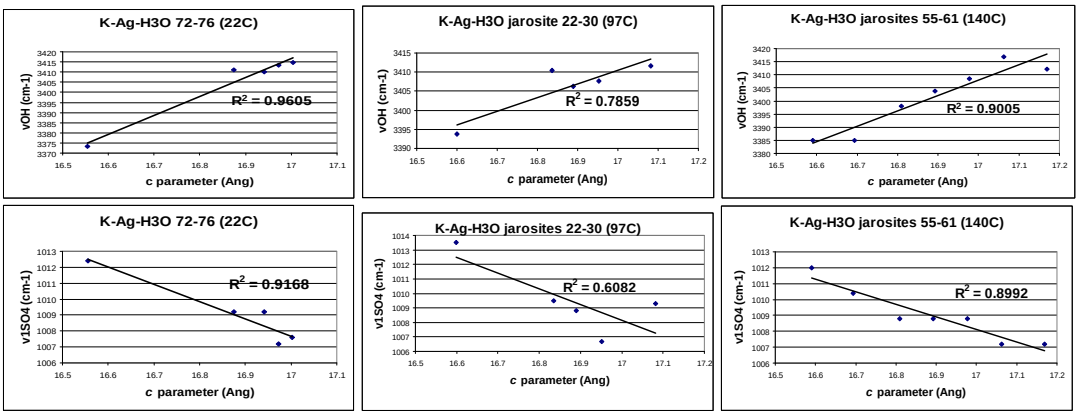

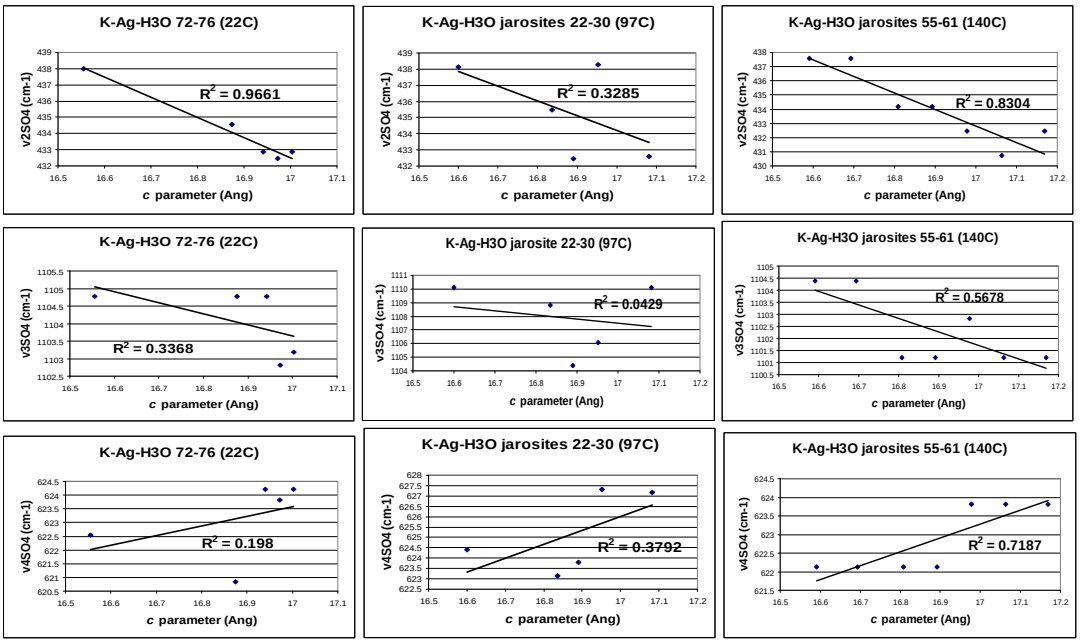

Figure 5.12 R^2 values of Raman wavenumbers (cm^{-1}) of modes νOH, ν_1SO_4, ν_2SO_4, ν_3SO_4 and ν_4SO_4 compared with refined *c* parameters for selected series of Na-Ag-H_3O-jarosite compounds synthesised at 22ºC, 97ºC and 140ºC.

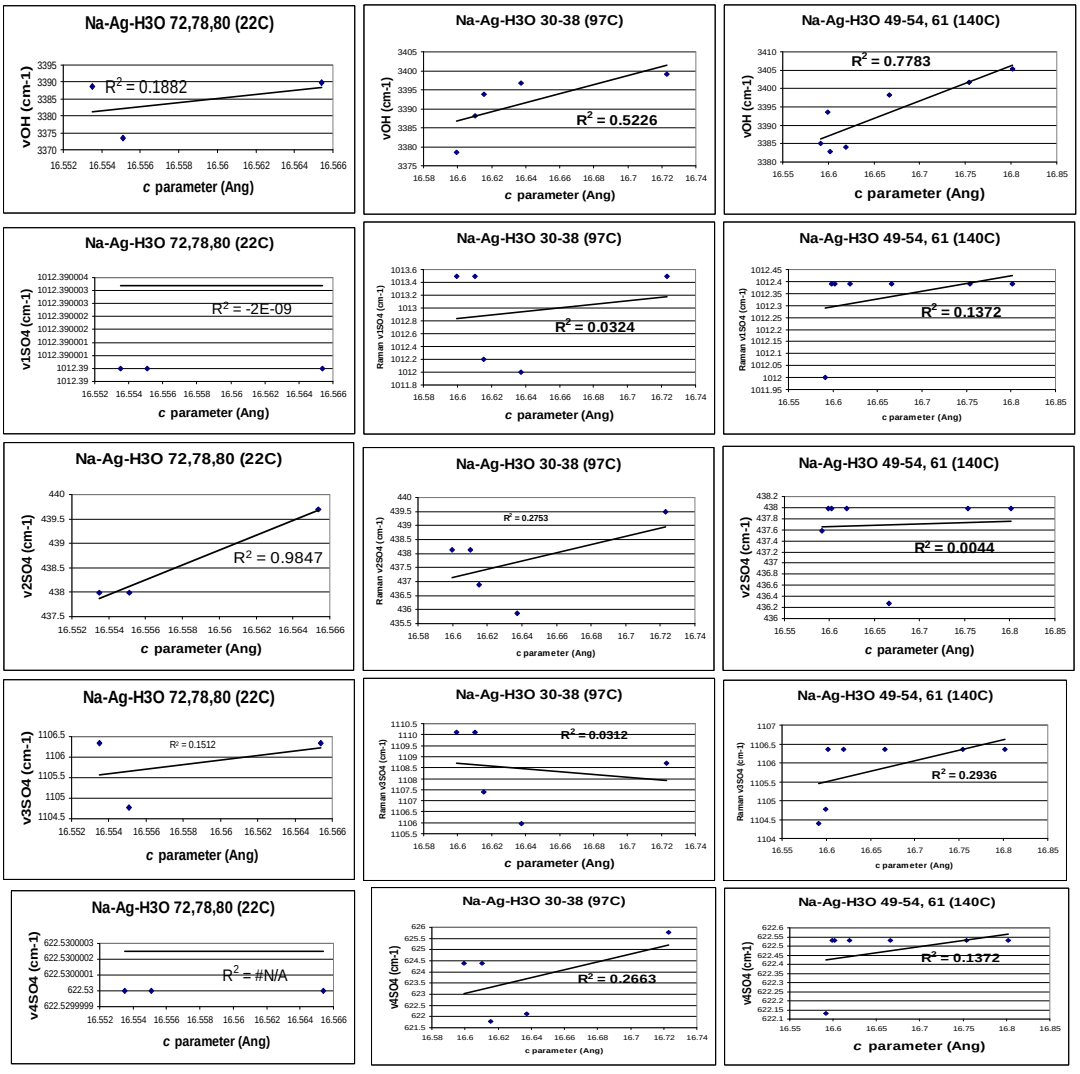

5.1.4 Possibility of solid solution in Ag-containing K-, Na- or Pb-jarosite compounds

The ICP-OES results show the different series of jarosite compounds have good linear relationships between the contents of the K, Na or Pb cation and the Ag cation in the products (see Tables 4.17, 4.18 and 4.19), if outliers of anomalous contents in some of the series are removed (Rollinson, 1993). Of the K-Ag-H_3O jarosite products, the R^2 values are: series 04-12 and 22-30 (both synthesised at 97ºC), 0.9877 and 0.996, respectively; series 57-61, 62-66, and 71 & 81-84 (all synthesised at 140ºC), 0.993, 0.7949 and 0.9918, respectively; and series 73-75 and 89-95 (both synthesised at 22ºC), 0.8981 and 0.9999, respectively. Of the Na-Ag-H_3O jarosite products, the R^2 values are: series 12-20 and 30-38 (both synthesised at 97ºC), 0.996 and 0.9374, respectively; series 50-54 & 61, 66-70, and 71 & 85-88 (all synthesised at 140ºC), 0.9989, 0.8916 and 0.9908, respectively; and series 77-79 and 95-101 (both synthesised at 22ºC), 0.9999 and 0.9989, respectively. The good linear relationships of these series indicate solid solution between synthetic Ag-H_3O-jarosite and both K-H_3O-jarosite and Na-H_3O-jarosite at low temperature (22ºC), elevated temperature (97ºC) and high temperature (140ºC) of synthesis. This finding is also supported by the partitioning coefficients for Ag in K-H_3O- and Na-H_3O-jarosites based on the combined data from the analysis techniques of *A*-site occupancies (see section 5.2.2).

The partitioning coefficients from the combined data also indicate solid solution between Ag-H_3O-jarosite and Pb-H_3O-jarosite in sample series JS43-48 & 61 (synthesised at 140ºC) and series 95 & 102-105 (synthesised at 22ºC); however, the low Pb contents make such a conclusion problematic. From the ICP-OES results,

the R^2 values for Pb-Ag-H_3O-jarosite products are: series 43-48 & 61, 0.9347; and series 95 & 102-105, 0.9582. Despite the good linear relationships indicated by these R^2 values, because the samples contain only low levels of Pb (*A*-site occupancies vary between 0 and 0.179 in the 140ºC series and 0 and 0.258 in the 22ºC series), this indicates problems of Pb entering the jarosite structure, probably because of the unit cell doubling to accommodate Pb^{2+} in the structure. One study has reported an incomplete solid solution exists between jarosite and plumbojarosite (Basciano and Peterson, 2010), with XRD analysis showing no peak broadening indicating non-homogeneity, only distinct peaks attributable to either jarosite or plumbojarosite. In the study's jarosite synthesis experiments involving solutions containing varying mixtures of K and Pb, it was found plumbojarosite first precipitates with 85 mol. % Pb in the solution and plumbojarosite only will precipitate with 99 mol. % Pb in the solution. However, other studies have reported substitution involving K^+ and Pb^{2+} to be extensive in jarosite (De Oliveira et al., 1996; Roca et al., 1999). Another study reports Pb-jarosite forms a solid-solution series with monovalent jarosites, but the series are not crystallographically perfect because order-disorder often results in superstructure effects in Pb-rich members, with a *c* axis of 34 Å (double the axis length of monovalent jarosites) in Pb-jarosite (Dutrizac and Jambor, 1984). In synthetic systems, the solid solution between Ag-Pb (± H_3O) and Ag-K (± H_3O) has been reported to be complete (Dutrizac and Jambor, 1984). In addition, extensive solid solution between Ag-rich and Pb-rich jarosites has been reported, but end-member compositions have not been achieved in syntheses because of partial replacement of non-ferrous metals by hydronium (Dutrizac and Jambor, 1984). It has been suggested, the solid solution series Pb-Ag-H_3O is disrupted by a region in which two jarosite phases (near end-member Pb-rich and Ag-rich phases) are present

(Dutrizac and Jambor, 1984). In this project, Pb-rich phases have not been achieved; the preference of H_3O over Pb for the jarosite *A* site has resulted, according to the ICP-AES results, in highest Pb occupancies of 0.179 (series 43-48 & 61) and 0.258 (series 95 & 102-107), from starting solutions containing 0.06 *M* Pb and 0.001 *M* Pb, respectively.

5.1.5 Other discussion of Ag-containing K-, Na- or Pb-jarosite compounds

5.1.5.1 *A*-O2 and *A*-O3 bond lengths

Rietveld refinement of the XRD data shows that, in the K-Ag-H_3O- and Na-Ag-H_3O-jarosite sample series synthesised at 22ºC and 140ºC, there are trends of generally declining bond lengths for both *A*-O2 and *A*-O3 as K^+ or Na^+ occupancy of the *A* site declines and Ag^+ occupancy increases (Table 5.15 and Figure 5.13). These results indicate the Ag^+ cation in the jarosite structure is smaller than both the K^+ cation and the Na^+ cation. In 12-fold coordination the ionic radius of K^+ is 1.64 Å (Shannon, 1976), Ag^+ is 1.48 Å (Dutrizac and Jambor, 2000) and H_3O^+ is 1.52 Å (Basciano and Peterson, 2008), so the results for the K-Ag-H_3O jarosite series indicate generally increasing bond lengths of *A*-O2 and *A*-O3 as the ionic radius of the cation occupying the *A* site increases (Basciano and Peterson, 2010). In K-Ag-H_3O jarosite sample series 55-61, synthesised at 140°C, sample 56 (K occupancy 0.71, Ag occupancy 0.09) has an *A*-O2 bond length of 2.9872 Å, which decreases to 2.9484 Å in sample 60 (K occupancy 0.34, Ag occupancy 0.55). For the same samples, the *A*-O3 (OH^-) bond lengths decrease from 2.8556 Å for sample 56 to 2.7559 Å for sample 60.

In Na-Ag-H_3O jarosite sample series 49-54 & 61, synthesised at 140°C, sample 50 (Na occupancy 0.16, Ag occupancy 0.23) has an *A*-O2 bond length of

3.0756 Å, which decreases to 2.9374 Å in sample 54, which has a higher Ag content (Na occupancy 0.04, Ag occupancy 0.66). However, the decreasing *A*-O2 bond length trend as Ag^+ increases, including the intermediate samples in the series, is not linear. The *A*-O2 bond length for the Ag-H_3O-jarosite sample in the series is 2.9593 Å, meaning an increase in bond length from sample 54, so the results are inconsistent. However, this is not the case with the *A*-O3 (OH^-) bond lengths for the same samples, which decrease consistently from 2.8043 Å for sample 50 to 2.7424 Å for sample 54. In these Na-Ag-H_3O jarosite series, if the ionic radius of Ag^+ is smaller than that of Na^+, this may mean Ag^+ is in 9-fold coordination (Ag^+ ionic radius 1.35-36 Å, compared with Na^+ 1.39 Å), rather than 12-fold (Ag^+ 1.48 Å), as reported by Groat *et al*. (2003). Another possible explanation for the *A*-O2 bond

Table 5.15. Changes in *A*-O2 and *A*-O3 bond lengths in selected[1] K-Ag-H_3O- and Na-Ag-H_3O-jarosite products as *A*-site cation occupancies vary.

K-Ag-H_3O-jarosite products synthesised at 140ºC			
Sample	***A*-site occupancy**	***A*-O2 (Å)**	***A*-O3 (Å)**
55	K 0.32, Ag 0.00	2.97785	2.84616
56	K 0.71, Ag 0.09	2.98724	2.85561
57	K 0.56, Ag 0.21	2.97751	2.85479
58	K 0.38, Ag 0.35	2.98459	2.85253
59	K 0.46, Ag 0.39	2.96464	2.82147
60	K 0.34, Ag 0.55	2.94844	2.75587
61	K 0.00, Ag 0.76	2.95930	2.73381
K-Ag-H_3O-jarosite products synthesised at 22ºC			
Sample	***A*-site occupancy**	***A*-O2 (Å)**	***A*-O3 (Å)**
73	K 0.67, Ag 0.00	3.00593	2.77891
74	K 0.61, Ag 0.08	3.02113	2.78448
75	K 0.37, Ag 0.19	2.99377	2.84001
76	K 0.37, Ag 0.26	3.0614	2.77527
72	K 0.00, Ag 0.74	2.9951	2.6808
Na-Ag-H_3O-jarosite products synthesised at 140ºC			
Sample	***A*-site occupancy**	***A*-O2 (Å)**	***A*-O3 (Å)**
49	Na 0.47, Ag 0.00	3.04325	2.80482
50	Na 0.16, Ag 0.23	3.0756	2.80433
51	Na 0.22, Ag 0.38	2.98579	2.70981
52	Na 0.17, Ag 0.45	2.84718	2.71940
53	Na 0.06, Ag 0.57	2.89087	2.71332
54	Na 0.04, Ag 0.66	2.93743	2.74239

61	Na 0.00, Ag 0.76	2.95930	2.73381
Na-Ag-H_3O-jarosite products synthesised at 22ºC			
Sample	***A*-site occupancy**	***A*-O2 (Å)**	***A*-O3 (Å)**
72	Na 0.00, Ag 0.74	2.9951	2.6808
77	n.d		
78	Na 0.09, Ag 0.61	2.92830	2.74412
79	n.d.		
80	Na 0.03, Ag 0.68	2.92698	2.73857

Key: 1 Selected samples are representative of low and high temperatures of synthesis.

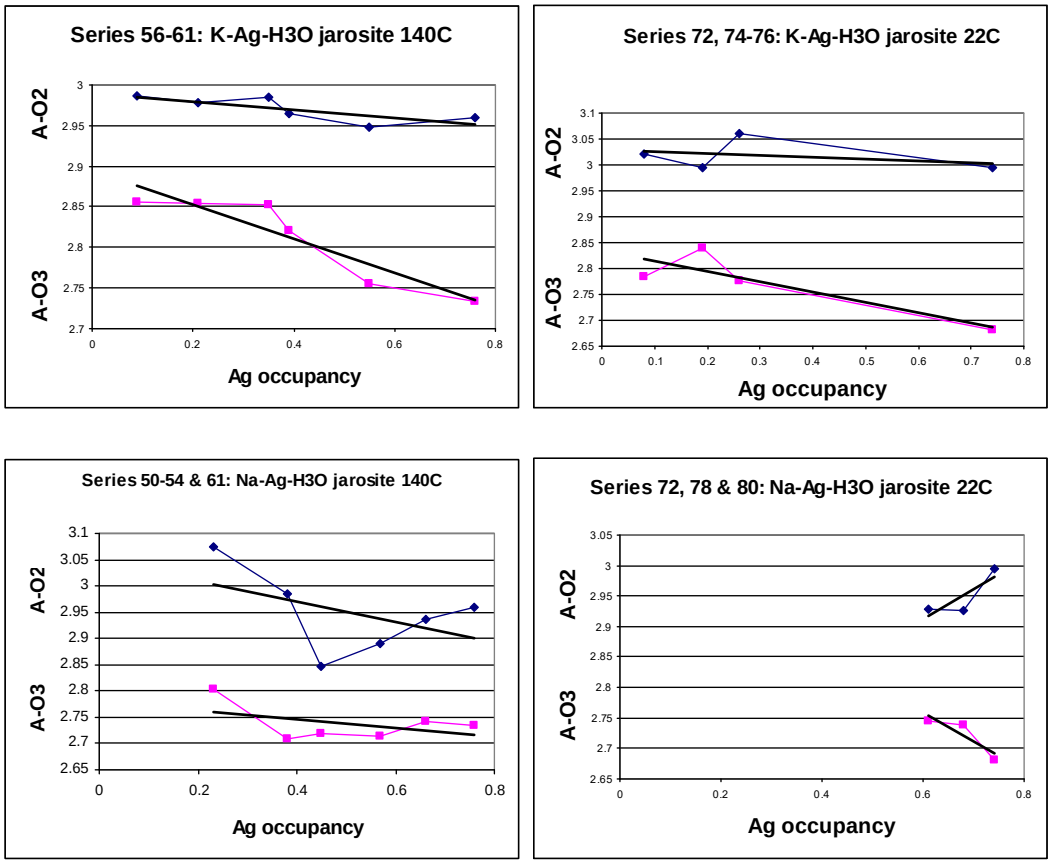

Figure 5.13. Changes in *A*-O2 and *A*-O3 bond lengths in K-Ag-H_3O- and Na-Ag-H_3O-jarosite series as *A*-site cation occupancies vary.

length trend is the proportion of H_3O^+ in the *A* site declines and vacancies increase as Na^+ declines, so reducing bond length. The results for Na-Ag-H_3O jarosite sample series 72, 78 & 80, synthesised at 22°C, shows a decreasing *A*-O3 bond length trend as Ag increases and an increasing *A*-O2 bond length trend.

5.1.5.2 O2 and O3 bond angles

Systematic changes of bond angles with Ag occupancy are evident in the Rietveld refinement results for both K-Ag-H_3O- and Na-Ag-H_3O-jarosite sample series. There are trends in the O2-*A*-O2, O3-*A*-O3 and O2-*A*-O3 bond angles in the K-Ag-H_3O-jarosite sample series, and trends in the O2-*A*-O2 and O2-*A*-O3 bond angles in the Na-Ag-H_3O-jarosite sample series (see Table 4.10). The O2-*A*-O2 bond angles

Table 5.16 Changes in O2-*A*-O2, O2-*A*-O3 and O3-*A*-O3 bond angles (in degrees) in selected[1] K-Ag-H_3O- and Na-Ag-H_3O-jarosite products

K-Ag-H_3O-jarosite products synthesised at 140ºC				
Sample	***A*-site occupancy**	**O2-*A*-O2**	**O2-*A*-O3**	**O3-*A*-O3**
55	K 0.32, Ag 0.00	70.188(2), 109.812(2)	74.242(5), 105.758(5)	59.383(5), 120.617(5)
56	K 0.71, Ag 0.09	68.300(2), 111.700(2)	72.288(6), 107.712(6)	59.323(6), 120.677(6)
57	K 0.56, Ag 0.21	68.094(2), 111.906(2)	71.120(6), 108.880(6)	60.858(6), 119.142(6)
58	K 0.38, Ag 0.35	67.549(1), 112.451(1)	70.265(2), 109.735(2)	61.249(2), 118.751(2)
59	K 0.46, Ag 0.39	67.364(1), 112.636(1)	69.883(3), 110.117(3)	61.527(3), 118.473(3)
60	K 0.34, Ag 0.55	66.585(2), 113.415(2)	68.456(7), 111.544(7)	62.347(8), 117.653(8)
61	K 0.00, Ag 0.76	66.843(1), 113.157(1)	68.356(5), 111.644(5)	63.013(5), 116.987(5)
K-Ag-H_3O-jarosite products synthesised at 22ºC				
Sample	***A*-site occupancy**	**O2-*A*-O2**	**O2-*A*-O3**	**O3-*A*-O3**
72	K 0.00, Ag 0.74	67.427(5), 112.573(5)	69.769(16), 110.231(16)	61.829(17), 118.171(17)
73	K 0.67, Ag 0.00	69.273(1), 110.727(1)	72.233(3), 107.767(3)	61.120(3), 118.880(3)
74	K 0.61, Ag 0.08	68.735(1), 111.265(1)	71.618(3), 108.382(3)	61.189(3), 118.811(3)
75	K 0.37, Ag 0.19	68.423(0), 111.577(0)	71.222(1), 108.778(1)	61.283(1), 118.717(1)
76	K 0.37, Ag 0.26	68.042(3), 111.958(3)	70.021(9), 109.979(9)	62.551(10), 117.449(10)
Na-Ag-H_3O-jarosite products synthesised at 140ºC				
Sample	***A*-site occupancy**	**O2-*A*-O2**	**O2-*A*-O3**	**O3-*A*-O3**
49	Na 0.47, Ag 0.00	69.767(0), 110.233(0)	73.628(1), 106.372(1)	59.683(1), 120.317(1)
50	Na 0.16, Ag 0.23	68.828(3), 111.172(3)	72.207(8), 107.793(8)	60.392(8), 119.608(8)
51	Na 0.22, Ag 0.38	69.487(3), 110.513(3)	71.805(7), 108.195(7)	62.180(7), 117.820(7)
52	Na 0.17, Ag 0.45	67.359(2), 112.641(2)	69.948(6), 110.052(6)	61.411(6), 118.589(6)
53	Na 0.06, Ag 0.57	66.727(2), 113.273(2)	69.003(6), 110.997(6)	61.736(6), 118.264(6)
54	Na 0.04, Ag 0.66	66.090(1), 113.910(1)	68.467(5), 111.533(5)	61.336(6), 118.664(6)
61	Na 0.00, Ag 0.76	66.843(1), 113.157(1)	68.356(5), 111.644(5)	63.013(5), 116.987(5)
Na-Ag-H_3O-jarosite products synthesised at 22ºC				
Sample	***A*-site occupancy**	**O2-*A*-O2**	**O2-*A*-O3**	**O3-*A*-O3**
72	Na 0.00, Ag 0.74	67.427(5), 112.573(5)	69.769(16), 110.231(16)	61.829(17), 118.171(17)
77	n.d			
78	Na 0.09, Ag 0.61	66.107(0), 113.893(0)	68.205(1), 111.795(1)	61.800(1), 118.200(1)
79	n.d.			
80	Na 0.03, Ag 0.68	65.764(1), 114.236(1)	67.264(3), 112.736(3)	62.621(3), 117.379(3)

Key: 1 Selected samples are representative of low and high temperatures of synthesis.

decrease from 70.188(2) degrees in the K-H_3O-jarosite product (sample 55, K occupancy 0.32) to 66.585(2) degrees in K-Ag-H_3O jarosite sample 60 (K occupancy

0.34, Ag 0.55); the angle is 66.843(1) degrees in the Ag-H_3O-jarosite product (sample 61, Ag occupancy 0.76) (see Table 5.16). The O3-*A*-O3 bond angle of K-H_3O-jarosite sample 55 is 59.383(5) degrees; there is then a trend of the angles increasing from 59.323(6) degrees in K-Ag-H_3O-jarosite sample 56 to 63.013(5) degrees in Ag-H_3O-jarosite sample 61. Trends are also seen in the O2-*A*-O3 bond angles of the K-Ag-H_3O jarosite sample series: in series 55-61, the angle decreases from 74.242(5) degrees to 68.356(5) degrees; in series 72-76, the angle decreases from 72.233(3) degrees (K occupancy 0.67) to 69.769(16) degrees (Ag occupancy 0.74). In the Na-Ag-H_3O jarosite product series, there is a general trend of O2-*A*-O2 bond angles decreasing from 69.767(0) degrees in sample 49 (Na occupancy 0.47, Ag 0) to 66.090(1) degrees in sample 54 (Na occupancy 0.04, Ag 0.66). There is no clear trend in the O3-*A*-O3 bond angles, although there is an overall non-linear increase from 59.683(1) degrees in sample 49 to 63.013(5) in sample 61. The O2-*A*-O3 bond angles show a trend of decreasing from 73.628(1) degrees in Na-H_3O-jarosite sample 49 to 68.356(5) degrees in Ag-H_3O-jarosite sample 61.

5.1.5.3 Cation selective occupancy of *A* site

The EMPA and ICP-AES results suggest that, at all temperatures of synthesis, the order of cation preference for occupancy of the *A* site in the jarosite crystal structure is K > H_3O > Ag > Na > Pb, which is consistent with the reported order of preference (Jambor, 1999). The partitioning coefficients for Ag in jarosites based on the *A*-site occupancies from the combined data from the analysis techniques also support this order of cation preference (see section 5.2.2). It is also consistent with reported PHREEQC data on the end-member solubility products (at 25ºC) of jarosite, hydronium jarosite and natrojarosite of $10^{-9.21}$, $10^{-5.39}$ and $10^{-5.28}$,

respectively (Glynn, 2000). However, the solubility products (at 298K) of jarosite, hydronium jarosite, argentojarosite and natrojarosite have been reported as $10^{-12.50}$, $10^{-8.67}$, $10^{-11.55}$ and $10^{-8.56}$, respectively (Gaboreau and Veillard, 2004), according to the following reaction: $A Fe_3(SO_4)_2(OH)_0 + 6H^+ \rightarrow A^+_{(aq)} + 3Fe^{3+}_{(aq)} + 2(SO_4)^{2-}_{(aq)} + 6(H_2O)_{(l)}$. Consequently, this indicates an order of K > Ag > H_3O > Na. From the results of EMPA and ICP-AES, in the Pb-Ag-H_3O compounds synthesised at 22ºC and 140ºC, the order of preference for occupancy of the *A* site is indicated as H_3O > Ag > Pb.

5.2 Capacity of natural jarosite minerals for Ag

The natural jarosite samples obtained for this project were found to contain only trace contents of Ag, even though many originated from mining areas known to contain Ag, such as Rio Tinto in Spain, Tintic Standard Mine in the United States and Laurion in Greece. EMPA detected Ag in only three out of 24 samples, including argentojarosite sample 34; the other two had Ag site occupancies of 0.001 and 0.003. Consequently, these samples provided no useful data on Ag in jarosite and natrojarosite.

5.3 Summary

- EMPA of jarosite compounds is problematical because potential errors of data interpretation occur as a result of particle size being smaller (< 1 μm) than the electron beam and thus causing interactions, resulting in substantial variation in the different readings of the composition of each compound;

- compositional data from the different analytical techniques (EMPA, ICP-AES and Rietveld refinement) used in this project indicate inconsistent trends in the *A*-site occupancies of the different jarosite series with increased temperature of synthesis, rather than simply increased cation occupancies with increased temperature of synthesis, as suggested by previous studies;
- the K-Ag-H_3O- and Na-Ag-H_3O-jarosite compound series have generally declining mean and median *A*-site occupancies for K + Ag and Na + Ag, respectively, and Ag-only as synthesis temperature increases from 22ºC to 97ºC, probably because of the different periods of synthesis of ~ 1 year and 4 hours, respectively; however, the occupancies generally increase as synthesis temperature rises from 97ºC to 140ºC, with the synthesis periods the same at the two temperatures;
- the Ag contents are substantially higher in Na-Ag-H_3O-jarosite compounds synthesised at 22ºC than in their equivalents synthesised at 97ºC and 140ºC, possibly because of the periods of synthesis of ~ 1 year at 22ºC and 4 hours at 97ºC and 140ºC;
- the Ag contents are generally relatively high in the Pb-Ag-H_3O-jarosite compounds synthesised at 22ºC compared with those synthesised at 140ºC, again probably because of different synthesis periods and the lower Pb concentrations in the starting solutions of compounds synthesised at 22ºC;
- EMPA and Rietveld refinement indicate no consistent relationship between synthesis temperature (22°C, 97°C and 140°C) and the proportion of *B*-site vacancies in the jarosite compounds;
- increasing concentrations of K, Na, Pb, and Ag in the synthesis starting solutions increase the K, Na, Pb, and Ag *A*-site occupancies of the jarosite products,

but the EMPA results have some anomalous contents, so the different series of compounds generally show only poor or fairly poor linear relationships between the concentrations of K, Na, Pb and Ag in the synthesis starting solutions and Ag content in the products;

- in the K-Ag-H_3O-jarosite compounds, the K content is consistently higher than the Ag content even when the Ag concentration in the starting solutions is three times the K concentration;
- in the Na-Ag-H_3O-jarosite compounds, the Ag content is higher than the Na content in the majority of them, even in some cases when the concentration of Na in the starting solutions is three times that of Ag;
- in the Pb-Ag-H_3O-jarosite compounds, the Ag content is consistently higher than the Pb content even when the concentration of Pb in the starting solutions is 2.5 times the concentration of Ag;
- comparison of the molar concentrations of Ag and K, Na or Pb in the synthesis starting solutions with their occupancies in the *A* site of the jarosite precipitates provides relative partitioning coefficients for Ag. The relative partitioning coefficients for Ag in the K-Ag-jarosites are, in general, less than 1 (the mean value of the seven series is 0.900), indicating that K is preferentially incorporated in the compounds relative to Ag. The lowest relative partitioning coefficients for Ag in the K-Ag-jarosites (0.669 and 0.714) are for the two series synthesised at low temperature (22ºC), indicating increased incorporation of K in the jarosite structure relative to Ag at lower temperature of synthesis. At 140ºC, Ag is slightly preferentially incorporated into the structure compared with K (the mean of the Ag partitioning coefficients for the three series is 1.038);

- the partitioning coefficients for Ag in the Na-Ag-jarosites are, in general, greater than 1 (the series average is 1.302), indicating that Ag is preferentially incorporated in these compounds. The two series synthesised at low temperature (22ºC) have the highest relative partitioning coefficients for Ag (1.458 and 1.506);
- the partitioning coefficients for Ag in the Pb-Ag-jarosites are, in general, greater than 1 (the mean of the two series is 1.166), indicating that Ag is preferentially incorporated in these compounds;
- the relative partitioning coefficients for Ag in the majority of the K-, Na- and Pb-Ag-jarosite series (12 out of a total of 16) are highest in the intermediate compounds synthesised from solutions with the lowest Ag concentrations in the respective series; therefore, there is a relatively high initial uptake of Ag into the jarosite compounds. The partitioning coefficients in the intermediate compounds then progressively decrease as the concentration of Ag is increased in the synthesis solutions, indicating that Ag concentration in the solutions is increasingly approaching saturation point relative to incorporation of Ag into the jarosite structure;
- the powder XRD data of the K-Ag-H_3O jarosite compounds show generally declining *d*-spacing values of the *hkl* 003 and 006 reflections as K content declines and Ag content increases, indicating decreases in the *c*-axis parameter caused by the smaller ionic radius of Ag substituting in the *A* site;
- the *d* values of the *hkl* 003 and 006 reflections of the Na-Ag-H_3O-jarosite compounds show generally declining *d* values for three of the series, another series shows an increasing *d*-value trend, and three series do not show consistent trends;

- the Pb-Ag-H_3O-jarosite compounds have *d* values of the *hkl* 003 and 006 reflections that are consistent with the low Pb contents and high H_3O contents but also show a generally declining trend as Ag occupancy increases;
- Rietveld refinement indicates the K-Ag-H_3O and Na-Ag-H_3O jarosite compounds show a trend of increasing unit-cell *a*-axis parameter and decreasing *c*-axis parameter as respectively K^+ and Na^+ occupancy of the *A* site declines and Ag^+ occupancy increases, which suggests the ionic radius of Ag^+ in jarosite is smaller than K^+ and Na^+;
- the isotropic displacement (U_{iso}) values from the Rietveld refinement of K-Ag-H_3O- and Na-Ag-H_3O-jarosite compounds show Ag has higher values than K and Na, respectively, in several samples, but no consistent relationship is indicated. Therefore, the data do not support the suggestion that the Ag^+ cation is smaller than K^+ and Na^+ and may be located, as has been reported, slightly off the *A* site because the void is too large for the Ag^+ ion, which tries to locally achieve lower, 9-fold coordination;
- Raman spectroscopy reveals that, for the v_1SO_4 band, there are increasing wavenumber trends as Ag content increases in the different K-Ag-H_3O-jarosite series synthesised at 22ºC, 97ºC and 140ºC, which is consistent with a smaller ionic radius and higher bonding energies. In two of the Na-Ag-H_3O-jarosite series (synthesised at 22ºC and 140ºC), there is no change in wavenumbers, whereas for series 30-38 (synthesised at 97ºC) there is no change in wavenumbers between the end-members but a general wavenumber increase in the intermediate members as Ag content increases. There is no change in wavenumbers in the Pb-Ag-H_3O-jarosite series;
- for the v_3SO_4 Raman band, there are increasing wavenumber trends as Ag content increases in the K-Ag-H_3O-jarosite series synthesised at 22ºC and 140ºC,

whereas in the series synthesised at 97ºC there is no change in wavenumber between the end-members and no clear trend in the wavenumbers of the intermediate members. In the Na-Ag-H_3O-jarosites, there is an increasing wavenumber trend as Ag content increases in the series synthesised at 97ºC and decreasing trends in the series synthesised at 22ºC and 140ºC. In the Pb-Ag-H_3O-jarosite series, there is an increasing wavenumber trend as Ag content increases;

- reportedly, Raman spectra of jarosite-group compounds are characterised by a tendency for wavenumbers assigned to vibrational modes $v_1(SO_4^{2-})$ and $v_3(SO_4^{2-})$, and three vibrational modes of Fe-O bonds, to decrease with an increase in the *c* unit-cell parameter, whereas wavenumbers assigned to $v_2(SO_4^{2-})$ and $v_4(SO_4^{2-})$ are independent of the value of *c*;
- wavenumbers assigned to vibrational modes $v_1(SO_4^{2-})$ and $v_3(SO_4^{2-})$ in K-Ag-H_3O-jarosite decrease as Ag content declines and the unit-cell *c* parameter increases, showing linear relationships (R^2 values) of 0.6082 and 0.0429, respectively, in series 22-30; 0.8992 and 0.5673, respectively, in sample series 55-61; and 0.9168 and 0.3368, respectively, in series 72-76;
- from the ICP-AES compositional results, good linear relationships between Ag and K content and Ag and Na content indicate solid solution between synthetic Ag-H_3O-jarosite and both K-H_3O-jarosite and Na-H_3O-jarosite at low temperature (22ºC), elevated temperature (97ºC) and high temperature (140ºC) of synthesis. This finding is also supported by the partitioning coefficients for Ag in K-H_3O- and Na-H_3O-jarosites based on the combined data from the analysis techniques of *A*-site occupancies;
- partitioning coefficients indicate solid solution between Ag-H_3O-jarosite and Pb-H_3O-jarosite in sample series JS43-48 & 61 (synthesised at 140ºC) and series 95

& 102-105 (synthesised at 22ºC); however, the low Pb contents make such a conclusion problematic;

- Rietveld refinement shows that, in the K-Ag-H_3O- and Na-Ag-H_3O-jarosite sample series synthesised at 22ºC and 140ºC, there are trends of generally declining bond lengths for both *A*-O2 and *A*-O3 as K^+ or Na^+ occupancy of the *A* site declines and Ag^+ occupancy increases, indicating the Ag^+ cation in the jarosite structure is smaller than both the K^+ cation and the Na^+ cation.

6 CONCLUSIONS AND RECOMMENDATIONS FOR FUTURE WORK

6.1 Conclusions

The aims of this study have been to determine the capacity of synthetic K-, Na- and Pb-jarosite compounds for Ag, by analysing the *A*-site contents and the characters of the Ag-bearing compounds. To achieve these aims, the objectives have been to determine the structural characteristics of the compounds of the solid solution series between Ag-H_3O-jarosite and respectively K-H_3O-jarosite, Na-H_3O-jarosite and Pb-H_3O-jarosite, and to compare the structures and characteristics of Ag-bearing jarosite compounds synthesised, under various conditions, at elevated temperatures (97ºC and 140ºC) and at a temperature characteristic of the surface environment (22ºC). One of the reasons for doing this has been to determine whether compounds synthesised at surface temperatures are more disordered and poorly crystalline than compounds made at elevated temperatures, as has been suggested by several authors (e.g., Swayze et al., 2008). In addition, understanding the differences in the bonding of Ag in different jarosite compounds may give important information on the potential release of Ag from these jarosites and the cycling of Ag in the natural environment. Silver is a valuable resource and the information gained in this study may also help resource geologists, mining engineers and environmental mineralogists to better understand the structural characteristics and potential economic value of naturally occurring Ag-bearing jarosite minerals.

The methods of jarosite synthesis used in this project have been successful in almost all cases, as indicated by XRD analysis, with only a few compounds showing sulphate contamination and in almost all cases this was removed by rewashing or rinsing with ammonium acetate. In addition, the XRD spectra of jarosite compounds

synthesised at low temperature (22ºC) (samples JS72-80 and 89-107) do not display problems of peak broadening and therefore inhomogeneity, with only JS77 and 78 showing some broadening of the more intense peaks (see Appendix E).

The analytical techniques have provided extensive data on the extent of Ag incorporation in the jarosite crystal structure in competition with K and Na during a variety of synthesis experiments. These data have provided information on the selective incorporation of K, Na and Ag in the jarosite structure, including partitioning coefficients. Data have also been provided on Ag incorporation into the jarosite structure in competition with Pb, and on the problems of synthesising Pb-containing jarosite compounds, particularly because of the low solubility and precipitation of $PbSO_4$. This problem of sulphate contamination of the jarosite products of synthesis resulted in this project's experiments with very low concentrations of Pb (0.00013-0.005 *M*) in sulphate synthesis starting solutions and hence resulted in low Pb content of the jarosite products, especially in the presence of Ag, which is preferentially incorporated in the crystal structure. Improved occupancies were achieved with up to 0.06 *M* Pb in the starting solutions; however, the highest Pb occupancies of the *A* site from the synthesis experiments in this project are only 0.168 (JS43D), 0.179 (JS43) and 0.258 (JS107). Other studies have reported that Pb-jarosite only precipitates with large amounts of Pb in the starting solution (Smith, 2004; Basciano, 2008).

One difficulty of analysis that has arisen is that EMPA of powder jarosite compounds is problematical because potential errors of data interpretation occur as a result of the particle size being smaller (< 1 μm) than the electron beam and so causing interactions. This resulted in substantial variation in the different EMPA readings of the composition of each jarosite compound. The standard deviations of

the compositions of the *A*-site cations from the EMPA readings are generally relatively high. This is indicated by the coefficient of variation (C, ratio of standard deviation of population to the mean) of the content the *A*-site cations in each sample: of the K-containing compounds, 45% have a C value of ≥ 20%; of the Na-containing compounds, 44% have a C value of ≥ 50%; and of the Pb-containing compounds, 70% have a C value of more than ≥ 50%. Of the compounds containing Ag, 78% have a C value of ≥ 20%.

Compositional data from the analytical techniques used (EMPA, ICP-AES and Rietveld refinement) indicate the trends in the *A*-site occupancies of the different jarosite compound series as temperature of synthesis increases are more complex than simply increased cation occupancies with higher temperature of synthesis, as suggested by previous studies. The K-Ag-H_3O-jarosite compound series have generally declining mean and median *A*-site occupancies of K + Ag with increase of synthesis temperature from 22ºC to 97ºC and from 22ºC to 140ºC, possibly because of the different periods of synthesis of ~ 1 year and 4 hours, respectively; however, the Ag-only occupancies generally increase with increase of synthesis temperature. The mean occupancies increase as synthesis temperature rises from 97ºC to 140ºC, with the synthesis periods being the same at the two temperatures. In the Na-Ag-H_3O-jarosite compound series, the mean Na + Ag and Ag-only *A*-site occupancies generally decrease as synthesis temperature increases from 22ºC to 97ºC and from 22ºC to 140ºC, again possibly because the period of synthesis at 22ºC is ~ 1 year compared with 4 hours at the higher temperatures. As temperature increases from 97ºC to 140ºC, the mean Na + Ag occupancies increase, whereas the Ag-only occupancies decrease. The mean Ag occupancies are generally relatively high in the Pb-Ag-H_3O-jarosite compounds synthesised at 22ºC compared with those

synthesised at 140ºC, again probably because of different synthesis periods and the lower Pb concentrations in the starting solutions of compounds synthesised at 22ºC.

EMPA and Rietveld refinement indicate no consistent relationship between synthesis temperature (22°C, 97°C or 140°C) and the proportion of *B*-site vacancies in the jarosite compounds, as has been suggested in previous studies.

In the synthesis experiments, increasing concentrations of K, Na, Pb, and Ag in the starting solutions result in increasing K, Na, Pb, and Ag contents of the jarosite compounds. However, because of anomalous contents in the EMPA results for some of the products, the different series of jarosite compounds generally show only poor or fairly poor linear relationships between the concentrations of K, Na, Pb and Ag in the synthesis starting solutions and the Ag content in the products, with only three series showing good linear relationships with R^2 values of ≥ 0.8356.

In the K-Ag-H_3O-jarosite compounds, the K content is consistently higher than the Ag content even when the Ag concentration in the starting solutions is three times the K concentration; this is an indicator of the selective incorporation of K in the jarosite structure compared with Ag. This finding is supported by the relative partitioning coefficients for Ag in the K-Ag-H_3O-jarosites, the comparison of the molar concentrations of Ag and K in the synthesis starting solutions with their molar concentrations in the *A* site of the jarosite precipitates. Based on the combined data from the analysis techniques, the relative partitioning coefficients for Ag in the K-Ag-H_3O-jarosites are, in general, less than 1 (series average 0.9), indicating that K is preferentially incorporated in the compounds relative to Ag. The lowest relative partitioning coefficients for Ag in the K-Ag-H_3O-jarosite compounds (0.669 and 0.714) are for the two series synthesised at low temperature (22ºC).

In the Na-Ag-H_3O-jarosite compounds, the Ag content is higher than the Na content in the majority of them, even in some cases when the concentration of Na in the starting solutions is three times that of Ag; this is an indicator of the selective incorporation of Ag in the jarosite structure compared with Na. The partitioning coefficients for Ag in the Na-Ag-H_3O-jarosites, which are, in general, greater than 1 (series average 1.3), also indicate that Ag is preferentially incorporated relative to Na. The two Na-Ag-H_3O-jarosite series synthesised at low temperature (22ºC) have the highest relative partitioning coefficients (1.458 and 1.506).

In the Pb-Ag-H_3O-jarosite compounds, the Ag content is consistently higher than the Pb content even when the concentration of Pb in the starting solutions is 2.5 times the concentration of Ag, indicating the selective incorporation of Ag in the jarosite structure compared with Pb. The partitioning coefficients for Ag in the Pb-Ag-H_3O-jarosites are, in general, greater than 1 (series average ~ 1.17), also indicating that Ag is preferentially incorporated.

The ICP-AES compositional results show good linear relationships between Ag and K content and Ag and Na content in the jarosite compounds, indicating solid solution between synthetic Ag-H_3O-jarosite and both K-H_3O-jarosite and Na-H_3O-jarosite at low temperature (22ºC), elevated temperature (97ºC) and high temperature (140ºC) of synthesis. This finding is also supported by the partitioning coefficients for Ag in K-H_3O- and Na-H_3O-jarosites based on the combined data from the analysis techniques of *A*-site occupancies. The partitioning coefficients also indicate solid solution between Ag-H_3O-jarosite and Pb-H_3O-jarosite in sample series JS43-48 & 61 (synthesised at 140ºC) and series 95 & 102-105 (synthesised at 22ºC); however, the low Pb contents make such a conclusion problematic.

The XRD main peaks and Rietveld refinement data provide useful information on how the proportion of Ag in the *A* site of jarosite compounds changes the unit cell's *a*- and *c*-axis parameters. This information will be valuable in the interpretation of XRD data on jarosite minerals from complex natural mineral assemblages (Basciano, 2008). The data from this project will inform the evaluation of data from XRD analysis of naturally occurring jarosite minerals and jarosites from mine and metallurgical processing wastes, including the evaluation of the proportion of Ag in the *A* site using variations in unit-cell *a*- and *c*-axis parameters as a guide. The powder XRD data of the K-Ag-H_3O jarosite compounds show generally declining *d*-spacing values of the *hkl* 003 and 006 reflections as K content declines and Ag content increases, indicating decreases in the *c*-axis parameter caused by the smaller ionic radius of Ag substituting in the *A* site. The *d* values of the *hkl* 003 and 006 reflections of the Na-Ag-H_3O-jarosite compounds generally decline as Ag content increases in three of the series, indicating decreases in the *c*-axis parameter; another series shows an increasing *d*-value trend and three series do not show consistent trends. The Pb-Ag-H_3O-jarosite compounds have *d* values of the *hkl* 003 and 006 reflections that are consistent with the low Pb contents and high H_3O contents, according to the JCPDS patterns and reported data, and also show a generally declining trend as Ag occupancy increases. In addition, Rietveld refinement of XRD data indicates the K-Ag-H_3O and Na-Ag-H_3O jarosite compounds show a trend of increasing *a* parameter and decreasing *c* parameter as K^+ or Na^+ occupancy of the *A* site declines and Ag^+ occupancy increases, which also suggests the ionic radius of Ag^+ in jarosite is smaller than those of K^+ and Na^+.

Raman spectroscopy enables comparison of the *c*-axis parameters of the different series of jarosite compounds with the wavenumbers of the assigned modes.

As a consequence, the wavenumbers may become indicators of changing bond strength as the varying Ag content alters the *c*-axis parameters. These results may provide data that create the potential to use Raman spectroscopy to characterise the composition of Ag-bearing natural jarosite compounds. A study has noted that studying synthesised minerals in different solid solution series allows recognition of the properties of more complex natural samples and interpretation of natural assemblages, including chemical composition (Basciano, 2008). In addition, another study reported systematic increases in characteristic Raman peaks of $v_1(SO_4)$, $v_3(SO_4)$ and $v_2(SO_4)$ and decreases in *v*OH peaks with increases in Na content in K/(K+Na) chemical composition ratios of K–Na jarosite solid solution compounds (Ling et al., 2016). The authors proposed using Raman peak positions of K–Na jarosite solid solution compounds as a guide to estimating compositional variation in K-Na-jarosites identified during in-situ and remote sensing measurements on Mars. Also, studies have used remote sensing to carry out spectral analyses to identify jarosite deposits (as analogues of environments on Mars), detecting jarosite absorption features at wavelengths 2.26 and 2.46 μm in northwest Canada (Battler et al., 2013) and ~ 2.26 μm in southern Utah, United States (Bell et al., 2010). Consequently, these studies suggest the potential to use the Raman spectroscopic data from this project to estimate the chemical composition of jarosites identified using remote sensing.

Raman spectra of jarosite-group compounds are characterised by a tendency for wavenumbers assigned to vibrational modes $v_1(SO_4^{2-})$ and $v_3(SO_4^{2-})$ to decrease with increases in the *c* unit-cell parameter, whereas wavenumbers assigned to $v_2(SO_4^{2-})$ and $v_4(SO_4^{2-})$ are independent of the value of *c*. Consequently, increasing

wavenumbers of modes $v_1(SO_4^{2-})$ and $v_3(SO_4^{2-})$ as Ag occupancy increases would be an indicator of a smaller ionic radius and shorter unit-cell *c* parameter.

Raman spectroscopy in this project has revealed that, for the v_1SO_4 band, there are increasing wavenumber trends as Ag content increases in the different K-Ag-H_3O-jarosite series synthesised at 22ºC, 97ºC and 140ºC, which is consistent with a smaller ionic radius and higher bonding energies. For the v_3SO_4 band, there are increasing wavenumber trends as Ag content increases in the K-Ag-H_3O-jarosite series synthesised at 22ºC and 140ºC, whereas in the series synthesised at 97ºC there is no change in wavenumber between the end-members and no clear trend in the wavenumbers of the intermediate members. In the K-Ag-H_3O-jarosites, the Raman results show the increase in the wavenumbers as Ag content increases and the unit-cell *c* parameter decreases has a stronger linear relationship (higher R^2 values) for vibrational mode $v_1(SO_4^{2-})$ than for mode $v_3(SO_4^{2-})$. For modes $v_1(SO_4^{2-})$and $v_3(SO_4^{2-})$, the R^2 values are 0.6082 and 0.0429, respectively, in series 22-30; 0.8992 and 0.5673, respectively, in sample series 55-61; and 0.9168 and 0.3368 in series 72-76. In two of the Na-Ag-H_3O-jarosite series (synthesised at 22ºC and 140ºC), there is no change in the wavenumbers of the v_1SO_4 band as Ag content increases, whereas for series 30-38 (synthesised at 97ºC) there is no change in wavenumbers between the end-members but a general wavenumber increase in the intermediate members as Ag content increases. In the Na-Ag-H_3O-jarosites, there is an increasing wavenumber trend for the v_3SO_4 band as Ag content increases in the series synthesised at 97ºC; however, there are decreasing wavenumber trends as Ag content increases in the series synthesised at 22ºC and 140ºC, indicating a larger ionic radius of Ag than Na and increasing *c* parameter. In the Pb-Ag-H_3O-jarosite series, there is no change in wavenumbers for the v_1SO_4 band as Ag content changes; however, there is an

increasing wavenumber trend for the v_3SO_4 band as Ag content increases, indicating shortening *c* parameters and a smaller ionic radius of Ag compared with Pb.

Rietveld refinement has also provided information on how the bond lengths and angles of the *A*-site cations, Fe, S and O in the jarosite structure alter with the occupancies of Ag, K and Na in the *A* site, as well as data on the atomic positions in the structure. Rietveld refinement shows that, in the K-Ag-H_3O- and Na-Ag-H_3O-jarosite sample series synthesised at 22ºC and 140ºC, there are trends of generally declining bond lengths for both *A*-O2 and *A*-O3 as K^+ or Na^+ occupancy of the *A* site declines and Ag^+ occupancy increases, indicating the Ag^+ cation in the jarosite structure is smaller than both the K^+ cation and the Na^+ cation.

In addition, Rietveld refinement has provided isotropic displacement (U_{iso}) values for the K-Ag-H_3O- and Na-Ag-H_3O-jarosite compounds, which show Ag has higher values than K and Na, respectively, in several samples, but do not indicate a consistent relationship. Therefore, the data do not support the suggestion that the Ag^+ cation is smaller than K^+ and Na^+ and may be located, as has been reported, slightly off the *A* site because the void is too large for the Ag^+ ion, which tries to locally achieve lower, 9-fold coordination.

6.2 Recommendations for future work

Further analysis of Pb-Ag-H_3O jarosite compounds by XRD and Rietveld refinement could be undertaken, including looking for any XRD peak broadening indicating non-homogeneity or for doubling of peaks.

Collection and analysis could be carried out of additional natural Ag-bearing jarosite samples to identify how incorporation of Ag alters the bonding and structure

of the minerals. The data from this project's synthesised solid solution jarosite compounds could be used to guide interpretation of natural assemblages.

Computer simulation studies have been used to model the incorporation of cations into the jarosite structure (Smith, 2004; Smith *et al.*, 2006a and 2006b). Such computational modelling of the jarosite structure could be carried out to calculate the energies involved in the chemical reactions in incorporation of K, Na, Pb, Ag and H_3O into the structure from various concentrations of cations in the synthesis solutions. This would enable evaluation of the incorporation of Ag into the structure relative to the competing cations. Similar modelling could be carried out of vacancies in the Fe site in the jarosite structure.

Analysis could be carried out of synthesised Ag-bearing jarosite compounds using X-ray absorption spectroscopy (XAS) to give insights into the bonding of Ag in jarosite. Extended X-ray Absorption Fine Structure (EXAFS) and X-ray Absorption Near Edge Structure (XANES) spectroscopic analyses are synchrotron radiation-based techniques that provide molecular-scale information on mineral local structure and binding forms (to other minerals and organic substances). The structures of K-Ag-H_3O, Na-Ag-H_3O and Pb-Ag-H_3O members of the synthetic argentojarosite-jarosite, argentojarosite-natrojarosite and argentojarosite-plumojarosite solid solution series, respectively, could be investigated using Ag K-edge and Na-edge, Fe K-edge and Na-edge, and Pb LIII-edge EXAFS and XANES spectroscopy. These experiments would address the bonding of Ag in the members jarosite solid solution series and whether or not it varies with the amount of Ag content and the presence of either K, Na or Pb. The experiments would also address whether the presence of Ag in the crystal structure modifies the bonding environment of Fe and Pb (in Pb-bearing varieties) in the lattice. Any differences in

the results for compounds formed at different synthesis temperatures (22ºC, 97ºC and140ºC) would also be investigated. Studies have previously modelled XAS data of jarosite minerals collected during experiments undertaken at the Synchrotron Radiation Source at Daresbury Laboratory (e.g., Hudson-Edwards et al., 2008).

REFERENCES

Amoros, J. L., Lunar, R. and Tavira, P., 1981. Jarosite: a silver-bearing mineral of the gossan of Rio Tinto (Huelva) and La Union (Cartagena, Spain). *Mineralium Deposita*, 16, 205-213.

Anthony, J. W., Bideaux, R. A., Bladh, K. W. and Nichols, M. C., 2003. *Handbook of Mineralogy*. Mineralogical Society of America, www.handbookofmineralogy.org.

Arslan, C. and Arslan, F., 2003. Thermochemical review of jarosite and goethite stability regions at 25 and 95ºC. *Turkish Journal of Engineering and Environmental Science*, 27, 45-52.

Baron, D. and Palmer, C. D., 1996. Solubility of jarosite at 4-35ºC. *Geochimica et Cosmochimica Acta*, 60(2), 185-195.

Baron, D. and Palmer, C. D., 2002. Solid-solution aqueous-solution reactions between jarosite ($KFe_3(SO_4)_2(OH)_6$) and it chromate analog. *Geochimica et Cosmochimica Acta*, 66(16), 2841-2853.

Basciano, L. C., 2008. Crystal chemistry of the jarosite group of minerals: solid solution and atomic structures. PhD thesis, Queen's University, Kingston, Ontario, Canada, published online.

Basciano, L. C. and Peterson, R. C., 2007. Jarosite-hydronium jarosite solid-solution series with full iron site occupancy: mineralogy and crystal chemistry. *American Mineralogist*, 92, 1464-1473.

Basciano, L. C. and Peterson, R. C., 2008. Crystal chemistry of the natrojarosite-jarosite and natrojarosite-hydronium jarosite solid-solution series: a synthetic study with full iron site occupancy. *American Mineralogist*, 93, 853-862.

Basciano, L. C. and Peterson, R. C., 2010. A crystallographic study of the incomplete solid-solution between plumbojarosite and jarosite. *Canadian Mineralogist*, 48, 651-659.

Battler, M. M., Osinski, G. R., Lim, D. S. S., Davila, A. F., Michel, F. A., Craig, M. A., Izawa, M. R. M., Leoni, L., Slater, G. F., Fairén, A. G., Preston, L. J. and Banerjee, N. R., 2013. Characterization of the acidic cold seep emplaced jarositic Golden Deposit, NWT, Canada, as an analogue for jarosite deposition on Mars. *Icarus*, 224, 382-398.

Becker, U. and Gasharova, B., 2001. AFM observations and simulations of jarosite growth at the molecular scale: probing the basis for the incorporation of foreign ions into jarosite as a storage mineral. *Physics and Chemistry of Minerals*, 28, 545-556.

Bell, J. H., Beitler Bowen, B. and Martini, B. A., 2010. Imaging spectroscopy of jarosite cement in the Jurassic Navajo Sandstone. *Remote Sensing of Environment*, 114, 2259-2270.

Bishop, J. L., and Murad, E., 2005. The visible and infrared spectral properties of jarosite and alunite. *American Mineralogist*, 90, 1100–1107.

Blowes, D. W., Ptacek, C. J., Jambor, J. L. and Weisener, C. G., 2003. The geochemistry of acid mine drainage. *Treatise on Geochemistry*, 9, 149-204.

Brophy, G. P., Scott, E. S. and Snellgrove, R. A., 1962. Sulphate studies II: solid solution between alunite and jarosite. *American Mineralogist*, 47, 112-126.

Brophy, G. P. and Sheridan, M. F., 1965. Sulphate studies IV: the jarosite-natrojarosite-hydronium jarosite solid solution series. *American Mineralogist*, 50, 1595-1607.

Brown, J. B., 1970. A chemical study of some synthetic potassium-hydronium jarosites. *Canadian Mineralogist*, 10, 696-703.

Brown, J. B., 1971. Jarosite-goethite stabilities at 25C, 1 atm. *Mineralium Deposita*, 6, 245-252.

Burger, P. V., Papike, J. J., Shearer, J. M. and Karner, J. M., 2009. Jarosite growth zoning as a recorder of fluid evolution. *Geochimica et Cosmochimica Acta*, 73, 3248-3259.

Cabri, L. J., 1987. The mineralogy of precious metals: new developments and metallurgical implications. *Canadian Mineralogist*, 25, 1-7.

Cadena Zamudio, J. L., undated. Jarocaza-3: Synthesis of jarositic nanotubes. Faculty of Geology, University of Barcelona. Paper published on internet.

Casas, J. M., Paipa, C., Godoy, I., Vargas, T., 2007. Solubility of sodium-jarosite and solution speciation in the system Fe(III)–Na–H_2SO_4–H_2O at 70ºC. *Journal of Geochemical Exploration*, 92, 111–119.

Craddock, P. T., 1995. *Early Metal Mining and Production*. Smithsonian Institution Press, Washington D.C., U.S.A.

Cruells, M., Roca, A., Patino, F., Salinas, E. and Rivera, I., 2000. Cyanidation kinetics of argentian jarosite in alkaline media. *Hydrometallurgy*, 55, 153-163.

Darke, K. E., Boyce, A. J., Clapperton, C. M., Fallick, A. E., Redwood, S. D. and Rice C. M., 1997. Supergene mineralization at the Koro Kollo Gold Mine, Bolivia. *Exploration and Mining Geology Journal*, 6(3), 209-221.

Desborough, G. A., Smith, K. S., Lowers, H. A., Swayze, G. A., Hammarstrom, J. M., Diehl, S. F., Driscoll, R. L. and Leinz, R. W., 2006. The use of synthetic jarosite as an analog for natural jarosite. Proceedings of the Seventh International Conference on Acid Rock Drainage (ICARD 7), St Louis, Missouri, USA, March 26-30, 2006, pp. 458-475.

Desborough, G. A., Smith, K. S., Lowers, H. A., Swayze, G. A., Hammarstrom, J. M., Diehl, S. F., Leinz, R. W. and Driscoll, R. L., 2010. Mineralogical and chemical characteristics of some natural jarosites. *Geochimica et Cosmochimica Acta*, 74, 1041-1056.

Drouet, C. and Navrotsky, A., 2003. Synthesis, characterization, and thermochemistry of K-Na-H_3O jarosites. *Geochimica et Cosmochimica Acta*, 67(11), 2063-2076.

Drouet, C., Pass, K. L., Baron, D., Draucker, S. and Navrotsky, A., 2004. Thermochemistry of jarosite-alunite and natrojarosite-natroalunite solid solutions. *Geochimica et Cosmochimica Acta*, 68(10), 2197-2205.

Dutrizac, J. E., 1980. The physical chemistry of iron precipitation in the zinc industry. *In:* Cigan, J. M., Mackey, T. S. and O'Keefe, T. J. (eds.), *Lead-Zinc-Tin '80: Proceedings of a World Symposium on Metallurgy and Environmental Control*. The Metallurgical Society of AIME (American Institute of Mining, Metallurgical and Petroleum Engineers, Inc.), Warrendale, Pennsylvania, U.S.A.

Dutrizac, J. E., 1983. Factors affecting alkali jarosite precipitation. *Metallurgical and Materials Transactions B*, 14(4), 531-539.

Dutrizac, J. E. and Jambor, J. L., 1984. Formation and characterization of argentojarosite and plumbojarosite and their relevance to metallurgical processing. *In:* Park, W. C., Hausen, D. M. and Hagni, R. D. (eds.), *Applied Mineralogy 1984: Proceedings of the Second International Congress on Applied Mineralogy in the Minerals Industry, Los Angeles, California, February 22-25, 1984*. The Metallurgical Society of AIME (the American Institute of Mining, Metallurgical and Petroleum Engineers, Inc.), Warrendale, Pennsylvania, U.S.A.

Dutrizac, J. E. and Jambor, J. L., 2000. Jarosites and their application in hydrometallurgy. *In:* Alpers, C. N., Jambor, J. L. and Nordstrom, D. K. (eds.), *Sulphate Minerals: Crystallography, Geochemistry and Environmental Significance. Reviews in Mineralogy and Geochemistry, volume 40*. Mineralogical Society of America Geochemical Society, Washington D.C., U.S.A.

Dutrizac, J. E. and Kaiman, S., 1976. Synthesis and properties of jarosite-type compounds. *Canadian Mineralogist*, 14, 151-158.

Elgersma, F., Witkamp, G. J., and van Rosmalen, G. M., 1993. Incorporation of zinc in continuous jarosite precipitation. *Hydrometallurgy*, 33, 313-339.

Fairchild, J. G., 1933. Artificial jarosites – the separation of potassium from cesium. *American Mineralogist*, 18, 543-547.

Figueiredo, M.-O. and Pereira da Silva, T., 2011. The positive environmental contribution of jarosite by retaining lead in acid mine drainage areas. *International Journal of Environmental Research and Public Health*, 8, 1575-1582.

Frost, R. L., Wills, R.-A., Weier, M. L. and Martens, W., 2005. Thermal decomposition of synthetic argentojarosite – implications for silver production in medieval times. *Thermochimica Acta*, 437, 30-33.

Frost, R., Wills, R-A., Weier, M. and Martens, W., 2006. A Raman spectroscopic study of selected natural jarosites. *Spectrochimica Acta*, 63, 1-8.

Gaboreau, S. and Veillard, P., 2004. Prediction of Gibbs free energy of formation of minerals of the alunite supergroup. *Geochimica et Cosmochimica Acta*, 68, 3307-3316.

Gasharova, B., Gottlicher, J. and Becker, U., 2005. Dissolution at the surface of jarosite: an in-situ AFM study. *Chemical Geology*, 215, 499-516.

Gill, R., 1997. Electron beam methods. *In:* Gill, R. (ed.), *Modern Analytical Geochemistry*. Addison Wesley Longman Limited, Harlow, England.

Groat, L. A., Jambor, J. L. and Pemberton, B. C., 2003. The crystal structure of argentojarosite, $AgFe_3(SO_4)_2(OH)_6$. *Canadian Mineralogist*, 41, 921-928.

Grohol, D. and Nocera, D. G., 2007. Magnetic disorder in the frustrated antiferromagnet jarosite arising from the $H_3O^{+\cdots}OH^-$ interaction. *Chemistry of Materials*, 19, 3061-3066.

Hahn, A. W., 1929. Silver-bearing minerals of some ores from the Tintic mining district. *AIME (American Institute of Mining Engineers) Transactions*, 77, 325-329. Published online at www.aimehq.org/search/docs/Volume%20085/085-42.pdf.

Han, H., Sun, W., Hu, Y., Jia, B. and Tang, H., 2014. Anglesite and silver recovery from jarosite residues through roasting and sulfidization-flotation in zinc hydrometallurgy. *Journal of Hazardous Materials*, 278, 49-54.

Hawthorne, F. C., Krivovichev, S. V. and Burns, P. C., 2000. Crystal chemistry of sulphate minerals. *In:* Alpers, C. N., Jambor, J. L. and Nordstrom, D. K. (eds.), *Sulphate Minerals: Crystallography, Geochemistry and Environmental Significance. Reviews in Mineralogy and Geochemistry, Vol. 40,* 405-452. Mineralogical Society of America Geochemical Society, Washington D.C., U.S.A.

Hendricks, S. B., 1937. The crystal structure of alunite and the jarosites. *American Mineralogist*, 22, 773-784.

Hudson-Edwards, K. A., Smith, A. M. L., Dubbin, W. E., Bennett, A. J., Murphy, P. J., Wright, K., 2008. Comparison of the structures of natural and synthetic Pb-Cu-jarosite-type compounds. *European Journal of Mineralogy*, 20, 241-252.

Jambor, J. L., 1999. Nomenclature of the alunite supergroup. *Canadian Mineralogist*, 37, 1323-1341.

Jamieson, H. E., Robinson, C., Alpers, C. N., Nordstrom, D. K., Poustovetov, A. and Lowers, H. A., 2005. The composition of coexisting jarosite-group minerals and water from the Richmond mine, Iron Mountain, California. *The Canadian Mineralogist*, 43, 1225-1242.

Ju, S., Zhang, L., Peng, J., Shi, Z., Guo, S., Liu, B. and Wang, Y., 2013. Thermodynamics of leaching roasted jarosite residue from zinc hydrometallurgy in NH_4Cl system. *Transactions of Nonferrous Metals Society of China*, 23, 1179-1183.

Kerolli-Mustafa, M., Fajkovic, H., Roncevic, S. and Curkovic, L., 2015. Assessment of metal risks from different depths of jarosite tailing waste of Trepca Zinc Industry, Kosovo based on BCR procedure. *Journal of Geochemical Exploration*, 148, 161-168.

Kubisz, J., 1970. Studies on synthetic alkali-hydronium jarosites: I. Synthesis of jarosite and natrojarosite. *Mineralogia Polonica*, 1, 47-59.

Leverett, P., McKinnon, A. R. and Williams P. A., 2005. Supergene geochemistry of the Endeavor Ore Body, Cobar, NSW, and relationships to other deposits in the Cobar Basin. *In:* Roach, I. C. (ed.), *Regolith 2005 – Ten Years of CRC LEME: Proceedings of CRC LEME Regional Regolith Symposia 2005*. The Cooperative Research Centre for Landscape Environments and Mineral Exploration, Australia, published online.

Lindsay, W. L., 1979. *Chemical Equilibria in Soils*. Wiley, New York.

Ling, Z., Cao, F., Ni, Y., Wu, Z., Zhang, J. and Li, B., 2016. Correlated analysis of chemical variations with spectroscopic features of the K–Na jarosite solid solutions relevant to Mars. *Icarus*, 271, 19-29.

Lottermoser, B. G., 2003. *Mine wastes: characterization, treatment and environmental impacts*. Springer-Verlag, Berlin Heidelberg.

Lowers, H., Desborough, G., Hammarstrom, J., Swayze, G., Smith, K. and Diehl, S., 2005. Not-so-routine electron probe microanalyses of jarosite. *Microscopic Microanalysis*, 11 (Suppl. 2).

Majzlan, J., Stevens, R., Boerio-Goates, J., Woodfield, B. F., Navrotsky, A., Burns, P. C., Crawford, M. K. and Amos, T. G., 2004. Thermodynamic properties, low-

temperature heat-capacity anomalies, and single-crystal X-ray refinement of hydronium jarosite, $(H_3O)Fe_3(SO_4)_2(OH)_6$. *Physics and Chemistry of Minerals*, 31, 518-531.

May, A., Sjoberg, J. J. and Baglin, E. G., 1973. Synthetic argentojarosite: physical properties and thermal behaviour. *American Mineralogist*, 58, 936-941.

Munsell, 2000. Munsell Soil Colour Charts. GretagMacbeth, NewYork.

Murphy, P. J., Smith, A. M. L., Hudson-Edwards, K. A., Dubbin, W. E., Wright, K., 2009. Raman and IR spectroscopic studies of alunite-supergroup compounds containing Al, Cr^{3+}, Fe^{3+} and V^{3+} at the *B* site. *The Canadian Mineralogist*, 47, 663-681.

Myneni, S. C. B., 2000. X-ray and vibrational spectroscopy of sulphate in earth materials. *In:* Alpers, C. N., Jambor, J. L. and Nordstrom, D. K. (eds.), *Sulphate Minerals: Crystallography, Geochemistry and Environmental Significance. Reviews in Mineralogy and Geochemistry, volume 40,* 113-172. Mineralogical Society of America Geochemical Society, Washington D.C., U.S.A.

Paktunc, D. and Dutrizac, J. E., 2003. Characterisation of arsenate-for-sulfate substitution in synthetic jarosite using X-ray diffraction and X-ray absorption spectroscopy. *The Canadian Mineralogist*, 41, 905-919.

Papike, J. J., Karner, J. M. and Shearer, C. K., 2006. Implications of Martian and terrestrial jarosite: a crystal chemical perspective. *Geochimica et Cosmochimica Acta*, 70, 1309-1321.

Papike, J. J., Burger, P. V., Karner, J. M., Shearer, C. K., and Lueth, V. W., 2007. Terrestrial analogs of martian jarosites: Major, minor element systematics and Na-K zoning in selected samples. *American Mineralogist*, 92, 444-447.

Parker, R. L., 1962. Isomorphous substitution in natural and synthetic alunite. *American Mineralogist*, 47, 127-136.

Patino, F., Salinas, E., Cruells, M. and Roca, A., 1998. Alkaline decomposition-cyanidation kinetics of argentian natrojarosite. *Hydrometallurgy*, 49, 323-336.

Powers, D. A., Rossman, G. R., Schugar, H. J. and Gray, H. B., 1975. Magnetic Behavior and Infrared Spectra of Jarosite, Basic Iron Sulfate, and Their Chromate Analogs. *Journal of Solid State Chemistry*, 13, 1-13.

Rattray, K. J., Taylor, M. R., Bevan, D. J. M., and Pring, A., 1996. Compositional segregation and solid solution in the lead-dominant alunite-type minerals from Broken Hills, N.S.W. *Mineralogical Magazine*, 60, 779-785.

Ripmeester, J. A., Ratcliffe, C. I., Dutrizac, J. E. and Jambor, J. L., 1986. Hydronium ion in the alunite-jarosite group. *Canadian Mineralogist*, 24, 435-437.

Roca, A., Vinals, J., Arranz, M. and Calero, J., 1999. Characterization and alkaline decomposition/cyanidation of beudantite-jarosite materials from Rio Tinto gossan ores. *Canadian Metallurgical Quarterly*, 38 (2), 93-103.

Rollinson, H. R., 1993. *Using Geochemical Data: evaluation, presentation, interpretation*. Pearson/Prentice Hall, Harlow, England.

RRUFF Project, Integrated Database of Raman Spectra, XRD and Chemistry Data, University of Arizona, USA, http://rruff.info/jarosite/display=default/

Sanchez, L., Cruells, M. and Roca, A., 1996. Sulphidization-cyanidation of jarosite species: applicability to the gossan ores of Rio Tinto. *Hydrometallurgy*, 42, 35-49.

Sasaki, K. and Konno, H., 2000. Morphology of jarosite-group compounds precipitated from biologically and chemically oxidized Fe ions. *Canadian Mineralogist*, 38, 45-56.

Sasaki, K., Tsunekawa, M. and Konno, H., 1995. Characterization of argentojarosite formed from biologically oxidized Fe^{3+} ions. *Canadian Mineralogist*, 33, 1311-1319.

Schwertmann, U. and Cornell, R. M., 2000. *Iron Oxides in the Laboratory: Preparation and Characterization*. Wiley-VCH, Weinheim, Germany.

Scott, K. M., 1987. Solid solution in, and classification of, gossan-derived members of the alunite-jarosite family, northwest Queensland, Australia. *American Mineralogist*, 72, 178-187.

Scott, K. M., 1990. Origin of alunite- and jarosite-group minerals in the Mt. Leyshon epithermal gold deposit, northeast Queensland, Australia. *American Mineralogist*, 75, 1176-1181.

Sejkora, J., Cejka, J., and Srein, V., 2001. Lead-dominant members of the crandallite group from Cinovec and Moldava deposits, Krusne hory Mts, Czech Republic. *Journal of the Czech Geological Society*, 46(1-2), 53-68.

Serna, C. J., Parada Cortina, C., Garcia Ramos, J. V., 1986. Infrared and Raman study of alunite-jarosite compounds. *Spectrochimica Acta*, 42A(6), 729-734.

Shannon, R. D., 1976. Revised effective radii and systematic studies of interatomic distances in halides and chalcogenides. *Acta Crystallographica*, A32, 751-767.

Smith, A. M. L., 2004. Mechanisms and products of the breakdown of contaminant element-bearing jarosites. Unpublished PhD thesis, Birkbeck College, University of London.

Smith, A. M. L., Hudson-Edwards, K. A., Dubbin, W. E. and Wright, K., 2006a. Dissolution of jarosite $[KFe_3(SO_4)_2(OH)_6]$ at pH 2 and 8: insights from batch experiments and computational modelling. *Geochimica et Cosmochimica Acta*, 70, 608-621.

Smith, A. M. L., Hudson-Edwards, K. A., Dubbin, W. E. and Wright, K., 2006b. Defects and impurities in jarosites: a computer simulation study. *Applied Geochemistry*, 21, 1251-1258.

Stoffregen, R. E., 1993. Stability relations of jarosite and natrojarosite at 150-250ºC. *Geochimica et Cosmochimica Acta*, 57, 2417-2429.

Stoffregen, R. E., Alpers, C. N. and Jambor, J. L., 2000. Alunite-jarosite crystallography, thermodynamics and geochronology. *In:* Alpers, C. N., Jambor, J. L. and Nordstrom, D. K. (eds.), *Sulphate Minerals: Crystallography, Geochemistry and Environmental Significance, Reviews in Mineralogy and Geochemistry, Vol. 40*. Mineralogical Society of America/Geochemical Society, Washington D.C., U.S.A.

Swayze, G. A., Desborough, G. A., Smith K. S., Lowers, H. A., Hammarstrom, J. M., Diehl, S. F., Leinz, R. W. and Driscoll, R. L., 2008. Understanding jarosite – from mine waste to Mars. *In:* Verplanck, P.L. (ed), *Understanding contaminants associated with mineral deposits: USGS Circular 1328*, pp. 8-13. US Geological Survey, Reston, Virginia.

Takeno, N., 2005. *Atlas of Eh-pH diagrams: intercomparison of thermodynamic databases*. Geological Survey of Japan Open File Report No. 419, National Institute of Advanced Industrial Science and Technology, Japan.

Tazaki, K., Mori, T. and Nonaka, T., 1992. Microbial jarosite and gypsum from corrosion of Portland cement concrete. *Canadian Mineralogist*, 30, 431-444.

Wang, H., Bigham, J. M., Jones, F. S. and Tuovinen, O. H., 2007. Synthesis and properties of ammoniojarosites prepared with iron-oxidizing acidophile microorganisms at 25-65°C. *Geochimica et Cosmochimica Acta*, 71, 155-164.

Welch, S. A., Christy, A. G., Kirste, D., Beavis, S. G. and Beavis, F., 2007. Jarosite dissolution I – trace cation flux in acid sulfate soils. *Chemical Geology*, 245, 183-197.

Welch, S. A., Kirste, D., Christy, A. G., Beavis, F. R. and Beavis, S. G., 2008. Jarosite dissolution II – reaction, kinetics, stoichiometry and acid flux. *Chemical Geology*, 254, 73-86.

Wills, A. S., Smith, A. M. L., Dubbin, W. E., Hudson-Edwards, K. A. and Wright, K., 2004. Interlayer exchange in the plumbo-jarosites: kagomé systems. *Journal of Magnetism and Magnetic Materials*, 272-276, 1300-1301.

APPENDIX A

Minerals of the alunite supergroup (total 48 minerals)
(Sources: Anthony et al., 2003; Groat et al., 2003; Basciano, 2008)

Jarosite Group Fe>Al

jarosite $KFe_3(SO_4)_2(OH)_6$
natrojarosite $NaFe_3(SO_4)_2(OH)_6$
hydronium jarosite $(H_3O)Fe_3(SO_4)_2(OH)_6$
ammoniojarosite $(NH_4)Fe_3(SO_4)_2(OH)_6$
argentojarosite $AgFe_3(SO_4)_2(OH)_6$
plumbojarosite $Pb[Fe_3(SO_4)_2(OH)_6]_2$
beaverite $PbCu(Fe,Al)_2(SO_4)_2(OH)_6$
dorallcharite $Tl_{0.8}K_{0.2}Fe_3(SO_4)_2(OH)_6$

Alunite Group Al>Fe

alunite $KAl_3(SO_4)_2(OH)_6$
natroalunite $NaAl_3(SO_4)_2(OH)_6$
ammonioalunite $(NH_4)Al_3(SO_4)_2(OH)_6$
schlossmacherite $(H_3O,Ca)Al_3(SO_4)_2(OH)_6$
minamiite $(Na,K,Ca)Al_3(SO_4)_2(OH)_6$
osarizawaite $PbCuAl_2(SO_4)_2(OH)_6$
walthierite $Ba_{0.5}Al_3(SO_4)_2(OH)_6$
huangite $Ca_{0.5}Al_3(SO_4)_2(OH)_6$

Beudantite Group Fe>Al

beudantite $PbFe_3[(As,S)O_4]_2(OH,H_2O)_6$
corkite $PbFe_3[(P,S)O_4]_2(OH,H_2O)_6$

Beudantite Group Al>Fe

hidalgoite $PbAl_3[(As,S)O_4]_2(OH,H_2O)_6$
hinsdalite $PbAl_3[(P,S)O_4]_2(OH)_6$
kemmlitzite $(Sr,Ce)Al_3[(As,S)O_4]_2(OH,H_2O)_6$
svanbergite $SrAl_3[(P,S)O_4]_2(OH,H_2O)_6$
woodhouseite $CaAl_3[(P,S)O_4]_2(OH,H_2O)_6$
weilerite $BaAl_3[(As,S)O_4](OH)_6$
gallobeudantite $PbGa_3[(As,S)O_4]_2(OH,H_2O)_6$

Crandallite Group Al>Fe

crandallite $CaAl_3(PO_4)_2(OH,H_2O)_6$
plumbogummite $PbAl_3(PO_4)_2(OH,H_2O)_6$
goyazite $SrAl_3(PO_4)_2(OH,H_2O)_6$
gorceixite $BaAl_3(PO_4)_2(OH,H_2O)_6$
arsenocrandallite $CaAl_3[(As,P)O_4]_2(OH,H_2O)_6$
phillipsbornite $PbAl_3(AsO_4)_2(OH,H_2O)_6$
arsenogoyazite $(Sr,Ca,Ba)Al_3[(As,P)O_4]_2(OH,H_2O$
arsenogorceixite $BaAl_3(AsO_4)(AsO_3{\bullet}OH)(OH)_6$
florencite-(Ce) $CeAl_3(PO_4)_2(OH)_6$
florencite-(La) $LaAl_3(PO_4)_2(OH)_6$
florencite-(Nd) $NdAl_3(PO_4)_2(OH)_6$
arsenoflorencite-(Ce) $CeAl_3(AsO_4,PO_4)_2(OH)_6$
arsenoflorencite-(La) $LaAl_3(AsO_4,PO_4)_2(OH)_6$
arsenoflorencite-(Nd) $NdAl_3(AsO_4,PO_4)_2(OH)_6$
waylandite $(Bi,Ca)Al_3(PO_4,SiO_4)_2(OH)_6$
eyelettersite $(Th,Pb)_{1-x}Al_3(PO_4,SiO_4)_2(OH)_6$
arsenowaylandite $(Bi,Ca)Al_3(AsO_4)_2(OH)_6$

Crandallite Group Fe>Al

benauite $SrFe_3(PO_4)_2(OH,H_2O)_6$
kintoreite $PbFe_3(PO_4)_2(OH,H_2O)_6$
lusungite $(Sr,Pb)Fe_3(PO_4)_2(OH,H_2O)_6$
zairite $BiFe_3(PO_4)_2(OH)_6$
dussertite $BaFe_3(AsO_4)_2(OH)_5$
segnitite $PbFe_3(AsO_4)_2(OH,H_2O)_6$

APPENDIX B: THEORY OF PHYSICAL AND CHEMICAL ANALYTICAL TECHNIQUES

B1 Scanning Electron Microscopy

The scanning electron microscope (SEM) is designed mainly for imaging, rather than compositional analysis. The SEM produces images by scanning an electron beam on a sample and producing a signal collected by an electron detector and displayed on a monitor. Spatial resolution better than 10 nm is available and SEM three-dimensional images have a large depth of field. The SEM is effective in the study of crystal morphology.

B2 X-ray diffraction

X-ray diffraction (XRD) is used to identify mineral samples by using a monochromatic X-ray beam generated by bombarding an anode with electrons and this beam is directed, via a collimator, on to a powdered sample. The beam causes the sample to emit characteristic X-rays diffracted at an angle 2θ (θ is the angle of incidence of the beam), which are directed on to a detector via a collimator and monochromator (removing fluorescence). An X-ray beam scan is produced by changing the angle between the source, sample and detector, and the 2θ degree angles are measured. This produces diffraction patterns of the crystalline substances in the sample, each having a unique pattern independent of other substances in the compound. A spectrum is generated of the X-ray intensity (counts) on the y axis with the 2θ degrees angle on the x axis. Using the known wavelength (λ) of X-rays from the anode, the 2θ angles and the order of reflection (n), Bragg's law ($n\lambda = 2d \sin \theta$) enables the unique spacing (d spacing) of each crystal lattice to be calculated, allowing identification of minerals using the Joint Committee for Powder Diffraction Standards' (JCPDS) reference patterns.

B3 Electron microprobe analysis

Electron microprobe analysis (EMPA) is used to identify minerals and to determine the concentrations of elements in the minerals. The technique can also be used to determine the textures of the minerals. In EMPA, samples are analysed as polished thin sections or resin blocks, with an outer coating of carbon to prevent charging. A spot beam of electrons is directed at the sample by an electron gun and filament. The electron beam excites electrons in the sample from their ground state by inelastic collisions (involving a loss of total kinetic energy); these collisions cause electrons to be ejected from inner electron shells of atoms in the sample. Electrons from higher shells of the atom fill the vacancies created in the inner shells and these transitions between energy levels generate X-rays with wavelengths characteristic of the element involved. Transitions into the K shell (innermost shell around the nucleus) from the outer orbital of the L shell (next shell out from the nucleus) are called $K\alpha_1$ transitions. EMPA also has a backscattered electron imaging system to enable the identification of mineral grains and their textures.

In energy dispersive X-ray spectrometry (EDS) mode, a solid-state semiconductor (silicon-lithium crystal) detector generates electrical pulses proportional to the photon energy of the characteristic X-rays detected. The photon energy (E) in kiloelectronvolts (keV) and X-ray wavelength (λ) are related by the equation $E\lambda = 12.398$. The pulses generated are processed into ‘channels’ of pulse counts by a multichannel analyser and the chemical composition of the sample is displayed as a spectrum of elements, with counts per second (intensity) plotted on the y axis and keV on the x axis. EDS enables simultaneous determination of the elements in a sample.

In wavelength dispersive X-ray spectrometry (WDS) mode, the characteristic X-rays are reflected by an analysing crystal according to wavelength and directed on to a detector. A range of analysing crystals, which are curved to ensure a consistent angle of incidence from the point source in the sample, is used to cover the entire range of elements. Layered synthetic microstructure (LSM) crystals are used, such as lithium fluoride (LiF), pentaerythritol (PET) or thallium acid phthalate (TAP) crystals. Analysis by WDS (5-8 min) takes longer than EDS (2 min) but the accuracy of WDS is an order of magnitude greater. The detection limits for the two systems are WDS 0.01 weight % and EDS 0.1-0.5 wt %. Each system makes corrections for dead time, background X-rays, spectral interference and matrix effects.

B4 Raman spectroscopy

Raman spectroscopy measures inelastic scattering – Raman scattering – of monochromatic light, in the visible, near infrared or near ultraviolet spectra range, from a laser on to a sample. Atoms possess quantised vibrational energy states, and Raman scattering occurs when incident light excites an electron from its ground state to a virtual energy state and it then relaxes into a vibrational excited state. Raman scattering is separated from the elastic Rayleigh scattered light by diffraction gratings and dispersion stages. The Raman scattered light is detected by a charge-coupled device or photon-counting photomultiplier tube. The counts are used to generate graphs of peaks and troughs that act as patterns that may be interpreted to reveal chemical composition and mineralogy. An advantage of the technique is that samples do not have to be fixed or sectioned and samples < 1 µm in diameter can be analysed.

B5 Inductively coupled plasma-atomic emission spectrometry

ICP-OES measures spectra of light emitted by atoms when excited electrons return to their ground states (lowest energy level). The emission or absorption of energy by electrons involves transitions between energy levels (orbitals). To jump up orbital levels requires energy input (absorption of heat), while dropping down levels gives off energy (photon of light). Electron energy levels, and the energy differences between them, are related to the charge on the nucleus (and the atomic number, Z). For each transition, light of a specific wavelength is generated, according to the energy involved, creating an emission spectral line characteristic of the element. To identify elements present, the lines are compared with standard lines for each element.

The light source is the ICP silica glass torch, which atomises the sample solution in argon plasma at up to 10,000 K, causing complete breakdown of atomic bonds, so minimising chemical interference. Argon gas is used because it is optically transparent, is chemically inert and has low thermal conductivity. The toroidal (doughnut-shaped) plasma is generated by argon gas being introduced through the outer glass tube of the coaxial torch, flowing through a radio-frequency magnetic field, produced by load coils around the torch, and being exposed to an electrical (Tesla) spark. The spark creates ‘seed’ electrons and ions, which oscillate in the RF field and collide, intensifying the ionisation. Eddy currents of free electrons are created that cause an ohmic (resistive) heating of the plasma up to about 10,000 K. The sample solution is mixed with argon gas in a nebuliser (atomiser) and then passes into a spray chamber, from which it is introduced through the torch’s inner glass tube into the plasma as an aerosol in the argon carrier gas.

The observation region is in the torch's tail flame (14-18 mm above the induction coil), where the temperature is 6000 K. An axial or radial system of transfer optics directs the light to a spectrometer. The spectrometer then directs the light on to a diffraction grating, which separates (diffracts) the emitted light by wavelength and focuses it on to a detector. The intensities (counts) of the emitted spectral lines provide a quantitative measure of analyte concentration and these are compared with standards.

Simultaneous systems have a polychromator spectrometer with a curved diffraction grating and up to 30 fixed detector channels that enable the simultaneous measurement of different wavelengths. The diffraction grating resolves the incident light into component wavelengths and the diffracted light is directed on to photomultipliers, aligned to a specific wavelength. The intensity of the signal on to the photomultiplier gives a measure of element concentration. Sequential systems focus the light on to a monochromator, which has a diffraction grating that is rotated under computer control to select wavelengths one element at a time. The diffracted light is focused on to a single photomultiplier tube, which determines the pre-selected wavelength (different tubes are needed for multiple elements). An analogue to digital converter (ADC) changes the voltage of the electrical signal produced by the photomultiplier into a digital signal for processing.

The temperature of the plasma of up to 10,000 K causes complete breakdown of the bonds between atoms, so minimising chemical interference. Matrix effects are minimised by matching standards to the unknowns. Background emissions can be measured by running an instrument blank.

APPENDIX C

Product weights of K-Ag jarosites synthesised at 22ºC, 97ºC and 140ºC, and the concentrations of K and Ag in the starting solutions

Sample	Concentration	Solution (ml)	Product, actual (g)	Product, ideal (g)
JS04[1]	0.22 *M* K, 0.00 *M* Ag	100	10.10	11.51
JS06[1]	0.165 *M* K, 0.055 *M* Ag	100	8.10	11.87
JS06D[1]	0.165 *M* K, 0.055 *M* Ag	100	4.90	11.87
JS08[1]	0.11 *M* K, 0.11 *M* Ag	100	8.50	12.25
JS10[1]	0.055 *M* K, 0.165 *M* Ag	100	8.20	12.64
JS10D[1]	0.055 *M* K, 0.165 *M* Ag	100	4.30	12.64
JS12[1]	0.00 *M* $M^{+,2+}$, 0.22 *M* Ag	100	8.15	13.05
JS22[2]	0.22 *M* K, 0.00 *M* Ag	100	9.48	11.51
JS24[2]	0.165 *M* K, 0.055 *M* Ag	100	8.15	11.87
JS24D[2]	0.165 *M* K, 0.055 *M* Ag	100	3.90	11.87
JS26[2]	0.11 *M* K, 0.11 *M* Ag	100	5.57	12.25
JS28[2]	0.055 *M* K, 0.165 *M* Ag	100	6.92	12.64
JS30[2]	0.00 *M* $M^{+,2+}$, 0.22 *M* Ag	100	6.20	13.05
JS40[2]	0.5 *M* K, 0.1 *M* Ag	100	2.14	17.42
JS55[3]	0.12 *M* K, 0.00 *M* Ag	100	3.95	6.04
JS56[3]	0.10 *M* K, 0.02 *M* Ag	100	3.94	6.09
JS57[3]	0.08 *M* K, 0.04 *M* Ag	100	4.69	6.26
JS58[3]	0.06 *M* K, 0.06 *M* Ag	100	4.52	6.39
JS59[3]	0.04 *M* K, 0.08 *M* Ag	100	3.18	6.51
JS60[3]	0.02 *M* K, 0.10 *M* Ag	100	4.73	6.64
JS61[3]	0.00 *M* $M^{+,2+}$, 0.12 *M* Ag	100	3.89	6.81
JS62[4]	0.22 *M* K, 0.00 *M* Ag	100	4.90	11.51
JS63[4]	0.165 *M* K, 0.055 *M* Ag	100	5.60	11.87
JS64[4]	0.11 *M* K, 0.11 *M* Ag	100	7.70	12.25
JS65[4]	0.055 *M* K, 0.165 *M* Ag	100	4.50	12.64
JS66[4]	0.00 *M* $M^{+,2+}$, 0.22 *M* Ag	100	4.50	13.05
JS71[5]	0.00 *M* $M^{+,2+}$, 0.22 *M* Ag	100	3.10	13.05
JS72[6]	0.00 *M* $M^{+,2+}$, 0.22 *M* Ag	100	4.60	13.05
JS73[6]	0.22 *M* K, 0.00 *M* Ag	100	5.00	11.51
JS74[6]	0.165 *M* K, 0.055 *M* Ag	100	4.40	11.87
JS75[6]	0.11 *M* K, 0.11 *M* Ag	100	4.30	12.25
JS76[6]	0.055 *M* K, 0.165 *M* Ag	100	5.30	12.64
JS81[5]	0.22 *M* K, 0.00 *M* Ag	100	5.35	11.51
JS82[5]	0.165 *M* K, 0.055 *M* Ag	100	7.20	11.87
JS83[5]	0.11 *M* K, 0.11 *M* Ag	100	5.90	12.25
JS84[5]	0.055 *M* K, 0.165 *M* Ag	100	3.50	12.64
JS89[7]	0.06 *M* K, 0.00 *M* Ag	200	2.60	6.04
JS90[7]	0.05 *M* K, 0.01 *M* Ag	200	3.70	6.09
JS91[7]	0.04 *M* K, 0.02 *M* Ag	200	4.10	6.26
JS92[7]	0.03 *M* K, 0.03 *M* Ag	200	2.90	6.39
JS93[7]	0.02 *M* K, 0.04 *M* Ag	200	3.90	6.51
JS94[7]	0.01 *M* K, 0.05 *M* Ag	200	2.90	6.64
JS95[7]	0.00 *M* $M^{+,2+}$, 0.06 *M* Ag	200	3.00	6.81

Notes: 1 Solutions contained 0.51 *M* $Fe_2(SO_4)_3.5H_2O$ and were heated at 97ºC and products were dried at 60ºC.
2 Solutions contained 0.51 *M* $Fe_2(SO_4)_3.5H_2O$ and were heated at 97ºC and products were dried at 110ºC.
3 Solutions contained 0.15 *M* $Fe_2(SO_4)_3.5H_2O$ and were heated at 140ºC and products were dried at 110ºC.
4 Samples were annealed at 140ºC and dried at 110ºC (from solutions originally containing 0.51 *M* $Fe_2(SO_4)_3.5H_2O$ and heated at 97ºC and products dried at 60ºC). 5 Samples were annealed at 140ºC and dried at 110ºC (from solutions originally containing 0.51 *M* $Fe_2(SO_4)_3.5H_2O$ and heated at 97ºC and products dried at 110ºC). 6 Solutions contained 0.51 *M* $Fe_2(SO_4)_3.5H_2O$ and were prepared at 22ºC and products were air dried. 7 Solutions contained 0.075 *M* $Fe_2(SO_4)_3.5H_2O$ and were prepared at 22ºC and products were air dried.

Product weights of Na-Ag jarosites synthesised at 22ºC, 97ºC and 140ºC, and the concentrations of Na and Ag in the starting solutions

Sample	Starting solution	Solution (ml)	Product, actual (g)	Product, ideal (g)
JS12[1]	0.00 M M^+, 0.22 M Ag	100	8.15	13.05
JS14[1]	0.22 M Na, 0.00 M Ag	100	4.45	10.94
JS16[1]	0.165 M Na, 0.055 M Ag	100	6.90	11.50
JS18[1]	0.11 M Na, 0.11 M Ag	100	7.20	12.02
JS20[1]	0.055 M Na, 0.165 M Ag	100	8.10	12.53
JS30[2]	0.00 M M^+, 0.22 M Ag	100	6.20	13.05
JS32[2]	0.22 M Na, 0.00 M Ag	100	3.72	10.94
JS34[2]	0.165 M Na, 0.055 M Ag	100	4.95	11.50
JS36[2]	0.11 M Na, 0.11 M Ag	100	3.20	12.02
JS38[2]	0.055 M Na, 0.165 M Ag	100	4.35	12.53
JS38D[2]	0.055 M Na, 0.165 M Ag	100	4.50	12.53
JS42[2]	0.5 M Na, 0.1 M Ag	100	2.48	16.97
JS49[3]	0.12 M Na, 0.00 M Ag	100	4.42	5.81
JS50[3]	0.10 M Na, 0.02 M Ag	100	3.13	5.90
JS51[3]	0.08 M Na, 0.04 M Ag	100	3.29	6.13
JS52[3]	0.06 M Na, 0.06 M Ag	100	3.46	6.31
JS53[3]	0.04 M Na, 0.08 M Ag	100	3.61	6.42
JS54[3]	0.02 M Na, 0.10 M Ag	100	2.82	6.62
JS61[3]	0.00 M M^+, 0.12 M Ag	100	3.89	6.81
JS66[4]	0.00 M M^+, 0.22 M Ag	100	4.50	13.05
JS67[4]	0.22 M Na, 0.00 M Ag	100	6.80	10.94
JS68[4]	0.165 M Na, 0.055 M Ag	100	8.10	11.50
JS69[4]	0.11 M Na, 0.11 M Ag	100	6.10	12.02
JS70[4]	0.055 M Na, 0.165 M Ag	100	5.80	12.53
JS71[5]	0.00 M M^+, 0.22 M Ag	100	3.10	13.05
JS72[6]	0.00 M M^+, 0.22 M Ag	100	4.60	13.05
JS77[6]	0.22 M Na, 0.00 M Ag	100	1.90	10.94
JS78[6]	0.165 M Na, 0.055 M Ag	100	1.85	11.50
JS79[6]	0.11 M Na, 0.11 M Ag	100	2.10	12.02
JS80[6]	0.055 M Na, 0.165 M Ag	100	2.90	12.53
JS85[5]	0.22 M Na, 0.00 M Ag	100	8.90	10.94
JS86[5]	0.165 M Na, 0.055 M Ag	100	7.10	11.50
JS87[5]	0.11 M Na, 0.11 M Ag	100	5.10	12.02
JS88[5]	0.055 M Na, 0.165 M Ag	100	4.00	12.53
JS95[7]	0.00 *M* $M^{+,2+}$, 0.06 *M* Ag	200	3.00	6.81
JS96[7]	0.06 *M* Na, 0.00 *M* Ag	200	1.00	5.81
JS97[7]	0.05 *M* Na, 0.01 *M* Ag	200	2.20	5.90
JS98[7]	0.04 *M* Na, 0.02 *M* Ag	200	3.00	6.13
JS99[7]	0.03 *M* Na, 0.03 *M* Ag	200	3.40	6.31
JS100[7]	0.02 *M* Na, 0.04 *M* Ag	200	3.50	6.42
JS101[7]	0.01 *M* Na, 0.05 *M* Ag	200	4.20	6.62

Notes: 1 Solutions contained 0.51 *M* $Fe_2(SO_4)_3.5H_2O$ and were heated at 97ºC and products were dried at 60ºC.
2 Solutions contained 0.51 *M* $Fe_2(SO_4)_3.5H_2O$ and were heated at 97ºC and products were dried at 110ºC.
3 Solutions contained 0.15 *M* $Fe_2(SO_4)_3.5H_2O$ and were heated at 140ºC and products were dried at 110ºC.
4 Samples were annealed at 140ºC and dried at 110ºC (from solutions originally containing 0.51 *M* $Fe_2(SO_4)_3.5H_2O$ and heated at 97ºC and products dried at 60ºC). 5 Samples were annealed at 140ºC and dried at 110ºC (from solutions originally containing 0.51 *M* $Fe_2(SO_4)_3.5H_2O$ and heated at 97ºC and products dried at 110ºC). 6 Solutions contained 0.51 *M* $Fe_2(SO_4)_3.5H_2O$ and were prepared at 22ºC and products were air dried. 7 Solutions contained 0.075 *M* $Fe_2(SO_4)_3.5H_2O$ and were prepared at 22ºC and products were air dried.

Product weights of Pb-Ag jarosites synthesised at 22ºC and 140ºC, plus the concentrations of Pb and Ag in the starting solutions

Sample	Starting solution	Solution (ml)	Product, actual (g)	Product, ideal (g)
JS43[1]	0.06 M Pb, 0.00 M Ag	100	2.87	9.94
JS43D[1]	0.06 M Pb, 0.00 M Ag	100	2.68	9.94
JS44[1]	0.05 M Pb, 0.02 M Ag	100	2.90	6.78
JS45[1]	0.04 M Pb, 0.04 M Ag	100	3.90	6.75
JS46[1]	0.03 M Pb, 0.06 M Ag	100	4.34	6.80
JS47[1]	0.02 M Pb, 0.08 M Ag	100	4.85	6.79
JS48[1]	0.01 M Pb, 0.10 M Ag	100	3.85	6.77
JS61	0.00 M M^{+}, 0.12 M Ag	100	3.89	6.81
JS95[2]	0.00 *M* $M^{+,2+}$, 0.06 *M* Ag	200	3.00	6.81
JS102[2]	0.00013 *M* Pb, 0.05 *M* Ag	200	3.20	5.94
JS103[2]	0.00032 *M* Pb, 0.05 *M* Ag	200	2.50	5.75
JS104[2]	0.001 *M* Pb, 0.05 *M* Ag	200	4.20	5.87
JS105[2]	0.005 *M* Pb, 0.05 *M* Ag	200	4.30	6.77
JS106[2]	0.001 *M* Pb, 0.05 *M* Ag	200	3.10	5.87
JS107[2,3]	0.001 *M* Pb, 0.00 *M* Ag	200	0.80	0.33 (5.23)

1 Samples contained 0.15 *M* $Fe_2(SO_4)_3.5H_2O$ and were prepared at 140ºC and product were dried at 110ºC.
2 Solutions contained 0.075 *M* $Fe_2(SO_4)_3.5H_2O$ and were prepared at 22ºC and products were air dried. Samples 106 and 107 involved slow addition of Pb over several months. 3 Figure in parentheses is for $(Pb_{0.25}[H_3O]_{0.5})Fe_3(SO_4)_2(OH)_6$.

APPENDIX D SECONDARY ELECTRON IMAGES

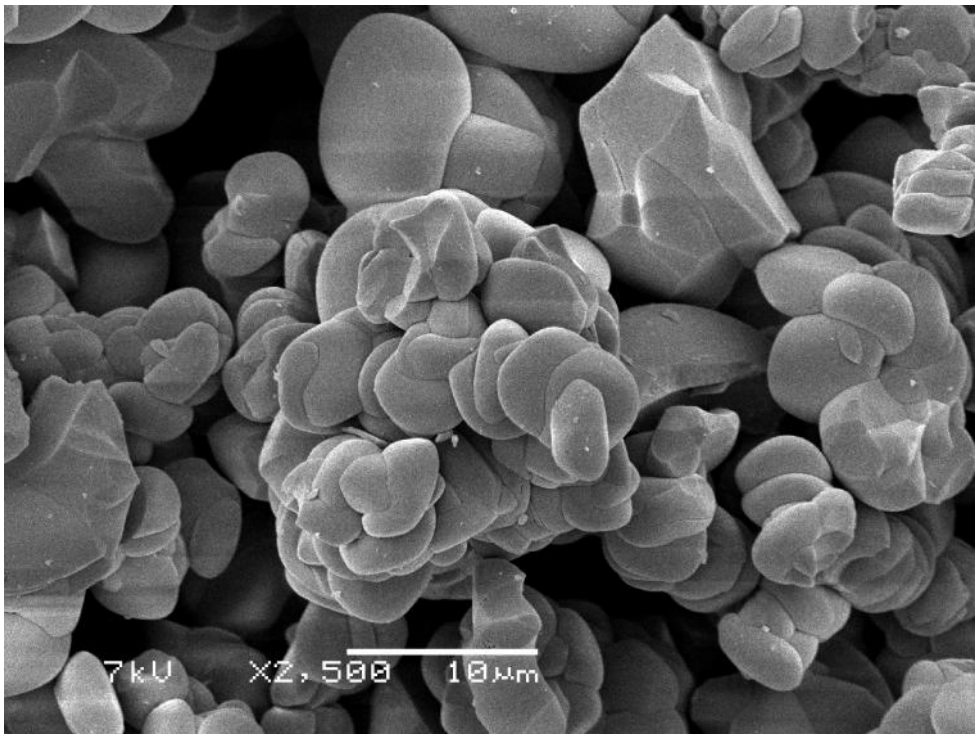

JS4 0.22 M K, 0.0 M Ag (dried at 60°C)

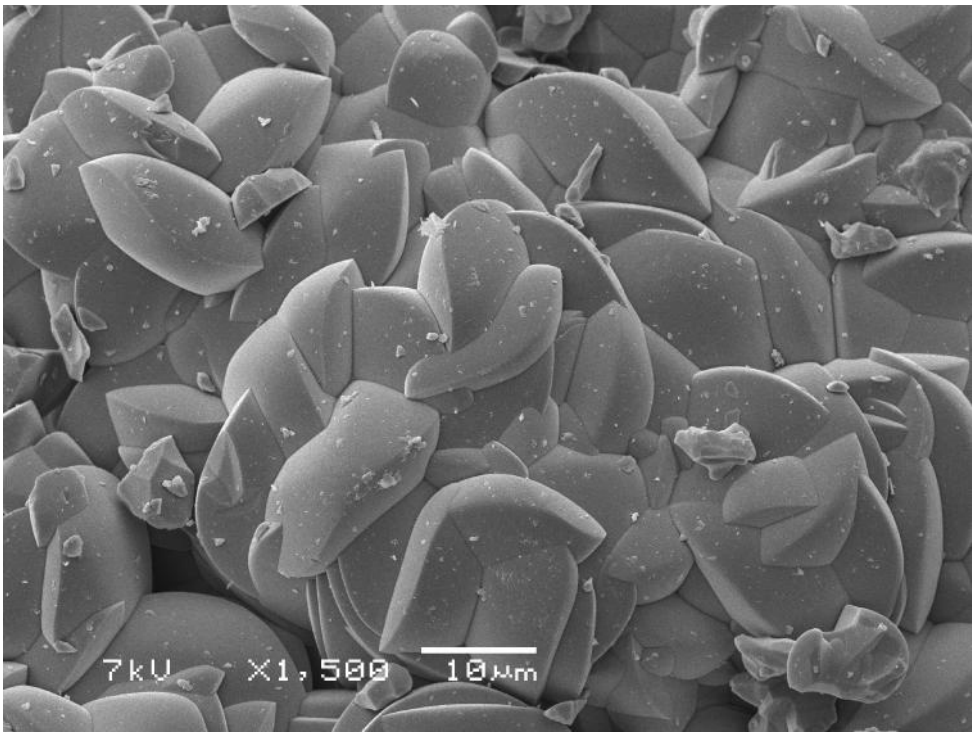

JS22 0.22 M K, 0.0 M Ag (dried at 110°C)

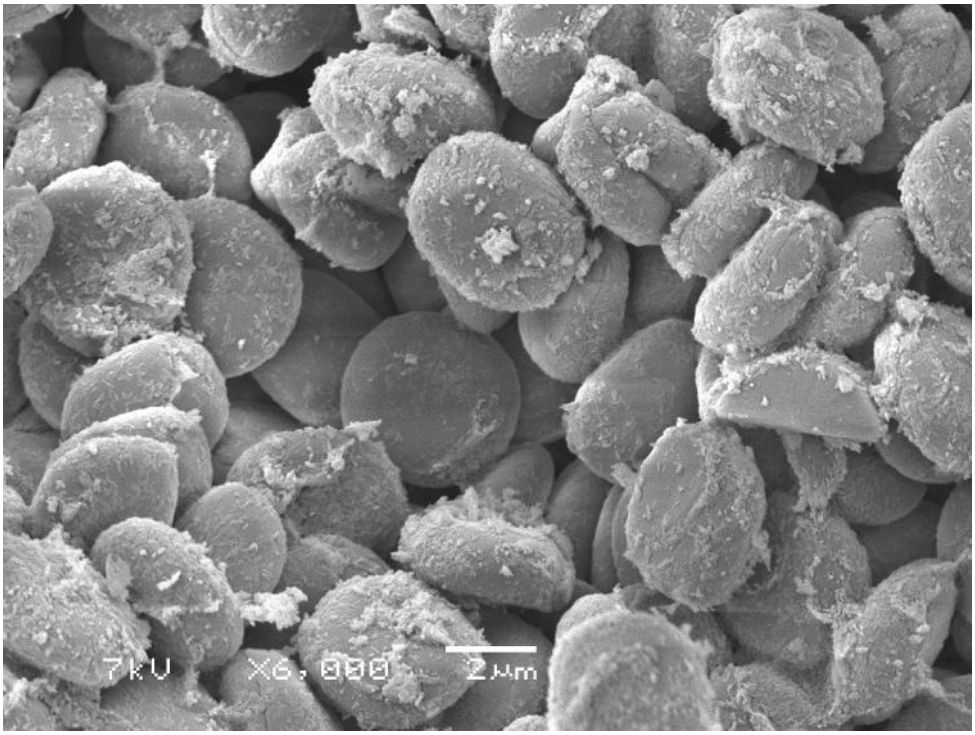

JS6 0.165 M K, 0.055 M Ag (dried at 60ºC)

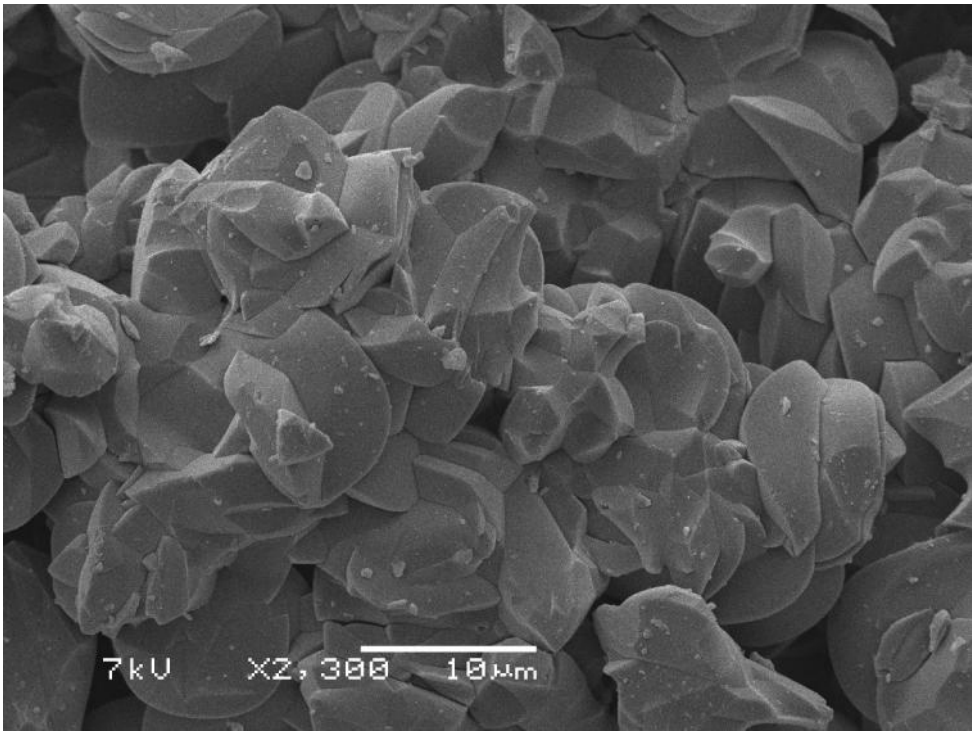

JS24 0.165 M K, 0.055 M Ag (dried at 110ºC)

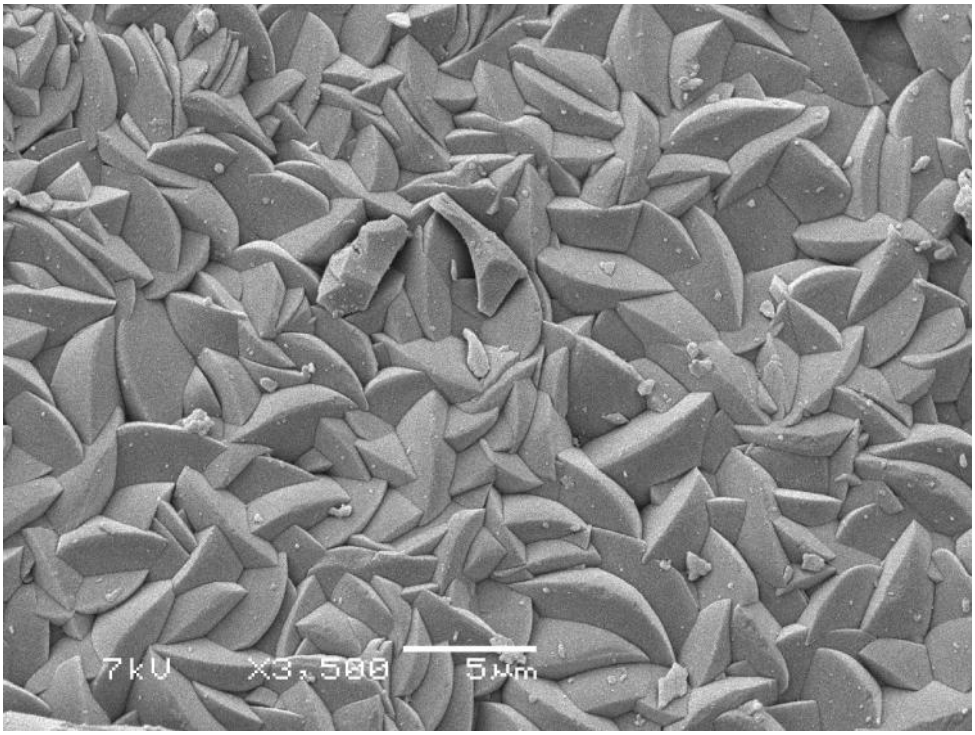

JS6D 0.165 M K, 0.055 M Ag (dried at 60ºC)

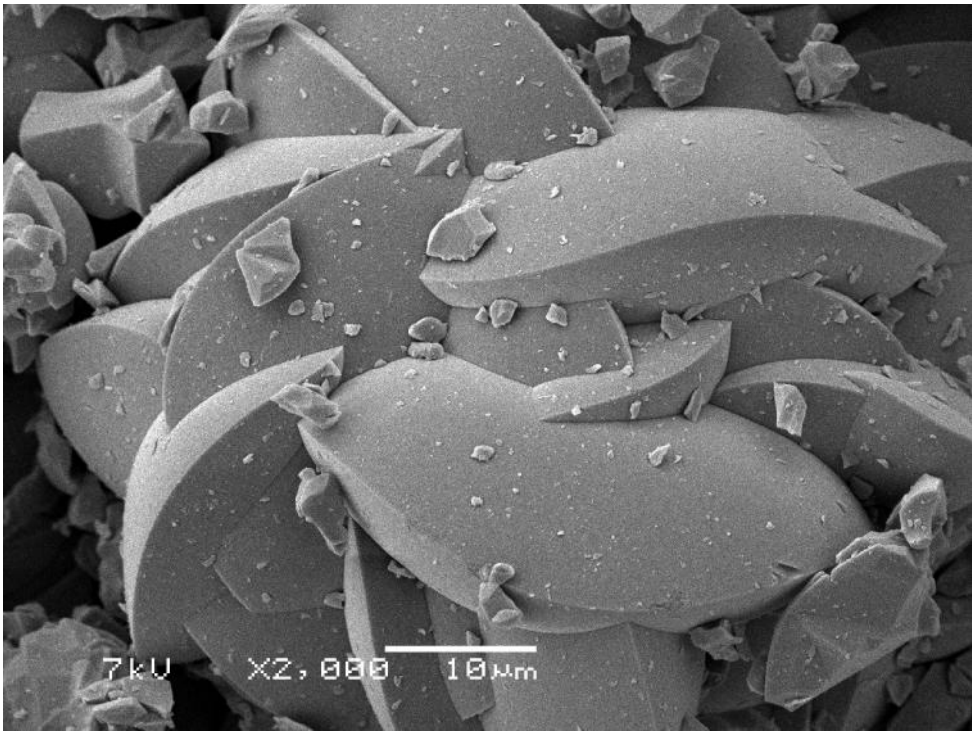

JS24D 0.165 M K, 0.055 M Ag (dried at 110ºC)

JS8 **0.11 M K, 0.11 M Ag (dried at 60ºC)**

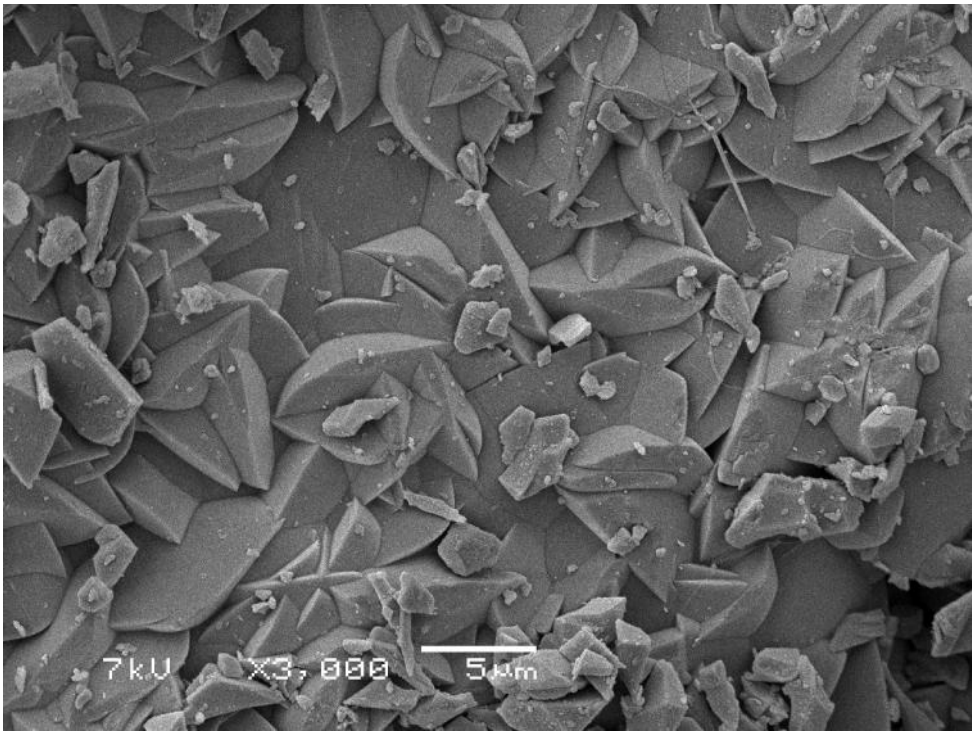

JS26 **0.11 M K, 0.11 M Ag (dried at 110ºC)**

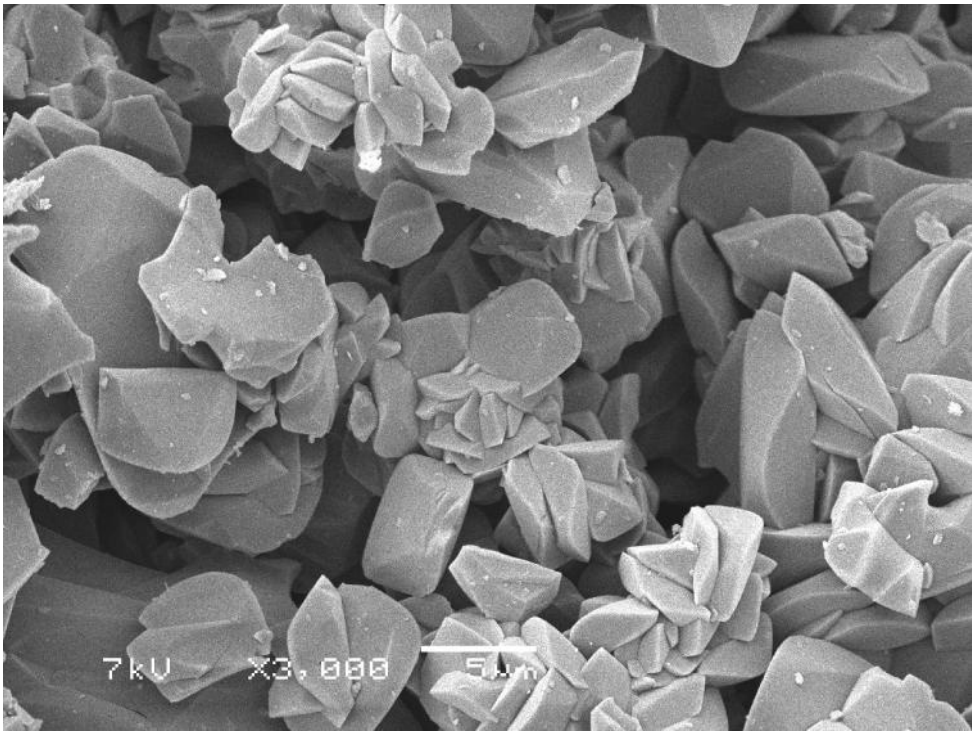

JS10 0.055 M K, 0.165 M Ag (dried at 60ºC)

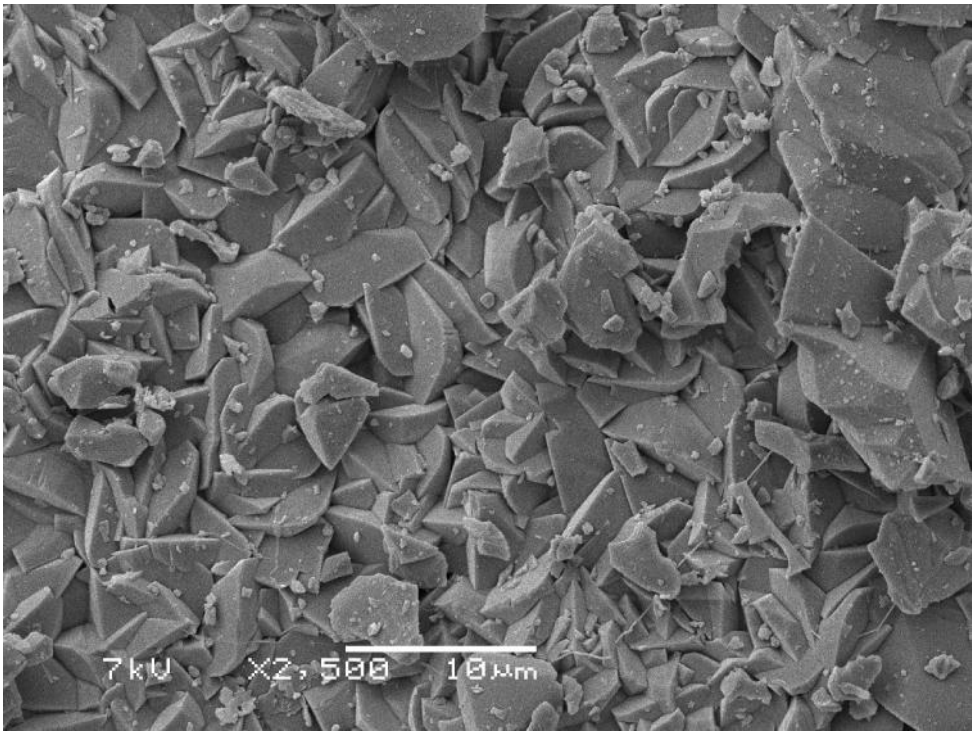

JS28 0.055 M K, 0.165 M Ag (dried at 110ºC)

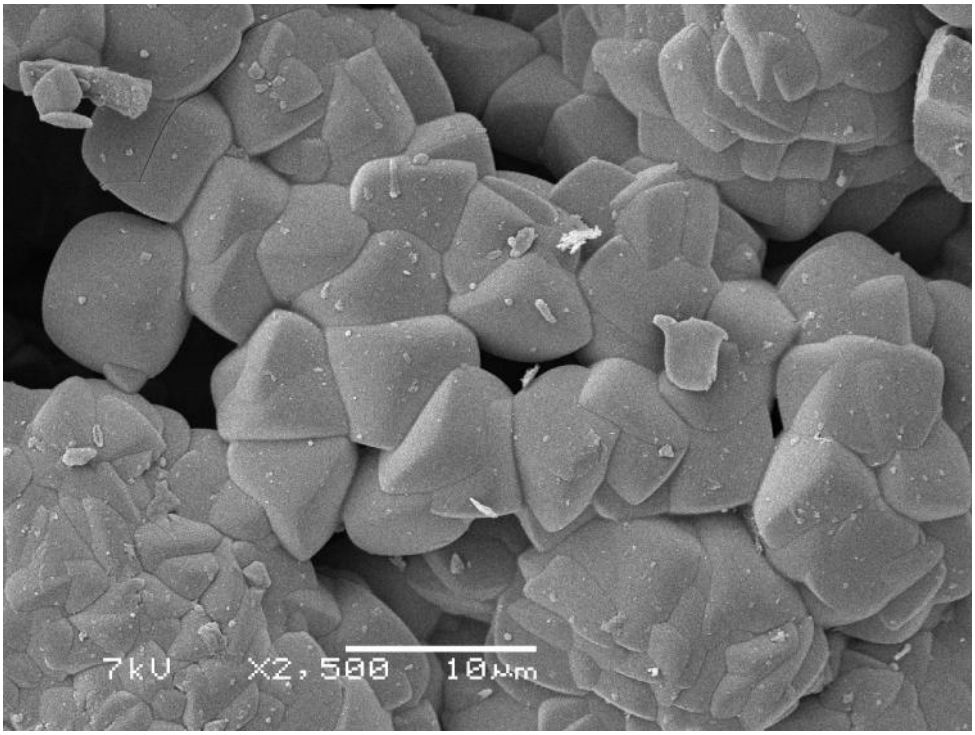

JS40 0.5 M K, 0.1 M Ag (dried at 110ºC)

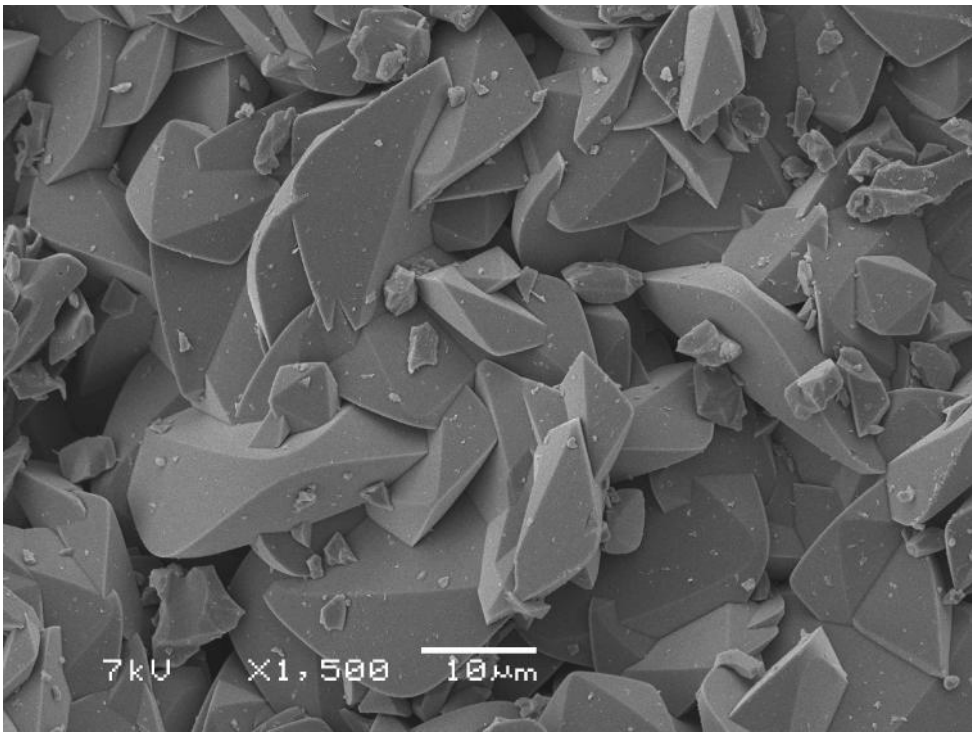

JS12 0.0 M K/Na, 0.22 M Ag (dried at 60ºC)

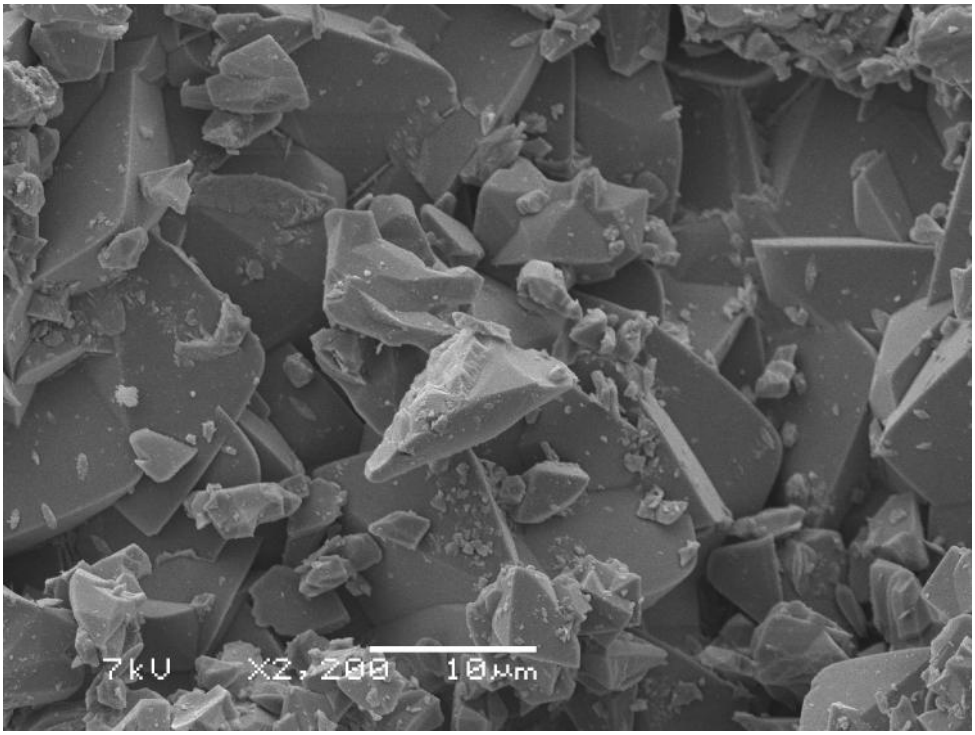

JS30 0.0 M K/Na, 0.22 M Ag (dried at 110ºC)

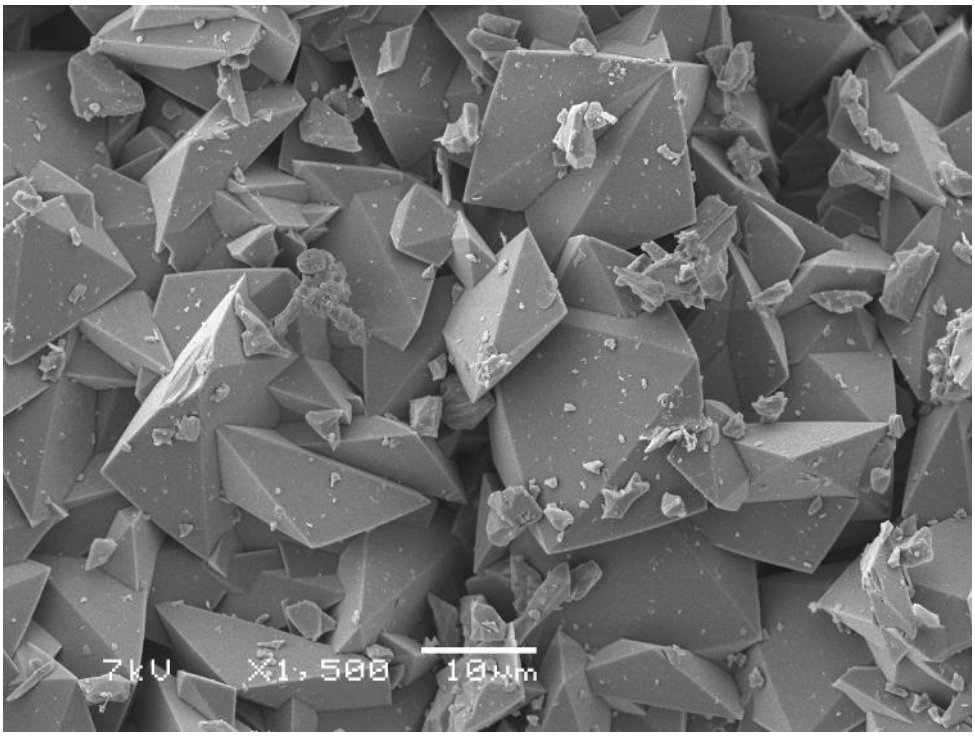

JS14 0.22 M Na, 0.0 M Ag (dried at 60ºC)

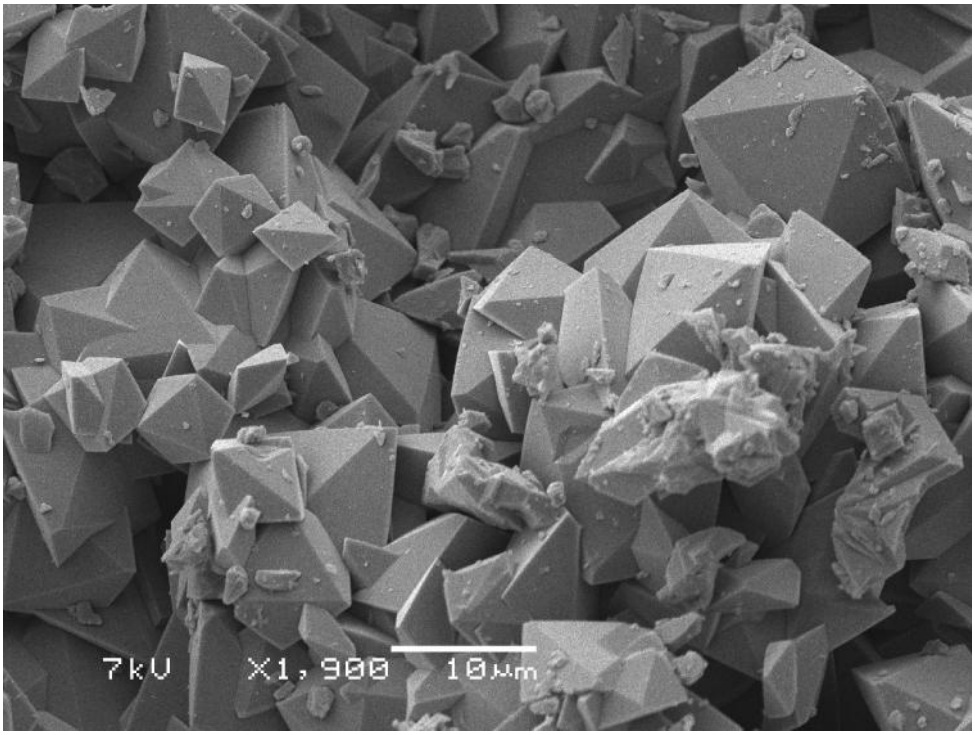

JS32 0.22 M Na, 0.0 M Ag (dried at 110ºC)

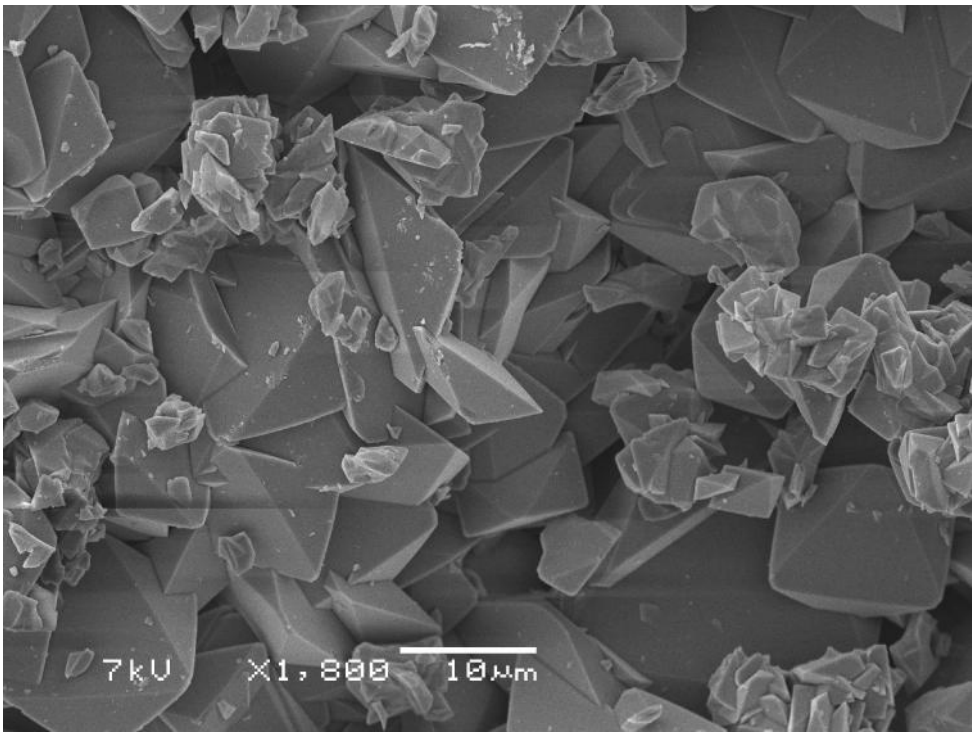

JS16 0.165 M Na, 0.055 M Ag (dried at 60ºC)

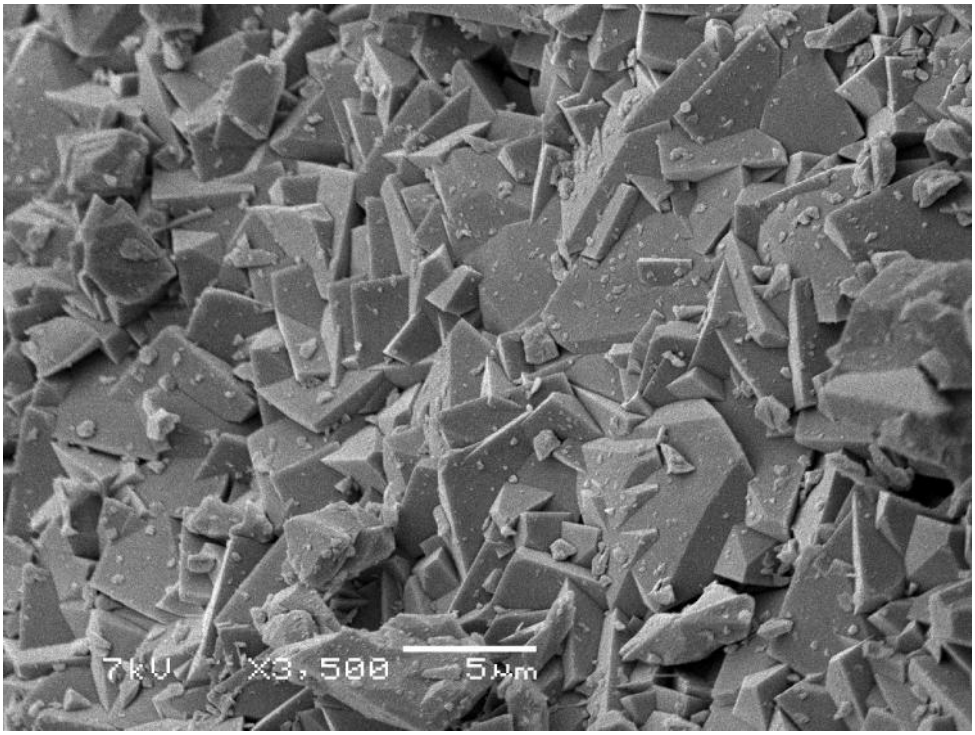

JS34 0.165 M Na, 0.055 M Ag (dried at 110ºC)

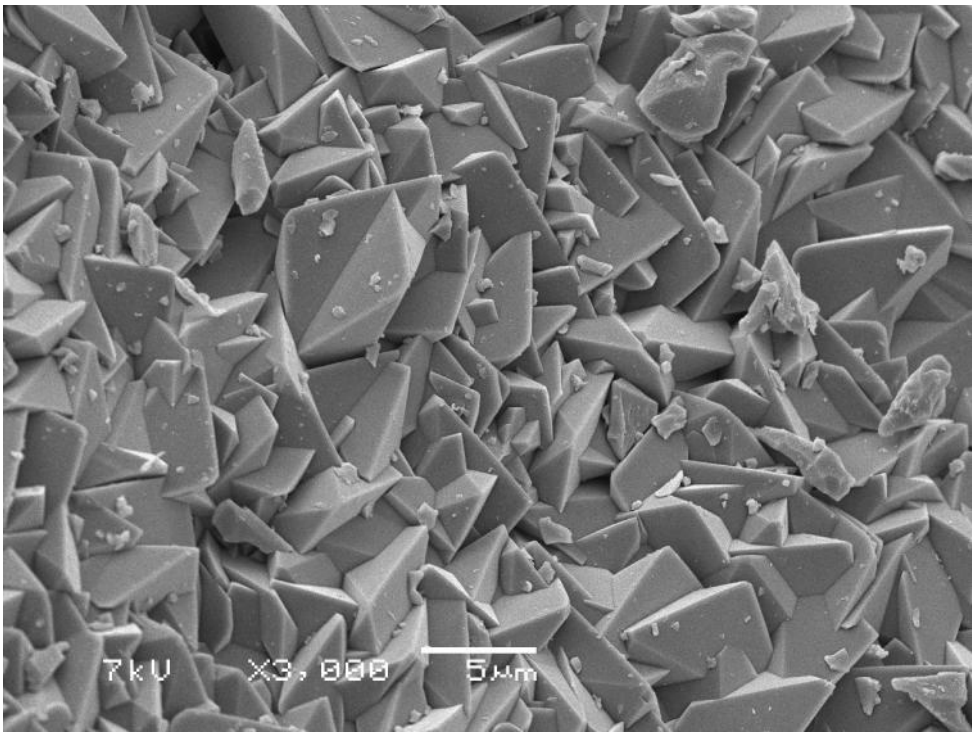

JS18 0.11 M Na, 0.11 M Ag (dried at 60ºC)

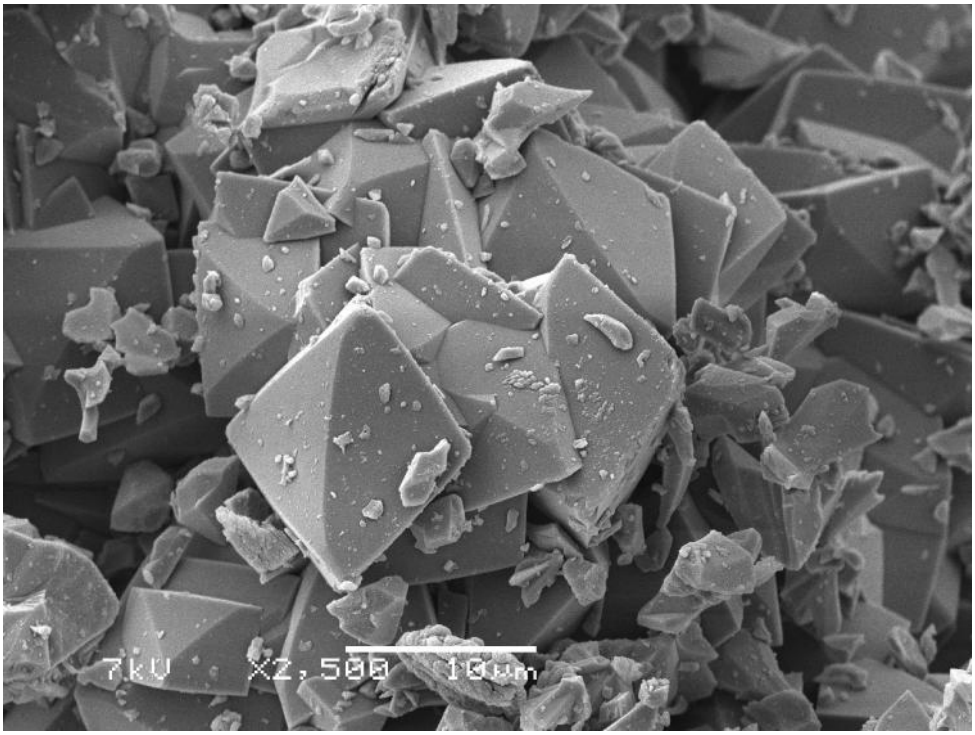

JS36 0.11 M Na, 0.11 M Ag (dried at 110ºC)

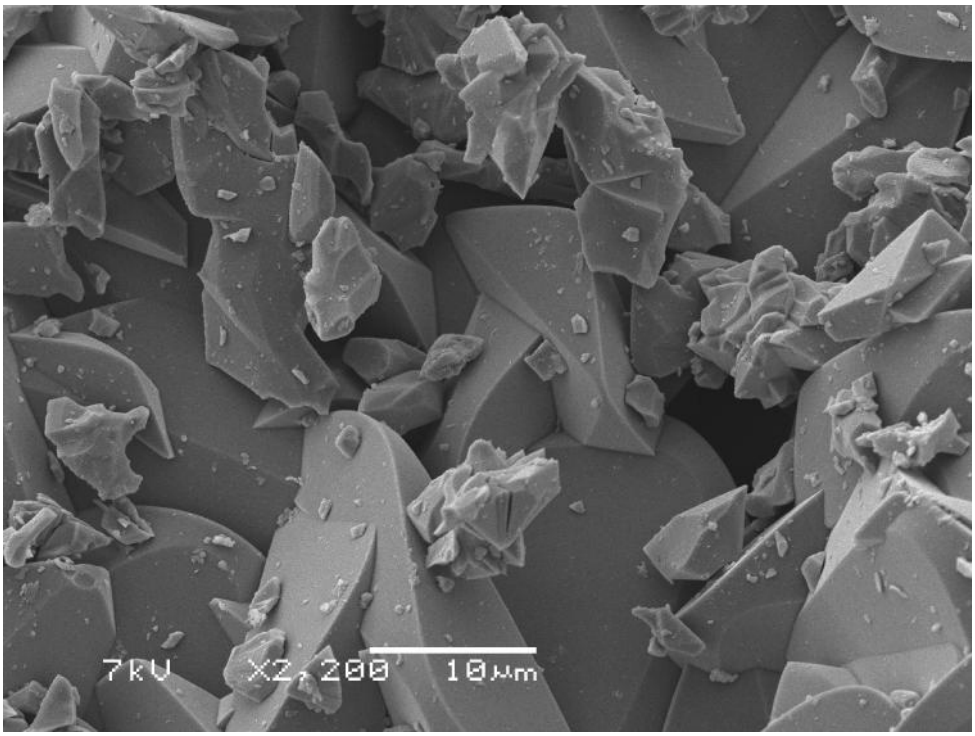

JS20 0.055 M Na, 0.165 M Ag (dried at 60ºC)

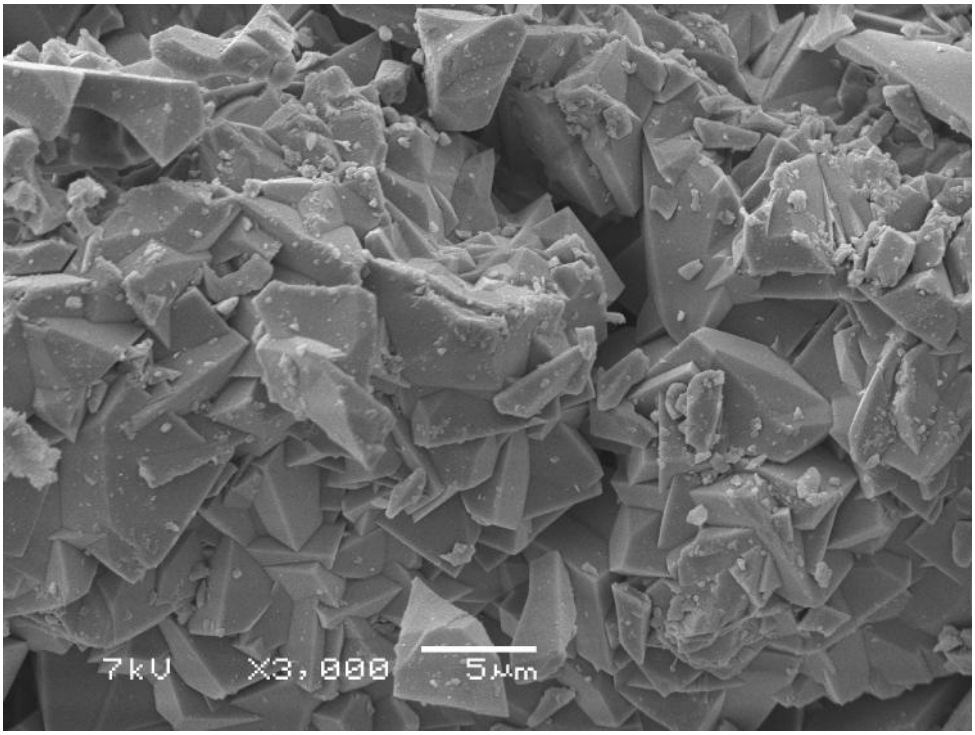

JS38 0.055 M Na, 0.165 M Ag (dried at 110ºC)

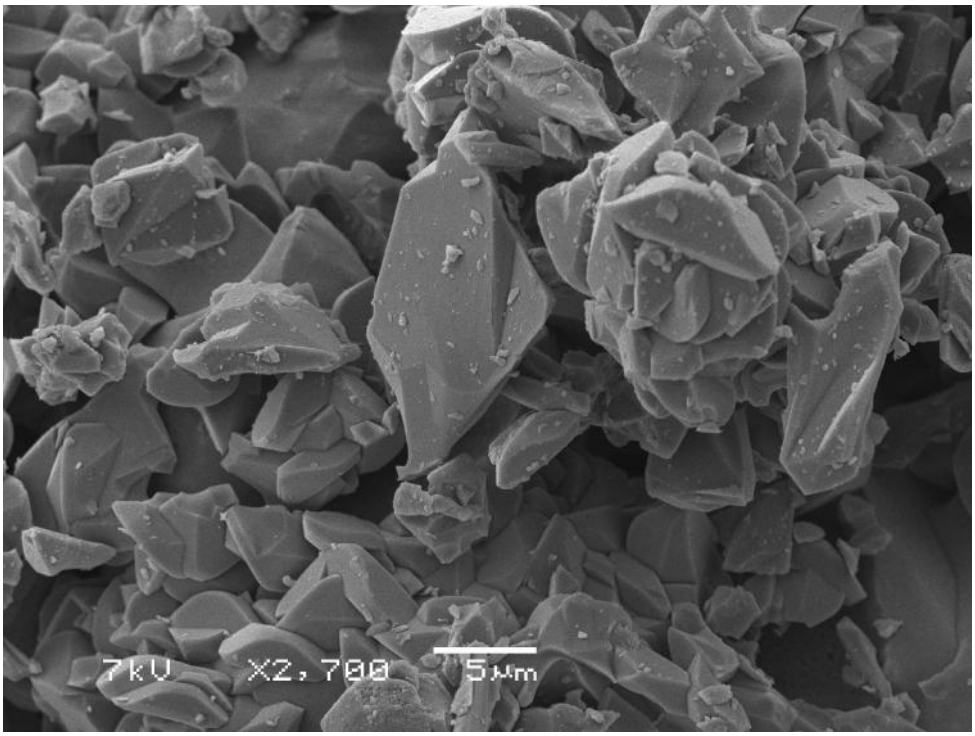

JS38D 0.055 M Na, 0.165 M Ag (dried at 110ºC)

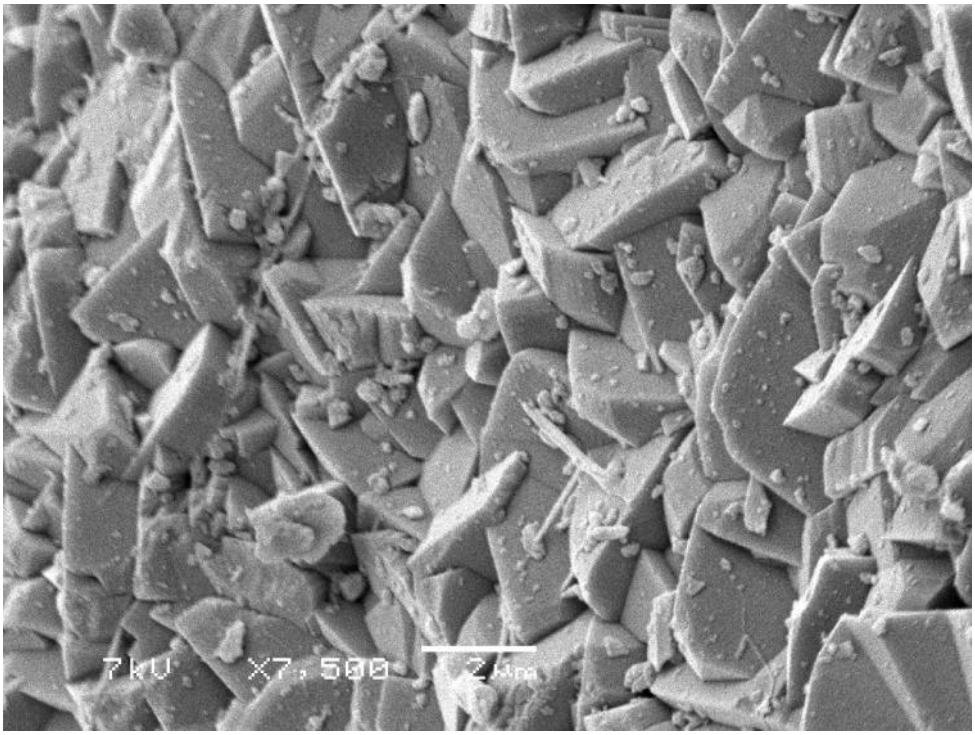

JS42 0.5 M Na, 0.1 M Ag (dried at 110ºC)

APPENDIX E XRD spectra of synthesised jarosite products (Cu radiation)

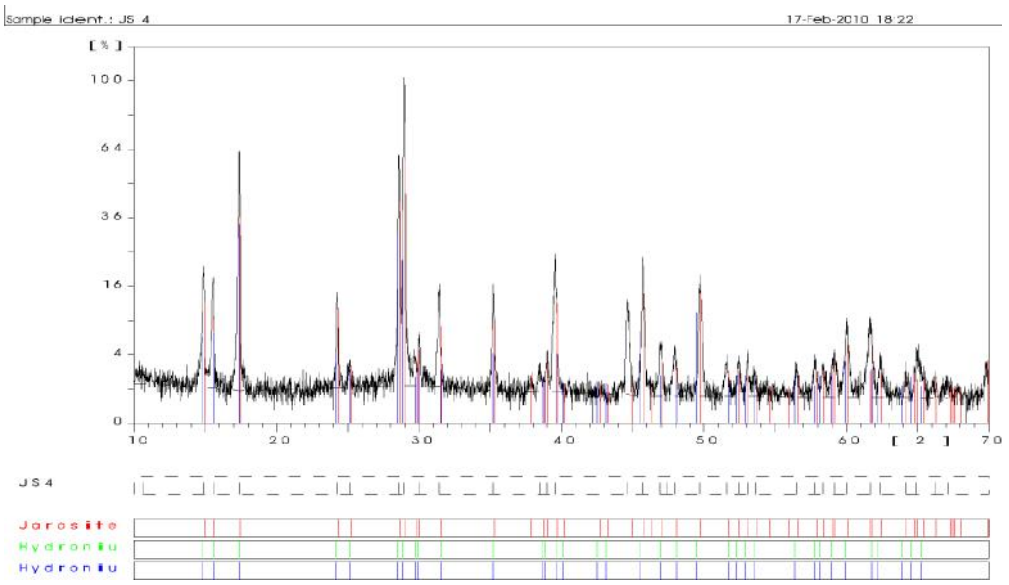

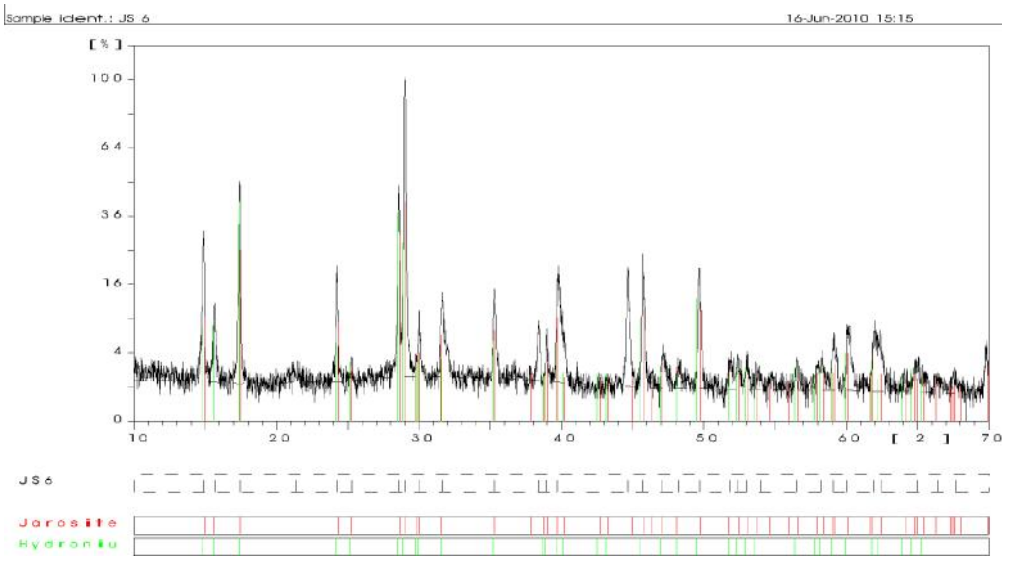

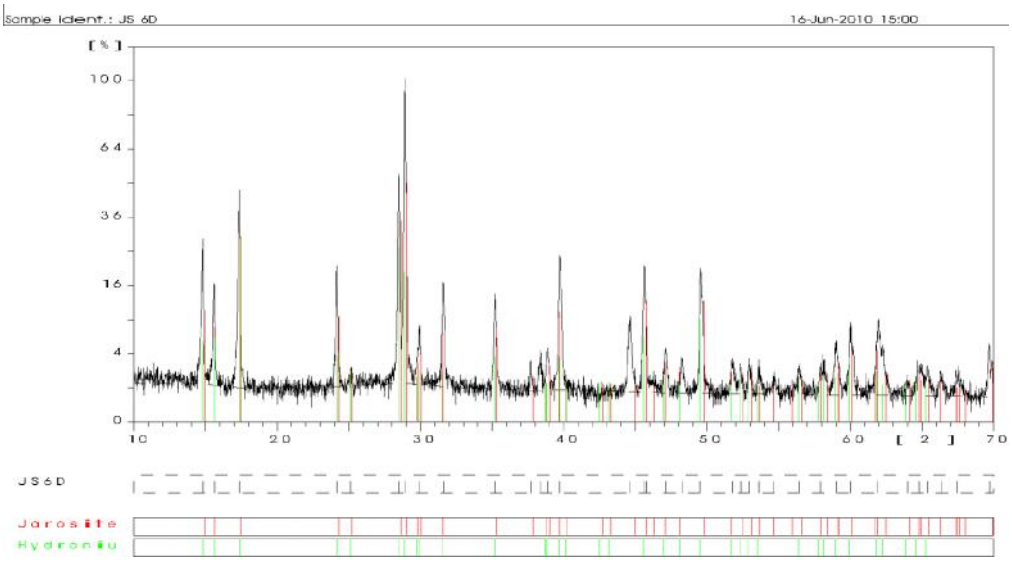

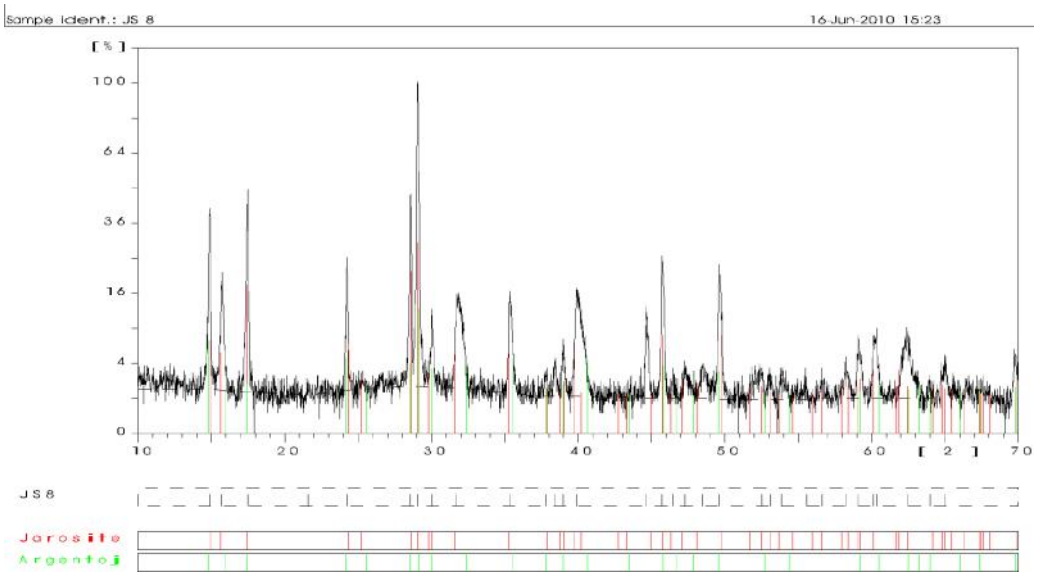
Sample Ident.: JS 8
16-Jun-2010 15:23
[%]
100
64
36
16
4
0
10
20
30
40
50
60
[2]
70
JS 8
Jarosite
Argentoj

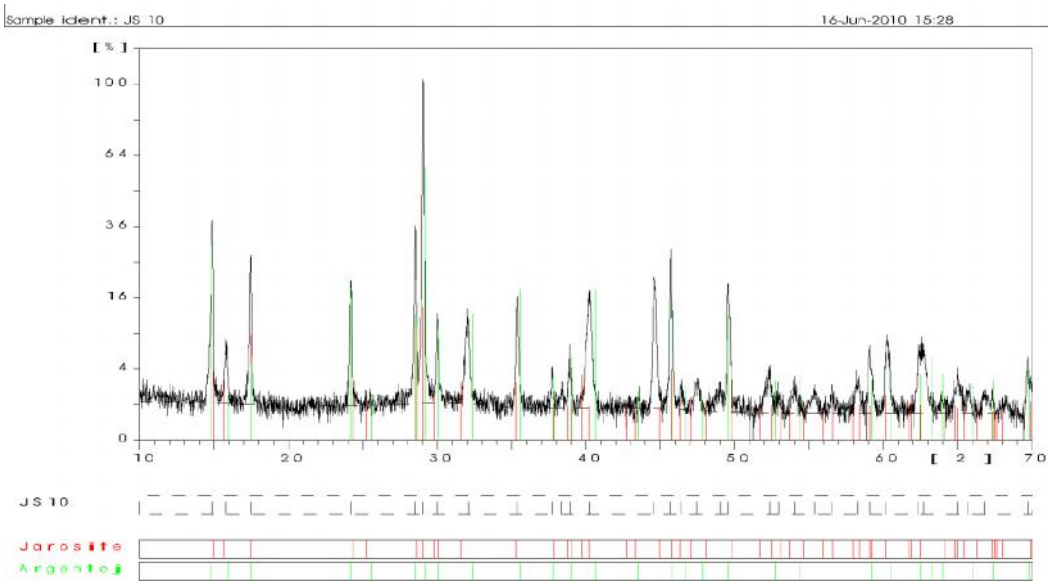
Sample Ident.: JS 10
16-Jun-2010 15:28
[%]
100
64
36
16
4
0
10
20
30
40
50
60
[2]
70
JS 10
Jarosite
Argentoj

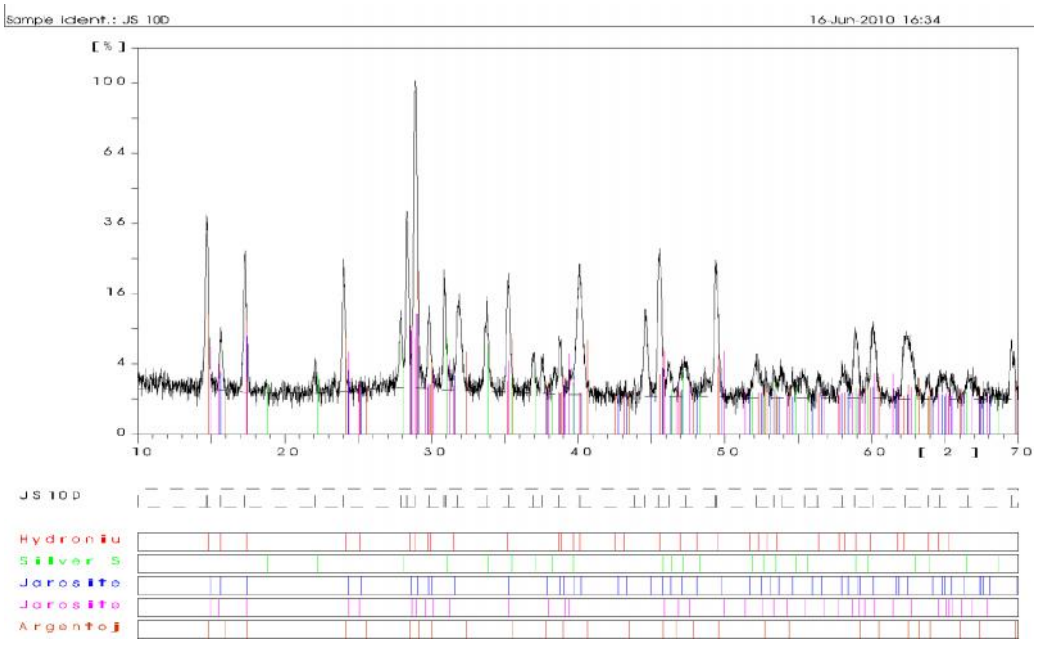
Sample Ident.: JS 10D
16-Jun-2010 16:34
[%]
100
64
36
16
4
0
10
20
30
40
50
60
[2]
70
JS 10D
Hydroniu
Silver S
Jarosite
Jarosite
Argentoj

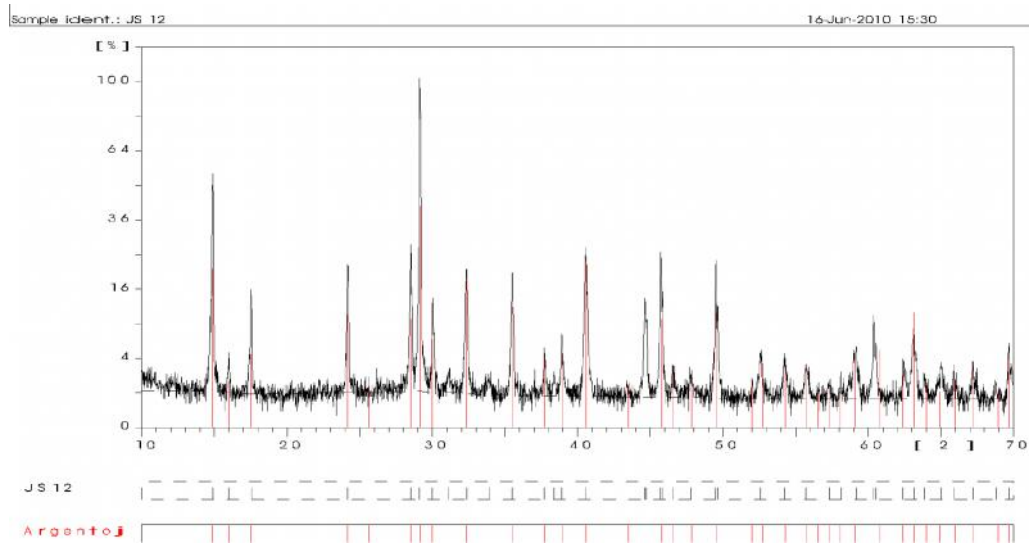
Sample Ident.: JS 12
16-Jun-2010 15:30
[%]
100
64
36
16
4
0
10
20
30
40
50
60
[2]
70
JS 12
Argentoj

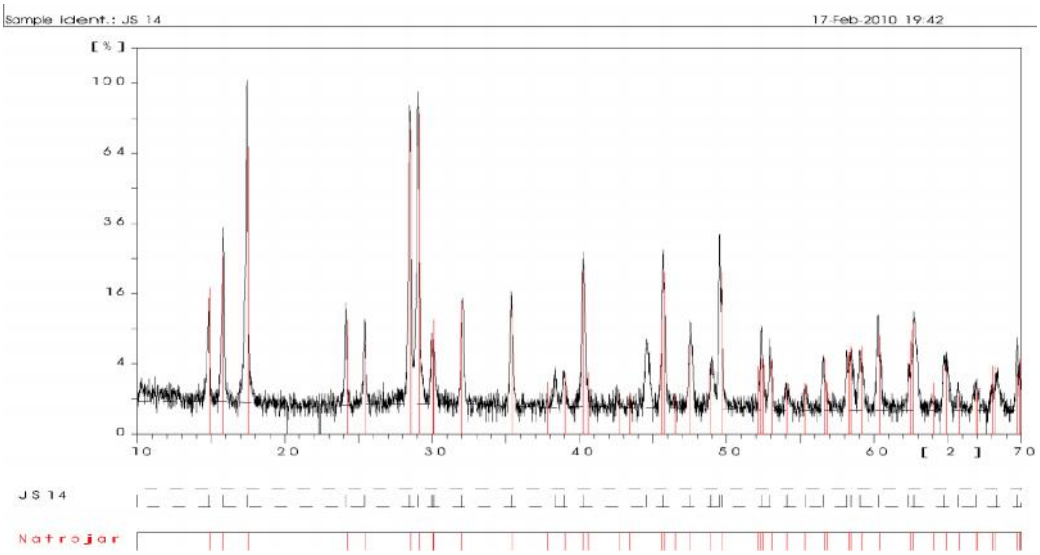
Sample Ident.: JS 14
17-Feb-2010 19:42
[%]
100
64
36
16
4
0
10
20
30
40
50
60
[2]
70
JS 14
Natrojar

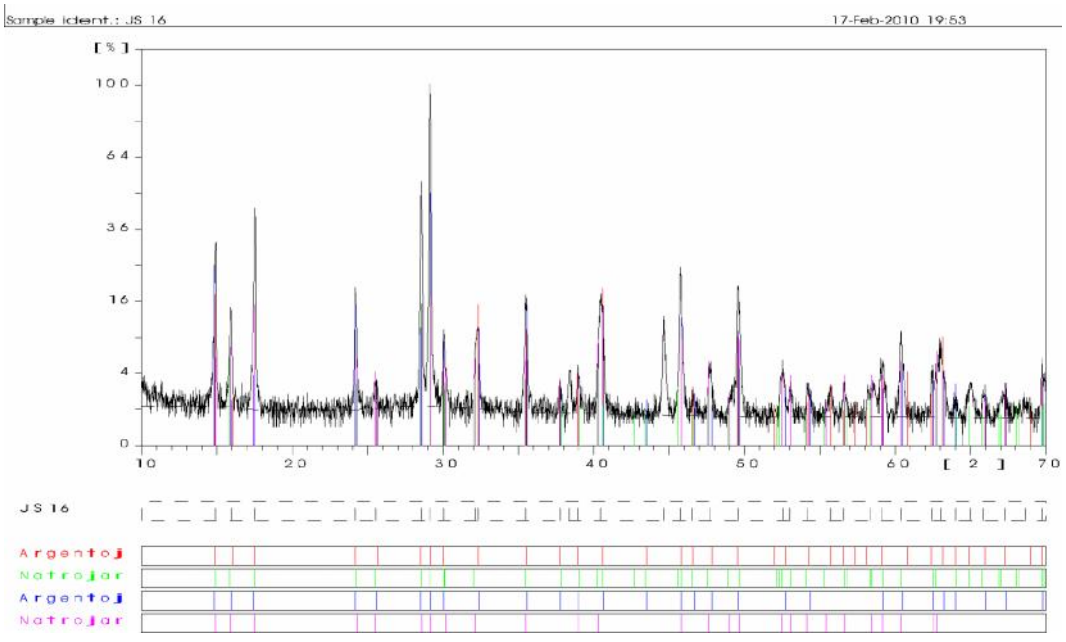
Sample Ident.: JS 16
17-Feb-2010 19:53
[%]
100
64
36
16
4
0
10
20
30
40
50
60
[2]
70
JS 16
Argentoj
Natrojar
Argentoj
Natrojar

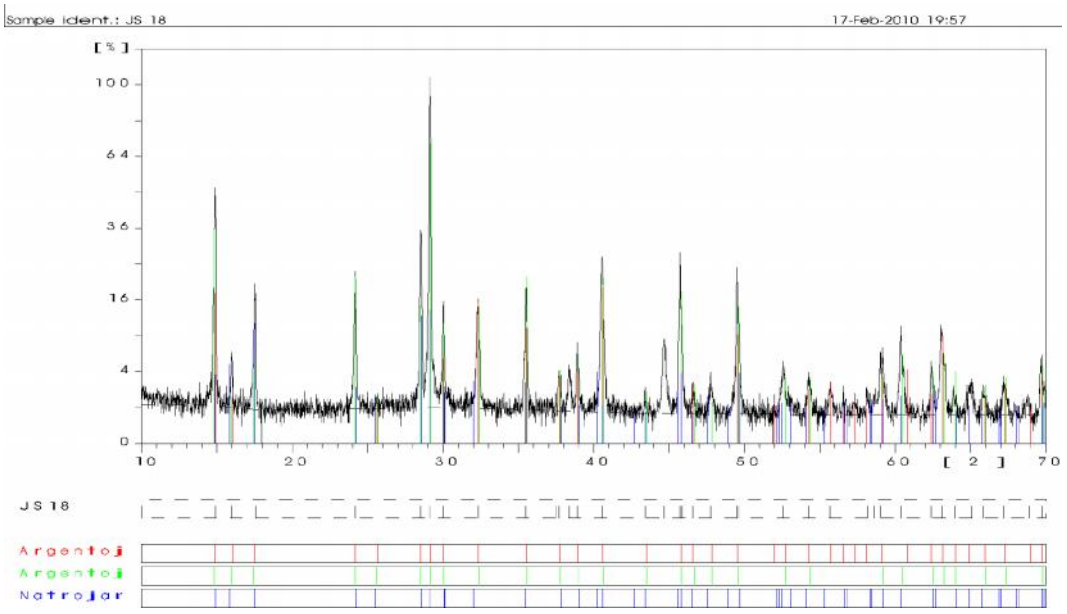
Sample ident.: JS 18
17-Feb-2010 19:57
[%]
100
64
36
16
4
0
10
20
30
40
50
60
[2]
70
JS18
Argentoj
Argentoj
Natrojar

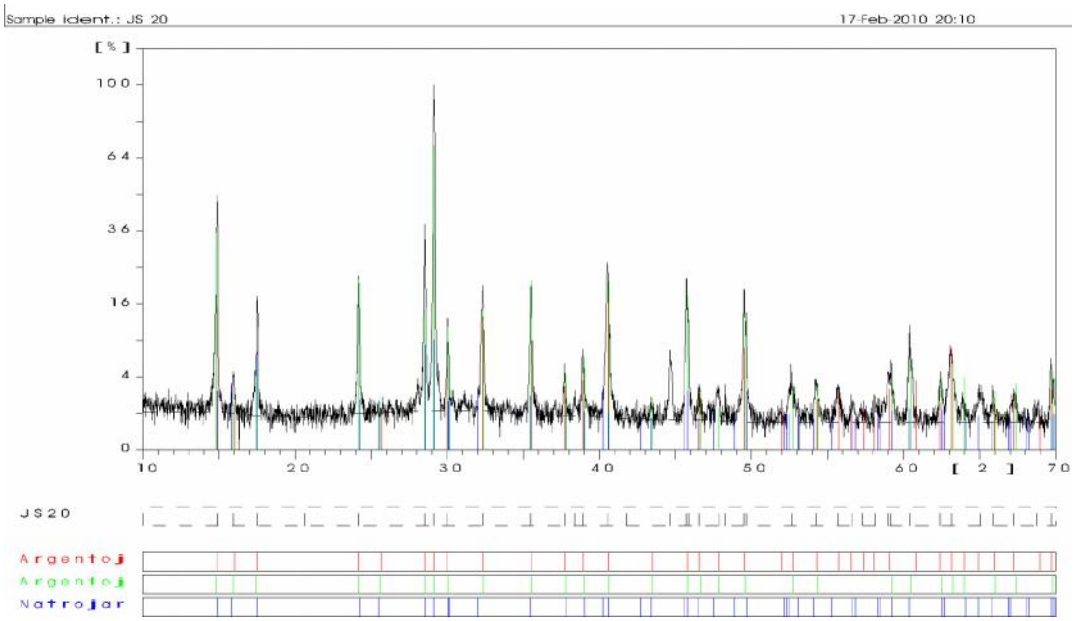
Sample ident.: JS 20
17-Feb-2010 20:10
[%]
100
64
36
16
4
0
10
20
30
40
50
60
[2]
70
JS20
Argentoj
Argentoj
Natrojar

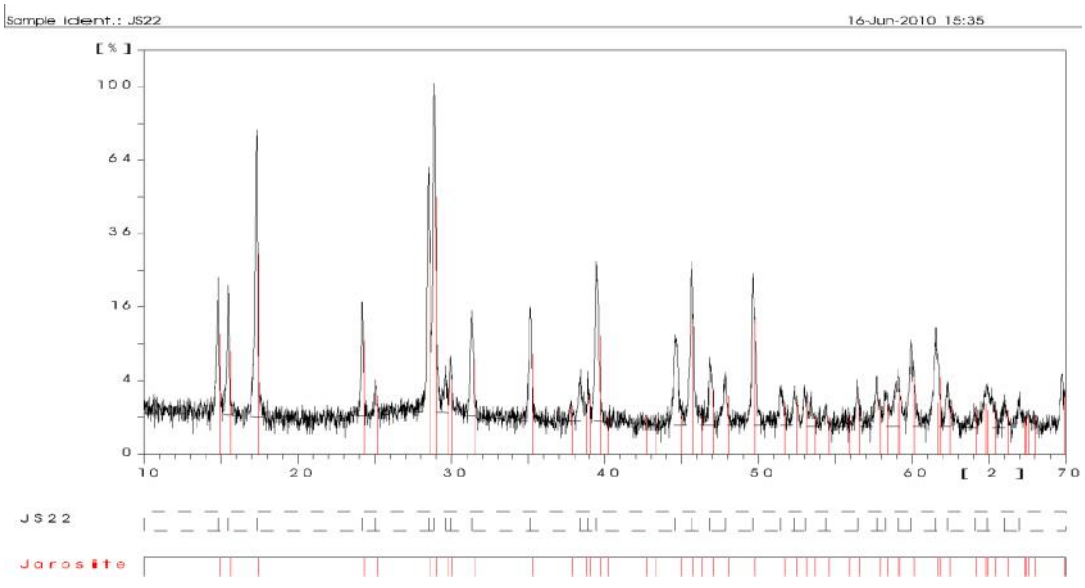
Sample ident.: JS22
16-Jun-2010 15:35
[%]
100
64
36
16
4
0
10
20
30
40
50
60
[2]
70
JS22
Jarosite

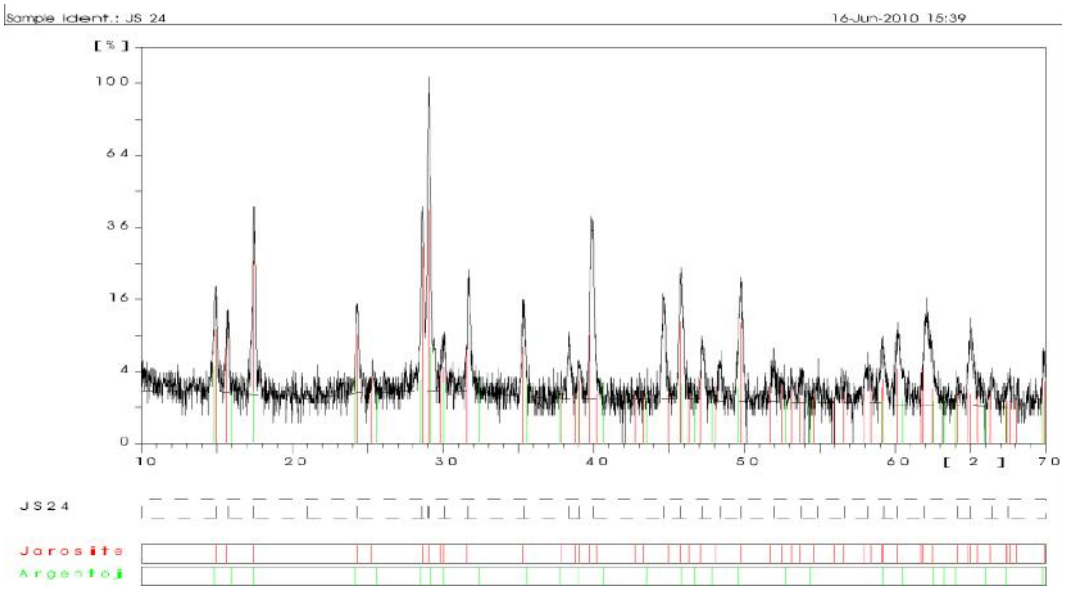
Sample ident.: JS 24
16-Jun-2010 15:39
[%]
100
64
36
16
4
0
10
20
30
40
50
60
[2]
70
JS24
Jarosite
Argentoj

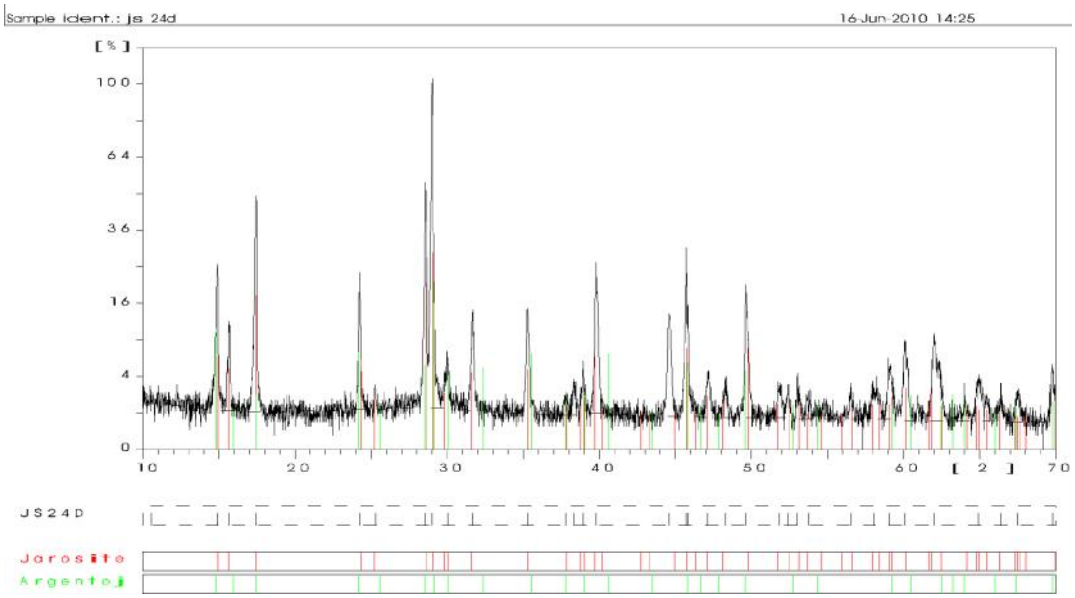
Sample ident.: js 24d
16-Jun-2010 14:25
[%]
100
64
36
16
4
0
10
20
30
40
50
60
[2]
70
JS24D
Jarosite
Argentoj

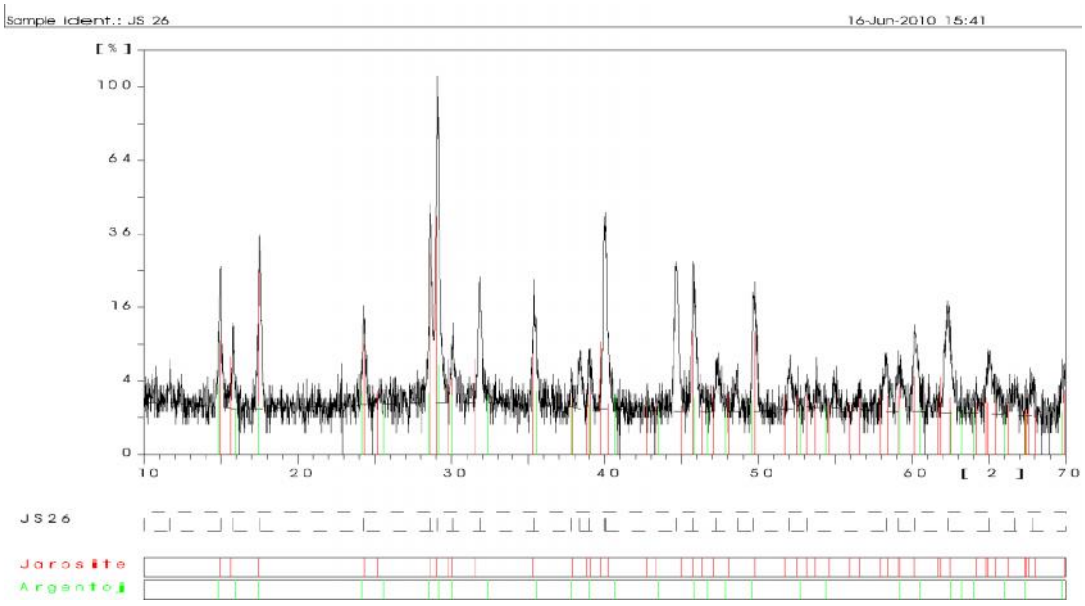
Sample ident.: JS 26
16-Jun-2010 15:41
[%]
100
64
36
16
4
0
10
20
30
40
50
60
[2]
70
JS26
Jarosite
Argentoj

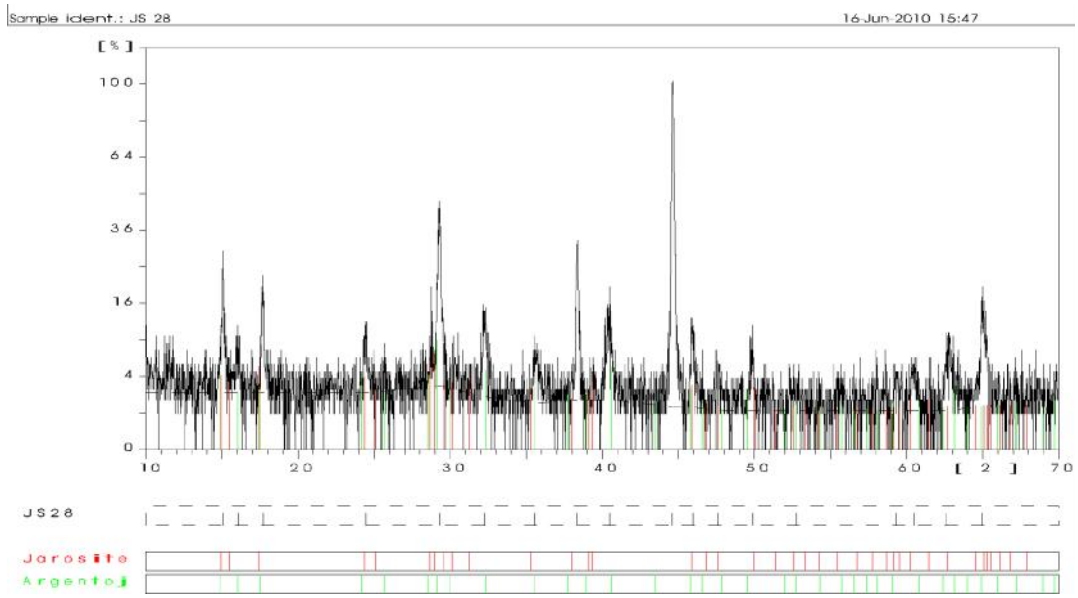
Sample Ident.: JS 28
16-Jun-2010 15:47
[%]
100
64
36
16
4
0
10
20
30
40
50
60
[2]
70
JS28
Jarosite
Argentoj

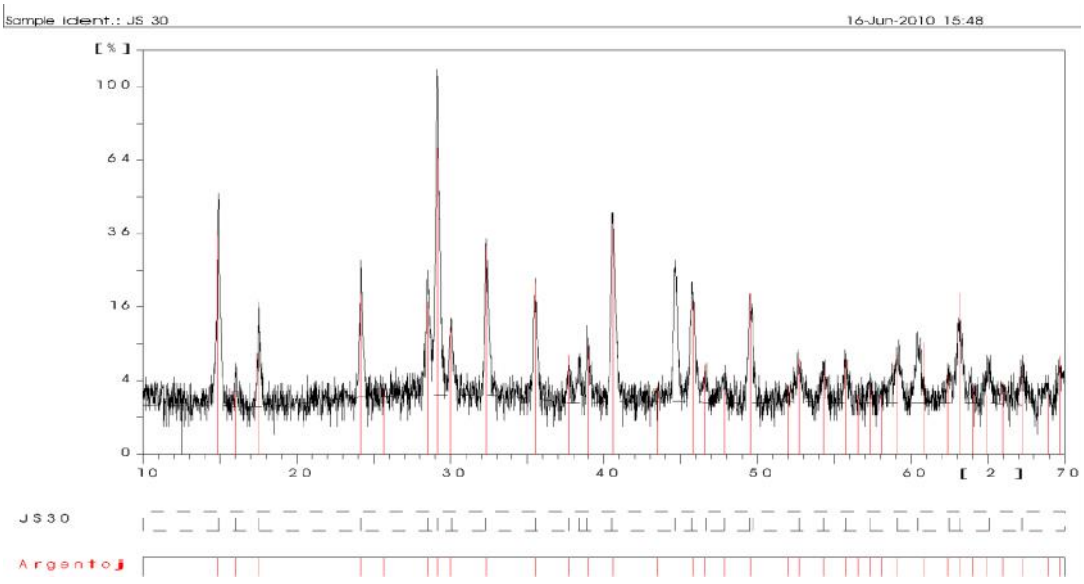
Sample Ident.: JS 30
16-Jun-2010 15:48
[%]
100
64
36
16
4
0
10
20
30
40
50
60
[2]
70
JS30
Argentoj

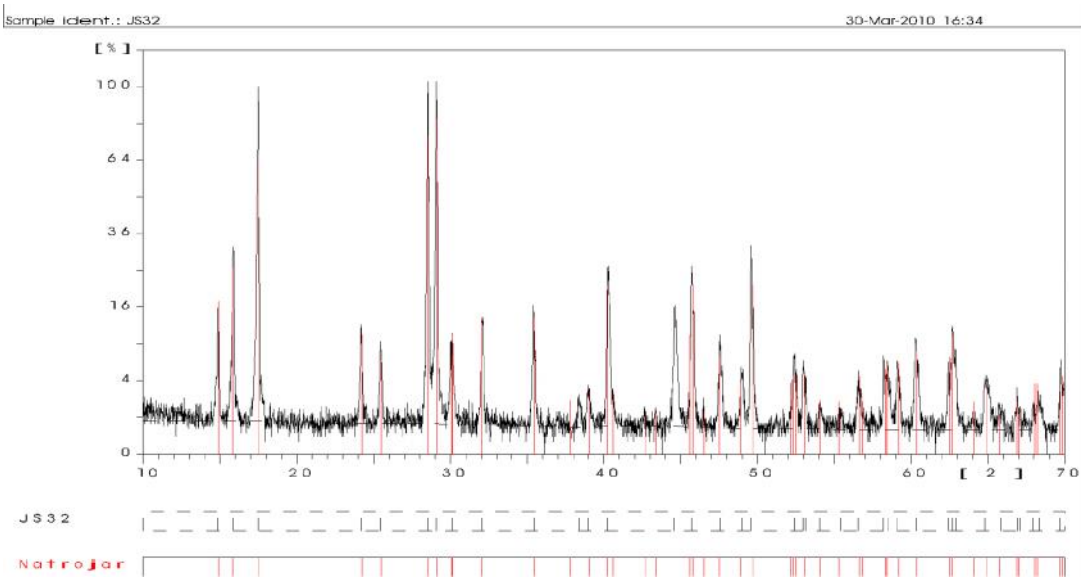
Sample Ident.: JS32
30-Mar-2010 16:34
[%]
100
64
36
16
4
0
10
20
30
40
50
60
[2]
70
JS32
Natrojar

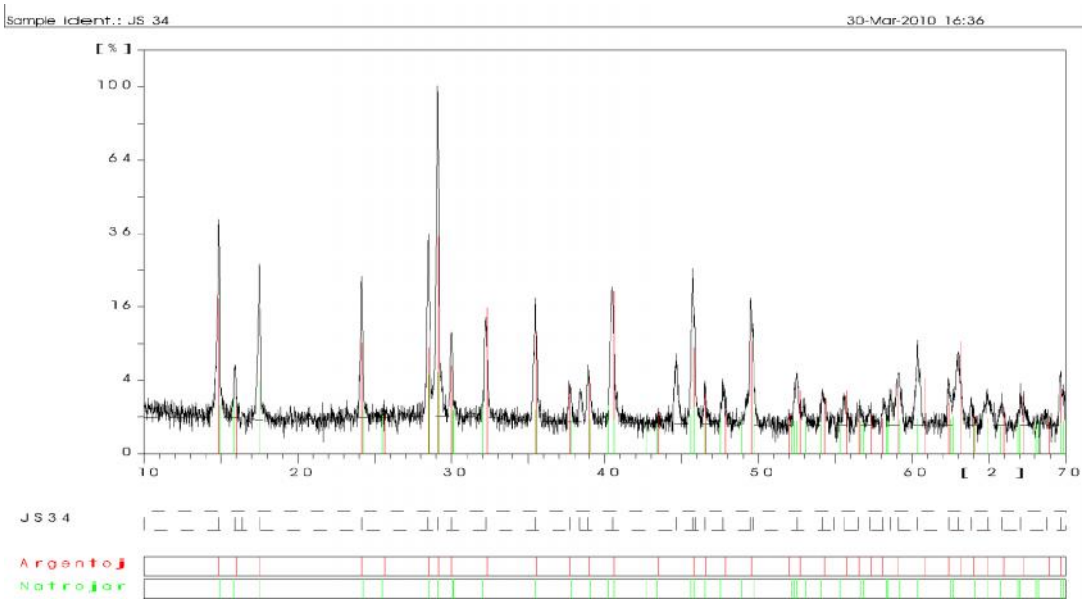
Sample Ident.: JS 34
30-Mar-2010 16:36
[%]
100
64
36
16
4
0
10
20
30
40
50
60
[2]
70
JS34
Argentoj
Natrojar

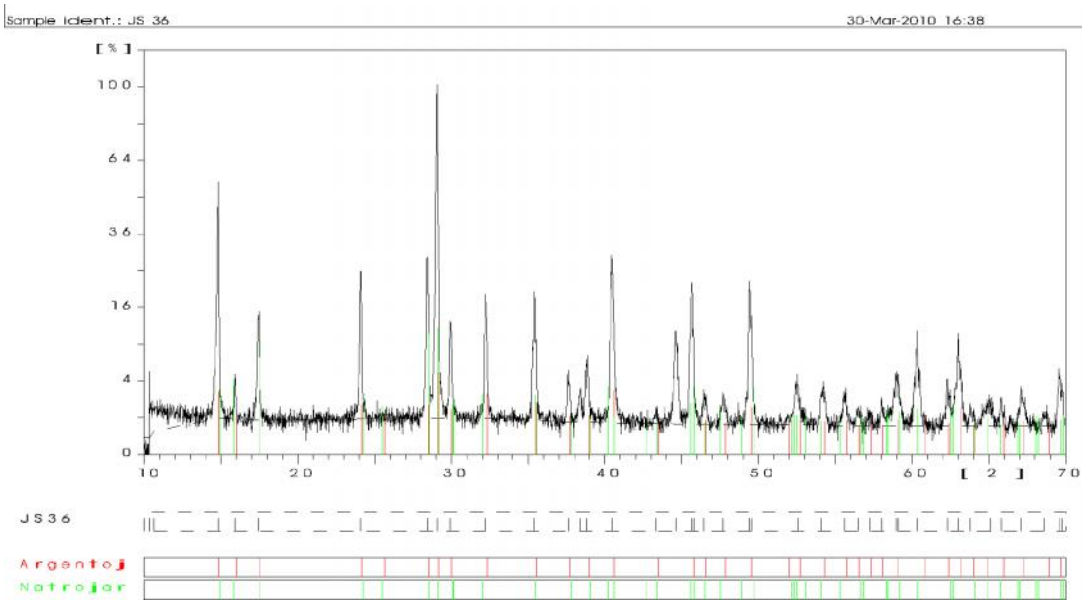
Sample Ident.: JS 36
30-Mar-2010 16:38
[%]
100
64
36
16
4
0
10
20
30
40
50
60
[2]
70
JS36
Argentoj
Natrojar

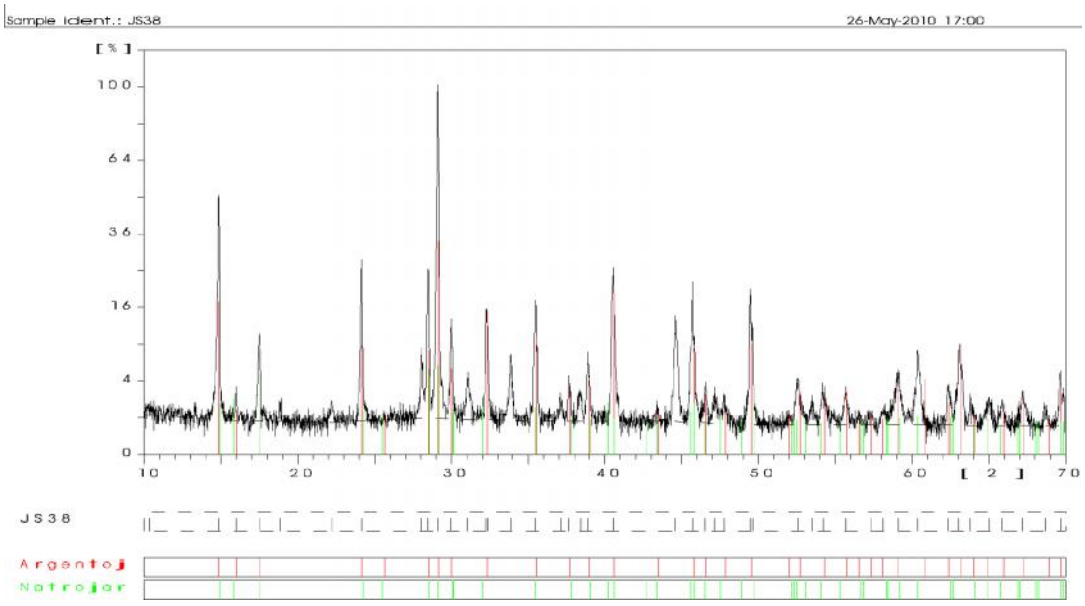
Sample Ident.: JS38
26-May-2010 17:00
[%]
100
64
36
16
4
0
10
20
30
40
50
60
[2]
70
JS38
Argentoj
Natrojar

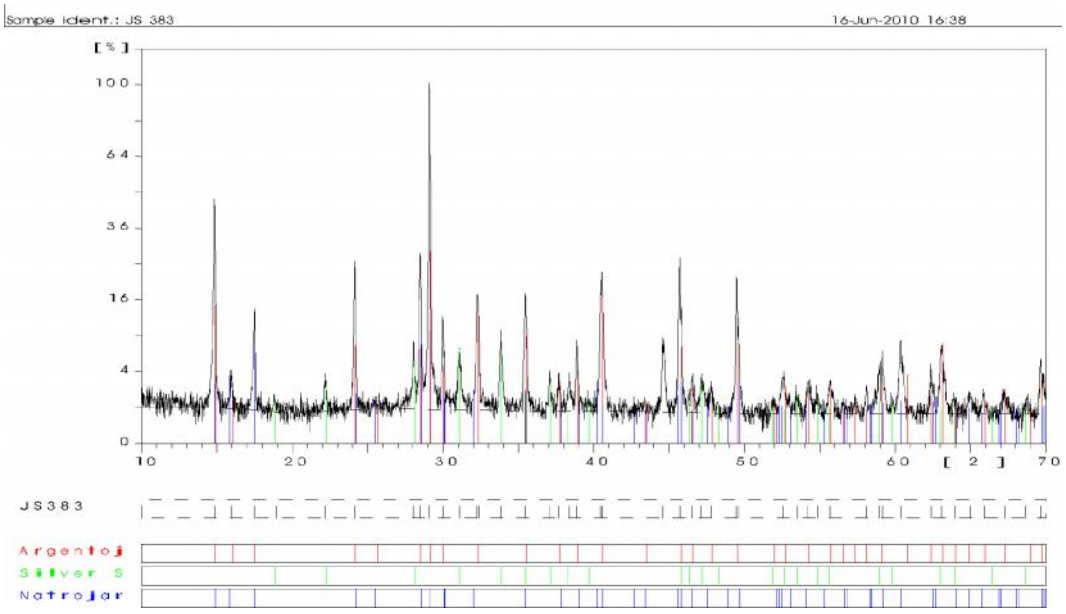
Sample ident.: JS 383
16-Jun-2010 16:38
[%]
100
64
36
16
4
0
10
20
30
40
50
60
[2]
70
JS383
Argentoj
Silver S
Natrojar

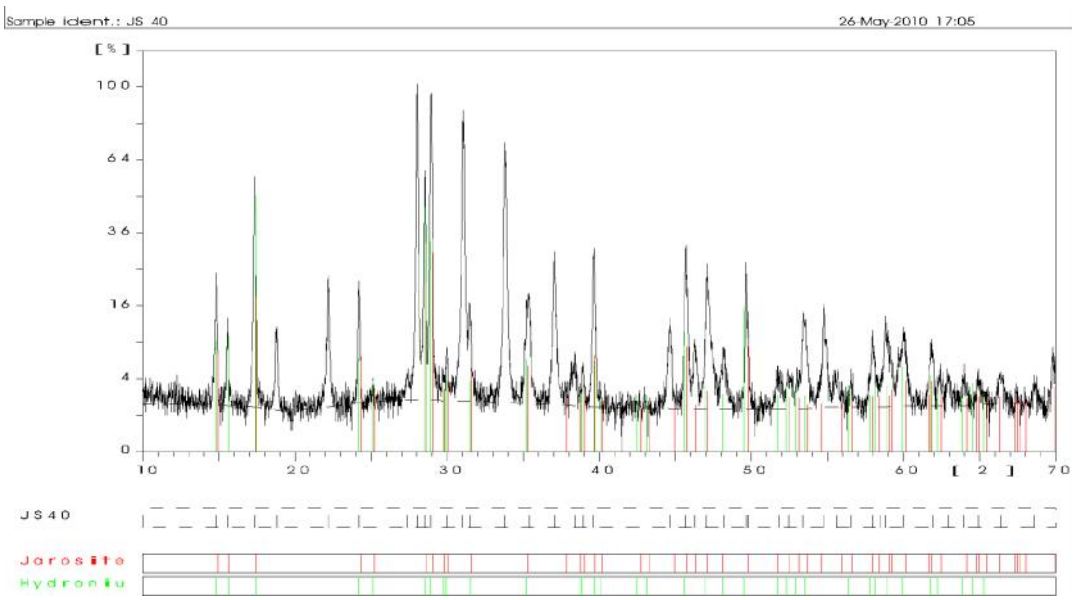
Sample ident.: JS 40
26-May-2010 17:05
[%]
100
64
36
16
4
0
10
20
30
40
50
60
[2]
70
JS40
Jarosite
Hydronium

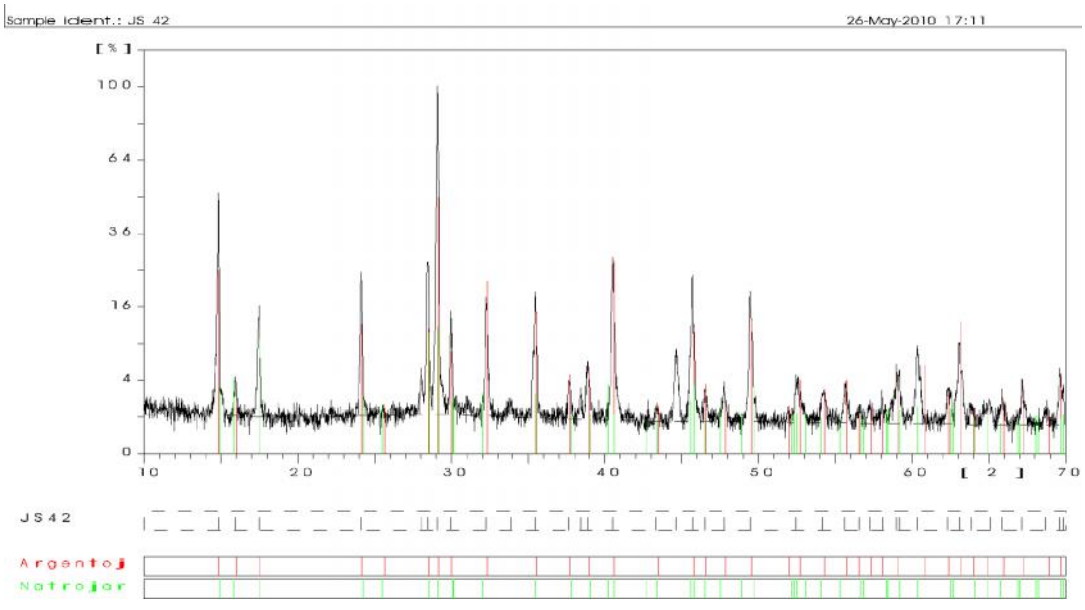
Sample ident.: JS 42
26-May-2010 17:11
[%]
100
64
36
16
4
0
10
20
30
40
50
60
[2]
70
JS42
Argentoj
Natrojar

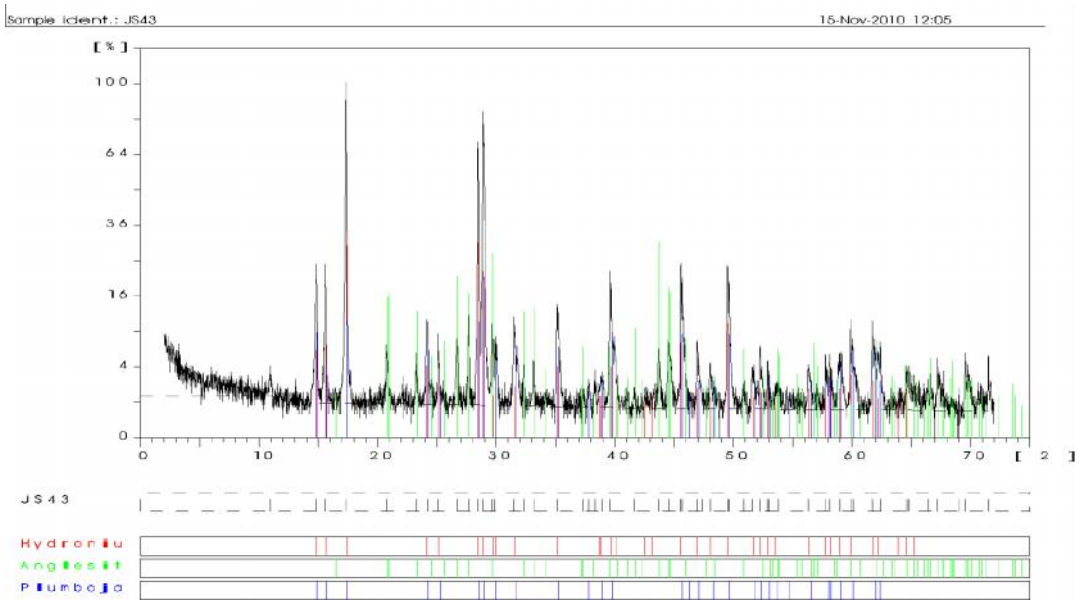
Sample ident.: JS43
15-Nov-2010 12:05
[%]
100
64
36
16
4
0
10
20
30
40
50
60
70
[2]
JS43
Hydroniu
Anglesit
Plumboja

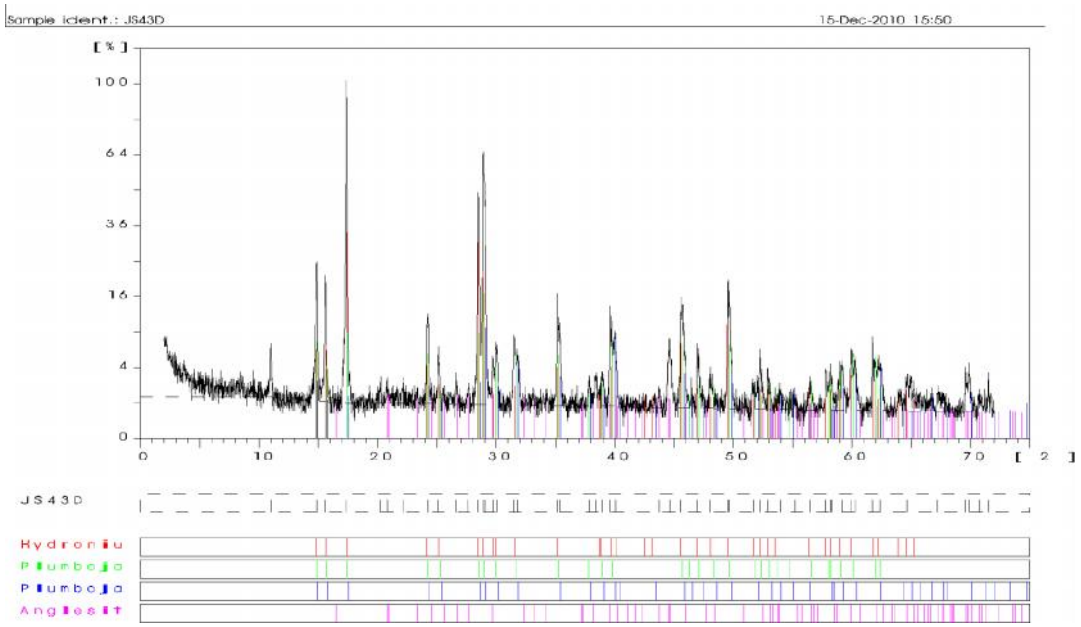
Sample ident.: JS43D
15-Dec-2010 15:50
[%]
100
64
36
16
4
0
10
20
30
40
50
60
70
[2]
JS43D
Hydroniu
Plumboja
Plumboja
Anglesit

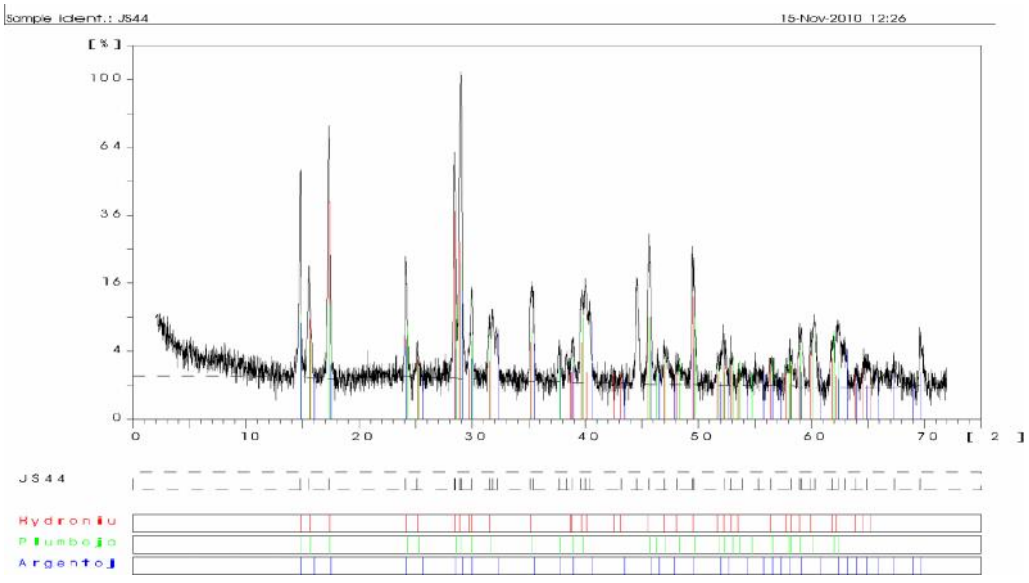
Sample ident.: JS44
15-Nov-2010 12:26
[%]
100
64
36
16
4
0
10
20
30
40
50
60
70
[2]
JS44
Hydroniu
Plumboja
Argentoj

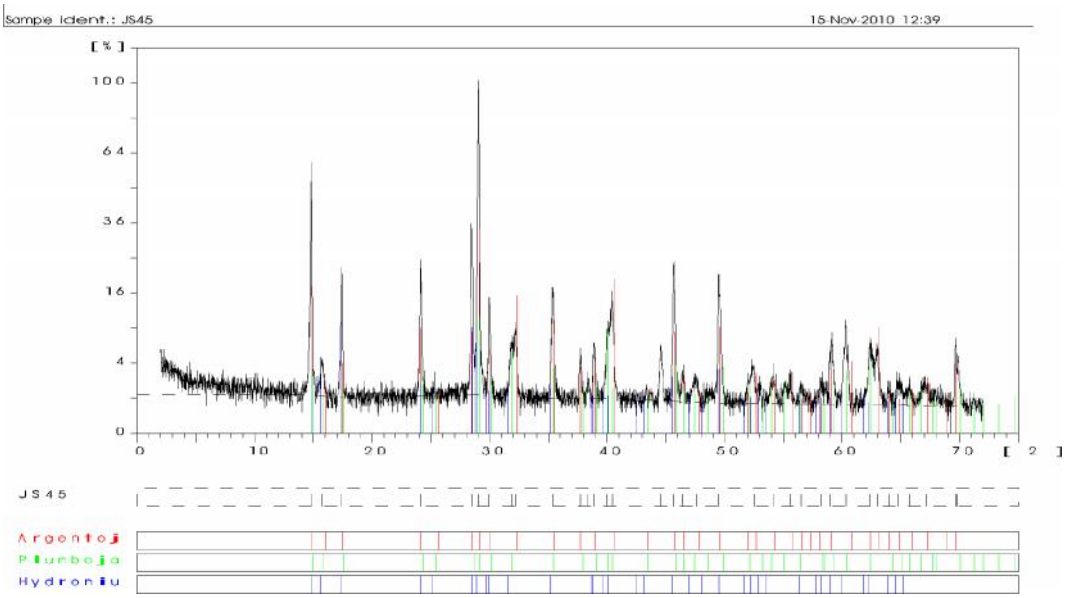
Sample Ident.: JS45
15-Nov-2010 12:39
[%]
100
64
36
16
4
0
0
10
20
30
40
50
60
70
[2]
JS45
Argentoj
Plumboja
Hydroniu

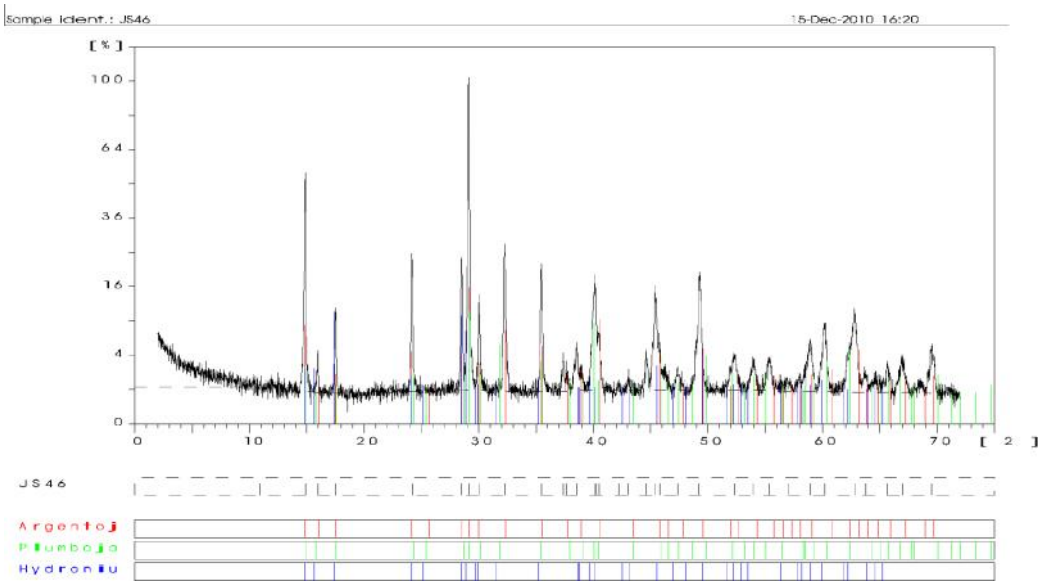
Sample Ident.: JS46
15-Dec-2010 16:20
[%]
100
64
36
16
4
0
0
10
20
30
40
50
60
70
[2]
JS46
Argentoj
Plumboja
Hydroniu

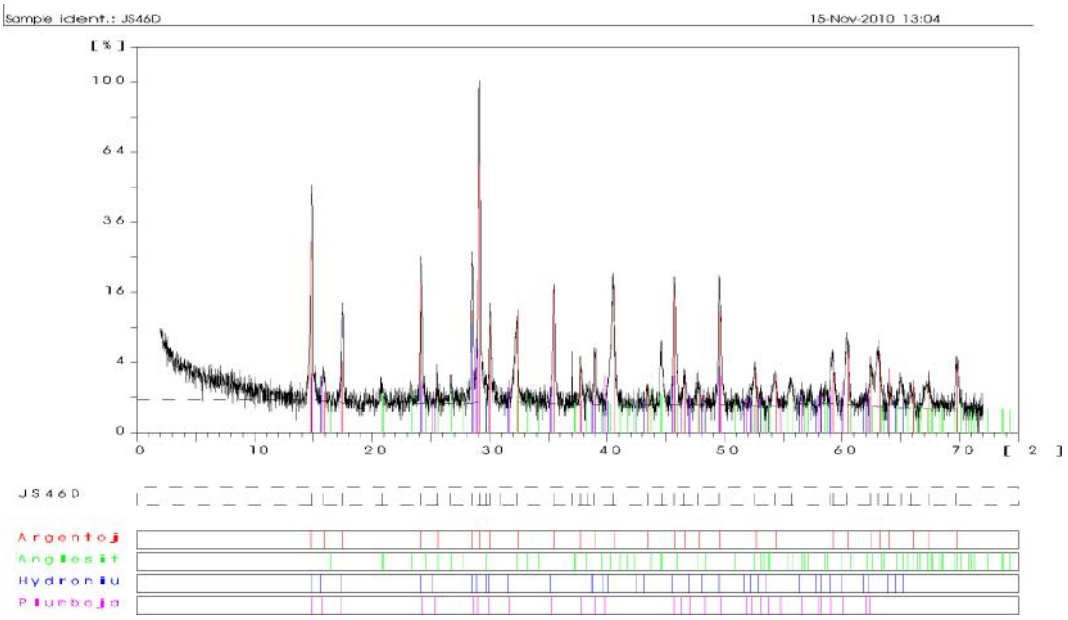
Sample Ident.: JS46D
15-Nov-2010 13:04
[%]
100
64
36
16
4
0
0
10
20
30
40
50
60
70
[2]
JS46D
Argentoj
Anglesit
Hydroniu
Plumboja

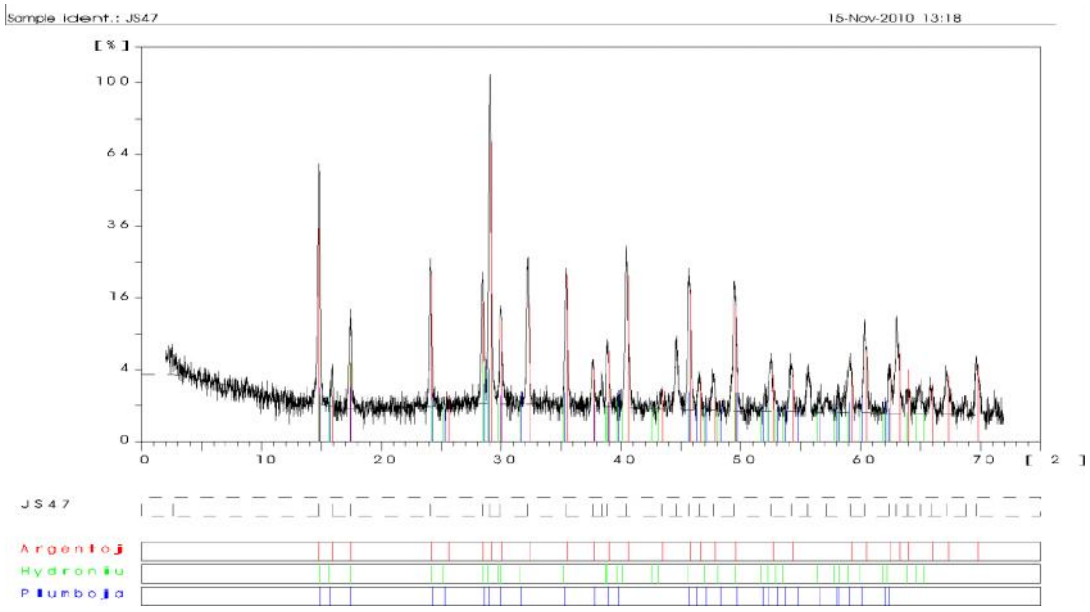
Sample ident.: JS47
15-Nov-2010 13:18
[%]
100
64
36
16
4
0
10
20
30
40
50
60
70
[2]
JS47
Argentoj
Hydroniu
Plumboja

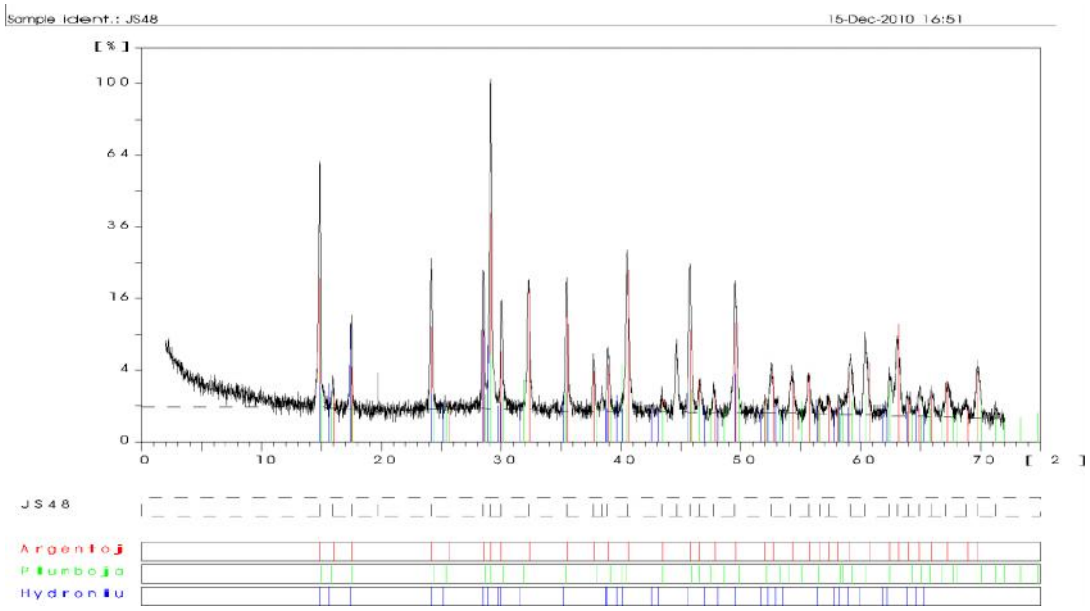
Sample ident.: JS48
15-Dec-2010 16:51
[%]
100
64
36
16
4
0
10
20
30
40
50
60
70
[2]
JS48
Argentoj
Plumboja
Hydroniu

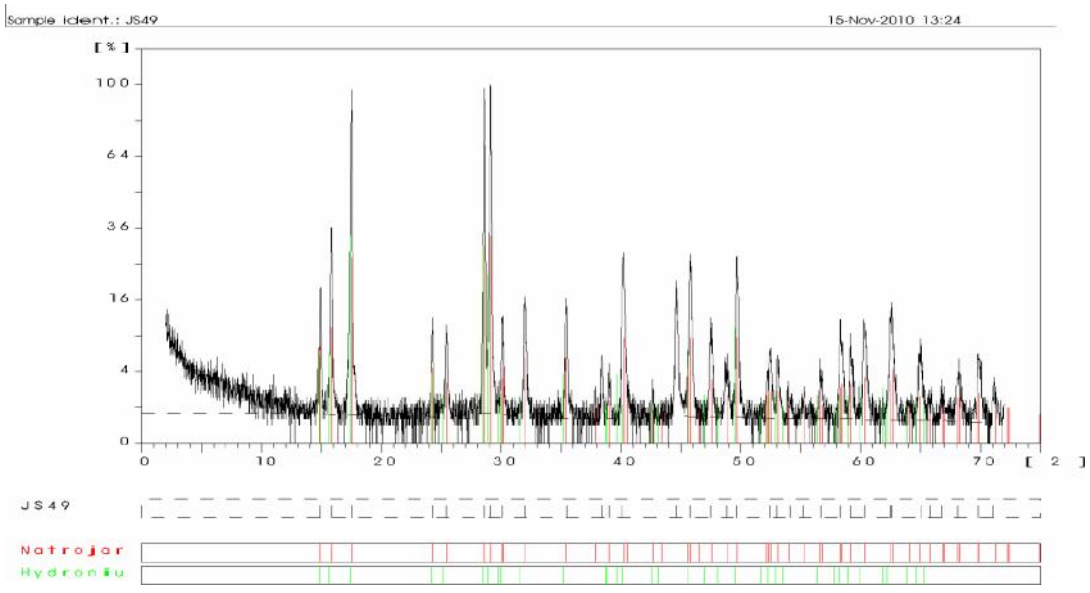
Sample ident.: JS49
15-Nov-2010 13:24
[%]
100
64
36
16
4
0
10
20
30
40
50
60
70
[2]
JS49
Natrojar
Hydroniu

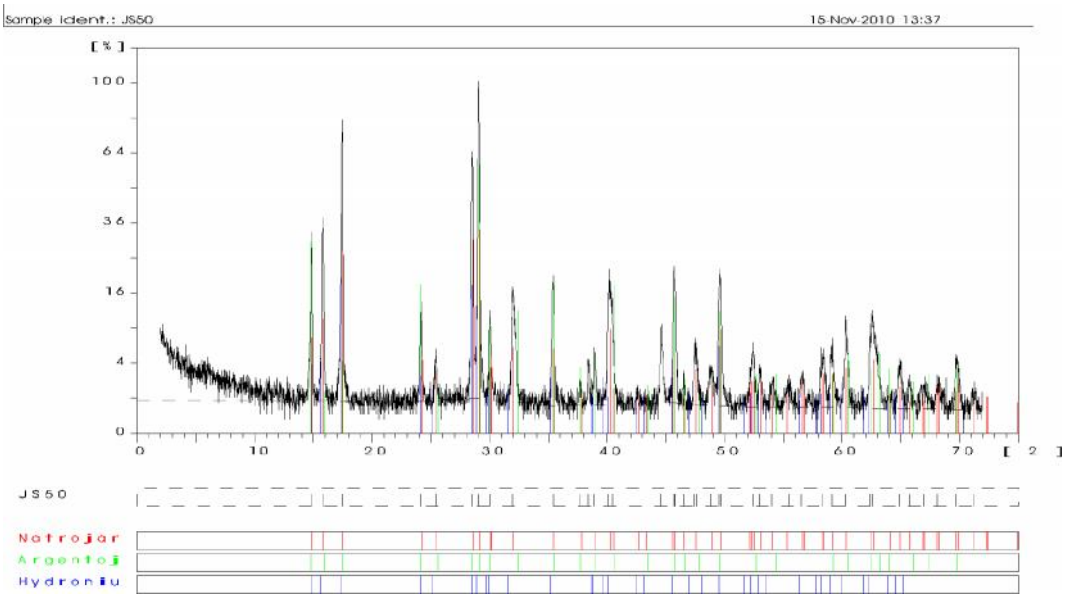
Sampe Ident.: JS50
15-Nov-2010 13:37
[%]
100
64
36
16
4
0
0
10
20
30
40
50
60
70
[2]
JS50
Natrojar
Argentoj
Hydroniu

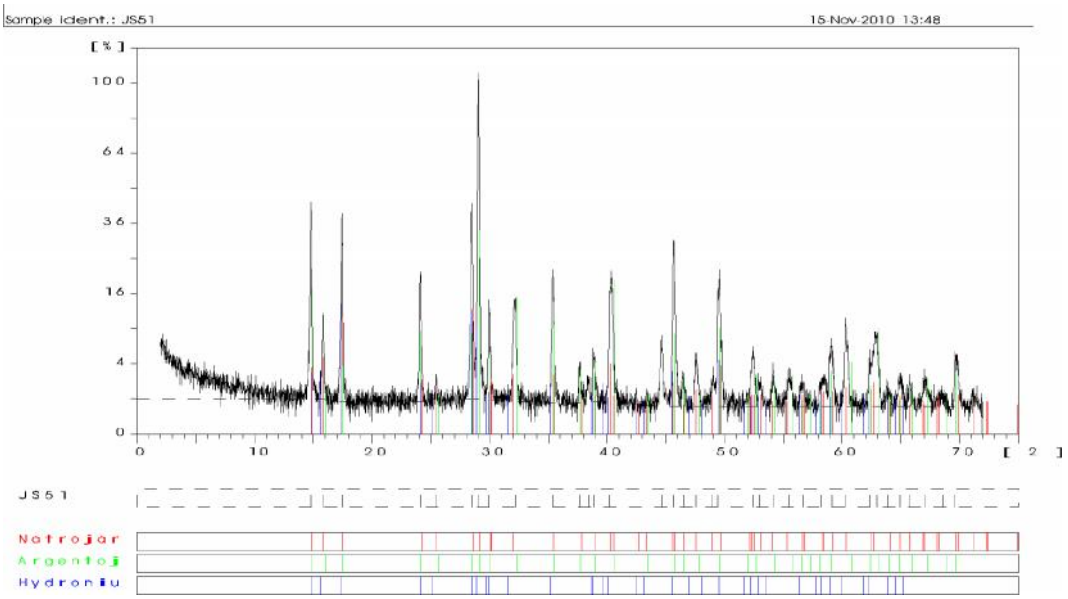
Sampe Ident.: JS51
15-Nov-2010 13:48
[%]
100
64
36
16
4
0
0
10
20
30
40
50
60
70
[2]
JS51
Natrojar
Argentoj
Hydroniu

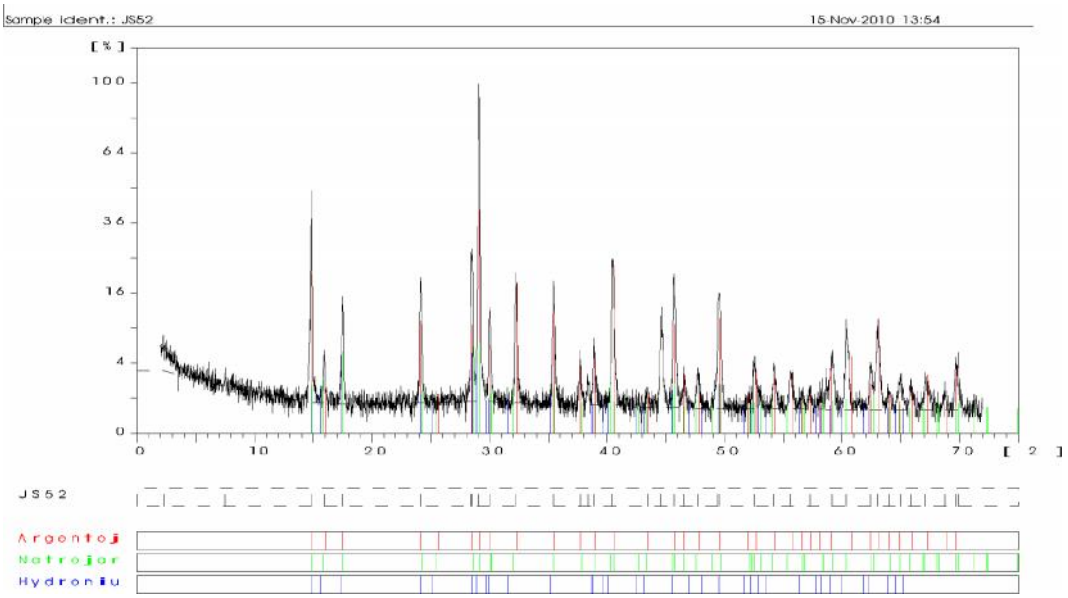
Sampe Ident.: JS52
15-Nov-2010 13:54
[%]
100
64
36
16
4
0
0
10
20
30
40
50
60
70
[2]
JS52
Argentoj
Natrojar
Hydroniu

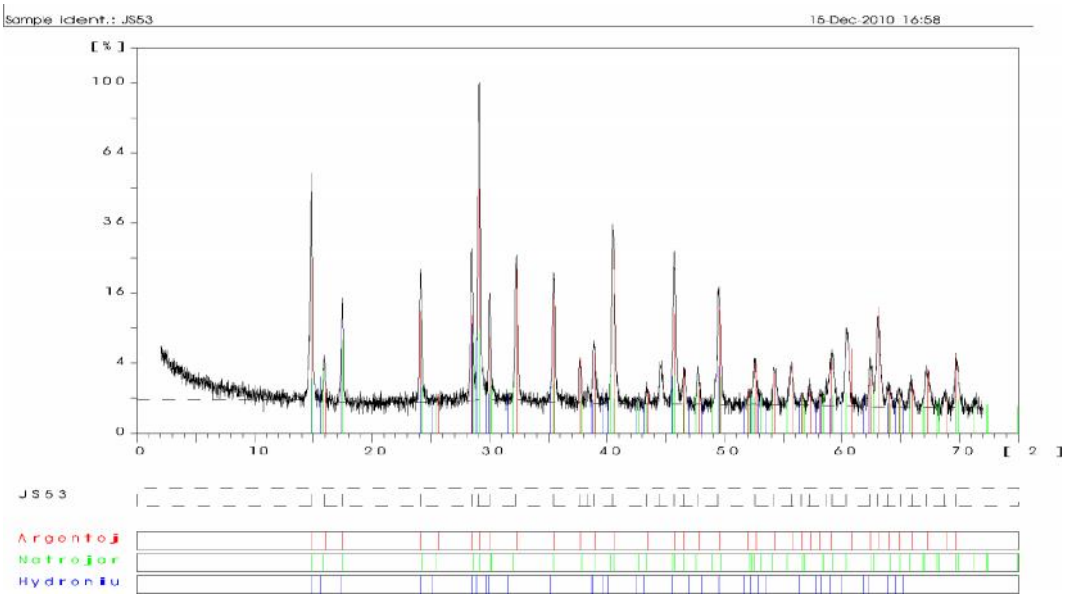
Sampe Ident.: JS53
15-Dec-2010 16:58
[%]
100
64
36
16
4
0
0
10
20
30
40
50
60
70
[2]
JS53
Argentoj
Natrojar
Hydroniu

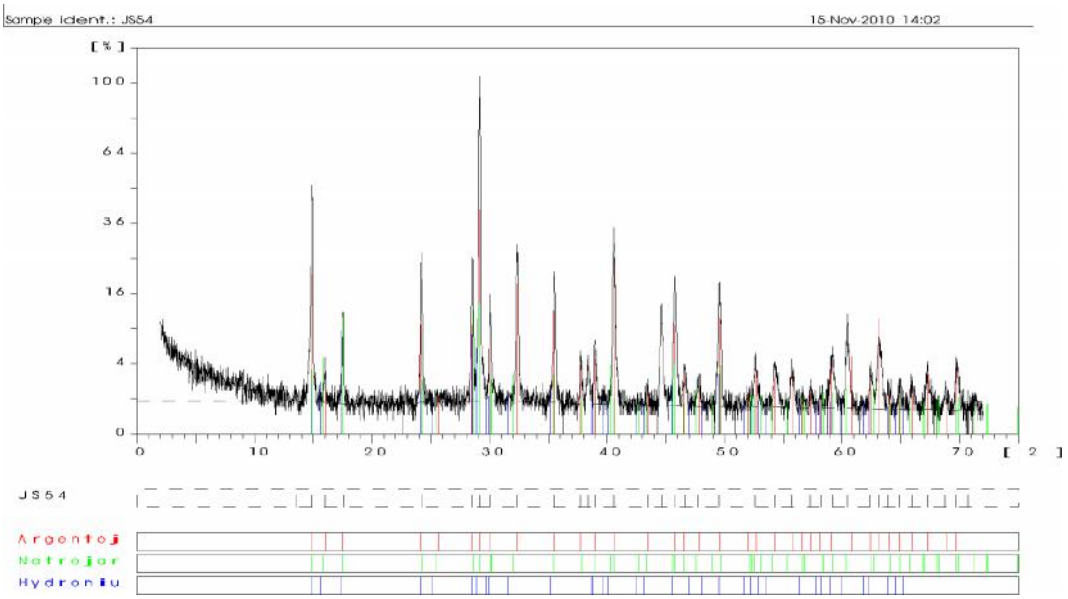
Sampe Ident.: JS54
15-Nov-2010 14:02
[%]
100
64
36
16
4
0
0
10
20
30
40
50
60
70
[2]
JS54
Argentoj
Natrojar
Hydroniu

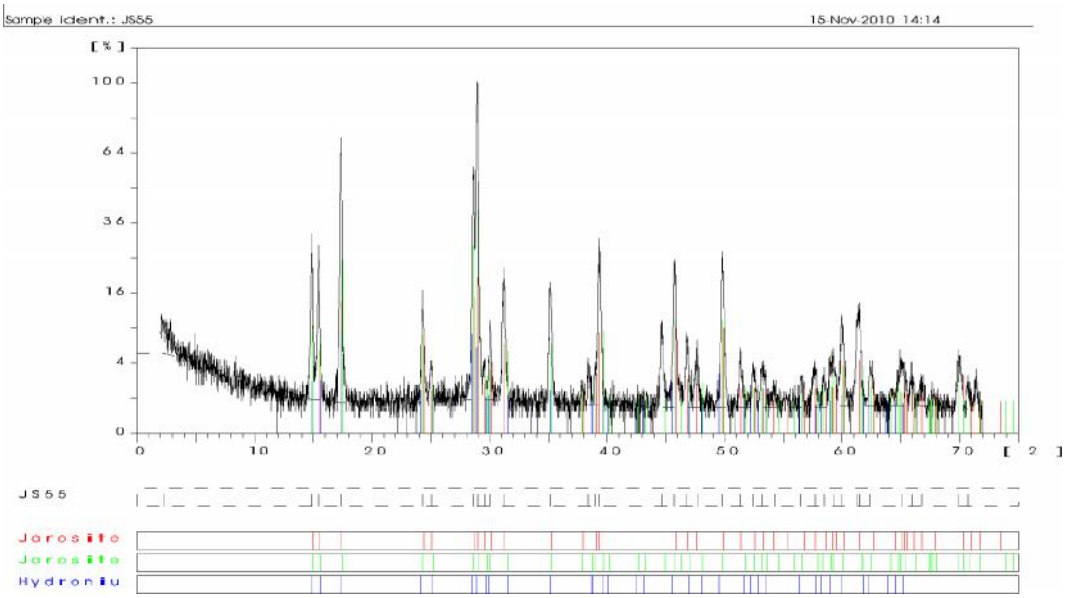
Sampe Ident.: JS55
15-Nov-2010 14:14
[%]
100
64
36
16
4
0
0
10
20
30
40
50
60
70
[2]
JS55
Jarosite
Jarosite
Hydroniu

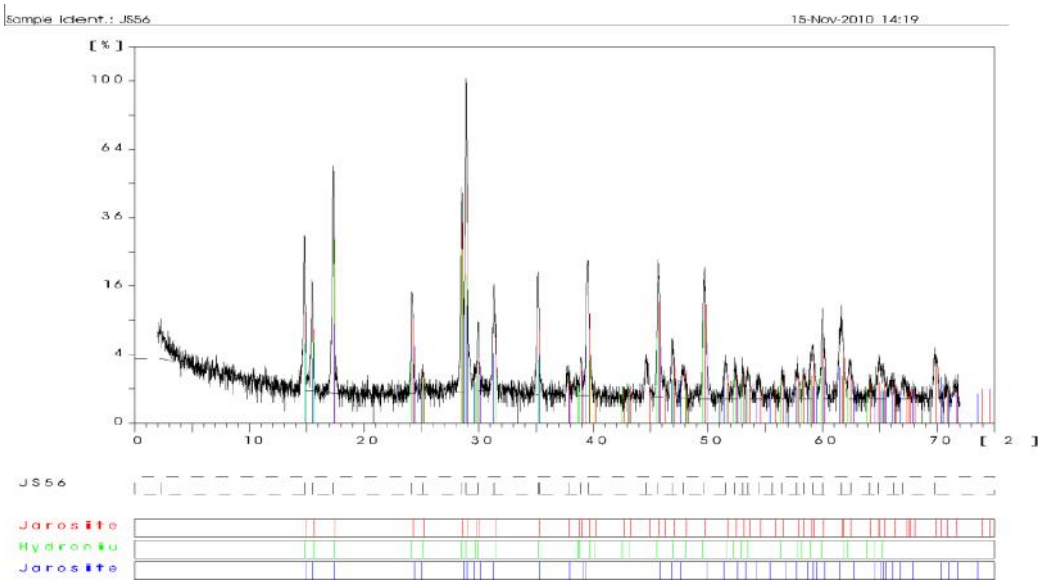
Sample ident.: JS56
15-Nov-2010 14:19
[%]
100
64
36
16
4
0
0
10
20
30
40
50
60
70
[2]
JS56
Jarosite
Hydronium
Jarosite

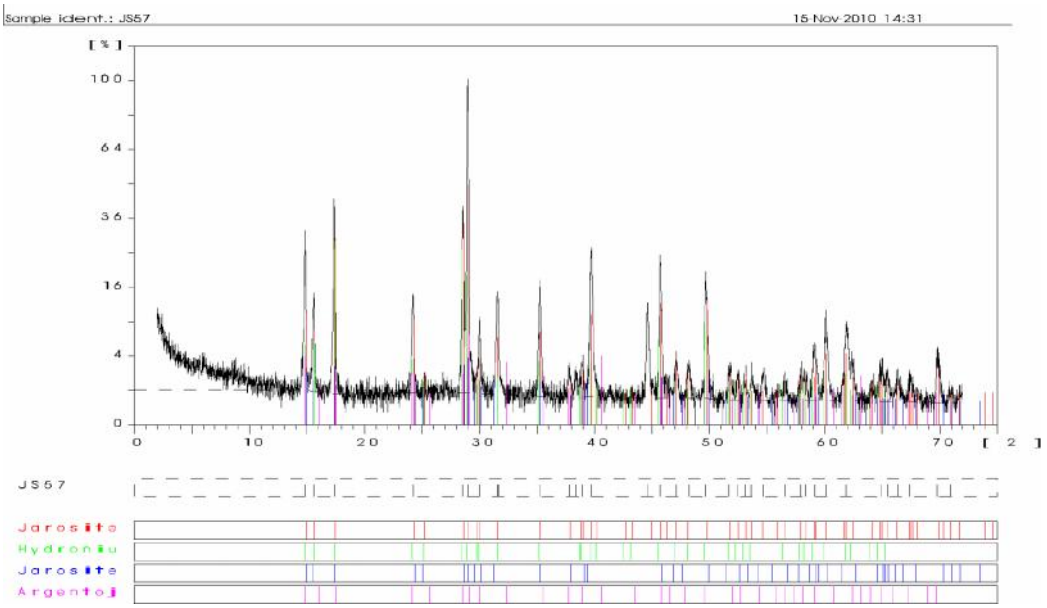
Sample ident.: JS57
15-Nov-2010 14:31
[%]
100
64
36
16
4
0
0
10
20
30
40
50
60
70
[2]
JS57
Jarosite
Hydronium
Jarosite
Argentoj

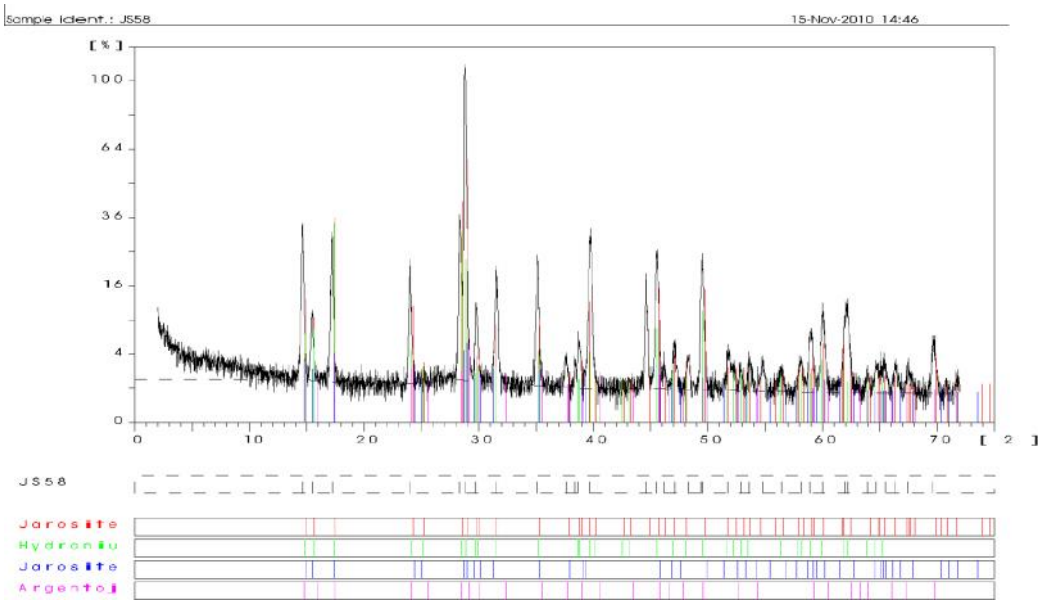
Sample ident.: JS58
15-Nov-2010 14:46
[%]
100
64
36
16
4
0
0
10
20
30
40
50
60
70
[2]
JS58
Jarosite
Hydronium
Jarosite
Argentoj

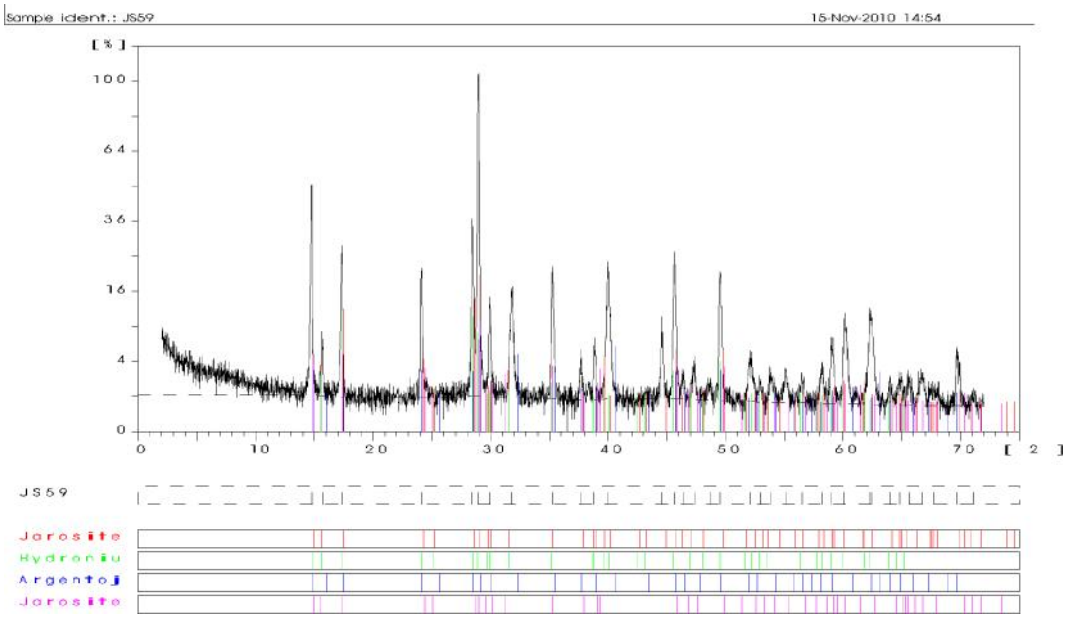
Sampe ident.: JS59
15-Nov-2010 14:54
[%]
100
64
36
16
4
0
0
10
20
30
40
50
60
70
[2]
JS59
Jarosite
Hydroniu
Argentoj
Jarosite

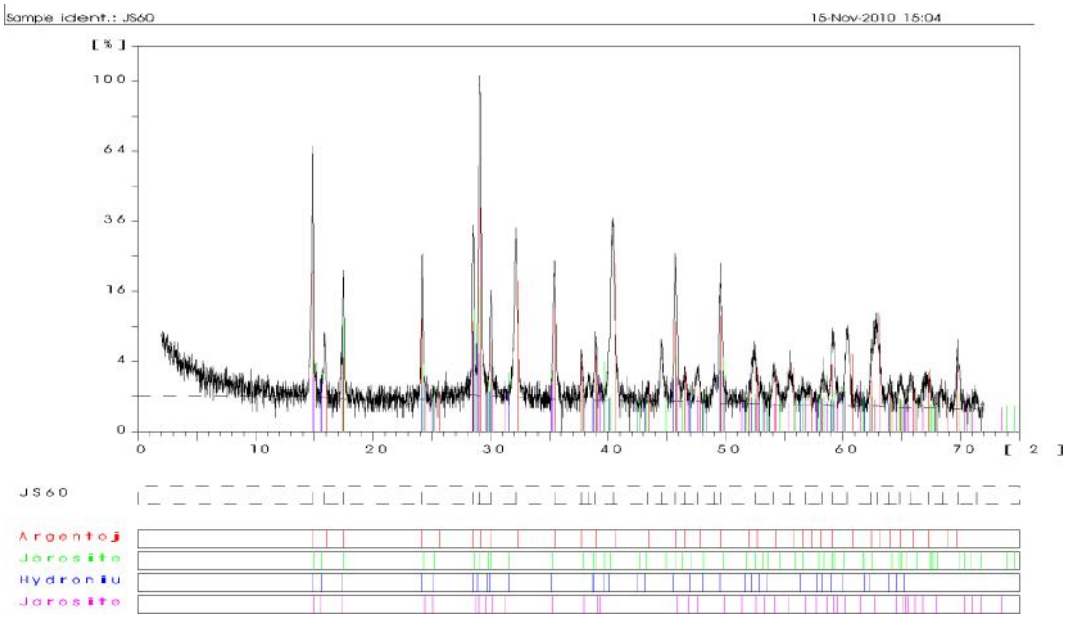
Sampe ident.: JS60
15-Nov-2010 15:04
[%]
100
64
36
16
4
0
0
10
20
30
40
50
60
70
[2]
JS60
Argentoj
Jarosite
Hydroniu
Jarosite

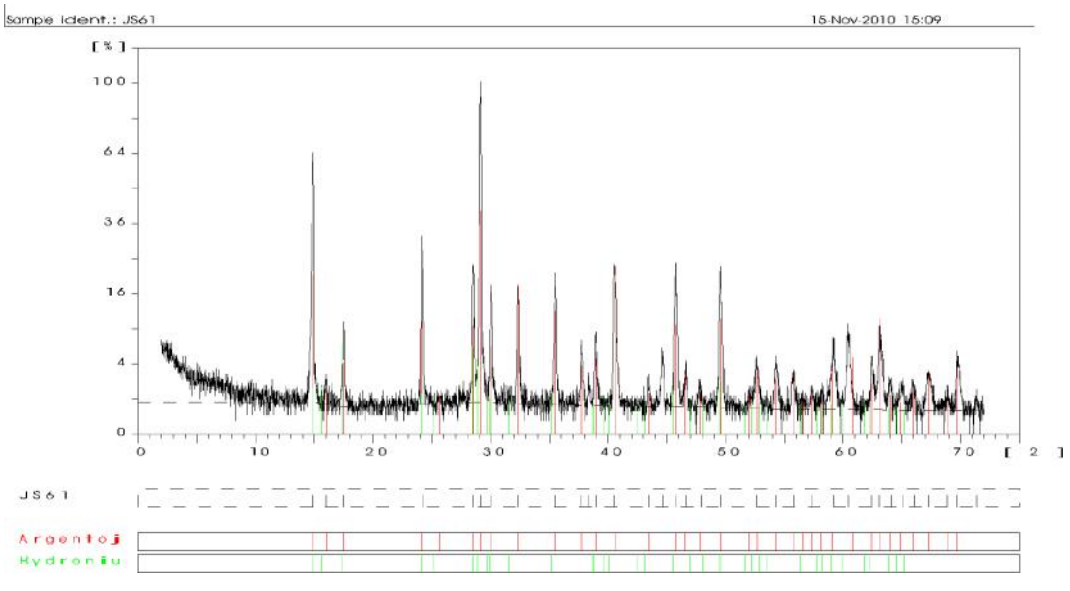
Sampe ident.: JS61
15-Nov-2010 15:09
[%]
100
64
36
16
4
0
0
10
20
30
40
50
60
70
[2]
JS61
Argentoj
Hydroniu

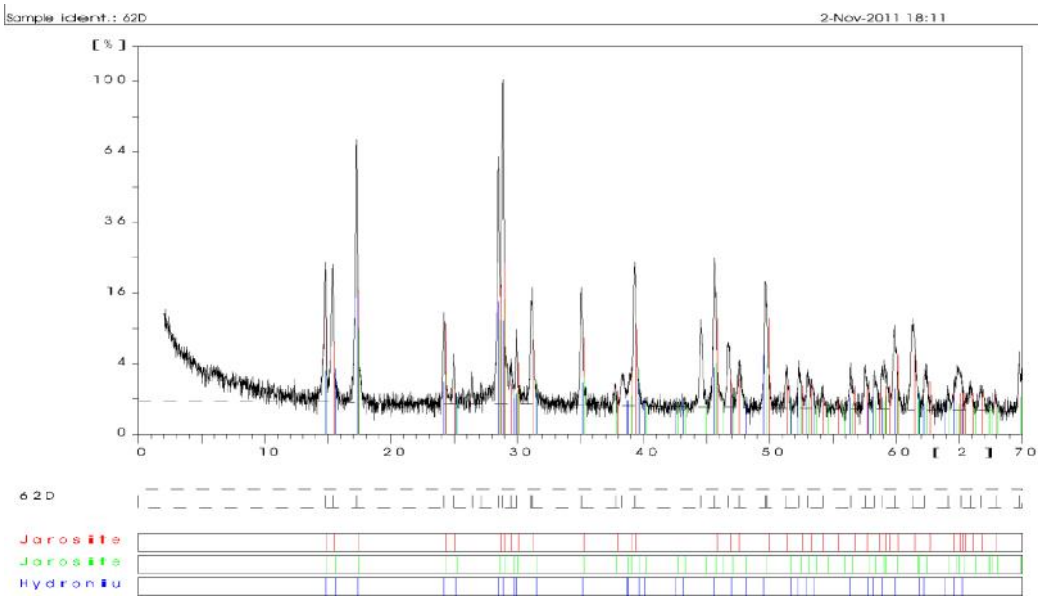
Sample Identf.: 62D
2-Nov-2011 18:11
[%]
100
64
36
16
4
0
10
20
30
40
50
60
[2]
70
62D
Jarosite
Jarosite
Hydroniu

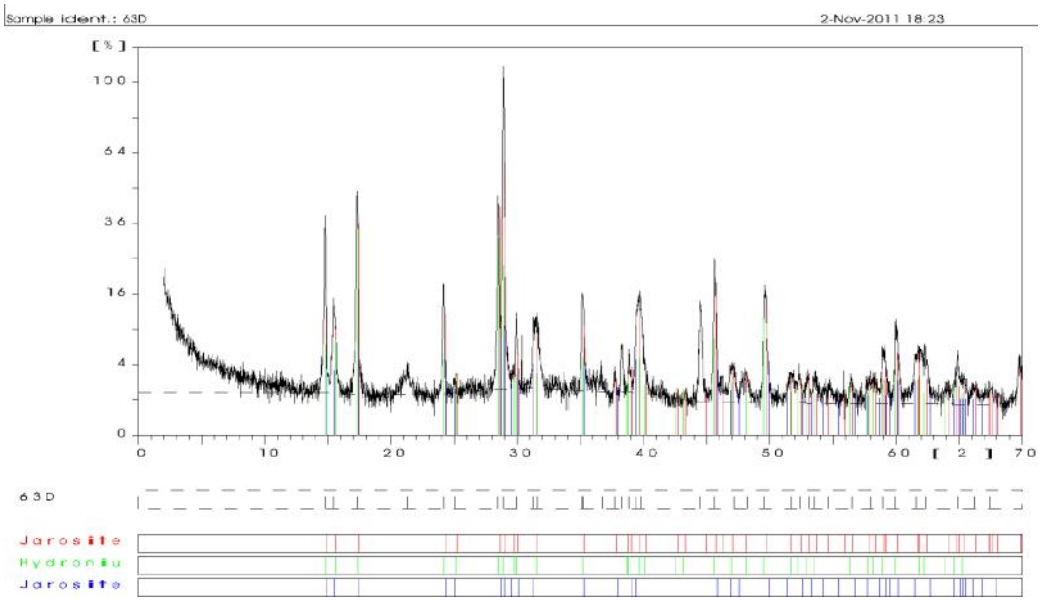
Sample Identf.: 63D
2-Nov-2011 18:23
[%]
100
64
36
16
4
0
10
20
30
40
50
60
[2]
70
63D
Jarosite
Hydroniu
Jarosite

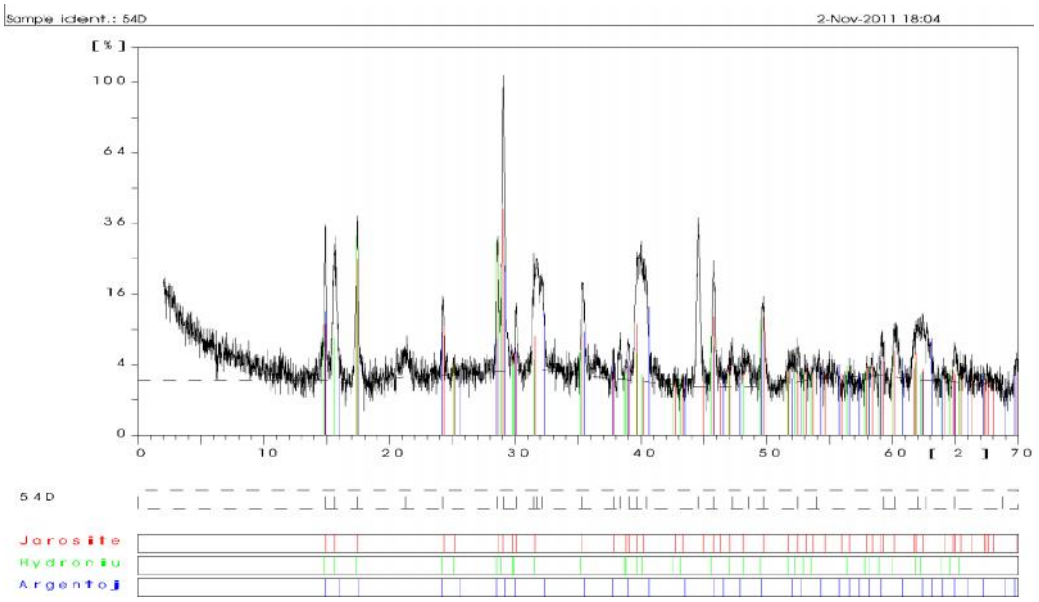
Sample Identf.: 54D
2-Nov-2011 18:04
[%]
100
64
36
16
4
0
10
20
30
40
50
60
[2]
70
54D
Jarosite
Hydroniu
Argento

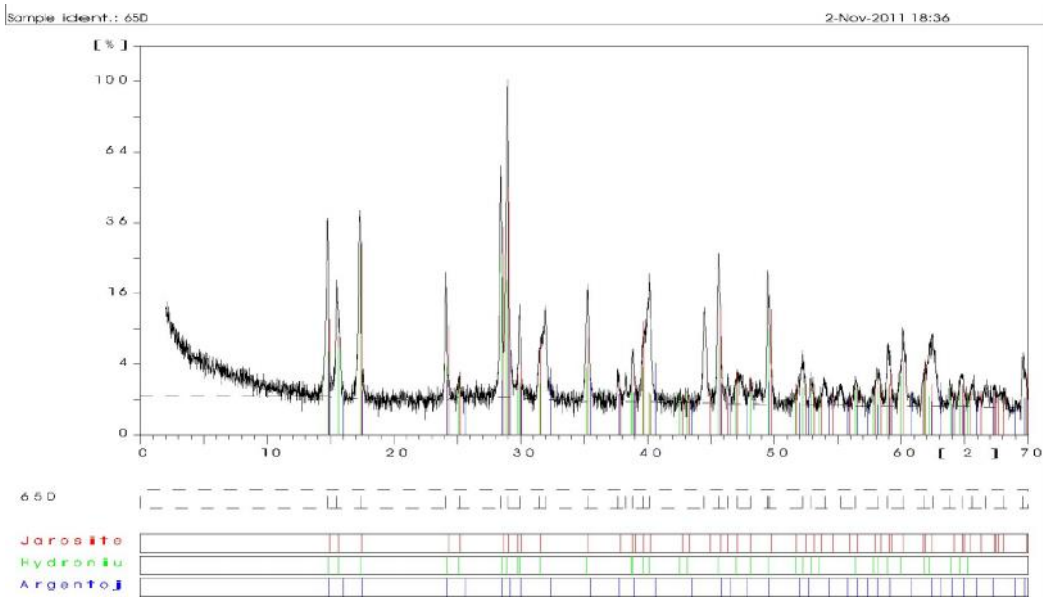
Sample ident.: 65D
2-Nov-2011 18:36
[%]
100
64
36
16
4
0
0
10
20
30
40
50
60
[2]
70
65D
Jarosite
Hydroniu
Argentoj

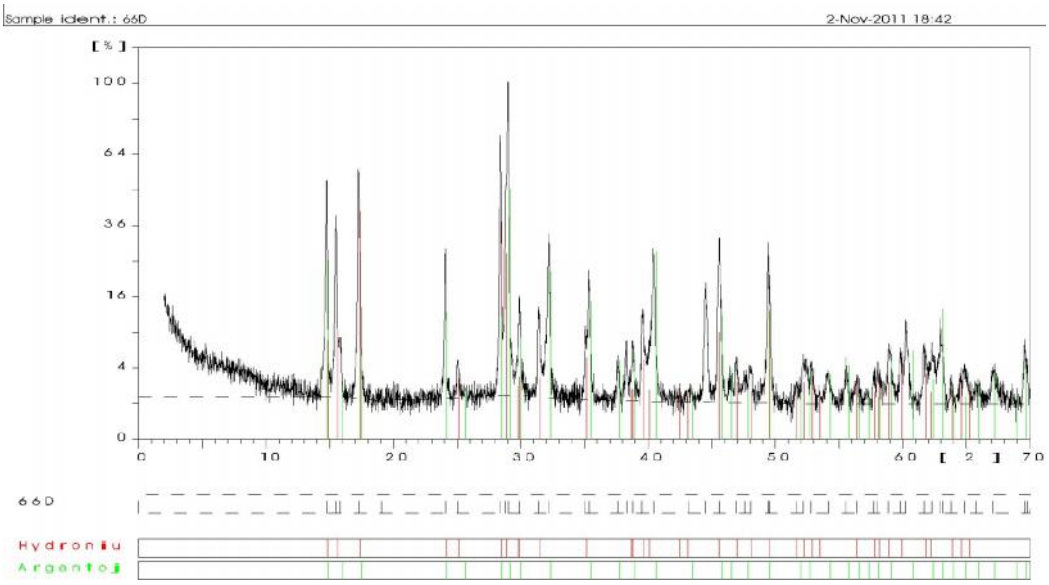
Sample ident.: 66D
2-Nov-2011 18:42
[%]
100
64
36
16
4
0
0
10
20
30
40
50
60
[2]
70
66D
Hydroniu
Argentoj

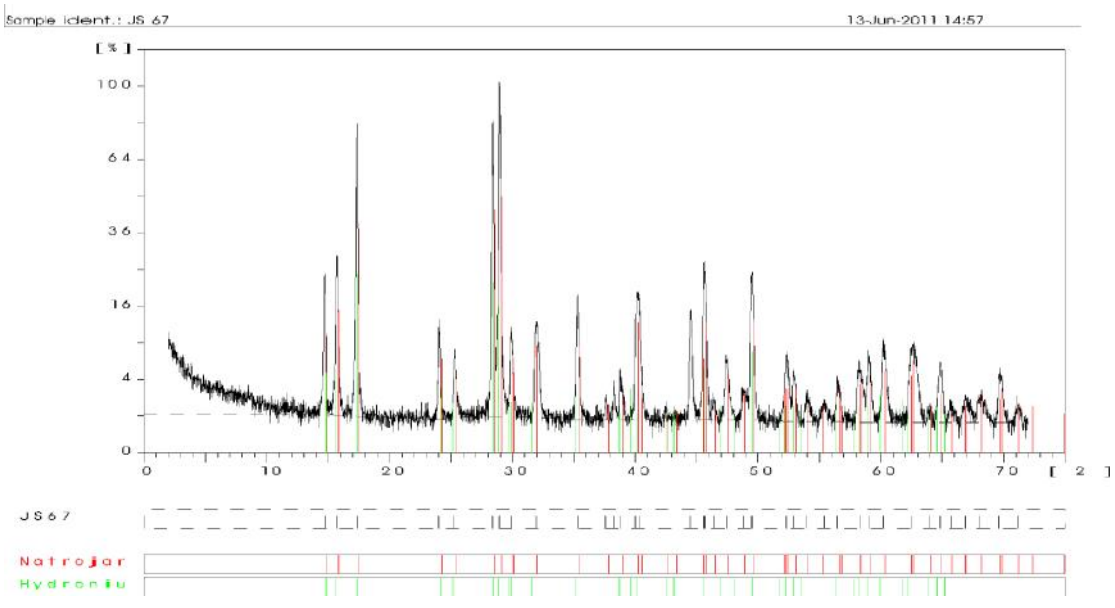
Sample ident.: JS 67
13-Jun-2011 14:57
[%]
100
64
36
16
4
0
0
10
20
30
40
50
60
70
[2]
JS67
Natrojar
Hydroniu

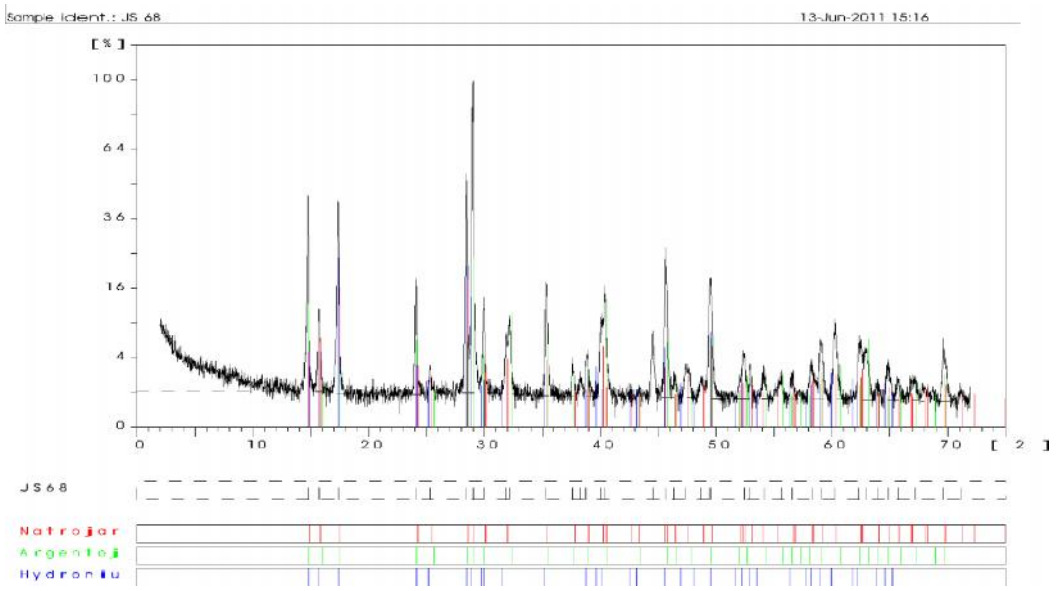
Sample Ident.: JS 68
13-Jun-2011 15:16
[%]
100
64
36
16
4
0
0
10
20
30
40
50
60
70
[2]
JS68
Natrojar
Argentoj
Hydroniu

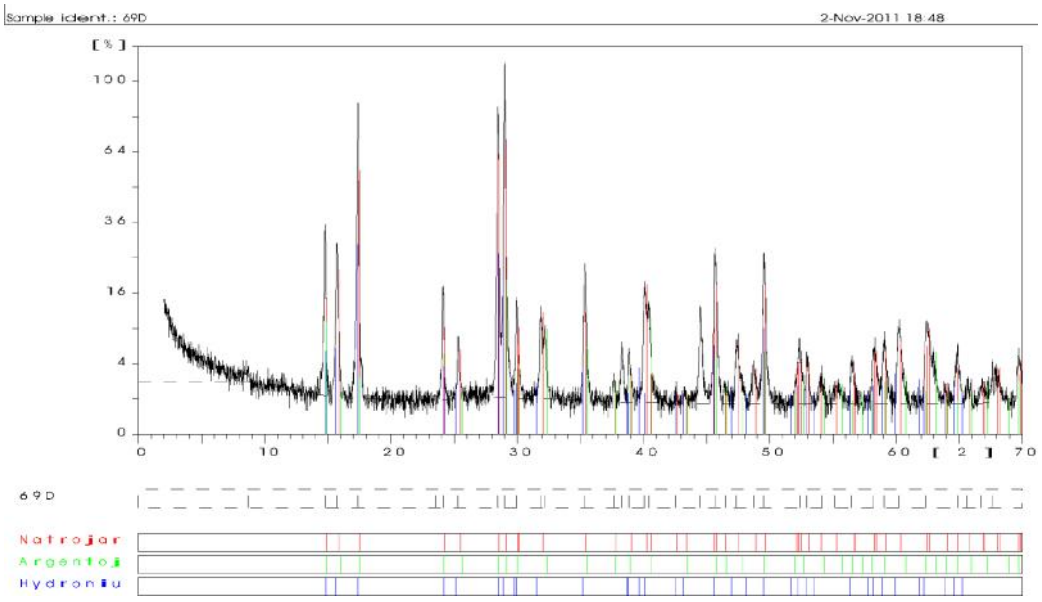
Sample Ident.: 69D
2-Nov-2011 18:48
[%]
100
64
36
16
4
0
0
10
20
30
40
50
60
[2]
70
69D
Natrojar
Argentoj
Hydroniu

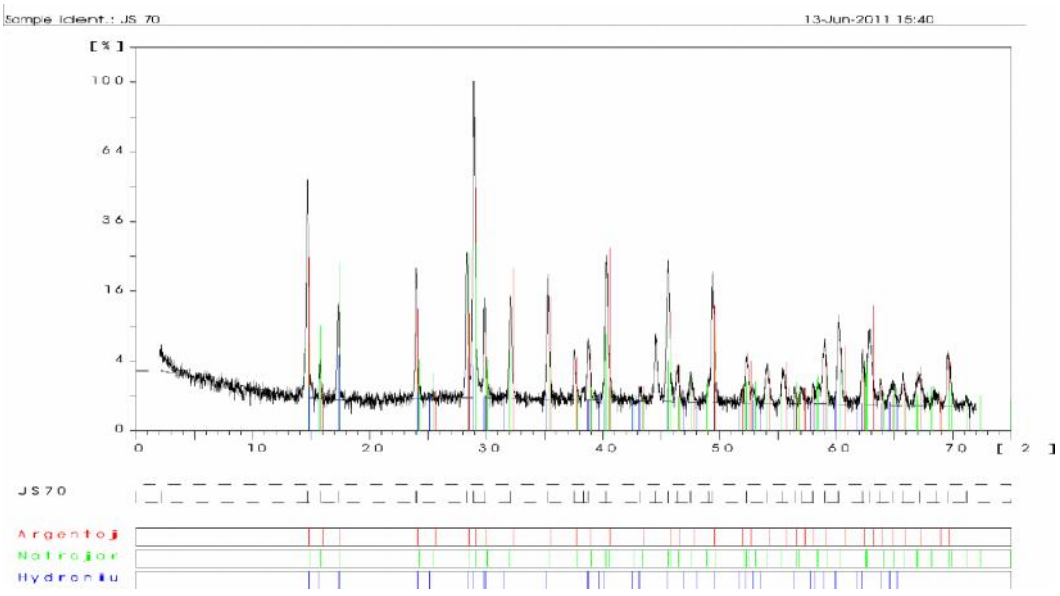
Sample Ident.: JS 70
13-Jun-2011 15:40
[%]
100
64
36
16
4
0
0
10
20
30
40
50
60
70
[2]
JS70
Argentoj
Natrojar
Hydroniu

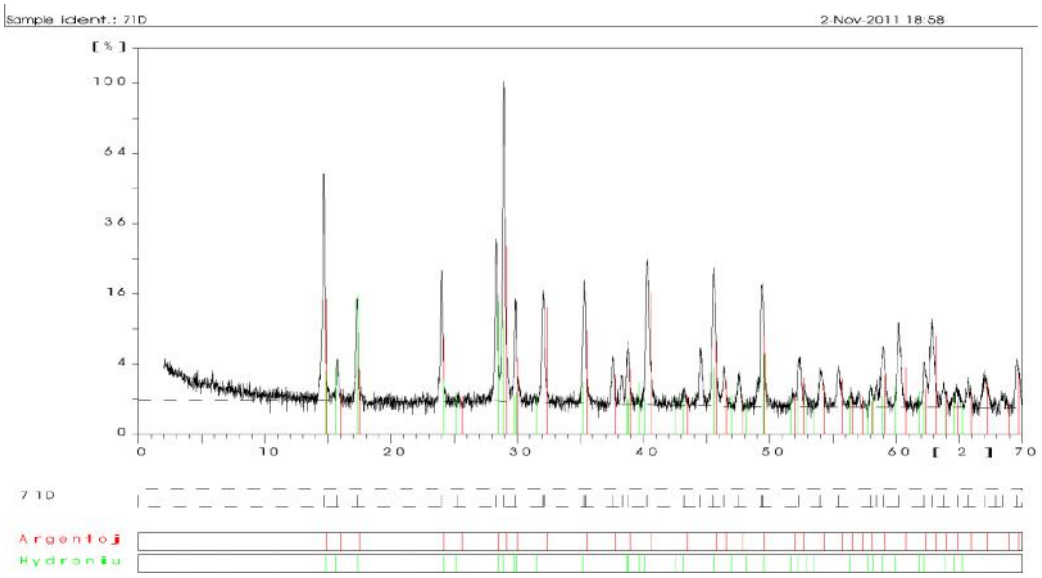
Sample Ident.: 71D
2-Nov-2011 18:58
[%]
100
64
36
16
4
0
0
10
20
30
40
50
60
[2]
70
71D
Argentoj
Hydroniu

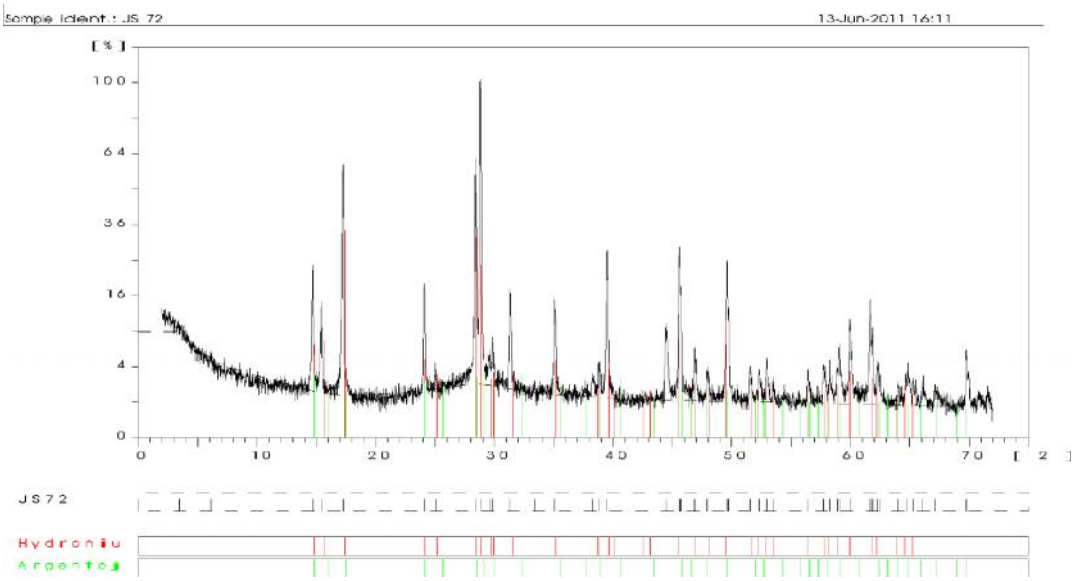
Sample Ident.: JS 72
13-Jun-2011 16:11
[%]
100
64
36
16
4
0
0
10
20
30
40
50
60
70
[2]
JS72
Hydroniu
Argentoj

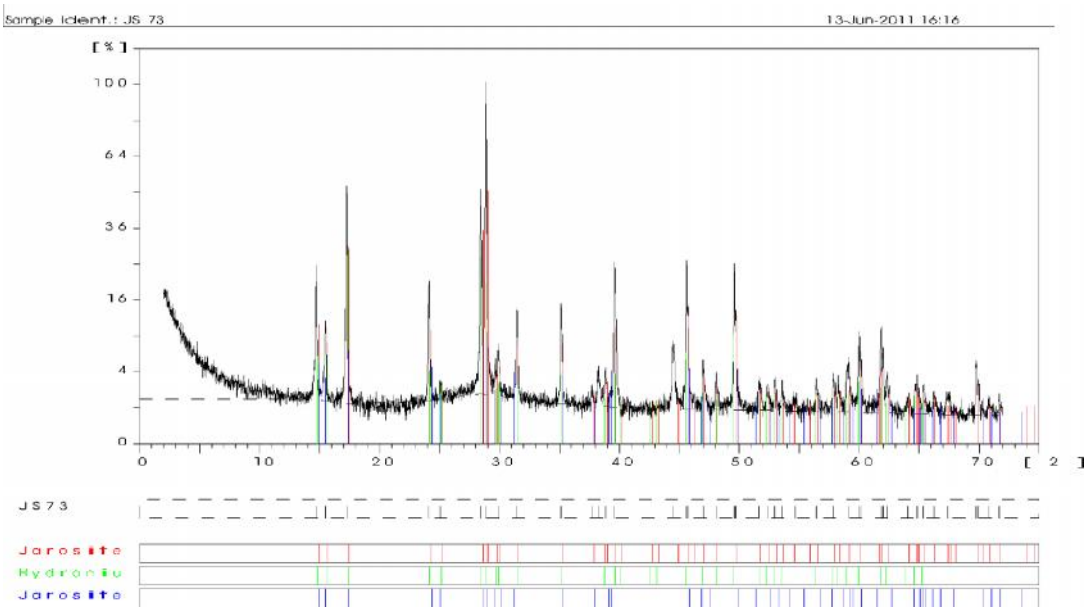
Sample Ident.: JS 73
13-Jun-2011 16:16
[%]
100
64
36
16
4
0
0
10
20
30
40
50
60
70
[2]
JS73
Jarosite
Hydroniu
Jarosite

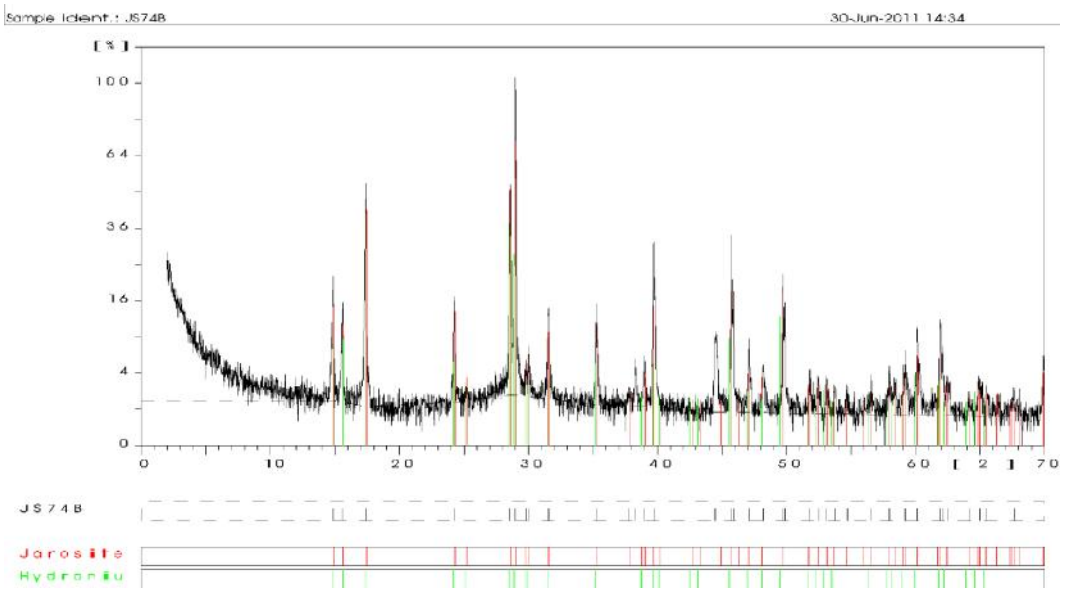
Sample Ident.: JS74B
30-Jun-2011 14:34
[%]
100
64
36
16
4
0
0
10
20
30
40
50
60
[2]
70
JS74B
Jarosite
Hydroniu

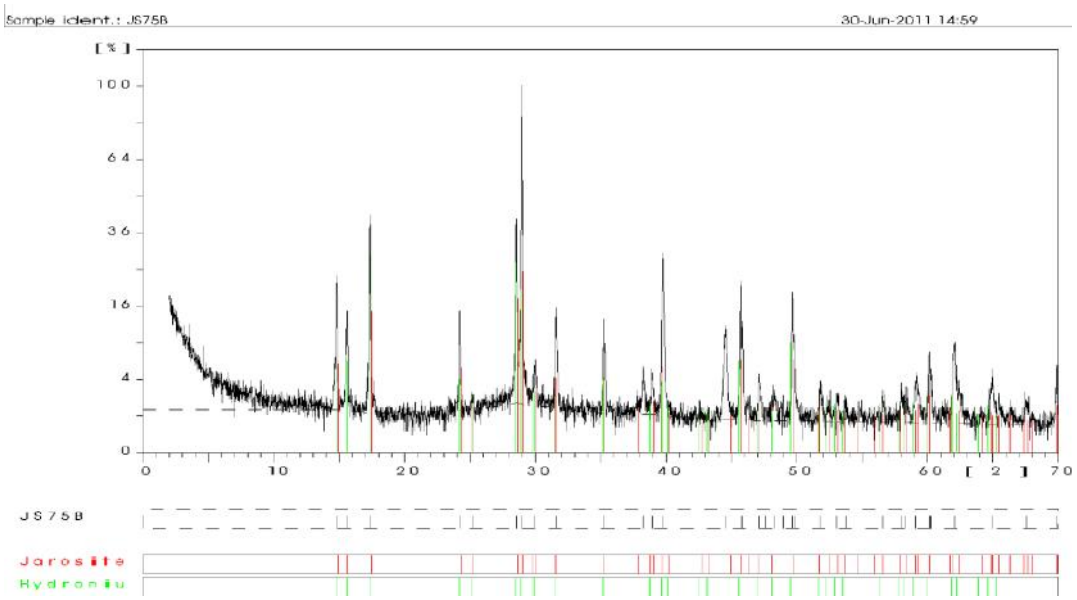
Sample Ident.: JS75B
30-Jun-2011 14:59
[%]
100
64
36
16
4
0
0
10
20
30
40
50
60
[2]
70
JS75B
Jarosite
Hydroniu

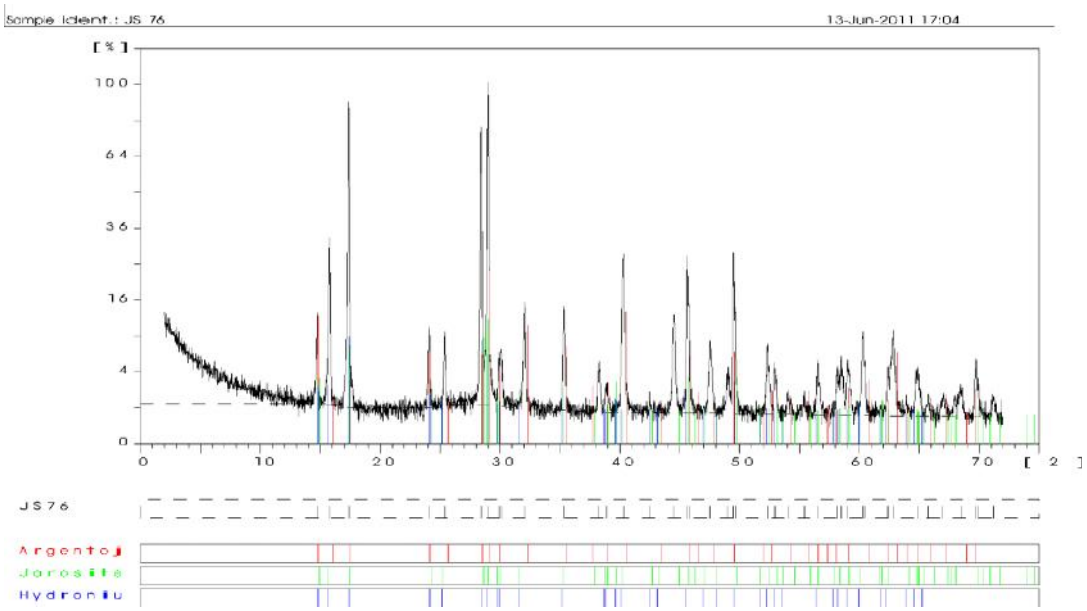
Sample Ident.: JS 76
13-Jun-2011 17:04
[%]
100
64
36
16
4
0
0
10
20
30
40
50
60
70
[2]
JS76
Argentoj
Jarosite
Hydroniu

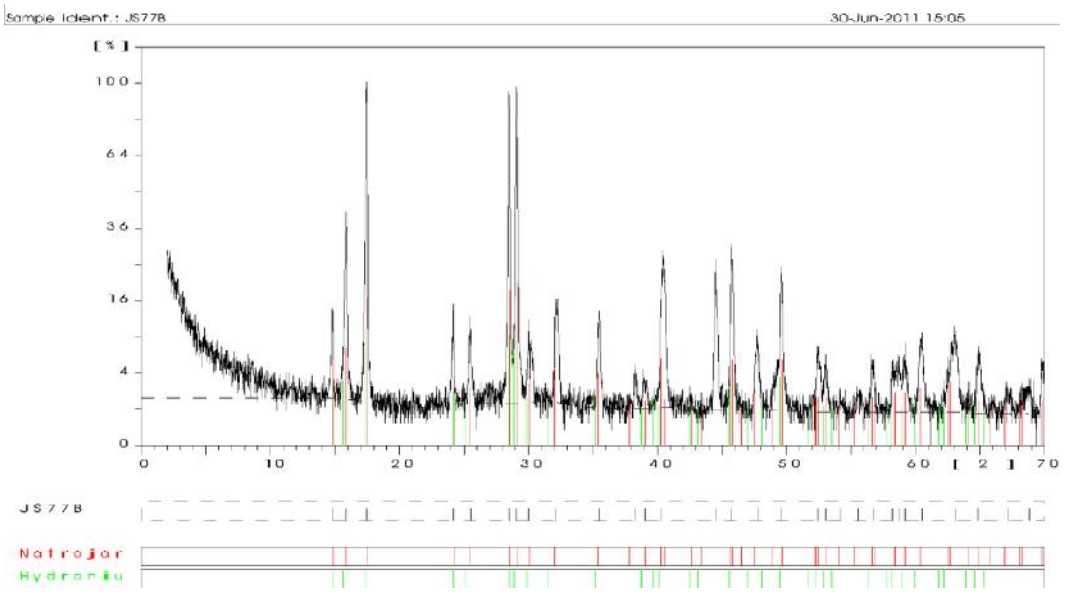
Sample Ident.: JS77B
30-Jun-2011 15:05
[%]
100
64
36
16
4
0
0
10
20
30
40
50
60
[2]
70
JS77B
Natrojar
Hydronatru

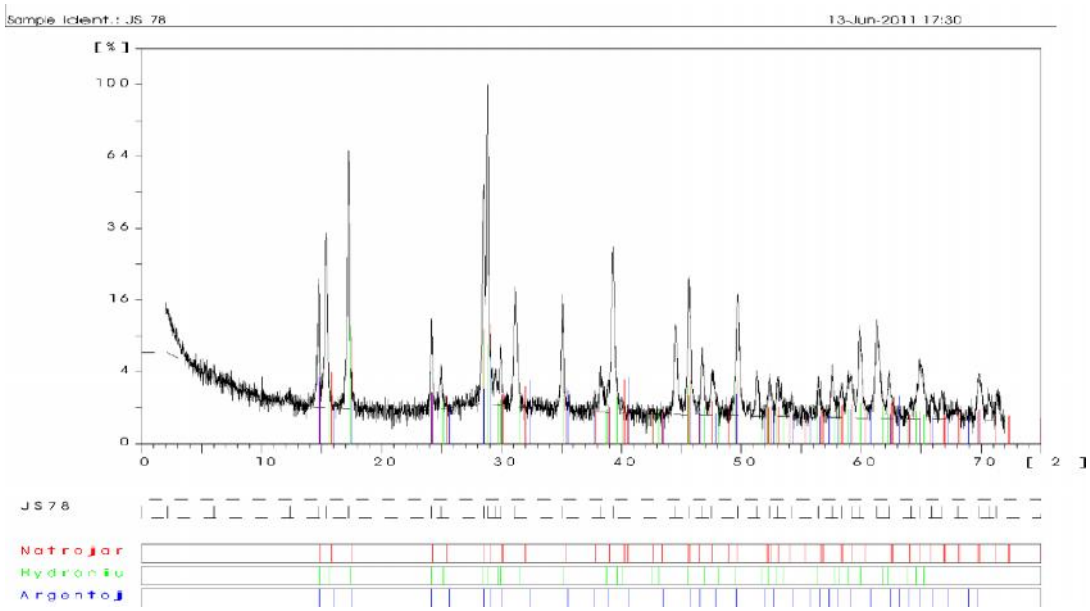
Sample Ident.: JS 78
13-Jun-2011 17:30
[%]
100
64
36
16
4
0
0
10
20
30
40
50
60
70
[2]
JS78
Natrojar
Hydronatru
Argentoj

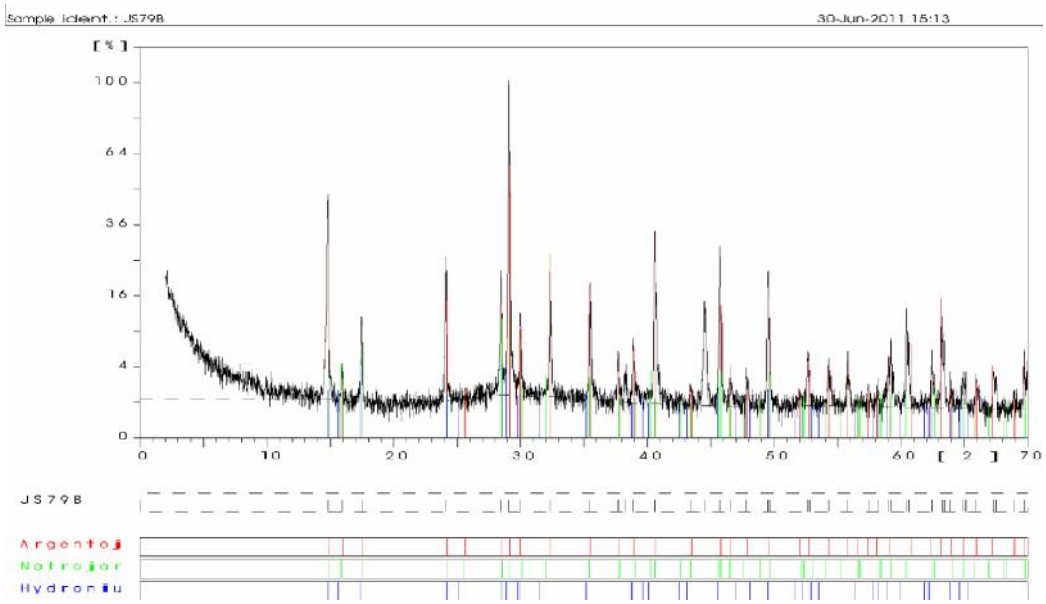
Sample Ident.: JS79B
30-Jun-2011 15:13
[%]
100
64
36
16
4
0
0
10
20
30
40
50
60
[2]
70
JS79B
Argentoj
Natrojar
Hydronatru

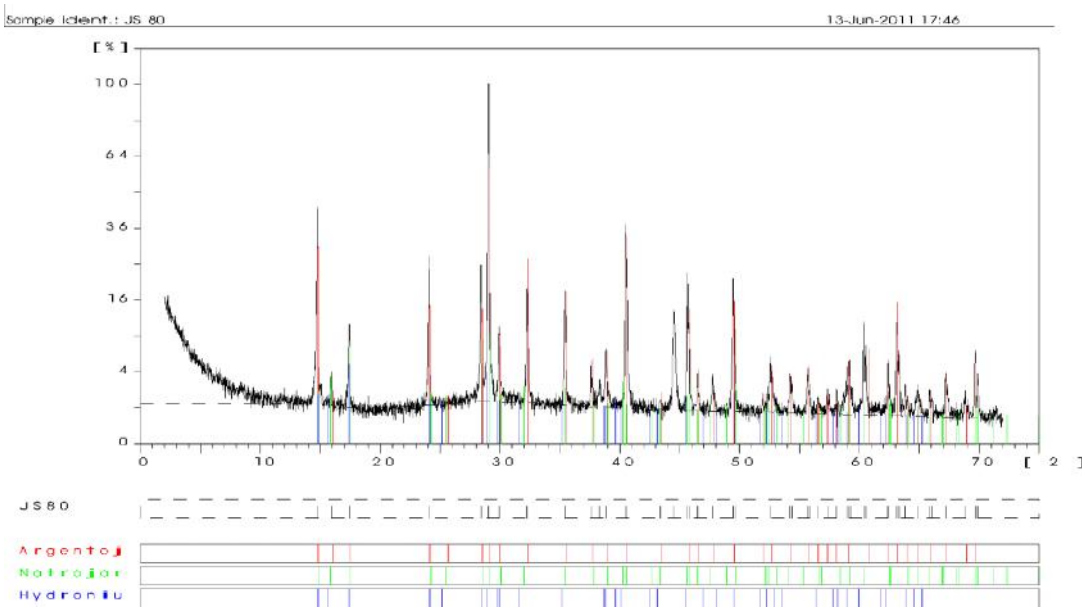
Sample Ident.: JS 80
13-Jun-2011 17:46
[%]
100
64
36
16
4
0
0
10
20
30
40
50
60
70
[2]
JS80
Argentoj
Natrojar
Hydroniu

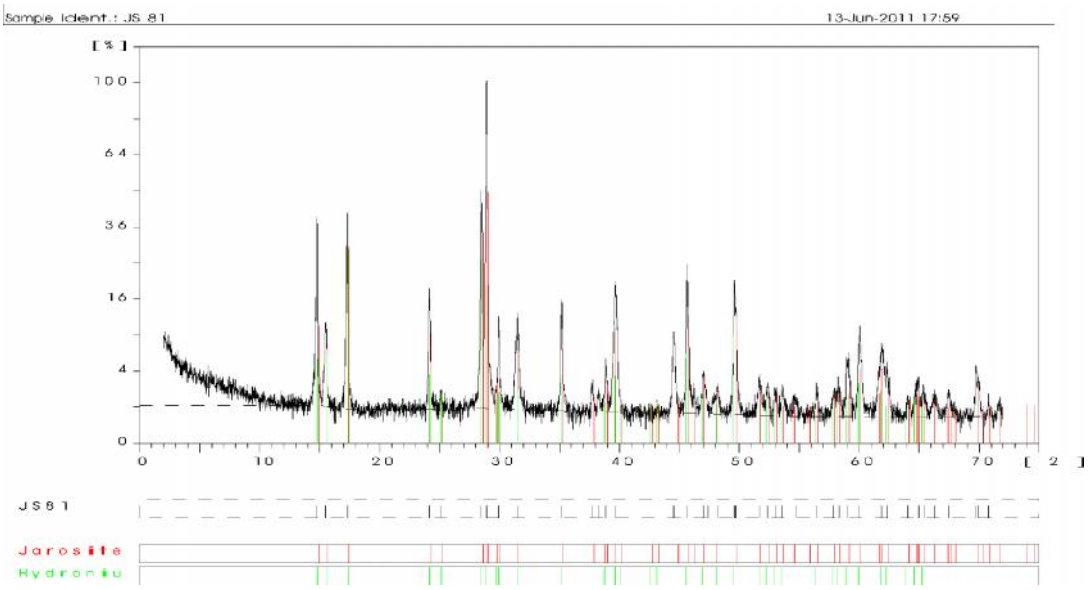
Sample Ident.: JS 81
13-Jun-2011 17:59
[%]
100
64
36
16
4
0
0
10
20
30
40
50
60
70
[2]
JS81
Jarosite
Hydroniu

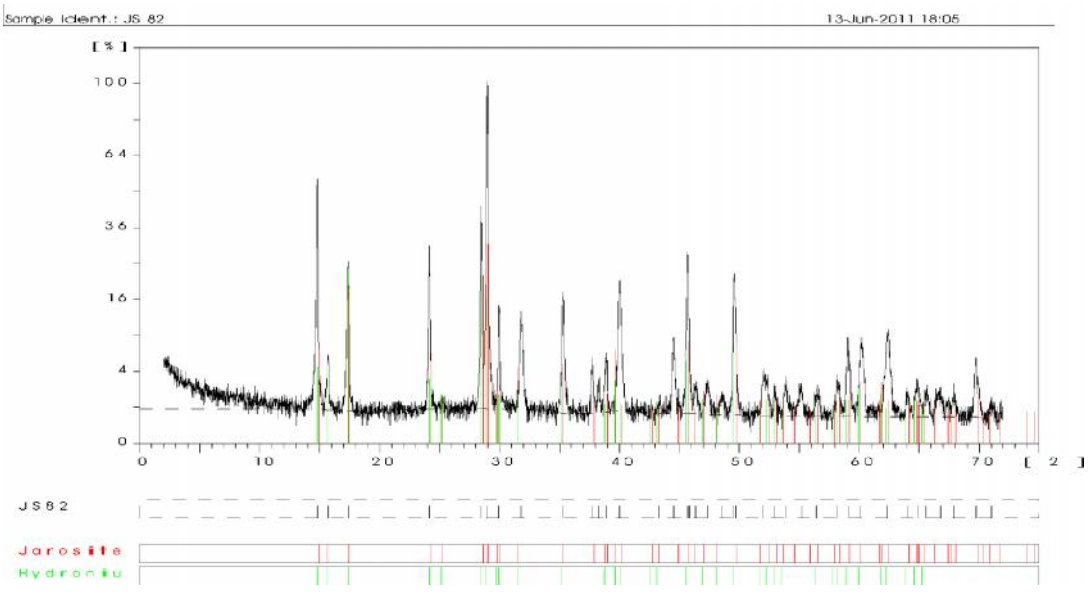
Sample Ident.: JS 82
13-Jun-2011 18:05
[%]
100
64
36
16
4
0
0
10
20
30
40
50
60
70
[2]
JS82
Jarosite
Hydroniu

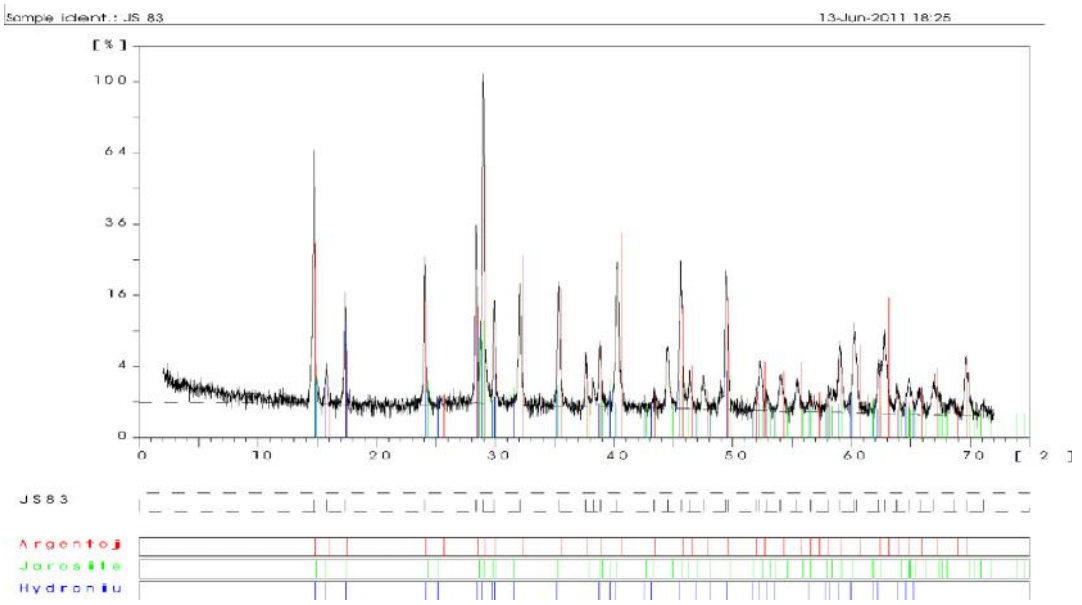
Sample Ident.: JS 83
13-Jun-2011 18:25
[%]
100
64
36
16
4
0
0
10
20
30
40
50
60
70
[2]
JS83
Argentoj
Jarosite
Hydroniu

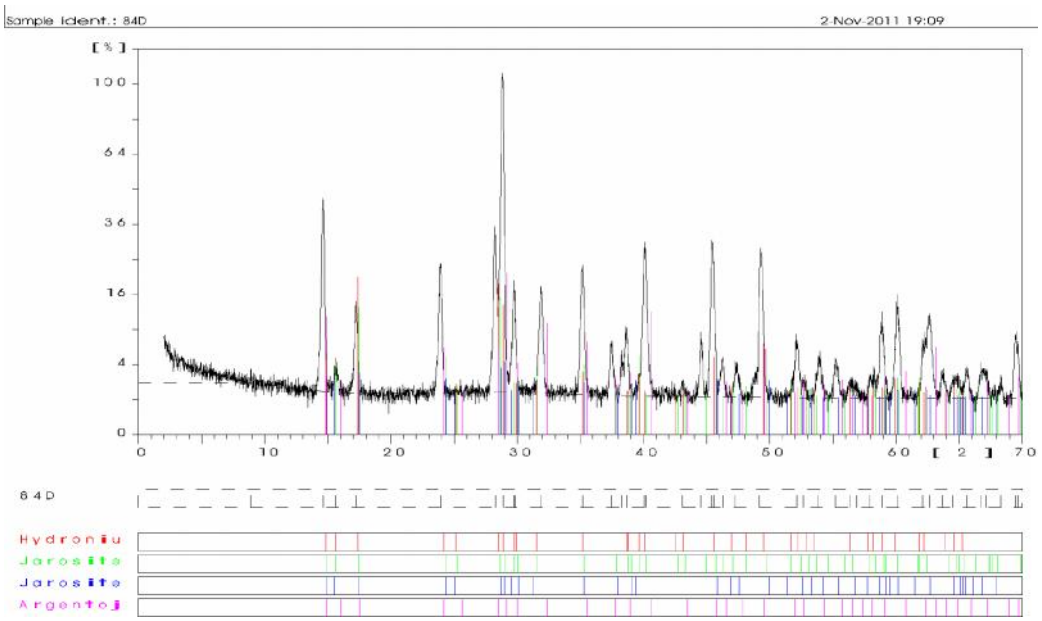
Sample Ident.: 84D
2-Nov-2011 19:09
[%]
100
64
36
16
4
0
0
10
20
30
40
50
60
[2]
70
84D
Hydroniu
Jarosite
Jarosite
Argentoj

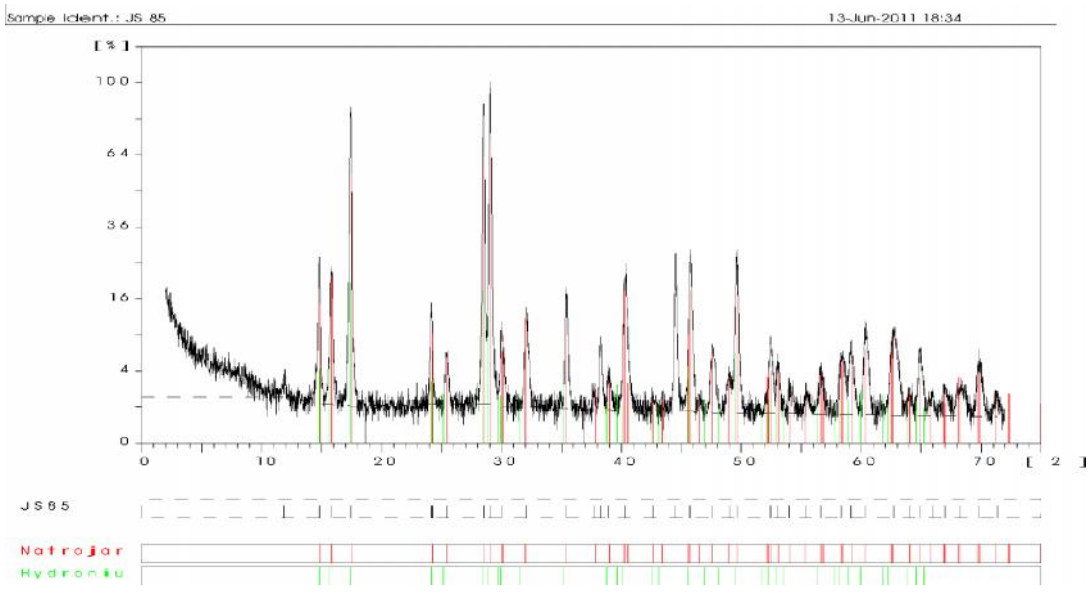
Sample Ident.: JS 85
13-Jun-2011 18:34
[%]
100
64
36
16
4
0
0
10
20
30
40
50
60
70
[2]
JS85
Natrojar
Hydroniu

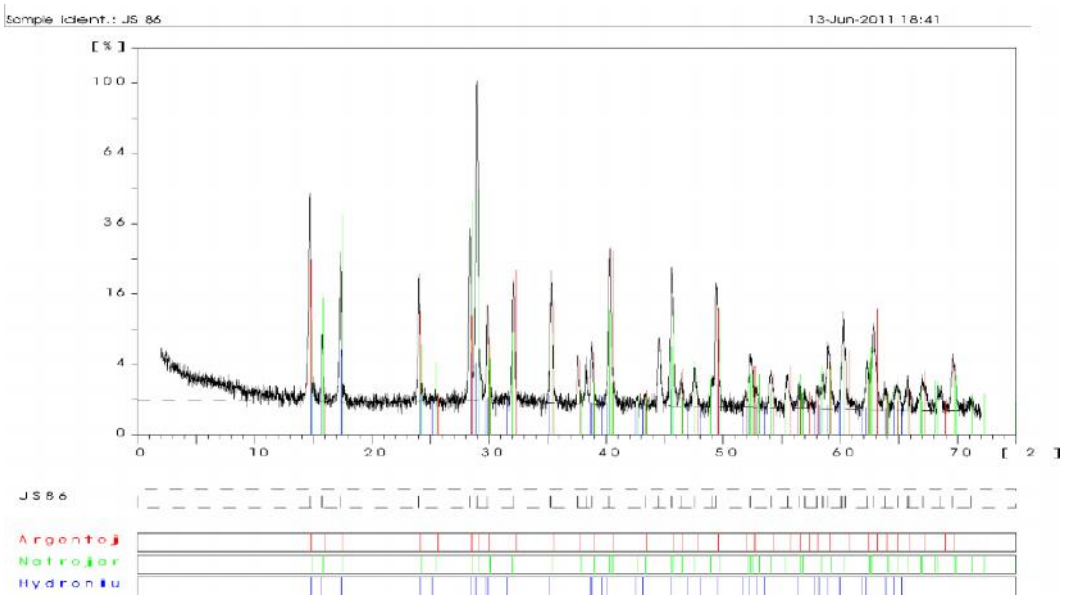
Sample Ident.: JS 86
13-Jun-2011 18:41
[%]
100
64
36
16
4
0
0
10
20
30
40
50
60
70
[2]
JS86
Argentoj
Natrojar
Hydroniu

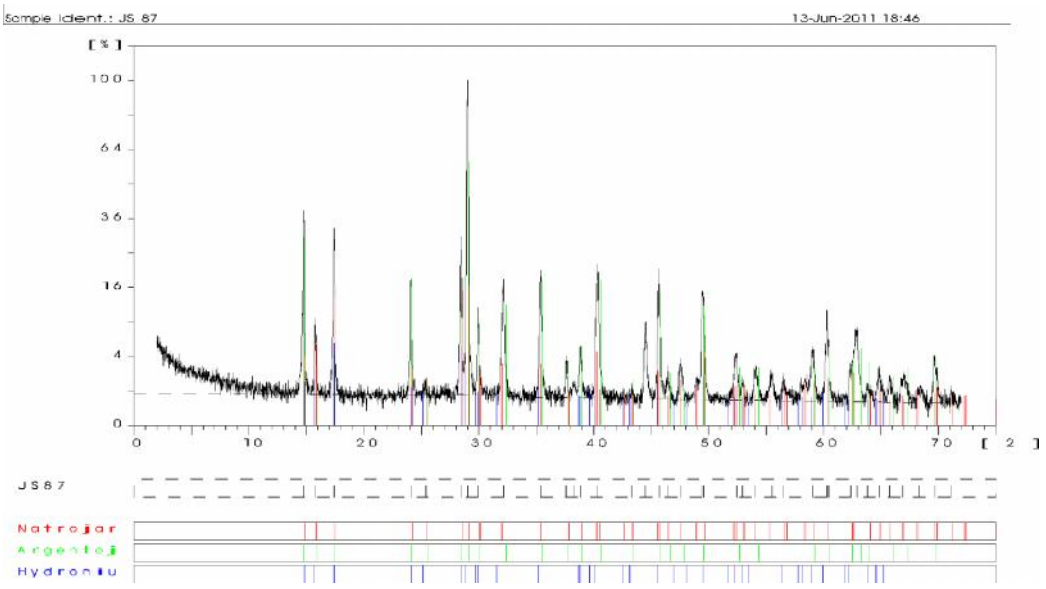
Sample Ident.: JS 87
13-Jun-2011 18:46
[%]
100
64
36
16
4
0
0
10
20
30
40
50
60
70
[2]
JS87
Natrojar
Argentoj
Hydroniu

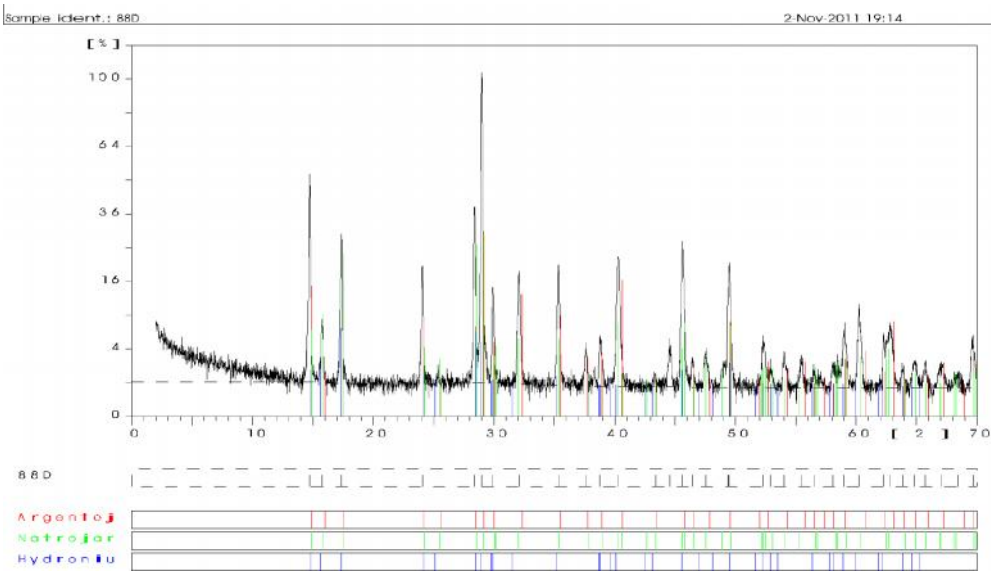
Sample Ident.: 88D
2-Nov-2011 19:14
[%]
100
64
36
16
4
0
0
10
20
30
40
50
60
[2]
70
88D
Argentoj
Natrojar
Hydroniu

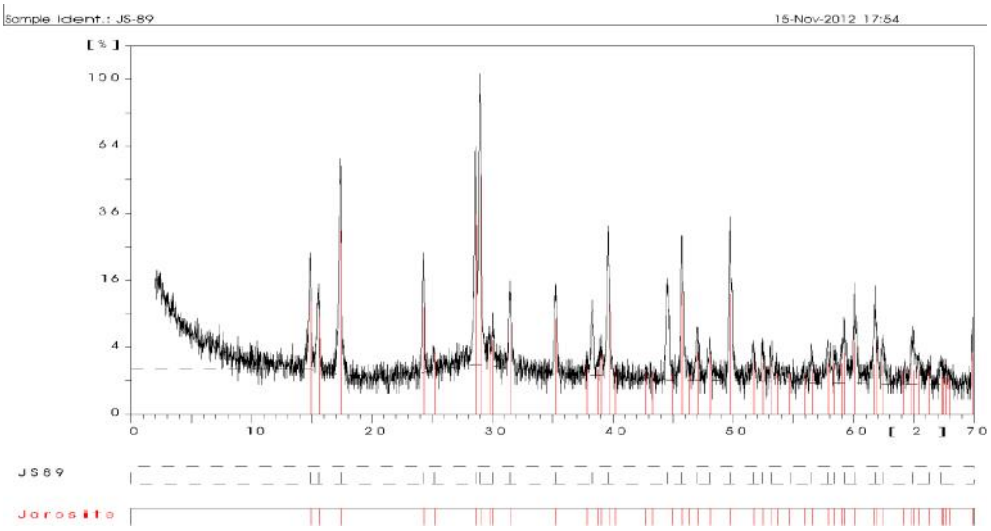
Sample Ident.: JS-89
15-Nov-2012 17:54
[%]
100
64
36
16
4
0
0
10
20
30
40
50
60
[2]
70
JS89
Jarosite

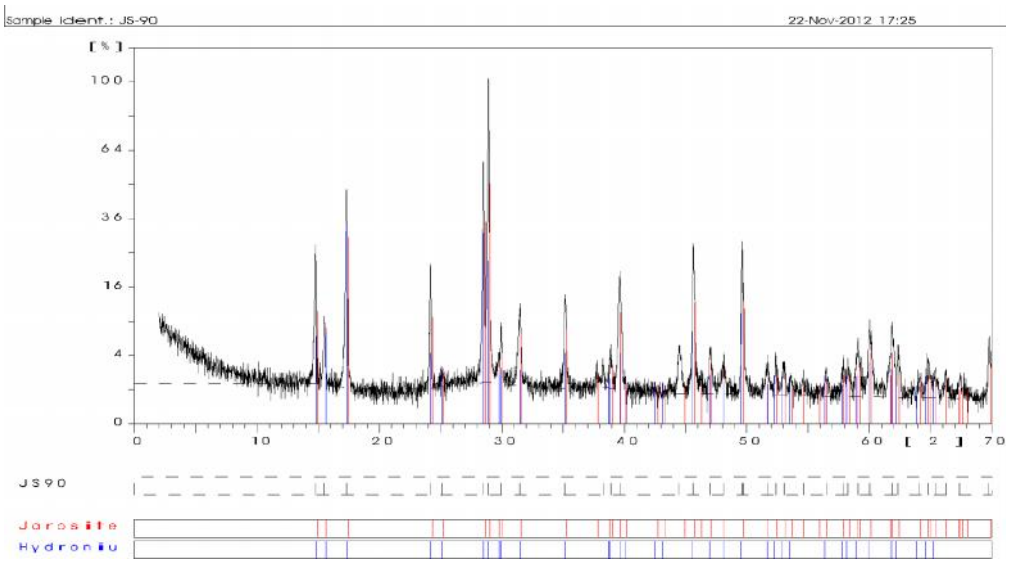
Sample Ident.: JS-90
22-Nov-2012 17:25
[%]
100
64
36
16
4
0
0
10
20
30
40
50
60
[2]
70
JS90
Jarosite
Hydronium

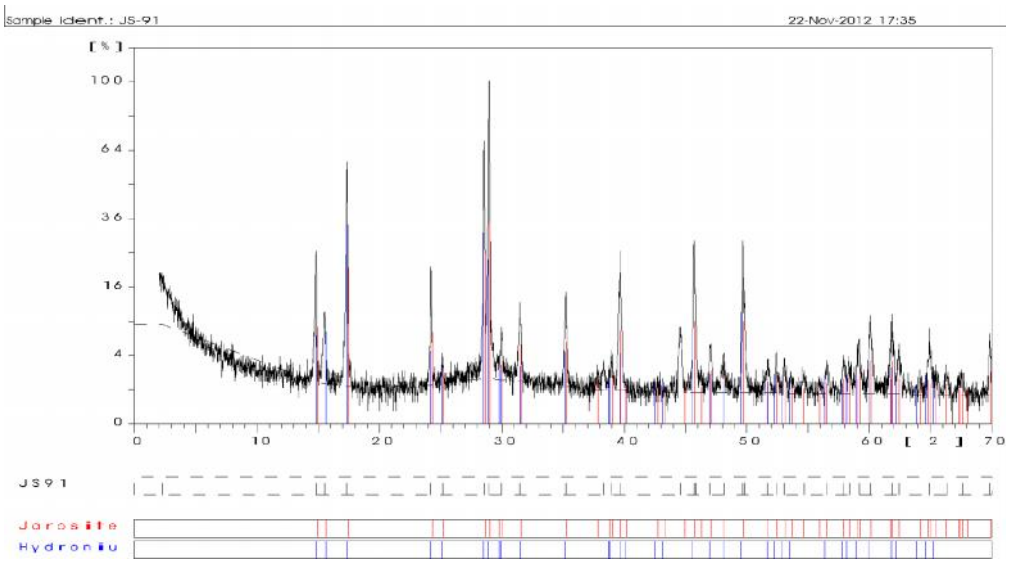
Sample Ident.: JS-91
22-Nov-2012 17:35
[%]
100
64
36
16
4
0
0
10
20
30
40
50
60
[2]
70
JS91
Jarosite
Hydronium

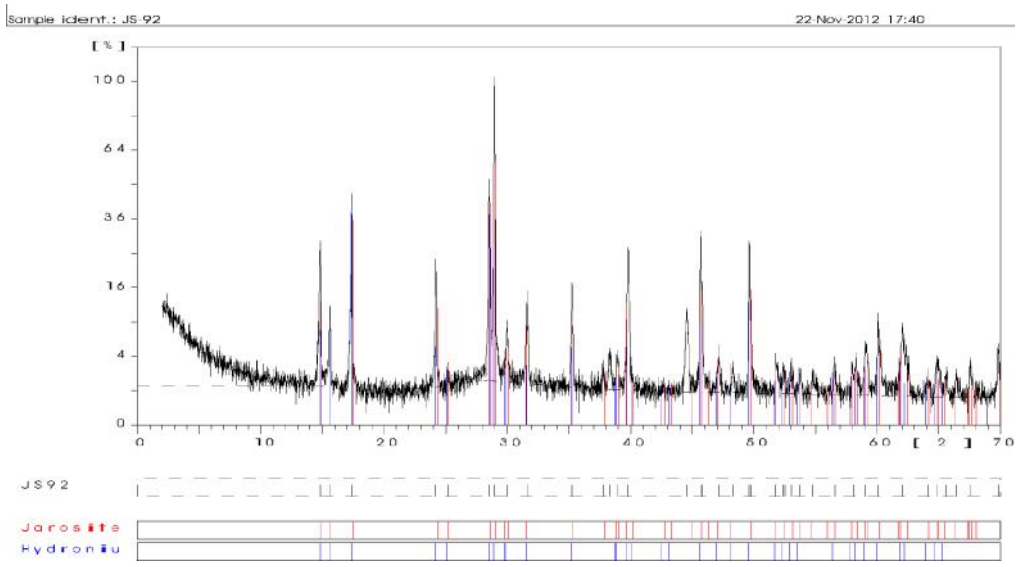
Sample ident.: JS-92
22-Nov-2012 17:40
[%]
100
64
36
16
4
0
0
10
20
30
40
50
60
[2]
70
JS92
Jarosite
Hydroniu

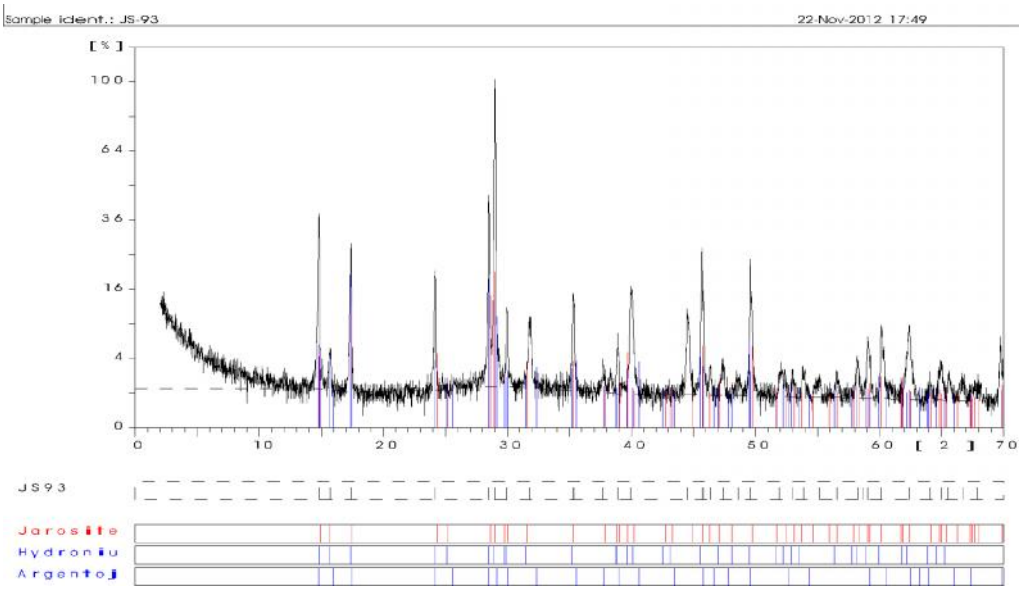
Sample ident.: JS-93
22-Nov-2012 17:49
[%]
100
64
36
16
4
0
0
10
20
30
40
50
60
[2]
70
JS93
Jarosite
Hydroniu
Argentoj

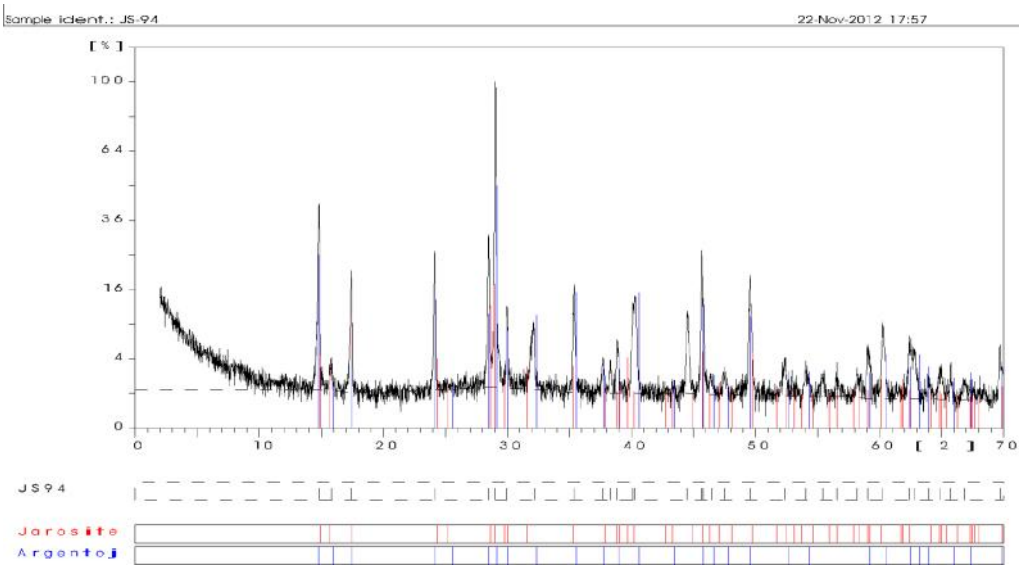
Sample ident.: JS-94
22-Nov-2012 17:57
[%]
100
64
36
16
4
0
0
10
20
30
40
50
60
[2]
70
JS94
Jarosite
Argentoj

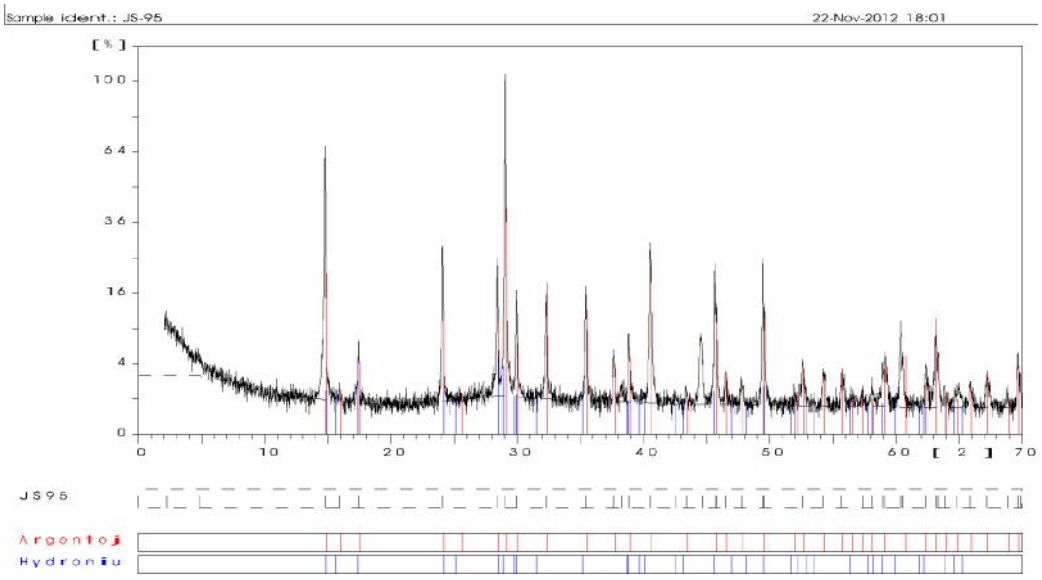
Sample ident.: JS-95
22-Nov-2012 18:01
[%]
100
64
36
16
4
0
10
20
30
40
50
60
[2]
70
JS95
Argentoj
Hydroniu

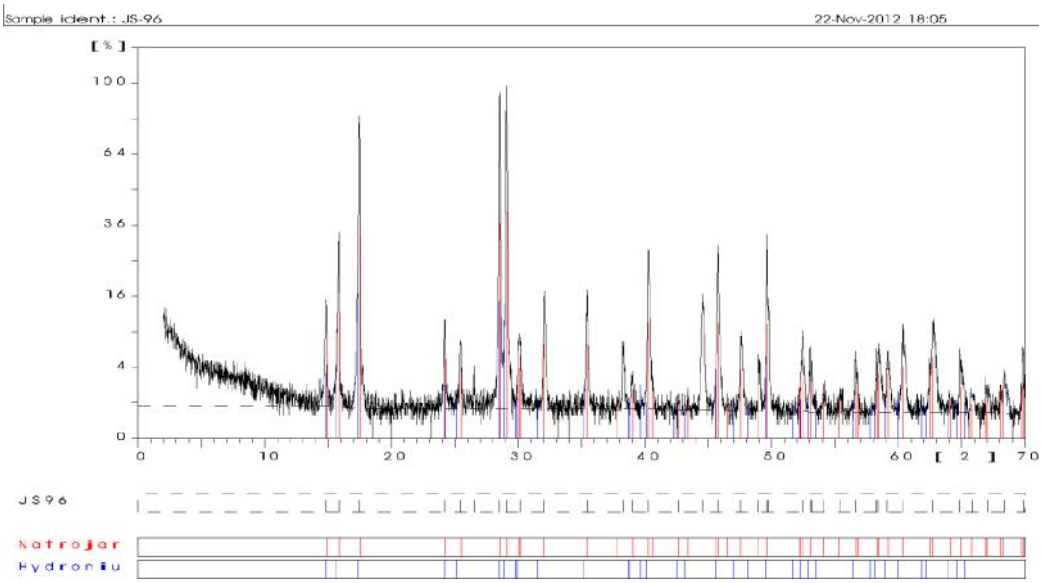
Sample ident.: JS-96
22-Nov-2012 18:05
[%]
100
64
36
16
4
0
10
20
30
40
50
60
[2]
70
JS96
Natrojar
Hydroniu

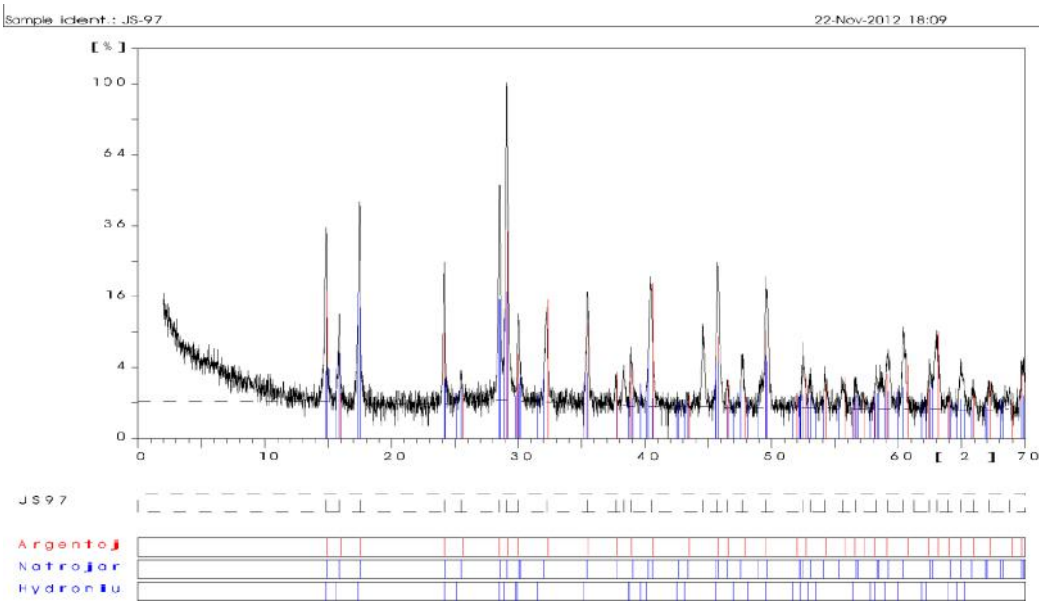
Sample ident.: JS-97
22-Nov-2012 18:09
[%]
100
64
36
16
4
0
10
20
30
40
50
60
[2]
70
JS97
Argentoj
Natrojar
Hydroniu

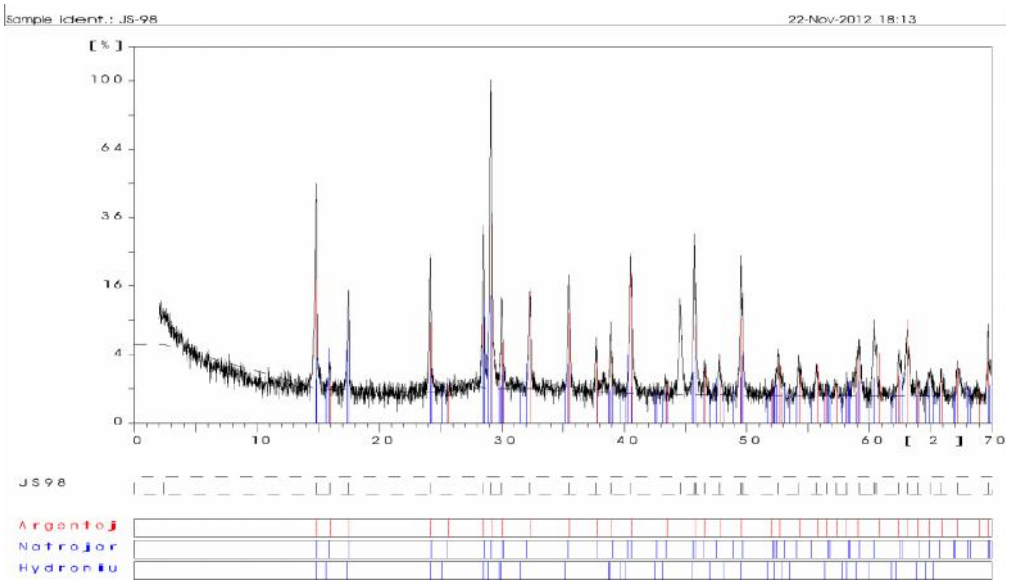
Sample ident.: JS-98
22-Nov-2012 18:13
[%]
100
64
36
16
4
0
0
10
20
30
40
50
60
[2]
70
JS98
Argentoj
Natrojar
Hydroniu

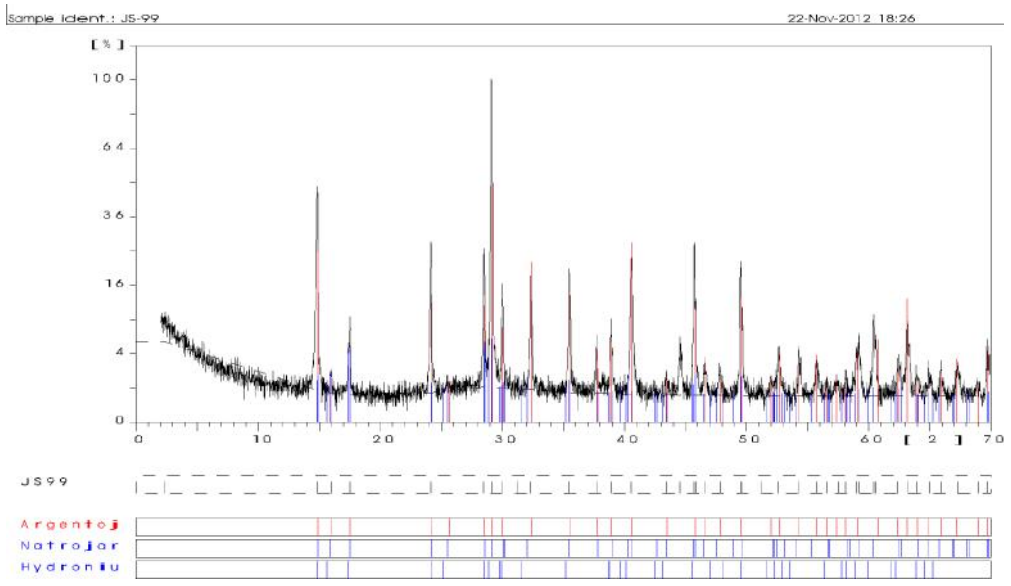
Sample ident.: JS-99
22-Nov-2012 18:26
[%]
100
64
36
16
4
0
0
10
20
30
40
50
60
[2]
70
JS99
Argentoj
Natrojar
Hydroniu

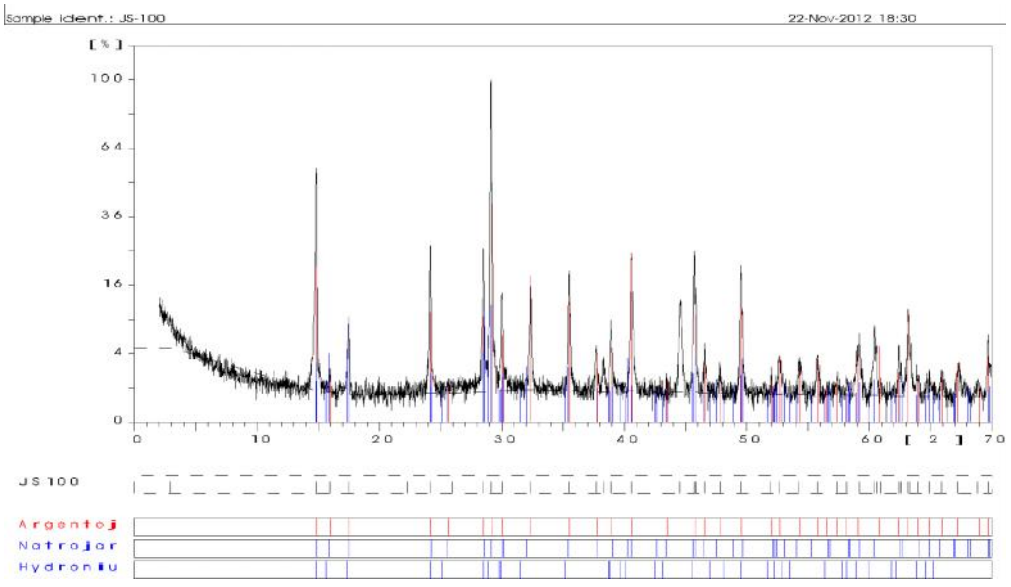
Sample ident.: JS-100
22-Nov-2012 18:30
[%]
100
64
36
16
4
0
0
10
20
30
40
50
60
[2]
70
JS100
Argentoj
Natrojar
Hydroniu

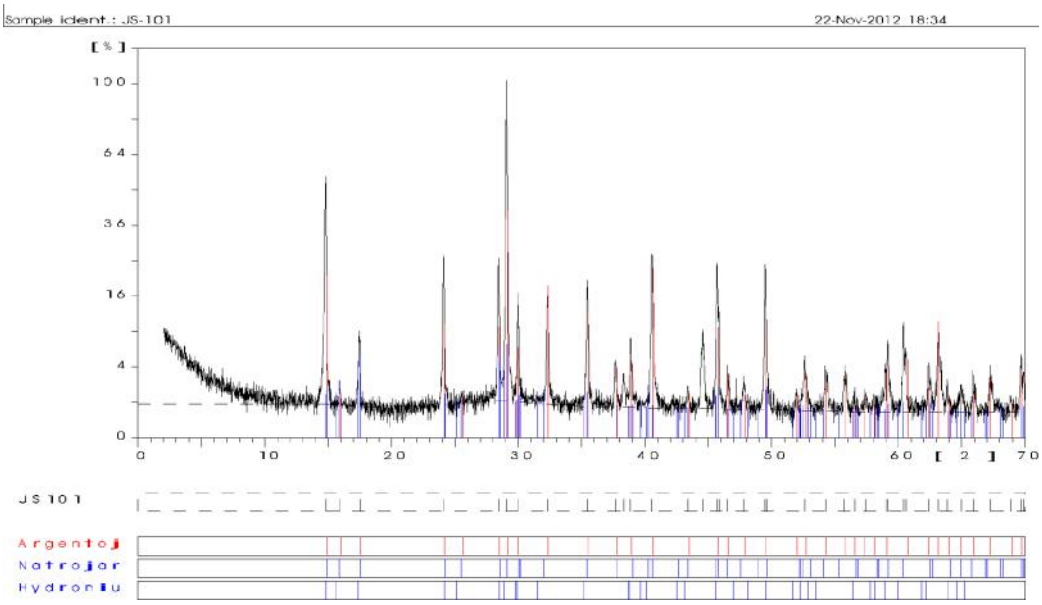
Sample ident.: JS-101
22-Nov-2012 18:34
[%]
100
64
36
16
4
0
0
10
20
30
40
50
60
[2]
70
JS 101
Argentoj
Natrojar
Hydroniu

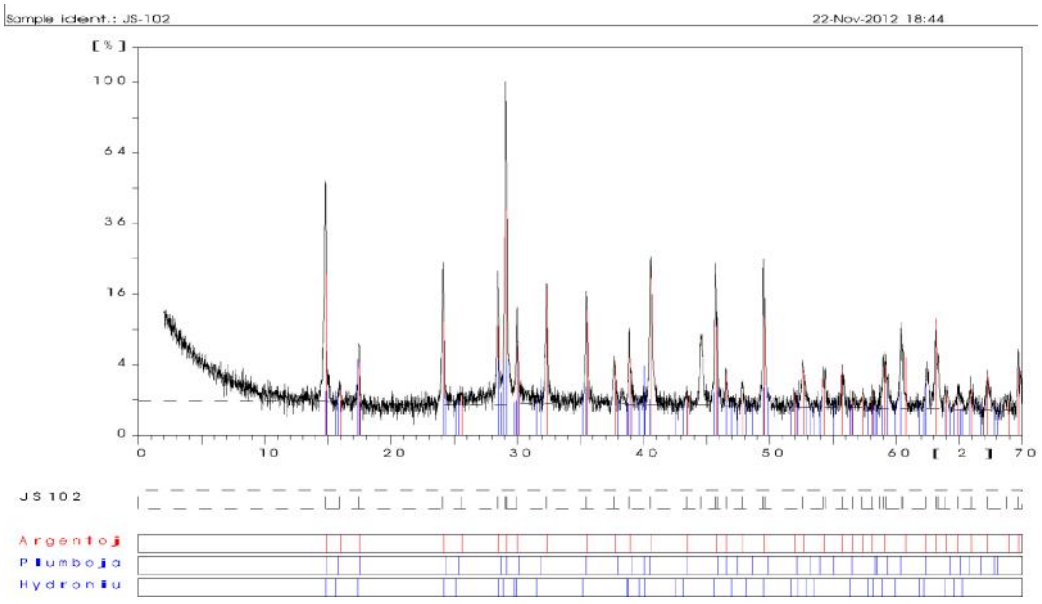
Sample ident.: JS-102
22-Nov-2012 18:44
[%]
100
64
36
16
4
0
0
10
20
30
40
50
60
[2]
70
JS 102
Argentoj
Plumboja
Hydroniu

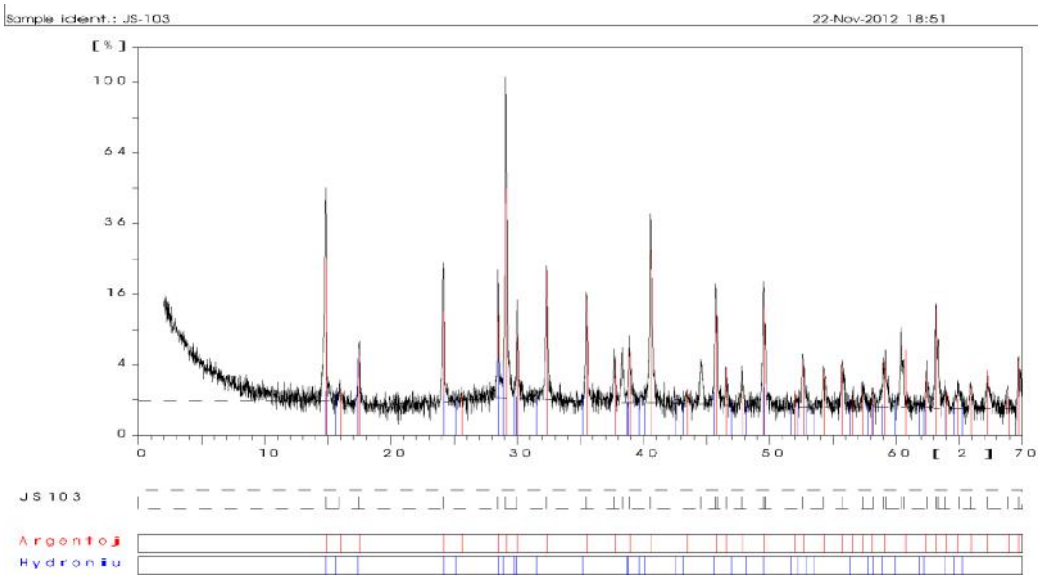
Sample ident.: JS-103
22-Nov-2012 18:51
[%]
100
64
36
16
4
0
0
10
20
30
40
50
60
[2]
70
JS 103
Argentoj
Hydroniu

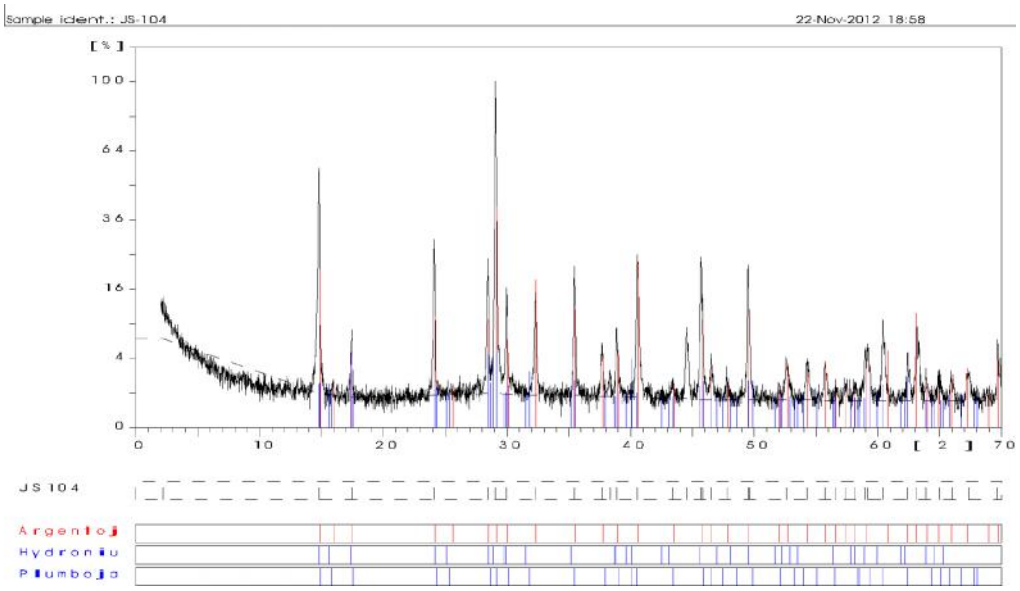
Sample ident.: JS-104
22-Nov-2012 18:58
[%]
100
64
36
16
4
0
0
10
20
30
40
50
60
[2]
70
JS 104
Argentoj
Hydroniu
Plumboja

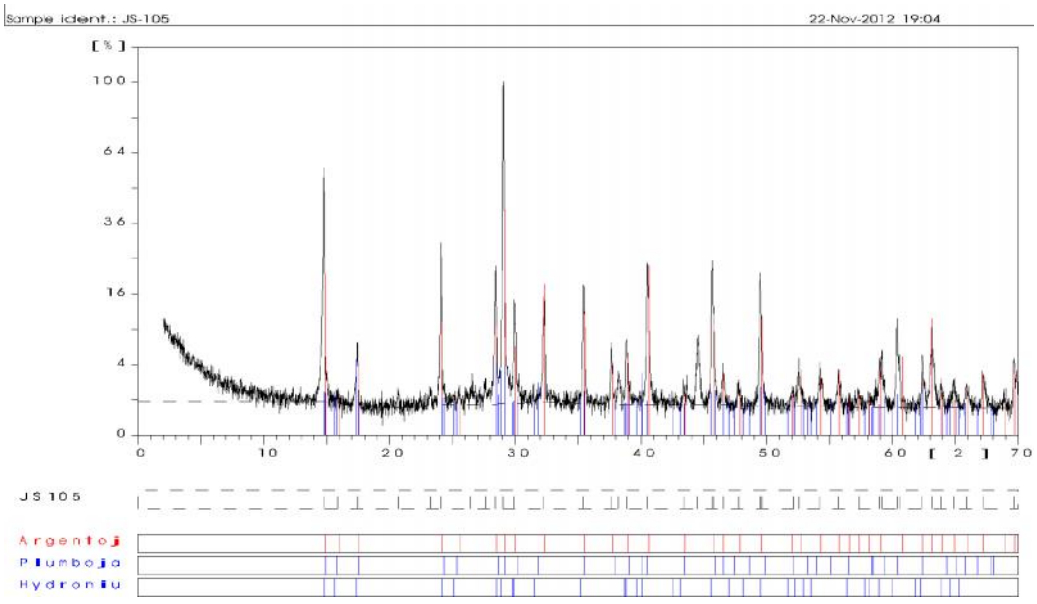
Sample ident.: JS-105
22-Nov-2012 19:04
[%]
100
64
36
16
4
0
0
10
20
30
40
50
60
[2]
70
JS 105
Argentoj
Plumboja
Hydroniu

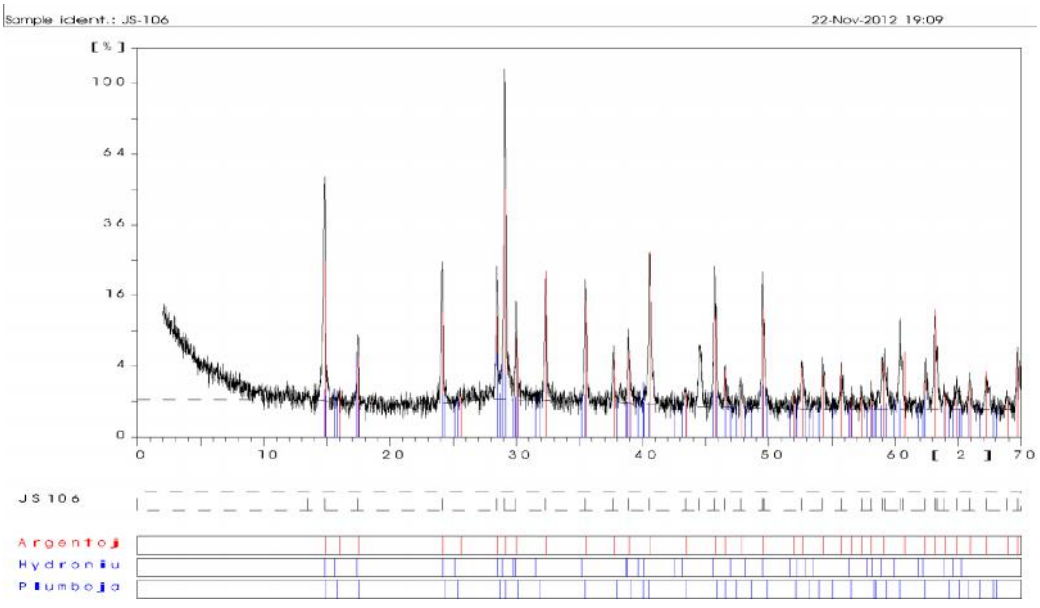
Sample ident.: JS-106
22-Nov-2012 19:09
[%]
100
64
36
16
4
0
0
10
20
30
40
50
60
[2]
70
JS 106
Argentoj
Hydroniu
Plumboja

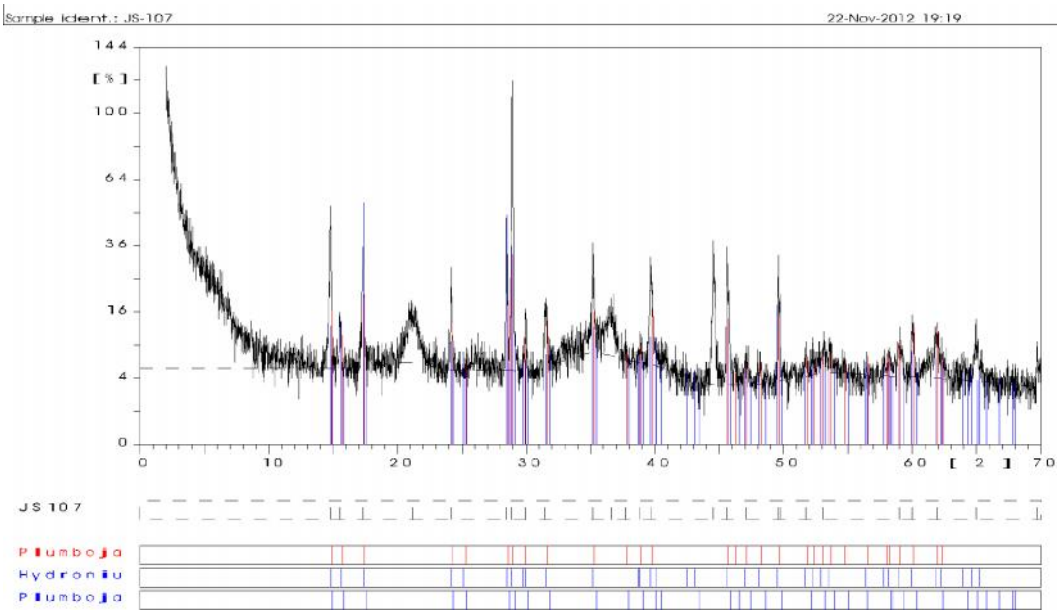
Sample Ident.: JS-107
22-Nov-2012 19:19
144
[%]
100
64
36
16
4
0
0
10
20
30
40
50
60
[2]
70
JS 107
Plumboja
Hydroniu
Plumboja

APPENDIX F Raman spectra of synthesised jarosite compounds

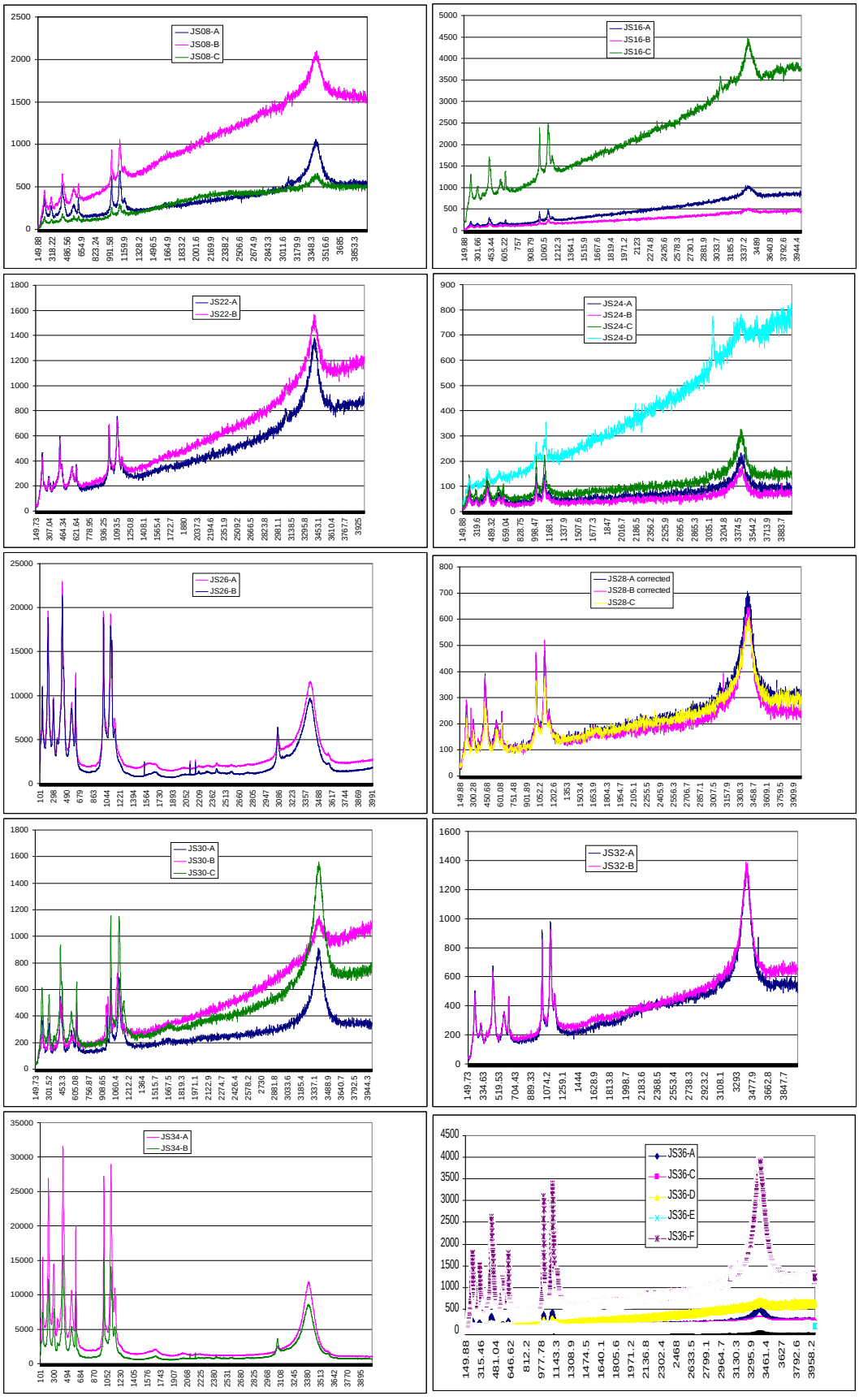

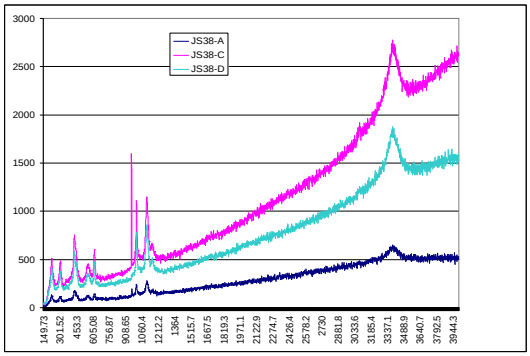
JS38-A
JS38-C
JS38-D

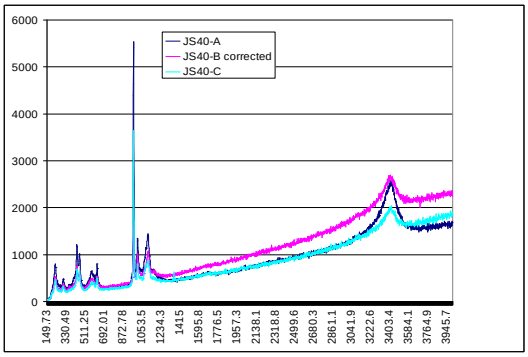
JS40-A
JS40-B corrected
JS40-C

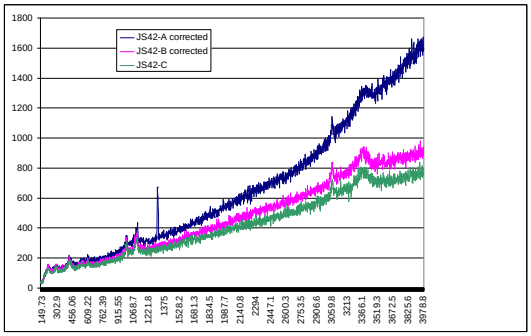
JS42-A corrected
JS42-B corrected
JS42-C

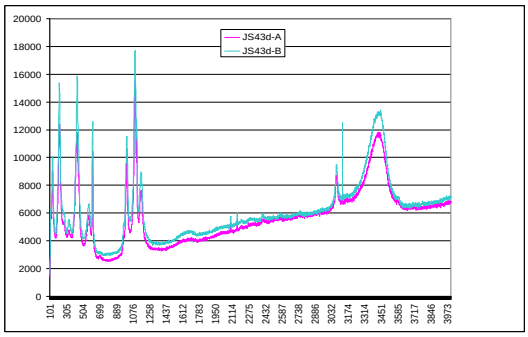
JS43d-A
JS43d-B

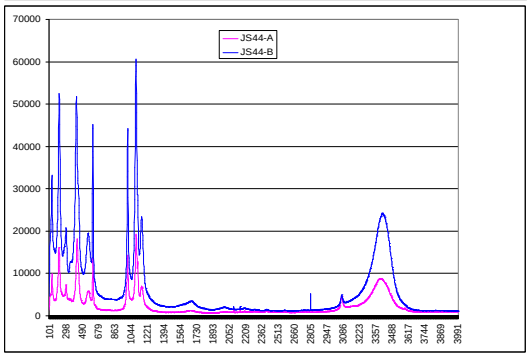
JS44-A
JS44-B

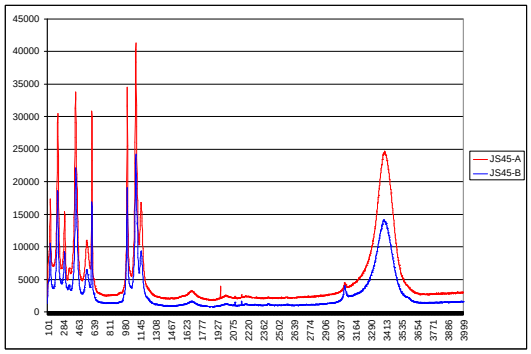
JS45-A
JS45-B

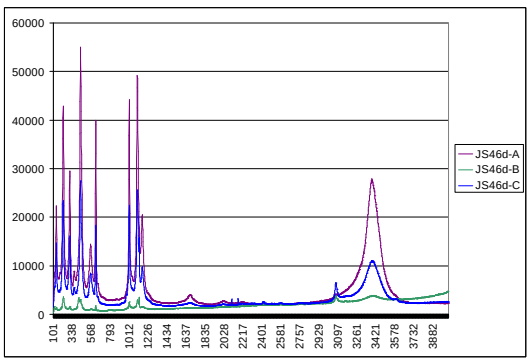
JS46d-A
JS46d-B
JS46d-C

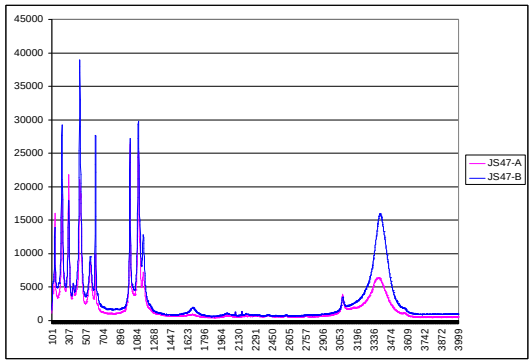
JS47-A
JS47-B

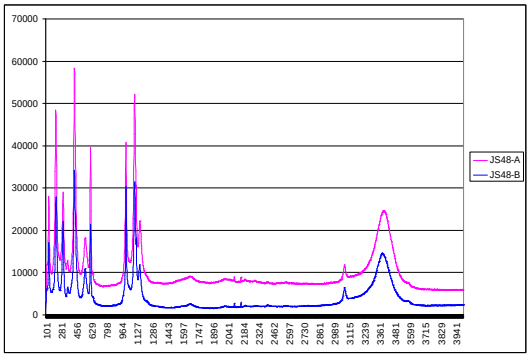
JS48-A
JS48-B

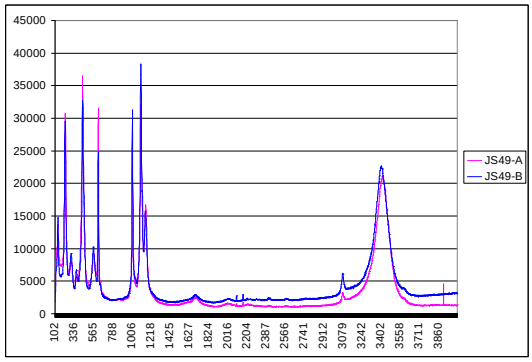
JS49-A
JS49-B

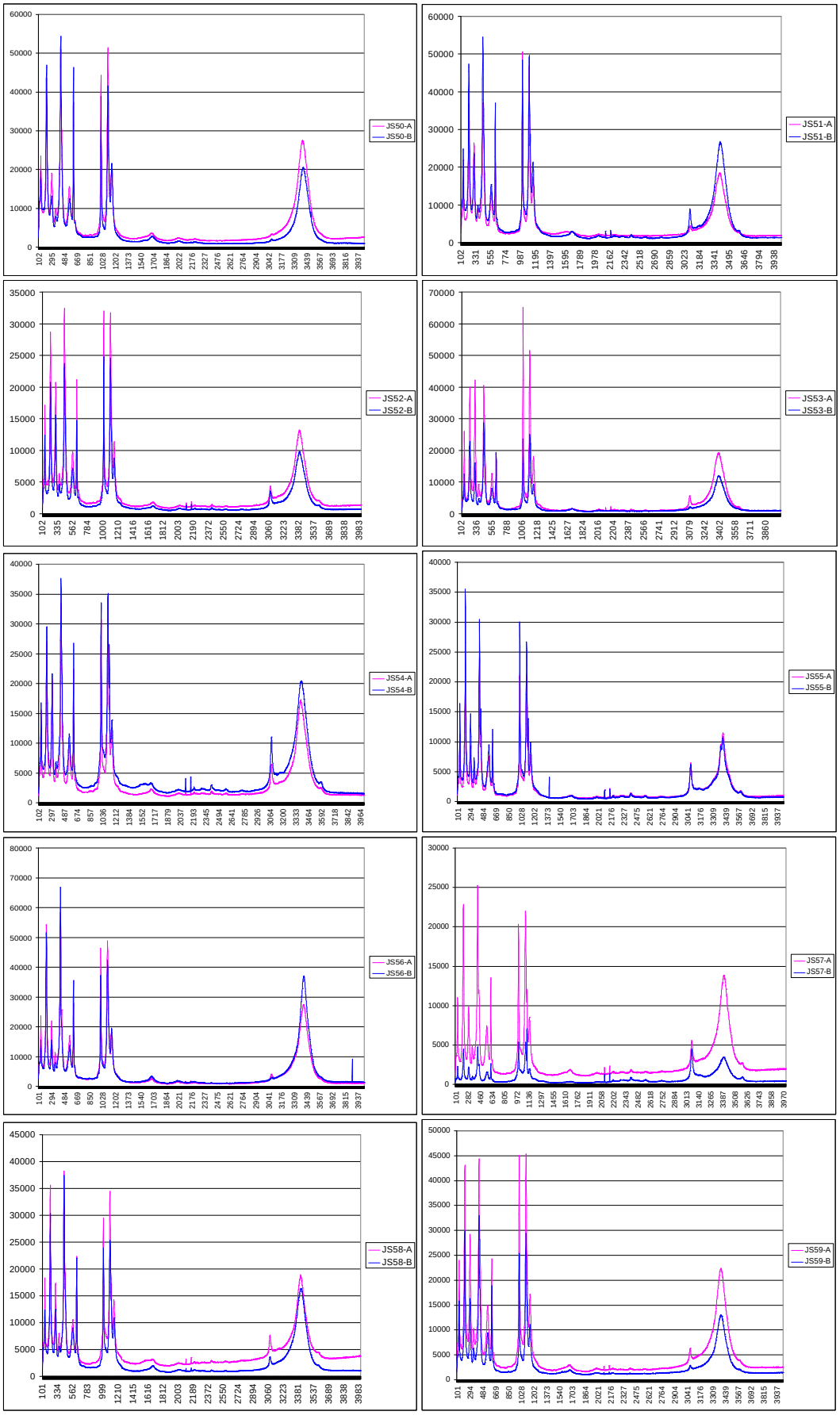
JS50-A
JS50-B
JS51-A
JS51-B
JS52-A
JS52-B
JS53-A
JS53-B
JS54-A
JS54-B
JS55-A
JS55-B
JS56-A
JS56-B
JS57-A
JS57-B
JS58-A
JS58-B
JS59-A
JS59-B

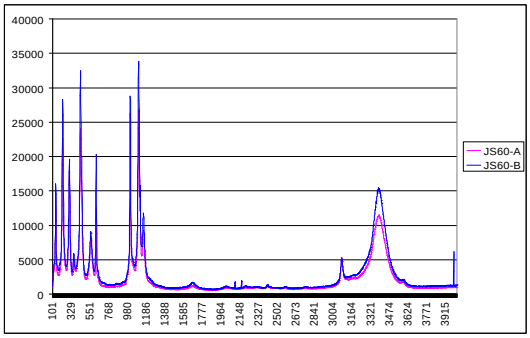
JS60-A
JS60-B

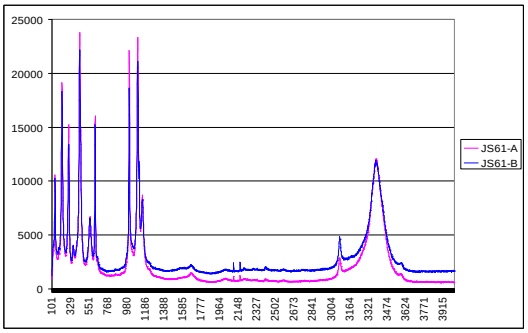
JS61-A
JS61-B

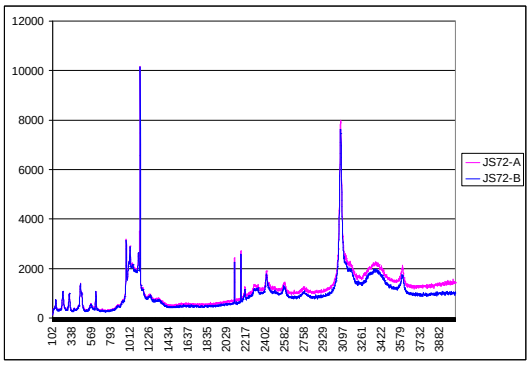
JS72-A
JS72-B

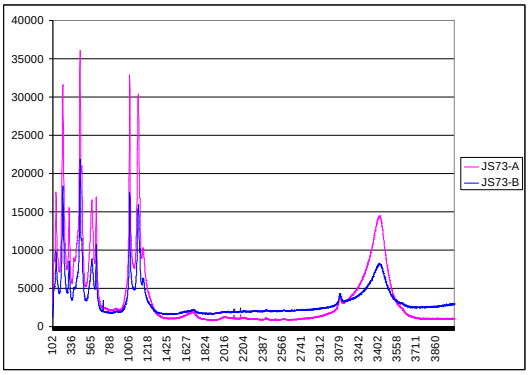
JS73-A
JS73-B

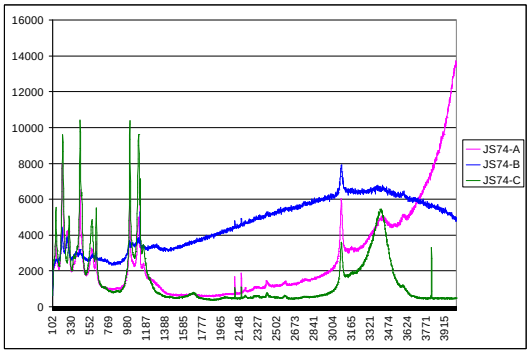
JS74-A
JS74-B
JS74-C

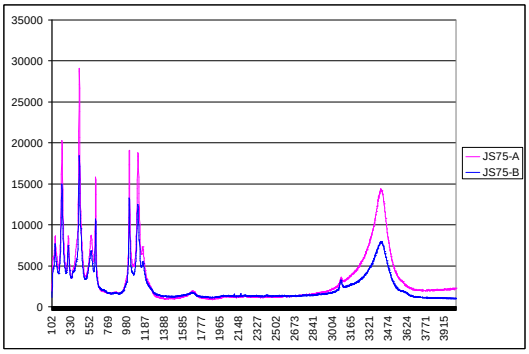
JS75-A
JS75-B

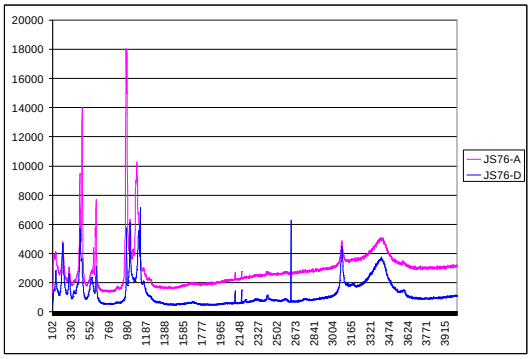
JS76-A
JS76-D

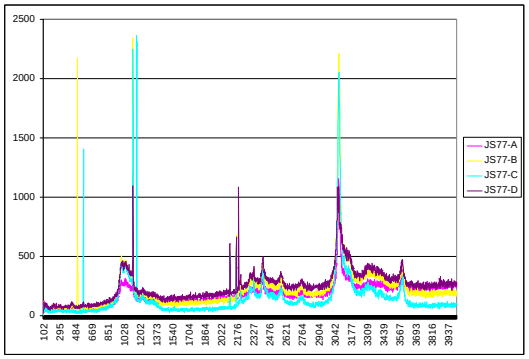
JS77-A
JS77-B
JS77-C
JS77-D

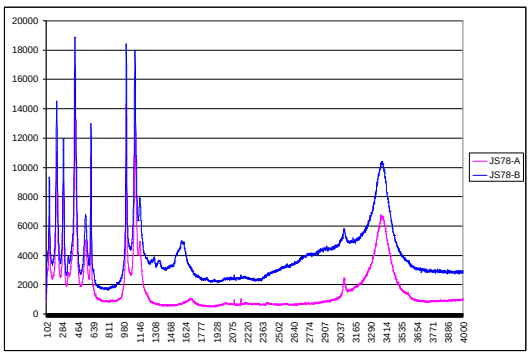
JS78-A
JS78-B

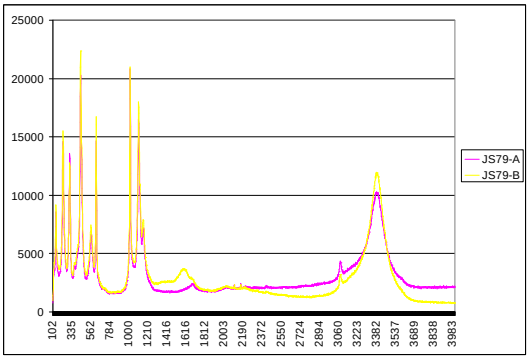
JS79-A
JS79-B

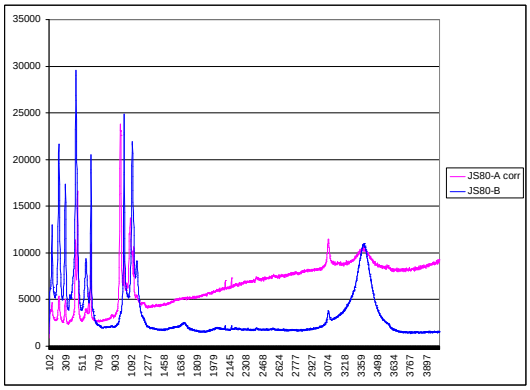
35000
30000
25000
20000
15000
10000
5000
0
102
309
511
709
903
1092
1277
1458
1636
1809
1979
2145
2308
2468
2624
2777
2927
3074
3218
3359
3498
3634
3767
3897
JS80-A corr
JS80-B

APPENDIX G

Potassium, Na, Pb and Ag occupancies of *A* site (based on the combined data) and concentration (*M*) in starting solutions, and partitioning coefficients for Ag in K-Ag, Na-Ag and Pb-Ag-jarosites between synthesis solutions and products.

Sample	Ag occ.	K occ.	(Ag/Ag+K)j	[Ag]sol.	[K]sol.	[Ag/Ag+K]sol.	P. coeff.
Solutions containing 0.51 M $Fe_2(SO_4)_3.5H_2O$ heated at 97ºC and products dried at 60ºC							
JS04	0	0.65	0	0	0.22	0	0
JS06	0.18	0.5	0.265	0.055	0.165	0.25	1.06
JS06D	0.15	0.52	0.224	0.055	0.165	0.25	0.896
JS08	0.3	0.41	0.423	0.11	0.11	0.5	0.846
JS10	0.41	0.25	0.621	0.165	0.055	0.75	0.828
JS10D	0.44	0.27	0.62	0.165	0.055	0.75	0.827
JS12	0.78	0	1	0.22	0	1	1
JS04-12			**3.153**			**3.5**	**0.901**
Solutions containing 0.51 M $Fe_2(SO_4)_3.5H_2O$ heated at 97ºC and products dried at 110ºC							
JS22	0	0.64	0	0	0.22	0	0
JS24	0.15	0.53	0.221	0.055	0.165	0.25	0.884
JS24D	0.14	0.52	0.212	0.055	0.165	0.25	0.848
JS26	0.25	0.44	0.362	0.11	0.11	0.5	0.724
JS28	0.56	0.27	0.675	0.165	0.055	0.75	0.9
JS30	0.63	0	1	0.22	0	1	1
JS22-30			**2.470**			**2.75**	**0.898**
JS40	0.04	0.26	0.133	0.1	0.5	0.167	0.796
Solutions containing 0.15 M $Fe_2(SO_4)_3.5H_2O$ heated at 140ºC and products dried at 110ºC							
JS55	0	0.43	0	0	0.12	0	0
JS56	0.16	0.7	0.186	0.02	0.1	0.167	1.114
JS57	0.23	0.47	0.329	0.04	0.08	0.333	0.988
JS58	0.34	0.38	0.472	0.06	0.06	0.5	0.944
JS59	0.45	0.29	0.608	0.08	0.04	0.667	0.912
JS60	0.68	0.16	0.81	0.1	0.02	0.833	0.972
JS61	0.85	0	1	0.12	0	1	1
JS55-61			**3.405**			**3.5**	**0.973**
Samples annealed at 140ºC and dried at 110ºC (from solutions originally containing 0.51 M $Fe_2(SO_4)_3.5H_2O$ heated at 97ºC and products dried at 60ºC)							
JS62	0	0.61	0	0	0.22	0	0
JS63	0.21	0.49	0.3	0.055	0.165	0.25	1.2
JS64	0.36	0.37	0.493	0.11	0.11	0.5	0.986
JS65	0.37	0.15	0.712	0.165	0.055	0.75	0.949
JS66	0.44	0	1	0.22	0	1	1
JS62-66			**2.505**			**2.5**	**1.002**
Samples annealed at 140ºC and dried at 110ºC (from solutions originally containing 0.51 M $Fe_2(SO_4)_3.5H_2O$ heated at 97ºC and products dried at 110ºC)							
JS71	0.76	0	1	0.22	0	1	1
JS81	0	0.6	0	0	0.22	0	0
JS82	0.24	0.44	0.353	0.055	0.165	0.25	1.412
JS83	0.46	0.29	0.613	0.11	0.11	0.5	1.226
JS84	0.68	0.09	0.883	0.165	0.055	0.75	1.177
JS71,81-84			**2.849**			**2.5**	**1.14**
Solutions containing 0.51 M $Fe_2(SO_4)_3.5H_2O$ were prepared at 22ºC and products air-dried at 22ºC							
JS72	0.63	0	1	0.22	0	1	1
JS73	0	0.78	0	0	0.22	0	0
JS74	0.06	0.68	0.081	0.055	0.165	0.25	0.324
JS75	0.14	0.64	0.179	0.11	0.11	0.5	0.358
JS76	0.26	0.37	0.413	0.165	0.055	0.75	0.551
JS72-76			**1.673**			**2.5**	**0.669**
Solutions containing 0.075 M $Fe_2(SO_4)_3.5H_2O$ were prepared at 22ºC and products air-dried at 22ºC							
JS89	0	0.73	0	0	0.06	0	0
JS90	0.05	0.69	0.068	0.01	0.05	0.167	0.407
JS91	0.1	0.65	0.133	0.02	0.04	0.333	0.399
JS92	0.15	0.6	0.2	0.03	0.03	0.5	0.4
JS93	0.35	0.43	0.449	0.04	0.02	0.667	0.673
JS94	0.52	0.28	0.65	0.05	0.01	0.833	0.78
JS95	0.85	0	1	0.06	0	1	1
JS89-95			**2.5**			**3.5**	**0.714**

Key: occ. = *A*-site occupation; j. = jarosite product; [Ag]sol. = concentration of Ag in starting solution (*M*); [K]sol. = concentration of K in starting solution (*M*); P. coeff. = partitioning coefficient.

Sample	Ag occ.	Na occ.	(Ag/Ag+Na)j	[Ag]sol.	[Na]sol.	[Ag/Ag+Na]sol.	P. coeff.
Solutions containing 0.51 M $Fe_2(SO_4)_3.5H_2O$ heated at 97ºC and products dried at 60ºC							
JS12	0.78	0	1	0.22	0	1	1
JS14	0	0.57	0	0	0.22	0	0
JS16	0.37	0.33	0.529	0.055	0.165	0.25	2.116
JS18	0.63	0.1	0.863	0.11	0.11	0.5	1.726
JS20	0.71	0.06	0.922	0.165	0.055	0.75	1.229
JS12-20			**3.314**			**2.5**	**1.326**
Solutions containing 0.51 M $Fe_2(SO_4)_3.5H_2O$ heated at 97ºC and products dried at 110ºC							
JS30	0.63	0	1	0.22	0	1	1
JS32	0	0.55	0	0	0.22	0	0
JS34	0.21	0.12	0.636	0.055	0.165	0.25	2.544
JS36	0.31	0.05	0.861	0.11	0.11	0.5	1.722
JS38	0.61	0.04	0.938	0.165	0.055	0.75	1.251
JS38D	0.65	0.07	0.903	0.165	0.055	0.75	1.204
JS30-38			**4.338**			**3.25**	**1.335**
JS42	0.7	0.09	0.886	0.1	0.5	0.167	5.305
Solutions containing 0.15 M $Fe_2(SO_4)_3.5H_2O$ heated at 140ºC and products dried at 110ºC							
JS49	0	0.47	0	0	0.12	0	0
JS50	0.25	0.33	0.431	0.02	0.1	0.167	2.581
JS51	0.47	0.2	0.701	0.04	0.08	0.333	2.105
JS52	0.67	0.09	0.882	0.06	0.06	0.5	1.764
JS53	0.77	0.04	0.951	0.08	0.04	0.667	1.426
JS54	0.83	0.01	0.988	0.1	0.02	0.833	1.186
JS61	0.85	0	1	0.12	0	1	1
JS49-54,61			**4.953**			**3.5**	**1.415**
Samples annealed at 140ºC and dried at 110ºC (from solutions originally containing 0.51 M $Fe_2(SO_4)_3.5H_2O$ heated at 97ºC and products dried at 60ºC)							
JS66	0.44	0	1	0.22	0	1	1
JS67	0	0.65	0	0	0.22	0	0
JS68	0.09	0.57	0.136	0.055	0.165	0.25	0.544
JS69	0.19	0.4	0.322	0.11	0.11	0.5	0.644
JS70	0.33	0.23	0.589	0.165	0.055	0.75	0.785
JS66-70			**2.047**			**2.5**	**0.819**
Samples annealed at 140ºC and dried at 110ºC (from solutions originally containing 0.51 M $Fe_2(SO_4)_3.5H_2O$ heated at 97ºC and products dried at 110ºC)							
JS71	0.76	0	1	0.22	0	1	1
JS85	0	0.57	0	0	0.22	0	0
JS86	0.35	0.29	0.547	0.055	0.165	0.25	2.188
JS87	0.5	0.17	0.746	0.11	0.11	0.5	1.492
JS88	0.56	0.11	0.836	0.165	0.055	0.75	1.115
JS71,85-88			**3.129**			**2.5**	**1.252**
Solutions containing 0.51 M $Fe_2(SO_4)_3.5H_2O$ were prepared at 22ºC and products air-dried at 22ºC							
JS72	0.63	0	1	0.22	0	1	1
JS77	0	0.67	0	0	0.22	0	0
JS78	0.42	0.11	0.792	0.055	0.165	0.25	3.168
JS79	0.48	0.06	0.889	0.11	0.11	0.5	1.778
JS80	0.82	0.03	0.965	0.165	0.055	0.75	1.287
JS72,77-80			**3.646**			**2.5**	**1.458**
Solutions containing 0.075 M $Fe_2(SO_4)_3.5H_2O$ were prepared at 22ºC and products air-dried at 22ºC							
JS95	0.85	0	1	0.06	0	1	1
JS96	0	0.68	0	0	0.06	0	0
JS97	0.41	0.37	0.526	0.01	0.05	0.167	3.15
JS98	0.68	0.14	0.829	0.02	0.04	0.333	2.489
JS99	0.8	0.04	0.952	0.03	0.03	0.5	1.904
JS100	0.81	0.02	0.976	0.04	0.02	0.667	1.463
JS101	0.83	0.01	0.988	0.05	0.01	0.833	1.186
JS95-101			**5.271**			**3.5**	**1.506**

Key: occ. = *A*-site occupation; j. = jarosite product; [Ag]sol. = concentration of Ag in starting solution (*M*); [Na]sol. = concentration of Na in starting solution (*M*); P. coeff. = partitioning coefficient.

Sample	Ag occ.	Pb occ.	(Ag/Ag+Pb)j	[Ag]sol.	[Pb]sol.	[Ag/Ag+Pb]sol.	P. coeff.
Solutions containing 0.15 M $Fe_2(SO_4)_3.5H_2O$ heated at 140ºC and products dried at 110ºC							
JS43	0	0.179	0	0	0.06	0	0
JS43D	0	0.168	0	0	0.06	0	0
JS44	0.281	0.081	0.776	0.02	0.05	0.286	2.713
JS45	0.502	0.082	0.86	0.04	0.04	0.5	1.72
JS46	0.701	0.046	0.938	0.06	0.03	0.667	1.406
JS46D	0.58	0.041	0.934	0.06	0.03	0.667	1.4
JS47	0.766	0.021	0.973	0.08	0.02	0.8	1.216
JS48	0.765	0.021	0.973	0.10	0.01	0.909	1.07
JS61	0.857	0	1	0.12	0	1	1
JS43-48,61			**6.454**			**4.829**	**1.337**
Solutions containing 0.075 M $Fe_2(SO_4)_3.5H_2O$ were prepared at 22ºC and products air-dried at 22ºC							
JS95	0.856	0	1	0.06	0	1	1
JS102	0.826	0.006	0.993	0.05	0.00013	0.998	0.995
JS103	0.822	0.028	0.967	0.05	0.00032	0.994	0.973
JS104	0.853	0.02	0.977	0.05	0.001	0.98	0.997
JS105	0.824	0.063	0.929	0.05	0.005	0.909	1.022
JS106	0.799	0.036	0.957	0.05	0.001	0.98	0.977
JS107	0	0.258	0	0	0.001	0	0
JS95,102-107			**5.823**			**5.861**	**0.994**

Key: occ. = *A*-site occupation; j. = jarosite product; [Ag]sol. = concentration of Ag in starting solution (*M*); [Pb]sol. = concentration of Pb in starting solution (*M*); P. coeff. = partitioning coefficient.

APPENDIX H Table of analytical precision (%) of ICP-AES results (parts per million) for samples and duplicates (dup) of K, Na, K-Ag, Na-Ag and Pb-Ag jarosites synthesised at 22ºC, 97ºC and 140ºC.

Sample	Na1	Na2	Na3	K1	K2	K3	Pb1	Pb2	Ag1	Ag2	Fe1	Fe2	Fe3	S1	S2
4	-	-	-	65289	35654	36924	-	-	-	-	257276	255882	257460	115752	114790
4 dup	-	-	-	103697	46588	47729	-	-	-	-	270472	266855	266936	117916	118596
Precision (%)	-	-	-	32	19	18	-	-	-	-	4	3	3	1	2
14	9880	22698	21321	-	-	-	-	-	-	-	268049	268607	269534	111777	111393
14 dup	8092	24230	22620	-	-	-	-	-	-	-	293411	290979	291306	115265	115177
Precision (%)	14	5	4	-	-	-	-	-	-	-	6	6	5	2	2
26	-	-	-	70211	29687	29873	-	-	44745	46139	257179	256644	257318	114030	112813
26 dup	-	-	-	64652	30497	31234	-	-	47639	48329	276839	275037	274654	115357	114838
Precision (%)	-	-	-	6	2	3	-	-	4	3	5	5	5	1	1
47	-	-	-	-	-	-	7004	6281	131528	133051	265361	264176	266757	102066	103233
47 dup	-	-	-	-	-	-	6751	5818	128586	131110	263455	261668	261269	99079	98539
Precision (%)	-	-	-	-	-	-	3	5	2	1	1	1	1	2	3
55	-	-	-	-	24235	24222	-	-	63954	66051	264703	263222	263624	110107	110160
55 dup	-	-	-	-	23957	24377	-	-	64723	65251	270455	267881	267751	109149	109245
Precision (%)	-	-	-	-	1	0	-	-	1	1	2	1	1	1	1
60	-	-	-	-	9283	10031	-	-	110903	109814	261590	259124	260512	100996	101250
60 dup	-	-	-	-	9374	9943	-	-	110942	111887	259916	258797	258620	102819	103581
Precision (%)	-	-	-	-	1	1	-	-	0	1	0	0	1	1	2
70	-	7684	7159	-	-	-	-	-	78507	78752	268274	270075	271926	104897	105014
70 dup	-	7785	7141	-	-	-	-	-	78942	79922	274293	272482	273232	105670	105669
Precision (%)	-	1	0	-	-	-	-	-	0	1	2	1	0	1	0
76	-	-	-	-	27426	28141	-	-	198798	196641	185628	186688	191473	109109	108762
76 dup	-	-	-	-	27200	28196	-	-	197935	194116	187560	189098	193397	109155	109412
Precision (%)	-	-	-	-	1	0	-	-	0	1	1	1	1	0	0
83	-	-	-	-	17818	17812	-	-	78103	80018	257481	260050	261473	102462	102181
83 dup	-	-	-	-	18922	18745	-	-	81893	83688	271113	272599	272291	107674	108190
Precision (%)	-	-	-	-	4	4	-	-	3	3	4	3	3	4	4
87	-	5040	4651	-	-	-	-	-	104338	105486	272842	272197	274682	107151	106823
87 dup	-	4865	4326	-	-	-	-	-	101322	104204	265976	266445	266723	102252	103592
Precision (%)	-	3	5	-	-	-	-	-	2	1	2	2	2	3	2
93	-	-	-	-	27288	27104	-	-	61334	62072	245309	245710	246982	104007	105087
93 dup	-	-	-	-	27967	28066	-	-	62727	63674	251675	252386	252231	107380	108050

Precision (%)	-	-	-	-	2	2	-	-	2	2	2	2	1	2	2
101	-	196	318	-	-	-	-		142966	143126	250465	252882	254117	101948	101433
101 dup	-	36	228	-	-	-	-	-	27613	27722	48696	51330	51422	20226	20679
Precision (%)	-	97	23	-	-	-	-	-	96	96	95	94	94	95	94
105	-	-	-	-	-	-	19930	19088	133255	132565	234795	234907	241860	95887	94800
105 dup	-	-	-	-	-	-	26545	26223	135387	133304	236747	238440	241012	96890	96022
Precision (%)	-	-	-	-	-	-	20	22	1	0	1	1	0	1	1

Key: Element and wavelength (nm) analysed: Na1 = Na 568.821; Na2 = Na 588.995; Na3 = Na 589.592; K1 = K 404.721; K2 = K 766.491; K3 = K 769.897; Pb1 = Pb 217.000; P2 = Pb 220.353; Ag1 = Ag 328.068; Ag2 = Ag 338.289; Fe1 = Fe 234.350; Fe2 = Fe 238.204; Fe3 = Fe 259.940; S1 = S 180.669; S2 = S 181.972.
Note: Precision (%) or coefficient of variation = (standard deviation divided by mean) times 100.

APPENDIX I EMPA chemical compositions (weight %) and site occupancies (and mean or average, ave), standard deviations (s) and coefficients of variation (C) of K-, Na-, Pb-, Ag-, K-Ag, Na-Ag and Pb-Ag jarosites synthesised at 22ºC, 97ºC and 140ºC.

	Chemical composition (wt %)								Site occupancy						
Analysis	**Na**	**K**	**Pb**	**Ag**	**Fe**	**S**	**O**	**Total**	**Na**	**K**	**Pb**	**Ag**	**H_3O**	**Fe**	**S**
4_1	0	1.769	0	0	24.163	8.233	19.61	53.775	0	0.35	0	0	0.65	3.37	2
4_4	0	2.347	0	0	25.759	11.707	25.383	65.196	0	0.33	0	0	0.67	2.53	2
4_5	0	2.113	0	0	29.71	12.719	27.983	72.525	0	0.27	0	0	0.73	2.68	2
4_9	0	3.084	0	0	33.334	12.172	28.401	76.991	0	0.42	0	0	0.58	3.14	2
4_12	0	1.369	0	0	30.281	12.954	28.347	72.951	0	0.17	0	0	0.83	2.68	2
4_19	0	2.244	0	0	25.893	8.844	21.116	58.097	0	0.42	0	0	0.58	3.39	2
4_20	0	2.428	0	0	19.581	6.35	15.611	43.97	0	0.62	0	0	0.38	3.54	2
								4_ave	0	0.37	0	0	0.63	3.04	2
								s	0	0.1411	0	0	0.1411	0.4104	0
								C	0	38.14	0	0	22.40	13.50	0
6_02	0	3.334	0	3.125	29.421	10.714	20.007	66.601	0	0.51	0	0.17	0.32	3.15	2
6_15	0	4.356	0	3.167	15.121	10.743	21.539	54.926	0	0.67	0	0.18	0.15	1.62	2
6_18	0	3.346	0	2.759	27.835	8.277	21.254	63.471	0	0.66	0	0.2	0.14	3.86	2
6_20	0	3.755	0	4.032	29.429	9.678	23.988	70.882	0	0.64	0	0.25	0.11	3.49	2
6_69	0	2.175	0	1.605	19.572	7.043	8.718	39.113	0	0.51	0	0.14	0.35	3.19	2
								6_ave	0	0.6	0	0.19	0.21	3.06	2
								s	0	0.0811	0	0.0409	0.1119	0.8549	0
								C	0	13.52	0	21.53	53.29	27.94	0
6D_2	0	1.18	0	1.012	32.696	12.19	26.751	75.009	0	0.16	0	0.05	0.79	3.08	2
6D_3	0	1.516	0	1.256	31.484	12.722	30.983	77.961	0	0.2	0	0.06	0.74	2.84	2
6D_8	0	2.498	0	2.11	26.694	9.233	22.135	62.67	0	0.44	0	0.14	0.42	3.32	2
6D_11	0	4.453	0	2.604	28.528	10.412	24.863	70.86	0	0.7	0	0.15	0.15	3.15	2
6D_17	0	1.088	0	0.695	15.234	5.392	12.709	35.118	0	0.33	0	0.08	0.59	3.24	2
6D_20	0	1.801	0	1.47	27.368	10.321	23.769	64.729	0	0.29	0	0.08	0.63	3.04	2
6D_23	0	2.128	0	0.978	35.142	14.044	29.383	81.675	0	0.25	0	0.04	0.71	2.87	2
6D_24	0	2.716	0	1.392	35.821	12.875	22.197	75.001	0	0.35	0	0.06	0.59	3.19	2

6D_26	0	2.462	0	1.296	35.859	13.425	26.728	79.77	0	0.3	0	0.06	0.64	3.07	2
6D_27	0	1.745	0	1.197	36.816	13.864	24.333	77.955	0	0.21	0	0.14	0.65	3.05	2
6D_28	0	2.126	0	0.987	29.691	12.345	19.284	64.433	0	0.28	0	0.05	0.67	2.76	2
6D_29	0	1.937	0	1.181	36.467	13.595	28.706	81.886	0	0.23	0	0.05	0.72	3.08	2
6D_31	0	1.868	0	1.088	35.227	13.938	30.539	82.66	0	0.22	0	0.05	0.73	2.9	2
6D_32	0	2.185	0	1.005	29.827	12.298	18.867	64.182	0	0.29	0	0.05	0.66	2.78	2
6D_33	0	2.261	0	1.138	20.546	7.989	17.17	49.104	0	0.46	0	0.08	0.46	2.95	2
6D_34	0	1.961	0	1.089	36.013	14.18	27.195	80.438	0	0.23	0	0.05	0.72	2.92	2
6D_35	0	2.144	0	1.182	34.339	14.39	22.512	74.567	0	0.24	0	0.05	0.71	2.74	2
6D_36	0	2.982	0	1.17	35.836	14.732	19.879	74.599	0	0.33	0	0.05	0.62	2.79	2
6D_37	0	1.995	0	1.045	36.969	14.218	23.539	77.766	0	0.23	0	0.04	0.73	2.99	2
6D_38	0	2.417	0	1.05	35.762	13.518	21.194	73.941	0	0.29	0	0.05	0.66	3.04	2
6D_39	0	1.801	0	0.772	35.637	14.205	23.358	75.773	0	0.21	0	0.03	0.76	2.88	2
6D_40	0	3.653	0	1.595	37.544	13.16	26.689	82.641	0	0.46	0	0.07	0.47	3.28	2
6D_41	0	1.715	0	1.025	35.44	13.272	27.236	78.688	0	0.21	0	0.05	0.74	3.07	2
6D_42	0	2.535	0	1.146	35.283	12.963	21.757	73.684	0	0.32	0	0.05	0.63	3.12	2
6D_43	0	2.01	0	1.413	35.003	13.015	26.086	77.527	0	0.25	0	0.06	0.69	3.09	2
6D_44	0	1.522	0	0.719	35.96	13.37	20.02	71.591	0	0.19	0	0.03	0.78	3.09	2
6D_45	0	1.873	0	1.125	33.988	13.509	13.17	63.665	0	0.23	0	0.05	0.72	2.89	2
6D_46	0	1.934	0	0.688	21.079	8.917	11.948	44.566	0	0.36	0	0.05	0.59	2.71	2
6D_48	0	2.341	0	1.077	35.226	14.526	12.334	65.504	0	0.26	0	0.04	0.7	2.78	2
6D_49	0	3.869	0	1.693	38.412	13.364	19.466	76.804	0	0.47	0	0.08	0.45	3.30	2
6D_50	0	2.534	0	1.45	30.724	12.868	20.429	68.005	0	0.32	0	0.07	0.61	2.74	2
6D_51	0	2.918	0	1.344	40.432	14.256	20.242	79.192	0	0.34	0	0.06	0.6	3.26	2
6D_52	0	2.051	0	0.907	36.974	14.282	30.031	84.245	0	0.24	0	0.04	0.72	2.97	2
6D_53	0	1.861	0	0.945	35.352	13.44	18.048	69.646	0	0.23	0	0.04	0.73	3.02	2
6D_56	0	1.047	0	0.377	12.393	5.109	19.484	38.41	0	0.34	0	0.04	0.62	2.78	2
6D_57	0	2.127	0	0.903	31.763	12.985	21.609	69.387	0	0.27	0	0.04	0.69	2.81	2
6D_59	0	1.747	0	0.931	31.199	12.231	12.444	58.552	0	0.23	0	0.05	0.72	2.93	2
6D_60	0	2.639	0	1.172	38.114	14.574	17.31	73.809	0	0.29	0	0.05	0.66	3.00	2
								6D_ave	0	0.30	0	0.06	0.64	2.99	2
								s	0	0.1024	0	0.0279	0.1219	0.1727	0
								C	0	34.13	0	46.5	19.05	5.69	0

8_01	0	2.596	0	5.908	26.07	9.571	25.245	69.39		0	0.44	0	0.37	0.19	3.13	2
8_02	0	2.928	0	5.91	30.996	12.058	24.4	76.292		0	0.4	0	0.29	0.31	2.94	2
8_03	0	2.18	0	4.179	26.243	10.91	18.568	62.08		0	0.33	0	0.23	0.44	2.76	2
8_04	0	2.67	0	7.204	26.861	11.478	22.511	70.724		0	0.38	0	0.37	0.25	2.69	2
8_05	0	1.698	0	6.268	29.64	11.131	21.648	70.385		0	0.25	0	0.33	0.42	3.06	2
8_06	0	1.408	0	5.621	24.874	10.231	10.07	52.204		0	0.23	0	0.33	0.44	2.79	2
8_07	0	1.849	0	4.897	30.838	12.226	27.753	77.563		0	0.25	0	0.24	0.51	2.9	2
8_11	0	2.471	0	5.783	25.352	11.703	22.503	67.812		0	0.35	0	0.29	0.36	2.49	2
8_12	0	2.761	0	5.506	30.251	12.571	23.97	75.059		0	0.36	0	0.26	0.38	2.76	2
8_13	0	1.496	0	4.381	29.936	11.185	17.767	64.765		0	0.22	0	0.23	0.55	3.07	2
8_16	0	0.888	0	5.511	24.556	10.941	16.19	58.086		0	0.13	0	0.3	0.57	2.58	2
8_19	0	1.921	0	6.171	34.391	13.049	22.263	77.795		0	0.24	0	0.28	0.48	3.03	2
									08_ave	0	0.3	0	0.29	0.41	2.85	2
									s	0	0.0913	0	0.0492	0.1165	0.2049	0
									C	0	30.43	0	16.97	28.41	7.19	0
10_1	0	2.404	0	7.087	42.841	12.881	25.155	90.368		0	0.23	0	0.11	0.66	3.04	2
10_2	0	2.438	0	5.323	47.227	14.329	28.271	97.588		0	0.23	0	0.11	0.66	3.1	2
10_3	0	2.341	0	6.243	42.572	13.169	25.193	89.518		0	0.2	0	0.11	0.69	2.94	2
10_4	0	1.764	0	2.952	38.471	13.614	26.455	83.256		0	0.23	0	0.14	0.63	3.02	2
10_5	0	1.499	0	11.168	50.716	17.447	22.816	103.646		0	0.22	0	0.11	0.67	3.05	2
10_6	0	2.199	0	4.666	41.354	14.585	31.084	93.888		0	0.19	0	0.08	0.73	3.02	2
10_11	0	2.431	0	3.822	38.25	13.958	27.67	86.131		0	0.22	0	0.13	0.65	2.9	2
10_12	0	1.736	0	3.862	35.28	14.086	26.824	81.788		0	0.22	0	0.09	0.69	3.08	2
10_13	0	3.532	0	10.125	56.44	21.517	49.751	141.365		0	0.2	0	0.11	0.69	3	2
10_14	0	3.419	0	4.081	42.565	13.839	26.299	90.203		0	0.2	0	0.09	0.71	3	2
10_15	0	2.986	0	3.513	41.144	13.999	25.586	87.228		0	0.2	0	0.13	0.67	3.04	2
10_17	0	2.845	0	5.523	45.181	16.145	32.461	102.155		0	0.22	0	0.12	0.66	3.11	2
10_18	0	1.714	0	4.37	38.027	14.338	31.497	89.946		0	0.19	0	0.08	0.73	2.95	2
10_19	0	2.955	0	3.47	42.433	12.23	21.338	82.426		0	0.23	0	0.1	0.67	3.1	2
10_20	0	2.644	0	5.496	37.755	14.23	27.439	87.564		0	0.23	0	0.11	0.66	3.04	2
10_31	0	2.329	0	5.708	37.363	13.075	25.816	84.291		0	0.29	0	0.16	0.55	3.15	2
10_32	0	1.074	0	8.449	41.417	12.223	27.215	90.378		0	0.2	0	0.16	0.64	2.88	2
10_33	0	1.473	0	5.893	37.205	13.024	28.903	86.498		0	0.27	0	0.28	0.45	3.01	2

10_36	0	2.973	0	4.613	42.057	13.256	26.893	89.792	0	0.22	0	0.15	0.63	3.12	2
10_38	0	3.332	0	5.236	44.242	14.167	28.369	95.346	0	0.2	0	0.18	0.62	3.04	2
10_40	0	1.4	0	3.308	38.324	13.667	30.084	86.785	0	0.3	0	0.23	0.47	3.05	2
10_43	0	2.353	0	4.638	37.412	13.839	29.705	87.947	0	0.28	0	0.2	0.52	3.1	2
10_44	0	1.711	0	2.922	36.146	14.143	30.493	85.415	0	0.2	0	0.12	0.68	2.93	2
10_46	0	2.079	0	4.308	37.47	14.015	30.325	88.197	0	0.24	0	0.18	0.58	3.07	2
10_49	0	3.4	0	5.929	68.356	26.732	54.564	158.981	0	0.21	0	0.13	0.66	2.94	2
10_55	0	2.824	0	6.557	37.903	13.914	28.811	90.009	0	0.33	0	0.28	0.39	3.13	2
								10_ave	0	0.23	0	0.14	0.63	3.03	2
								s	0	0.0364	0	0.0548	0.0863	0.0730	0
								C		15.83	0	39.14	13.70	2.41	0
10D_3	0	1.14	0	2.132	24.496	9.593	21.773	59.134	0	0.2	0	0.13	0.67	2.93	2
10D_7	0	1.864	0	2.591	29.781	13.171	28.822	76.229	0	0.23	0	0.12	0.65	2.6	2
10D_8	0	1.381	0	4.722	26.94	11.085	24.955	69.083	0	0.2	0	0.25	0.55	2.79	2
10D_10	0	2.644	0	8.752	29.422	12.737	28.685	82.24	0	0.34	0	0.41	0.25	2.65	2
10D_17	0	1.312	0	2.575	33.781	13.821	30.825	82.314	0	0.16	0	0.11	0.73	2.81	2
10D_26	0	1.631	0	3.153	38.177	13.906	29.762	86.629	0	0.19	0	0.13	0.68	3.15	2
10D_28	0	1.496	0	4.613	37.212	13.503	16.626	73.45	0	0.18	0	0.2	0.62	3.16	2
10D_32	0	0.729	0	2.506	23.517	8.082	10.619	45.453	0	0.15	0	0.1	0.75	3.34	2
10D_34	0	2.44	0	5.904	57.493	20.623	28.729	115.189	0	0.19	0	0.17	0.64	3.2	2
10D_35	0	1.605	0	4.618	36.988	13.629	30.844	87.684	0	0.19	0	0.2	0.61	3.12	2
10D_43	0	1.512	0	3.304	42.478	14.757	34.583	96.634	0	0.17	0	0.13	0.7	3.3	2
10D_44	0	2.777	0	4.494	39.638	14.381	23.752	85.042	0	0.32	0	0.19	0.49	3.16	2
10D_45	0	2.196	0	4.426	38.121	14.26	25.956	84.959	0	0.25	0	0.18	0.57	3.07	2
10D_47	0	2.038	0	3.301	37.906	14.195	32.993	90.433	0	0.24	0	0.14	0.62	3.07	2
10D_48	0	1.625	0	3.325	36.998	14.155	26.326	82.429	0	0.19	0	0.14	0.67	3	2
10D_52	0	3.238	0	6.061	37.878	15.039	19.864	82.08	0	0.35	0	0.24	0.41	2.89	2
10D_53	0	1.634	0	2.77	35.897	13.588	35.857	89.746	0	0.2	0	0.12	0.68	3.03	2
10D_54	0	2.768	0	6.387	46.447	16.77	37.038	109.41	0	0.27	0	0.23	0.5	3.18	2
10D_56	0	0.922	0	4.286	36.919	13.106	27.919	83.152	0	0.12	0	0.19	0.69	3.23	2
10D_60	0	1.925	0	3.779	36.733	14.006	24.976	81.419	0	0.23	0	0.16	0.61	3.01	2
10D_61	0	1.504	0	2.486	36.124	13.655	29.449	83.218	0	0.18	0	0.11	0.71	3.04	2
								10D_ave	0	0.22	0	0.17	0.61	3.03	2

								s	0	0.0609	0	0.0702	0.1182	0.1982	0
								C	0	27.68	0	41.29	19.38	6.54	0
12_29	0	0	0	15.504	57.935	21.96	49.183	144.582		0	0	0	0.42	0.58	3.03	2
12_31	0	0	0	6.215	36.707	13.69	27.565	84.177		0	0	0	0.27	0.73	3.08	2
12_42	0	0	0	5.175	35.627	12.946	27.179	80.927		0	0	0	0.24	0.76	3.16	2
									12_ave	0	0	0	0.31	0.69	3.09	2
									s	0	0	0	0.0964	0.0964	0.0656	0
									C	0	0	0	31.10	13.97	2.12	0
14_25	0.791	0	0	0	37.312	14.299	20.237	72.639		0.15	0	0	0	0.85	3	2
14_26	0.754	0	0	0	36.989	14.433	24.01	76.186		0.15	0	0	0	0.85	2.94	2
14_45	1.238	0	0	0	42.872	15.946	28.246	88.302		0.22	0	0	0	0.78	3.09	2
									14_ave	0.17	0	0	0	0.83	3.01	2
									s	0.0404	0	0	0	0.0404	0.0755	0
									C	23.76	0	0	0	4.87	2.51	0
16_1	0.359	0	0	3.299	24.676	10.608	23.317	62.259		0.09	0	0	0.18	0.73	2.67	2
16_2	0.308	0	0	3.803	27.162	10.807	24.348	66.428		0.08	0	0	0.21	0.71	2.89	2
16_9	0.369	0	0	4.389	25.771	10.863	24.098	65.49		0.09	0	0	0.24	0.67	2.72	2
16_10	0.185	0	0	2.658	29.723	10.565	24.592	67.723		0.05	0	0	0.15	0.8	3.23	2
16_12	0.23	0	0	3.767	23.419	9.892	21.877	59.185		0.06	0	0	0.23	0.71	2.72	2
16_18	0.285	0	0	2.388	29.043	10.671	24.569	66.956		0.07	0	0	0.13	0.8	3.13	2
16_20	0.24	0	0	2.474	26.019	11.081	24.308	64.122		0.06	0	0	0.13	0.81	2.7	2
16_23	1.098	0	0	1.931	38.6	13.548	27.654	82.831		0.23	0	0	0.08	0.69	3.27	2
16_26	0.473	0	0	2.384	38.065	13.262	26.478	80.662		0.1	0	0	0.11	0.79	3.3	2
16_31	0.935	0	0	1.98	37.458	13.242	23.08	76.695		0.2	0	0	0.09	0.71	3.25	2
									16_ave	0.1	0	0	0.16	0.74	2.99	2
									s	0.0615	0	0	0.0574	0.0525	0.2711	0
									C	61.5	0	0	35.88	7.09	9.07	0
18_3	0.274	0	0	4.396	32.947	13.639	30.277	81.533		0.06	0	0	0.19	0.75	2.77	2
18_4	0.137	0	0	5.411	30.43	11.281	26.085	73.344		0.03	0	0	0.29	0.68	3.1	2
18_8	0.244	0	0	3.665	23.178	9.477	21.184	57.748		0.07	0	0	0.23	0.7	2.8	2

18_15	0.165	0	0	4.125	32.494	11.177	26.404	74.365		0.04	0	0	0.22	0.74	3.34	2
18_21	0.283	0	0	3.444	27.458	11.146	24.903	67.234		0.07	0	0	0.18	0.75	2.83	2
18_22	0.203	0	0	4.082	27.132	11.629	25.551	68.597		0.05	0	0	0.21	0.74	2.68	2
									18_ave	0.05	0	0	0.22	0.73	2.92	2
									s	0.0163	0	0	0.0390	0.0294	0.2496	0
									C	32.60	0	0	17.73	4.03	8.55	0
20_1	0.114	0	0	3.563	37.91	13.362	31.167	86.116		0.02	0	0	0.16	0.82	3.26	2
20_2	0.32	0	0	4.295	38.678	13.213	31.288	87.794		0.07	0	0	0.19	0.74	3.36	2
20_3	0.64	0	0	4.297	37.774	12.82	30.554	86.085		0.14	0	0	0.2	0.66	3.38	2
20_6	0.085	0	0	4.085	29.899	13.47	29.061	76.6		0.02	0	0	0.18	0.8	2.55	2
20_7	0.074	0	0	5.414	29.478	12.077	26.952	73.995		0.02	0	0	0.27	0.71	2.8	2
20_8	0.131	0	0	6.967	33.627	13.363	30.199	84.287		0.03	0	0	0.31	0.66	2.89	2
20_9	0.066	0	0	5.973	34.7	13.539	30.675	84.953		0.01	0	0	0.26	0.73	2.94	2
20_14	0.145	0	0	4.714	32.58	11.586	27.076	76.101		0.03	0	0	0.24	0.73	3.23	2
20_15	0.13	0	0	5.358	25.92	11.739	25.461	68.608		0.03	0	0	0.27	0.7	2.54	2
20_16	0.119	0	0	4.551	32.012	10.745	25.633	73.06		0.03	0	0	0.25	0.72	3.42	2
20_17	0.128	0	0	4.503	36.019	13.068	30.261	83.979		0.03	0	0	0.2	0.77	3.16	2
20_19	0.121	0	0	4.194	36.509	13.154	30.503	84.481		0.03	0	0	0.19	0.78	3.19	2
									20_ave	0.04	0	0	0.23	0.74	3.06	2
									s	0.0351	0	0	0.0460	0.0505	0.3103	0
									C	87.75	0	0	20.00	6.82	10.14	0
22_1	0	1.854	0	0	34.989	14.608	32.27	83.721		0	0.21	0	0	0.79	2.75	2
22_2	0	1.897	0	0	35.321	15.09	33.095	85.403		0	0.21	0	0	0.79	2.69	2
22_3	0	1.848	0	0	34.28	14.701	32.205	83.034		0	0.21	0	0	0.79	2.68	2
22_4	0	3.013	0	0	36.035	15.277	33.808	88.133		0	0.32	0	0	0.68	2.71	2
22_5	0	2.295	0	0	34.703	14.256	31.752	83.006		0	0.26	0	0	0.74	2.8	2
22_6	0	1.908	0	0	32.101	13.466	29.746	77.221		0	0.23	0	0	0.77	2.74	2
22_7	0	1.871	0	0	32.884	14.515	31.532	80.802		0	0.21	0	0	0.79	2.6	2
22_8	0	2.234	0	0	32.574	14.558	31.581	80.947		0	0.25	0	0	0.75	2.57	2
22_9	0	1.712	0	0	31.962	14.442	31.126	79.242		0	0.19	0	0	0.81	2.54	2
22_10	0	1.88	0	0	32.577	14.734	31.775	80.966		0	0.21	0	0	0.79	2.54	2
22_11	0	1.735	0	0	33.286	13.832	30.597	79.45		0	0.21	0	0	0.79	2.76	2

22_12	0	2.031	0	0	33.841	14.8	32.266	82.938	0	0.23	0	0	0.77	2.63	2
22_13	0	1.749	0	0	34.394	14.534	31.967	82.644	0	0.2	0	0	0.8	2.72	2
22_14	0	1.891	0	0	32.439	14.323	31.121	79.774	0	0.22	0	0	0.78	2.6	2
22_15	0	2.481	0	0	36.157	14.612	34.439	85.989	0	0.28	0	0	0.72	2.84	2
22_16	0	2.115	0	0	33.356	14.777	32.109	82.357	0	0.23	0	0	0.77	2.59	2
22_17	0	2.069	0	0	34.614	14.199	31.595	82.477	0	0.24	0	0	0.76	2.8	2
22_18	0	1.472	0	0	34.452	12.352	28.662	76.938	0	0.2	0	0	0.8	3.2	2
22_19	0	1.361	0	0	32.865	14.639	31.609	80.474	0	0.15	0	0	0.85	2.58	2
22_20	0	1.419	0	0	32.913	14.547	31.496	80.375	0	0.16	0	0	0.84	2.6	2
22_21	0	1.205	0	0	36.651	13.638	31.162	82.656	0	0.14	0	0	0.86	3.09	2
22_22	0	2.408	0	0	37.292	14.075	24.472	78.247	0	0.28	0	0	0.72	3.04	2
22_23	0	1.707	0	0	37.82	13.715	23.695	76.937	0	0.2	0	0	0.8	3.17	2
22_24	0	1.566	0	0	38.181	14.469	28.091	82.307	0	0.18	0	0	0.82	3.03	2
22_25	0	1.91	0	0	36.807	14.334	30.605	83.656	0	0.22	0	0	0.78	2.95	2
22_26	0	1.555	0	0	35.689	14.333	29.806	81.383	0	0.18	0	0	0.82	2.86	2
22_27	0	1.462	0	0	38.187	14.363	27.769	81.781	0	0.17	0	0	0.83	3.05	2
22_28	0	1.958	0	0	41.376	14.298	24.057	81.689	0	0.22	0	0	0.78	3.32	2
22_29	0	2.837	0	0	36.34	14.625	27.583	81.385	0	0.32	0	0	0.68	2.85	2
22_30	0	1.853	0	0	36.877	14.338	28.88	81.948	0	0.21	0	0	0.79	2.95	2
22_31	0	1.645	0	0	37.486	14.221	27.509	80.861	0	0.19	0	0	0.81	3.03	2
22_32	0	2.576	0	0	41.055	14.176	25.832	83.639	0	0.3	0	0	0.7	3.32	2
22_33	0	1.512	0	0	38.868	14.598	28.936	83.914	0	0.17	0	0	0.83	3.06	2
22_34	0	1.651	0	0	37.236	14.037	28.456	81.38	0	0.19	0	0	0.81	3.05	2
22_35	0	1.595	0	0	37.531	13.255	28.293	80.674	0	0.2	0	0	0.8	3.25	2
22_36	0	2.12	0	0	39.743	14.315	25.806	81.984	0	0.24	0	0	0.76	3.19	2
22_37	0	1.685	0	0	37.982	14.222	28.033	81.922	0	0.19	0	0	0.81	3.07	2
22_38	0	1.83	0	0	37.981	14.058	26.809	80.678	0	0.21	0	0	0.79	3.1	2
22_39	0	1.954	0	0	37.363	14.211	25.989	79.517	0	0.23	0	0	0.77	3.02	2
22_40	0	1.58	0	0	38.721	14.375	29.41	84.086	0	0.18	0	0	0.82	3.09	2
22_41	0	1.51	0	0	38.07	14.032	28.645	82.257	0	0.18	0	0	0.82	3.11	2
22_42	0	1.811	0	0	36.075	14.404	28.729	81.019	0	0.21	0	0	0.79	2.88	2
22_43	0	2.055	0	0	33.893	13.561	25.713	75.222	0	0.25	0	0	0.75	2.87	2
22_44	0	1.922	0	0	36.31	13.672	27.808	79.712	0	0.23	0	0	0.77	3.05	2
22_45	0	1.854	0	0	36.893	14.141	25.139	78.027	0	0.21	0	0	0.79	3	2

22_46	0	2.073	0	0	36.657	13.528	23.535	75.796		0	0.25	0	0	0.75	3.11	2
22_47	0	1.857	0	0	38.466	13.535	25.225	79.083		0	0.22	0	0	0.78	3.26	2
22_48	0	2.032	0	0	37.77	13.292	26.891	79.985		0	0.25	0	0	0.75	3.26	2
22_49	0	1.836	0	0	36.779	13.948	28.434	80.997		0	0.22	0	0	0.78	3.03	2
22_50	0	1.884	0	0	37.984	13.284	24.104	77.256		0	0.23	0	0	0.77	3.28	2
22_51	0	2.321	0	0	38.011	13.552	26.139	80.023		0	0.28	0	0	0.72	3.22	2
22_52	0	2.044	0	0	36.493	14.499	24.139	77.175		0	0.23	0	0	0.77	2.89	2
22_53	0	2.522	0	0	37.281	14.191	27.484	81.478		0	0.29	0	0	0.71	3.02	2
22_54	0	2.846	0	0	37.781	13.982	25.708	80.317		0	0.33	0	0	0.67	3.1	2
22_55	0	3.168	0	0	38.954	14.322	23.107	79.551		0	0.36	0	0	0.64	3.12	2
22_56	0	2.588	0	0	39.615	14.147	23.98	80.33		0	0.3	0	0	0.7	3.21	2
22_57	0	2.056	0	0	36.573	13.25	23.321	75.172		0	0.25	0	0	0.75	3.17	2
22_58	0	3.031	0	0	37.96	14.062	24.532	79.585		0	0.35	0	0	0.65	3.1	2
22_59	0	1.878	0	0	37.644	14.17	26.265	79.957		0	0.22	0	0	0.78	3.05	2
22_60	0	2.793	0	0	38.991	14.214	25.256	81.244		0	0.32	0	0	0.68	3.15	2
22_61	0	2.186	0	0	35.754	14.051	21.577	73.568		0	0.26	0	0	0.74	2.92	2
									22_ave	0	0.23	0	0	0.77	2.95	2
									s	0	0.0486	0	0	0.0486	0.2248	0
									C	0	21.13	0	0	6.31	7.62	0
24_1	0	1.554	0	0.838	16.889	8.596	18.087	45.964		0	0.3	0	0.06	0.64	2.26	2
24_3	0	2.014	0	2.576	32.987	12.355	28.549	78.481		0	0.27	0	0.12	0.61	3.07	2
24_4	0	1.823	0	1.75	21.75	8.203	19.014	52.54		0	0.36	0	0.13	0.51	3.04	2
24_6	0	1.794	0	1.822	31.284	14.816	31.644	81.36		0	0.2	0	0.07	0.73	2.42	2
24_7	0	1.834	0	1.235	31.599	11.19	26.271	72.129		0	0.27	0	0.07	0.66	3.24	2
24_9	0	1.083	0	0.994	26.876	14.738	30.057	73.748		0	0.12	0	0.04	0.84	2.09	2
24_11	0	1.346	0	1.339	18.585	11.617	23.09	55.977		0	0.19	0	0.07	0.74	1.84	2
24_13	0	1.703	0	0.968	16.132	9.386	19.093	47.282		0	0.3	0	0.06	0.64	1.97	2
24_14	0	1.635	0	1.737	24.636	11.743	25.1	64.851		0	0.23	0	0.09	0.68	2.41	2
24_15	0	1.707	0	1.128	24.309	11.796	25.055	63.995		0	0.24	0	0.06	0.7	2.37	2
24_17	0	1.79	0	1.117	19.209	12.196	24.209	58.521		0	0.24	0	0.05	0.71	1.81	2
									24_ave	0	0.25	0	0.07	0.68	2.41	2
									s	0	0.0644	0	0.0281	0.0839	0.5026	0
									C	0	25.76	0	40.14	12.34	20.85	0

24D_2	0	1.155	0	1.009	39.161	14.975	33.949	90.249	0	0.13	0	0.04	0.83	3	2
24D_17	0	4.736	0	3.089	40.523	13.808	33.478	95.634	0	0.56	0	0.13	0.31	3.37	2
24D_19	0	1.405	0	1.412	40.626	14.879	26.27	92.626	0	0.15	0	0.06	0.79	3.14	2
24D_21	0	3.127	0	2.409	37.761	13.546	22.304	79.147	0	0.38	0	0.11	0.51	3.2	2
24D_24	0	2.1	0	1.695	35.051	13.978	26.508	79.332	0	0.25	0	0.07	0.68	2.88	2
24D_27	0	2.085	0	1.942	35.319	12.844	22.407	74.597	0	0.27	0	0.09	0.64	3.16	2
24D_28	0	2.926	0	1.365	36.998	13.658	22.257	77.204	0	0.35	0	0.06	0.59	3.11	2
24D_29	0	2.102	0	1.439	35.089	12.536	22.391	73.557	0	0.27	0	0.07	0.66	3.21	2
24D_30	0	1.917	0	1.318	37.322	13.631	25.738	79.926	0	0.23	0	0.06	0.71	3.14	2
24D_31	0	1.958	0	1.865	35.429	12.853	20.817	72.922	0	0.25	0	0.09	0.66	3.16	2
24D_32	0	1.585	0	1.569	34.326	13.499	25.108	76.087	0	0.19	0	0.07	0.74	2.92	2
24D_33	0	2.376	0	1.692	39.564	13.966	21.58	79.178	0	0.28	0	0.07	0.65	3.25	2
24D_34	0	1.882	0	1.716	37.181	13.862	26.754	81.395	0	0.22	0	0.07	0.71	3.08	2
24D_35	0	1.787	0	1.339	35.182	13.638	27.16	79.106	0	0.21	0	0.06	0.73	2.96	2
24D_36	0	1.892	0	1.346	36.743	14.024	28.291	82.296	0	0.22	0	0.06	0.72	3.01	2
24D_37	0	2.111	0	1.753	35.647	13.844	28.089	81.444	0	0.25	0	0.08	0.67	2.96	2
24D_38	0	2.158	0	2.243	36.262	13.19	26.563	80.416	0	0.27	0	0.1	0.63	3.16	2
24D_39	0	2.298	0	1.602	36.091	13.987	27.664	81.642	0	0.27	0	0.07	0.66	2.96	2
24D_40	0	1.76	0	1.643	34.864	14.086	27.533	79.886	0	0.2	0	0.07	0.73	2.84	2
24D_41	0	2.008	0	1.448	32.474	13.373	23.692	72.995	0	0.25	0	0.06	0.69	2.79	2
24D_42	0	1.969	0	1.837	35.084	12.817	23.555	75.262	0	0.25	0	0.09	0.66	3.14	2
24D_43	0	1.939	0	2.31	35.131	13.354	23.983	76.717	0	0.24	0	0.1	0.66	3.02	2
24D_44	0	1.982	0	2.186	36.142	13.856	26.511	80.677	0	0.23	0	0.09	0.68	2.99	2
24D_45	0	2.515	0	2.662	35.752	13.593	25.899	80.421	0	0.3	0	0.12	0.58	3.02	2
24D_46	0	1.89	0	2.034	35.071	13.27	26.298	78.563	0	0.23	0	0.09	0.68	3.03	2
24D_47	0	2.462	0	1.616	36.858	12.873	20.095	73.904	0	0.31	0	0.07	0.62	3.22	2
24D_48	0	1.697	0	1.788	35.385	13.721	25.986	78.577	0	0.2	0	0.08	0.72	2.96	2
24D_49	0	3.1	0	3.106	37.915	14.409	14.746	73.276	0	0.35	0	0.13	0.52	3.02	2
24D_51	0	5.238	0	4.767	31.927	12.682	33.283	87.897	0	0.68	0	0.22	0.1	2.89	2
24D_53	0	6.985	0	4.869	32.154	12.938	35.004	91.95	0	0.89	0	0.22	0	2.85	2
24D_54	0	4.243	0	3.017	31.425	13.507	33.711	85.903	0	0.52	0	0.13	0.35	2.67	2
24D_56	0	2.016	0	1.214	32.386	13.959	23.554	73.129	0	0.24	0	0.05	0.71	2.66	2
24D_57	0	2.634	0	2.239	38.861	13.602	23.425	80.761	0	0.32	0	0.1	0.58	3.28	2

24D_59	0	2.667	0	1.905	39.493	13.361	20.827	78.253		0	0.33	0	0.08	0.59	3.39	2
									24D_ave	0	0.3	0	0.09	0.61	3.04	2
									s	0	0.1521	0	0.0402	0.1768	0.1753	0
									C	0	50.70	0	44.67	28.98	5.77	0
26_2	0	1.912	0	1.314	27.481	12.069	26.428	69.204		0	0.26	0	0.06	0.68	2.61	2
26_3	0	2.134	0	2.39	29.478	13.278	28.934	76.214		0	0.26	0	0.11	0.63	2.55	2
26_4	0	1.698	0	1.113	30.891	12.262	27.635	73.599		0	0.23	0	0.05	0.72	2.89	2
26_7	0	2.01	0	1.936	32.009	11.702	27.242	74.899		0	0.28	0	0.1	0.62	3.14	2
26_10	0	2.307	0	1.767	35.132	12.799	29.827	81.832		0	0.3	0	0.08	0.62	3.15	2
26_12	0	1.478	0	1.822	36.274	12.96	30.229	82.763		0	0.19	0	0.08	0.73	3.21	2
26_20	0	1.439	0	0.429	34.27	13.235	29.958	79.331		0	0.18	0	0.02	0.8	2.97	2
									26_ave	0	0.24	0	0.07	0.69	2.93	2
									s	0	0.0450	0	0.0308	0.0683	0.2649	0
									C	0	18.75	0	44.00	9.90	9.04	0
28_1	0	1.959	0	2.467	35.691	13.478	30.984	84.579		0	0.24	0	0.11	0.65	3.04	2
28_2	0	1.849	0	4.294	38.321	13.277	31.433	89.174		0	0.23	0	0.19	0.58	3.31	2
28_3	0	1.528	0	2.064	35.087	14.082	31.596	84.357		0	0.18	0	0.09	0.73	2.86	2
28_4	0	1.688	0	2.691	32.748	13.913	30.752	81.792		0	0.2	0	0.11	0.69	2.7	2
28_5	0	2.432	0	4.814	39.848	14.038	33.303	94.435		0	0.28	0	0.2	0.52	3.26	2
28_6	0	1.891	0	2.247	35.701	13.836	31.495	85.17		0	0.22	0	0.1	0.68	2.96	2
28_7	0	1.6	0	1.866	36.35	13.435	30.99	84.241		0	0.2	0	0.08	0.72	3.11	2
28_8	0	1.746	0	2.911	36.694	13.496	31.287	86.134		0	0.21	0	0.13	0.66	3.12	2
28_9	0	1.583	0	1.99	36.738	13.783	31.627	85.721		0	0.19	0	0.09	0.72	3.06	2
28_10	0	1.506	0	2.351	35.294	13.203	30.358	82.712		0	0.19	0	0.11	0.7	3.07	2
28_11	0	1.458	0	1.434	35.718	13.981	32.166	84.757		0	0.17	0	0.08	0.75	2.93	2
28_12	0	1.761	0	1.986	35.776	14.043	31.777	85.343		0	0.21	0	0.08	0.71	2.93	2
28_13	0	1.704	0	2.03	36.647	13.656	31.44	85.477		0	0.2	0	0.09	0.71	3.08	2
28_14	0	1.477	0	1.718	35.817	13.75	31.273	84.035		0	0.18	0	0.07	0.75	2.99	2
28_15	0	1.723	0	2.411	35.632	13.818	31.425	85.009		0	0.2	0	0.1	0.7	2.96	2
28_16	0	2.069	0	1.955	38.975	13.668	33.101	89.768		0	0.25	0	0.12	0.63	3.27	2
28_17	0	1.663	0	1.639	35.619	13.367	30.677	82.965		0	0.2	0	0.07	0.73	3.06	2
28_18	0	1.838	0	2.148	36.005	14.199	31.105	85.295		0	0.21	0	0.09	0.7	2.91	2

28_19	0	1.714	0	1.96	37.561	14.033	32.263	87.531		0	0.2	0	0.08	0.72	3.07	2
28_20	0	1.462	0	1.501	36.506	14.076	31.939	85.484		0	0.17	0	0.06	0.77	2.98	2
									28_ave	0	0.21	0	0.1	0.69	3.03	2
									s	0	0.0272	0	0.0363	0.0597	0.1445	0
									C	0	12.95	0	36.30	8.65	4.77	0
30_3	0	0	0	6.553	33.867	12.23	28.497	81.147		0	0	0	0.32	0.68	3.18	2
30_9	0	0	0	4.237	37.462	13.971	31.959	87.629		0	0	0	0.18	0.82	3.08	2
30_17	0	0	0	5.126	36.291	13.518	31.013	85.948		0	0	0	0.23	0.77	3.08	2
30_18	0	0	0	4.658	37.516	14.088	32.181	88.443		0	0	0	0.2	0.8	3.06	2
30_19	0	0	0	4.715	37.858	13.895	31.995	88.463		0	0	0	0.2	0.8	3.13	2
30_47	0	0	0	7.036	36.755	13.276	29.239	86.306		0	0	0	0.32	0.68	3.18	2
									30_ave	0	0	0	0.24	0.76	3.12	2
									s	0	0	0	0.0627	0.0627	0.0531	0
									C	0	0	0	26.13	8.25	1.7	0
32_21	1.601	0	0	0	29.452	11.2	24.941	67.194		0.4	0	0	0	0.6	3.02	2
32_22	1.57	0	0	0	32.467	12.616	24.956	71.609		0.35	0	0	0	0.65	2.95	2
32_23	1.344	0	0	0	30.386	12.816	30.651	75.197		0.29	0	0	0	0.71	2.72	2
32_24	0.886	0	0	0	29.88	12.621	30.144	73.531		0.2	0	0	0	0.8	2.72	2
32_25	1.757	0	0	0	30.54	11.664	28.086	72.047		0.42	0	0	0	0.58	3.01	2
32_26	1.082	0	0	0	33.842	12.803	26.367	74.094		0.24	0	0	0	0.76	3.03	2
32_28	0.938	0	0	0	31.726	12.406	22.969	68.039		0.21	0	0	0	0.79	2.94	2
32_29	1.281	0	0	0	34.739	13.431	20.905	70.356		0.27	0	0	0	0.73	2.97	2
32_30	1.206	0	0	0	25.315	10.474	20.628	57.623		0.32	0	0	0	0.68	2.77	2
32_31	0.938	0	0	0	30.379	12.833	30.461	74.611		0.2	0	0	0	0.8	2.72	2
32_32	0.899	0	0	0	29.466	12.003	25.901	68.269		0.21	0	0	0	0.79	2.82	2
32_33	0.944	0	0	0	29.015	11.626	28.846	70.431		0.23	0	0	0	0.77	2.87	2
32_34	1.852	0	0	0	30.572	11.859	27.815	72.098		0.44	0	0	0	0.56	2.96	2
32_35	1.171	0	0	0	27.726	12.682	24.509	66.088		0.26	0	0	0	0.74	2.51	2
32_36	0.845	0	0	0	28.667	11.983	25.214	66.709		0.2	0	0	0	0.8	2.75	2
32_37	0.964	0	0	0	27.401	11.64	25.671	65.678		0.23	0	0	0	0.77	2.7	2
32_38	0.609	0	0	0	29.585	12.168	31.595	73.957		0.14	0	0	0	0.86	2.79	2
32_39	1.5	0	0	0	31.193	11.831	28.477	73.001		0.35	0	0	0	0.65	3.03	2

32_40	1.455	0	0	0	28.44	11.807	28.713	70.416		0.34	0	0	0	0.66	2.77	2
32_41	1.616	0	0	0	24.44	9.862	20.029	55.947		0.46	0	0	0	0.54	2.85	2
32_42	1.043	0	0	0	29.525	11.562	24.167	66.297		0.25	0	0	0	0.75	2.93	2
32_43	1.288	0	0	0	29.713	11.565	25.48	68.046		0.31	0	0	0	0.69	2.95	2
32_44	1.178	0	0	0	26.948	11.591	28.517	68.234		0.28	0	0	0	0.72	2.67	2
32_45	1.159	0	0	0	28.493	11.343	30.872	71.867		0.28	0	0	0	0.72	2.88	2
32_46	1.625	0	0	0	28.05	11.359	24.896	65.93		0.4	0	0	0	0.6	2.84	2
32_47	1.578	0	0	0	30.69	11.956	27.538	71.762		0.37	0	0	0	0.63	2.95	2
32_48	1.444	0	0	0	26.496	11.509	29.845	69.294		0.35	0	0	0	0.65	2.64	2
32_49	1.415	0	0	0	28.849	10.863	28.447	69.574		0.36	0	0	0	0.64	3.05	2
32_50	0.993	0	0	0	26.421	11.544	26.126	65.084		0.24	0	0	0	0.76	2.63	2
32_51	1.485	0	0	0	23.951	10.146	19.933	55.515		0.41	0	0	0	0.59	2.71	2
32_52	1.29	0	0	0	17.386	7.932	13.502	40.11		0.45	0	0	0	0.55	2.52	2
32_53	0.774	0	0	0	25.619	11.477	30.721	68.591		0.19	0	0	0	0.81	2.56	2
32_54	0.664	0	0	0	24.199	11.75	29.539	66.152		0.16	0	0	0	0.84	2.36	2
32_55	1.535	0	0	0	26.63	9.849	16.442	54.456		0.43	0	0	0	0.57	3.1	2
32_56	1.669	0	0	0	26.376	10.823	31.543	70.411		0.43	0	0	0	0.57	2.8	2
32_57	1.147	0	0	0	23.011	11.129	30.1	65.387		0.29	0	0	0	0.71	2.37	2
32_58	1.44	0	0	0	24.818	10.749	28.702	65.709		0.37	0	0	0	0.63	2.65	2
32_59	1.301	0	0	0	24.494	10.923	24.965	61.665		0.33	0	0	0	0.67	2.57	2
32_60	0.898	0	0	0	24.559	11.21	30.342	67.009		0.22	0	0	0	0.78	2.52	2
									32_ave	0.3	0	0	0	0.7	2.78	2
									s	0.0894	0	0	0	0.0894	0.1907	0
									C	29.80	0	0	0	12.77	6.86	0
34_36	0.156	0	0	3.193	30.689	12.346	21.252	67.636		0.04	0	0	0.15	0.81	2.85	2
34_37	0.203	0	0	2.557	31.219	11.736	27.521	73.236		0.05	0	0	0.13	0.82	3.05	2
34_38	0.231	0	0	2.485	29.891	11.601	24.952	69.16		0.06	0	0	0.13	0.81	2.96	2
34_39	0.281	0	0	3.982	31.413	11.514	26.92	74.11		0.07	0	0	0.21	0.72	3.13	2
34_40	0.589	0	0	3.827	32.852	11.792	24.98	74.04		0.14	0	0	0.19	0.67	3.2	2
34_41	1.499	0	0	1.815	28.299	10.701	22.311	64.625		0.39	0	0	0.1	0.51	3.04	2
34_42	0.202	0	0	3.297	29.408	11.213	25.01	69.13		0.05	0	0	0.17	0.78	3.01	2
34_46	0.208	0	0	3.022	33.554	12.194	21.07	70.048		0.05	0	0	0.15	0.8	3.16	2
34_47	0.566	0	0	2.759	32.481	11.748	15.897	63.451		0.13	0	0	0.14	0.73	3.17	2

34_48	0.189	0	0	2.542	30.946	11.2	12.747	57.624		0.05	0	0	0.13	0.82	3.17	2
34_51	0.653	0	0	3.219	32.015	11.507	24.115	71.509		0.16	0	0	0.17	0.67	3.19	2
34_53	0.295	0	0	2.851	33.399	12.798	17.103	66.446		0.06	0	0	0.13	0.81	3	2
34_54	0.256	0	0	2.425	35.253	12.875	27.5	78.309		0.06	0	0	0.11	0.83	3.14	2
34_56	0.34	0	0	2.927	33.719	12.909	22.611	72.506		0.07	0	0	0.13	0.8	3	2
34_57	0.227	0	0	4.803	35.823	12.992	26.473	80.318		0.05	0	0	0.22	0.73	3.17	2
34_61	0.46	0	0	2.455	33.799	12.335	24.523	73.572		0.1	0	0	0.12	0.78	3.15	2
34_62	0.732	0	0	1.99	23.405	9.198	12.808	48.133		0.22	0	0	0.13	0.65	2.92	2
34_66	0.212	0	0	2.078	25.159	10.866	22.196	60.511		0.05	0	0	0.11	0.84	2.66	2
34_67	0.454	0	0	3.579	26.889	10.557	19.598	61.077		0.12	0	0	0.2	0.68	2.92	2
34_69	0.441	0	0	2.815	32.071	11.58	17.223	64.13		0.11	0	0	0.14	0.75	3.18	2
34_70	0.205	0	0	1.711	22.493	10.166	1.889	36.464		0.06	0	0	0.1	0.84	2.54	2
34_71	0.369	0	0	2.9	32.089	12.195	26.227	73.78		0.08	0	0	0.14	0.78	3.02	2
34_72	0.398	0	0	3.037	32.554	12.016	22.726	70.731		0.09	0	0	0.15	0.76	3.11	2
									34_ave	0.1	0	0	0.15	0.75	3.03	2
									s	0.0776	0	0	0.0336	0.0790	0.1701	0
									C	77.60	0	0	22.40	10.53	5.61	0
36_2	0.145	0	0	4.278	33.413	12.039	27.963	77.838		0.03	0	0	0.21	0.76	3.19	2
36_6	0.11	0	0	4.569	33.788	12.708	29.08	80.255		0.02	0	0	0.21	0.77	3.05	2
36_20	0.24	0	0	7.43	24.951	9.965	22.698	65.284		0.07	0	0	0.44	0.49	2.87	2
									36_ave	0.04	0	0	0.29	0.67	3.04	2
									s	0.0265	0	0	0.1328	0.1589	0.1604	0
									C	66.25	0	0	45.79	23.72	5.28	0
38_1	0.059	0	0	7.34	37.209	13.8	31.804	90.212		0.01	0	0	0.32	0.67	3.1	2
38_3	0	0	0	6.038	42.095	15.764	36.103	100		0	0	0	0.23	0.77	3.07	2
38_7	0.056	0	0	6.226	41.649	15.872	36.183	99.986		0.01	0	0	0.23	0.76	3.01	2
38_12	0.102	0	0	4.811	36.878	13.79	31.601	87.182		0.02	0	0	0.21	0.77	3.07	2
38_20	0.073	0	0	7.104	36.468	13.712	31.525	88.882		0.01	0	0	0.31	0.68	3.05	2
									38_ave	0.01	0	0	0.26	0.73	3.06	2
									s	0.0071	0	0	0.0510	0.0505	0.0332	0
									C	71.00	0	0	19.62	6.92	1.08	0

38D_1	0.079	0	0	3.764	34.468	13.118	34.051	100.252	0.02	0	0	0.17	0.81	3.02	2
38D_2	0.119	0	0	3.641	34.737	11.613	31.917	96.914	0.03	0	0	0.19	0.78	3.43	2
38D_3	0.346	0	0	4.463	24.088	8.234	22.638	70.092	0.12	0	0	0.32	0.56	3.36	2
38D_6	0.252	0	0	4.209	34.25	13.87	35.178	102.437	0.05	0	0	0.18	0.77	2.84	2
38D_7	0.124	0	0	4.418	36.593	14.143	36.517	107.477	0.02	0	0	0.19	0.79	2.97	2
38D_8	0.108	0	0	3.479	35.096	14.156	35.852	103.732	0.02	0	0	0.15	0.83	2.85	2
38D_9	0.35	0	0	9.643	30.86	11.206	30.246	95.53	0.09	0	0	0.51	0.4	3.16	2
38D_10	0.115	0	0	2.773	34.974	12.538	33.33	98.719	0.03	0	0	0.13	0.84	3.2	2
38D_11	0.238	0	0	7.02	34.429	13.309	34.617	104.368	0.05	0	0	0.31	0.64	2.97	2
38D_12	0.08	0	0	4.324	35.4	14.199	36.091	105.265	0.02	0	0	0.18	0.8	2.86	2
38D_13	0.142	0	0	4.151	33.031	14.153	35.062	100.695	0.03	0	0	0.17	0.8	2.68	2
38D_14	0.254	0	0	5.352	33.117	12.922	33.383	99.221	0.05	0	0	0.25	0.7	2.94	2
38D_16	0.17	0	0	9.299	38.588	12.886	35.834	113.315	0.04	0	0	0.43	0.53	3.44	2
38D_17	0.116	0	0	4.226	34.618	13.339	34.491	101.626	0.02	0	0	0.19	0.79	2.98	2
38D_18	0.085	0	0	2.532	36.019	13.373	34.979	102.425	0.02	0	0	0.11	0.87	3.09	2
38D_21	0.13	0	0	3.781	33.506	13.952	34.924	100.652	0.03	0	0	0.17	0.8	2.97	2
								38D_ave	0.04	0	0	0.23	0.73	3.05	2
								s	0.0283	0	0	0.1109	0.1319	0.2195	0
								C	70.75	0	0	48.22	18.07	7.20	0
40_4	0	2.704	0	1.05	32.985	12.309	28.506	77.554	0	0.36	0	0.05	0.59	3.08	2
40_9	0	2.094	0	0.729	34.622	14.315	31.83	83.59	0	0.24	0	0.03	0.73	2.78	2
40_11	0	1.112	0	0.733	34.05	13.673	30.505	80.073	0	0.13	0	0.03	0.84	2.86	2
40_18	0	2.648	0	0.647	34.86	14.601	32.434	85.19	0	0.3	0	0.03	0.67	2.74	2
								40_ave	0	0.26	0	0.04	0.7	2.87	2
								s	0	0.0981	0	0.01	0.1053	0.1518	0
								C	0	37.73	0	0.25	15.04	5.29	0
42_5	0.275	0	0	3.813	37.284	13.794	31.707	86.873	0.06	0	0	0.16	0.78	3.1	2
42_7	0.269	0	0	4.359	39.254	13.752	32.249	89.883	0.05	0	0	0.19	0.76	3.28	2
42_11	0.258	0	0	4.517	29.176	10.986	25.229	70.166	0.07	0	0	0.24	0.69	3.05	2
42_12	0.244	0	0	5.138	39.764	14.287	33.245	92.678	0.05	0	0	0.21	0.74	3.2	2
42_13	0.321	0	0	6.161	37.746	14.015	32.364	90.607	0.06	0	0	0.26	0.68	3.09	2
42_15	0.217	0	0	3.886	38.386	13.508	31.574	87.571	0.04	0	0	0.17	0.79	3.26	2

42_16	0.249	0	0	4.466	33.669	13.959	30.959	83.302		0.05	0	0	0.19	0.76	2.77	2
42_19	0.247	0	0	4.257	33.806	14.326	21.845	84.167		0.05	0	0	0.18	0.77	2.71	2
42_20	0.249	0	0	3.684	36.383	13.131	31.44	84.887		0.05	0	0	0.17	0.78	3.18	2
									42_ave	0.05	0	0	0.2	0.75	3.07	2
									s	0.0086	0	0	0.0339	0.0397	0.2033	0
									C	17.40	0	0	16.95	5.29	6.62	0
44_1	0	0	1.412	5.426	25.827	10.486	34.1	77.251		0	0	0.042	0.308	0.608	2.828	2
44_3	0	0	0.647	3.271	23.716	9.985	31.668	69.287		0	0	0.02	0.195	0.785	2.727	2
44_4	0	0	0.279	2.941	25.001	10.204	32.834	71.259		0	0	0.008	0.171	0.821	2.813	2
44_8	0	0	1.756	3.996	26.835	10.927	35.379	78.893		0	0	0.05	0.217	0.733	2.819	2
									44_ave	0	0	0.03	0.223	0.747	2.797	2
									s	0	0	0.0194	0.0599	0.0931	0.0469	0
									C	0	0	64.67	26.86	12.46	1.68	0
45_07	0	0	0.149	6.578	19.645	6.444	15.772	48.588		0	0	0.007	0.607	0.386	3.5	2
45_40	0	0	0.159	10.376	22.828	12.664	16.546	62.573		0	0	0.004	0.487	0.509	2.069	2
45_41	0	0	0.483	5.653	19.384	10.697	18.516	54.733		0	0	0.014	0.314	0.672	2.08	2
45_61	0	0	0	0.411	1.56	0.64	1.66	4.271		0	0	0	0.382	0.618	2.798	2
									45_ave	0	0	0.006	0.448	0.546	2.61	2
									s	0	0	0.0059	0.1279	0.1265	0.6834	0
									C	0	0	98.33	28.55	23.17	26.18	0
47_46	0	0	0.311	14.181	25.787	13.288	17.882	71.449		0	0	0.007	0.634	0.359	2.23	2
47_47	0	0	0.116	20.792	33.609	17.328	17.355	89.2		0	0	0.002	0.713	0.285	2.23	2
47_48	0	0	0.111	20.78	37.484	16.228	19.163	93.766		0	0	0.002	0.761	0.237	2.65	2
47_52	0	0	0.096	20.737	32.386	15.362	19.986	88.567		0	0	0.002	0.802	0.196	2.42	2
47_54	0	0	0.183	18.805	29.279	13.981	21.826	84.074		0	0	0.004	0.8	0.196	2.40	2
47_55	0	0	0.036	16.999	28.851	14.329	25.658	85.873		0	0	0.001	0.705	0.294	2.31	2
47_56	0	0	0.929	8.729	31.21	12.174	23.349	76.391		0	0	0.024	0.426	0.55	2.94	2
47_57	0	0	0.273	19.353	37.553	17.692	18.128	92.999		0	0	0.005	0.65	0.345	2.44	2
47_58	0	0	0	14.887	29.339	15.415	18.704	78.345		0	0	0	0.574	0.426	2.19	2
47_61	0	0	0	20.227	32.292	15.254	22.762	90.535		0	0	0	0.788	0.212	2.43	2
47_62	0	0	0	19.258	31.089	15.627	20.462	86.436		0	0	0	0.733	0.267	2.28	2

47_63	0	0	0.507	17.185	36.347	14.96	21.108	90.107	0	0	0.01	0.68	0.31	2.79	2
47_65	0	0	0.208	13.242	33.459	15.881	16.907	79.697	0	0	0.004	0.496	0.5	2.42	2
47_67	0	0	0.286	17.935	43.012	20.771	15.526	97.53	0	0	0.004	0.513	0.483	2.38	2
47_68	0	0	0.186	18.771	41.232	19.731	15.13	95.05	0	0	0.003	0.565	0.432	2.40	2
47_69	0	0	0.124	14.63	29.094	15.344	6.016	65.208	0	0	0.003	0.567	0.43	2.18	2
47_70	0	0	0.131	19.916	28.578	15.033	20.313	83.971	0	0	0.003	0.788	0.209	2.18	2
47_72	0	0	0.17	14.808	29.09	13.602	29.016	86.686	0	0	0.004	0.647	0.349	2.46	2
47_74	0	0	0.061	23.112	37.29	16.429	24.887	101.779	0	0	0.001	0.836	0.163	2.61	2
47_75	0	0	0	16.548	42.64	18.773	29.487	107.448	0	0	0	0.524	0.476	2.61	2
47_76	0	0	0.143	14.036	20.14	8.566	21.742	64.627	0	0	0.005	0.974	0.021	2.7	2
47_77	0	0	0	27.062	41.47	16.803	25.135	110.47	0	0	0	0.957	0.043	2.83	2
47_80	0	0	2.393	17.23	36.008	18.957	13.844	88.432	0	0	0.039	0.54	0.421	2.18	2
47_81	0	0	0.257	14.603	34.005	12.987	15.286	77.138	0	0	0.006	0.668	0.326	3	2
47_82	0	0	0.184	17.981	28.528	14.441	25.726	86.86	0	0	0.004	0.69	0.306	2.27	2
47_83	0	0	0.111	20.282	35.716	16.616	23.337	96.062	0	0	0.002	0.726	0.272	2.47	2
47_84	0	0	0.701	19.755	43.595	20.516	16	100.567	0	0	0.011	0.572	0.417	2.44	2
47_87	0	0	0.097	17.364	40.195	17.036	26.73	101.422	0	0	0.002	0.606	0.392	2.71	2
47_88	0	0	0.109	14.964	35.188	15.389	5.593	71.243	0	0	0.002	0.578	0.42	2.63	2
47_89	0	0	1.607	14.125	48.576	21.056	24.192	109.556	0	0	0.024	0.399	0.577	2.65	2
47_90	0	0	0.127	18.242	32.673	16.123	22.996	90.161	0	0	0.002	0.673	0.325	2.33	2
47_91	0	0	0	15.842	24.695	11.687	29.403	81.627	0	0	0	0.806	0.194	2.43	2
47_92	0	0	0.081	13.148	28.578	14.436	17.061	73.304	0	0	0.002	0.541	0.457	2.27	2
47_93	0	0	0.688	7.747	40.323	20.701	20.556	90.015	0	0	0.01	0.222	0.768	2.24	2
								47_ave	0	0	0.006	0.652	0.342	2.46	2
								s	0	0	0.0082	0.1546	0.1511	0.2243	0
								C	0	0	136.67	23.71	44.18	9.12	0
48_8	0	0	0.224	5.715	27.994	10.07	26.071	70.064	0	0	0.007	0.337	0.656	3.19	2
48_12	0	0	0.061	5.881	25.739	10.051	25.187	66.925	0	0	0.002	0.348	0.65	2.94	2
48_17	0	0	0.168	4.162	27.568	10.048	25.753	67.699	0	0	0.005	0.246	0.749	3.15	2
48_21	0	0	0.315	5.068	28.251	10.367	26.568	70.579	0	0	0.009	0.291	0.7	3.13	2
48_24	0	0	0.72	4.755	28.386	10.441	26.747	71.039	0	0	0.021	0.271	0.708	3.12	2
								48_ave	0	0	0.009	0.299	0.693	3.11	2
								s	0	0	0.0073	0.0433	0.0407	0.0966	0

									C	0	0	81.11	14.48	5.87	3.11	0
49_1	2.28	0	0	0	22.767	10.605	34.495	70.147		0.6	0	0	0	0.4	2.46	2
49_14	1.887	0	0	0	18.234	9.344	33.376	62.841		0.56	0	0	0	0.44	2.24	2
49_18	2.014	0	0	0	20.351	10.568	35.497	68.43		0.53	0	0	0	0.47	2.21	2
49_20	2.089	0	0	0	19.947	10.28	35.297	67.613		0.57	0	0	0	0.43	2.23	2
									49_ave	0.56				0.44	2.29	2
									s	0.0289	0	0	0	0.0289	0.1173	0
									C	5.16	0	0	0	6.57	5.12	0
50_1	1.749	0	0	3.887	33.201	13.674	28.924	81.435		0.36	0	0	0.17	0.47	2.79	2
50_2	0.965	0	0	3.551	30.105	12.212	21.782	68.615		0.22	0	0	0.17	0.61	2.83	2
50_3	1.296	0	0	4.876	30.397	13.127	24.979	74.675		0.28	0	0	0.22	0.5	2.66	2
50_4	0.48	0	0	3.983	34.616	13.578	36.113	88.77		0.1	0	0	0.17	0.73	2.93	2
50_5	0.48	0	0	5.382	35.009	13.649	24.836	79.356		0.1	0	0	0.23	0.67	2.94	2
50_6	0.756	0	0	4.128	33.398	13.678	31.019	82.979		0.15	0	0	0.18	0.67	2.8	2
50_10	1.337	0	0	6.742	31.463	12.614	24.259	76.415		0.3	0	0	0.32	0.38	2.86	2
50_14	1.872	0	0	2.989	32.228	13.629	24.194	74.912		0.38	0	0	0.13	0.49	2.71	2
50_15	1.943	0	0	3.281	32.287	13.477	26.4	77.388		0.4	0	0	0.15	0.45	2.75	2
50_18	0.599	0	0	5.15	34.2	13.741	33.5	87.19		0.12	0	0	0.22	0.66	2.86	2
50_19	1.386	0	0	4.734	32.964	13.159	27.167	79.41		0.29	0	0	0.21	0.5	2.88	2
50_20	0.572	0	0	9.913	33.705	12.565	29.586	86.341		0.13	0	0	0.47	0.4	3.08	2
50_21	2.347	0	0	2.96	29.896	13.027	19.008	67.238		0.5	0	0	0.14	0.36	2.63	2
50_22	0.645	0	0	7.898	34.443	12.938	28.084	84.008		0.14	0	0	0.36	0.5	3.06	2
50_23	0.6	0	0	5.895	34.363	13.287	32.486	86.631		0.13	0	0	0.26	0.61	2.97	2
50_24	1.381	0	0	4.351	30.526	12.557	30.991	79.806		0.31	0	0	0.21	0.48	2.79	2
50_25	0.904	0	0	4.587	34.97	14.264	27.945	82.67		0.18	0	0	0.19	0.63	2.81	2
50_27	0.515	0	0	4.648	33.618	13.279	31.158	83.218		0.11	0	0	0.21	0.68	2.91	2
50_29	1.628	0	0	6.034	30.618	13.324	19.916	71.52		0.34	0	0	0.27	0.39	2.64	2
50_30	1.593	0	0	7.493	27.053	13.135	22.111	71.385		0.34	0	0	0.34	0.32	2.36	2
50_32	0.9	0	0	4.863	34.221	13.445	30.303	83.732		0.19	0	0	0.21	0.6	2.92	2
50_33	1.495	0	0	3.207	34.311	13.099	28.527	80.639		0.32	0	0	0.15	0.53	3	2
50_34	0.836	0	0	8.823	33.166	12.99	28.898	84.713		0.18	0	0	0.4	0.42	2.93	2
50_37	0.725	0	0	6.272	33.635	13.596	26.224	80.452		0.15	0	0	0.27	0.58	2.84	2

50_39	2.011	0	0	3.875	34.079	13.701	30.356	84.022		0.41	0	0	0.17	0.42	2.86	2
50_40	0.723	0	0	5.693	33.57	14.13	23.018	77.134		0.14	0	0	0.24	0.62	2.73	2
50_42	1.488	0	0	5.143	34.068	13.799	33.8	88.298		0.3	0	0	0.22	0.48	2.83	2
50_43	1.8	0	0	2.866	33.132	13.402	35.939	87.139		0.37	0	0	0.13	0.5	2.84	2
50_44	0.645	0	0	4.664	34.564	13.83	32.452	86.155		0.13	0	0	0.2	0.67	2.87	2
50_45	2.011	0	0	3.199	33.718	13.302	33.981	86.211		0.42	0	0	0.14	0.44	2.91	2
50_46	1.215	0	0	5.708	33.445	13.654	24.224	78.246		0.25	0	0	0.25	0.5	2.81	2
50_47	1.509	0	0	3.137	32.227	13.282	28.26	78.415		0.32	0	0	0.14	0.54	2.79	2
50_48	1.99	0	0	3.932	33.81	13.35	32.522	85.604		0.42	0	0	0.18	0.4	2.91	2
50_49	1.626	0	0	3.907	31.51	12.918	30.616	80.577		0.35	0	0	0.18	0.47	2.8	2
50_50	1.029	0	0	4.342	34.779	14.167	23.334	77.651		0.2	0	0	0.18	0.62	2.82	2
50_51	1.638	0	0	5.81	32.613	12.247	27.816	80.124		0.37	0	0	0.28	0.35	3.06	2
50_53	0.925	0	0	4.755	34.873	13.613	31.44	85.606		0.19	0	0	0.21	0.6	2.94	2
50_54	1.451	0	0	5.533	32.508	13.345	25.148	77.985		0.3	0	0	0.25	0.45	2.8	2
50_55	0.535	0	0	6.274	34.751	13.468	30.087	85.115		0.11	0	0	0.28	0.61	2.96	2
50_56	0.764	0	0	4.947	33.97	13.47	25.5	78.651		0.16	0	0	0.22	0.62	2.9	2
50_58	0.648	0	0	11.588	28.815	11.61	27.003	79.664		0.16	0	0	0.59	0.25	2.85	2
50_59	0.644	0	0	11.174	33.104	12.355	23.827	81.104		0.15	0	0	0.54	0.31	3.08	2
50_60	0.739	0	0	3.609	33.532	12.997	28.137	79.014		0.16	0	0	0.17	0.67	2.96	2
									50_ave	0.25	0	0	0.24	0.51	2.85	2
									s	0.1111	0	0	0.1031	0.1181	0.1327	0
									C	44.44	0	0	42.96	23.16	4.66	0
51_5	0.796	0	0	8.387	30.184	12.672	26.361	78.4		0.18	0	0	0.39	0.43	2.73	2
51_6	0.552	0	0	9.305	31.366	12.171	31.748	85.142		0.13	0	0	0.45	0.42	2.96	2
51_12	0.317	0	0	5.013	29.691	12.546	29.805	77.372		0.07	0	0	0.24	0.69	2.72	2
51_13	0.487	0	0	8.682	30.253	12.336	33.782	85.54		0.11	0	0	0.42	0.47	2.82	2
51_14	0.851	0	0	4.727	31.802	12.801	34.05	84.231		0.19	0	0	0.22	0.59	2.85	2
51_15	0.748	0	0	5.887	30.891	12.402	33.067	82.995		0.17	0	0	0.28	0.55	2.86	2
51_16	0.724	0	0	6.983	30.892	12.557	28.325	79.481		0.16	0	0	0.33	0.51	2.82	2
51_17	1.748	0	0	3.806	30.843	11.892	33.248	81.537		0.41	0	0	0.19	0.4	2.98	2
51_22	0.267	0	0	4.537	34.228	12.926	33.38	85.338		0.06	0	0	0.21	0.73	3.04	2
51_23	0.538	0	0	7.016	31.562	12.871	25	76.987		0.12	0	0	0.32	0.56	2.82	2
51_24	0.302	0	0	5.065	33.224	12.654	34.68	85.925		0.07	0	0	0.24	0.69	3.01	2

51_25	0.577	0	0	8.053	32.002	13.138	26.936	80.706	0.12	0	0	0.36	0.52	2.8	2
51_26	0.312	0	0	6.392	32.732	12.983	33.952	86.371	0.07	0	0	0.29	0.64	2.89	2
51_27	0.655	0	0	6.286	31.695	12.505	35.41	86.551	0.15	0	0	0.3	0.55	2.91	2
51_28	0.766	0	0	4.758	32.733	13.78	29.622	81.659	0.16	0	0	0.21	0.63	2.73	2
51_29	0.319	0	0	4.918	33.549	12.948	30.903	82.637	0.07	0	0	0.23	0.7	2.97	2
51_30	0.63	0	0	8.017	30.767	12.314	32.303	84.031	0.14	0	0	0.39	0.47	2.87	2
51_31	1.366	0	0	5.713	29.99	12.181	27.15	76.4	0.31	0	0	0.28	0.41	2.83	2
51_33	0.368	0	0	4.211	32.576	13.017	26.665	76.837	0.08	0	0	0.19	0.73	2.87	2
51_34	1.838	0	0	4.385	30.592	12.78	25.837	75.432	0.4	0	0	0.2	0.4	2.75	2
51_35	1.036	0	0	8.996	28.303	12.38	27.037	77.752	0.23	0	0	0.43	0.44	2.62	2
51_37	1.115	0	0	6.35	30.945	12.602	30.137	81.149	0.25	0	0	0.3	0.45	2.82	2
51_39	1.45	0	0	4.839	31.345	13.195	27.118	77.947	0.31	0	0	0.22	0.47	2.73	2
51_41	0.643	0	0	5.368	31.706	13.041	34.747	85.505	0.14	0	0	0.24	0.62	2.79	2
51_42	0.789	0	0	4.486	32.269	12.8	33.822	84.166	0.17	0	0	0.21	0.62	2.89	2
51_44	0.409	0	0	9.11	30.619	12.764	30.644	83.546	0.09	0	0	0.42	0.49	2.75	2
51_46	0.728	0	0	8.083	33.46	12.477	33.781	88.529	0.16	0	0	0.39	0.45	3.08	2
51_48	0.709	0	0	7.21	28.008	12.217	27.674	75.818	0.16	0	0	0.35	0.49	2.63	2
51_51	0.188	0	0	4.354	33.216	12.307	31.709	81.774	0.04	0	0	0.21	0.75	3.1	2
51_53	0.46	0	0	5.508	31.059	12.904	33.568	83.499	0.1	0	0	0.25	0.65	2.76	2
51_54	0.529	0	0	8.023	30.797	11.913	28.894	80.156	0.12	0	0	0.4	0.48	2.97	2
51_56	0.996	0	0	6.795	31.457	12.385	31.898	83.531	0.22	0	0	0.33	0.45	2.92	2
51_57	0.537	0	0	4.515	33.533	13.16	31.115	82.86	0.11	0	0	0.2	0.69	2.93	2
51_58	0.54	0	0	4.25	32.536	12.764	28.858	78.948	0.12	0	0	0.2	0.68	2.93	2
51_59	0.249	0	0	5.695	32.958	13.13	33.086	85.118	0.05	0	0	0.26	0.69	2.88	2
51_60	0.633	0	0	6.934	31.457	12.711	29.924	81.659	0.14	0	0	0.32	0.54	2.84	2
								51_ave	0.16	0	0	0.29	0.55	2.86	2
								s	0.0894	0	0	0.0808	0.1107	0.1145	0
								C	55.88	0	0	27.86	20.13	4.00	0
52_1	0.158	0	0	5.068	34.196	13.669	35.862	88.953	0.03	0	0	0.22	0.75	2.87	2
52_2	0.182	0	0	7.575	33.164	13.107	27.359	81.387	0.04	0	0	0.34	0.62	2.9	2
52_4	0.141	0	0	3.802	34.012	14.081	30.578	82.614	0.03	0	0	0.16	0.81	2.77	2
52_8	0.181	0	0	8.576	33.466	12.947	33.518	88.688	0.04	0	0	0.39	0.57	2.97	2
52_9	0.225	0	0	12.516	29.461	11.74	28.191	82.133	0.05	0	0	0.63	0.32	2.88	2

52_13	0.251	0	0	12.01	30.16	12.488	28.15	83.059	0.06	0	0	0.57	0.37	2.77	2
52_21	0.168	0	0	4.93	33.295	12.776	35.001	86.17	0.04	0	0	0.23	0.73	2.99	2
52_22	0.224	0	0	11.838	31.4	12.401	29.949	85.812	0.05	0	0	0.57	0.38	2.91	2
52_24	0.199	0	0	5.249	33.642	13.974	27.976	81.04	0.04	0	0	0.22	0.74	2.76	2
52_25	0.122	0	0	7.149	33.48	13.865	32.5	87.116	0.02	0	0	0.31	0.67	2.77	2
52_32	0.247	0	0	8.004	31.588	12.842	33.206	85.887	0.05	0	0	0.37	0.58	2.82	2
52_33	0.22	0	0	5.37	33.52	13.257	30.787	83.154	0.05	0	0	0.24	0.71	2.9	2
52_34	0.186	0	0	7.155	31.839	13.041	29.578	81.799	0.04	0	0	0.33	0.63	2.8	2
52_36	0.244	0	0	8.55	32.46	12.657	32.743	86.654	0.05	0	0	0.4	0.55	2.94	2
52_38	0.276	0	0	5.347	32.968	13.4	34.135	86.126	0.06	0	0	0.24	0.7	2.82	2
52_40	0.291	0	0	8.932	31.246	12.2	31.699	84.368	0.07	0	0	0.44	0.49	2.94	2
52_41	0.367	0	0	13.491	30.408	11.654	26.647	82.567	0.09	0	0	0.69	0.22	3	2
52_45	0.145	0	0	4.951	32.035	12.091	38.458	87.68	0.03	0	0	0.24	0.73	3.04	2
52_48	0.223	0	0	10.848	32.897	12.572	28.575	85.115	0.05	0	0	0.51	0.44	3	2
52_49	0.13	0	0	9.372	30.765	12.301	32.868	85.436	0.03	0	0	0.45	0.52	2.87	2
52_50	0.257	0	0	7.328	28.972	11.589	35.741	83.887	0.06	0	0	0.38	0.56	2.87	2
52_51	0.134	0	0	5.893	33.932	13.174	38.787	91.92	0.03	0	0	0.27	0.7	2.96	2
52_54	0.195	0	0	7.026	33.456	13.333	28.86	82.87	0.04	0	0	0.31	0.65	2.88	2
52_55	0.136	0	0	11.597	28.079	11.298	30.007	81.117	0.03	0	0	0.61	0.36	2.85	2
52_60	0.229	0	0	7.644	31.518	12.717	36.214	88.322	0.05	0	0	0.36	0.59	2.85	2
52_74	0.177	0	0	5.495	46.629	27.447	0.556	80.304	0.03	0	0	0.28	0.69	2.88	2
52_80	0.26	0	0	6.356	45.815	26.084	0.201	78.716	0.05	0	0	0.34	0.61	2.97	2
52_81	0.315	0	0	6.935	45.235	25.473	0.484	78.442	0.06	0	0	0.38	0.56	3.01	2
52_83	0.317	0	0	4.134	45.686	27.007	0.354	77.498	0.06	0	0	0.21	0.73	2.87	2
52_85	0.24	0	0	4.642	42.487	23.771	0.812	71.952	0.05	0	0	0.27	0.68	3.02	2
								52_ave	0.05	0	0	0.37	0.58	2.9	2
								s	0.0148	0	0	0.1394	0.1464	0.0816	0
								C	29.60	0	0	37.68	25.24	2.81	0
53_1	0.129	0	0	5.47	34.204	13.764	32.584	86.151	0.03	0	0	0.24	0.73	2.85	2
53_2	0.038	0	0	6.014	32.161	12.356	33.922	84.491	0.01	0	0	0.29	0.7	2.99	2
53_3	0.091	0	0	4.081	35.003	13.922	31.423	84.52	0.02	0	0	0.17	0.81	2.89	2
53_6	0.105	0	0	4.408	35.036	13.583	28.395	81.527	0.02	0	0	0.19	0.79	2.96	2
53_7	0.119	0	0	6.509	31.171	12.559	29.455	79.813	0.03	0	0	0.31	0.66	2.85	2

53_9	0.069	0	0	4.22	32.721	13.061	28.949	79.02	0.01	0	0	0.19	0.8	2.88	2
53_11	0.161	0	0	6.319	30.987	13.09	24.823	75.38	0.03	0	0	0.29	0.68	2.72	2
53_12	0.136	0	0	7.869	31.758	12.393	30.909	83.065	0.03	0	0	0.38	0.59	2.94	2
53_14	0.196	0	0	7.119	33.831	12.703	21.955	75.804	0.04	0	0	0.33	0.63	3.06	2
53_15	0.205	0	0	7.118	32.439	12.858	27.597	80.217	0.04	0	0	0.33	0.63	2.9	2
53_18	0.132	0	0	5.421	33.705	13.288	31.316	83.862	0.03	0	0	0.24	0.73	2.91	2
53_21	0.203	0	0	5.073	31.838	12.545	35.563	85.222	0.05	0	0	0.24	0.71	2.91	2
53_23	0.078	0	0	5.15	32.292	12.477	38.58	88.577	0.02	0	0	0.25	0.73	2.97	2
53_24	0.1	0	0	4.138	33.231	14.248	30.135	81.852	0.02	0	0	0.17	0.81	2.68	2
53_25	0.176	0	0	9.63	32.945	12.671	26.674	82.096	0.04	0	0	0.45	0.51	2.99	2
53_26	0.095	0	0	5.167	34.132	13.767	28.007	81.168	0.02	0	0	0.22	0.76	2.85	2
53_32	0.071	0	0	5.812	32.48	13.263	31.371	82.997	0.01	0	0	0.26	0.73	2.81	2
53_34	0.2	0	0	4.568	32.839	13	29.966	80.573	0.04	0	0	0.21	0.75	2.9	2
53_35	0.163	0	0	8.355	32.862	12.537	24.629	78.546	0.04	0	0	0.4	0.56	3.01	2
53_36	0.099	0	0	4.728	32.718	13.739	32.596	83.88	0.02	0	0	0.2	0.78	2.73	2
53_37	0.133	0	0	6.847	33.134	13.353	29.192	82.659	0.03	0	0	0.3	0.67	2.85	2
53_38	0.112	0	0	7.016	30.757	12.688	34.015	84.588	0.02	0	0	0.33	0.65	2.78	2
53_39	0.165	0	0	5.66	33.598	13.606	26.801	79.83	0.03	0	0	0.25	0.72	2.84	2
53_42	0.105	0	0	5.375	33.568	13.375	29.704	82.127	0.02	0	0	0.24	0.74	2.88	2
53_45	0.105	0	0	8.708	32.544	13.107	22.713	77.177	0.02	0	0	0.39	0.59	2.85	2
53_47	0.121	0	0	11.123	29.467	11.919	23.899	76.529	0.03	0	0	0.55	0.42	2.84	2
53_48	0.248	0	0	10.471	29.665	11.189	24.159	75.732	0.06	0	0	0.56	0.38	3.04	2
53_50	0.147	0	0	9.342	33.864	12.729	33.014	89.096	0.03	0	0	0.44	0.53	3.05	2
53_52	0.134	0	0	4.225	33.557	13.547	30.7	82.163	0.03	0	0	0.19	0.78	2.84	2
53_54	0.099	0	0	5.306	34.096	12.909	29.369	81.779	0.02	0	0	0.24	0.74	3.03	2
53_55	0.191	0	0	10.479	26.909	11.241	31.825	80.645	0.05	0	0	0.55	0.4	2.75	2
								53_ave	0.03	0	0	0.3	0.67	2.89	2
								s	0.0120	0	0	0.1127	0.1200	0.0997	0
								C	40.00	0	0	37.57	17.91	3.45	0
54_2	0.049	0	0	14.292	27.295	10.921	34.328	86.885	0.01	0	0	0.78	0.21	2.87	2
54_3	0.022	0	0	7.671	33.47	13.393	27.845	82.401	0	0	0	0.34	0.66	2.87	2
54_4	0.079	0	0	6.057	31.39	13.061	29.303	79.89	0.02	0	0	0.28	0.7	2.76	2
54_7	0.066	0	0	9.892	32.042	12.388	32.382	86.77	0.01	0	0	0.47	0.52	2.97	2

54_8	0.075	0	0	5.698	33.194	13.334	33.836	86.137	0.02	0	0	0.25	0.73	2.86	2
54_9	0.092	0	0	5.023	32.115	12.834	27.099	77.163	0.02	0	0	0.23	0.75	2.87	2
54_10	0.037	0	0	8.702	32.809	13.272	25.899	80.719	0.01	0	0	0.39	0.6	2.84	2
54_12	0.067	0	0	9.11	33.225	12.811	26.838	82.051	0.01	0	0	0.42	0.57	2.98	2
54_13	0.102	0	0	7.263	32.473	13.248	30.296	83.382	0.02	0	0	0.33	0.65	2.81	2
54_14	0.051	0	0	9.081	33.374	13.986	18.568	75.06	0.01	0	0	0.39	0.6	2.74	2
54_16	0.063	0	0	6.081	29.57	11.449	34.177	81.34	0.02	0	0	0.32	0.66	2.97	2
54_17	0.07	0	0	6.978	29.9	12.21	28.998	78.156	0.02	0	0	0.34	0.64	2.81	2
54_18	0.089	0	0	9.899	33.105	13.336	29.806	86.235	0.02	0	0	0.44	0.54	2.85	2
54_25	0.053	0	0	4.316	31.76	11.996	31.499	79.624	0.01	0	0	0.21	0.78	3.04	2
54_27	0.021	0	0	7.341	29.694	11.246	34.907	83.209	0.01	0	0	0.39	0.6	3.03	2
54_28	0.12	0	0	7.079	28.118	10.645	31.989	77.951	0.03	0	0	0.4	0.57	3.03	2
54_30	0.055	0	0	5.184	33.883	13.418	30.605	83.145	0.01	0	0	0.23	0.76	2.9	2
54_31	0.065	0	0	7.541	31.288	12.644	29.31	80.848	0.01	0	0	0.35	0.64	2.84	2
54_33	0.097	0	0	4.812	30.737	12.571	30.347	78.564	0.02	0	0	0.23	0.75	2.81	2
54_34	0.073	0	0	6.198	32.648	13.603	29.906	82.428	0.01	0	0	0.27	0.72	2.76	2
54_35	0.085	0	0	11.321	29.677	11.977	27.676	80.736	0.02	0	0	0.56	0.42	2.84	2
54_36	0.088	0	0	8.961	29.767	11.936	31.631	82.383	0.02	0	0	0.45	0.53	2.86	2
54_37	0.069	0	0	7.265	30.69	11.571	30.096	79.691	0.02	0	0	0.37	0.61	3.05	2
54_38	0.079	0	0	5.172	32.256	13.631	31.921	83.059	0.02	0	0	0.23	0.75	2.72	2
54_39	0.078	0	0	5.816	32.901	13.091	29.633	81.519	0.02	0	0	0.26	0.72	2.89	2
54_41	0.083	0	0	8.81	30.722	12.632	24.175	76.422	0.02	0	0	0.41	0.57	2.79	2
54_46	0.051	0	0	6.998	32.432	13.325	29.664	82.47	0.01	0	0	0.31	0.68	2.79	2
54_47	0.089	0	0	10.659	30.902	12.78	28.756	83.186	0.02	0	0	0.5	0.48	2.78	2
54_48	0.068	0	0	8.59	29.933	12.896	26.36	77.847	0.01	0	0	0.4	0.59	2.66	2
54_51	0.05	0	0	14.064	26.937	10.187	33.844	85.082	0.01	0	0	0.82	0.17	3.04	2
54_53	0.047	0	0	6.449	29.018	11.922	35.248	82.684	0.01	0	0	0.32	0.67	2.79	2
54_54	0.052	0	0	9.794	32.474	13.483	23.161	78.964	0.01	0	0	0.43	0.56	2.77	2
54_55	0.007	0	0	7.728	32.598	13.315	28.801	82.449	0	0	0	0.35	0.65	2.81	2
54_58	0.06	0	0	10.965	29.023	11.924	24.71	76.682	0.01	0	0	0.55	0.44	2.79	2
54_59	0.08	0	0	5.037	32.813	13.335	34.749	86.014	0.02	0	0	0.22	0.76	2.83	2
54_60	0.03	0	0	5.329	33.132	13.469	35.014	86.974	0.01	0	0	0.24	0.75	2.82	2
									54_ave	0.01	0	0	0.38	0.61	2.86	2
									s	0.0065	0	0	0.1402	0.1394	0.0988	0

								C	65.00	0	0	36.89	22.85	3.45	0
55_1	0	2.757	0	0.008	28.024	11.848	40.393	83.03	0	0.38	0	0	0.62	2.72	2
55_2	0	3.061	0	0.009	27.792	11.997	41.756	84.615	0	0.42	0	0	0.58	2.66	2
55_7	0	3.283	0	0.028	27.001	10.6	35.903	76.815	0	0.51	0	0	0.49	2.92	2
55_10	0	2.92	0	0	28.142	12.476	34.531	78.069	0	0.38	0	0	0.62	2.59	2
55_11	0	3.69	0	0	25.879	11.104	34.385	75.058	0	0.54	0	0	0.46	2.68	2
55_37	0	2.543	0	0	21.761	11.619	39.207	75.13	0	0.36	0	0	0.64	2.15	2
55_57	0	2.985	0	0.01	21.024	10.938	40.048	75.005	0	0.45	0	0	0.55	2.21	2
								55_ave	0	0.43	0	0	0.57	2.56	2
								s	0	0.0692	0	0	0.0692	0.2802	0
								C	0	16.09	0	0	12.14	10.95	0
56_1	0	2.708	0	1.799	14.048	6.724	31.919	57.198	0	0.66	0	0.16	0.18	2.4	2
56_2	0	3.216	0	1.865	13.982	7.011	31.418	57.492	0	0.75	0	0.16	0.09	2.29	2
56_11	0	2.883	0	1.729	13.525	6.716	30.785	55.638	0	0.7	0	0.15	0.15	2.31	2
								56_ave	0	0.7	0	0.16	0.14	2.33	2
								s	0	0.0451	0	0.0058	0.0458	0.0586	0
								C	0	6.44	0	3.63	32.71	2.52	0
57_2	0	2.468	0	2.729	32.679	12.516	25.673	76.065	0	0.53	0	0.21	0.26	3	2
57_6	0	3.695	0	4.822	24.947	9.613	22.33	65.407	0	0.63	0	0.3	0.07	2.98	2
57_28	0	2.619	0	4.016	19.064	8.423	15.182	49.304	0	0.51	0	0.28	0.21	2.6	2
								57_ave	0	0.56	0	0.26	0.18	2.86	2
								s	0	0.0643	0	0.0473	0.0985	0.2254	0
								C		11.48	0	18.19	54.72	7.88	0
58_5	0	2.426	0	3.013	32.56	11.816	32.517	82.332	0	0.34	0	0.15	0.51	3.16	2
58_16	0	3.538	0	6.474	29.936	10.921	29.366	80.235	0	0.53	0	0.35	0.12	3.15	2
58_19	0	2.481	0	2.826	34.523	12.419	37.459	89.708	0	0.33	0	0.14	0.53	3.19	2
58_27	0	2.676	0	3.712	28.164	10.384	26.004	70.94	0	0.42	0	0.21	0.37	3.11	2
58_32	0	2.159	0	3.948	14.216	6.345	14.263	40.931	0	0.56	0	0.37	0.07	2.57	2
58_42	0	2.283	0	5.013	19.317	7.404	14.662	48.679	0	0.51	0	0.4	0.09	3	2
58_48	0	2.414	0	5.038	21.328	8.32	15.836	52.936	0	0.48	0	0.36	0.16	2.94	2

58_60	0	2.656	0	3.105	30.197	11.1	27.755	74.813		0	0.39	0	0.17	0.44	3.12	2
58_83	0	4.086	0	7.175	32.624	17.467	24.573	85.925		0	0.38	0	0.24	0.38	2.14	2
58_84	0	4.887	0	8.097	36.744	17.472	21.048	88.248		0	0.46	0	0.28	0.26	2.41	2
58_89	0	4.828	0	8.357	30.492	14.646	23.05	81.373		0	0.54	0	0.34	0.12	2.39	2
									58_ave	0	0.45	0	0.27	0.28	2.83	2
									s	0	0.0781	0	0.0915	0.1666	0.3641	0
									C	0	18.20	0	35.52	62.39	13.49	0
59_1	0	1.735	0	7.154	18.891	7.396	29.831	65.007		0	0.38	0	0.57	0.05	2.93	2
59_2	0	1.907	0	3.473	21.865	9.296	34.748	71.289		0	0.34	0	0.22	0.44	2.7	2
59_3	0	1.754	0	5.989	19.915	8.173	27.732	63.563		0	0.35	0	0.44	0.21	2.8	2
59_4	0	2.02	0	5.235	20.756	8.61	29.327	65.948		0	0.38	0	0.36	0.26	2.77	2
59_5	0	1.927	0	6.881	21.171	8.639	29.527	68.145		0	0.37	0	0.47	0.16	2.81	2
59_6	0	1.985	0	7.144	19.144	8.357	27.587	64.217		0	0.39	0	0.51	0.1	2.63	2
59_7	0	2.007	0	4.917	22.564	9.545	35.349	74.382		0	0.34	0	0.31	0.35	2.71	2
59_8	0	2.406	0	4.304	23.458	9.214	28.733	68.115		0	0.43	0	0.28	0.29	2.92	2
59_9	0	2.008	0	4.514	23.425	9.975	26.322	66.244		0	0.33	0	0.26	0.41	2.7	2
59_10	0	2.028	0	4.682	23.735	9.767	32.869	73.081		0	0.34	0	0.28	0.38	2.79	2
59_11	0	2.563	0	6.68	24.599	9.762	34.397	78.001		0	0.43	0	0.41	0.16	2.89	2
59_12	0	2.769	0	6.385	20.242	8.338	26.696	64.43		0	0.54	0	0.46	0	2.79	2
59_13	0	1.809	0	5.126	18.8	8.275	33.422	67.432		0	0.36	0	0.37	0.27	2.61	2
59_15	0	1.675	0	2.799	22.894	9.027	34.636	71.031		0	0.3	0	0.18	0.52	2.91	2
59_19	0	1.609	0	4.633	19.518	7.635	31.028	64.423		0	0.35	0	0.36	0.29	2.93	2
59_21	0	1.746	0	3.41	21.081	8.737	36.052	71.026		0	0.33	0	0.23	0.44	2.77	2
59_22	0	1.762	0	7.01	21.258	8.68	35.424	74.134		0	0.33	0	0.48	0.19	2.81	2
59_24	0	1.683	0	2.651	21.788	9.391	40.822	76.335		0	0.29	0	0.17	0.54	2.66	2
59_25	0	2.589	0	4.824	23.722	9.429	36.648	77.212		0	0.45	0	0.3	0.25	2.89	2
59_26	0	1.82	0	4.478	20.925	8.791	28.042	64.056		0	0.34	0	0.3	0.36	2.73	2
									59_ave	0	0.37	0	0.35	0.28	2.79	2
									s	0	0.0579	0	0.1140	0.1489	0.1008	0
									C	0	15.65	0	32.57	53.18	3.61	0
60_37	0	1.059	0	8.599	21.976	8.285	28.898	68.817		0	0.21	0	0.62	0.17	3.05	2
60_42	0	1.002	0	4.395	16.109	6.321	24.066	51.893		0	0.26	0	0.41	0.33	2.93	2

60_43	0	0.977	0	7.218	17.579	6.741	21.893	54.408		0	0.24	0	0.64	0.12	2.99	2
60_44	0	0.529	0	6.056	12.372	5.293	12.29	36.54		0	0.16	0	0.68	0.16	2.68	2
60_50	0	0.605	0	6.548	13.919	5.904	6.952	33.928		0	0.17	0	0.66	0.17	2.71	2
									60_ave	0	0.21	0	0.6	0.19	2.87	2
									s	0	0.0432	0	0.1096	0.0809	0.1674	0
									C	0	20.57	0	18.27	42.58	5.83	0
61_17	0	0	0	3.685	9.196	3.733	9.063	27.656		0	0	0	0.59	0.41	2.83	2
61_32	0	0	0	2.994	10.614	4.004	9.911	29.807		0	0	0	0.44	0.56	3.04	2
61_48	0	0	0	3.624	11.109	4.258	10.511	31.893		0	0	0	0.51	0.49	3	2
61_50	0	0	0	3.4	11.046	4.385	10.662	31.87		0	0	0	0.46	0.54	2.89	2
61_56	0	0	0	2.777	11.074	4.255	10.431	30.92		0	0	0	0.39	0.61	2.99	2
61_57	0	0	0	2.502	12.688	4.813	11.806	34.54		0	0	0	0.31	0.69	3.03	2
61_58	0	0	0	11.898	26.133	9.334	23.954	76.943		0	0	0	0.76	0.24	3.21	2
61_59	0	0	0	14.212	25.907	9.634	24.494	79.823		0	0	0	0.88	0.12	3.09	2
61_60	0	0	0	12.058	29.108	9.542	25.31	82.283		0	0	0	0.75	0.25	3.5	2
61_61	0	0	0	13.031	25.513	9.459	24.007	77.501		0	0	0	0.82	0.18	3.1	2
61_65	0	0	0	5.738	13.287	6.378	14.599	42.861		0	0	0	0.53	0.47	2.39	2
61_66	0	0	0	11.601	28.267	10.778	26.836	83.566		0	0	0	0.64	0.36	3.01	2
61_71	0	0	0	10.071	23.89	8.6	21.937	69.639		0	0	0	0.7	0.3	3.19	2
61_72	0	0	0	8.345	19.807	8.575	20.349	61.339		0	0	0	0.58	0.42	2.65	2
61_74	0	0	0	13.999	28.118	10.003	25.802	83.973		0	0	0	0.83	0.17	3.23	2
61_79	0	0	0	13.787	24.849	8.884	22.973	75.841		0	0	0	0.92	0.08	3.21	2
									61_ave	0	0	0	0.63	0.37	3.02	2
									s	0	0	0	0.1848	0.1848	0.2550	0
									C	0	0	0	29.33	49.95	8.44	0
62_05	0	4.189	0	0.022	23.623	9.149	20.38	57.363		0	0.75	0	0	0.25	2.96	2
62_06	0	0.803	0	0.036	5.645	2.455	7.066	16.005		0	0.54	0	0	0.46	2.64	2
62_07	0	3.931	0	0.022	30.274	12.935	14.597	61.759		0	0.5	0	0	0.5	2.69	2
62_10	0	3.933	0	0.012	36.487	14.132	12.055	66.619		0	0.46	0	0	0.54	2.96	2
62_11	0	3.123	0	0.026	35.154	13.847	1.669	53.819		0	0.37	0	0	0.63	2.91	2
62_12	0	3.955	0	0.041	28.482	11.325	5.054	48.857		0	0.57	0	0	0.43	2.89	2
62_18	0	3.598	0	0	27.447	10.288	11.319	52.652		0	0.57	0	0	0.43	3.06	2

62_19	0	4.3	0	0	29.875	11.186	10.147	55.508		0	0.63	0	0	0.37	3.07	2
62_20	0	3.974	0	0.006	27.698	11.093	8.286	51.057		0	0.59	0	0	0.41	2.87	2
62_28	0	2.403	0	0.009	17.272	7.383	10.613	37.68		0	0.53	0	0	0.47	2.69	2
62_30	0	2.052	0	0.038	15.423	5.954	9.243	32.71		0	0.57	0	0	0.43	2.97	2
									62_ave	0	0.55	0	0	0.45	2.88	2
									s	0	0.0962	0	0	0.0962	0.1484	0
									C	0	17.49	0	0	21.38	5.15	0
63_49	0	1.429	0	2.671	10.758	5.578	9.112	29.548		0	0.42	0	0.28	0.3	2.21	2
63_50	0	0.512	0	0.688	6.271	2.481	8.06	18.012		0	0.34	0	0.16	0.5	2.9	2
63_53	0	3.153	0	4.51	13.733	7.995	9.68	39.071		0	0.54	0	0.32	0.14	2.29	2
63_63	0	0.11	0	0.153	1.028	0.486	4.423	6.2		0	0.37	0	0.19	0.44	2.43	2
									63_ave	0	0.42	0	0.24	0.34	2.46	2
									s	0	0.0881	0	0.0750	0.1603	0.3087	0
									C	0	20.98	0	31.25	47.15	12.55	0
64_4	0	1.688	0	5.839	29.533	11.318	15.022	60.466		0	0.24	0	0.31	0.45	3	2
64_6	0	2.456	0	6.426	31.709	12.276	13.408	63.268		0	0.33	0	0.31	0.36	2.97	2
64_7	0	2.429	0	7.619	34.701	13.851	16.287	71.296		0	0.29	0	0.33	0.38	2.88	2
64_8	0	2.278	0	6.217	30.728	13.283	16.264	65.326		0	0.28	0	0.28	0.44	2.66	2
64_10	0	2.13	0	5.815	26.164	10.203	11.77	53.437		0	0.34	0	0.34	0.32	2.94	2
64_12	0	1.418	0	5.135	22.372	9.931	15.385	51.666		0	0.23	0	0.31	0.46	2.59	2
64_14	0	0.646	0	1.637	9.412	3.64	5.544	19.935		0	0.29	0	0.27	0.44	2.97	2
64_18	0	1.348	0	4.947	24.364	10.472	11.246	49.662		0	0.21	0	0.28	0.51	2.67	2
64_19	0	1.825	0	5.797	26.21	11.537	15.85	58.228		0	0.26	0	0.3	0.44	2.61	2
64_20	0	1.721	0	5.479	27.065	10.855	10.439	52.745		0	0.26	0	0.3	0.44	2.86	2
64_21	0	1.621	0	5.326	24.942	9.902	14.049	53.273		0	0.27	0	0.32	0.41	2.89	2
64_22	0	0.827	0	3.419	15.163	6.321	18.52	42.611		0	0.21	0	0.32	0.47	2.75	2
64_26	0	1.899	0	5.858	26.445	11.24	13.282	55.81		0	0.28	0	0.31	0.41	2.7	2
64_27	0	1.899	0	4.419	22.693	9.302	14.2	50.101		0	0.33	0	0.28	0.39	2.8	2
64_29	0	0.705	0	2.476	9.867	5.06	9.196	25.992		0	0.31	0	0.39	0.3	3.02	2
64_30	0	2.732	0	5.026	31.906	13.217	14.447	63.901		0	0.34	0	0.23	0.43	2.77	2
64_33	0	1.78	0	5.869	28.349	12.281	14.243	59.338		0	0.24	0	0.28	0.48	2.65	2
64_35	0	1.409	0	4.805	23.133	9.717	12.289	48.834		0	0.24	0	0.29	0.47	2.73	2

64_36	0	1.587	0	5.185	20.188	9.134	13.184	46.91		0	0.28	0	0.34	0.38	2.54	2
64_38	0	2.274	0	6.435	33.179	13.838	14.696	66.834		0	0.27	0	0.28	0.45	2.75	2
64_39	0	2.376	0	5.792	31.985	14.36	23.326	74.116		0	0.27	0	0.24	0.49	2.56	2
64_40	0	2.346	0	6.876	35.724	15.36	17.93	74.254		0	0.25	0	0.27	0.48	2.67	2
64_41	0	0.892	0	3.127	18.126	7.536	16.025	43.752		0	0.19	0	0.25	0.56	2.76	2
64_44	0	1.418	0	5.127	24.561	9.906	10.382	48.826		0	0.23	0	0.31	0.46	2.85	2
64_45	0	2.046	0	4.615	23.281	10.276	14.94	52.494		0	0.33	0	0.27	0.4	2.6	2
64_46	0	2.153	0	5.216	34.454	15.09	9.333	62.364		0	0.23	0	0.21	0.56	2.62	2
64_62	0	0.027	0	0.132	0.581	0.23	2.536	3.506		0	0.19	0	0.34	0.47	2.9	2
64_75	0	0.031	0	0.185	0.667	0.294	4.484	5.661		0	0.17	0	0.37	0.46	2.6	2
									64_ave	0	0.26	0	0.3	0.44	2.76	2
									s	0	0.0471	0	0.0402	0.0600	0.1453	0
									C	0	18.12	0	13.40	13.64	5.26	0
65_04	0	1.857	0	6.326	25.885	9.867	5.18	49.115		0	0.31	0	0.38	0.31	3.01	2
65_10	0	2.82	0	4.753	24.099	9.236	18.276	59.184		0	0.5	0	0.31	0.19	3	2
65_35	0	0.261	0	3.741	14.766	6.464	6.478	31.71		0	0.07	0	0.34	0.59	2.62	2
									65_ave	0	0.29	0	0.34	0.37	2.88	2
									s	0	0.2155	0	0.0351	0.2053	0.2223	0
									C	0	74.31	0	10.32	55.49	7.72	0
66_05	0	0	0	6.377	32.466	12.287	17.797	69.927		0	0	0	0.31	0.69	3.03	2
66_15	0	0	0	7.855	16.348	7.194	12.756	44.153		0	0	0	0.65	0.35	2.61	2
66_24	0	0	0	5.925	26.423	10.086	10.32	52.754		0	0	0	0.35	0.65	3.01	2
66_39	0	0	0	7.539	26.263	10.138	13.17	56.724		0	0	0	0.44	0.56	2.97	2
									66_ave	0	0	0	0.44	0.56	2.91	2
									s	0	0	0	0.1517	0.1517	0.1982	0
									C	0	0	0	34.48	27.09	6.81	0
67_4	3.093	0	0	0.013	24.438	9.621	10.291	47.628		0.81	0	0	0	0.19	2.92	2
67_8	2.378	0	0	0	34.862	13.212	13.973	64.425		0.5	0	0	0	0.5	3.03	2
67_11	4.362	0	0	0	33.518	13.077	5.61	56.587		0.93	0	0	0	0.07	2.94	2
67_21	1.635	0	0	0.007	19.114	8.492	15.715	44.963		0.54	0	0	0	0.46	2.58	2
67_23	1.26	0	0	0.008	22.355	8.676	0.754	33.053		0.41	0	0	0	0.59	2.96	2

67_49	3.1	0	0	0	32.194	12.277	17.635	65.206		0.7	0	0	0	0.3	3.01	2
									67_ave	0.65	0	0	0	0.35	2.91	2
									s	0.1993	0	0	0	0.1993	0.1654	0
									C	30.66	0	0	0	56.94	5.68	0
68_07	0.905	0	0	1.233	17.974	7.108	15.611	42.831		0.36	0	0	0.1	0.54	2.9	2
68_13	0.894	0	0	0.736	8.732	3.656	4.559	18.577		0.68	0	0	0.12	0.2	2.74	2
68_21	2.353	0	0	4.985	30.383	11.925	14.553	64.199		0.55	0	0	0.25	0.2	2.93	2
68_23	1.147	0	0	0.293	17.081	7.524	11.645	37.69		0.43	0	0	0.02	0.55	2.61	2
68_25	1.677	0	0	0.628	15.845	7.266	6.011	31.427		0.64	0	0	0.05	0.31	2.5	2
68_33	1.098	0	0	0.106	16.526	7.163	7.011	31.904		0.43	0	0	0.01	0.56	2.65	2
68_43	1.448	0	0	3.563	21.11	8.48	0.512	35.113		0.48	0	0	0.25	0.27	2.86	2
68_45	3.83	0	0	0.029	29.802	11.725	9.534	54.92		0.91	0	0	0	0.09	2.92	2
68_48	1.628	0	0	0.015	15.861	7.025	5.805	30.334		0.65	0	0	0	0.35	2.59	2
									68_ave	0.57	0	0	0.09	0.34	2.74	2
									s	0.1699	0	0	0.1008	0.1732	0.1633	0
									C	29.81	0	0	112.00	50.94	5.96	0
69_01	1.006	0	0	0.323	16.725	6.593	8.252	32.899		0.43	0	0	0.03	0.54	2.91	2
69_02	1.502	0	0	0.918	38.352	13.458	22.208	76.438		0.31	0	0	0.04	0.65	3.27	2
69_03	1.955	0	0	0.69	35.293	13.064	17.6	68.602		0.42	0	0	0.03	0.55	3.1	2
69_11	0.771	0	0	2.982	37.205	12.934	19.172	73.064		0.03	0	0	0.14	0.83	3.3	2
69_16	2.092	0	0	1.369	30.938	10.989	13.231	58.601		0.53	0	0	0.07	0.4	3.23	2
69_22	0.296	0	0	10.241	29.599	11.477	13.862	65.575		0.07	0	0	0.53	0.4	2.96	2
69_23	1.756	0	0	0.724	38.292	13.403	21.386	75.561		0.37	0	0	0.03	0.6	3.28	2
69_29	1.243	0	0	1.98	37.172	13.097	18.414	71.906		0.26	0	0	0.09	0.65	3.26	2
									69_ave	0.3	0	0	0.12	0.58	3.16	2
									s	0.1759	0	0	0.1701	0.1414	0.1545	0
									C	58.63	0	0	141.75	24.38	4.89	0
70_1	2.064	0	0	3.27	32.794	12.267	10.05	60.445		0.47	0	0	0.16	0.37	3.07	2
70_3	0.205	0	0	9.199	23.617	10.147	8.613	51.781		0.06	0	0	0.54	0.4	2.67	2
70_6	0.966	0	0	3.839	31.381	12.055	18.575	66.816		0.22	0	0	0.19	0.59	2.99	2
70_23	0.101	0	0	4.999	8.672	4.231	17.629	35.632		0.07	0	0	0.7	0.23	2.35	2

70_30	0.826	0	0	0.998	14.388	6.537	5.493	28.242		0.35	0	0	0.09	0.56	2.53	2
									70_ave	0.23	0	0	0.33	0.44	2.72	2
									s	0.1778	0	0	0.2678	0.1475	0.3045	0
									C	77.30	0	0	81.15	33.52	11.19	0
71_2	0	0	0	12.418	26.608	13.475	20.164	72.665		0	0	0	0.55	0.45	2.26	2
71_8	0	0	0	9.13	19.598	9.259	20.185	58.172		0	0	0	0.59	0.41	2.43	2
71_19	0	0	0	11.085	19.725	9.897	10.016	50.723		0	0	0	0.67	0.33	2.29	2
71_22	0	0	0	16.388	25.176	13.022	18.57	73.156		0	0	0	0.75	0.25	2.2	2
71_23	0	0	0	12.901	20.895	10.227	18.851	62.874		0	0	0	0.75	0.25	2.35	2
71_24	0	0	0	12.039	20.503	10.155	14.427	57.124		0	0	0	0.7	0.3	2.31	2
71_25	0	0	0	12.905	26.23	11.591	22.681	73.407		0	0	0	0.66	0.34	2.6	2
									71_ave	0	0	0	0.66	0.34	2.35	2
									s	0	0	0	0.0759	0.0759	0.1321	0
									C	0	0	0	11.50	22.32	5.62	0
72_7	0	0	0	9.399	12.981	5.728	22.105	50.213		0	0	0	0.98	0.02	2.6	2
72_82	0	0	0	0.439	13.21	5.787	1.275	20.711		0	0	0	0.05	0.95	2.62	2
72_84	0	0	0	0.695	21.57	8.674	1.646	32.585		0	0	0	0.05	0.95	2.85	2
72_104	0	0	0	9.394	9.121	3.416	12.639	34.57		0	0	0	1.05	0	3.07	2
72_120	0	0	0	12.491	21.051	7.895	17.31	58.747		0	0	0	1.01	0	3.06	2
									72_ave	0	0	0	0.63	0.37	2.84	2
									s	0	0	0	0.5282	0.5282	0.2277	0
									C	0	0	0	83.84	142.76	8.02	0
73_41	0	1.923	0	0	32.453	14.577	32.975	81.928		0	0.22	0	0	0.78	2.56	2
73_42	0	4.467	0	0	36.445	14.505	29.266	84.683		0	0.51	0	0	0.49	2.88	2
73_43	0	1.63	0	0	30.633	11.711	25.284	69.258		0	0.23	0	0	0.77	3	2
73_48	0	1.999	0	0	33.808	13.647	37.357	86.811		0	0.24	0	0	0.76	2.84	2
73_49	0	1.746	0	0	35.425	13.641	39.245	90.057		0	0.21	0	0	0.79	2.98	2
73_50	0	2.498	0	0	33.929	14.641	31.379	82.447		0	0.28	0	0	0.72	2.66	2
73_52	0	1.437	0	0	31.773	14.56	19.96	67.73		0	0.16	0	0	0.84	2.51	2
73_53	0	3.279	0	0	36.036	14.49	29.969	83.774		0	0.37	0	0	0.63	2.86	2
73_54	0	1.99	0	0	35.184	14.443	27.948	79.565		0	0.23	0	0	0.77	2.8	2

73_55	0	1.493	0	0	34.041	13.758	33.139	82.431	0	0.18	0	0	0.82	2.84	2
73_56	0	2.987	0	0	34.714	14.247	13.639	65.587	0	0.34	0	0	0.66	2.8	2
73_57	0	1.854	0	0	32.202	14.066	23.226	71.348	0	0.22	0	0	0.78	2.63	2
73_61	0	3.603	0	0	37.664	14.524	20.714	76.505	0	0.41	0	0	0.59	2.98	2
73_62	0	3.799	0	0	36.139	14.584	22.461	76.983	0	0.43	0	0	0.57	2.84	2
73_65	0	5.096	0	0	32.328	14.368	21.733	73.525	0	0.58	0	0	0.42	2.58	2
73_67	0	3.02	0	0	30.572	14.322	21.138	69.052	0	0.35	0	0	0.65	2.45	2
73_69	0	3.028	0	0	32.146	13.102	11.767	60.043	0	0.38	0	0	0.62	2.82	2
73_73	0	2.326	0	0	32.385	14.431	24.786	73.928	0	0.26	0	0	0.74	2.58	2
73_74	0	3.257	0	0	34.812	14.861	23.231	76.161	0	0.36	0	0	0.64	2.69	2
73_75	0	2.089	0	0	32.068	12.846	29.525	76.528	0	0.27	0	0	0.73	2.87	2
73_76	0	2.029	0	0	32.545	12.84	30.098	77.512	0	0.26	0	0	0.74	2.91	2
73_77	0	1.908	0	0	32.057	13.004	32.568	79.537	0	0.24	0	0	0.76	2.83	2
73_78	0	2.22	0	0	32.11	12.798	29.072	76.2	0	0.28	0	0	0.72	2.88	2
73_79	0	3.38	0	0	33.705	13.078	27.384	77.547	0	0.42	0	0	0.58	2.96	2
73_82	0	3.095	0	0	32.909	13.006	28.724	77.734	0	0.39	0	0	0.61	2.9	2
73_83	0	3.105	0	0	31.991	12.888	29.862	77.846	0	0.4	0	0	0.6	2.85	2
73_84	0	2.123	0	0	31.615	13.066	29.934	76.738	0	0.27	0	0	0.73	2.78	2
73_85	0	2.761	0	0	33.464	12.91	27.669	76.804	0	0.35	0	0	0.65	2.98	2
73_86	0	2.684	0	0	36.392	14.733	21.968	75.777	0	0.3	0	0	0.7	2.84	2
73_87	0	2.847	0	0	37.092	14.818	23.248	78.005	0	0.32	0	0	0.68	2.87	2
73_88	0	3.908	0	0	40.987	15.246	16.752	76.893	0	0.42	0	0	0.58	3.09	2
73_89	0	4.248	0	0	42.183	16.718	25.104	88.253	0	0.42	0	0	0.58	2.9	2
73_90	0	3.72	0	0	42.32	15.934	16.224	78.198	0	0.38	0	0	0.62	3.05	2
73_91	0	3.44	0	0	38.447	14.612	15.179	71.678	0	0.39	0	0	0.61	3.02	2
73_92	0	3.478	0	0	38.139	14.925	22.64	79.182	0	0.38	0	0	0.62	2.93	2
73_93	0	3.404	0	0	36.733	14.076	13.724	67.937	0	0.4	0	0	0.6	3	2
73_94	0	3.145	0	0	37.192	14.848	23.659	78.844	0	0.35	0	0	0.65	2.88	2
73_95	0	1.963	0	0	34.256	14.566	16.688	67.473	0	0.22	0	0	0.78	2.7	2
73_96	0	5.308	0	0	35.2	14.405	18.006	72.919	0	0.24	0	0	0.76	2.81	2
73_97	0	5.207	0	0	34.844	15.205	13.86	69.116	0	0.56	0	0	0.44	2.63	2
73_98	0	3.357	0	0	35.516	15.368	16.147	70.388	0	0.36	0	0	0.64	2.65	2
73_101	0	2.413	0	0	35.698	15.534	6.206	59.851	0	0.25	0	0	0.75	2.64	2
73_102	0	2.65	0	0	35.566	15.1	8.618	61.934	0	0.29	0	0	0.71	2.7	2

73_103	0	2.152	0	0	35.404	15.043	20.678	73.277		0	0.23	0	0	0.77	2.7	2
73_104	0	2.498	0	0	37.763	15.659	22.498	78.418		0	0.26	0	0	0.74	2.77	2
73_107	0	3.453	0	0	34.452	14.611	22.282	74.798		0	0.39	0	0	0.61	2.71	2
73_108	0	3.806	0	0	37.907	16.083	19.69	77.486		0	0.39	0	0	0.61	2.71	2
									73_ave	0	0.32	0	0	0.68	2.8	2
									s	0	0.0952	0	0	0.0952	0.1500	0
									C	0	29.75	0	0	14.00	5.36	0
74_3	0	2.31	0	0.329	13.726	5.094	5.825	27.284		0	0.74	0	0.04	0.22	3.09	2
74_9	0	2.089	0	0.849	30.71	11.528	28.841	74.017		0	0.3	0	0.04	0.66	3.06	2
74_28	0	3.622	0	1.069	21.412	8.999	23.814	58.916		0	0.66	0	0.07	0.27	2.73	2
74_31	0	3.076	0	0.777	16.924	7.514	11.116	39.407		0	0.67	0	0.06	0.27	2.59	2
74_36	0	2.462	0	0.62	11.45	4.68	18.367	37.579		0	0.86	0	0.08	0.06	2.81	2
74_47	0	4.443	0	1.194	31.587	12.114	26.965	76.303		0	0.6	0	0.06	0.34	2.99	2
									74_ave	0	0.64	0	0.06	0.3	2.88	2
									s	0	0.1881	0	0.0160	0.1985	0.2000	0
									C	0	29.39	0	26.67	66.17	6.94	0
75_1	0	3.015	0	3.397	34.02	13.107	24.331	77.87		0	0.38	0	0.15	0.47	2.98	2
75_4	0	2.848	0	2.698	33.476	12.784	25.205	77.011		0	0.37	0	0.13	0.5	3.01	2
75_9	0	2.424	0	1.689	34.544	13.497	28.037	80.191		0	0.29	0	0.07	0.64	2.94	2
75_11	0	1.696	0	1.114	15.136	6.295	25.587	49.828		0	0.44	0	0.11	0.45	2.76	2
75_26	0	2.6	0	2.077	30.466	11.676	17.066	63.885		0	0.37	0	0.11	0.52	3	2
75_35	0	2.289	0	1.544	34.589	13.613	29.65	81.685		0	0.28	0	0.07	0.65	2.92	2
75_36	0	2.608	0	1.649	33.094	13.281	23.9	74.532		0	0.32	0	0.07	0.61	2.86	2
75_38	0	2.19	0	2.107	32.824	12.821	28.799	78.741		0	0.28	0	0.1	0.62	2.94	2
75_40	0	3.333	0	2.121	34.193	13.351	21.399	74.397		0	0.41	0	0.09	0.5	2.94	2
									75_ave	0	0.35	0	0.1	0.55	2.93	2
									s	0	0.0588	0	0.0283	0.0782	0.0774	0
									C	0	16.80	0	28.30	14.22	2.64	0
76_92	0	2.546	0	2.525	29.597	12.041	8.19	54.899		0	0.35	0	0.12	0.53	2.82	2
76_93	0	2.549	0	2.605	28.603	11.605	14.968	60.33		0	0.36	0	0.13	0.51	2.83	2
76_94	0	2.683	0	2.357	28.695	11.202	24.302	69.239		0	0.39	0	0.13	0.48	2.94	2

76_99	0	2.394	0	2.912	31.385	11.72	37.534	85.945		0	0.33	0	0.15	0.52	3.07	2
76_100	0	2.244	0	3.373	28.089	10.824	24.961	69.491		0	0.34	0	0.19	0.47	2.98	2
76_103	0	2.776	0	3.035	30.355	12.407	27.096	75.669		0	0.37	0	0.15	0.48	2.81	2
76_104	0	2.58	0	2.448	29.255	11.726	24.297	70.306		0	0.36	0	0.12	0.52	2.86	2
76_105	0	2.993	0	3.432	31.467	11.984	25.942	75.818		0	0.41	0	0.17	0.42	3.01	2
									76_ave	0	0.36	0	0.15	0.49	2.92	2
									s	0	0.0262	0	0.0251	0.0364	0.0987	0
									C	0	7.28	0	16.73	7.43	3.38	0
77_21	1.327	0	0	0	26.385	11.293	37.233	76.238		0.33	0	0	0	0.67	2.68	2
77_22	2.586	0	0	0	24.999	9.471	13.496	50.552		0.76	0	0	0	0.24	3.03	2
77_28	1.382	0	0	0	22.521	9.363	21.334	54.6		0.41	0	0	0	0.59	2.76	2
77_39	1.658	0	0	0	25.856	9.992	25.451	62.957		0.46	0	0	0	0.54	2.97	2
									77_ave	0.49	0	0	0	0.51	2.86	2
									s	0.1878	0	0	0	0.1878	0.1667	0
									C	38.33	0	0	0	36.82	5.83	0
78_41	0.173	0	0	0.598	31.471	11.986	15.143	59.371		0.04	0	0	0.03	0.93	3.01	2
78_43	0.053	0	0	0.541	34.844	13.174	17.045	65.657		0.01	0	0	0.02	0.97	3.04	2
78_49	0.186	0	0	0.466	35.135	13.148	17.302	66.237		0.04	0	0	0.02	0.94	3.07	2
78_55	0.273	0	0	0.356	35.13	13.663	6.909	56.331		0.06	0	0	0.02	0.92	2.95	2
78_77	0.237	0	0	7.684	22.199	8.463	18.894	57.477		0.08	0	0	0.54	0.38	3.01	2
78_114	0	0	0	13.264	23.218	10.277	17.189	63.948		0	0	0	0.77	0.05	2.59	2
78_118	0	0	0	8.203	23.087	8.537	12.042	51.869		0	0	0	0.57	0.29	3.1	2
78_120	0	0	0	15.595	29.861	10.796	16.693	72.945		0	0	0	0.86	0	3.18	2
78_123	0	0	0	12.199	26.143	12.841	12.591	63.774		0	0	0	0.56	0.3	2.34	2
78_127	0	0	0	10.948	18.125	8.394	4.496	41.963		0	0	0	0.78	0.07	2.48	2
									78_ave	0.05	0	0	0.42	0.53	2.88	2
									s	0.0298	0	0	0.3550	0.4095	0.2933	0
									C	59.60	0	0	84.52	77.26	10.18	0
79_60	0.244	0	0	6.626	24.489	9.89	25.939	67.188		0.07	0	0	0.4	0.53	2.84	2
79_62	0.13	0	0	9.988	21.054	9.89	23.61	64.672		0.04	0	0	0.6	0.36	2.44	2
79_63	0.163	0	0	11.069	26.79	10.848	44.915	93.785		0.04	0	0	0.61	0.35	2.84	2

79_70	0.268	0	0	5.508	27.193	10.373	21.267	64.609		0.07	0	0	0.32	0.61	3.01	2
									79_ave	0.06	0	0	0.48	0.46	2.78	2
									s	0.0173	0	0	0.1452	0.1284	0.2420	0
									C	28.83	0	0	30.25	27.91	8.71	0
80_75	0.078	0	0	6.8	24.415	9.289	34.748	75.33		0.02	0	0	0.33	0.65	3.01	2
80_76	0.18	0	0	11.755	25.671	11.091	23.84	72.537		0.04	0	0	0.56	0.4	2.65	2
80_77	0.137	0	0	10.898	26.931	12.033	23.771	73.77		0.03	0	0	0.54	0.43	2.56	2
80_78	0.139	0	0	15.558	23.912	11.002	34.011	84.622		0.04	0	0	0.84	0.12	2.49	2
80_79	0.106	0	0	16.513	29.043	12.909	33.655	92.226		0.02	0	0	0.63	0.35	2.58	2
80_80	0.212	0	0	16.487	28.694	12.351	28.502	86.246		0.04	0	0	0.78	0.18	2.63	2
80_81	0.149	0	0	14.906	27.956	13.679	35.169	91.859		0.03	0	0	0.65	0.32	2.35	2
80_82	0.348	0	0	16.723	26.738	11.929	33.205	88.943		0.08	0	0	0.82	0.1	2.51	2
80_83	0.081	0	0	8.532	28.847	12.002	35.248	84.71		0.02	0	0	0.42	0.56	2.76	2
80_84	0.215	0	0	10.191	28.738	13.156	20.766	73.066		0.05	0	0	0.45	0.5	2.5	2
80_86	0.139	0	0	10.995	25.17	10.252	12.547	59.103		0.04	0	0	0.63	0.33	2.82	2
80_88	0.098	0	0	8.639	34.399	13.804	16.141	73.081		0.01	0	0	0.37	0.62	2.86	2
80_89	0.064	0	0	10.209	34.922	14.183	22.556	81.934		0.01	0	0	0.42	0.57	2.83	2
80_90	0.056	0	0	10.569	36.345	14.082	17.492	78.544		0.01	0	0	0.45	0.54	2.96	2
80_91	0.054	0	0	10.425	33.537	13.835	17.572	75.423		0.01	0	0	0.44	0.55	2.78	2
80_92	0.15	0	0	12.877	33.575	13.282	19.592	79.476		0.03	0	0	0.52	0.45	2.9	2
80_100	0.079	0	0	10.381	23.241	10.333	15.279	59.313		0.02	0	0	0.59	0.39	2.58	2
80_107	0.105	0	0	12.49	33.527	13.338	23.334	82.794		0.02	0	0	0.56	0.42	2.89	2
80_113	0.052	0	0	9.662	28.72	10.732	13.023	62.189		0.01	0	0	0.48	0.51	2.73	2
									80_ave	0.03	0	0	0.55	0.42	2.7	2
									s	0.0178	0	0	0.1466	0.1592	0.1834	0
									C	59.33	0	0	26.65	37.90	6.79	0
81_5	0	0.163	0	0.047	1.072	0.399	4.455	6.136		0	0.67	0	0	0.26	3.08	2
81_31	0	3.206	0	0	27.836	11.181	6.767	48.99		0	0.47	0	0	0.53	2.86	2
81_33	0	3.301	0	0.023	17.073	7.769	1.081	29.247		0	0.7	0	0	0.3	2.52	2
81_37	0	2.899	0	0.02	32.354	11.634	5.491	52.398		0	0.41	0	0	0.59	3.19	2
81_38	0	1.905	0	0.02	12.981	4.683	2.779	22.368		0	0.67	0	0	0.33	3.18	2
81_39	0	1.802	0	0.01	9.891	3.92	8.877	24.5		0	0.75	0	0	0.25	2.9	2

81_40	0	1.719	0	0.001	9.752	4.708	6.364	22.544		0	0.6	0	0	0.4	2.38	2
81_44	0	1.866	0	0.002	12.415	4.912	7.376	26.571		0	0.62	0	0	0.38	2.9	2
81_47	0	1.049	0	0.007	7.139	3.006	9.08	20.281		0	0.57	0	0	0.43	2.73	2
81_48	0	3.926	0	0	24.964	9.989	6.254	45.133		0	0.64	0	0	0.36	2.87	2
81_54	0	1.972	0	0.026	9.591	4.153	6.863	22.605		0	0.78	0	0	0.22	2.65	2
81_58	0	4.534	0	0	26.07	9.907	9.459	49.97		0	0.75	0	0	0.25	3.02	2
									81_ave	0	0.64	0	0	0.36	2.86	2
									s	0	0.1119	0	0	0.1119	0.2514	0
									C	0	17.48	0	0	31.08	8.79	0
82_6	0	0.296	0	0.205	1.026	0.576	7.479	9.582		0	0.84	0	0.21	0	2.05	2
82_26	0	0.063	0	0.1	0.452	0.26	3.734	4.609		0	0.4	0	0.23	0.37	2	2
82_35	0	3.177	0	2.198	18.196	9.019	9.014	41.604		0	0.58	0	0.14	0.28	2.32	2
82_36	0	1.825	0	1.844	22.17	9.043	9.66	44.542		0	0.33	0	0.12	0.55	2.81	2
82_37	0	4.884	0	3.339	38.089	14.046	5.547	65.905		0	0.57	0	0.14	0.29	3.11	2
82_42	0	2.567	0	2.899	36.597	13.746	22.014	77.823		0	0.31	0	0.13	0.56	3.06	2
82_43	0	2.551	0	2.701	37.318	13.557	35.144	91.271		0	0.31	0	0.12	0.57	3.16	2
82_44	0	2.952	0	3.328	41.444	16.091	29.952	93.767		0	0.3	0	0.12	0.58	2.96	2
82_49	0	2.127	0	2.442	18.179	7.199	18.185	48.261		0	0.48	0	0.2	0.32	2.9	2
82_50	0	2.091	0	3.38	26.208	9.91	13.01	54.599		0	0.35	0	0.2	0.45	3.04	2
82_51	0	1.602	0	1.553	31.278	13.521	16.911	64.865		0	0.19	0	0.07	0.74	2.66	2
82_53	0	1.479	0	1.083	13.554	6.495	3.698	26.309		0	0.37	0	0.1	0.53	2.4	2
82_54	0	2.187	0	1.902	33.934	12.692	14.195	64.91		0	0.28	0	0.09	0.63	3.07	2
82_60	0	1.063	0	1.191	7.406	3.998	0.411	14.069		0	0.44	0	0.18	0.38	2.13	2
82_62	0	2.293	0	2.158	29.307	11.873	2.031	47.662		0	0.32	0	0.11	0.57	2.83	2
									82_ave	0	0.4	0	0.14	0.46	2.7	2
									s		0.1608	0	0.0484	0.1843	0.4116	0
									C	0	40.20	0	34.57	40.07	15.24	0
83_1	0	3.925	0	10.58	38.158	16.258	33.828	102.749		0	0.4	0	0.39	0.21	2.69	2
83_2	0	2.909	0	6.337	31.276	16.267	7.132	63.921		0	0.29	0	0.23	0.48	2.21	2
83_24	0	0.091	0	0.48	1.423	0.678	13.769	16.441		0	0.22	0	0.42	0.36	2.41	2
83_26	0	2.457	0	12.265	28.084	14.673	15.673	73.152		0	0.27	0	0.5	0.23	2.2	2
83_27	0	0.075	0	0.356	0.93	0.468	15.224	17.053		0	0.26	0	0.45	0.29	2.28	2

83_31	0	1.991	0	8.38	19.165	8.897	13.365	51.798		0	0.37	0	0.56	0.07	2.47	2
									83_ave	0	0.3	0	0.43	0.27	2.38	2
									s	0	0.0691	0	0.1129	0.1398	0.1878	0
									C	0	23.03	0	26.26	51.78	7.89	0
84_21	0	0.907	0	13.097	26.287	15.028	25.895	81.214		0	0.1	0	0.52	0.38	2.01	2
84_23	0	1.029	0	17.097	20.849	11.951	23.253	74.179		0	0.14	0	0.85	0.01	2	2
84_26	0	0.909	0	11.613	32.072	17.284	35.728	97.606		0	0.09	0	0.4	0.51	2.13	2
84_27	0	0.407	0	13.292	23.101	10.144	29.502	76.446		0	0.07	0	0.78	0.15	2.61	2
									84_ave	0	0.1	0	0.64	0.26	2.19	2
									s	0	0.0294	0	0.2127	0.2247	0.2878	0
									C	0	29.40	0	33.23	86.42	13.14	0
85_1	1.682	0	0	0	26.068	10.287	24.399	62.436		0.46	0	0	0	0.54	2.91	2
85_5	1.908	0	0	0	18.764	7.571	12.767	41.01		0.7	0	0	0	0.3	2.85	2
85_6	2.719	0	0	0	25.613	11.474	4.453	44.259		0.66	0	0	0	0.34	2.56	2
85_7	2.923	0	0	0	31.306	12.863	21.604	68.696		0.63	0	0	0	0.37	2.79	2
85_8	2.385	0	0	0	25.246	10.702	15.037	53.37		0.62	0	0	0	0.38	2.71	2
85_16	1.612	0	0	0	22.034	8.823	11.891	44.36		0.51	0	0	0	0.49	2.87	2
85_17	2.475	0	0	0	29.875	12.332	15.189	59.871		0.56	0	0	0	0.44	2.78	2
85_19	1.137	0	0	0	20.563	8.331	12.289	42.32		0.38	0	0	0	0.62	2.83	2
85_20	1.338	0	0	0	20.184	9.11	14.153	44.785		0.41	0	0	0	0.59	2.54	2
									85_ave	0.55	0	0	0	0.45	2.76	2
									s	0.1141	0	0	0	0.1141	0.1322	2
									C	20.75	0	0	0	25.36	4.79	0
86_64	0.307	0	0	6.735	17.811	7.266	17.035	49.154		0.12	0	0	0.55	0.33	2.81	2
86_65	0.199	0	0	4.42	12.682	5.448	16.372	39.119		0.1	0	0	0.48	0.42	2.67	2
86_67	0.528	0	0	6.515	26.994	10.659	22.782	67.478		0.14	0	0	0.36	0.5	2.91	2
86_68	0.585	0	0	7.56	19.951	8.563	11.16	47.819		0.19	0	0	0.52	0.29	2.67	2
86_69	0.264	0	0	2.644	10.016	4.697	5.334	22.946		0.16	0	0	0.33	0.51	2.45	2
86_73	0.534	0	0	10.069	26.612	10.246	18.394	65.855		0.15	0	0	0.58	0.27	2.98	2
86_77	0.423	0	0	8.578	24.58	10.355	14.651	58.587		0.11	0	0	0.49	0.4	2.73	2
86_78	0.395	0	0	5.431	17.331	7.629	9.529	40.315		0.14	0	0	0.42	0.44	2.61	2

86_81	1.278	0	0	0.962	11.977	5.16	8.38	27.757		0.69	0	0	0.11	0.2	2.66	2
86_91	2.592	0	0	0.205	27.17	10.782	14.379	55.128		0.67	0	0	0.01	0.32	2.89	2
86_92	2.394	0	0	0.218	21.502	8.827	7.418	40.359		0.76	0	0	0.01	0.23	2.8	2
									86_ave	0.29	0	0	0.35	0.36	2.73	2
									s	0.2672	0	0	0.2127	0.1056	0.1532	0
									C	92.14	0	0	60.77	29.33	5.61	0
87_1	0.252	0	0	9.647	22.032	9.586	18.001	59.545		0.07	0	0	0.6	0.33	2.64	2
87_2	0.429	0	0	10.029	24.359	10.481	17.295	62.593		0.11	0	0	0.57	0.32	2.67	2
87_3	0.465	0	0	8.676	22.154	8.777	18.599	58.671		0.15	0	0	0.59	0.26	2.9	2
87_4	0.701	0	0	8.813	24.015	10.082	12.545	56.156		0.19	0	0	0.52	0.29	2.73	2
87_5	0.277	0	0	9.159	26.523	11.092	15.268	62.319		0.07	0	0	0.49	0.44	2.75	2
87_6	0.21	0	0	10.05	24.902	11.008	18.325	64.495		0.05	0	0	0.54	0.41	2.6	2
87_7	0.103	0	0	2.098	3.452	2.046	4.061	11.76		0.14	0	0	0.61	0.25	1.94	2
87_8	0.209	0	0	4.284	8	4.193	3.525	20.211		0.14	0	0	0.61	0.25	2.19	2
87_9	0.476	0	0	9.203	22.106	10.042	14.781	56.608		0.13	0	0	0.54	0.33	2.53	2
87_10	0.211	0	0	7.309	15.229	7.311	7.901	37.961		0.08	0	0	0.59	0.33	2.39	2
87_11	0.293	0	0	2.117	3.687	2.132	4.47	12.699		0.38	0	0	0.59	0.03	1.99	2
87_12	0.167	0	0	2.915	4.975	2.705	4.869	15.631		0.17	0	0	0.64	0.19	2.11	2
87_13	0.109	0	0	2.375	6.231	2.639	8.171	19.525		0.12	0	0	0.53	0.35	2.71	2
87_14	0.148	0	0	0.697	1.978	1.086	5.243	9.152		0.38	0	0	0.38	0.24	2.09	2
87_15	0.07	0	0	0.534	1.618	0.784	8.008	11.014		0.25	0	0	0.4	0.35	2.37	2
87_16	0.352	0	0	11.257	25.947	11.327	19.649	68.532		0.09	0	0	0.59	0.32	2.63	2
87_17	1.356	0	0	6.289	25.821	9.494	24.769	67.729		0.4	0	0	0.39	0.21	3.12	2
87_18	1.006	0	0	6.146	26.985	9.918	24.696	68.751		0.28	0	0	0.37	0.35	3.12	2
87_19	0.352	0	0	9.545	25.324	10.986	18.032	64.239		0.09	0	0	0.52	0.39	2.65	2
87_20	0.213	0	0	10.371	25.574	11.138	18.522	65.818		0.05	0	0	0.55	0.4	2.64	2
87_21	0.24	0	0	10.097	26.038	10.96	18.77	66.105		0.06	0	0	0.55	0.39	2.73	2
87_22	0.905	0	0	6.921	23.955	10.449	16.445	58.675		0.24	0	0	0.39	0.37	2.63	2
87_23	0.284	0	0	8.956	24.99	9.169	25.01	68.409		0.09	0	0	0.54	0.37	3.13	2
87_24	0.292	0	0	8.534	26.569	9.837	22.509	67.741		0.08	0	0	0.52	0.4	3.1	2
87_25	0.2	0	0	1.932	6.603	2.966	8.649	20.35		0.19	0	0	0.39	0.42	2.56	2
87_26	0.074	0	0	0.795	2.059	0.978	6.247	10.153		0.21	0	0	0.16	0.63	2.42	2
87_27	0.267	0	0	0.622	2.42	1.264	3.3	7.917		0.14	0	0	0.29	0.57	2.2	2

87_28	0.311	0	0	2.225	6.15	3.334	5.512	17.532		0.26	0	0	0.4	0.34	2.18	2
87_29	0.135	0	0	0.955	2.161	1.283	5.434	9.968		0.29	0	0	0.44	0.27	1.93	2
87_30	0.146	0	0	3.329	5.717	3.025	3.55	15.767		0.13	0	0	0.65	0.22	2.17	2
									87_ave	0.17	0	0	0.50	0.33	2.53	2
									s	0.1014	0	0	0.1139	0.1118	0.3556	0
									C	59.65	0	0	22.78	33.88	14.06	0
88_1	0.66	0	0	7.97	23.801	10.488	16.482	59.563		0.18	0	0	0.45	0.37	2.61	2
88_2	0.624	0	0	10.173	23.941	10.067	13.403	58.208		0.17	0	0	0.6	0.23	2.73	2
88_3	0.829	0	0	8.737	23.129	9.529	13.166	55.39		0.24	0	0	0.55	0.21	2.79	2
88_4	0.819	0	0	9.496	25.919	10.447	16.425	63.106		0.22	0	0	0.54	0.24	2.85	2
88_5	0.533	0	0	8.609	23.417	10.341	17.3	60.2		0.14	0	0	0.49	0.37	2.6	2
88_6	0.275	0	0	10.022	23.893	10.286	21.705	66.181		0.07	0	0	0.58	0.35	2.67	2
88_7	0.423	0	0	6.589	19.806	8.897	15.427	51.142		0.13	0	0	0.44	0.43	2.56	2
88_9	0.293	0	0	8.18	23.444	9.935	17.578	59.43		0.08	0	0	0.49	0.43	2.71	2
88_10	0.243	0	0	7.983	26.633	11.522	16.463	62.844		0.06	0	0	0.41	0.53	2.65	2
88_11	0.701	0	0	6.71	20.997	9.656	17.418	55.482		0.2	0	0	0.41	0.39	2.5	2
88_16	0.636	0	0	6.373	22.421	9.684	22.934	62.048		0.18	0	0	0.39	0.43	2.66	2
88_17	0.574	0	0	5.673	16.124	7.372	12.767	42.51		0.05	0	0	0.49	0.46	2.51	2
88_19	0.53	0	0	6.906	17.852	8.362	11.528	45.178		0.18	0	0	0.49	0.33	2.45	2
88_21	0.654	0	0	5.329	17.654	7.51	14.513	45.66		0.24	0	0	0.42	0.34	2.7	2
88_22	0.313	0	0	10.037	23.942	10.586	18.002	62.88		0.08	0	0	0.56	0.36	2.6	2
88_23	0.259	0	0	8.474	23.245	9.849	21.758	63.839		0.07	0	0	0.51	0.42	2.71	2
88_26	0.409	0	0	8.056	20.195	9.239	16.044	53.931		0.12	0	0	0.52	0.36	2.51	2
88_27	1.058	0	0	6.199	23.724	10.325	21.454	62.76		0.29	0	0	0.36	0.35	2.64	2
88_28	0.305	0	0	8.981	21.966	9.663	22.149	63.064		0.09	0	0	0.55	0.36	2.61	2
88_29	0.293	0	0	10.399	24.193	10.677	18.076	63.638		0.08	0	0	0.58	0.33	2.6	2
									88_ave	0.14	0	0	0.49	0.37	2.63	2
									s	0.0711	0	0	0.0699	0.0775	0.1003	0
									C	50.79	0	0	14.27	20.95	3.81	0
89_11	0	1.029	0	0	8.221	3.033	23.783	36.066		0	0.56	0	0	0.44	3.11	2
89_13	0	2.842	0	0	10.94	6.994	26.739	47.515		0	0.67	0	0	0.33	1.8	2
89_14	0	3.181	0	0.003	14.178	8.181	32.39	57.933		0	0.64	0	0	0.36	1.99	2

89_18	0	2.334	0	0.009	13.487	8.56	27.337	51.727		0	0.45	0	0	0.55	1.81	2
89_26	0	2.504	0	0.008	12.511	7.877	19.272	42.172		0	0.52	0	0	0.48	1.82	2
89_32	0	2.213	0	0.02	13.331	8.366	27.511	51.441		0	0.43	0	0	0.57	1.83	2
									89_ave	0	0.55	0	0	0.45	2.06	2
									s	0	0.0977	0	0	0.0977	0.5192	0
									C	0	17.76	0	0	21.71	25.20	0
90_1	0	4.07	0	0.783	27.909	12.701	11.411	56.875		0	0.53	0	0.04	0.43	2.52	2
90_2	0	4.007	0	0.998	30.073	13.67	17.158	65.906		0	0.48	0	0.04	0.48	2.53	2
90_3	0	4.357	0	0.928	29.703	13.673	14.625	63.286		0	0.52	0	0.04	0.44	2.49	2
90_4	0	4.422	0	1.013	32.022	13.661	22.349	73.467		0	0.52	0	0.04	0.44	2.69	2
90_5	0	3.446	0	0.66	29.247	13.022	20.523	66.898		0	0.43	0	0.03	0.54	2.58	2
90_6	0	3.282	0	0.763	28.154	12.072	27.432	71.703		0	0.45	0	0.04	0.51	2.68	2
90_7	0	3.676	0	0.743	26.898	12.223	16.859	60.399		0	0.49	0	0.04	0.47	2.53	2
90_8	0	3.519	0	0.76	29.364	13.16	16.899	63.702		0	0.44	0	0.03	0.53	2.56	2
90_9	0	3.434	0	0.6	28.762	13.141	21.684	67.621		0	0.43	0	0.03	0.54	2.51	2
90_10	0	3.1	0	0.666	26.571	11.807	16.38	58.524		0	0.43	0	0.03	0.54	2.58	2
90_11	0	4.237	0	1.141	30.651	13.6	11.429	61.058		0	0.51	0	0.05	0.44	2.59	2
90_12	0	3.534	0	0.844	30.009	13.508	19.774	67.669		0	0.43	0	0.04	0.53	2.55	2
90_13	0	5.941	0	1.014	28.147	11.535	18.468	65.105		0	0.84	0	0.05	0.11	2.8	2
90_16	0	4.104	0	0.914	19.255	9.667	6.351	40.291		0	0.7	0	0.06	0.24	2.29	2
90_17	0	4.08	0	1.135	21.856	10.111	11.618	48.8		0	0.66	0	0.07	0.27	2.48	2
90_18	0	5.865	0	1.08	27.442	12.412	19.706	66.505		0	0.78	0	0.05	0.17	2.54	2
90_19	0	3.726	0	0.888	18.353	8.375	15.681	47.023		0	0.73	0	0.06	0.21	2.52	2
90_20	0	4.308	0	1.122	26.116	11.516	13.879	56.941		0	0.61	0	0.06	0.33	2.6	2
90_21	0	4.46	0	1.863	26.604	11.43	20.548	64.905		0	0.64	0	0.1	0.26	2.67	2
90_23	0	4.842	0	1.322	28.02	11.452	22.202	67.838		0	0.69	0	0.07	0.24	2.81	2
90_24	0	3.283	0	0.782	28.12	12.816	19.465	64.466		0	0.42	0	0.04	0.54	2.52	2
90_30	0	4.319	0	1.03	28.049	11.953	24.777	70.128		0	0.59	0	0.05	0.36	2.69	2
									90_ave	0	0.56	0	0.05	0.39	2.58	2
									s	0	0.1279	0	0.0168	0.1392	0.1134	0
									C	0	22.84	0	33.6	35.69	4.40	0
91_1	0	2.239	0	0.276	33.386	14.335	29.82	80.056		0	0.26	0	0.01	0.73	2.67	2

91_2	0	4.524	0	0.785	34.569	12.878	32.041	84.797	0	0.58	0	0.04	0.38	3.08	2
91_3	0	5.783	0	0.74	32.762	12.163	20.691	72.139	0	0.78	0	0.04	0.18	3.09	2
91_5	0	2.871	0	0.652	34.842	12.494	31.443	82.302	0	0.38	0	0.03	0.59	3.2	2
91_6	0	3.726	0	0.706	32.543	11.778	25.718	74.471	0	0.52	0	0.04	0.44	3.17	2
91_9	0	1.628	0	0.418	8.537	4.895	9.562	25.04	0	0.55	0	0.05	0.4	2	2
91_10	0	3.66	0	0.867	22.667	10.501	22.067	59.762	0	0.57	0	0.05	0.38	2.48	2
91_11	0	4.155	0	1.41	34.301	12.475	23.312	75.653	0	0.55	0	0.07	0.38	3.16	2
91_12	0	5.031	0	1.415	32.713	11.934	25.883	76.976	0	0.69	0	0.07	0.24	3.15	2
91_15	0	3.805	0	1.207	22.397	10.651	24.26	62.32	0	0.59	0	0.07	0.34	2.41	2
91_16	0	4.309	0	1.171	17.606	9.211	25.866	58.163	0	0.77	0	0.08	0.15	2.19	2
91_17	0	5.043	0	1.193	32.295	13.033	20.611	72.175	0	0.63	0	0.05	0.32	2.84	2
91_18	0	2.146	0	0.466	26.485	11.933	22.726	63.756	0	0.29	0	0.02	0.69	2.55	2
91_19	0	3.472	0	1.16	20.462	9.725	22.694	57.513	0	0.59	0	0.07	0.34	2.42	2
91_20	0	3.693	0	1.121	15.627	7.219	21.779	49.439	0	0.84	0	0.09	0.07	2.49	2
91_21	0	3.054	0	0.614	32.472	11.691	28.394	76.225	0	0.43	0	0.03	0.54	3.19	2
91_22	0	3.498	0	0.764	31.358	13.235	10.48	59.335	0	0.43	0	0.03	0.54	2.72	2
91_23	0	2.941	0	0.495	32.234	12.374	19.975	68.019	0	0.39	0	0.02	0.59	2.99	2
91_24	0	2.378	0	0.34	27.658	11.022	28.346	69.744	0	0.35	0	0.02	0.63	2.88	2
91_25	0	3.868	0	0.637	31.513	11.637	16.514	64.169	0	0.55	0	0.03	0.42	3.11	2
91_26	0	3.007	0	0.522	31.625	13.401	17.396	65.951	0	0.37	0	0.02	0.61	2.71	2
91_27	0	3.11	0	0.444	21.204	8.019	29.285	62.062	0	0.64	0	0.03	0.33	3.04	2
91_28	0	4.445	0	0.631	28.749	11.092	27.532	72.449	0	0.66	0	0.03	0.31	2.98	2
91_29	0	2.766	0	0.398	28.2	10.597	23.569	65.53	0	0.43	0	0.02	0.55	3.06	2
91_31	0	2.619	0	0.489	33.304	13.373	25.946	75.731	0	0.32	0	0.02	0.66	2.86	2
91_33	0	4	0	1.197	26.394	10.509	33.238	75.338	0	0.62	0	0.07	0.31	2.88	2
91_34	0	4.848	0	1.306	31.575	12.031	25.616	75.376	0	0.66	0	0.06	0.28	3.01	2
91_35	0	3.381	0	1.377	32.222	12.251	23.898	73.129	0	0.45	0	0.07	0.48	3.02	2
91_36	0	3.006	0	1.848	41.323	16.32	18.256	80.799	0	0.3	0	0.07	0.63	2.91	2
91_42	0	2.976	0	1.922	43.698	15.966	19.912	84.482	0	0.31	0	0.07	0.62	3.14	2
91_43	0	2.154	0	0.973	43.276	16.61	25.559	88.572	0	0.21	0	0.03	0.76	2.99	2
91_50	0	2.419	0	0.951	37.186	15.176	17.38	73.112	0	0.26	0	0.04	0.7	2.81	2
91_52	0	2.605	0	1.252	38.278	15.732	6.285	64.152	0	0.27	0	0.05	0.68	2.79	2
91_56	0	4.435	0	1.178	36.546	14.711	21.979	78.849	0	0.49	0	0.05	0.46	2.85	2
91_57	0	2.76	0	1.346	38.223	14.296	18.081	74.706	0	0.32	0	0.06	0.62	3.07	2

91_58	0	3.1	0	0.742	22.631	9.512	27.108	63.093		0	0.53	0	0.05	0.42	2.73	2
91_59	0	2.974	0	1.022	37.759	13.859	34.809	90.423		0	0.35	0	0.04	0.61	3.13	2
91_63	0	1.882	0	0.537	36.145	14.191	20.559	73.314		0	0.22	0	0.02	0.76	2.92	2
91_64	0	4.86	0	1.181	36.756	15.06	20.669	78.526		0	0.53	0	0.05	0.42	2.8	2
91_65	0	3.862	0	0.781	36.477	14.894	19.87	75.884		0	0.43	0	0.03	0.54	2.81	2
									91_ave	0	0.48	0	0.04	0.48	2.91	2
									s	0	0.1640	0	0.0205	0.1755	0.2820	0
									C	0	34.17	0	51.25	36.56	9.69	0
92_38	0	3.321	0	2.584	36.345	14.254	33.027	89.531		0	0.38	0	0.11	0.51	2.93	2
92_40	0	1.993	0	1.367	35.987	13.159	28.731	81.237		0	0.25	0	0.06	0.69	3.14	2
92_43	0	3.068	0	2.331	47.594	17.991	19.299	90.283		0	0.28	0	0.08	0.64	3.04	2
92_55	0	2.069	0	1.95	40.041	14.746	20.639	79.445		0	0.23	0	0.08	0.69	3.12	2
92_61	0	2.952	0	2.61	34.887	12.867	34.401	87.717		0	0.38	0	0.12	0.5	3.11	2
92_65	0	2.789	0	1.499	36.57	14.85	27.921	83.629		0	0.31	0	0.06	0.63	2.83	2
									92_ave	0	0.31	0	0.09	0.6	3.03	2
									s	0	0.0641	0	0.0251	0.0851	0.1238	0
									C	0	20.68	0	27.89	14.18	4.09	0
93_2	0	2.671	0	2.671	35.98	13.457	21.432	76.211		0	0.33	0	0.12	0.55	3.07	2
93_5	0	3.189	0	2.648	32.861	12.957	4.975	56.63		0	0.4	0	0.12	0.48	2.91	2
93_6	0	2.747	0	2.965	35.095	13.852	0.864	55.523		0	0.33	0	0.13	0.54	2.91	2
93_7	0	4.015	0	3.367	34.302	12.807	13.288	67.779		0	0.51	0	0.16	0.33	3.07	2
93_12	0	2.541	0	1.87	35.278	13.752	32.208	85.649		0	0.3	0	0.08	0.62	2.95	2
93_14	0	2.48	0	1.845	37.232	14.534	35.641	91.732		0	0.28	0	0.08	0.64	2.94	2
93_15	0	3.286	0	2.393	31.793	12.552	24.374	74.398		0	0.43	0	0.11	0.46	2.91	2
93_19	0	1.969	0	1.582	34	14.364	38.319	90.234		0	0.22	0	0.07	0.71	2.72	2
93_21	0	1.902	0	1.72	30.572	12.791	36.526	83.511		0	0.24	0	0.08	0.68	2.74	2
93_22	0	1.975	0	2.252	37.039	13.855	36.897	92.018		0	0.23	0	0.1	0.67	3.07	2
93_25	0	2.596	0	2.051	34.746	14.117	34.521	88.031		0	0.3	0	0.09	0.61	2.83	2
93_27	0	4.001	0	4.402	29.312	12.363	12.318	62.396		0	0.53	0	0.21	0.26	2.72	2
93_31	0	4.195	0	5.018	26.68	10.521	1.786	48.2		0	0.65	0	0.28	0.07	2.91	2
93_32	0	2.471	0	2.202	28.874	11.167	12.37	57.084		0	0.36	0	0.12	0.52	2.97	2
93_34	0	1.687	0	1.448	31.751	12.605	41.398	88.889		0	0.22	0	0.07	0.71	2.89	2

93_35	0	2.713	0	2.595	35.553	13.976	18.645	73.482		0	0.32	0	0.11	0.57	2.92	2
									93_ave	0	0.35	0	0.12	0.53	2.91	2
									s	0	0.1235	0	0.0558	0.1765	0.1128	0
									C	0	35.29	0	46.50	33.30	3.88	0
94_2	0	0.236	0	0.518	6.757	3.591	38.765	49.867		0	0.11	0	0.08	0.81	2.16	2
94_3	0	0.028	0	0.631	2.266	1.198	19.814	23.937		0	0.03	0	0.31	0.66	2.18	2
94_5	0	0.228	0	1.219	2.953	1.58	46.229	52.209		0	0.23	0	0.46	0.31	2.14	2
94_6	0	0.04	0	0.174	0.581	0.328	31.671	32.794		0	0.2	0	0.32	0.48	2.09	2
94_9	0	0.88	0	1.438	7.18	4.061	25.838	39.397		0	0.32	0	0.23	0.45	2.03	2
94_10	0	1.228	0	3.591	12.044	6.711	16.02	39.594		0	0.3	0	0.32	0.38	2.06	2
94_12	0	0.169	0	0.397	2.28	1.136	21.757	25.739		0	0.23	0	0.21	0.56	2.24	2
94_13	0	0.08	0	0.549	1.765	0.936	29.571	32.901		0	0.14	0	0.33	0.53	2.17	2
94_14	0	0.228	0	0.365	4.043	2.343	25.543	32.522		0	0.15	0	0.09	0.76	1.98	2
94_16	0	0.032	0	0.194	4.373	2.43	28.914	35.943		0	0.02	0	0.05	0.93	2.09	2
94_18	0	0.041	0	0.143	0.592	0.323	24.343	25.442		0	0.2	0	0.26	0.54	2.12	2
94_19	0	0.061	0	0.126	1.351	0.711	20.437	22.686		0	0.14	0	0.1	0.76	2.19	2
94_20	0	0.031	0	0.134	1.964	1.079	30.706	31.986		0	0.05	0	0.07	0.88	2.09	2
94_21	0	0.346	0	3.243	16.346	8.345	60.974	89.254		0	0.07	0	0.23	0.7	2.25	2
94_22	0	0.863	0	1.772	16.025	8.404	68.068	95.132		0	0.17	0	0.13	0.7	2.19	2
94_23	0	0.158	0	0.651	6.616	3.481	41.101	52.007		0	0.07	0	0.11	0.82	2.18	2
94_24	0	0.393	0	1.565	3.804	2.102	38.353	46.217		0	0.3	0	0.44	0.26	2.08	2
94_25	0	0.186	0	1.411	3.171	1.741	40.012	46.521		0	0.17	0	0.48	0.35	2.09	2
94_26	0	0.089	0	0.575	2.173	1.177	8.596	10.502		0	0.12	0	0.29	0.59	2.12	2
94_27	0	0.211	0	1.613	2.981	1.739	32.473	39.017		0	0.2	0	0.55	0.25	1.98	2
94_28	0	0.355	0	3.767	9.693	5.258	53.435	72.508		0	0.11	0	0.43	0.46	2.12	2
94_29	0	0.609	0	2.758	4.633	2.513	14.525	25.389		0	0.4	0	0.65	0	2.12	2
									94_ave	0	0.17	0	0.28	0.53	2.12	2
									s	0	0.0994	0	0.1696	0.2357	0.0720	0
									C	0	58.47	0	60.57	44.47	3.40	0
95_4	0	0	0	9.973	30.807	11.659	19.008	71.447		0	0	0	0.51	0.49	3.03	2
95_7	0	0	0	12.662	27.72	10.84	17.406	68.628		0	0	0	0.69	0.31	2.94	2
95_9	0	0	0	8.578	31.372	12.078	10.98	63.008		0	0	0	0.42	0.58	2.98	2

95_12	0	0	0	11.798	33.855	13.252	10.243	69.148		0	0	0	0.53	0.47	2.93	2
95_19	0	0	0	9.643	30.494	11.594	10.69	62.421		0	0	0	0.49	0.51	3.02	2
95_25	0	0	0	11.338	24.788	9.388	19.566	65.08		0	0	0	0.72	0.28	3.03	2
95_26	0	0	0	6.529	29.824	11.447	8.421	56.221		0	0	0	0.34	0.66	2.99	2
95_27	0	0	0	5.99	32.692	12.238	9.88	60.8		0	0	0	0.29	0.71	3.07	2
95_29	0	0	0	10.693	26.92	10.7	16.916	65.229		0	0	0	0.59	0.41	2.89	2
95_30	0	0	0	6.594	31.295	11.81	1.752	51.451		0	0	0	0.33	0.67	3.04	2
95_32	0	0	0	13.893	30.571	11.998	33.912	90.374		0	0	0	0.69	0.31	2.93	2
95_35	0	0	0	10.309	26.349	9.614	29.588	75.86		0	0	0	0.64	0.36	3.15	2
95_36	0	0	0	18.24	31.225	13.104	16.956	79.525		0	0	0	0.89	0.11	2.74	2
95_37	0	0	0	9.522	21.406	8.281	21.628	60.837		0	0	0	0.73	0.27	2.97	2
									95_ave	0	0	0	0.56	0.44	2.98	2
									s	0	0	0	0.1768	0.1768	0.0960	0
									C	0	0	0	31.57	40.18	3.22	0
96_31	2.842	0	0	0	45.656	16.753	34.657	99.908		0.47	0	0	0	0.53	3.13	2
96_32	2.87	0	0	0	30.181	11.352	20.377	64.78		0.71	0	0	0	0.29	3.05	2
96_36	2.17	0	0	0	22.221	8.38	7.712	40.483		0.72	0	0	0	0.28	3.04	2
96_39	3.208	0	0	0	34.629	12.736	12.276	62.849		0.7	0	0	0	0.3	3.12	2
96_40	3.057	0	0	0	31.202	12.004	14.314	60.577		0.71	0	0	0	0.29	2.98	2
96_41	1.08	0	0	0	28.299	10.583	23.601	63.564		0.28	0	0	0	0.72	3.07	2
96_42	2.133	0	0	0	37.306	14.777	20.102	74.318		0.4	0	0	0	0.6	2.9	2
96_44	2.093	0	0	0	29.161	11.098	22.249	64.601		0.53	0	0	0	0.47	3.02	2
96_48	2.006	0	0	0	30.535	11.569	26.779	70.889		0.48	0	0	0	0.52	3.03	2
96_49	2.798	0	0	0	30.512	11.29	19.536	64.136		0.69	0	0	0	0.31	3.1	2
96_51	1.806	0	0	0	32.335	12.587	15.143	61.871		0.4	0	0	0	0.6	2.95	2
96_52	2.172	0	0	0	29.557	11.063	22.328	65.12		0.55	0	0	0	0.45	3.07	2
96_53	3.725	0	0	0	35.161	13.515	23.26	75.661		0.77	0	0	0	0.23	2.99	2
96_55	2.036	0	0	0	30.757	11.354	22.993	67.14		0.5	0	0	0	0.5	3.11	2
96_56	2.311	0	0	0	25.938	9.67	20.704	58.623		0.67	0	0	0	0.33	3.08	2
96_57	1.197	0	0	0	37.662	13.751	32.044	84.654		0.24	0	0	0	0.76	3.14	2
96_59	2.655	0	0	0	32.764	12.238	14.087	61.744		0.61	0	0	0	0.39	3.07	2
96_60	2.263	0	0	0	26.821	10.772	14.687	54.543		0.59	0	0	0	0.41	2.86	2
									96_ave	0.56	0	0	0	0.44	3.04	2

								s	0.1567	0	0	0	0.1567	0.0783	0
								C	27.98	0	0	0	35.61	2.58	0
97_33	0.452	0	0	14.341	31.417	11.971	12.331	70.512	0.11	0	0	0.71	0.18	3.01	2
97_48	0.615	0	0	16.62	45.356	17.169	2.305	82.065	0.1	0	0	0.58	0.32	3.03	2
97_50	0.309	0	0	5.48	32.715	12.106	18.682	69.292	0.07	0	0	0.27	0.66	3.1	2
97_56	0.744	0	0	5.696	33.637	13.138	15.32	68.535	0.16	0	0	0.26	0.58	2.94	2
								97_ave	0.11	0	0	0.46	0.43	3.02	2
								s	0.0374	0	0	0.2258	0.2235	0.0658	0
								C	34.00	0	0	49.09	51.98	2.18	0
98_55	0.507	0	0	12.397	30.526	11.754	14.844	70.028	0.12	0	0	0.63	0.25	2.98	2
98_56	0.775	0	0	20.042	46.474	17.623	20.882	105.796	0.12	0	0	0.68	0.2	3.03	2
98_57	0.274	0	0	8.062	28.088	10.847	23.586	70.857	0.07	0	0	0.44	0.49	2.97	2
98_58	0.344	0	0	9.339	28.325	10.86	24.453	73.321	0.09	0	0	0.51	0.4	2.99	2
98_59	0.346	0	0	7.547	34.005	13.73	19.252	74.88	0.07	0	0	0.33	0.6	2.84	2
98_60	0.257	0	0	10.029	28.342	10.768	19.73	69.126	0.07	0	0	0.55	0.38	3.02	2
98_61	0.397	0	0	12.598	28.586	10.284	19.132	70.997	0.11	0	0	0.73	0.16	3.19	2
98_62	0.39	0	0	12.941	26.618	9.909	19.584	69.442	0.11	0	0	0.78	0.11	3.08	2
98_63	0.427	0	0	18.182	44.737	16.449	38.888	118.683	0.07	0	0	0.66	0.27	3.12	2
98_64	0.264	0	0	4.665	26.472	9.413	27.772	68.586	0.08	0	0	0.29	0.63	3.23	2
98_65	0.266	0	0	6.829	26.179	9.943	21.883	65.1	0.07	0	0	0.41	0.52	3.02	2
98_66	0.235	0	0	7.791	33.505	11.945	18.676	72.152	0.05	0	0	0.39	0.56	3.22	2
98_67	0.293	0	0	12.241	27.318	10.349	17.422	67.623	0.08	0	0	0.7	0.22	3.03	2
98_68	0.308	0	0	11.701	22.893	8.513	20.629	64.044	0.1	0	0	0.82	0.08	3.09	2
98_69	0.429	0	0	13.459	28.449	11.297	19.39	73.024	0.11	0	0	0.71	0.18	2.89	2
98_71	0.439	0	0	11.621	26.335	9.94	16.528	64.863	0.12	0	0	0.69	0.19	3.04	2
98_72	0.385	0	0	10.742	23.156	9.309	12.447	56.039	0.12	0	0	0.69	0.19	2.86	2
98_73	0.27	0	0	10.859	37.939	13.253	33.092	95.413	0.06	0	0	0.76	0.18	3.29	2
98_74	0.445	0	0	10.042	31.996	11.405	20.482	74.37	0.11	0	0	0.52	0.37	3.22	2
98_75	0.226	0	0	8.981	23.931	9.373	28.161	70.658	0.07	0	0	0.57	0.36	2.93	2
98_76	0.254	0	0	6.173	22.986	8.28	18.514	56.207	0.09	0	0	0.44	0.47	3.19	2
98_77	0.209	0	0	7.323	18.994	8.628	24.012	59.166	0.07	0	0	0.5	0.43	2.53	2
98_78	0.073	0	0	4.949	18.829	8.994	9.833	42.678	0.02	0	0	0.33	0.65	2.4	2

98_79	0.383	0	0	7.146	14.535	6.876	26.152	55.092		0.16	0	0	0.62	0.22	2.43	2
98_80	0.362	0	0	20.28	46.451	18.348	50.461	135.902		0.06	0	0	0.66	0.28	2.91	2
98_81	0.105	0	0	5.66	23.941	9.94	28.611	68.257		0.03	0	0	0.34	0.63	2.77	2
98_82	0.311	0	0	9.167	25.563	10.15	23.549	68.748		0.09	0	0	0.54	0.37	2.89	2
98_83	0.443	0	0	10.746	27.323	11.185	15.408	65.105		0.11	0	0	0.57	0.32	2.8	2
98_84	0.134	0	0	3.342	21.429	8.538	26.086	59.529		0.04	0	0	0.23	0.73	2.88	2
									98_ave	0.09	0	0	0.55	0.36	2.96	2
									s	0.0312	0	0	0.1612	0.1815	0.2228	0
									C	34.67	0	0	29.31	50.42	7.53	0
99_55	0.141	0	0	14.118	31.882	12.86	23.715	80.166		0.03	0	0	0.65	0.32	2.85	2
99_56	0.144	0	0	16.429	37.253	14.079	19.288	85.128		0.03	0	0	0.69	0.28	3.04	2
99_58	0.221	0	0	14.321	28.861	15.346	13.139	66.727		0.04	0	0	0.55	0.41	2.16	2
99_59	0.108	0	0	13.771	27.901	14.043	15.674	66.895		0.02	0	0	0.58	0.4	2.28	2
99_60	0.184	0	0	17.041	35.332	12.768	18.201	81.13		0.04	0	0	0.79	0.17	3.18	2
99_61	0.064	0	0	13.085	31.966	11.913	15.831	69.26		0.01	0	0	0.65	0.34	3.08	2
99_62	0.158	0	0	15.886	32.727	13.167	16.813	75.527		0.03	0	0	0.72	0.25	2.85	2
99_63	0.158	0	0	15.842	32.298	13.757	17.795	76.811		0.03	0	0	0.68	0.29	2.7	2
99_65	0.134	0	0	10.625	33.629	14.409	22.721	78.39		0.03	0	0	0.44	0.53	2.68	2
99_66	0.196	0	0	11.167	35.159	17.047	10.987	69.279		0.03	0	0	0.39	0.58	2.37	2
99_68	0.145	0	0	14.945	36.164	14.474	19.813	83.085		0.03	0	0	0.61	0.36	2.87	2
99_69	0.072	0	0	11.922	35.382	15.128	18.203	77.263		0.01	0	0	0.47	0.52	2.69	2
99_71	0.115	0	0	10.813	26.596	11.686	16.044	60.614		0.03	0	0	0.55	0.42	2.61	2
99_72	0.143	0	0	15.884	34.626	12.691	16.929	77.411		0.03	0	0	0.74	0.23	3.13	2
99_73	0.118	0	0	8.105	36.671	17.882	18.546	77.232		0.02	0	0	0.27	0.71	2.35	2
99_75	0.054	0	0	4.246	32.871	13.282	26.603	73.526		0.01	0	0	0.19	0.8	2.84	2
99_76	0.112	0	0	14.677	35.522	14.411	19.001	80.979		0.02	0	0	0.61	0.37	2.83	2
99_78	0.088	0	0	12.466	37.669	13.49	28.165	90.621		0.02	0	0	0.55	0.43	3.21	2
99_79	0.163	0	0	13.984	33.315	14.387	20.387	79.271		0.03	0	0	0.58	0.39	2.66	2
99_81	0.177	0	0	14.67	30.946	15.49	11.195	67.404		0.03	0	0	0.56	0.41	2.29	2
99_82	0.157	0	0	15.286	34.67	13.519	21.197	82.474		0.03	0	0	0.67	0.3	2.94	2
99_83	0.188	0	0	16.19	34.987	14.778	10.758	72.867		0.04	0	0	0.65	0.31	2.72	2
99_84	0.145	0	0	14.159	32.652	13.506	23.021	80.876		0.03	0	0	0.62	0.35	2.78	2
									99_ave	0.03	0	0	0.57	0.4	2.74	2

									s	0.0088	0	0	0.1440	0.1485	0.2972	0
									C	29.33	0	0	25.26	37.13	10.85	0
100_54	0.136	0	0	13.983	28.376	10.657	13.631	66.783		0.04	0	0	0.78	0.18	3.06	2
100_55	0.019	0	0	10.684	24.992	9.482	13.512	58.689		0.01	0	0	0.67	0.32	3.03	2
100_62	0.084	0	0	15.025	38.661	14.089	20.162	88.021		0.02	0	0	0.63	0.35	3.15	2
100_63	0.1	0	0	17.575	34.888	13.596	6.128	72.287		0.02	0	0	0.77	0.21	2.95	2
100_69	0.079	0	0	11.487	33.635	12.167	18.696	76.064		0.02	0	0	0.56	0.42	3.17	2
100_71	0.056	0	0	7.646	32.533	11.677	22.605	74.517		0.01	0	0	0.39	0.6	3.2	2
100_74	0.088	0	0	11.411	28.705	10.872	20.473	71.549		0.02	0	0	0.62	0.36	3.03	2
100_77	0.04	0	0	12.08	22.307	8.676	10.343	53.446		0.01	0	0	0.83	0.16	2.95	2
100_80	0.068	0	0	8.534	31.737	11.524	14.217	66.08		0.02	0	0	0.44	0.54	3.16	2
									100_ave	0.02	0	0	0.63	0.35	3.08	2
									s	0.0093	0	0	0.1510	0.1537	0.0955	0
									C	46.50	0	0	23.97	43.91	3.10	0
101_31	0.045	0	0	7.293	29.818	11.531	21.322	70.009		0.01	0	0	0.38	0.61	2.97	2
101_32	0.15	0	0	12.494	28.147	10.446	23.976	75.213		0.04	0	0	0.71	0.25	3.09	2
101_33	0.037	0	0	6.427	33.737	13.193	17.522	70.916		0.01	0	0	0.29	0.7	2.94	2
101_34	0.039	0	0	9.634	31.786	11.865	13.822	67.146		0.01	0	0	0.48	0.51	3.08	2
101_36	0.056	0	0	8.405	34.221	13.04	30.16	85.882		0.01	0	0	0.38	0.61	3.01	2
101_37	0.096	0	0	10.214	34.112	13.016	11.063	68.501		0.02	0	0	0.47	0.51	3.01	2
101_40	0.088	0	0	7.321	27.507	9.978	8.528	53.422		0.02	0	0	0.44	0.54	3.16	2
101_43	0.025	0	0	4.011	23.921	9.014	10.969	47.94		0.01	0	0	0.21	0.78	2.48	2
101_44	0.097	0	0	4.437	26.916	9.72	8.398	49.568		0.03	0	0	0.27	0.7	3.18	2
101_47	0.109	0	0	15.086	38.265	13.333	17.713	84.506		0.02	0	0	0.67	0.31	3.29	2
101_52	0.111	0	0	13.175	31.773	11.475	17.302	73.836		0.03	0	0	0.68	0.29	3.18	2
101_55	0	0	0	8.774	26.053	9.273	8.097	52.197		0	0	0	0.56	0.44	3.23	2
101_57	0.017	0	0	14.823	36.786	13.859	6.982	72.467		0	0	0	0.64	0.36	3.05	2
101_61	0.062	0	0	9.473	31.394	11.453	17.949	70.331		0.02	0	0	0.49	0.49	3.15	2
101_64	0.035	0	0	15.127	31.605	11.024	13.296	71.087		0.01	0	0	0.82	0.17	3.29	2
									101_ave	0.02	0	0	0.5	0.48	3.07	2
									s	0.0112	0	0	0.1785	0.1804	0.1971	0
									C	56.00	0	0	35.70	37.58	6.42	0

102_5	0	0	0.174	12.079	30.071	11.544	14.329	59.194		0	0	0.005	0.622	0.373	2.99	2
102_17	0	0	0.491	8.391	33.831	12.707	8.27	53.78		0	0	0.012	0.393	0.595	3.06	2
102_19	0	0	0.132	9.057	34.616	12.934	21.292	67.944		0	0	0.003	0.416	0.581	3.07	2
102_20	0	0	0.087	12.193	33.297	12.471	15.115	63.437		0	0	0.002	0.581	0.417	3.07	2
102_27	0	0	0.175	11.603	32.274	12.243	5.068	51.815		0	0	0.004	0.563	0.433	3.03	2
102_30	0	0	0.077	5.647	33.206	13.624	19.71	61.639		0	0	0.002	0.246	0.752	2.8	2
102_31	0	0	0.142	8.694	33.724	12.716	2.979	48.338		0	0	0.003	0.406	0.591	3.04	2
102_32	0	0	0.082	4.973	35.746	13.652	13.476	57.282		0	0	0.002	0.217	0.781	3.01	2
102_34	0	0	0.152	11.862	32.704	12.793	19.886	67.42		0	0	0.004	0.551	0.445	2.93	2
102_38	0	0	0.056	9.015	31.8	12.384	14.706	58.303		0	0	0.001	0.433	0.566	2.95	2
102_50	0	0	0.193	11.192	34.138	13.322	22.434	81.279		0	0	0.004	0.5	0.496	2.94	2
									102_ave	0	0	0.004	0.448	0.548	2.99	2
									s	0	0	0.0030	0.1322	0.1326	0.0812	0
									C	0	0	75.00	29.51	24.20	2.72	0
103_10	0	0	0.109	10.714	36.714	13.4	24.589	85.526		0	0	0.0025	0.475	0.5225	3.15	2
103_13	0	0	0.09	7.653	29.092	11.157	24.246	72.238		0	0	0.0025	0.408	0.5895	2.99	2
103_16	0	0	0.087	12.596	34.984	12.672	25.576	85.915		0	0	0.002	0.59	0.408	3.17	2
103_23	0	0	0.122	7.877	22.831	9.473	13.181	53.484		0	0	0.004	0.49	0.506	2.77	2
									103_ave	0	0	0.003	0.491	0.506	3.02	2
									s	0	0	0.0009	0.0752	0.0749	0.1851	0
									C	0	0	30.00	15.32	14.80	6.13	0
104_20	0	0	0.512	9.042	31.449	11.616	17.949	70.568		0	0	0.014	0.463	0.523	3.11	2
104_31	0	0	1.267	11.908	23.794	8.542	23.794	69.305		0	0	0.046	0.83	0.124	3.2	2
104_33	0	0	0	16.722	29.819	10.605	11.415	68.561		0	0	0	0.94	0.06	3.23	2
104_34	0	0	1.203	14.86	25.914	9.508	2.732	54.217		0	0	0.039	0.93	0.031	3.13	2
104_35	0	0	0.887	15.256	27.862	10.401	11.796	66.202		0	0	0.026	0.872	0.102	3.08	2
									104_ave	0	0	0.025	0.807	0.168	3.15	2
									s	0	0	0.0186	0.1974	0.2017	0.0628	0
									C	0	0	74.40	24.46	120.06	1.99	0
105_1	0	0	0.91	8.843	21.519	8.537	18.22	58.029		0	0	0.033	0.616	0.351	2.89	2

105_3	0	0	0.727	9.83	14.888	6.84	15.489	47.774	0	0	0.033	0.854	0.113	2.5	2
105_12	0	0	0.582	10.034	15.076	7.052	17.8	50.544	0	0	0.026	0.846	0.128	2.45	2
105_17	0	0	0.745	10.925	15.55	7.346	18.764	53.33	0	0	0.031	0.884	0.085	2.43	2
105_19	0	0	0.793	11.096	15.279	7.02	18.175	52.363	0	0	0.035	0.94	0.025	2.5	2
105_30	0	0	3.227	7.194	10.214	4.804	6.661	32.1	0	0	0.19	0.81	0	2.44	2
105_37	0	0	0.701	10.053	18.939	7.185	25.892	62.77	0	0	0.03	0.832	0.138	3.03	2
105_38	0	0	0.58	9.182	18.161	7.216	20.932	56.071	0	0	0.025	0.756	0.219	2.89	2
105_39	0	0	0.866	9.672	20.952	7.399	25.612	64.501	0	0	0.036	0.777	0.187	3.25	2
105_40	0	0	0.765	9.953	19.977	7.747	26.968	65.41	0	0	0.031	0.764	0.205	2.96	2
								105_ave	0	0	0.047	0.808	0.145	2.73	2
								s	0	0	0.0504	0.0881	0.1020	0.3023	0
								C	0	0	107.23	10.90	70.34	11.07	0
106_2	0	0	0.794	14.02	30.413	10.882	16.107	72.216	0	0	0.023	0.766	0.211	3.21	2
106_8	0	0	0.856	8.716	34.105	12.096	24.966	80.739	0	0	0.022	0.428	0.55	3.24	2
106_9	0	0	0.95	6.075	31.886	12.288	24.996	76.195	0	0	0.024	0.294	0.682	2.98	2
106_18	0	0	0.244	8.89	36.727	12.781	28.317	86.959	0	0	0.006	0.413	0.581	3.3	2
106_21	0	0	0.248	9.535	35.761	12.593	25.464	83.601	0	0	0.006	0.45	0.544	3.26	2
106_22	0	0	0.22	7.747	33.546	12.196	28.492	82.201	0	0	0.006	0.378	0.616	3.16	2
106_27	0	0	1.345	13.671	45.329	15.81	43.872	120.027	0	0	0.026	0.514	0.46	3.29	2
106_30	0	0	0.684	12	33.539	11.872	16.375	74.47	0	0	0.018	0.601	0.381	3.24	2
106_34	0	0	1.12	10.071	33.763	11.968	20.589	77.511	0	0	0.029	0.5	0.471	3.24	2
								106_ave	0	0	0.018	0.483	0.499	3.21	2
								s	0	0	0.0093	0.1374	0.1404	0.0968	0
								C	0	0	51.67	28.45	28.14	3.02	0
107_1	0	0	1.487	0.032	30.04	3.56	7.582	42.701	0	0	0.029	0	0.971	2.15	2
107_7	0	0	1.436	0.059	38.523	3.338	10.369	53.725	0	0	0.03	0	0.97	2.94	2
107_10	0	0	1.219	0.018	38.754	2.871	9.092	51.954	0	0	0.029	0	0.971	3.44	2
107_18	0	0	1.339	0.066	39.042	2.763	8.018	51.228	0	0	0.033	0	0.967	3.6	2
107_32	0	0	1.659	0.062	41.585	3.795	8.447	55.548	0	0	0.03	0	0.97	2.8	2
107_40	0	0	0.894	0.022	21.291	2.172	5.477	29.856	0	0	0.028	0	0.972	2.5	2
								107_ave	0	0	0.03	0	0.97	2.91	2
								s	0	0	0.0017	0	0.0017	0.5506	0
								C	0	0	5.67	0	0.18	18.92	0

APPENDIX J ICP-AES compositions (parts per million) of K, Na, Pb, Ag, K-Ag, Na-Ag and Pb-Ag jarosites synthesised at 22ºC, 97ºC and 140ºC.

Sample	Na	K	Pb	Ag	Fe	S
4	-	47729	-	-	266936	117916
6	-	33570	-	33312	277200	110614
6D	-	36783	-	28817	259212	116404
8	-	28041	-	55504	262938	110932
10	-	16874	-	77305	262280	110799
10D	-	17463	-	79717	252697	107035
12	-	-	-	134206	240715	102017
14	23425	-	-	-	291899	115265
16	12936	-	-	68936	284810	112064
18	3542	-	-	108223	242973	102730
20	2114	-	-	122589	241607	102295
22	-	46134	-	-	267781	118667
24	-	36627	-	28422	258954	113311
24D	-	36732	-	27878	261274	115882
26	-	31234	-	48329	275037	115357
28	-	18084	-	102315	245031	109395
30	-	-	-	166157	221906	97430
32	22821	-	-	-	290990	116444
34	6140	-	-	99541	277627	107479
36	1192	-	-	127912	262431	106332
38	510	-	-	176680	242868	107814
38D	1818	-	-	143122	255975	109826
40	-	27916	-	309964	145889	111276
42	3160	-	-	122781	237188	103547
43	-	-	61635	-	278116	106299
43D	-	-	53572	-	270582	98683
44	-	-	27991	50382	279068	106430
45	-	-	29230	90604	275724	106721
46	-	-	15300	123130	272864	104474
46D	-	-	14078	103757	269840	106461
47	-	-	7004	133051	264176	102066
48	-	-	6986	133507	271107	103581
50	13493	-	-	47973	300731	113561
51	7879	-	-	84434	267552	105833
52	3435	-	-	120738	272310	106646
53	1522	-	-	137391	274275	105754
54	485	-	-	140886	260604	100556
55	-	24377	-	65251	268696	109149
57	-	31861	-	42725	272441	111862
58	-	24661	-	61656	261214	106292
59	-	18827	-	81998	264237	107182
60	-	10031	-	110359	260512	100996
61	-		-	150657	266529	104541
62D	-	41230	-		272711	109083
63D	-	27634	-	33440	272603	93150
64D	-	21193	-	56430	281084	93729
65D	-	9437	-	66864	276320	106441
66D	-	-	-	79722	282742	107229
67	23882	-	-	-	309695	113862
68	20796	-	-	23926	297479	113689
69D	16441	-	-	36137	311674	113342
70	7684	-	-	78752	271000	104897
71D	-	-	-	132215	270206	103975
72	-	-	-	341857	158931	96906

73	-	54617	-		241507	115402
74	-	47208	-	12016	248705	113395
75	-	42983	-	25976	240196	110611
76	-	28196	-	196025	189098	109155
77	28421	-	-		298320	119820
78	4165	-	-	122353	239400	102630
79	1080	-	-	129493	230677	96053
80	884	-	-	312655	161823	96668
81	-	40876	-	-	275562	112426
82	-	30547	-	45627	284693	113757
83	-	17818	-	80018	260050	102462
84D	-	5500	-	120610	270179	105568
85	22992	-	-	-	289671	111598
86	22512	-	-	14573	296800	112911
87	4865	-	-	102763	266723	102252
88D	4495	-	-	103213	285472	110222
89	-	47406	-	-	230042	106101
90	-	49498	-	10523	261396	117556
91	-	41719	-	18156	247635	105910
92	-	37765	-	26014	233569	102780
93	-	27288	-	62072	246000	104007
94	-	17668	-	90307	241526	102384
95	-	-	-	138281	240926	96546
96	27849	-	-	-	300064	114260
97	13273	-	-	69379	261800	101478
98	4906	-	-	114586	248490	99738
99	1421	-	-	125991	234323	93869
100	593	-	-	135153	244316	98658
101	318	-	-	143126	252488	101948
102	-	-	1839	143016	251476	103021
103	-	-	9072	137716	250565	99695
104	-	-	6286	140451	248749	97903
105	-	-	19509	132910	237187	95887
106	-	-	11223	129708	233848	96484
107	-	-	38799	-	398754	46687